Mfd, une protéine impliquée dans la virulence de B. cereus et une nouvelle cible pour le développement d'antibiotiques

Delphine Cormontagne

THÈSE DE DOCTORAT

NNT : 2023UPASB021

université PARIS-SACLAY

Mfd, une protéine impliquée dans la virulence de *B. cereus* et une nouvelle cible pour le développement d'antibiotiques.

Mfd, a protein involved in B. cereus virulence and a new target for the development of innovative antimicrobials.

Thèse de doctorat de l'université Paris-Saclay
École doctorale n°581, agriculture, alimentation, biologie, environnement, santé (ABIES)
Spécialité de doctorat : Microbiologie
Graduate School : Biosphera. Référent : AgroParisTech

Thèse préparée à l'UMR **Micalis Institute** (Université Paris-Saclay, INRAE, AgroParisTech) sous la direction de **Nalini RAMA RAO**, Directrice de Recherche, la co-direction de **Thierry NAAS**, PU-PH,
le co-encadrement de **Seav-ly TRAN**, Chercheuse.

Thèse soutenue à Paris-Saclay, le 23 mars 2023

Delphine CORMONTAGNE

Composition du Jury

Membres du jury avec voix délibérative

Olivier DUSSURGET Professeur, Université Paris-Cité	Président
Anne BRISABOIS Directrice de Recherche, Anses	Rapporteur & Examinatrice
Nathalie CONNIL Maîtresse de Conférences (HDR), Université de Rouen	Rapporteur & Examinatrice
Florence DOUCET POPULAIRE PU-PH, Hôpital A. Béclère (Université Paris-Saclay)	Examinatrice

université PARIS-SACLAY

ÉCOLE DOCTORALE
Agriculture, alimentation, biologie, environnement, santé (ABIES)

Titre : Mfd, une protéine impliquée dans la virulence de *B. cereus* et une nouvelle cible pour le développement d'antibiotiques.

Mots clés : Mfd, virulence, *Bacillus cereus*, antibiotique

Résumé : Mfd est une protéine bactérienne fortement conservée et impliquée dans de nombreux processus comme la réparation de l'ADN, la mutagénèse ou encore la virulence.

Bacillus cereus est une bactérie responsable d'intoxications alimentaires, mais également un pathogène opportuniste pouvant causer des infections non gastro-intestinales sévères chez les personnes immunodéprimées comme les nouveau-nés prématurés. La pathogénie de *B. cereus* est multifactorielle, un des facteurs impliquée dans sa virulence est la protéine Mfd. Par l'étude de souches cliniques et environnementales de *B. cereus*, nous avons pu montrer que Mfd joue un rôle majeur dans la virulence des souches cliniques et que son implication semble être étroitement liée à sa séquence / structure fonctionnelle. Une modification de cette dernière pourrait engendrer une variation dans la virulence d'une souche. Ces données contribuent à une meilleure compréhension des mécanismes de virulence de *B. cereus* et permettent de suggérer Mfd comme un facteur global de virulence.

Grâce à son rôle dans la virulence et la mutagénèse, Mfd est une cible prometteuse pour le développement de nouveaux antibiotiques. Nous avons montré qu'un inhibiteur de Mfd, le NM102, a une activité antimicrobienne sur *K. pneumonia* et *P. aeruginosa* exclusivement dans un contexte d'infection sans induire de toxicité dans l'hôte. En plus de cette activité, le NM102 est aussi capable d'inhiber la fonction de Mfd dans la mutagénèse ce qui réduit la fréquence d'apparition de résistance aux antibiotiques. Ces résultats permettent de proposer une alternative prometteuse pour lutter contre la résistance des bactéries aux antibiotiques qui constituent un problème de santé global et alarmant.

Title: Mfd, a protein involved in *B. cereus* virulence and a new target for the development of innovative antimicrobials

Keywords: Mfd, virulence, *Bacillus cereus*, antibiotics

Abstract: Mfd is a conserved bacterial protein implicated in various processes such as DNA repair, mutagenesis and virulence.

Bacillus cereus is a bacteria known to cause food-borne outbreaks but it is also an opportunistic pathogen responsible for severe local and systemic infections in immunocompromised humans and neonates. *B. cereus* pathogenicity is multifactorial and the Mfd protein is implicated in virulence. With the study of environmental and clinical strains, we were able to show an essential role of Mfd in the clinical strains' virulence. Its role seems to be linked to the Mfd sequence and structure and its modification could induce a variation in the pathogenicity of a strain. These data contribute to a better understanding of the mechanisms underlying *B. cereus* virulence and allow to suggest Mfd as a potential universal virulence factor.

Due to its role in virulence and mutagenesis, Mfd is a promising target for the development of new antimicrobial drugs. We identified an inhibitor of Mfd called NM102 showing an antimicrobial activity against *K. pneumonia* and *P. aeruginosa* exclusively in a context of infection, without inducing toxicity to the host. Furthermore, NM102 also inhibits Mfd's function in mutagenesis leading to a decrease of antimicrobial resistance. This represents a promising alternative therapeutic strategy to fight against antimicrobial resistance which constitutes an urgent and alarming health issue.

Remerciements

J'ai réalisé ce travail au sein de l'Institut Micalis de l'INRAE de Jouy-en-Josas sous la direction de la Dr Nalini Rama Rao, du Dr Thierry Naas et l'encadrement de la Dr Seav-ly Tran.

Je souhaite tout d'abord remercier Nalini, Thierry et Seav-ly pour tout ce que j'ai pu apprendre à leur côté avec tous les conseils que j'ai reçus et tout le temps qu'ils m'ont dédié le long de cette thèse. Grâce à eux j'ai énormément évolué et progressé.

Je remercie les membres de l'équipe PIMs, passés et présents, pour leurs conseils, leur accueil et leur joie de vivre. Rozenn Dervyn pour tout ce qu'elle m'a enseigné et Jasmina Vidic pour son énergie et son enthousiasme. Je tiens à remercier plus particulièrement Lucie Lebreuilly qui a souffert au côté de Nalini dans la relecture de mon manuscrit et avec qui j'ai passé d'excellents moments au labo mais aussi en dehors.

Je remercie Gwenaelle Andre-Leroux et Samantha Samson de l'équipe Maiage pour leur implication dans mon projet mais aussi leur bonne humeur tout au long de nos réunions.

Je remercie le directeur d'unité Philippe Noirot pour m'avoir accueillie au sein de l'INRAE Micalis de Jouy-en-Josas.

Je remercie également l'école Doctorale ABIES, son directeur et directeur adjoint Alexandre Pery et Pierre Larraufie et mon comité de thèse, la Dr Alexandra Gruss, le Pr Olivier Dussurget et la Dr Caroline Pénicaut pour leur précieuse aide et leurs bons conseils.

Je remercie la Dr Anne Brisabois, la Dr Nathalie Connil, la Pr Florence Doucet Populaire et le Pr Olivier Dussurget pour avoir accepté de faire partie de mon jury de thèse.

Je remercie l'équipe informatique du bureau d'à côté, Frank Gérard, Momar Mbow et Emmanuel Cuervo pour nos discussions souvent pleines d'humour mais toujours là pour aider en cas de besoin.

Je remercie mes amis qui ont été à mes côtés de nombreuses années dont ces trois dernières années, qui m'ont supportée, qui m'ont forcée à arrêter de travailler et à socialiser tout au long de mon doctorat.

Enfin je remercie ma famille qui m'a soutenue, qui a toujours été là et qui m'a forcée aussi à prendre des vacances.

Table des matières

Table des figures et tableaux

Abréviations

ABC	ATP-Binding Cassette
ADN	Acide DésoxyriboNucléique
AP	Site Abasique
ARN	Acide RiboNucléique
ARS	Agences Régionales de Santé
ATP	Adénosine TriPhosphate
ATUn	Autorisation Temporaires d'Utilisation nominative
BER	Base Excision Repar
BLSE	β-Lactamases à Spectre Etendu
BMR	Bactéries Multi Résistantes
CMI	Concentration Minimum D'inhibition
DO	Déclaration Obligatoire
ECDC	European Centre for Disease Prevention
EFSA	European Food Safety Authority
EMA	European Medicines Agency
EPS	ExoPolySaccharides
ESKAPE	*Enterococcus faecium*, *Staphylococcus aureus*, *Klebsiella pneumoniae*, *Acinetobacter baumanni*, *Pseudomonas aeruginosa* et *Enterobacter spp*.
FDA	Food and Drug Administration
GLASS	Global Antimicrobial Resistance Surveillance System
LPS	LipoPolySaccharides
MATE	Multidrug And Toxic compound Extrusion
Mfd	Mutation Frequency Decline
MFS	Major Facilitator Superfamily
NER	Nucleotide Excision Repair
NO	Oxyde Nitrique
OMS	Organisation Mondiale de la Santé
ONERBA	Observatoire Nationale de l'Epidémiologie de la Résistance Bactérienne aux Antibiotiques
PLGA	Poly(D-L lactide-co-glycolide)
PLP	Protéines de Liaison des Pénicillines
PME	Petites et Moyennes Entreprises
RID	RNAP Interaction Domain
RND	Resistance-Nodulation-cell Division
SMR	Small Multidrug Resistance
TIAC	Toxi-Infections Alimentaires Collectives
TRCF	Transcription Repair Coupling Factor
TRG	Translocation in RecG
UV	Ultra Violet

INTRODUCTION

Projet de thèse :

Lors de ma thèse je me suis focalisée sur l'étude de Mfd (Mutation Frequency Decline), une protéine bactérienne fortement conservée et impliquée dans de nombreux processus tels que la réparation de l'ADN, la mutagénèse ou encore la virulence.

Dans un premier axe, j'ai cherché à comprendre l'implication de Mfd dans la virulence de *Bacillus cereus*. *B. cereus* est un pathogène opportuniste surtout reconnu dans les toxi-infections alimentaires collectives, mais il est aussi capable de causer des infections sévères non gastro-intestinales notamment chez les nouveau-nés ou encore les personnes immunodéprimées. De nombreux facteurs de virulence ont déjà été décrits chez *B. cereus*, dont la pathogénie est clairement multifactorielle. Parmi ces facteurs, Mfd est impliquée dans la capacité de *B. ce*reus à résister au système immunitaire de l'hôte. Pourtant, le gène *mfd* est présent chez toutes les souches de *B. cereus*, quelle que soit la pathogénie des souches. En outre, la séquence protéique de Mfd étant fortement conservée, on la retrouve dans toutes ces souches avec très peu de différences sur sa séquence. Mon but était donc d'étudier si les quelques différences sur la séquence de Mfd pourraient être à l'origine d'une modification de sa conformation et/ou de son activité engendrant ainsi des différences dans la virulence des souches. J'ai ainsi utilisé une collection de souches comportant des souches environnementales et des souches isolées de patients, et j'ai caractérisé les relations structure/fonction de leur Mfd.

Mon second axe d'étude a été d'utiliser Mfd en tant que nouvelle cible bactérienne pour le développement de nouveaux antibiotiques. En effet, il existe actuellement une crise majeure dans le traitement d'infections due à la présence d'une forte résistance de certaines bactéries aux traitements antibiotiques. Cette antibiorésistance concerne de nombreuses bactéries ce qui peut rendre, dans certaines situations, les traitements actuels complètement inefficaces. Il y a un besoin urgent de nouvelles molécules agissant sur de nouvelles cibles pour lesquelles les bactéries n'ont pas encore mis en place de mécanismes de résistance. Au sein de notre équipe, nous proposons Mfd comme nouvelle cible pour le développement d'antimicrobiens innovants. En effet, Mfd est présente et conservée chez les bactéries et absente chez les eucaryotes. Par ailleurs son rôle a été démontré dans la virulence bactérienne par sa capacité à réparer les dommages sur l'ADN engendrés par la réponse immunitaire de l'hôte infecté. Pour finir, des études récentes ont mis en évidence un rôle de Mfd dans la capacité des bactéries à promouvoir l'antibiorésistance. Ainsi, l'inhibition de l'activité de Mfd par des nouvelles molécules inhibitrices permettrait (1) une diminution de la réparation des dommages ADN causés par la réponse immunitaire, (2) une diminution de la mutagénèse et par conséquent une diminution de la fréquence d'apparition de résistances, (3) une diminution de la virulence de certaines souches. Mfd est nécessaire à la survie bactérienne uniquement en condition de stress. Par conséquent, son

inhibition ne devrait pas être bactéricide en dehors de la zone d'inflammation, ce qui devrait limiter la pression sur les bactéries et donc limiter l'apparition de résistances. En outre, ces nouvelles molécules ne devraient pas impacter les bactéries bénéfiques du microbiote en dehors de la zone d'inflammation. Dans cette optique, j'ai étudié l'efficacité d'inhibiteurs de Mfd sur des souches faisant partie du groupe ESKAPE, un groupe de bactéries jouant un rôle majeur dans l'antibiorésistance, en utilisant et développant différents modèles *in vitro* et *in vivo*.

Chapitre 1 : Présentation de la protéine Mfd

1. Réparation de l'ADN

Les bactéries rencontrent des facteurs endogènes (espèces réactives de l'oxygène et du nitrogène) et exogènes (produits chimiques, irradiation, stress oxydatif ou nitrogène induit lors de la réponse immunitaire) qui peuvent induire des dommages sur leur ADN. Les systèmes de réparation de ces dommages sont donc primordiaux pour la survie de la bactérie. Selon les types de dommages induits, les bactéries ont mis en place différentes voies de réparation de l'ADN. Parmi ces voies de réparation, on retrouve majoritairement :

- La réparation par excision de base (BER pour « Base Excision Repair »)
- La réparation par excision de nucléotides (NER pour « Nucleotide Excision Repair »)
- La recombinaison homologue
- La jonction d'extrémités non homologues

1.1. Réparation par excision de base

Il s'agit de la voie de réparation la plus communément utilisée dans la réparation de dommages causés sur une seule base. La réparation par excision de base est démarrée par une ADN glycosylase qui reconnait la lésion et clive la liaison osidique, permettant le retrait de la base endommagée et la formation d'un site abasique (sites AP). Ce site dénué de base à ses extrémités 5' et 3' est pris en charge par des AP endonucléases et AP lyases. Par l'action d'une polymérase et d'une ligase, la base manquante est rajoutée et les extrémités sont jointes (Dalhus et al. 2009).

1.2. Réparation par excision de nucléotides

Cette voie est conservée chez les procaryotes et les eucaryotes et nécessite les endonucléases formant le complexe UvrABC. La réparation par excision de nucléotides est induite en réponse à différents stress tels que les UV, le stress nitrogène ou encore la réponse SOS. Les dommages sur l'ADN sont reconnus par UvrA et UvrB. La dissociation de UvrA permet le recrutement de UvrC et le complexe UvrBC va cliver les liaisons phosphodiester autour de la lésion afin de retirer entre 10 et 15 nucléotides. Le retrait de ces nucléotides est facilité par une hélicase (UvrD). La réparation, comme pour la voie par excision de base, va se finir par l'action d'une polymérase et d'une ligase (Figure 1) (Ha and Edwards 2021). Il a aussi été montré que la protéine Mfd est impliquée dans cette voie de réparation en facilitant le recrutement du complexe UvrAB, cette implication de Mfd sera développée dans une partie prochaine.

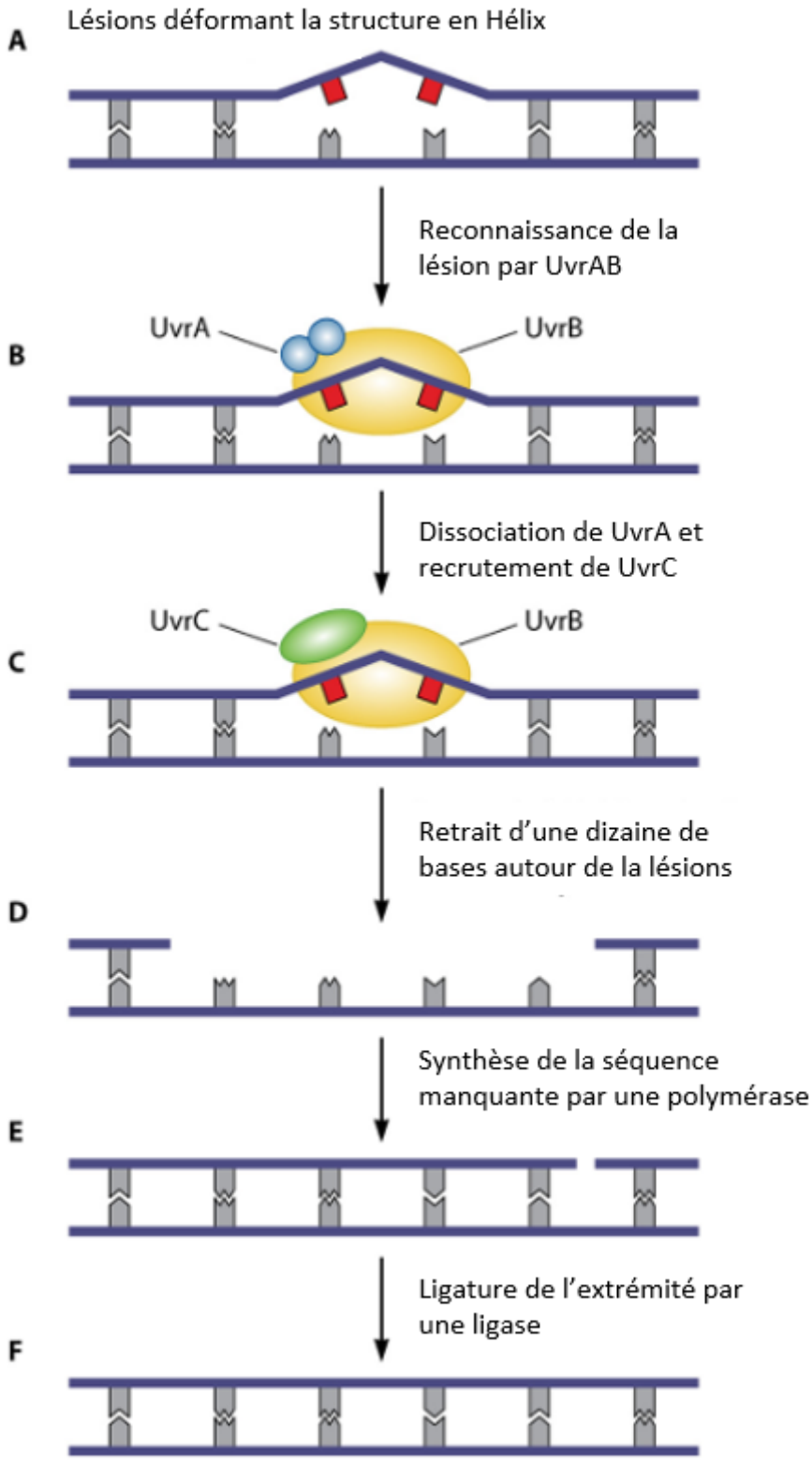

Figure 1 : Modèle de la réparation par excision de nucléotides.
La lésion est reconnue par le complexe UvrAB, le recrutement de UvrC va entrainer le retrait d'une dizaine de bases autour de la lésion. Une polymérase va revenir synthétiser la séquence manquante et une ligase va lier l'extrémité 5' avec le reste du brin (Ha and Edwards 2021).

1.3. Recombinaison homologue

La recombinaison homologue est la voie la plus communément utilisée dans la réparation de cassures doubles brins. Cette voie de réparation est très conservée et nécessite la présence d'une seconde copie de la séquence à réparer qui servira de modèle. La recombinaison homologue commence par une reconnaissance de la cassure double brin et une dégradation de l'ADN par le complexe RecBCD (Dillingham and Kowalczykowski 2008). C'est sur l'ADN simple brin généré à l'issue de cette dégradation que vient se lier des protéines RecA, formant un filament. Ce filament de RecA utilise l'ADN simple brin comme guide pour trouver une séquence homologue. Une fois que cela est fait, l'extrémité 3' simple brin est utilisée comme amorce par une polymérase qui va se servir de la séquence homologue comme matrice pour la synthèse d'un nouveau brin. À l'issue de cette synthèse, l'ADN va former des jonctions Holliday qui sont reconnues par la protéine RecG, une hélicase, permettant la séparation des deux ADN doubles brins (Kuzminov 1999).

1.4. Jonction d'extrémités non homologues

Cette voie de réparation est aussi utilisée dans la réparation de cassures doubles brins en absence d'une seconde copie de la séquence d'ADN endommagée. Elle effectue une ligature des extrémités de la cassure par le recrutement des homodimères Ku et d'une ligase. Il est aussi possible que les extrémités de la cassures soient dégradées par RecBCD puis reliées par une ligase (Chayot et al. 2010).

2. Rôle de Mfd dans la réparation de l'ADN

Mfd « Mutation Frequency Decline », aussi appelée TRCF « Transcription Repair Coupling Factor », est une protéine impliquée dans la réparation de l'ADN chez les bactéries suivant la voie de réparation par excision de nucléotides et qui est fortement conservée.

Plusieurs fonctions de Mfd ont été décrites via son interaction avec l'ARN polymérase lors de la transcription. En effet, différents problèmes peuvent émerger durant ce processus. L'ARN polymérase est notamment capable de faire machine arrière au lieu de continuer à avancer et Mfd a été montrée comme étant capable de sauver la transcription du gène en forçant l'ARN polymérase à continuer à aller de l'avant. Sur les transcrits, l'extrémité 3' n'est alors pas placée correctement et Mfd forcerait l'ARN messager à reprendre sa place et ainsi permettre la continuation de l'élongation (Park, Marr, and Roberts 2002).

L'implication de Mfd dans la réparation de l'ADN par excision de nucléotides lors de la transcription a déjà été décrite (Figure 2) (Selby and Sancar 1993; Selby 2017). Dans sa conformation inactive, Mfd est capable de reconnaitre l'ARN polymérase qui est bloquée au niveau d'une lésion sur l'ADN. Son interaction avec l'ARN polymérase induit un changement de conformation qui lui permet de passer en

configuration active. Dans cette conformation, Mfd présente une activité ATPase plus importante, une meilleure affinité avec l'ADN et une activité de translocase. Suite à l'interaction entre Mfd et l'ARN polymérase, cette dernière (toujours liée à l'ARN) se dissocie de l'ADN. La protéine Mfd va alors favoriser le recrutement d'UvrA et UvrB au site de la lésion où un complexe entre Mfd, ARN polymérase, UvrA et UvrB se forme. Uniquement UvrB va rester sur le site du dommage et permettre le recrutement d'UvrC qui effectuera deux incisions sur la séquence ADN (Moolenaar et al. 2000). La réparation va ensuite continuer via l'hélicase UvrD, l'ADN polymérase I et une ligase (Caron, Kushner, and Grossman 1985).

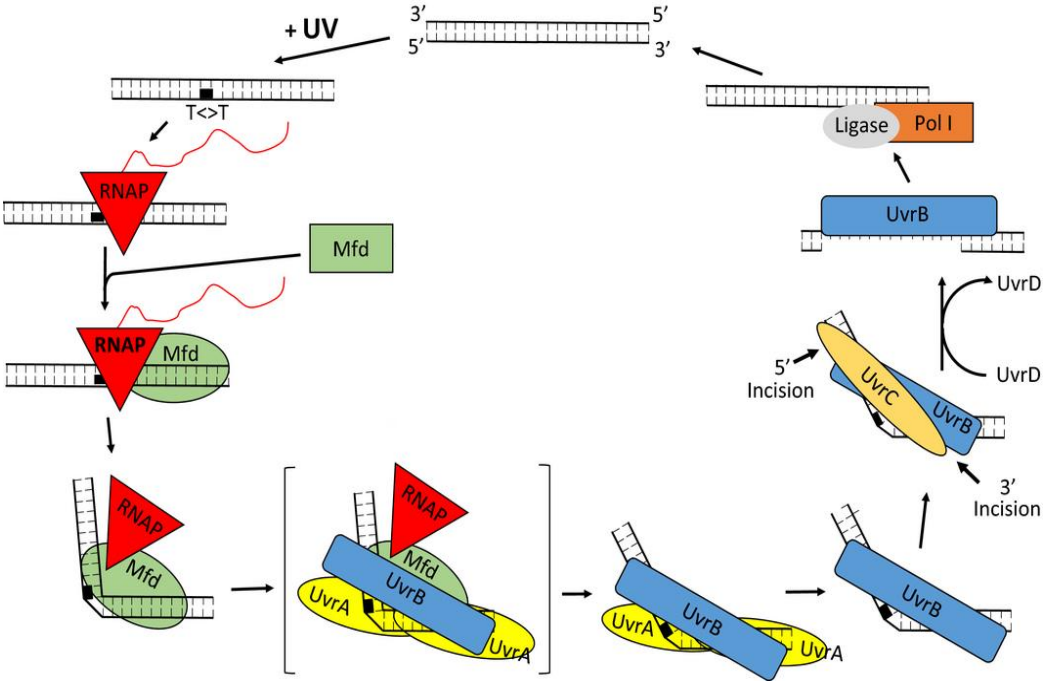

Figure 2 : Schéma de la réparation de l'ADN impliquant Mfd chez E. coli
Lors de la transcription de l'ADN, à la rencontre d'une lésion sur l'ADN l'ARN polymérase se bloque. Mfd se lie à l'ARN polymérase. Suite à cette interaction l'ARN va se détacher de l'ARN polymérase qui quant à elle reste au niveau de la lésion. Dans cette conformation Mfd va permettre le recrutement d'UvrA par son domaine d'homologie à UvrB. UvrB en s'associant avec UvrA va permettre la dissociation de Mfd et de l'ARN polymérase. Les protéines UvrA et UvrB vont par la suite permettre de commencer le processus de réparation de l'ADN (Selby 2017).

3. Structure de Mfd

Mfd est une large protéine multifonctionnelle de 130 kDa. Elle contient des motifs caractéristiques de la super famille II des hélicases. Elle est composée de huit domaines structuraux qui peuvent se diviser en 5 modules fonctionnels (Figure 3) :

- La région N-terminale de Mfd est divisée en trois domaines (1A, 1B et 2). Le domaine 2 (D2) se situe entre les domaines 1A (D1a) et 1B (D1b) et a une forte homologie de séquence avec une partie de la protéine UvrB impliquée dans la liaison UvrA/UvrB. Les trois domaines (1A, 1B et 2) suivent une conformation similaire à trois des quatre domaines de UvrB. Le domaine 1A possède partiellement un domaine ATPase dégénéré similaire à RecA que porte UvrB. Le

domaine 1B contient lui aussi des éléments structuraux de UvrB. Par contre, Mfd n'a pas d'homologie avec le 4eme domaine d'UvrB qui comprend la seconde partie du domaine ATPase similaire à RecA et donne à UvrB son activité hélicase. Bien que le domaine 1A possède des motifs d'un site ATPase, il lui manque des motifs structuraux majeurs pour la fixation de l'ATP et son hydrolyse (Assenmacher et al. 2006). C'est grâce à ces homologies que Mfd est capable de recruter la protéine UvrA, une protéine nécessaire à la réparation par excision de nucléotides. Les domaines 1A et 1B ont aussi été montrés comme étant capables de reconnaitre la présence d'un dommage sur l'ADN (Deaconescu et al. 2006).

- Le module d'interaction avec l'ARN polymérase est porté sur le domaine 4 (D4). C'est par ce domaine que la protéine Mfd est capable de se lier avec la sous-unité β de l'ARN polymérase arrêtée au site d'une lésion de l'ADN (Deaconescu et al. 2006).
- Le module de translocation se trouve au niveau des domaines 5 (D5) et 6 (D6). C'est sur ce module que l'on retrouve des motifs caractéristiques de la super famille II des hélicases. Cette région hélicase a une forte similarité à celle de la protéine RecG. Néanmoins, Mfd n'est pas capable de produire une activité hélicase, elle ne peut pas séparer les deux brins de l'ADN mais elle présente une activité translocase ATP-dépendante. C'est une caractéristique que Mfd partage avec RecG (Deaconescu et al. 2006). À droite des motifs hélicases se trouve un motif TRG (Translocation in RecG) qui est aussi impliqué dans l'activité translocase de Mfd. Des mutations sur le motif TRG entrainent la non-dissociation de l'ARN polymérase sur l'ADN (Chambers, Smith, and Savery 2003). Le motif TRG est aussi impliqué dans la transduction de l'énergie de l'hydrolyse de l'ATP (Deaconescu, Savery, and Darst 2007).
- À l'extrémité C-terminale de Mfd se trouve le domaine 7 (D7). Il s'agit d'un élément régulateur qui inhibe l'activité de Mfd. En conformation inactive, D7 recouvre le domaine D2 bloquant l'interaction entre Mfd et UvrA. C'est seulement lorsque Mfd s'associe à une ARN polymérase que sa conformation change et que le domaine 7 ne bloque plus l'accès au domaine 2 (Deaconescu, Savery, and Darst 2007). La délétion du domaine 7 de Mfd a été montrée comme rendant la protéine constitutionnellement active. L'activité ATPase devient cinq fois plus importante lorsque le domaine 7 est tronqué par rapport à la protéine entière (Smith, Szczelkun, and Savery 2007).
- Le seul domaine qui ne semble pas avoir de fonction particulière est le domaine 3 (D3). Il semble être flexible et peu conservé d'espèce en espèce avec de nombreuses délétions et insertions de séquences. Chez certaines bactéries comme *T. maritima* il est même totalement absent (Deaconescu et al. 2006).

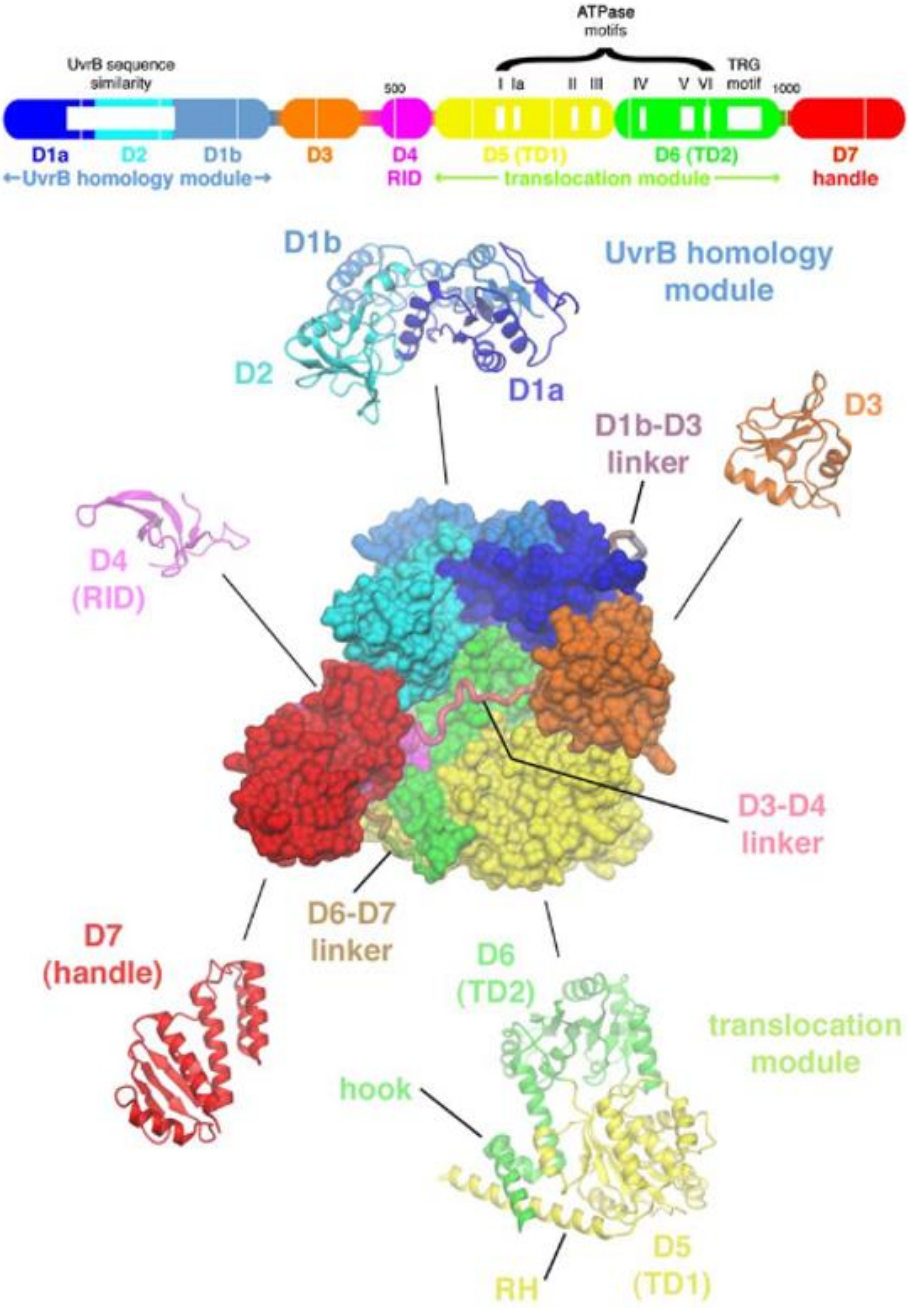

Figure 3 : Domaines structuraux et fonctionnels de la protéine Mfd
La protéine Mfd est composée de 1148 acides aminés, de 8 domaines structuraux D1, D2, D3, D4, D5, D6 et D7 et 5 modules fonctionnels comprenant une région d'homologie avec la protéine UvrB, un domaine d'interaction avec l'ARN polymérase, un module de translocation qui contient des motifs pour une activité hélicase et le domaine qui permet de modifier la conformation de Mfd et ainsi régule l'activité de Mfd. (Deaconescu et al. 2006)

La partie C-terminale de la protéine (du domaine 4 au domaine 7) à une activité ATPase et moteur plus importante que la protéine entière. L'activité ATPase est multipliée par vingt-deux avec une protéine tronquée de Mfd n'ayant que l'extrémité C-terminale. De plus, l'ARN polymérase est dissociée de l'ADN plus rapidement (<10 secondes) avec seulement la partie C-terminale de Mfd qu'avec la protéine entière (~80 secondes). Les parties N-terminale et C-terminale semblent être indépendantes au niveau de leurs fonctions. Leurs interactions sont néanmoins nécessaires pour la réparation de l'ADN, la

stabilité de la protéine et il s'agit aussi d'un moyen pour limiter l'activité de Mfd (Murphy et al. 2009). L'interaction entre les parties N-terminale et C-terminale est un interrupteur qui permet de réguler les fonctions de Mfd durant la réparation de l'ADN lors de la transcription.

4. Mfd comme facteur de transcription

Peu après la découverte de l'implication de Mfd dans la réparation de l'ADN, il était apparent que cette protéine pouvait être impliquée dans d'autres processus tels que la répression de la transcription. Mfd a été montrée comme étant impliquée dans la répression catabolique puisque la mutation de *mfd* chez *B. subtilis* entraine une diminution de l'inhibition de l'opéron *hut.* Cet opéron est impliqué dans la régulation de l'utilisation de l'histidine. En présence de glucose, lorsque la répression catabolique est induite, l'expression de l'opéron est treize fois moins importante qu'en condition où la répression catabolique n'est pas induite. Chez le mutant, cette répression n'est que quatre fois moins importante (Zalieckas et al. 1998). Également chez *B. subtilis*, la délétion de *mfd* entraine une diminution de la répression du régulateur CodY (Belitsky and Sonenshein 2011).

Grâce à sa capacité à sauver des complexes ARN polymérase bloqués dû au manque de nucléotides et non à un dommage, Mfd est considérée comme un facteur de transcription général (Park, Marr, and Roberts 2002). Il a récemment été décrit que la protéine Mfd seule était capable de se déplacer sur l'ADN à une vitesse de 7bp/s sur une longueur de 200 paires de bases. Mfd, après avoir localisé et débloqué un complexe d'élongation, peut continuer à avancer derrière celui-ci à une vitesse plus faible. Dans ce cas elle ne peut rattraper le complexe d'élongation que s'il se retrouve de nouveau bloqué avant la dissociation de Mfd de l'ADN. Si le complexe d'élongation s'arrête fréquemment et ne peut pas s'échapper, Mfd peut ainsi aider la transcription. Dans le cas où il y a une faible concentration de nucléotides libres et l'ARN polymérase fait de nombreuses pauses, Mfd est aussi capable de favoriser la terminaison de la transcription. Lorsque la concentration de nucléotides remonte, Mfd va alors avoir plutôt un rôle d'appui dans la transcription où elle va simplement faire diminuer les temps de pause de l'ARN polymérase. Enfin dans le cas où les nucléotides sont en abondance, Mfd n'aura pas d'impact sur le taux de transcription puisque l'ARN polymérase fait rarement des pauses. La limitation sur la distance sur laquelle Mfd est capable de se déplacer seule sur l'ADN est intéressante. Puisque Mfd ne peut se déplacer que sur 200 paires de bases, cela diminue les chances de rentrer en contact et gêner d'autres processus se déroulant sur l'ADN. La dispersion rapide de Mfd permet aussi de garder une quantité suffisante de Mfd libre qui va pouvoir s'associer avec des ARN polymérases (Le et al. 2018). Ceci est particulièrement important lorsque l'on note qu'il y a environ 20 % de Mfd qui sont retrouvées sur l'ADN, libres, en non interaction avec l'ARN polymérase malgré un nombre de copies très inférieur (dizaines de copies pour des milliers d'ARN polymérase) (Ho, van Oijen, and Ghodke 2018). Il est

intéressant de noter que Mfd ne va interagir qu'avec les complexes d'élongation et non avec ceux d'initiation. Cela s'explique par la présence du facteur sigma qui durant l'initiation de la transcription va induire une gêne stérique empêchant l'interaction de l'ARN polymérase et de l'ADN avec Mfd (Park, Marr, and Roberts 2002). Lors de la transcription, il est aussi possible que l'ARN polymérase rencontre sur son passage une protéine liée sur l'ADN. Sans Mfd, l'ARN polymérase attendrait que la protéine se détache par elle-même de l'ADN avant de pouvoir continuer l'élongation, tandis qu'en présence de Mfd, grâce à son activité de translocation, l'ARN polymérase va pouvoir être déplacée (Roberts and Park 2004)

Il a aussi été montré récemment qu'en effectuant une immunoprécipitation de la chromatine suivie d'un séquençage à haut débit sur des bactéries en phase exponentielle de croissance de *B. subtilis*, on observe que Mfd est associée à environ cinq cents gènes. De nombreux sites d'association de Mfd avec l'ADN et l'ARN polymérase sont retrouvés au niveau de régions complexes à transcrire tels que des ARN non codants, des ARN anti sens, des « riboswitch » ou encore des sites de pauses de la transcription (Ragheb et al. 2021). L'étude de *B. subtilis* en phase stationnaire montre qu'en condition de stress disulfure (qui est un type de stress oxydatif), la délétion de *mfd* entraine une diminution ou une augmentation d'expression d'un certain nombre de gènes contrôlant de nombreux processus cellulaires tels la mobilité du flagelle, la protéolyse, le métabolisme des antibiotiques et de l'acide carboxylique, le transport de sodium ou encore la biosynthèse de glutamine, d'isoprenoïde, d'iosine monophosphate et de surfactine (Martin et al. 2021).

5. Mfd comme facteur d'évolvabilité

La première description de Mfd a montré son implication dans la suppression de mutations chez *E. coli* suite à une irradiation aux UV (Filippov and Zagoruiko 1978 ; Witkin 1994). Dans cette première étude, la perte de Mfd entraine une augmentation de la fréquence d'apparition de mutations. Ce phénotype n'est pas visible sur les souches mutantes pour *uvr,* ce qui laisse penser que sa fonction dépend d'Uvr. Une souche contenant une délétion de *mfd* présente un taux de mutations cinq fois plus important suite à une irradiation aux UV qu'une souche sauvage (Selby and Sancar 1994). La diminution de mutations est attribuée à son rôle dans la réparation par excision de nucléotides.

Des études plus récentes ont montré que Mfd a un rôle pro-mutagène durant la phase exponentielle et stationnaire de croissance des bactéries en condition de stress chez *B. subtilis* (Ragheb et al. 2019; Million-Weaver et al. 2015; Paul et al. 2013; Gomez-Marroquin et al. 2016; Martin et al. 2011; Ross et al. 2006; Pybus et al. 2010).

L'implication de Mfd en phase exponentielle de croissance augmente l'évolvabilité de *B. subtilis* avec le développement de résistances aux antibiotiques. Ce phénomène a pu être observé sur des bactéries

à coloration Gram positive et à coloration Gram négative et concerne des antibiotiques ayant différents mécanismes d'action (Ragheb et al. 2019; Han et al. 2008; Lee et al. 2009). Ragheb *et al* a montré, en mesurant l'apparition de résistance à la rifampicine, que des souches ayant une délétion de *mfd,* ont un taux de mutation de 2 à 5 fois moins important que leurs souches sauvages (Figure 4). Même en condition d'infection sur des cellules CaCo-2, la fréquence de mutation de *S. typhimurium Δmfd* est cinq fois moins importante que chez la souche sauvage. L'effet de Mfd sur la mutagénèse est donc conservé en condition de croissance et de réplication chez l'hôte. Dans cette même étude, Mfd a été montrée comment accélérant l'apparition de résistances à différents antibiotiques tels que la rifampicine, la phosphomycine, la triméthoprime, la kanamycine et la vancomycine. L'apparition des résistances est de 6 à 21 fois plus rapide chez la souche sauvage que chez le mutant de *S. typhimurium*. De plus, les auteurs ont aussi montré que cette acquisition de résistance semblerait être dépendante de l'interaction de Mfd avec la sous unité β de l'ARN polymérase et de UvrA (Ragheb et al. 2019).

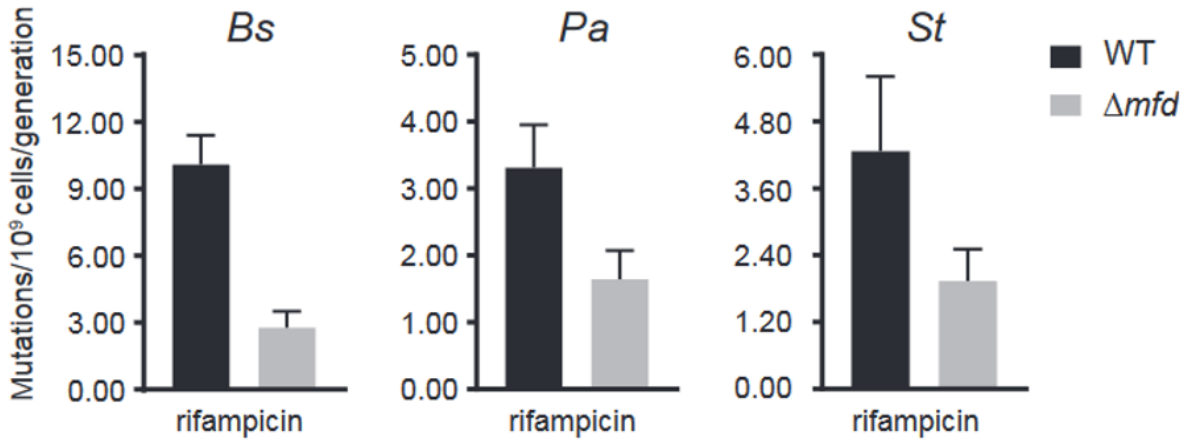

Figure 4 : Mfd promeut la mutagénèse dans diverses espèces bactériennes (Bs : Bacillus subtillis, Pa : Pseudomonas aeruginosa, St : Salmonella typhimurium) (Ragheb et al. 2019)

Une étude sur *C. jejuni* a montré que la délétion de *mfd* entraine un taux de mutations spontanées induisant une résistance à la ciprofloxacine cent fois moins important que chez la souche sauvage. La surexpression de *mfd* quant à elle provoque une augmentation de la fréquence de mutations (Han et al. 2008). Chez *H. pylori,* une autre étude a révélé que le gène *mfd* est nécessaire pour la réparation de l'ADN, la recombinaison de l'ADN mais aussi dans la résistance aux antibiotiques. Les doses minimales inhibitrices pour différents antibiotiques ont été mesurées sur un mutant *mfd* et sur une souche sauvage. Le mutant s'est montré plus sensible à un certain nombre d'antibiotiques comme la ciprofloxacine et le métronidazole où il est quatre fois plus sensible que la souche sauvage. Le mutant est aussi plus sensible à la mitomycine C, ce qui révèle que Mfd est impliquée dans la réparation de cassures double-brins de l'ADN (Lee et al. 2009). Dû à son implication dans le développement de résistance, Mfd devient une cible dans le développement de composés anti évolvabilité. Mfd est considérée comme une cible particulièrement intéressante puisqu'en absence de stress, la délétion de

Mfd n'entraine pas de changement évolutif. Par son faible impact en absence de stress, l'utilisation d'inhibiteurs contre Mfd devrait théoriquement limiter l'apparition de résistances.
Malgré toutes ces études, les mécanismes précis derrière la mutagénèse associée à Mfd restent beaucoup moins bien compris que son implication dans la réparation de l'ADN.

6. Rôle dans la virulence

L'équipe de la Dr Nalini Rama Rao a mis en évidence un rôle de Mfd dans la virulence de *B. cereus* et *S. flexneri*. L'effet de la délétion de *mfd* a tout d'abord été testé chez *B. cereus* dans un modèle d'infection d'insectes (*B. mori*). L'absence de Mfd provoque une diminution drastique de la virulence de *B. cereus* (Figure 5A). Les souches ont également été testées sur des cellules de types monocytes et seulement la souche sauvage s'est montrée capable de survivre (Figure 5B). Les défenses immunitaires communes entre l'insecte et les cellules se concentrent sur la sécrétion d'espèces réactives de l'oxygène ou du nitrogène. Alors que l'absence d'espèces réactives de l'oxygène n'entraine pas de changement de phénotype de la souche mutante, l'inhibition de la réponse nitrogène provoque une survie du mutant dans les cellules. Ce résultat a aussi été obtenu dans un modèle *in vitro* de stress nitrogène. En présence de ce stress, la survie du mutant diminue tandis que celle de la souche sauvage est inchangée (Figure 5C). L'implication de Mfd dans la virulence de *B. cereus* face à un stress nitrogène a été confirmée chez la souris. Le mutant n'est pas virulent sur des souris sauvages mais le devient lorsqu'il infecte des souris déficientes dans la production d'espèces réactives du nitrogène (Figure 5D). Il est connu que la réponse nitrogène entraine des dommages sur l'ADN. Pour savoir si Mfd est impliquée dans la réparation de ces dommages, les souches sauvages et mutantes de *B. cereus* ont subi un stress nitrogène et l'état de leur ADN a été observé via une migration sur gel en pulse field (Figure 5E). On peut voir qu'il y a une dégradation de l'ADN chez la souche mutante exposée à un stress nitrogène qui n'est pas présente chez la souche sauvage (Guillemet et al. 2016). Il semblerait donc que l'un des rôles de Mfd dans la virulence soit son implication dans la réparation de dommages causés par la réponse nitrogène de l'hôte. Mfd donnerait à la bactérie une résistance face à la réponse immunitaire.

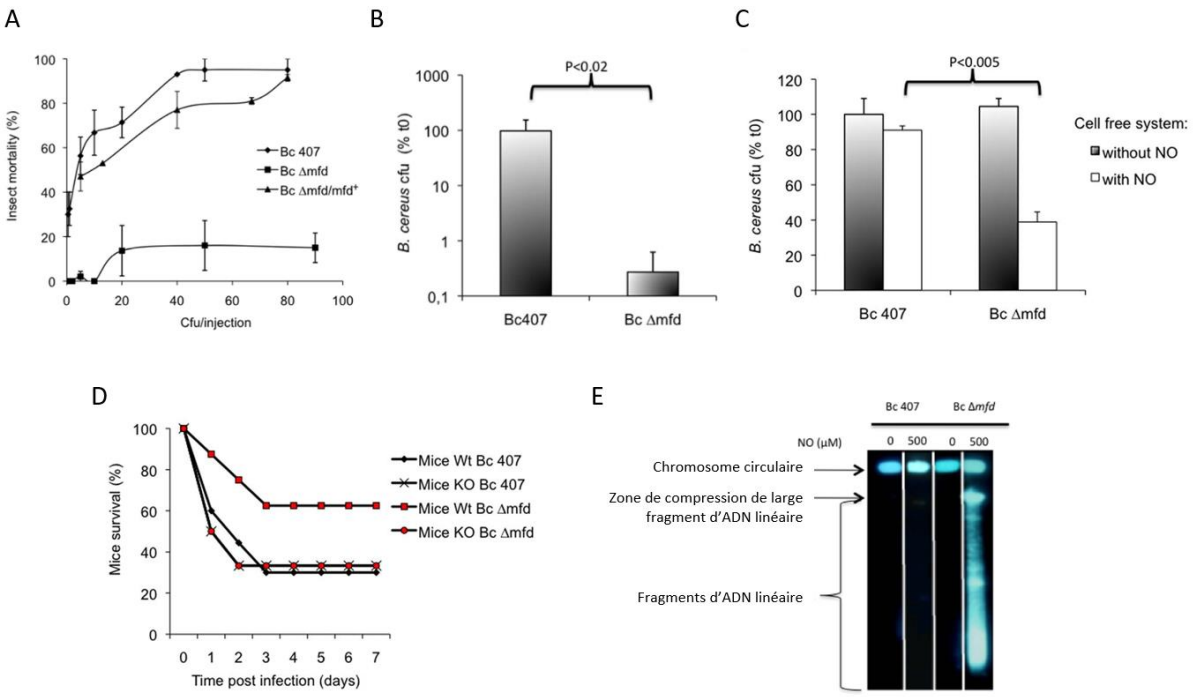

Figure 5 : Effet de Mfd chez B. cereus sur sa virulence dans un modèle insecte (A), sur sa survie intracellulaire (B), sur sa survie en présence d'un stress nitrique in vitro (C), sur sa virulence dans un modèle murin sur des souris sauvages ou déficientes dans la production d'espèces réactives du nitrogène (D) et sur l'intégrité de son ADN en réponse à un stress nitrogène (E) (Guillemet et al. 2016).

D'autres inducteurs de stress bactérien provoquant une mutagénèse ont été testés tels que la mitomycine C ou encore les UV sans montrer de différence de survie entre la souche sauvage et le mutant *mfd* chez *B. cereus.* Mfd n'a pas non plus été montrée comme étant impliquée dans la résistance au peptide antimicrobien cecropin A (Darrigo et al. 2016) ou à la réponse au stress oxydatif (Schalow, Courcelle, and Courcelle 2012). L'infection de macrophages isolés de la moelle osseuse de souris sauvages ou déficientes dans la production d'espèces réactives du nitrogène montre que la survie du mutant n'est possible que dans les macrophages provenant des souris déficientes pour la réponse nitrogène. RecBC (AddAB chez *B. cereus*) est également impliqué dans la résistance au stress nitrogène contrairement à UvrA. En effet, un mutant pour *addAB* chez *B. cereus* est plus sensible à un stress nitrogène qu'un mutant pour *uvrA* qui a le même niveau de survie qu'une souche sauvage. Un double mutant *uvrA* et *mfd* montre un même niveau de survie qu'un mutant simple *mfd* et le double mutant *addAB* et *mfd* n'est pas plus sensible au stress nitrogène que les mutants simples. Par conséquent, les rôles de Mfd dans la résistance au stress nitrogène généré par l'hôte lors d'une infection par *B. cereus* semblent être liés aux voies de réparation des cassures doubles brins impliquant RecBC plutôt que dans la voie de réparation de l'ADN par excision de nucléotides dans laquelle le rôle de Mfd a déjà été décrit (Figure 6).

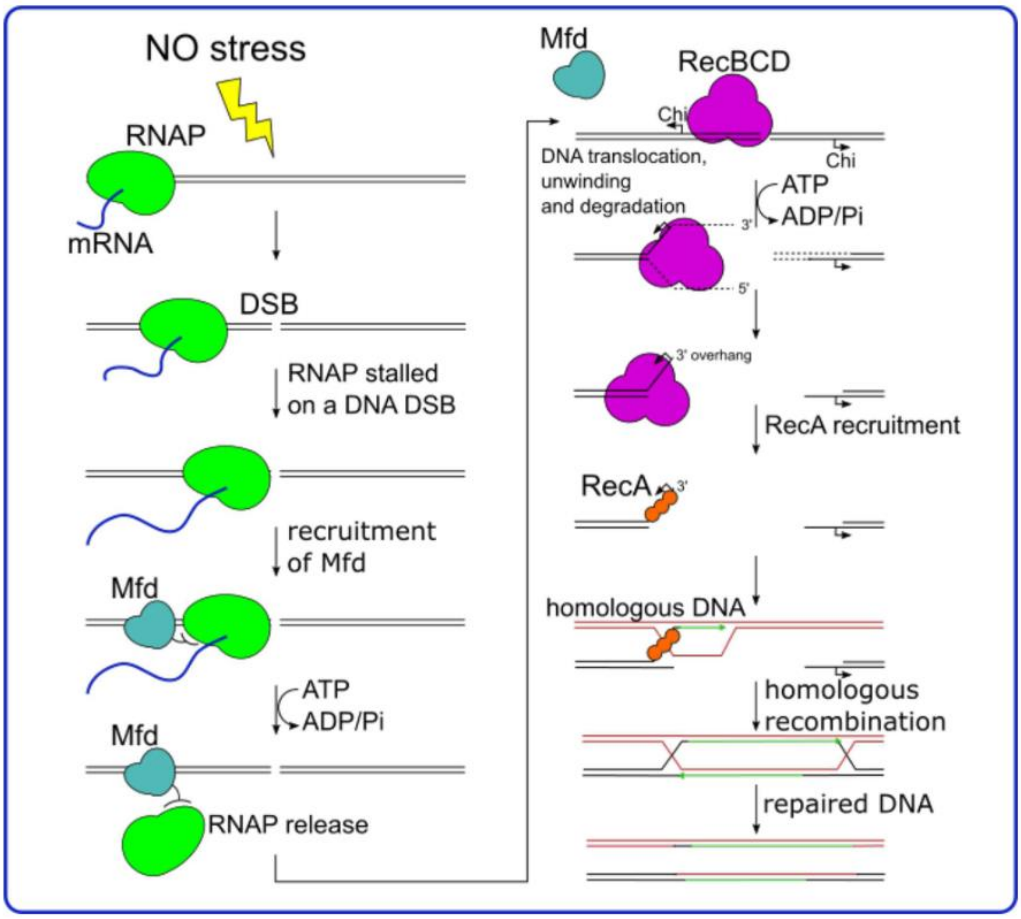

Figure 6 : Rôle de Mfd en réponse à un stress nitrogène (Darrigo et al. 2016)

Mon projet de thèse se concentre sur la protéine Mfd. D'un côté je me suis intéressée à son implication dans la virulence de *B. cereus* pour mieux comprendre le rôle de Mfd dans la virulence de cette bactérie. Et d'autre part, mes recherches ont porté sur l'utilisation de Mfd comme cible thérapeutique dans le développement de nouveaux composés antimicrobiens.

Chapitre 2 : *Bacillus cereus*

1. Caractérisation du groupe

Bacillus cereus sensu lato (Embranchement : *Firmicutes*, Classe : *Bacilli*, Ordre : *Bacillales*, Famille : *Bacillaceae*) est un groupe de bactéries comprenant plus d'une vingtaine d'espèces dont huit sont principalement décrites (Figure 7) :

- *B. cereus sensu stricto* est considéré comme étant un pathogène opportuniste de l'Homme et des animaux. Depuis 2012, il s'agit du second agent pathogène responsable ou suspecté des toxi-infections alimentaires collectives en France (France 2021). *B. cereus sensu stricto* entraine des symptômes de type émétique ou diarrhéique et peut entraîner chez des patients immunodéprimés ou vulnérables des affections plus sévères voire mortelles (Bottone 2010; Drobniewski 1993).
- *B. mycoïdes* et *B. pseudomycoïdes* sont deux espèces non pathogènes associées au système racinaire des plantes (Bargabus et al. 2003; Yi et al. 2018).
- *B. weihenstephanensis* est une espèce psychrotolérante capable de se développer à de basses températures (entre 4 °C et 7 °C) (Lechner et al. 1998). Certaines souches peuvent induire des infections d'origines alimentaires grâce à leur capacité à produire une toxine émétique identique à celle produite par *Bacillus cereus sensu stricto* (Stenfors Arnesen et al. 2011; Guerin et al. 2017).
- *B. anthracis* est l'espèce responsable de la maladie du charbon, une zoonose infectant de nombreux hôtes tels que les mammifères y compris l'Homme (Mock and Fouet 2001).
- *B. thuringiensis* est un entomopathogène qui infecte un grand nombre d'insectes tels que les vers à soie. Son génome est quasiment identique à celui de *B. cereus sensu stricto*, sa différence porte sur sa capacité à former des inclusions parasporales (protéines Cry) qui sont toxiques pour certains invertébrés (Schnepf et al. 1998).
- *B. cytotoxicus* est caractérisé par un chromosome de petite taille par rapport aux autres espèces du groupe et possède le gène *cytK-1* codant pour une entérotoxine induisant des toxi-infections alimentaires collectives graves (Guinebretiere et al. 2013; Lapidus et al. 2008; Lopez et al. 2015).
- *B. toyonensis* est utilisé comme probiotique pour certains animaux (Jimenez et al. 2013).

La classification de *B. cereus* a récemment évolué grâce au séquençage et à l'analyse des séquences en effectuant la moyenne d'identité nucléotidique (ANI pour « average nucleotide identity). Avant 1998, il n'y avait que quatre espèces définies comme étant la source de différentes pathogénies ou présentant une morphologie de colonies différentes. Par la suite, deux différentes espèces de *B. cereus*

ont émergé grâce à des analyses moléculaires basées sur le séquençage des gènes 16S et 23S de l'ADN ribosomique. Puis, il a fallu attendre 2010 avant de voir deux nouvelles espèces être proposées et 2013 avant que deux autres soient validées et publiées, augmentant le nombre officiel d'espèces de *B. cereus* à huit. Depuis, le nombre d'espèces n'a cessé d'augmenter grâce au séquençage de génomes entiers. Etant donné que les méthodes d'identification des espèces du groupe ne sont pas standardisées, il est fort probable que sa taxonomie continue d'évoluer.

Le groupe *B. cereus* est ubiquitaire et peut être retrouvé dans le sol (qui est son réservoir primaire), les aliments, les insectes ou encore les mammifères (Ceuppens, Boon, and Uyttendaele 2013; Jensen et al. 2003; Stenfors Arnesen, Fagerlund, and Granum 2008; Guinebretiere et al. 2013). On retrouve *B. cereus* sous forme de spores ou de cellules végétatives. L'infection d'un hôte peut se faire via une contamination d'aliments ingérés, de l'air inhalé ou encore en pénétrant dans l'organisme via une plaie. Lors d'une infection, les bactéries vont entrer en germination et se multiplier à l'intérieur de l'hôte en le dégradant, ce qui peut entrainer sa mort. Les bactéries vont par la suite être disséminées dans l'environnement, via l'hémolymphe, le sang ou les selles de l'hôte, et sporuler (Jensen et al. 2003; Vilas-Boas, Peruca, and Arantes 2007). *B. cereus* requière un milieu riche pour germer et se multiplier. Dans l'environnement, sa prolifération est vraisemblablement restreinte à quelques niches où les nutriments sont concentrés tels que la rhizosphère (zone du sol autour des racines des plantes), les eaux usées ou encore le fumier (Jensen et al. 2003).

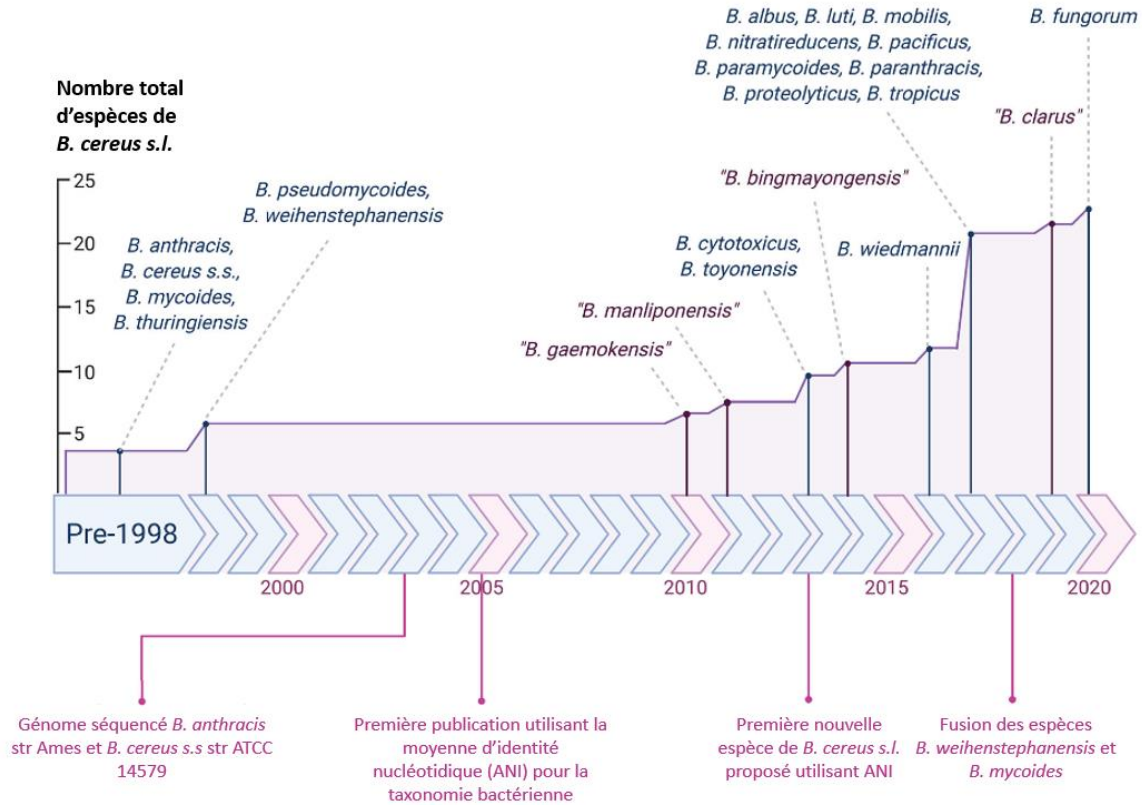

Figure 7 : Chronologie de la taxonomie de B. cereus jusqu'à 2020 (Carroll et al. 2022).

1.1. Bactérie

Les espèces du groupe *B. cereus* sont des bactéries à coloration Gram positive, anaérobies facultatives, qui peuvent être mobiles grâce à une ciliature péritriche ou immobiles (quelques espèces de *B. anthracis* et *B. mycoïdes* sont immobiles (Stenfors and Granum 2001)). Morphologiquement, ce sont des bacilles de 3 µm de long pour 1 µm de large (Figure 8). Elles sont constituées d'une membrane interne et d'un peptidoglycane épais ayant la fonction de maintenir la forme de la cellule. Génétiquement, leur génome fait entre 5,3 et 5,9 Mb et a un faible pourcentage de bases GC (~35 %). Ce groupe présente aussi des caractéristiques biochimiques telles que la résistance à la polymyxine, l'incapacité à métaboliser le mannitol ou encore le fait que la plupart des souches sont capables de synthétiser une lécithinase (phospholipase C).

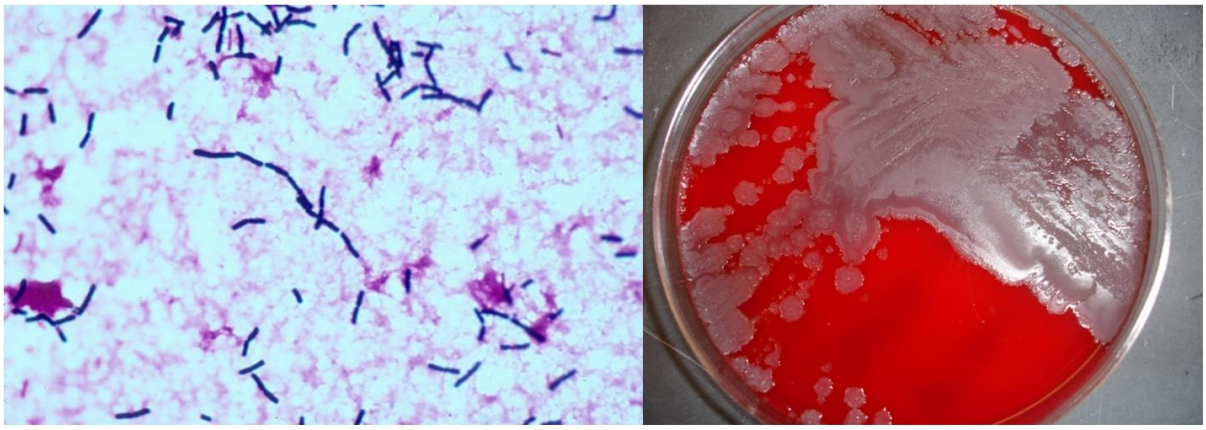

Figure 8 : Vue microscopique observée en coloration de Gram (à gauche) et colonies sur une gélose au sang (à droite) de B. cereus (Bottone 2010)

1.2. Spore

En parallèle de leur forme végétative qui est métaboliquement active, les membres du groupe *B. cereus* sont capables de former des endospores lors de conditions environnementales défavorables. Il s'agit d'une forme dormante, inactive, qui redevient une forme végétative via un processus de germination lorsque l'environnement est à nouveau favorable. Les spores sont constituées d'un noyau interne entouré d'une membrane interne, d'un cortex qui est entouré par la membrane externe et enfin d'une couche externe supplémentaire (Kutima and Foegeding 1987). La couche externe est composée de protéines et d'une petite quantité de lipides et de glucides. Ces derniers permettent à la spore de résister aux agents oxydants et aux produits chimiques en bloquant les molécules toxiques (Setlow 2006). Les spores sont aussi très résistantes à la dessiccation, aux radiations, à de nombreux agents stérilisants tels que la chaleur (résistant à une température supérieure à 80 °C pendant 10 minutes), aux métaux lourds ou encore aux antibiotiques. La spore représente donc un moyen de survie très efficace pour *B. cereus* et est aussi considérée comme un bon élément de dissémination.

1.3. Biofilms

Les biofilms sont des communautés bactériennes vivant sous une forme collective qui leur confère différents avantages face à leur environnement. Les bactéries présentes dans les biofilms forment une matrice composée d'exopolysaccharides (EPS), de protéines et d'ADN (Flemming and Wingender 2010). Ces écosystèmes microbiens sont ubiquitaires et caractérisés par leur tolérance aux biocides et leur persistance. La résistance des biofilms aux procédures de nettoyage–désinfection, largement documentée, est un problème crucial auquel se heurte l'industrie agroalimentaire (Solveig Langsrud 2003; Gopal et al. 2015). La formation de biofilm est un trait commun partagé entre les membres du groupes *B. cereus*. Le flagelle est un élément de la bactérie qui joue un rôle majeur en favorisant notamment l'adhésion des cellules, le passage des nutriments et l'expansion du biofilm (Ramarao and Lereclus 2006; Houry et al. 2010; Houry et al. 2012). Bien que les biofilms de *B. cereus* soient principalement composés de cellules végétatives, durant la maturation de celui-ci, des spores sont formées (Wijman et al. 2007; Faille et al. 2014). Le gène *spo0A*, impliqué dans la sporulation, a même été montré comme jouant un rôle dans la formation de biofilms chez *B. subtilis*. Cela a mis en évidence que la sporulation et la formation de biofilms sont liées (Hamon and Lazazzera 2001). Certains biofilms de *B. cereus* peuvent même atteindre un pourcentage de spores supérieur à 50 % (Faille et al. 2014). La formation de spores dans le biofilm peut s'expliquer par une forte densité cellulaire ainsi qu'un manque de nutriments (van Gestel, Nowak, and Tarnita 2012). La germination lente des spores pourrait contribuer à une augmentation de la résistance de *B. cereus* aux méthodes de nettoyage et de désinfection utilisées (Lindsay, Brozel, and Von Holy 2006). Ces spores au sein des biofilms peuvent alors devenir des contaminants dans des produits alimentaires.

2. Pathogénicité du groupe *B. cereus*

Parmi tous les membres du groupes *B. cereus*, quatre sont connus en tant que pathogènes : *B. thuringiensis*, *B. anthracis*, *B. cytotoxicus* et *B. cereus*.

2.1. *B. thuringiensis*

B. thuringiensis est un entomopathogène utilisé comme bioinsecticide. Cette espèce est utilisée pour contrôler les insectes nuisibles dans l'agriculture et dans la lutte contre les moustiques (Marrone 1994). Son pouvoir pathogène est notamment lié à la production de protéines Cry pour « crystal » (ce sont des inclusions cristallines aussi appelées δ-endotoxines). Il existe des centaines de gènes codant pour la protéine Cry, constituant de nombreuses familles qui sont référencées dans une base de données (http://www.lifesci.sussex.ac.uk/home/Neil_Crickmore/Bt/). Les protéines Cry ciblent un grand nombre d'insectes et d'espèces d'invertébrés (acariens, nématodes). Lors de l'ingestion, les inclusions

du cristal protéique de *B. thuringiensis* sont solubilisées par le pH alcalin de l'intestin des insectes. Cette solubilisation provoque la formation de protoxines qui après clivage via des protéases de l'hôte (telles que trypsine ou chymotrypsine) vont devenir des toxines actives. Les toxines Cry vont se fixer sur plusieurs récepteurs spécifiques de l'épithélium intestinal entrainant la formation de pores membranaires qui vont provoquer la lyse de la cellule (Barbara H. Knowles 1987; Schnepf et al. 1998; Bravo et al. 2011; Vachon, Laprade, and Schwartz 2012).

B. thuringiensis produit aussi deux autres protéines pouvant agir en parallèle des toxines Cry. Il s'agit des protéines Vip « Vegetative Insecticidal Proteins » et Cyt (toxines cytolitique). Les protéines Cyt sont décrites comme ayant un mode d'action similaire aux toxines Cry (Bravo, Gill, and Soberon 2007; Palma et al. 2014). Les toxines Vip quant à elles sont synthétisées durant la phase végétative de croissance de la bactérie. On compte trois familles : Vip1, Vip2 et Vip3. Ce sont des toxines binaires, les familles 1 et 2 sont actives contre les coléoptères tandis que la famille 3 est active contre les lépidoptères (Chakroun et al. 2016).

2.2. *B. anthracis*

B. anthracis est un pathogène de classe 3, c'est-à-dire un micro-organisme qui peut provoquer une maladie grave chez l'Homme et constituer un danger pour les personnes directement exposées à celui-ci. Il est l'agent responsable de la maladie du charbon, une zoonose affectant les mammifères qui est transmissible à l'Homme et potentiellement mortelle.

Il existe trois types de pathologies : intestinales, cutanées et pulmonaires (Dixon et al. 1999). Les infections de type intestinal et cutané restent généralement localisées. Elles se traduisent par un œdème et une nécrose de la peau. En absence de traitement, la létalité associée à ces formes se porte entre 25 et 60 % pour la forme intestinale et à 20 % pour la forme cutanée. Avec traitement, elle devient inférieure à 1 % (Santé publique France). La pathologie pulmonaire est la plus sévère des trois formes et peut entrainer une défaillance multi-organes. Les spores de *B. anthracis* rejoignent les ganglions lymphatiques par l'intermédiaire des macrophages où elles vont germer (Guidi-Rontani et al. 1999; Sanz et al. 2008). La létalité de cette forme varie entre 80 et 100 % et entraine le décès des patient en trois jours (Santé publique France). Le traitement de *B. anthracis* repose sur une utilisation d'antibiotiques le plus précocement possible.

Les facteurs de virulence majeurs sont encodés sur deux plasmides : pXO1 (182kb) et pXO2 (96kb) (Hu et al. 2009; Pilo and Frey 2011). Le plasmide pXO1 contient deux gènes codant pour deux toxines binaires : une métalloprotéase à zinc « Lethal Factor – LF » et une adénylate cyclase calmoduline-dépendante « Oeadema Factor –EF ». Lorsque ces deux protéines sont couplées à l'antigène protecteur PA (lui aussi synthétisé par le plasmide pXO1), elles forment la toxine létale LF-PA et la toxine oedéamateuse EF-PA. La partie PA permet l'adhésion des toxines aux récepteurs des cellules

hôtes, entrainant l'internalisation des toxines et la lyse des cellules (Moayeri et al. 2003). Le plasmide pXO2 porte quant à lui l'opéron *capBCADE* qui permet la synthèse des enzymes formant la capsule d'acide γ-poly-D-glutamique (PGDA). Cette capsule est essentielle puisqu'elle confère à la bactérie la capacité d'échapper au système immunitaire de l'hôte.

2.3. *B. cereus*

2.3.1. *Infections gastro-intestinales*

B. cereus sensus stricto, (*B. cereus* pour le reste du manuscrit) et *B. cytotoxicus* sont tous les deux responsables de toxi-infections alimentaires collectives (TIAC) chez l'Homme provoquant des infections gastro-intestinales (Glasset et al. 2016). On définit un foyer de TIAC par l'apparition d'au moins deux cas présentant des symptômes et une origine d'infection similaires. En France, les TIAC sont à déclaration obligatoire (DO) de la part des médecins et des responsables d'établissement de restauration collective auprès de l'administration, soit par les Agences Régionales de Santé (ARS), soit par les Directions Départementales de la Protection des Populations (DDPP) (décret n°86-770 du 10 juin 1986). Les TIAC sont considérées comme confirmées lorsque l'agent pathogène est isolé à partir d'un prélèvement d'origine humaine ou des restes alimentaires. Les TIAC sont suspectées lorsque le pathogène n'a pas été confirmé mais suspecté grâce à un algorithme prenant en compte les signes cliniques, la durée d'incubation et le type d'aliments consommés (Santé publique France).

Les infections gastro-intestinales peuvent se présenter sous deux types de symptômes.

- Le syndrome diarrhéique est engendré par une intoxication suivant la synthèse de toxines par les bactéries végétatives dans l'intestin. L'infection se fait par le biais de spores ou de cellules végétatives présentes dans des produits laitiers, des purées de légumes, des crudités ou encore des plats à base de viandes. Le plus souvent, les bactéries vont être ingérées sous forme végétative mais peuvent aussi être sous forme de spores (Clavel et al. 2004) qui dans l'intestin vont germer, se multiplier et produire des entérotoxines. Les symptômes d'une infection par *B. cereus* vont apparaitre plusieurs heures après l'ingestion (de 5 à 24 h) et se manifestent par des douleurs abdominales et une diarrhée profuse (Stenfors Arnesen, Fagerlund, and Granum 2008). Les infections sont généralement bénignes avec une rémission dans les 24 h sans avoir besoin de traitement. Cependant, des cas de décès ont déjà été rapportés (Dierick et al. 2005; Messelhausser et al. 2014; Naranjo et al. 2011).
- Le syndrome émétique est le résultat d'une intoxination provoquée par le céréulide. Il s'agit d'une toxine synthétisée par certaines souches de *B. cereus* et préformée dans les aliments. La toxine va causer des nausées et vomissements rapidement après l'ingestion des aliments (de 30 minutes à 6 h) et a déjà entrainé des décès dus à des insuffisances hépatiques (Dierick et al. 2005; Mahler et al. 1997). On va retrouver le céréulide dans des plats à base d'aliments

amylacés comme le riz ou les pâtes préparés à l'avance et conservés à température ambiante ou mal réfrigérés qui sont réchauffés rapidement avant la consommation. Les spores présentes lors de la préparation vont entrer en germination lors du stockage de l'aliment et vont produire la toxine émétique (Ehling-Schulz, Fricker, and Scherer 2004). Le céréulide est très résistant à la chaleur et n'est pas détruit lors du réchauffage. Il n'est pas non plus dégradé par le pH acide de l'estomac ou par les enzymes digestives (Alonzo, Magarvey, and Schmeing 2015). Il semblerait que la synthèse du céréulide soit uniquement associée à certaines souches spécifiques de *B. cereus* (Hoton et al. 2009).

B. cytotoxicus se différencie de *B. cereus* par sa température de croissance comprise entre 20 °C et 50 °C, l'absence d'hydrolyse de l'amidon et également l'absence de croissance dans des milieux artificiels ne contenant pas de tryptophane. La caractérisation majeure de cette espèce se trouve dans la production de la cytotoxine CytK1 (Guinebretiere et al. 2013).

Les TIAC sont une préoccupation majeure dans les secteurs de l'agroalimentaire et de la santé. En 2005, *B. cereus* représentait la quatrième cause de TIAC en France (Delmas G 2006). Depuis 2012, *B. cereus* est le second pathogène suspecté ou confirmé des TIAC reportées. Le nombre de TIAC associé à *B. cereus* a continué à augmenter au cours des années, rattrapant quasiment le nombre de TIAC associé à *S. aureus* (Figure 9) (France 2021).

Selon un rapport de Santé Publique France, en 2019, 1 783 TIAC ont été déclarés en France, touchant un total de 15 641 personnes, dont 4 % (609) se sont présentées à l'hôpital et 0,08 % (12) en sont décédées. Lorsque l'on compare le nombre de cas notifiés, on remarque une augmentation de 8,6 % (+153 TIAC déclarées) par rapport à 2018. Sur les 12 décès recensés, 6 sont suspectés d'avoir été causés par *B. cereus*, touchant des personnes âgées (France 2021).

En 2019, l'Autorité européenne de sécurité des aliments (EFSA: European Food Safety Authority) a recensé 5 940 TIAC sur 33 pays européen. *B. cereus* était le troisième agent pathogène responsable de ces infections et sur les 60 cas mortels, il en est responsable de 12 %. En 2021, l'implication de *B. cereus* dans la proportion de cas mortels a légèrement diminué jusqu'à 3 % (https://www.efsa.europa.eu/en/microstrategy/FBO-dashboard).

Néanmoins, de manière générale, l'incidence des infections alimentaires à *B. cereus* est sous-estimée car il n'est pas systématiquement recherché en cas de TIAC dans de nombreux pays. La France est l'un des pays portant le plus d'attention à *B. cereus*. En effet, si on regarde les données de 2019, 52 % des TIAC reportées impliquant *B. cereus* viennent de la France et représentent 86 % des cas mortels décomptés.

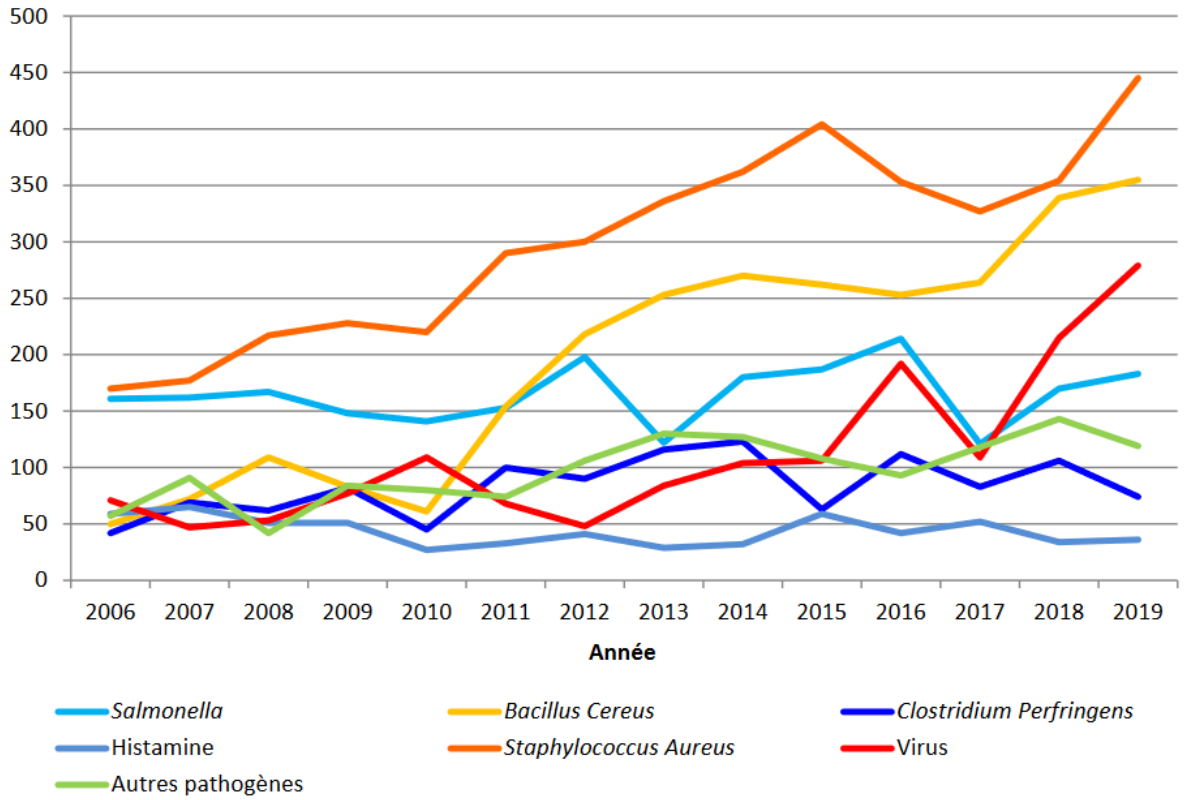

Figure 9 : Nombre de TIAC déclarées selon l'agent pathogène suspecté ou confirmé entre 2006 et 2019 (France 2021).

En plus d'avoir un coût humain, les TIAC ont aussi un impact économique important. En effet, pour les entreprises agro-industrielles, le rappel de produits contaminés entraine des pertes financières importantes. Par exemple, en 2009, le rappel de produits à bases de cacahuètes contaminés par *Salmonella* a entrainé un cout de 70 millions de dollars à l'entreprise et a aussi entrainé sa faillite (Hussain and Dawson 2013).

2.3.2. *Infections non gastro-intestinales*

B. cereus est aussi considéré comme étant un pathogène opportuniste de plus en plus reconnu. Les infections non gastro-intestinales sont plus rares mais elles sont aussi plus graves (Bottone 2010).

Les infections non gastro-intestinales représentent des infections locales ou systémiques non liées au tractus intestinal. Ces infections ne sont pas à déclaration obligatoire. Il est donc plus difficile de mesurer le risque et l'incidence de *B. cereus* dans les infections non gastro-intestinales en France ou dans le monde. Il existe néanmoins un grand nombre d'études de cas qui montre *B. cereus* comme l'agent responsable d'infections locales et systémiques ainsi que de son implication dans des cas mortels (Kato et al. 2016).

B. cereus a été montré comme étant à l'origine :

- D'endophtalmies (Hemady et al. 1990; Helgason et al. 2000). L'endophtalmie est une infection oculaire entrainant une diminution de l'acuité visuelle à la suite d'une infection microbienne

traumatique ou systémique de l'intérieur de l'œil (Callegan et al. 1999). La gravité de l'infection varie en fonction du pathogène et la rapidité du traitement.

- De parodontites pouvant induire une dégradation des dents (Rasko et al. 2007).
- D'infections du système nerveux central où il peut provoquer des hémorragies méningées (Kawatani et al. 2009) ainsi que des abcès au niveau du cerveau (Nishikawa et al. 2009).
- D'infections au cœur localisées (endocardites, péricardites) ou générales (bactériémies) (Akesson, Hedstrom, and Ripa 1991; Arnaout et al. 1999; Miller et al. 1997)
- De méningites chez les nouveau-nés et en particulier les prématurés (Cormontagne et al. 2021)
- D'infections locales à la suite d'un traumatisme dues à la présence de spores dans l'environnement ou acquises en tant qu'agent pathogène secondaire à l'hôpital.
- Plusieurs cas d'infections fulminantes similaires à *B. anthracis* ont déjà été reportés alors que les individus étaient en bonne santé (Avashia et al. 2007; Hoffmaster et al. 2006). Les souches isolées possédaient le gène de virulence *pagA* qui est porté par le plasmide pXO1 de *B. anthracis*. Il a donc été montré que des souches de *B. cereus* possédant des gènes codant pour des facteurs de virulence retrouvés chez *B. anthracis* peuvent être à l'origine d'infections pulmonaires sévères.

Toutes ces pathologies montrent que *B. cereus* est un pathogène qui doit être pris en compte sérieusement lors de son isolement dans des prélèvements cliniques et ne pas être considéré comme un contaminant.

Dû à sa présence ubiquitaire, *B. cereus* peut être retrouvé dans l'environnement hospitalier où il pose un réel problème. De nombreux cas d'infections nosocomiales ont été rapportés chez des patients hospitalisés, souvent immunodéprimés. Une grande variété de sources de contamination a été identifiée tels que des équipements de filtration de l'air et de ventilation, le matériel de bronchoscopie, le linge, les gants, les mains ou encore les ballons de ventilation manuelle au sein des services de réanimation (Barrie et al. 1994; Hsueh et al. 1999; Van Der Zwet et al. 2000; Bryce et al. 1993; Hernaiz et al. 2003; Moyer et al. 2009). Dans des cas de bactériémies ou de septicémies, des contaminations via des cathéters ont été documentées (Kuroki et al. 2009). Grâce à sa capacité à former des biofilms (Auger et al. 2009), *B. cereus* peut facilement adhérer à la surface des cathéters et provoquer des infections persistantes. La décontamination de ces biofilms est compliquée puisqu'un traitement antibiotique ne sera efficace que sur les bactéries détachées du biofilm tandis que celles au sein du biofilm seront protégées de l'action thérapeutique (Stewart et al. 2001). Entre sa capacité à former des biofilms et à sporuler, *B. cereus* est capable d'échapper aux traitements et de persister dans l'environnement hospitalier.

Parmi les infections nosocomiales, *B. cereus* est particulièrement dangereux pour les nouveau-nés prématurés. Lorsque l'on regarde des études de cas dans la littérature, on peut voir que ces infections entrainent une forte mortalité chez les nouveau-nés (40 % des cas) (Annexe 1) (Cormontagne et al. 2021). Les nouveau-nés prématurés ayant un système immunitaire immature sont plus sensibles aux infections qui se développent, la plupart du temps, dans les dix premiers jours de vie.

En 2016, dix nouveau-nés infectés par *B. cereus* ont été identifiés en Île de France sur cinq hôpitaux différents. Le lait maternel pasteurisé avait été suspecté comme possible contaminant et des études ont été faites sur des lots de lait incriminés. Ces tests ont mis en évidence la présence de *B. cereus* mais la comparaison des souches cliniques et environnementales a révélé une grande diversité génotypique, rendant impossible l'identification d'une source de contamination commune. De plus, certains des cas n'avaient même pas reçu de lait pasteurisé provenant du lactarium. Néanmoins, bien qu'aucune corrélation n'a pas pu être établie entre les souches cliniques et environnementales, on ne peut pas exclure leur possible dangerosité. Ces cas ont entrainé un arrêt du fonctionnement du lactarium pendant l'enquête sur la source de contamination. Cinq cents litres de lait maternel pasteurisé ont dû être jetés bien que de nombreux nouveau-nés ayant reçu ce lait n'ont jamais développé d'infections. Au final, la source de contamination n'a jamais pu être identifiée.

3. Toxines et facteurs de virulence

Un pathogène est défini par sa capacité à infecter un hôte en lui provoquant des effets délétères. Même des bactéries qui ne sont pas normalement pathogènes peuvent le devenir lorsqu'ils infectent des hôtes affaiblis. Afin d'infecter son hôte, la bactérie peut employer de multiples stratégies pour créer des conditions qui seront favorables pour sa survie.

Les gènes de virulence bactérienne peuvent être divisés en trois classes (Wassenaar and Gaastra 2001) :

- Des gènes de virulence codant pour des protéines telles que des toxines qui vont être directement impliquées dans la dégradation des tissus de l'hôte. Ce sont des gènes qui ne sont pas présents ou exprimés dans des souches hypovirulentes.
- Des gènes impliqués dans la colonisation de l'hôte et/ou dans le contournement du système immunitaire. Ces gènes vont permettre l'établissement du cycle infectieux au sein de l'hôte.
- Des gènes codants pour l'ensemble des produits nécessaires à l'activité des facteurs des deux premières catégories. On retrouve dans cette catégorie des gènes de maturation tels que des protéines chaperonnes, des gènes impliqués dans la sécrétion des facteurs de virulence, des gènes impliqués dans l'approvisionnement de l'agent pathogène en nutriment ou encore des gènes impliqués dans la régulation de l'expression des gènes de virulence.

Les souches de *B. cereus* ont des niveaux de pathogénicité très variables. Des souches peuvent être inoffensives pour l'Homme alors que d'autres peuvent engendrer une pathologie grave pouvant amener au décès de l'hôte. De nombreux facteurs ont été mis en évidence comme étant potentiellement impliqués dans la virulence de la bactérie. Parmi ces facteurs, on retrouve notamment le céréulide, les entérotoxines Nhe, Hbl et EntFM, les « pore forming toxins » CytK et HlyII, les phospholipases PI-PLC, PC-PLC et SM-PLC, les protéases InhA1 et NprA, les régulateurs de l'expression des facteurs de virulence ou encore la protéine Mfd.

En termes de santé publique, il est nécessaire de connaitre le risque que représentent les souches isolées, que ce soit au niveau de l'industrie agroalimentaire ou dans les hôpitaux. Ainsi, il est important de savoir si une souche retrouvée dans leur environnement présente un danger afin de mettre en œuvre les mesures de prévention et de décontamination adaptées. La virulence de *B. cereus* est multifactorielle et de nombreux facteurs de virulence ont été décrits et étudiés, néanmoins, ils n'expliquent toujours pas entièrement la virulence de *B. cereus.* Certaines souches peuvent posséder ces facteurs mais être apovirulentes tandis que d'autres peuvent n'en présenter aucun et être hypervirulentes. De plus, les facteurs de virulence peuvent agir de différentes manières, ils ne vont pas nécessairement directement être toxiques pour l'hôte mais un bon nombre d'entre eux (HlyII, Mfd, InhA1 ou encore NprA) augmentent la résistance de *B. cereus* face au système immunitaire. Les travaux sur la compréhension de la virulence de cette bactérie sont donc essentiels pour détecter de manière efficace les souches pathogènes et les différencier des souches non pathogènes.

3.1. Le céréulide

Le céréulide est une toxine responsable du syndrome émétique causé par *B. cereus*. Il s'agit d'un petit polypeptide cyclique composé de 12 acides aminés (Agata et al. 1994) qui est le produit d'une synthèse peptidique non-ribosomale (Ehling-Schulz, Fricker, and Scherer 2004). La machinerie enzymatique nécessaire à l'assemblage de la toxine est codée par le locus *ces* qui fait 24 kb. Ce locus est notamment utilisé en tant que marqueur pour identifier les souches productrices de la toxine émétique. Le locus *ces* est porté par un plasmide pBCE de 270 kb ayant des similarités avec pXO1 de *B. anthracis* (Ehling-Schulz et al. 2006; Rasko et al. 2007).

La toxine est extrêmement stable et est capable de résister à un pH acide jusqu'à pH 2 ainsi qu'à de hautes températures (121 °C pendant 15 min). Cela lui permet de ne pas être détruit par l'acide gastrique, les enzymes protéolytiques du tractus intestinal ou encore la cuisson des aliments (Agata et al. 1994; Shinagawa et al. 1996). Étant un ionophore de potassium, le céréulide peut traverser les membranes. Par ce transport, il induit le gonflement des mitochondries, inhibant de cette façon leur activité (Mikkola et al. 1999). Cette toxine est capable d'entrainer l'apoptose de multiples types cellulaires comme notamment les cellules hépatiques (Yokoyama et al. 1999) et les cellules NK de la

réponse immunitaire (Paananen et al. 2002). Le symptôme de vomissements causé par la toxine émétique est dû à l'activation du nerf vague suite à la fixation du céréulide sur des récepteurs spécifiques (Agata et al. 1995).

3.2. Les entérotoxines

3.2.1. *L'hémolysine BL*

L'hémolysine BL (Hbl) fut la première entérotoxine de *B. cereus* identifiée. Elle est composée de trois sous unités incluant deux composants lytiques L2 et L1 codés par *hblC* et *hblD* et la protéine de liaison B codée par *hblA* (Beecher and Macmillan 1991; Thompson et al. 1984; Ryan, Macmillan, and Zilinskas 1997). Hbl est une toxine hémolytique, cytotoxique, dermonécrotique qui entraine une augmentation de la perméabilité vasculaire. L'entérotoxine est cytotoxique pour les cellules intestinales mais aussi pour les erythrocytes (Beecher and MacMillan 1990), les cellules épithéliales rénales Vero (Granum and Lund 1997), le tissu dermique (Thompson et al. 1984) et rétinal (Beecher et al. 1995; Beecher and Wong 2000). L'interaction des trois sous unités est nécessaire pour la formation de pores transmembranaires permettant le passage d'eau, d'ions et de molécules de faible poids moléculaire (Beecher and Wong 1997).

3.2.2. *L'entérotoxine Nhe*

L'entérotoxine Nhe « Non-Hemolytic Enterotoxin » est elle aussi un complexe protéique tripartite composé de NheA, NheB et NheC codées par l'opéron *nheABC* (Granum, O'Sullivan, and Lund 1999). Nhe est tout aussi cytotoxique que Hbl mais n'a pas son caractère hémolytique. Comme Hbl, sa propriété cytotoxique est due à l'assemblage des trois protéines qui la compose, formant des pores transmembranaires qui entrainent la lyse osmotique des cellules. Nhe est considérée comme étant la toxine diarrhéique majeure de *B. cereus* à cause de la forte corrélation entre la cytotoxicité des filtrats de culture d'un grand nombre de souches sur des cellules Vero et leur concentration en Nhe (Moravek et al. 2006). Il a été décrit que les gènes codant pour Nhe sont présents dans toutes les souches de *B. cereus* mais exprimés à différents niveaux (Fagerlund et al. 2007; Moravek et al. 2006; Ngamwongsatit et al. 2008).

3.2.3. *L'entérotoxine FM*

L'entérotoxine FM (EntFM) a été identifiée comme étant responsable de perméabilité vasculaire chez le lapin, d'infiltrations sur des anses ligaturées de lapins et de toxicité sur les cellules épithéliales Vero (Shinagawa et al. 1991). Il a été démontré que EntFM est une peptidase membranaire impliquée dans la mobilité et la morphologie de *B. cereus*. De ce fait, elle a été renommée CwpFM (Cell wall peptidase).

Cette entérotoxine permet l'adhésion des bactéries aux cellules épithéliales et participe à la formation de biofilms, ce qui est essentiel dans la virulence de *B. cereus* chez l'insecte (Tran et al. 2010).
Une étude portée sur 39 séquences de CwpFM a montré que l'on ne retrouve qu'une seule copie du gène dans les différentes souches de *B. cereus* et que sa séquence est fortement conservée. L'étude *in silico* des séquences montre qu'il y a néanmoins une différence entre la séquence de souches non pathogènes par rapport à la séquence de souches isolées dans des TIAC au niveau de deux modules fonctionnels. Ces deux motifs pourraient induire une variation dans la pathogénicité d'une souche. La relation séquence/structure/fonction de CwpFM semble jouer un rôle important dans la virulence de *B. cereus* (annexe 2) (Tran et al. 2020).

3.3. Les « pore forming toxins »

3.3.1. *La cytotoxine K*

La cytotoxine K 1 (CytK1) fut identifiée pour la première fois en 1998 après un isolement d'une toxi-infection alimentaire causant la mort de trois personnes en France (Lund, De Buyser, and Granum 2000). Codée par *cytK*, cette protéine appartient à la famille des protéines à structure en tonneau β capables de former des pores. CytK est nécrotique, hémolytique et cytotoxique pour l'épithélium intestinal (Hardy, Lund, and Granum 2001). Il existe deux variants de CytK : CytK1 et CytK2. Ces deux variants présentent 89 % d'identité. Néanmoins, des études ont montré que le variant CytK2 est 5 fois moins cytotoxique que CytK1 sur des cellules Caco-2 et Vero (Fagerlund et al. 2004).

3.3.2. *L'hémolysine II*

L'hémolysine II (HlyII) codée par *hem2* est comme CytK une protéine ayant une structure en tonneau β. Elle est capable de former des pores transmembranaires de petite taille permettant le passage d'anions (Andreeva et al. 2006). HlyII peut s'insérer dans des membranes de différents types cellulaires et ne semble pas avoir besoin de récepteurs spécifiques. Son effet cytotoxique a été montré sur érythrocytes, des cellules neuronales, épithéliales, des macrophages, des monocytes et des cellules dendritiques (Andreeva et al. 2006; Sinev et al. 1993; Tran and Ramarao 2013).
Des observations *in vitro* et *in vivo* chez l'insecte ont montré que la formation de pores par HlyII dans la membrane des cellules phagocytaires entraîne leur apoptose et permet ainsi à *B. cereus* de contourner les défenses immunitaires de l'hôte (Tran et al. 2011; Tran et al. 2013). Le gène *hlyII* est surexprimé lorsque la bactérie est dans un environnement présentant peu de fer. L'apoptose des hémocytes et des macrophages permettrait le relargage du fer qu'ils contiennent (Tran et al. 2013).

3.4. Les phospholipases

Les phospholipases C jouent des rôles variés dans la virulence des bactéries pathogènes (Titball 1998). Les phospholipases sont capables d'induire une lyse des cellules via une activité enzymatique. Elles sont aussi associées à la dégradation des tissus et à l'altération de la signalisation cellulaire (Drobniewski 1993). *B. cereus* produit trois phospholipases C : la phosphatidylinositol phospholipase C (PI-PLC), la phosphatidylcholine phospholipase C (PC-PLC) et la sphingomyélinase (SM-PLC). Ces deux dernières sont actives séparément mais sont aussi capables de s'associer créant la céréolysine AB qui a une activité hémolytique (Gilmore et al. 1989).

3.5. Les protéases

Les protéases ont un rôle majeur dans la virulence bactérienne. Elles ont des rôles très variés tels que l'activation de toxines, la lyse de protéines, la protection contre le système immunitaire ou encore l'interférence avec la signalisation cellulaire (Miyoshi and Shinoda 2000). *B. cereus* exprime une cinquantaine de protéases dont deux majeures qui sont produites en fin de phase stationnaire : NprA et InhA1 (Chitlaru et al. 2006).

InhA1 est une métalloprotéase à zinc, sécrétée, interférant avec les défenses immunitaires de l'hôte en hydrolysant des peptides antimicrobiens (Dalhammar and Steiner 1984). InhA1 est absorbée à la surface de l'exosporium (l'enveloppe la plus externe de la spore) (Charlton et al. 1999) et permet aux spores de s'échapper des macrophages après leur internalisation (Ramarao and Lereclus 2005). En plus du gène *inhA1*, le génome de *B. cereus* contient deux gènes paralogues *inhA2* et *inhA3*. *inhA2* et *inh3* possèdent respectivement 66 % et 73 % d'homologie à *inhA1*. Tous les deux contiennent un domaine de fixation au zinc. InhA2 pourrait protéger *B. cereus* des peptides antimicrobiens synthétisés par les cellules épithéliales intestinales de l'insecte *Galleria mellonella* (Fedhila et al. 2006). Le rôle de InhA3 dans la virulence de *B. cereus* quant à lui reste encore méconnu (Guillemet et al. 2010).

NprA est aussi une métalloprotéase « thermolysin-like » de la famille des peptidases M4. NprA pourrait être impliquée dans la virulence en clivant des composants tissulaires comme l'élastine, la fibronectine ou encore des protéines impliquées dans la coagulation sanguine (Chung et al. 2006). Il a été montré récemment que NprA et InhA1 font partie du sécrétome de *B. cereus* et que la sécrétion de NprA ne peut avoir lieu sans InhA1. NprA est composée d'un peptide signal de 24kDa et d'un domaine C-terminal de 35 kD. Dans le sécrétome, NprA est retrouvée sous une forme à 35 kDa. InhA1 a été montrée comme étant responsable du clivage de NprA, lui permettant de prendre sa forme mature qui sera sécrétée. De plus, l'infection de macrophages a montré que NprA et InhA1 sont essentielles pour la sortie des spores phagocytées hors des macrophages (Haydar et al. 2018). Ces deux protéases jouent donc un rôle important dans la résistance de *B. cereus* à la réponse du système immunitaire de l'hôte.

3.6. Les régulateurs de l'expression des facteurs de virulence

3.6.1. *PlcR*

L'expression de la plupart des facteurs de virulence décrits précédemment est régulée par un régulateur transcriptionnel PlcR (Phospholipase C Regulator). C'est le cas des toxines diarrhéiques Nhe et Hbl, de CytK, des phospholipases PI-PLC, PC-PLC et SM-PLC, des paralogues de NprA (mais pas NprA elle-même), de la métalloprotéase InhA2 (mais pas InhA1 ni InhA3), et de plusieurs bactériocines (Agaisse et al. 1999; Gohar et al. 2008). PlcR est reconnu comme le régulateur majeur de la virulence de *B. cereus*. Son régulon compte au total 45 gènes, dispersés sur le chromosome. Leur expression est activée en début de phase stationnaire par la fixation de PlcR à une séquence dans leur région promotrice. C'est une séquence palindromique spécifique et fortement conservée TATGnAnnnnTnCAT(A) nommée boîte PlcR (Gohar et al. 2008). L'expression de PlcR s'autorégule par l'intermédiaire du peptide PapR qui est codé par un gène situé en aval de *plcR* (Slamti and Lereclus 2002). Au moment du passage en phase stationnaire de croissance, les facteurs de virulence régulés directement ou indirectement par PlcR représentent plus de 80 % de la quantité de protéines extracellulaires de *B. cereus* (Gohar et al. 2002).

3.6.2. *NprR*

Comme PlcR, le régulon de NprR contient de nombreux gènes codant des enzymes dégradatives : protéases, estérases, lipases, chitinases et une chitosanase. C'est notamment un régulateur de l'expression de NprA. Le gène *nprR* est en opéron avec le gène codant son peptide activateur, *nprX* (Perchat et al. 2011). L'expression de *nprR* seul (en absence de *nprX*) réduit de cinq fois l'efficacité de la sporulation. La sporulation est restaurée en ajoutant le peptide NprX en début de phase stationnaire (Perchat et al. 2016).

3.6.3. *Spo0A*

Spo0A est un régulateur transcriptionnel pléiotrope présent chez toutes les bactéries sporulantes (Galperin et al. 2012). Il y est qualifié de régulateur global (« master regulator ») car les régulons et les différenciations sous son contrôle sont nombreux. Chez *B. subtilis*, Spo0A influence la transcription de plus de 500 gènes, dont 121 contrôlés directement par Spo0A (Molle et al. 2003; Fawcett et al. 2000). Lorsque des signaux (densité cellulaire, carences nutritionnelles, etc) activent les kinases, celles-ci déclenchent une cascade de phosphorylations, impliquant les facteurs Spo0B et Spo0F, qui aboutit à la phosphorylation de Spo0A. L'accumulation de Spo0A~P active la transcription d'au moins sept gènes dont *sigF* et *sigE*, codant respectivement les facteurs σF et σE. Ces facteurs contrôlent l'entrée en sporulation et le passage d'un à deux compartiments cellulaires (préspore et cellule mère) dans lesquels la transcription des gènes est différemment régulée (Patrick J. Piggot 2002). Spo0A~Préprime

également la transcription de nombreux gènes possédant une « boite Spo0A » (site de fixation de Spo0A sur l'ADN). Ces gènes, sous le contrôle de Spo0A, peuvent être impliqués dans de nombreux processus comme la motilité, la formation de biofilms et la sporulation (Fujita, Gonzalez-Pastor, and Losick 2005; Grau et al. 2015; Piggot and Hilbert 2004). Spo0A est également connu pour agir comme répresseur de la transcription de *plcR* (Lereclus et al. 2000).

3.7. Îlot de pathogénicité du plasmide pAH187

L'étude d'une collection de souches isolées de patients infectés avec *B. cereus* a mis en évidence un îlot de pathogénicité sur le plasmide pAH187. Des nouveaux biomarqueurs des souches cliniques (araC, gshAB, BCQ_PI180) (Kavanaugh et al. 2022) ont été identifiés sur la séquence de ce plasmide. La région contenant ces biomarqueurs a alors été considérée comme un possible îlot de pathogénicité, ce qui a été confirmé par des test *in vivo* chez la larve *Galleria mellonella*. En effet, la délétion de cet îlot a entrainé une diminution de la virulence de *B. cereus*. Cette délétion a aussi révélé une diminution de la germination chez le mutant par rapport à la souche contenant le plasmide entier. L'îlot identifié sur le plasmide pAH187 joue donc un rôle essentiel non seulement dans la virulence mais aussi la germination de *B. cereus* (annexe 3) (Dervyn et al. 2021).

3.8. La protéine Mfd

Récemment, la protéine Mfd « Mutation Frequency Decline » a été mise en évidence comme étant impliquée dans la virulence de *B. cereus*. Il a été montré que la délétion du gène *mfd* entraine une perte de virulence (Guillemet et al. 2016). Mfd, par son implication dans la réparation de l'ADN, permet à *B. cereus* de résister à la réponse immunitaire et plus particulièrement à la réponse nitrogène de l'hôte qui entraîne des lésions sur l'ADN bactérien (cf Chapitre 1).

Chapitre 3 : Les antibiotiques et l'antibiorésistance

1. Les maladies infectieuses

Les maladies infectieuses sont causées par des microorganismes (Virus, bactéries, parasites, champignons…). Ces pathogènes peuvent entrainer des infections locales comme une infection cutanée ou ils peuvent provoquer des infections systémiques qui sont généralisées. Naturellement, notre système immunitaire est équipé pour combattre ces pathogènes, mais il n'est pas toujours en mesure de maîtriser l'infection. Avant le 20ème siècle et la découverte des antibiotiques, les maladies infectieuses étaient la première cause de mortalité dans le monde (Cohen 2000). Un enfant né en 1900 avait 10 % de chance de mourir entre 1 et 4 ans à cause d'une pneumonie ou d'une maladie diarrhéique. Le manque d'hygiène publique ou personnelle, la consommation d'eau, d'aliments ou de lait contaminés étaient des facteurs majeurs dans la transmission de ces infections.

Parmi les maladies infectieuses causant des épidémies sévères, on retrouve de nombreuses bactéries comme *Yersinia pestis,* l'agent responsable de la peste qui a causé au moins trois pandémies connues. Il est estimé que la seconde pandémie (appelée la peste noire) aurait engendré la mort de plus de 200 millions de personnes en Europe et Asie de l'Est. Cette pandémie aurait décimé 30 % de la population européenne de l'époque (Piret and Boivin 2020). Outre *Yersinia pestis*, on retrouve aussi les *Rickettsies* (famille de bactéries responsable du typhus), *Mycobacterium tuberculosis* (agent responsable de la tuberculose), *Vibrio cholerae* (agent responsable du choléra), *Salmonella typhi* (agent responsable de la fièvre typhoïde), *Streptococcus pyogenes* (agent responsable de la scarlatine) et *Corneybacterium diphtheriae* (agent responsable de la diphtérie) comme espèces bactériennes responsables d' épidémies majeures (Mercer 2021).

L'amélioration de la qualité de la nourriture et de l'eau ainsi que la mise en place de règles sanitaires et d'hygiènes a fortement augmenté l'espérance de vie. Entre 1700 et 1900, cette espérance de vie moyenne est passée de 17 à 52 ans en Angleterre (Piret and Boivin 2020). L'amélioration de la santé humaine a continué d'augmenter grâce à la découverte des antibiotiques.

2. Histoire des antibiotiques

L'utilisation de microbes produisant des antibiotiques dans le traitement d'infections remonte à plusieurs millénaires. Des cataplasmes à partir de pain moisi ou de miel étaient utilisés pour traiter des plaies ouvertes en Serbie, en Chine, en Grèce et en Egypte il y a plus de 2000 ans. Un papyrus datant de 1500 ans avant l'ère commune est la preuve la plus ancienne d'un document médical qui inclut notamment ces méthodes de traitement (Haas 1999).

L'antibiose entre bactéries a été décrite bien avant la découverte d'antibiotiques. Par exemple, Louis Pasteur avait proposé que les microbes étaient capables de produire des substances mortelles pour d'autres bactéries (Brunel 1951). Néanmoins, il faudra attendre 1908 et Paul Ehrlich pour voir apparaitre le développement de médicaments antimicrobiens. Paul Ehrlich, un médecin allemand, a mis au point un dérivé de l'arsenic non toxique, efficace contre la syphilis s'appelant l'arséphénamine et commercialisé sous le nom de Salvarsan (Gelpi, Gilbertson, and Tucker 2015).

En 1928, Alexander Fleming identifie *Penicillium notatum* comme étant capable d'inhiber la croissance bactérienne. Il concentre la substance antibactérienne et la nomme « pénicilline » (Fleming 2001). Il faudra néanmoins attendre 1945 pour avoir une production industrielle et une commercialisation de la pénicilline pure.

En 1936, Gerhard Domagk, un scientifique poursuivant les travaux de Paul Ehrlich à l'institut Bayer en Allemagne, découvre le sulfamidochrysoïdine aussi nommé « prontosil ». Ce composé est une pro drogue qui nécessite l'activité d'une estérase *in vivo* pour être activé (Otten 1986). Il s'agit du premier antibiotique de la classe des sulfamides. Cette classe d'antibiotique fut aussi la première à être efficace sur un large spectre de bactéries.

À partir de là, les travaux sur les antibiotiques deviennent de plus en plus présents et la découverte de nouvelles classes d'antibiotiques se poursuit jusque dans les années 80. Les travaux de Waksman sur les Actinomycètes en tant que producteurs de nombreux antibiotiques tels que la néomycine et la streptomycine (les premiers agents efficaces contre la tuberculose) ont initié l'âge d'or de la découverte d'antibiotiques entre les années 40 et 60 (Figure 10) (Waksman, Schatz, and Reynolds 2010). La plupart des antibiotiques découverts durant cette période sont toujours utilisés de nos jours.

L'introduction des antibiotiques a révolutionné le domaine médical du 20ème siècle. En plus du traitement de maladies infectieuses, les antibiotiques ont rendu possible de nombreuses avancées dans des procédures médicales telles que le traitement contre le cancer, la transplantation d'organes ou plus généralement la bonne réalisation de chirurgies. Il a été calculé que la découverte et l'utilisation des antibiotiques a entrainé une augmentation de l'espérance de vie de plus de vingt ans (Hutchings, Truman, and Wilkinson 2019).

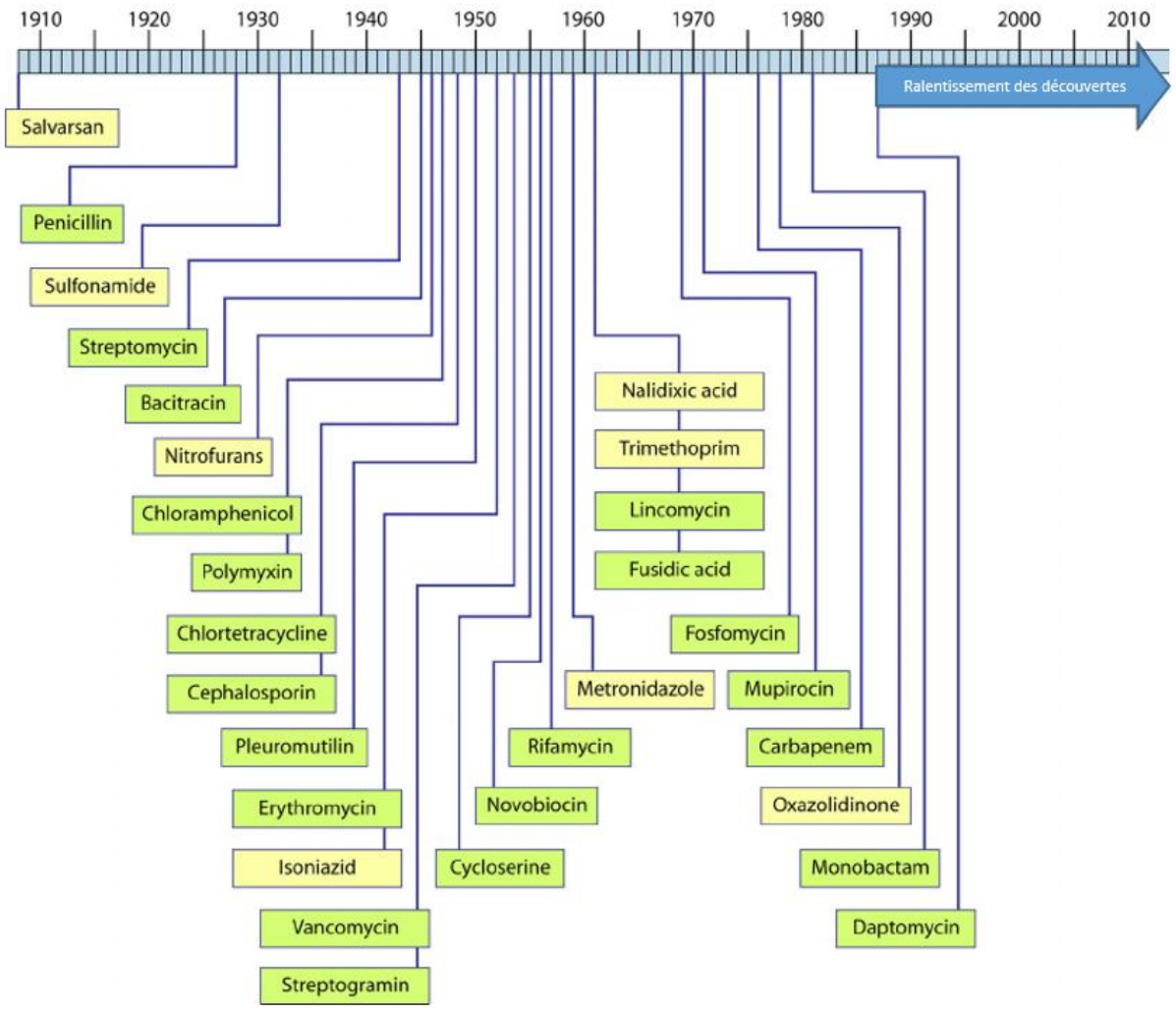

Figure 10 : Chronologie de la découverte des antibiotiques entre 1910 et 2010 (Silver 2011).

3. Cibles actuelles des antibiotiques

Les antibiotiques sont des petites molécules qui inhibent des mécanismes essentiels à la survie ou à la multiplication des bactéries. Ils sont bactéricides lorsqu'ils ciblent la survie et sont bactériostatiques lorsqu'ils bloquent la multiplication bactérienne. Ces antibiotiques ciblent principalement six voies essentielles des bactéries (Figure 11), ce qui les classe dans différents groupes (tableau 1).

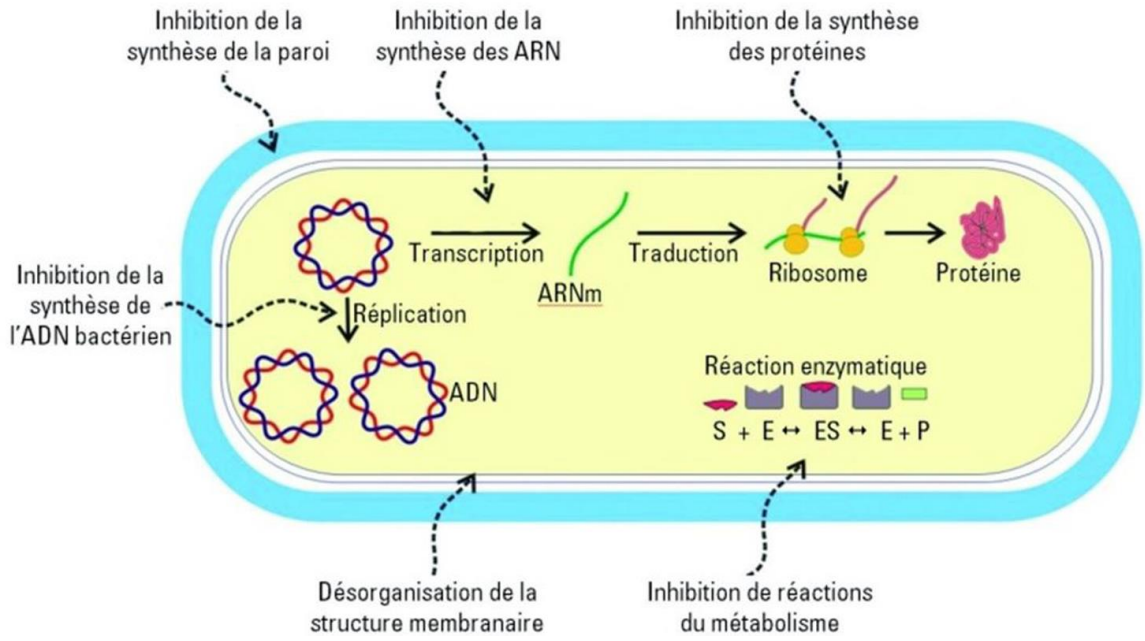

Figure 11 : Voies essentielles ciblées par les antibiotiques.(Bordeaux 2019).

3.1. La paroi bactérienne

La paroi est une particularité de la cellule procaryote. Elle lui permet de conserver sa forme et de résister à la pression osmotique. La paroi bactérienne est composée de peptidoglycane et sa synthèse est inhibée par les β-lactamines et les glycopeptides. Le peptidoglycane est composé de deux sucres, le N-acétylglucosamine et l'acide N-acétyl muramique et d'un pentapeptides qui se termine par deux résidus D-alanine. Ces trois éléments sont reliés lors de la synthèse du peptidoglycane par des transpeptidases appelées protéines de liaison aux pénicillines (PLP). C'est en se fixant sur les PLP, grâce à une structure similaire aux deux D-alanine, que les antibiotiques de cette famille vont inhiber l'activité transpeptidase et bloquer la synthèse de la paroi (Yocum, Rasmussen, and Strominger 1980).

3.2. La polarité de la membrane

La polarité de la membrane permet aux bactéries d'avoir une perméabilité sélective afin de maintenir une homéostasie qui est nécessaire à la conservation d'énergie. Cette polarité est formée grâce à un gradient d'ions de part et d'autre de la membrane. La gramicidine et la polymixine modifient la perméabilité cationique de la membrane, ce qui annule le gradient de proton. Cette action induit une perméabilité et une désorganisation de la membrane. Le contenu intracellulaire peut alors sortir, ce qui entraine la mort de la bactérie (Shatri and Tadi 2022).

3.3. Traduction des protéines

La traduction des protéines est un processus impliquant de nombreux acteurs comme l'ARN messager, les ARN de transfert et des ribosomes. Ces derniers sont composés de deux sous unités appelées 30S et 50S. Certains antibiotiques peuvent cibler ces sous unités et ainsi inhiber le processus de traduction.

Les aminoglycosides et les tétracyclines inhibent la sous unité 30S, la première famille en se liant de manière irréversible (Krause et al. 2016) et la seconde en bloquant l'association de l'ARNt avec le ribosome (Chopra and Roberts 2001). Les macrolides et les lincosamides, quant à eux, inhibent la sous unité 50S en se liant de manière réversible (Patel and Hashmi 2022; Murphy, Bistas, and Le 2022).

3.4. L'ADN

La réplication et la conservation de l'intégrité de l'ADN sont primordiales à la survie des bactéries. L'ADN gyrase fait partie de la famille des topoisomérases. Ce sont des enzymes qui vont contrôler la structure de l'ADN et on les retrouve dans de nombreux processus cellulaires tels que la transcription et la réplication. Les antibiotiques de la famille des quinolones (dont les fluoroquinolones) vont inhiber l'ADN gyrase et la topoisomérase IV. Les fluoroquinolones vont intéragir avec une région appelé QRDR des toposiomérases et vont ainsi créer des changements de conformations induisant l'inhibition de l'activité des enzymes (Blondeau 2004). Le métronidazole quant à lui interagit avec l'ADN et induit une perte de la structure hélicoïdale de l'ADN et des dommages sur l'ADN (Weir and Le 2022).

3.5. Transcription de l'ARN

La transcription est essentielle à la survie des bactéries puisqu'elle permet la synthèse d'ARN messager qui va pouvoir être utilisé dans la traduction et donc la synthèse de protéines. La rifampicine est un antibiotique qui inhibe l'ARN polymérase, soit en bloquant le passage pour l'élongation au bout 5' de l'ADN soit en diminuant l'affinité de l'ARN polymérase avec les transcrits (Beloor Suresh, Rosani, and Wadhwa 2022). La fidaxomicine, va quant à elle, inhiber l'initiation de la transcription en se fixant au niveau du complexe ADN/ARN polymérase (Zhanel, Walkty, and Karlowsky 2015).

3.6. Voies métaboliques

Les voies métaboliques permettent la synthèse de molécules nécessaires au bon fonctionnement de la cellule. Cela peut être la synthèse de lipides, de glucides, d'ATP et bien d'autres. Les voies métaboliques sont au centre de la survie de tous les organismes. Le traitement principal induisant une inhibition de la synthèse d'acide folique est une combinaison d'antibiotiques, le sulfamethoxazole qui inhibe la dihydroptéroate synthase et le triméthoprime qui inhibe l'enzyme dihydrofolate réductase. Les deux composés ensemble créés un effet en synergie anti-acide folique (Kemnic and Coleman 2022). De manière plus spécifique, l'isoniazide est une prodrogue qui, lorsque activée, va former un complexe avec NADH et inhiber l'acide gras synthase et ainsi la synthèse d'acide myolique (Timmins and Deretic 2006). Ce dernier est un composant essentiel de la paroi mycobactérienne et est donc utilisé exclusivement pour le traitement des infections à *Mycobacteriaceae*.

Tableau 1 : Liste des grands groupes d'antibiotiques actuels

Mode d'action	Groupe d'antibiotiques

Inhibiteur de la synthèse de la paroi	β-Lactamines
	Carbapénèmes Céphalosporines Monobactames Pénicillines
	Glycopeptides
	Fosfomycine
Dépolarisation de la membrane	Lipopeptides
	Gramicidine
	Polymixine
Inhibiteur de la synthèse de protéines	Interaction avec la sous unité ribosomale 30S
	Aminoglycosides Tétracyclines
	Interaction avec la sous unité ribosomale 50S
	Chloramphénicol Lincosamides Macrolides Oxazolidinones Streptogramines
Inhibiteur de la synthèse d'ADN	Quinolones
	Fluoroquinolones
	Métronidazole
Inhibiteur de la transcription de l'ADN	Rifampicine
	Fidaxomicine
Inhibiteur du métabolisme	Sulfonamides
	Triméthoprime
	Nitrofuranes

4. Apparition et propagation de l'antibiorésistance

4.1. L'antibiorésistance

La résistance aux antibiotiques ou l'antibiorésistance survient lorsque les bactéries deviennent moins sensibles ou complètement résistantes aux traitements antibactériens. Cette résistance aux antibiotiques est devenue un problème majeur de santé publique en médecine humaine et animale puisque les infections causées par des souches résistantes sont de plus en plus difficiles à traiter.

L'antibiorésistance est un phénomène qui est apparu dès la mise à disposition des antibiotiques, mais il faudra attendre 1998 avant que l'OMS reconnaisse officiellement qu'il s'agit d'un problème à traiter (Organization 1998). Depuis, la surveillance de l'antibiorésistance a pris de l'ampleur. En France, l'ONERBA (l'Observatoire Nationale de l'Epidémiologie de la Résistance Bactérienne aux Antibiotiques) et Santé Publique France s'occupent de rassembler les données de surveillance du pays depuis respectivement 1997 et 1999 (Aubry Damon H 2000). En Europe, c'est l'ECDC (le Centre européen de

prévention et de contrôle des maladies) qui s'occupe de regrouper les données de surveillance des pays européen. Ils ont un atlas en ligne regroupant les données de chaque année. Si on s'intéresse à *K. pneumoniae*, une entérobactérie responsable d'infections nosocomiales (contractées à l'hôpital) de plus en plus résistante aux antibiotiques, on observe une augmentation du pourcentage d'isolats résistants aux carbapénèmes qui sont les antibiotiques de derniers recours dans les infections sévères à bactérie à coloration Gram négative dans de nombreux pays en Europe. Ce pourcentage atteint jusqu'à 70 % dans les bactériémies en Grèce (Figure 12). Certains pays comme la Roumanie ou l'Italie sont passés de 0 à 46 %, et 0 à 30 % d'isolats résistants recensés entre 2006 et 2021. Même dans des pays conservant un faible pourcentage de souches résistantes comme la France, on recense huit fois plus d'isolats résistants aux carbapénèmes en 2021 par rapport à 2005. Cette augmentation est liée à une diffusion autochtone de souches, d'épidémies hospitalières et dans 50 % des cas, à une importation de souches par le biais de séjours et d'hospitalisation dans des zones endémiques.

En 2015, l'OMS a mis en place un système de surveillance à l'échelle internationale appelé GLASS (« Global Antimicrobial Resistance Surveillance System ») qui a pour mission d'assurer une approche standardisée dans la collecte, l'analyse, l'interprétation et le partage de données entre pays dans le but d'améliorer les mesures de préventions et de réponses face aux infections résistantes aux antibiotiques (https://www.who.int/initiatives/glass).

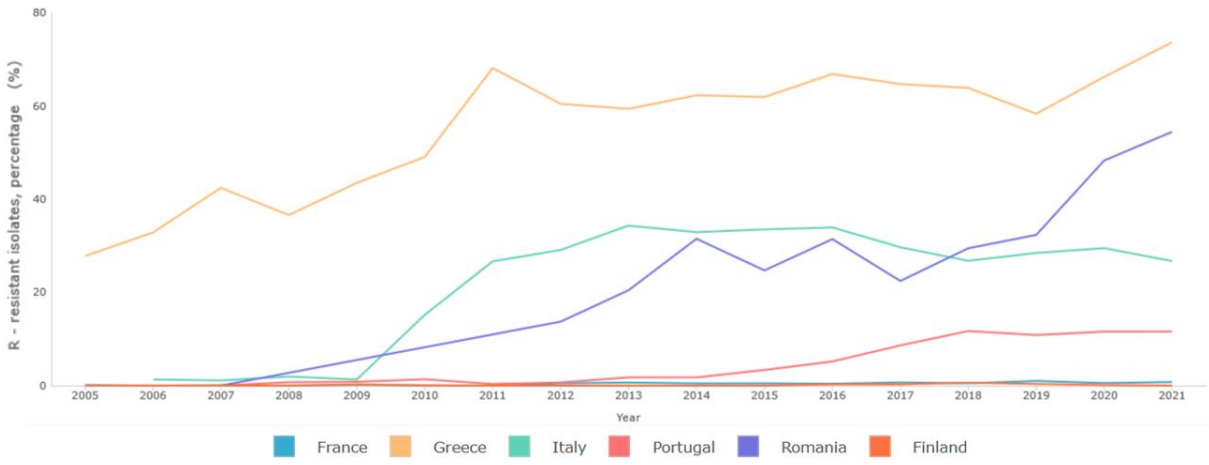

Figure 12 : Pourcentages d'isolats résistants de K. pneumoniae aux antibiotiques de la famille des carbapénèmes en Europe entre 2005 et 2021 (données d'ECDC).

4.2. Impact socio-économique

En 2020, la consommation moyenne d'antibiotiques était de 16,4 doses journalières pour 1000 habitants en Europe. Néanmoins, cette consommation varie énormément d'un pays à un autre. Les Pays-Bas ne sont qu'à 8,5 doses alors que Chypre est à 28,9 doses. Bien que la consommation d'antibiotiques reste haute, il est aussi important de noter qu'elle a tout de même diminué de 22,6 %

entre 2014 et 2020. Cette diminution a majoritairement eu lieu entre 2019 et 2020 dû à la pandémie du COVID-19 (2022).

Malgré la diminution de la quantité d'antibiotiques utilisés en 2021, le nombre d'infections impliquant des souches résistantes a augmenté pour tous les pathogènes en Europe par rapport à 2020. La plus forte hausse a été observée pour *Acinetobacter* spp. pour lequel on retrouve une augmentation de 43 % des cas. Ce nombre de cas a augmenté de 21 % pour *E. faecium*, 14 % pour *E. faecalis*, 9,4 % pour *S. aureus*, 8,2 % pour *P. aeruginosa*, 8,1 % pour *K. pneumoniae* et 2,8 % pour *E. coli*. Le nombre de cas de *K. pneumoniae* résistants aux carbapénèmes continue aussi d'augmenter alors qu'il s'agit de la dernière ligne de défense utilisée dans son traitement (https://www.ecdc.europa.eu/en/publications-data/surveillance-antimicrobial-resistance-europe-2021).

Une étude récente menée dans 204 pays a estimé qu'environ 4,95 millions des décès dans le monde seraient associés à des bactéries résistantes aux antibiotiques en 2019 et dont 1,3 millions seraient directement causées par les bactéries (Antimicrobial Resistance 2022). L'étude Burden, réalisée par Santé Publique France estime qu'en 2012, 158 000 cas d'infections étaient causés par des bactéries multi-résistantes parmi lesquels 16 000 infections invasives (méningites, bactériémies, septicémies) et 12 500 décès ont été associés à ces infections. Sept bactéries multirésistantes ont été étudiées lors de cette étude : *S. aureus* résistant à la méticilline, des entérocoques résistants à la vancomycine, *E. coli* et *K. pneumoniae* résistant aux céphalosporines de 3ème génération, *K. pneumoniae*, *Acinetobacter spp.* et *P. aeruginosa* résistants aux carbapénèmes. Ces bactéries appartiennent au groupe ESKAPE (https://www.santepubliquefrance.fr/maladies-et-traumatismes/infections-associees-aux-soins-et-resistance-aux-antibiotiques/resistance-aux-antibiotiques/donnees/).

Dans le rapport O'Neil, ministre de la Santé sous James Cameron, en Angleterre, il a été estimé que si rien n'est fait pour combattre l'antibiorésistance, les bactéries résistantes aux antibiotiques pourraient entrainer plus de 10 millions de morts par an dans le monde en 2050 au lieu des 700 000 estimés en 2014 (Figure 13). Ce nombre représenterait un mort toutes les trois secondes dans le monde à cause d'une bactérie résistante et représenterait un coût de l'ordre de 100 000 milliards de dollars (O'Neill 2016). Ce rapport alarmant a mis en exergue la nécessité de nouveaux antibiotiques et de nouvelles approches thérapeutiques. Malheureusement, l'innovation dans ce domaine représente un fort coût pour les industriels et, avec l'émergence rapide de résistances, les nouveaux candidats médicaments deviennent rapidement obsolètes ce qui rend cette recherche peu rentable à l'heure actuelle.

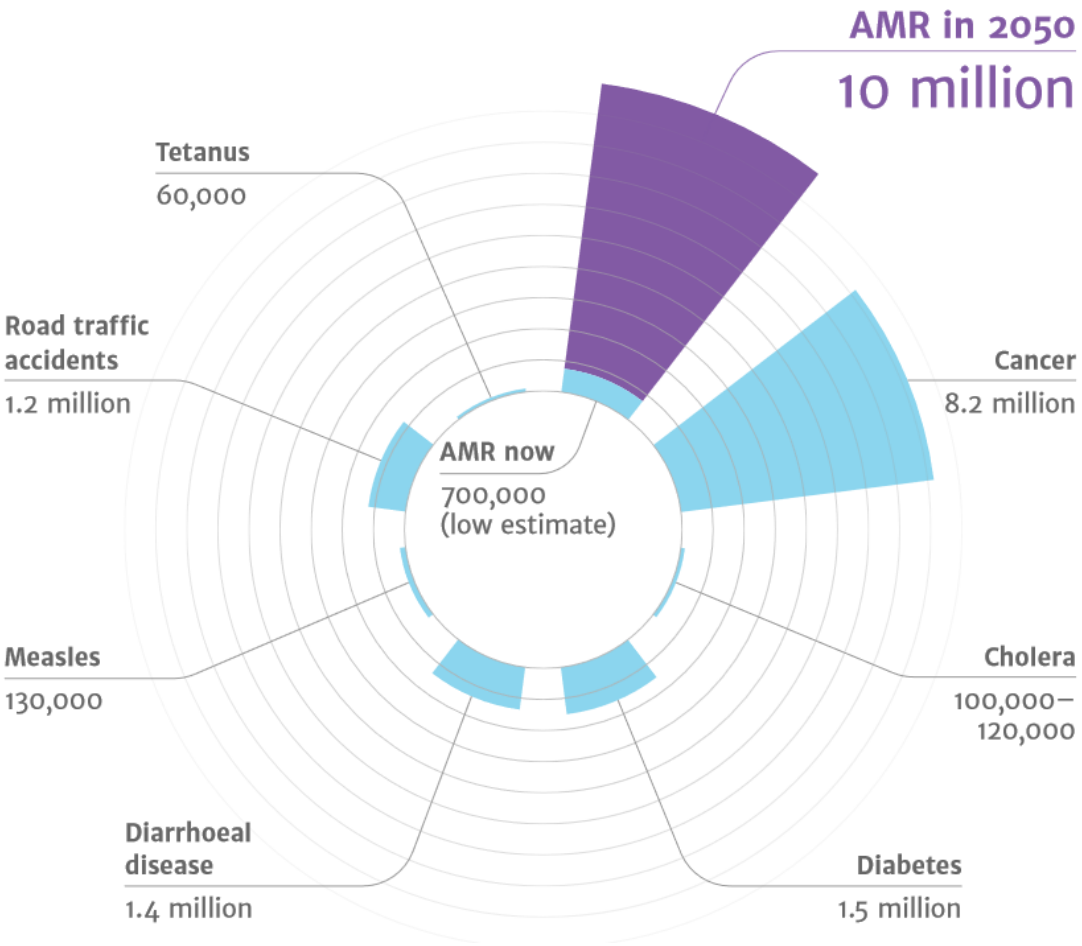

Figure 13 : Prédiction de l'impact des bactéries résistantes aux antibiotiques sur les causes de mortalité (O'Neill 2016)

4.3. Groupe ESKAPE

Les souches résistantes aux antibiotiques ont une plus grande prévalence en environnement hospitalier où les patients dont les défenses sont altérées sont particulièrement vulnérables aux infections bactériennes. Bien que de nombreuses bactéries restent sensibles à la plupart de nos traitements, un groupe particulier de bactéries résistantes a émergé. Dans les hôpitaux des pays développés et en développement, ce groupe composé d'*Enterococcus faecium*, *Staphylococcus aureus* (SARM), *Klebsiella pneumoniae*, *Acinetobacter baumanni*, *Pseudomonas aeruginosa* et *Enterobacter spp.*, est surnommé « les bactéries ESKAPE » (Rice 2008).

Les bactéries ESKAPE sont d'une importance capitale, elles sont à l'origine de la majorité des infections nosocomiales provoquant des maladies graves qui peuvent entrainer le décès du patient telles que bactériémies, infections du tractus urinaire, pneumonies, méningites et infections de plaies cutanées. L'intégralité du groupe ESKAPE fait partie de la liste publiée par l'OMS en 2022 nommant les bactéries pour lesquels il est urgent de développer de nouvelles solutions thérapeutiques (Figure 14) (WHO 2022). *A. baumannii*, *P. aeruginosa* et les entérobactéries (incluant *K. pneumoniae*) sont placées dans

la première catégorie avec une priorité critique tandis que *S. aureus* et *E. faecium* sont classées dans la catégorie d'en dessous avec une priorité élevée.

Les pathogènes du groupe ESPAKE sont retrouvés dans de nombreuses niches environnementales. Des études ont identifié des souches résistantes dans du sable, de l'eau de mer, des eaux usées industrielles ou municipales, des décharges, des légumes, des plats préparés et des irrigations d'eau (Akanbi et al. 2017; Michael et al. 2013; Hrenovic et al. 2017; Ebomah and Okoh 2020; Verraes et al. 2013). Cela est probablement dû au rejet des eaux usées, de déchets hospitaliers ou agricoles incorrectement jetés et traités ou encore à l'activité humaine comme des baignades dans des réserves d'eaux naturelles (Hrenovic et al. 2017). Ces bactéries résistantes deviennent donc de plus en plus communes dans notre environnement.

Les études au sein de notre laboratoire se concentrent principalement sur *K. pneumoniae* et *P. aeruginosa*, deux bactéries considérées comme une priorité critique par l'OMS.

4.3.1. Klebsiella pneumoniae

K. pneumoniae est une bactérie à coloration Gram négative et appartient à la famille des Entérobactéries. Il s'agit d'un pathogène opportuniste surtout nosocomial et impliqué dans de nombreux types d'infections : pneumonies nosocomiales, infections urinaires, infections hépato-biliaires et des bactériémies. Cette bactérie est présente dans l'eau, sur les plantes, le sol, la peau, les muqueuses et le tube digestif humain. Sa transmission dite oro-fécale se fait par contact avec des objets souillés, des contacts inter humains (manuportage) ou encore des végétaux contaminés.

La résistance naturelle aux antimicrobiens est principalement due aux pompes à efflux et à l'expression d'une pénicillinase à spectre restreint (SHV). La capacité de *K. pneumoniae* à coloniser l'environnement hospitalier, y compris la moquette, les éviers, les fleurs et diverses surfaces, ainsi que la peau des patients et du personnel hospitalier, a été identifiée comme un facteur majeur de propagation de cette bactérie (Podschun and Ullmann 1998). *K. pneumoniae* peut acquérir du matériel génétique par l'intermédiaire de plasmides de multi-résistance. Il n'est pas rare d'isoler, même en France, des souches devenues résistantes à l'ensemble de l'arsenal thérapeutique anti-infectieux. Les infections par *K. pneumoniae* représentent environ 10 % des infections bactériennes traitées dans le domaine hospitalier (Piano et al. 2019).

4.3.2. Pseudomonas aeruginosa

P. aeruginosa est aussi une bactérie à coloration Gram négative ubiquitaire. C'est un pathogène des plantes, des animaux et de l'Homme. Elle est associée à des maladies graves et des infections acquises à l'hôpital telles que la pneumonie sous ventilation, des infections cutanées et des bactériémies. Cette bactérie ubiquitaire est retrouvée dans le sol, l'eau, la flore cutanée et la plupart des environnements

créés par l'Homme. Elle est également présente sur les équipements médicaux, y compris les cathéters, provoquant des infections nosocomiales. *P. aeruginosa* est capable de coloniser de nombreuses surfaces et produire des biofilms durables. Ce pathogène est naturellement résistant à un grand nombre d'antibiotiques y compris certaines ß-lactamines, car il produit une β-lactamase (céphalosporinase de type AMPC) qui n'est pas inhibée par l'acide clavulanique (un inhibiteur de β-lactamase) (Lodge et al. 1990). Les infections causées par *P. aeruginosa* représentent environ 7 % des cas reportés au NHSF (« National Healthcare Safety Network ») (Weiner et al. 2016).

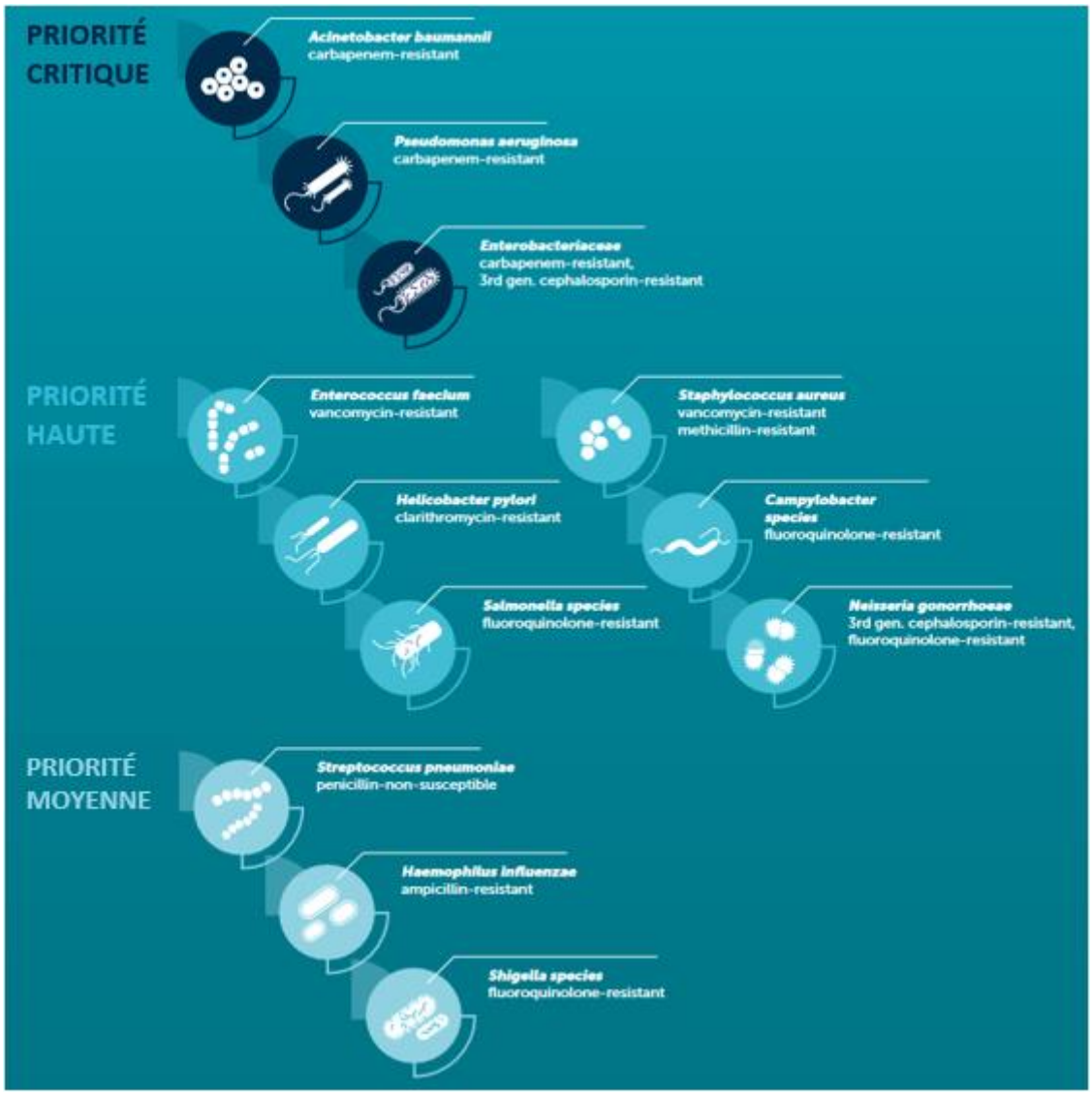

Figure 14 : Liste des pathogènes prioritaires pour le développement d'agents antimicrobiens (WHO 2022)

4.4. Causes de la crise actuelle

Une des causes de l'émergence de la résistance aux antibiotiques est l'utilisation irraisonnée et massive des antibiotiques dans tous les compartiments ; humain, animal et environnemental (agriculture). À l'exception de la famille des carbapénèmes, des représentants des autres familles d'antibiotiques sont utilisés à la fois chez l'Homme et l'animal.

En Médecine humaine, les antibiotiques sont réservés aux traitements d'infections bactériennes et à de la prophylaxie, notamment en pré et post opératoire. Cette utilisation est similaire pour les animaux de compagnie. Bien qu'interdit en France, de nombreux pays dans le monde continuent, en élevage, en agriculture ou en aquaculture, à utiliser des antibiotiques en prohylaxie par l'intermédaire de l'eau ou leur nourriture, afin de limiter les risques d'infection ou en métaphylaxie pour traiter tout un groupe présentant quelques individus malades (1999). En outre, et bien que cet usage soit controversé, les antibiotiques sont aussi utilisés comme facteur de croissance. Au lieu de traiter des individus malades ou à risque, les antibiotiques sont administrés sur de longues périodes de temps, dans des concentrations sous létales afin d'améliorer la production de viande. Le temps d'exposition dépend de l'organisme traité, que ce soit pour les plantes ou pour les animaux, il s'étend quasiment sur toute la durée de vie de ceux-ci. Ces conditions favorisent le développement et la propagation de résistances à l'intérieur des élevages (Collignon and McEwen 2019). Le rejet d'eaux usées contenant des résidus d'antibiotiques entraine aussi l'apparition de souches résistantes dans l'environnement et dans l'eau de rivières, qui sera ensuite bue par les animaux sauvages.

Tous ces points provoquent une dispersion de souches résistantes dans notre environnement au lieu d'une localisation limitée au domaine hospitalier. C'est pourquoi il y a aujourd'hui le concept d'une seule santé appelée « One Health » où il faut agir sur plusieurs fronts et ne pas se limiter uniquement à des actions humaines (Figure 15). Avec cette notion d'une seule santé, l'utilisation d'antibiotiques comme facteurs de croissance dans les aliments pour animaux a été interdite au sein de l'union européenne en 2006 (IP/05/1687). Cela est récemment allé plus loin puisque depuis 2022, l'utilisation prophylactique d'antibiotique a aussi été interdite (UE 2019).

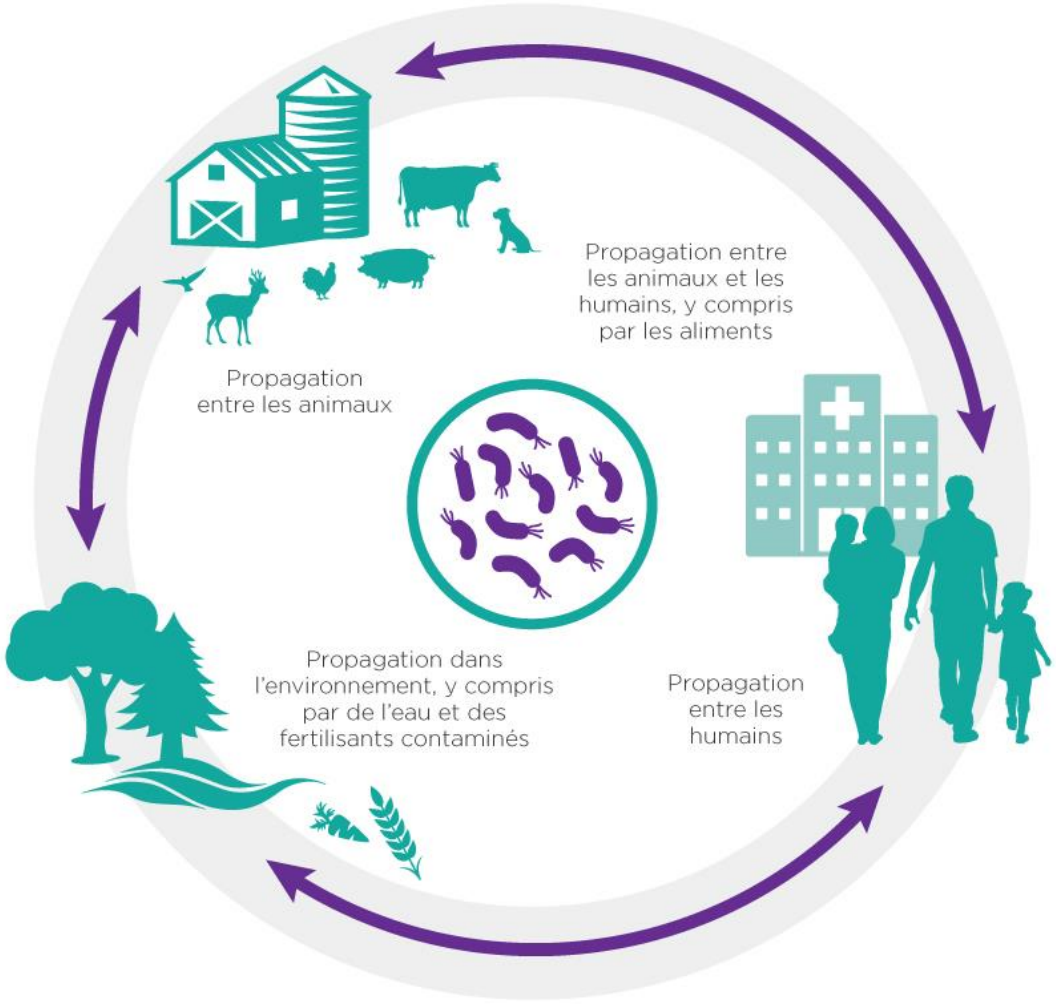

Figure 15 : Liens de la résistance aux antimicrobiens avec l'approche une seule santé (SantéCanada 2017).

5. Mécanismes de résistances aux antibiotiques

Les bactéries en tant que telles ne sont pas susceptibles ou résistantes de manière uniforme. Il existe certaines espèces bactériennes capables de résister naturellement à certains antibiotiques tandis que d'autres bactéries peuvent acquérir ces résistances à travers les différentes voies d'échange de matériel génétique (transformation, transposition et conjugaison) ou encore des mutations spontanées. Cette acquisition peut être temporaire ou permanente.

Bien que nous ayons de nombreux antibiotiques disponibles pour le traitement d'infections, il existe des résistances connues pour chacun d'entre eux.

L'étude des bactéries résistantes aux antibiotiques a permis de mieux comprendre les mécanismes de résistance qui ont été mis en place. On peut séparer ces mécanismes de résistance aux antibiotiques en quatre catégories : (1) la réduction de la perméabilité, (2) la modification de la cible, (3) l'inactivation de l'antibiotique et (4) l'efflux des molécules (Figure 16).

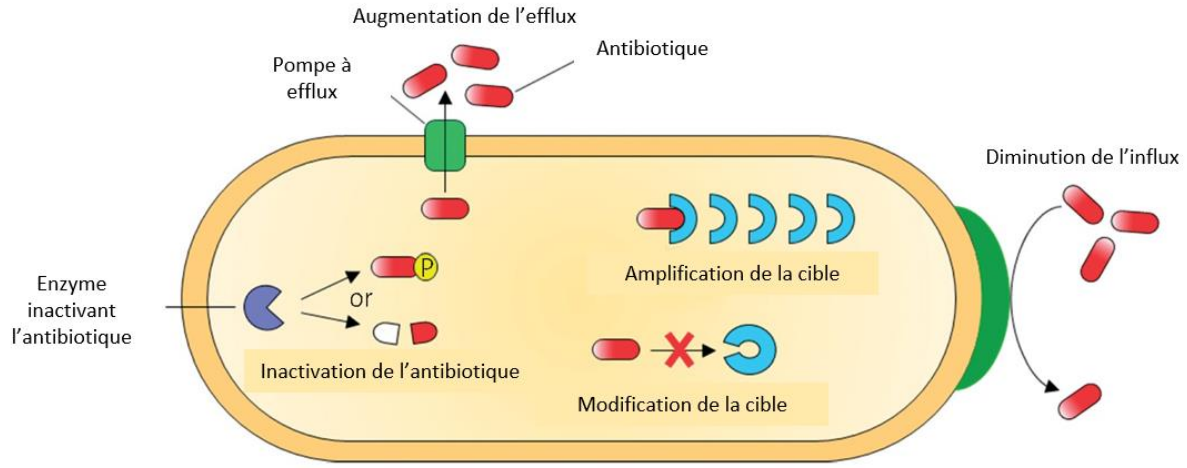

Figure 16 : Mécanismes généraux de la résistance aux antibiotiques

5.1. Réduction de la perméabilité

La structure et les fonctions de la couche de lipopolysaccharides (LPS) chez les bactéries à coloration Gram négative forment une barrière pour le passage de certains types de molécules. Cela donne à ces bactéries une résistance innée sur un large panel d'antibiotiques comme les β-lactamines et les fluoroquinolones (Pages 2004). Les mycobactéries ont une couche externe de la paroi riche en lipides, cette particularité facilite le passage des molécules hydrophobes mais rend aussi ce passage difficile pour les molécules hydrophiles (Lambert 2002). On note aussi que toutes les bactéries n'ayant pas de paroi comme les mycoplasmes sont aussi résistantes à tous les antibiotiques ciblant la paroi (Liu et al. 2014).

Pour que de petites molécules passent à travers la membrane, les bactéries ont des porines. Il existe deux façons pour limiter le passage des molécules : une diminution du nombre de porines ou des mutations qui augmentent la sélectivité de ces canaux (Kumar and Schweizer 2005). Les entérobactéries sont connues comme devenant de sensibilité diminuée voire résistantes aux carbapénèmes en diminuant ou en mutant leurs porines. Par exemple, chez *E. cloacae*, la résistance au méropénème est due à la disparation de porines (Cornaglia et al. 1996). Chez *N. gonorrhoeae*, des mutations sur le gène codant pour la porine ont été montrées comme étant responsables de la résistance aux β-lactamines et à la tétracycline (Gill et al. 1998).

5.2. Modification de la cible

S. aureus, une bactérie à coloration Gram positive, normalement sensible à la vancomycine, a mis en place des mécanismes de résistance comme la synthèse d'enzymes détruisant l'extrémité D-Ala-D-Ala du peptidoglycane auquel se lie la vancomycine ou encore en modifiant le dipeptide qui devient alors D-Ala-D-Ser (Miller, Munita, and Arias 2014). Il s'agit de l'un des mécanismes connus qui est impliqué dans la résistance à la vancomycine. Le génome de *S. aureus* peut aussi contenir un gène de résistance

appelé *mecA* qui code la protéine PBP2a, une nouvelle protéine liant les pénicillines (PLP). Cette protéine est plus résistante aux β-lactamides que la version native. Cette modification est responsable de la résistance à la méthicilline avec des fois, des résistances croisées à la streptomycine, la tétracycline et l'érythromycine (Grundmann et al. 2006).

La modification des PLP est un mécanisme répandu chez les bactéries à coloration Gram positive. La présence d'une mutation dans les PLP induit une baisse de l'affinité des antibiotiques de la famille des β-lactamines. La résistance de *E. faecium* à l'ampicilline et celle de *S. pneumoniae* à la pénicilline est due à ce mécanisme (Kapoor, Saigal, and Elongavan 2017).

Pour les antibiotiques ciblant les sous unités ribosomiques, l'apparition de résistances peut être causée par une modification des ribosomes, une méthylation via l'expression des méthylases codées par les gènes *erm* (Bactéries à coloration Gram positive) ou Arm (bactéries à coloration Gram négative) ou par une protection des ribosomes (Roberts 2004).

Une modification de la structure de l'ADN gyrase ou de la topoisomérase IV dans la région QRDR, région fixant les quinolones, entraine une diminution ou élimine la capacité de l'antibiotique à s'associer (Redgrave et al. 2014).

Pour la résistance aux molécules ciblant les voies métaboliques, ce sont des mutations au niveau du site actif d'enzymes (comme la dihydropteroate synthase ou la dihydrofolate reductase) impliquées dans la synthèse d'acide folique qui vont diminuer l'affinité de l'inhibiteur avec sa cible (Huovinen et al. 1995).

5.3. Inactivation de l'antibiotique

Les bactéries ont deux possibilités pour inactiver une molécule, soit entrainer sa dégradation, soit la modifier par l'ajout de groupement chimique.

Les β-lactamases sont un large groupe d'hydrolases. Ces enzymes vont cibler les β-lactamines qu'elles vont hydrolyser. Le cycle aromatique des β-lactamines s'ouvre et empêche la fixation des molécules sur les PLP. Il existe des β-lactamases spécifiques pour tous les types de β-lactamines. Les pénicillinases vont dégrader uniquement les β-lactamines de la famille des pénicillines, les céphalosporinases dégradent les céphalosporines et les carbapénemases, les carbapénèmes. Plus récemment, des β-lactamases à spectre étendu (BLSE) ont été découvertes. Elles confèrent une résistance croisée aux pénicillines, aux céphalosporines et à l'aztréonam (monobactame), mais pas aux carbapénèmes. Les gènes codant pour ces BLSEs sont portés par des plasmides qui codent pour d'autres résistances, ce qui rend ces bactéries multirésistantes (BMR). Les BLSE sont retrouvées principalement chez les entérobactéries mais également chez d'autres pathogènes à coloration Gram négative tels que *P. aeruginosa* et *A. baumannii* (Hakemi Vala et al. 2014; Bush and Jacoby 2010).

L'inactivation par modification chimique se fait par l'ajout de groupement acétyle, phosphoryle ou adényle. Il y a un grand nombre de transférases qui ont été identifiées. L'acétylation semble être le mécanisme le plus utilisé et est connu pour être utilisé contre les aminoglycosides, le chloramphénicol, les streptogramines et les fluoroquinolones. Le phosphorylation et l'adénylation sont principalement connues comme étant utilisées contre les aminoglycosides (Schwarz et al. 2004; Robicsek et al. 2006; Ramirez and Tolmasky 2010).

5.4. Efflux des molécules

Les bactéries possèdent des pompes à efflux, certaines constitutivement exprimées, d'autres induites ou surexprimées sous certains stimuli environnementaux. Ces pompes sont capables d'expulser un grand nombre de molécules. La plupart des bactéries possèdent de nombreuses pompes différentes. Il y a cinq grandes familles de pompes à efflux :

- La famille des transporteurs ABC « ATP-binding cassette » : ils transportent des acides aminés, des ions, des polysaccharides, des protéines et des sucres. Chez *V. cholerae*, une pompe ABC (VceAB) a été montrée comme étant impliquée dans la résistance d'antibiotiques (Colmer, Fralick, and Hamood 1998).
- La famille des transporteurs MATE « multidrug and toxic compound extrusion » : cette famille utilise un gradient sodium pour transporter des cations, les fluoroquinolones et quelques aminoglycosides (Kuroda and Tsuchiya 2009).
- La famille des transporteurs SMR « small multidrug resistance » : ils transportent des cations lipophiles. Ces pompes ont peu de substrats et donc peu d'antibiotiques ont été montrés comme étant transportés par celles-ci. On retrouve seulement quelques β-lactamines et aminoglycosides (Yerushalmi, Lebendiker, and Schuldiner 1995).
- La famille des transporteurs MFS « major facilitator superfamily » : ils transportent des anions, des métabolites, des sucres et aussi certains antibiotiques tels que les macrolides et la tétracycline. Ces pompes ont la plus grande diversité de substrats avec différentes pompes laissant passer des antibiotiques spécifiques (Kumar, Mukherjee, and Varela 2013).
- La famille des transporteurs RND « resistance-nodulation-cell division » : ils transportent des détergents, des colorants, des métaux lourds, des solvants et de nombreux autres substrats dont des nombreux antibiotiques. Certaines pompes vont être spécifiques à un antibiotique tandis que d'autres vont avoir un plus large panel de substrats. La pompe MexAB-OprM chez *P. aeruginosa* confère une résistance aux β-lactamines, au chloramphénicol, à la tétracycline, au triméthoprim, au sulfamethoxazole et à certaines fluorquinolones (Li, Nikaido, and Poole 1995).

5.5. Autres : Formation de biofilms

La formation de biofilms peut protéger les bactéries contre l'action des antiseptiques et antibiotiques. La matrice des biofilms contient des polysaccharides, des protéines et de l'ADN bactérien. Cette matrice empêche la pénétration des antimicrobiens dans le biofilm et donc d'atteindre les bactéries. Pour rendre l'efficacité aux antibiotiques, il est nécessaire de détruire le biofilm. De plus, les bactéries à l'intérieur de ces biofilms ont un métabolisme ralenti rendant les antibiotiques ciblant les cellules en croissance ou se divisant inefficacent. Un autre aspect des biofilms à prendre en considération dans l'antibiorésistance est le transfert de gènes qui est facilité dû à la proximité des bactéries. Il peut donc y avoir un échange des gènes de résistance dans la communauté bactérienne (Mah 2012; Soto 2013; Van Acker, Van Dijck, and Coenye 2014).

6. Quel futur pour le traitement des infections ?

Après « l'âge d'or des antibiotiques », l'ensemble des acteurs pharmaceutiques ont été confrontés à des défis scientifiques majeurs pour la mise au point de nouveaux antibiotiques, notamment en ce qui concerne les bactéries à coloration Gram négative. De plus, les industries pharmaceutiques ont perdu l'intérêt pour ce secteur qui ne promettait pas une croissance importante du marché et des bénéfices. Le ralentissement de la recherche de nouveaux antibiotiques naturels a aussi été accompagné par une augmentation de criblage haut débit pour découvrir des molécules synthétiques mais la plupart de ces recherches ont été sans succès. Par exemple, la compagnie GlaxoSmithKline (GSK) a effectué 70 criblages haut débit entre 1995 et 2001 pour obtenir seulement 5 candidats potentiels (Payne et al. 2007). Ce désintérêt des grandes sociétés pharmaceutiques a suscité des inquiétudes parmi la communauté scientifique et les pouvoirs publiques (Cars 2014).

Depuis les années 2000, une seule nouvelle classe d'antibiotiques a été commercialisée : les diaryquinolines. Il existe actuellement un seul membre, la bedaquiline qui est utilisée dans le traitement contre des souches de *Mycobacterium tuberculosis* multi-résistantes.

En 2022, l'OMS a publié un rapport sur le développement de nouvelles molécules thérapeutiques. Ils ont recensé en essai clinique 45 antibiotiques en combinaison avec une nouvelle entité et 32 nouveaux agents antibactériens non traditionnels. Sur les 45 antibiotiques, 27 sont actifs contre les pathogènes prioritaires de l'OMS mais seulement 2 sont actifs contre les bactéries Gram-négatives multi résistantes. Dans les combinaisons testées, on retrouve notamment des β-lactamines combinées avec des inhibiteurs de β-lactamases (WHO 2022).

Depuis le 1er juillet 2017, seulement 17 nouveaux antibiotiques ont été approuvés par la FDA « Food and Drug Administration » ou l'EMA (agence européenne des médicaments). Sur ces nouveaux médicaments approuvés, 80 % appartiennent à des classes d'antibiotiques déjà existantes et

présentent des risques importants de développement de résistances croisées. Les développeurs de nouveaux médicaments sont principalement des PME (petites et moyennes entreprises) réparties mondialement avec cependant une majorité en Europe (50,4 %) et en Amérique (37,2 %). Dans les agents non traditionnels développés, on retrouve des bactériophages, des inhibiteurs de virulence, des composés immunomodulateurs, des agents potentialisateurs et des peptides antimicrobiens. De nos jours, le développement s'effectue sur un spectre d'efficacité très restreint puisque 43,8 % des molécules ciblent un seul agent pathogène Concernant les nouveaux agents bactériens non traditionnels, on retrouve 6 anticorps, 9 issues de bactériophages, 11 modulateurs du microbiome, 2 immunomodulateur et 6 agents divers (Figure 17) (WHO 2022).

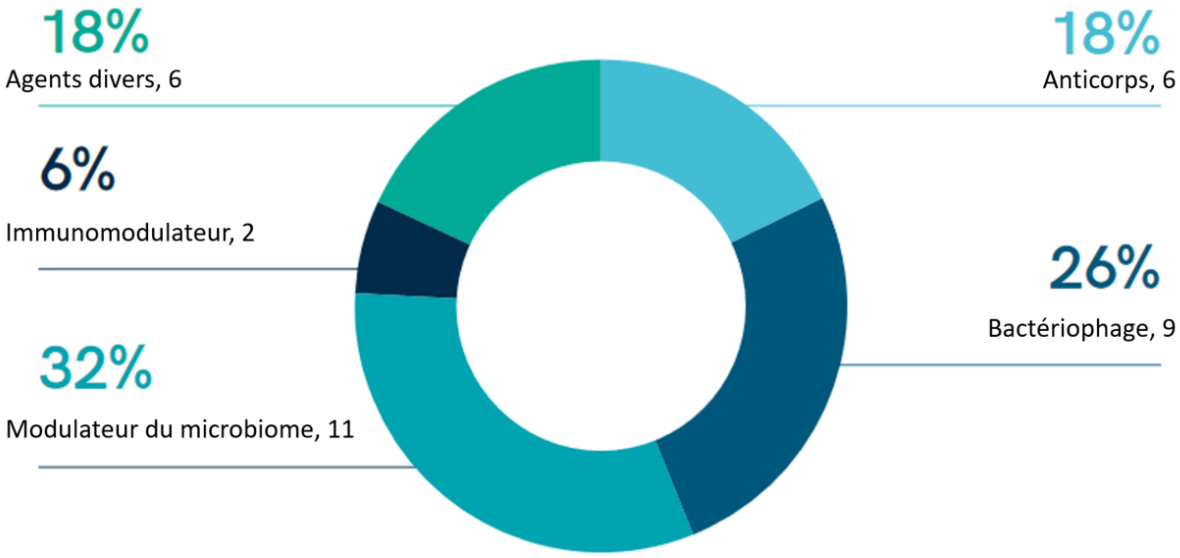

Figure 17 : Catégories des antibiotiques non traditionnels en essai clinique (WHO 2022).

Les bactériophages sont des virus qui vont infecter et se répliquer dans les bactéries. Il y a deux options dans la thérapie utilisant les bactériophages, soit utiliser les lysines produites qui sont capables de dégrader la paroi bactérienne, soit utiliser un cocktail de phages spécifiques pour un pathogène ou avec un spectre plus étendu. Depuis leur découverte en 1915, les bactériophages ont été utilisés pour traiter des infections par l'Europe centrale, la France et l'ancienne union soviétique (Summers 2012). En France, leur utilisation est très contrôlée et ils ne peuvent être utilisés qu'avec une ATUn (Autorisation Temporaires d'Utilisation nominative) mais en Russie ou en Géorgie, leur utilisation dans le traitement d'infections causées par *K. pneumoniae* est courante (Sulakvelidze, Alavidze, and Morris 2001).

Une autre stratégie actuellement développée est l'antivirulence, ce concept se base sur l'inhibition de facteurs de virulence bactériens plutôt que sur un effet bactéricide. Sans cette pression, il est possible que le développement de résistances soit fortement réduit. Les molécules antivirulentes ciblent généralement des toxines ou des protéines impliquées dans l'adhésion, la formation de biofilms, la sécrétion de toxines ou la détection du quorum (Cegelski et al. 2008). Chez *E. coli*, l'adhésine FimH,

présente dans les pili, est une cible utilisée pour inhiber l'adhésion des bactéries et la formation de biofilms. Des mannosides biphényles ont été identifiés comme inhibiteurs de FimH et sont capables de réduire l'adhésion des bactéries sur l'épithélium de la vessie chez la souris (Cusumano et al. 2011). Certaines de ces molécules antivirulentes sont des anticorps. Par exemple, l'anticorps AR-301 est en développement pour le traitement d'infections par *S. aureus* car il cible les α-toxines secrétées et permet ainsi de protéger les cellules impliquées dans la réponse immunitaire ('AR-301 (Tosatoxumab)')('AR-301 (Tosatoxumab)')(249). L'anticorps monoclonal bezlotoxumab se fixe sur la toxine B de *C. difficile* et a été approuvé en 2016 pour une utilisation thérapeutique (Wilcox et al. 2017). De manière complémentaire, en plus de l'inhibition directe des toxines, il y a aussi des études sur l'inhibition des systèmes de sécrétion des toxines comme le système de sécrétion de type III présent sur les bactéries à coloration Gram négative. Les anticorps KB001 et MEDI3902 sont en phase 2 des tests cliniques et ciblent la protéine PcrV de ce système de sécrétion (Milla et al. 2014; DiGiandomenico et al. 2014). Les molécules impliquées dans la communication entre bactéries sont aussi considérées comme des facteurs de virulence puisqu'une grande concentration de ces signaux va avoir un impact sur la formation de biofilm, sur la motilité et la sécrétion d'enzymes capable de dégrader l'hôte. Chez *P. aeruginosa* une de ces molécules est la PQS « Pseudomonas Quinolone Signal ». Sa synthèse est effectuée grâce à un groupe d'enzyme appelé PqsABCDEH et l'inhibition de PsqD permet la réduction de la formation de biofilms (Storz et al. 2012).

Il existe de nombreux peptides antimicrobiens naturels (Rima et al. 2021) en développement actuellement dont la teixobactine. Il s'agit d'un inhibiteur de la paroi découvert chez *Eleftheria terrae* qui est efficace contre *S. aureus*, *S. pyogenes*, *S. agalactiae*, *B. anthracis*, *C. difficile*, *P. acnes* et *M. tuberculosis*. Il est aussi efficace sur des souches résistantes de *S. aureus*, *E. faecalis*, *E. faecium* et *S. pneumoniae*. Des premiers tests ont montré que la teixobactine n'était pas toxique sur des cellules NIH et HepG2 à une concentration bien supérieure à la dose inhibitrice déterminée sur les bactéries. De plus, en présence d'une concentration faible, sur une période de 27 jours, *S. aureus* n'a pas développé de résistance au peptide. Néanmoins, la teixobactine n'est pas efficace sur les bactéries à coloration Gram négative (Ling et al. 2015). Malgré cela, ce peptide reste un candidat très prometteur en tant que nouvel antibiotique. Un autre peptide en développement est la darabactine. Identifié chez *Phostorhabdus khanii*, il s'agit d'un inhibiteur de BamA, une chaperonne et translocatrice qui s'occupe du repliement des protéines présentes sur la membrane externe. Ce peptide est efficace sur des bactéries à coloration Gram négative telles que *P. aeruginosa*, *K. pneumoniae*, *E. coli*, *S. typhimurium*, *M. catarrhalis* ou encore *A. baumannii*. Ce peptide a aussi l'avantage de ne pas être toxique pour les cellules HepG2, FaDu et HEK293 ainsi que sur le microbiote (même les bactéries à coloration Gram négative tel que les *Bacteroides*). Bien que prometteur, des mutations sur le gène de *bamA* entrainent l'apparition de résistance à la darabactine. Une étude sur *E. coli* a montré qu'après seulement trois

jours de passage, la concentration minimale inhibitrice augmente (Imai et al. 2019). Les SNAPPs (polymère de peptides antimicrobiens) sont aussi une piste explorée actuellement car ils sont efficaces contre des infections induites par *A. baumannii* tout en étant non toxiques pour l'hôte (Lam et al. 2016). L'un des médicaments récemment approuvé est l'irresistin-16, cette molécule est à large spectre agissant sur les bactéries à coloration Gram négative et positive. Elle impacte l'intégrité de la membrane bactérienne ainsi que la synthèse d'acide folique (Martin et al. 2020).

Toutes ces pistes de recherche montrent que le développement d'antimicrobiens est à nouveau en plein essor. Néanmoins, de nouvelles cibles suivant des stratégies thérapeutiques innovantes restent encore à explorer. Les nouvelles molécules doivent être spécifiques des cibles d'origines bactériennes afin d'éviter une toxicité chez l'hôte. Le développement de stratégies avec un mode d'action indirect permettrait de limiter un développement rapide de résistances en diminuant la pression pour leur développement.

C'est dans ce contexte que s'inscrit mon projet de thèse et que nous proposons Mfd, une protéine conservée, comme cible pour le développement de nouvelles molécules antimicrobiennes. Étant non essentielle à la survie bactérienne, son inhibition ne tuerait pas directement les bactéries mais diminuerait leur résistance au système immunitaire au site de l'inflammation.

RÉSULTATS

Partie 1 : Étude de Mfd dans la virulence de *B. cereus*

1. Résumé article 1

B. cereus est le second agent responsable de TIAC en Europe. Par ailleurs, certaines souches induisent des infections locales ou systémiques graves qui peuvent parfois entrainer la mort chez des patients immunodéprimés ou des nouveau-nés. La pathogénicité des souches *B. cereus* varie énormément, de non pathogènes à fortement virulentes. De nombreux facteurs ont été identifiés comme CytK, Nhe, Hbl, InhA1, CwpFM ou encore Mfd qui contribuent à la virulence des souches. Mfd est impliquée dans la résistance de *B. cereus* au stress nitrique produit lors de la réponse immunitaire. En effet, Mfd permet la réparation des dommages de l'ADN causés par ce stress et de ce fait favorise la survie de *B. cereus*. Mfd est une protéine ubiquitaire dont la structure 3D est connue. Elle comprend huit domaines structuraux et cinq modules fonctionnels. Mfd a été décrite chez plusieurs modèles bactériens comme étant impliquée dans la réparation de l'ADN, dans la mutagénèse, dans la régulation de la transcription et dans la virulence bactérienne.

Mon premier objectif a consisté à étudier le lien entre la séquence, la structure et le rôle de Mfd dans la virulence de *B. cereus*. Pour cela, j'ai comparé la séquence protéique des Mfd d'une collection de 22 souches de *B. cereus* : 10 souches environnementales (n'ayant pas engendré de pathologies) et 12 souches cliniques (issues de patients infectés). Dans les 22 souches, Mfd présente une séquence de 1150 acides aminés sans aucune insertion ou délétion. Il existe 57 différences d'acides aminés entre ces 22 Mfd, ce qui correspond à un ratio de différences de 0,048.

Basé sur ces différences de séquences, nous avons établi un alignement MAFFT qui permet de classer les séquences protéiques selon leur degré d'identité. À partir de ce classement, nous avons observé que les Mfd se classent en deux groupes. De manière intéressante, ces 2 groupes de Mfd correspondent aux deux types de souches : environnementales d'un côté et cliniques de l'autre. Ce regroupement des souches suggère qu'il y aurait une corrélation entre la séquence de Mfd et la virulence d'une souche.

Afin d'étudier cette hypothèse, je me suis intéressée aux deux souches dont les Mfd sont les plus éloignées : la souche S50 (environnementale) et la souche S53 (clinique). Les Mfd de ces deux souches présentent 98 % d'identité avec seulement 28 différences entre leurs séquences. Pour savoir si cette différence de séquence pourrait induire une différence dans la virulence, j'ai construit plusieurs mutants de *B. cereus*. J'ai tout d'abord utilisé la souche de référence du laboratoire, Bc407 et son mutant Bc407*Δmfd*. Dans ce dernier, j'ai complémenté le gène *mfd* absent par le gène *mfd* issu soit de la souche S50, soit de la souche S53. Par ailleurs j'ai construit les mutants Δ*mfd* des souches S50 et S53 que j'ai ensuite complémentés avec le gène *mfd* à nouveau des souches S50 ou S53.

Pour tester l'impact de ces mutations et complémentations, j'ai utilisé le modèle insecte *B. eri* qui est sensible aux infections par *B. cereus*. J'ai montré que la souche S50 est moins virulente que la souche clinique S53 pour l'insecte. Puis j'ai montré que pour la souche virulente S53, la délétion de *mfd* entraine une perte de virulence par rapport à la souche sauvage, suggérant un rôle important de Mfd dans la virulence de cette souche. La complémentation de *mfd* de la souche mutante de S53 restaure partiellement le phénotype de la souche sauvage. Dans la souche Bc407 Δ*mfd* qui est atténuée dans sa virulence par rapport à la souche sauvage, la complémentation par *mfd* de S50 ne restaure pas la virulence de la souche, alors que la complémentation par *mfd* de S53 redonne à la souche sa capacité à tuer les insectes. Ainsi, *mfd* de la souche S53 est suffisant pour conférer la virulence de *B. cereus*, contrairement à *mfd* de la souche S50. Il y a donc un lien entre la séquence de *mfd* et son implication dans la virulence.

En collaboration avec l'unité Maiage, une étude *in silico* plus approfondie des séquences des Mfd des souches S50 et S53 a permis d'identifier quatre différences qui pourraient potentiellement être à l'origine d'une différence structurale entre les Mfd. Deux de ces quatre différences se trouvent au niveau du domaine D2 et pourraient entrainer une modification conformationnelle de la protéine tandis que les deux autres se trouvant sur les domaines D5 et D6 pourraient provoquer un changement d'activité de la protéine. Pour étudier ces différences, j'ai fait une complémentation de la souche S53 Δ*mfd* avec une séquence modifiée de son gène *mfd* au niveau de ces 4 acides aminés (modifications correspondant aux acides aminés retrouvés dans la Mfd de la souche S50). Nos résultats préliminaires suggèrent que cette souche est aussi virulente que la souche sauvage S53 et que cette Mfd mutée est donc toujours fonctionnelle. Il ne semblerait pas que ces mutations soient, seules, à l'origine de la différence de virulence entre les souches S50 et S53.

À l'issue de cette étude, nous avons pu montrer qu'il y a bien une virulence liée à Mfd et que cette virulence varie de souche à souche. L'impact de Mfd sur la virulence ne s'explique pas simplement par une absence ou une présence du gène mais il semblerait qu'il s'agisse d'un système plus complexe lié à sa séquence et donc peut-être à sa structure et/ou à son activité. Nous savons que Mfd est impliquée dans de nombreux processus cellulaires, c'est pourquoi une modification de sa conformation ou de son activité pourrait avoir des conséquences sur la résistance au système immunitaire via la réparation de l'ADN ou encore sur l'expression de facteurs de virulence via son rôle dans la transcription. Mfd étant une protéine ubiquitaire, l'étude de sa compréhension ne servirait pas uniquement à la lutte contre *B. cereus* mais sur un large panel de bactéries. Mfd pourrait être un facteur global de virulence et la compréhension de la relation séquence/virulence d'une souche est un outil important dans la lutte contre les infections bactériennes et la détection de souches virulentes.

2. Article 1: The sequence and structure of the Mfd protein dictates its role during virulence

Soumission prochaine à Microorganisms

The sequence and structure of the Mfd protein dictates its role during virulence

D. Cormontagne[1+], S. Samson[1,2+], S. Albert[1,2], SL. Tran[1], G. André[2]* and N. Ramarao[1]*

[1]Université Paris-Saclay, INRAE, Micalis Institute, 78350, Jouy-en-Josas, France

[2]Université Paris-Saclay, INRAE, MaIAGE, 78350, Jouy-en-Josas, France

*Correspondence to nalini.ramarao@inrae.fr and gwenaelle.andre@inrae.fr

+these authors contributed equally to this work

Key words

Mfd; virulence factor, *Bacillus cereus*; insect assays; multiple sequence alignment; homology remodeling

Abstract

The Mfd (Mutation Frequency Decline) protein is primarily known as a ubiquitous RNA-polymerase (RNAP)-associated factor, first responsible for removing RNAP stalled onto DNA lesions, then for recruiting UvrA of the NER (Nucleic Excision Repair) complex, ensuing boosting DNA repair, in both Gram positive and Gram negative bacteria. Also, it was recently reported in both *E. coli* and *B. subtilis* that Mfd regulates transcription in time and in hard-to-transcribe regions, especially those that express structured regulatory RNAs. Also, DNA translocase Mfd is an evolvability factor that thrives mutagenesis and accelerates antibio-resistance through hypermutation development. In addition, we have previously demonstrated, that Mfd is a virulence factor for *B. cereus* and *S. flexneri* confering resistance to the host nitrogen immune response. Our knowledge about Mfd mainly relies on biochemical studies, and we lack information about Mfd functions in living cells and its role during bacterial virulence. Markedly, our work recapitulates how a molecular analysis and a 3D homology modeling of Mfd sequences from clinical and non-clinical bacterial strains, selected upon their utmost discrepancy, gives clues to decipher the sequence/structure/activity relationship of this complex protein. These data provide hints into the macromolecular phenotype associated with the Mfd protein. This allows a better understanding of the various roles plaid by this complex protein during bacterial adaptation and virulence.

Introduction

As the second causative agent of food-born outbreaks (FBO) in Europe [1], the virulence of the Gram positive bacteria *Bacillus cereus* is essential to be mastered at cellular and at molecular levels. Despite the ubiquitous presence of *B. cereus* in nature, the pathogenicity of a strain varies widely from avirulent to pathogenic [2]. *B. cereus* has been shown to cause severe local and systemic infections in humans, especially in immunocompromised people [3] and preterm neonates [4]. With its persistence over long periods of time in the environment, *B. cereus* is also responsible for many nosocomial infections [4, 5]. Many factors have already been identified and described as implicated in virulence, such as the cytotoxin K (CytK), the non-haemolytic enterotoxin (Nhe), the haemolysin BL (Hbl) [6-9] or enzymatic proteins such as InhA1 and CwpFM [10, 11]. Other factors are also implicated in *B. cereus* virulence and we have identified the Mutation Frequency Decline (Mfd) protein as a decisive determinant during bacterial pathogenesis [12].

Mfd is a highly conserved protein implicated in DNA repair *via* its interaction with the RNA polymerase (RNAP) [13]. Mfd is recruited at DNA damages sites where the RNAP is stalled. The protein has two main roles, timely regulated, the first one is to push the RNAP forward to dislocate it from the DNA template [13], the second role is subsequently to recruit UvrA in order to start DNA repair by the Nucleus Excision Repair pathway [14]. Mfd can also bind RNAP in the absence of exogenous damage, and cells lacking Mfd do not always display increased sensitivity to DNA-damaging agents. Moreover, even though Mfd is known to promote DNA repair, it paradoxically increases mutagenesis in specific contexts, such as at regions of replication-transcription conflicts and in stationary-phase mutagenesis. Accordingly, Mfd has been associated with the development of antibiotic resistance in *Campylobacter jejuni* and *Helicobacter pylori* [15, 16], and suggested as an evolvability factor that promotes hypermutation in bacteria, thus accelerating the evolution of antimicrobial resistance (AMR) [17]. Furthermore, Mfd thrives virulence in the Gram-positive *B. cereus* as well as in the Gram-negative *Shigella flexneri* species, and confers resistance to nitric oxide (NO) stress, a key step in the immune response, following infections [12, 18, 19].

The structure of the Mfd protein has been solved [14, 20]. Mfd is a multi-functional nanomachine of 1150 amino-acid residues, 3D arranged in eight structural domains and organized into 6 functional modules. At the N terminal of the protein, the D1a-D2-D1b region has its D2 domain homologous to the UvrB protein, thus allowing the recruitment and binding

to UvrA [14, 21]. Accordingly, it is called the UvrB-homology module. The D3 domain is of unknown function and often empassed with the D1a-D2-D1b domains as the N-terminal domain (NTD) [14]. The D4 domain is the RNAP Interacting Domain (RID), which specifically binds to the RNAP β subunit protrusion [14]. The D5 and D6 domains, respectively called TD1 and TD2 (Translocation Domain), hold the translocation module. This latter module is structurally homologous to helicases of the superfamily 2 (SF2), such as RecG [14], and shares both ATP binding and DNA binding sites. Even though this module presents a helicase motif VI, it acts as a double strand DNA translocase to push the stalled RNAP forward [22]. Finally, the D7 domain is of unknown function but could be a regulatory domain, as it holds Mfd back into a repressed and inactive conformation, hence preventing any ATP-ase activity. Indeed, within this arrangement, D2 and D7 domains are locked in together, rendering D2-mediated binding between Mfd and UvrA impossible [23].

We have previously shown that Mfd confers bacterial resistance to the host nitrogen (NO) response [12]. Production of reactive nitrogen species is a key step in the immune response following infections [19]. NO induces lesions to bacterial DNA, thus limiting bacterial growth within hosts. Mfd is involved in the DNA repair, ensuing NO-induced DNA damages, and is thus required for bacterial resistance to the host-NO-response. Consequently, a *B. cereus* mutant lacking Mfd is severely impaired in its virulence capacity in cell and animal models. As Mfd is widely conserved in the bacterial kingdom, these data highlight a mechanism possibly ubiquitous in bacteria to overcome the mutagenic host immune response.

In this study, we report a correlation between the sequence/structure of Mfd and its role in *B. cereus* virulence. Within a collection of strains displaying distinct pathological capability, we evaluated the impact of Mfd on the virulence and documented the hypothesis of a possible correlation between Mfd sequence signature and virulence phenotype. Accordingly, our data provide a better understanding of the structure/function relationship of Mfd on bacterial virulence and point out residue positions that could be critical for the dynamic remodeling along its functional cycle.

Methods

Bacterial strains and mutant construction.

The bacterial strain *B. thuringiensis* 407 Cry- (Bc 407) was used as a model for *B. cereus.* This strain has been cured of its plasmid, is acrystalliferous, and shows high phylogenic and

phenotypic similarity with the *B. cereus* reference strain ATCC 14579 and is therefore considered as a *B. cereus* strain [24]. The Bc 407 *Δmfd* was obtained through double homologous recombination using the thermosensitive vector pMAD and is described elsewhere [12].

Two strain libraries were used for the study. The first one is composed of 10 environmental strains collected from various sources that did not induced any infection [25]. The second is composed of 12 clinical strains isolated from 12 infected patients [26] (Tab 1, 2).

The S50 *Δmfd* and S53 *Δmfd* strains were obtained by double homologous recombination using the pAT113 plasmid [27] since it is not replicative in *B. cereus*. The upstream and downstream fragments of *mfd* from each strain and a tetracycline resistance cassette were cloned inside pAT113 by Genecust (Boynes, France). The two plasmids (pAT113_Δmfd_S50 and pAT113_Δmfd_S53) were transformed into the *E. coli* HB101 strain and then transferred by conjugation into the S50 and S53 strains. The donor strain and the receptor strain were mixed together at a ratio of (5:1) on a sterile membrane filter with a pore size of 0.45 µm (HAWP02500 Milipore) placed on BHI plates and incubated overnight at 37°C. After mating, the bacteria were resuspended and incubated at least 30' in 1.5 mL of colicine, centrifuged 5' at 3000 g, the supernatant discarded and resuspended again in 1.5 mL of colicine. The mutants were selected on BHI plates supplemented with 150 µg/mL of tetracycline and verified by PCR using primers upstream and downstream from the cloning region:

For S50: (5' – GTATGGGAATCGATCGTCCG – 3') and (5' – TTACAGACTTGCGCTCTTCC – 3')

For S53: (5' – GCATGGGAATTGATCGTCCG – 3') and (5' – AACTGGCAGCAGTATTGACC – 3').

All the complemented strains were obtained by using the pAT28 plasmid [28]. The sequence of *mfd* from the S50 and the S53 strains, as well as a modified sequence for the S53 strain, mfd_S53*, where four amino acids were permuted between the S50 and the S53 *mfd* sequences (Met131 → Ile131, Asp210 → Glu210, Tyr505 → His505 and Glu615 → Gly615) were cloned inside pAT28 by Genecust. The plasmids (pAT28_mfd_S50, pAT28_mfd_S53 and pAT28_mfd_S53*) were transformed into the *E. coli* HB101 strain and transferred into Bc 407 and S53 strains by conjugation as described above. The selection was done on BHI plates supplemented with 300 µg/mL of spectinomycin and verified by PCR using primers located on the plasmid:

(5' – CCCAGTCACGACGTTGTAAAA CG – 3') and (5' – AGCGGATAACAATTTCACACAGG – 3')

Sequence alignment

The multiple sequence alignment (MSA) of the 22 sequences of *mfd* was carried out using the algorithm MAFFT available from EMBL-EBI webtools, with Clustal output format (https://www.ebi.ac.uk/Tools/msa/mafft/). It was selected for its high precision, with its default FFT-NS-i parameters v7.487. Mfd sequences were grouped based on their identity.

Insect assay

Fourth instar silkworm larvae *Bombyx eri* were purchased from "L'office pour les insectes et leur environnement" (OPIE, Guyancourt, France). Larvae were reared with *Ligustrum vulgare* or *Ligustrum japonicum* until they reached 0.6 – 0.9 g. Prior to the assays, *B. eri* larvae were starved overnight and randomly distributed in groups of 10 to 15 per conditions. *B. cereus* strains were grown in LB medium at 37°C under agitation at 180 rpm until early exponential growth phase. Bacterial cultures were diluted in Phosphate Saline Buffer (PBS) to obtain 1.10^3 - $3,2.10^3$ CFU/injection. Larvae were injected with 20 µL of bacterial suspension in the haemolymphe *via* the last pro-leg. The injections were performed using a 1 mL hypodermic syringe with a 0.5 x 25 mm needle and an automated syringe pump (KD Scientific KDS 100). Post-injection, larvae were placed at 28°C for 24h where the survival rate was monitored.

***In silico* study of Mfd**

The Mfd protein structures of strains of *B. cereus* S50 and S53 were homology modelled using the sequence of Mfd from *E. coli strain K12* and MODELLER software version 9.18 (Dali and Blundell, 1993). Four distinct conformations were selected upon their relevance within the functional cycle, namely conformation L0 for "load zero state" (PDB code 2EYQ) [14], L2 (PDB code 6X2F), C1 (PDB code 6X2N) and C5 (PDB code 6X50), for first and last steps of the "nucleotide hydrolysis Cycle", respectively. Per template/strain, hundred models were computed, then the five best models were selected according to the MODELLER function and DOPE scores, and eventually, one model was kept upon stereochemical quality using PROCHECK v.6 (https://saves.mbi.ucla.edu/), and visual inspection using PyMOL v.2.5.2 (Schrödinger, LLC.: https://pymol.org/2/). Per template/strain, every model was 3D aligned onto D4 chosen as reference immobile segment, and using PyMOL, then substitutions were mapped. To evaluate the distortion per module, the commands align and angle from the PyMOL Plugin "angle between domains" were used.

Results

The sequences of Mfd clustered the strains according to their virulence

The prevalence of the *mfd* gene was evaluated using Blast, in a panel of *B. cereus* strains, either coming from environmental sources or isolated from infected patients. An *mfd* gene coding for an Mfd protein sequence was found for each of the 22 strains (not shown). The 22 Mfd protein sequences were retrieved, aligned and grouped according to their identity (Fig. 1). Overall, the MSA shows 98% of sequence identity, including 57 substitutions along the 1150 residues, with neither insertion nor deletion. This corresponds to a mutation ratio of 0.048. Beyond this high identity feature, the MSA separates the sequences in 3 main groups (yellow, red and blue in Fig. 1 and Fig. 2): one group contains Mfd from environmental strains (blue), a second one contains Mfd from clinical strains (yellow), and three sequences (red), coming from both clinical and not clinical strains intertwin at the median position called "twilight zone", due to strong similarity at these borders.

This clustering, within highly similar sequences, suggests a possible correlation between sequences of Mfd and virulence of a strain. To document this hypothesis, the Mfd from the two strains S50 (for the environmental group) and S53 (for the clinical group) that are the most distinct, hence that aggregate the most numerous differences, were selected for experimental tracking of virulence. S50 and S53 are positioned at the extremities of the MSA, and cumulate a total of 28 mutations.

Mfd is implicated in B. cereus virulence in vivo

First, the virulence of the two strains S50 and S53 was assessed in the insect *Bombyx eri* infection model (Fig. 3A). Infection with the S50 strain led to over 90% of insect survival, whereas infection with the S53 strain showed a decrease in insect survival to 28%. Thus, the S53 strain is virulent in this model while the S50 is not.

Then, we aimed to document the role of Mfd in strain virulence by comparing insect survival in the wild type strains and the Δ*mfd* mutants. No difference in virulence was observed between the S50 and the S50Δ*mfd* strains, with none of them inducing a significant decrease in insect survival (Fig. 3B). By contrast, the S53Δ*mfd* mutant was strongly impaired in its virulence capacity compared to the wild type S53 strain, with insect survival reaching 53% and 28%, respectively (Fig. 3C). Furthermore, complementation of the S53Δ*mfd* mutant by *mfd* of

the S53 strain partially restored the virulence. These data suggest that Mfd plays an essential role in promoting virulence of pathogenic strains.

The sequence/structure of Mfd dictates virulence

The impact of the Mfd proteins from the two strains was assessed on the laboratory strain Bc407 (Fig. 4). A deletion of *mfd* in the Bc407 strain induces a decrease of virulence compared to the wild type, confirming the role of Mfd in the virulence of this strain, as previously described [12]. The complementation of the Bc407Δ*mfd* mutant with the *mfd* sequence of the S50 strain did not lead to an increased virulence. By contrast, the complementation of the Bc407Δ*mfd* mutant with the *mfd* sequence of the S53 strain induced an increase of virulence to a level similar to the one obtained with the wild type Bc407 strain. These data further confirm that the Mfd protein differs from one strain to another and that the role of Mfd in the pathogenicity of a strain is linked to its sequence.

In silico analysis of Mfd sequences and structures

The alignment of the Mfd sequences from strains S50 and S53 revealed 98% identity. Overall, the 28 counted differences are unpredictably disseminated along the 7 domains (Fig. 5). Table 3 compiles the number, amino-acid residue substitution and domain location for each mutation. The most conserved domains are D4 and D5 with a single substitution per domain, while D3, D6 and D7 domains show 3, 2 and 3 differences, respectively. Domains D1a, D2 and D1b are more prone to substitutions and this module gathered 60% of the differences, with 17 out of 28 mutations between the two sequences. S53 contains 6 mutations into charged residues. Overall, there is no difference in positively charged residues in both strains and only three more negatively charged residues in S53 (185 *vs* 182), which does not impact the pI of 5.4 for both strains. Those substitutions were mapped onto Mfd_{S50} and Mfd_{S53} homology modeled from the auto-repressed conformation of $Mfd_{E.coli}$. The discrepancies are disseminated in the structure, nevertheless two sets of residues cluster in 3D. One gathers $Lys51_{S53}$ and $His115_{S53}$, both in D1a, to connect with $Asp304_{S53}$ in D1b, the other assembles together $Met131_{S53}$, $Ser238_{S53}$ and $Asn292_{S53}$ that belong to D1a, D2, D1b, respectively. These nexuses suggest that they could participate to mobilize the three subdomains into a more rigid module. $Asp210_{S53}$ of D2 is located in the center of Mfd, where it interacts with a polar segment of the D3-D4 super linker. Also, $Glu439_{S53}$, $Ile442_{S53}$ and $Leu466_{S53}$ of domain D3 are

interesting because they share an interface with UvrB-like module. Similarly, $Tyr505_{S53}$ of D4 points towards D5, and $Glu615_{S53}$ of D5 forms a salt bridge with $Lys422_{S53}$ from D3. The remaining mutations in coils are inserted inside or at the junction between functional modules. Because, we assume that these substitutions could be involved in the conformational remodelling of the protein, through rigid body motions of the modules, we document the possible impact of those mutations along the structural rearrangement. Accordingly, we selected four critical conformations of $Mfd_{E.\ coli}$, coming either from crystallographic or from cryo-EM experiments, and used them as conformational templates for Mfd_{S53} along this structure/function course. The first conformation is called L0 (load zero) and describes the auto-repressed inactive structure (PDB code: 2EYQ) [29], the second is called L2 and refers to the Mfd loaded onto RNAP and double strand DNA (PDB code 6X2F), the third and fourth are called C1 and C5, and correspond to the first and last steps of the nucleotide hydrolysis cycle, respectively (PDB code 6X2N and 6X50) [30]. From conformations L0, L2, C1 to C5, the angles, rms deviations and displacements were evaluated for Mfd full length and within each module (Fig. 6). These measurements, and especially the rms measured per module that is always lower that 1.3 Å, emphasize that UvrB-like enlarged to D3, D4 and D7 move each as one entity block, only D5/D6 translocase module undergoes an internal conformational change but this amplitude is rather small. The largest remodelings occur between conformations L0 and L2 then C1, and evidence that the modules move rigid blocks. Indeed, the first movement is triggered by UvrB-like enlarged to D3 module that unlocks from D7. It is highlighted by the extension of the super D4-D5 linker -also called relay helix- that unfolds from helix and expand to position the two modules more than 25 Å far from each other. The second change is the elongation of D4 that pops out of the Mfd core due to the unwinding of super linker D3-D4. As a conclusion, due to their location within coils, most of the substitutions could tune the internal flexibility within each module and adjust cautiously the remodeling. Reversely the largest conformational changes could be supported by the two central super linkers that connect D3 to D4 and D4 to D5 (relay helix).

Study of relation sequence/structure in the virulence of S53

The S53*Δmfd* strain complemented with its own entire *mfd* showed an increased virulence capacity compared to the S53*Δmfd* strain to a level almost similar to the wild type strain. Then, the impact of Mfd amino acid sequence was assessed on the S53*Δmfd* strain. We

complemented the strain with a modified sequence of *mfd* leading to a modification of the amino acid sequence: four amino acids where changed to the ones present on the Mfd from the S50 strain. Met131 was changed to Ile131, Asp210 to Glu210, Tyr505 to His505 and Glu615 to Gly615 since those permutations could potentially lead to conformational or activity modification as stated previously. The mutant complemented with the modified sequence showed a virulence significantly higher than the S53*Δmfd* strain and similar to the wild type strain (Fig. 3C). Thus, those mutations are not sufficient to explain the difference of virulence between the S50 and S53 strains.

Discussion

This study reports the importance of the Mfd sequence in the virulence of *B. cereus*. Despite a very high homology degree, we show that a few modifications can induce a change of virulence. We did an in-depth study of the Mfd sequences in order to identify the source of this change in virulence. Hence, we combine *in vitro* sequence investigation with *in silico* sequence/structure analysis. *In silico*, we showed that there is a clear distinction in the Mfd sequences between environmental and clinical strains. Stepping further into a molecular comprehension of this trait, we hypothesize that few modifications, critically positioned in the 3D structure, could induce a change in the remodeling of Mfd along its functional cycle and result in distinct virulence. Particularly, we now proposed the rational mutations of Met131, Asp210, His505 and Glu615 residues that differ between S50 and S53, because they could tune Mfd structural remodeling or partnering and thus alleviate Mfd functions. Their role could be similar to Arg165 in D2 domain of *S. typhimurium* and Leu499 for L499R in RID of *E. coli*, whose mutations into Ala and Arg could alter their interaction with D7 and RID, respectively [17]. D3-D4 super linker and RH are strictly conserved, hence emphasizing their crucial role, possibly to trigger the revolution of Mfd throughout the structure/function cycle. Also, we cannot exclude that any change in their sphere of interaction along the cycle could not have tremendous functional consequences. Overall, how this could correlate to the virulence is hard to explain and dissecting the conformational clock of Mfd-dependent transcription is a challenge that has been addressed [20, 30]. Nevertheless, our description is a first step and their identification as functional *per se* domains is an advance.

In parallel, we demonstrated *in vivo* that deleting *mfd* from a clinical strain induces a clear increase of the insect survival while that same mutation has no impact on the environmental

strain. Hence, our study confirms Mfd as a virulence factor but reinforces the role of the activity of the protein in itself where slight modifications on the sequence could induce a change of activity. Markedly, we did observe a similar clustering between Mfd from virulent *Listeria monocytogenes* as compared to *Listeria innocua* (Supp Fig. 1). These results highlight a possible universal difference in the Mfd sequences of virulent strains compared to non-pathogenic ones. This feature could lead to propose Mfd as biomarker for virulence phenotype.

Figure legends

Fig 1: Mdf sequences alignment from *B. cereus* strains

The Mfd sequence of 10 environmental and 12 clinical strains of *B. cereus* were aligned using the algorithm MAFFT available from EMBL-EBI webtools, with Clustal output format. The sequences were ordered depending of the differences found. Each colour represents different phylogenetic groups.

Fig 2: Phylogenic tree

The Mfd sequence of 10 environmental and 12 clinical strains of *B. cereus* were aligned using the algorithm MAFFT available from EMBL-EBI webtools, with Clustal output format. The sequences were ordered depending of the differences found and the corresponding phylogenic tree was build.

Fig 3: Implication of Mfd in the difference of virulence between S50 and S53 strains

B. eri larvea were injected with S50, S53, S50*Δmfd*, S53*Δmfd,* S53*ΔmfdΩmfd_53* and S53 *ΔmfdΩmfd_53** in early exponential phase and insect survival rate was monitored 24h post injection. Error bars show SEM and P value is calculated using Mann-Whitney test (** $p < 0.01$; **** $p < 0.0001$).

Fig 4: Impact of *mfd* complementation in the virulence of Bc407 strain in insect

B. eri larvea were injected with Bc407, Bc407 *Δmfd*, Bc407 *ΔmfdΩmfd_50* and Bc407 *ΔmfdΩmfd_53* in early exponential phase. Survival rate was monitored 24h post injection. Error bars show SEM and P value is calculated using Mann-Whitney test (**** $p<0.0001$, * $p<0.05$).

Fig 5: Mapping of the mutations between Mfd of S50 and S53 strains on the homology model of S53

The homology model of Mfd, built on sequence of S53 representative of the clinical group, is shown as surface. The modules are colored with respect to a color code that runs along the paper with D1a in dark blue, D2 in cyan, D1b in blue, D3 in orange, RID D4 in pink, TD1-D5 in green, D6 in yellow, D7 in red. Each module except the highly conserved D4-D6 is highlighted as a cartoon within a close view where the substitutions are displayed with dots.

Upper part: close view of the nexus within the N-terminal domain and the role of Met131. Lower part: close view of the salt-bridged interactions connecting Asp210 from D2 to the D3-D4 super linker.

Fig. 6: Mapping of Mfd of S53 in the different Mfd conformations

Homology modeling of Mfd from S53 in four critical conformations: L0 (load zero) that describes the auto-repressed inactive structure (PDB code: 2EYQ), L2 that refers to the Mfd loaded onto RNAP and double strand DNA (PDB code 6X2F), C1 and C5 corresponding to the first and last steps of the nucleotide hydrolysis cycle, respectively (PDB code 6X2N and 6X50).

Sup Fig 1: Mdf sequence alignment from *L. monocytogenes* and *L. innocua* strains

The Mfd sequences of 27 *L. innocua* strains and 32 *L. monocytogenes* strains were aligned using the algorithm MAFFT available from EMBL-EBI webtools, with Clustal output format. That way the sequences were ordered depending of the differences found. Each colour represents different phylogenetic groups.

References

1. Journal, T.E., *The Community Summary Report on Food-Borne Outbreaks in The European Union in 2007.* EFSA Journal, 2009. **271**.
2. Stenfors Arnesen, L.P., A. Fagerlund, and P.E. Granum, *From soil to gut: Bacillus cereus and its food poisoning toxins.* FEMS Microbiol Rev, 2008. **32**(4): p. 579-606.
3. Bottone, E.J., *Bacillus cereus, a volatile human pathogen.* Clin Microbiol Rev, 2010. **23**(2): p. 382-98.
4. Cormontagne, D., et al., *Bacillus cereus Induces Severe Infections in Preterm Neonates: Implication at the Hospital and Human Milk Bank Level.* Toxins (Basel), 2021. **13**(2).
5. Glasset, B., et al., *Bacillus cereus-induced food-borne outbreaks in France, 2007 to 2014: epidemiology and genetic characterisation.* Euro Surveill, 2016. **21**(48).
6. Lund, T., M.L. De Buyser, and P.E. Granum, *A new cytotoxin from Bacillus cereus that may cause necrotic enteritis.* Mol Microbiol, 2000. **38**(2): p. 254-61.
7. Fagerlund, A., et al., *Bacillus cereus Nhe is a pore-forming toxin with structural and functional properties similar to the ClyA (HlyE, SheA) family of haemolysins, able to induce osmotic lysis in epithelia.* Microbiology (Reading), 2008. **154**(Pt 3): p. 693-704.
8. Lund, T. and P.E. Granum, *Characterisation of a non-haemolytic enterotoxin complex from Bacillus cereus isolated after a foodborne outbreak.* FEMS Microbiol Lett, 1996. **141**(2-3): p. 151-6.
9. Beecher, D.J., et al., *Extracellular virulence factors in Bacillus cereus endophthalmitis: methods and implication of involvement of hemolysin BL.* Infect Immun, 1995. **63**(2): p. 632-9.
10. Haydar, A., et al., *InhA1-Mediated Cleavage of the Metalloprotease NprA Allows Bacillus cereus to Escape From Macrophages.* Front Microbiol, 2018. **9**: p. 1063.
11. Tran, S.L., et al., *Structural Modeling of Cell Wall Peptidase CwpFM (EntFM) Reveals Distinct Intrinsically Disordered Extensions Specific to Pathogenic Bacillus cereus Strains.* Toxins (Basel), 2020. **12**(9).
12. Guillemet, E., et al., *The bacterial DNA repair protein Mfd confers resistance to the host nitrogen immune response.* Sci Rep, 2016. **6**: p. 29349.
13. Roberts, J. and J.S. Park, *Mfd, the bacterial transcription repair coupling factor: translocation, repair and termination.* Curr Opin Microbiol, 2004. **7**(2): p. 120-5.
14. Deaconescu, A.M., et al., *Structural basis for bacterial transcription-coupled DNA repair.* Cell, 2006. **124**(3): p. 507-20.
15. Han, J., et al., *Key role of Mfd in the development of fluoroquinolone resistance in Campylobacter jejuni.* PLoS Pathog, 2008. **4**(6): p. e1000083.
16. Lee, G.H., et al., *The Helicobacter pylori Mfd protein is important for antibiotic resistance and DNA repair.* Diagn Microbiol Infect Dis, 2009. **65**(4): p. 454-6.
17. Ragheb, M.N., et al., *Inhibiting the Evolution of Antibiotic Resistance.* Mol Cell, 2019. **73**(1): p. 157-165 e5.
18. Darrigo, C., et al., *The Bacterial Mfd Protein Prevents DNA Damage Induced by the Host Nitrogen Immune Response in a NER-Independent but RecBC-Dependent Pathway.* PLoS One, 2016. **11**(10): p. e0163321.
19. Porrini, C., N. Ramarao, and S.L. Tran, *Dr. NO and Mr. Toxic - the versatile role of nitric oxide.* Biol Chem, 2020. **401**(5): p. 547-572.

20. Brugger, C., et al., *Molecular determinants for dsDNA translocation by the transcription-repair coupling and evolvability factor Mfd.* Nat Commun, 2020. **11**(1): p. 3740.
21. Assenmacher, N., et al., *Structural basis for transcription-coupled repair: the N terminus of Mfd resembles UvrB with degenerate ATPase motifs.* J Mol Biol, 2006. **355**(4): p. 675-83.
22. Park, J.S., M.T. Marr, and J.W. Roberts, *E. coli Transcription repair coupling factor (Mfd protein) rescues arrested complexes by promoting forward translocation.* Cell, 2002. **109**(6): p. 757-67.
23. Deaconescu, A.M., N. Savery, and S.A. Darst, *The bacterial transcription repair coupling factor.* Curr Opin Struct Biol, 2007. **17**(1): p. 96-102.
24. Lereclus, D., et al., *Transformation and expression of a cloned delta-endotoxin gene in Bacillus thuringiensis.* FEMS Microbiol Lett, 1989. **51**(1): p. 211-7.
25. Kamar, R., et al., *Pathogenic potential of Bacillus cereus strains as revealed by phenotypic analysis.* J Clin Microbiol, 2013. **51**(1): p. 320-3.
26. Glasset, B., et al., *Bacillus cereus, a serious cause of nosocomial infections: Epidemiologic and genetic survey.* PLoS One, 2018. **13**(5): p. e0194346.
27. Trieu-Cuot, P., et al., *An integrative vector exploiting the transposition properties of Tn1545 for insertional mutagenesis and cloning of genes from gram-positive bacteria.* Gene, 1991. **106**(1): p. 21-7.
28. Trieu-Cuot, P., et al., *A pair of mobilizable shuttle vectors conferring resistance to spectinomycin for molecular cloning in Escherichia coli and in gram-positive bacteria.* Nucleic Acids Res, 1990. **18**(14): p. 4296.
29. Sali, A. and T.L. Blundell, *Comparative protein modelling by satisfaction of spatial restraints.* J Mol Biol, 1993. **234**(3): p. 779-815.
30. Kang, J.Y., et al., *Structural basis for transcription complex disruption by the Mfd translocase.* Elife, 2021. **10**.

Tab. 1 : Environmental strains used in this study

Strains	Origin
INRA PF (S9)	Milk protein
I13 (S10)	Cooked rice
INRA 5 (S11)	Pasteurized zucchini purée
INRA C64 (S12)	Pasteurized vegetables
ADRIA I3 (S13)	Cooked foods
INRA A3 (S38)	Startch
INRA SL' (S44)	Soil
I2 (S46)	Dried fruit
ADRIA I21 (S50)	Cooked foods
WSBC 10204 (S52)	Pasteurized milk

Tab. 2 : Clinical strains used in this study

Strains	Origin	Outcome
09CEB13BAC (S6)	Blood culture, New born	ND
09CEB14BAC (S7)	Blood culture, New born	ND
09CEB33BAC (S8)	Cutaneous, New born	ND
12CEB31BAC (S14)	Blood bulture, New born	Death
13CEB06BAC (S15)	Arterial catheter, New born	ND
09CEB11BAC (S16)	Blood culture, New born	Death
09CEB31BAC (S17)	Central catheter, New born	ND
09CEB12BAC (S53)	Meninge, New born	Death
09CEB17BAC (S55)	Neo-natal unit	
09CEB34BAC (S59)	Gastric tube, New born	ND
09CEB36BAC (S61)	Central catheter, New born	ND
09CEB37BAC (S62)	Neo-natal intensive care unit	

ND : Not disclosed

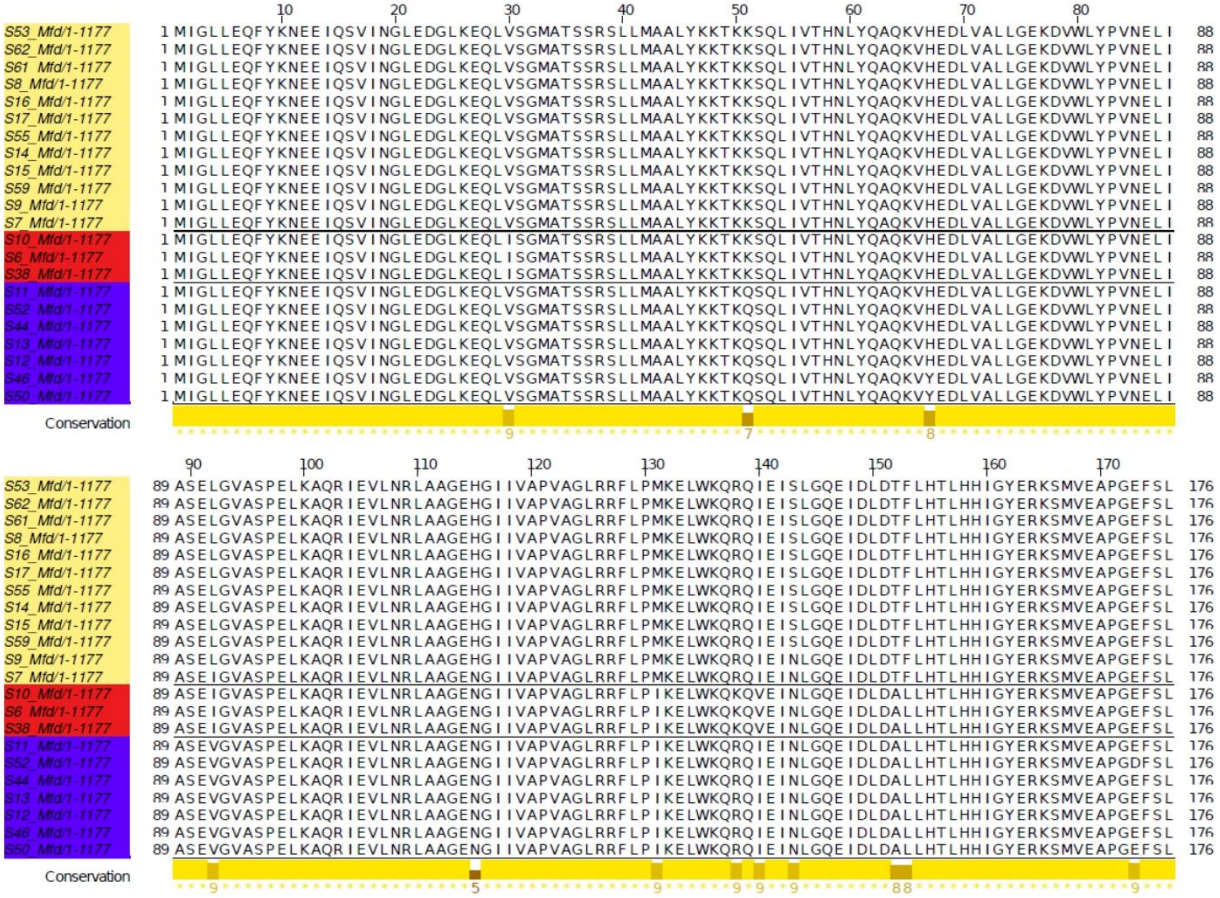

Fig 1

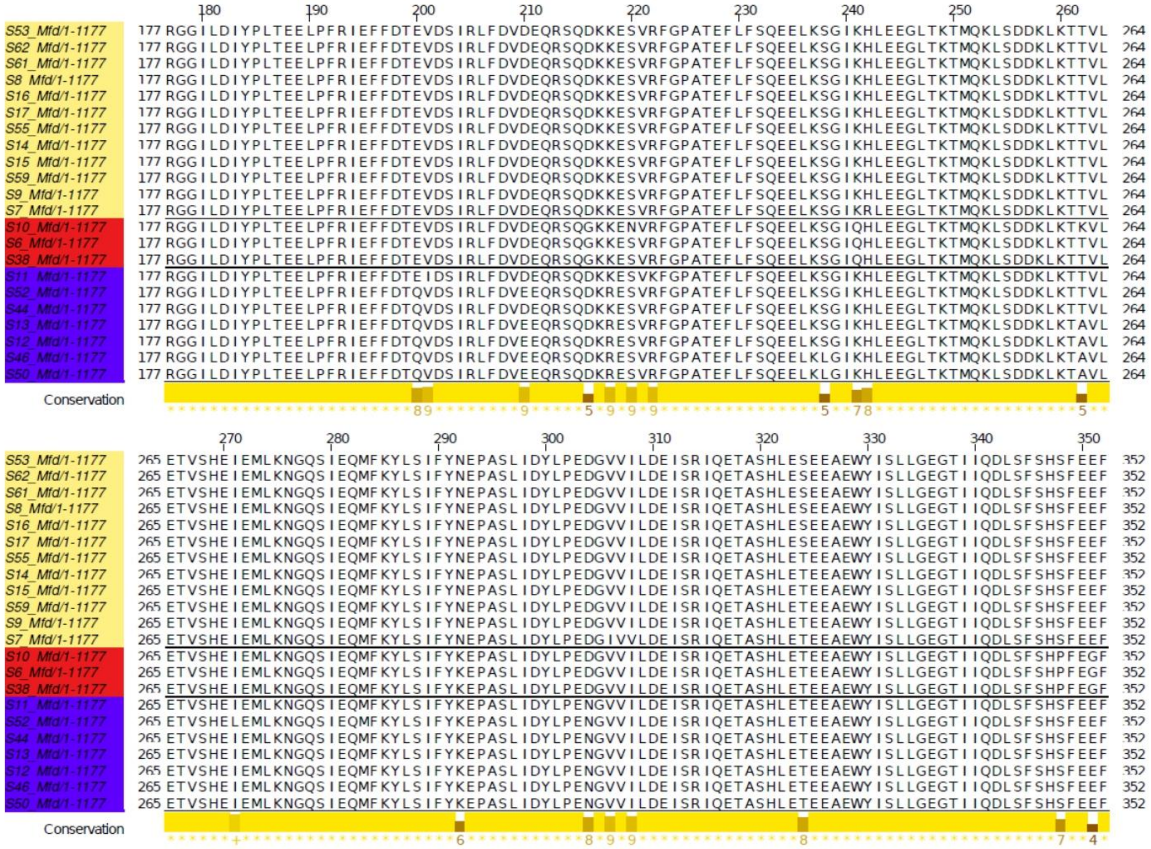
S53_Mfd/1-1177
S62_Mfd/1-1177
S61_Mfd/1-1177
S8_Mfd/1-1177
S16_Mfd/1-1177
S17_Mfd/1-1177
S55_Mfd/1-1177
S14_Mfd/1-1177
S15_Mfd/1-1177
S59_Mfd/1-1177
S9_Mfd/1-1177
S7_Mfd/1-1177
S10_Mfd/1-1177
S6_Mfd/1-1177
S38_Mfd/1-1177
S11_Mfd/1-1177
S52_Mfd/1-1177
S44_Mfd/1-1177
S13_Mfd/1-1177
S12_Mfd/1-1177
S46_Mfd/1-1177
S50_Mfd/1-1177
Conservation

Fig 1

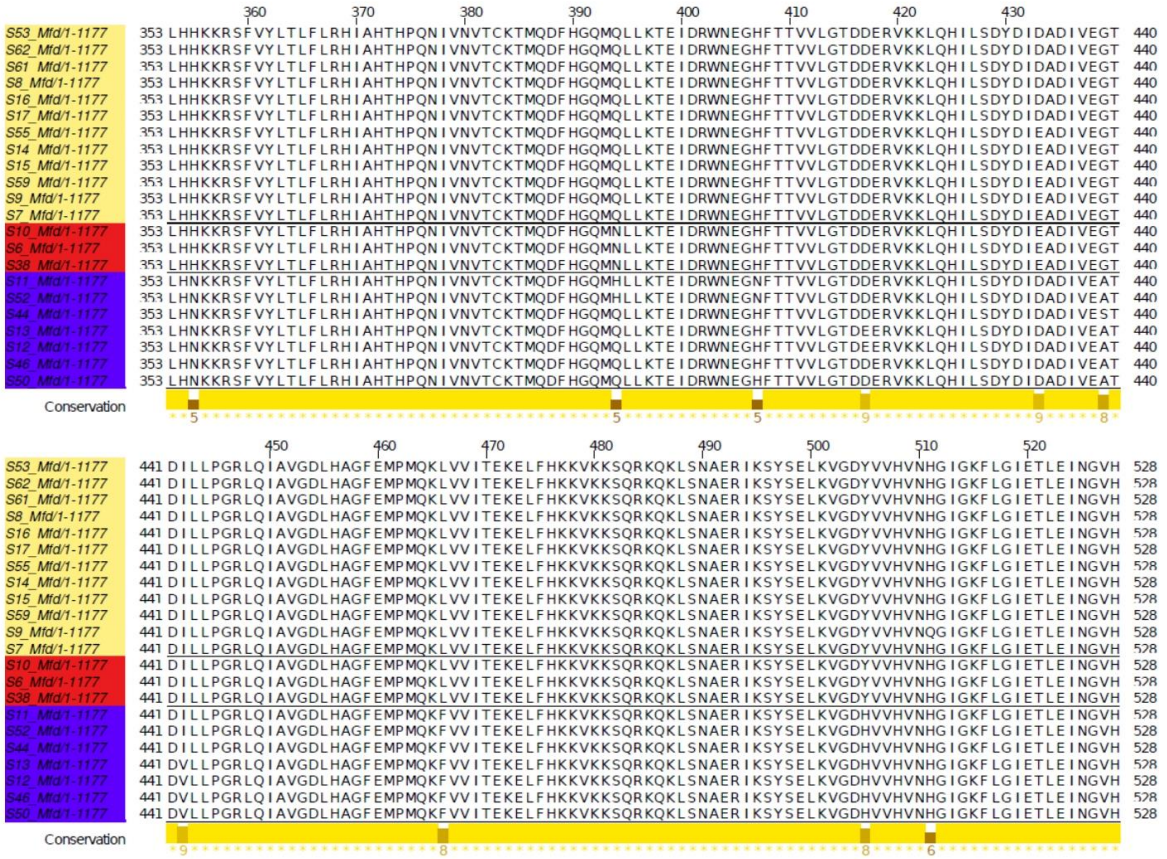
S53_Mfd/1-1177
S62_Mfd/1-1177
S61_Mfd/1-1177
S8_Mfd/1-1177
S16_Mfd/1-1177
S17_Mfd/1-1177
S55_Mfd/1-1177
S14_Mfd/1-1177
S15_Mfd/1-1177
S59_Mfd/1-1177
S9_Mfd/1-1177
S7_Mfd/1-1177
S10_Mfd/1-1177
S6_Mfd/1-1177
S38_Mfd/1-1177
S11_Mfd/1-1177
S52_Mfd/1-1177
S44_Mfd/1-1177
S13_Mfd/1-1177
S12_Mfd/1-1177
S46_Mfd/1-1177
S50_Mfd/1-1177
Conservation

Fig 1

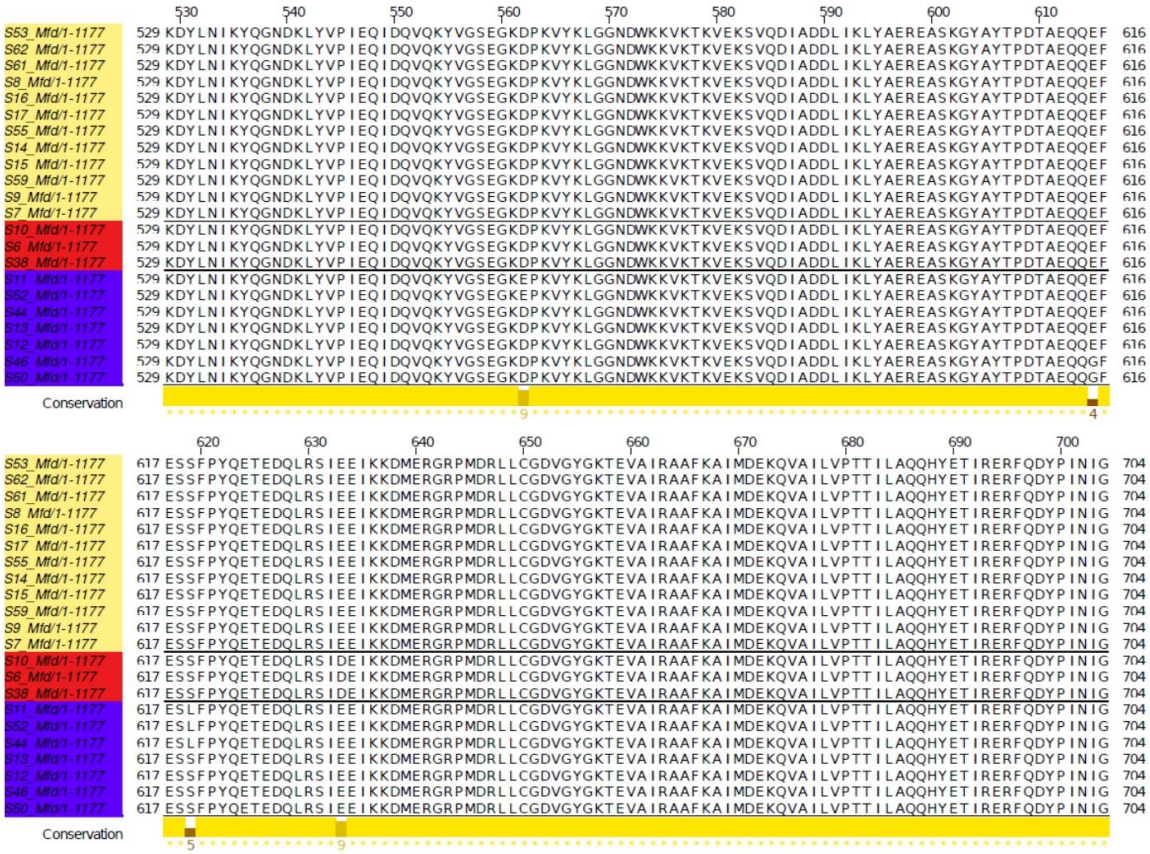
530 540 550 560 570 580 590 600 610
S53_Mfd/1-1177 529 KDYLNIKYQGNDKLYVPIEQIDQVQKYVGSEGKDPKVYKLGGNDWKKVKTKVEKSVQDIADDLIKLYAEREASKGYAYTPDTAEQQEF 616
S62_Mfd/1-1177 529 KDYLNIKYQGNDKLYVPIEQIDQVQKYVGSEGKDPKVYKLGGNDWKKVKTKVEKSVQDIADDLIKLYAEREASKGYAYTPDTAEQQEF 616
S61_Mfd/1-1177 529 KDYLNIKYQGNDKLYVPIEQIDQVQKYVGSEGKDPKVYKLGGNDWKKVKTKVEKSVQDIADDLIKLYAEREASKGYAYTPDTAEQQEF 616
S8_Mfd/1-1177 529 KDYLNIKYQGNDKLYVPIEQIDQVQKYVGSEGKDPKVYKLGGNDWKKVKTKVEKSVQDIADDLIKLYAEREASKGYAYTPDTAEQQEF 616
S16_Mfd/1-1177 529 KDYLNIKYQGNDKLYVPIEQIDQVQKYVGSEGKDPKVYKLGGNDWKKVKTKVEKSVQDIADDLIKLYAEREASKGYAYTPDTAEQQEF 616
S17_Mfd/1-1177 529 KDYLNIKYQGNDKLYVPIEQIDQVQKYVGSEGKDPKVYKLGGNDWKKVKTKVEKSVQDIADDLIKLYAEREASKGYAYTPDTAEQQEF 616
S55_Mfd/1-1177 529 KDYLNIKYQGNDKLYVPIEQIDQVQKYVGSEGKDPKVYKLGGNDWKKVKTKVEKSVQDIADDLIKLYAEREASKGYAYTPDTAEQQEF 616
S14_Mfd/1-1177 529 KDYLNIKYQGNDKLYVPIEQIDQVQKYVGSEGKDPKVYKLGGNDWKKVKTKVEKSVQDIADDLIKLYAEREASKGYAYTPDTAEQQEF 616
S15_Mfd/1-1177 529 KDYLNIKYQGNDKLYVPIEQIDQVQKYVGSEGKDPKVYKLGGNDWKKVKTKVEKSVQDIADDLIKLYAEREASKGYAYTPDTAEQQEF 616
S59_Mfd/1-1177 529 KDYLNIKYQGNDKLYVPIEQIDQVQKYVGSEGKDPKVYKLGGNDWKKVKTKVEKSVQDIADDLIKLYAEREASKGYAYTPDTAEQQEF 616
S9_Mfd/1-1177 529 KDYLNIKYQGNDKLYVPIEQIDQVQKYVGSEGKDPKVYKLGGNDWKKVKTKVEKSVQDIADDLIKLYAEREASKGYAYTPDTAEQQEF 616
S7_Mfd/1-1177 529 KDYLNIKYQGNDKLYVPIEQIDQVQKYVGSEGKDPKVYKLGGNDWKKVKTKVEKSVQDIADDLIKLYAEREASKGYAYTPDTAEQQEF 616
S10_Mfd/1-1177 529 KDYLNIKYQGNDKLYVPIEQIDQVQKYVGSEGKDPKVYKLGGNDWKKVKTKVEKSVQDIADDLIKLYAEREASKGYAYTPDTAEQQEF 616
S6_Mfd/1-1177 529 KDYLNIKYQGNDKLYVPIEQIDQVQKYVGSEGKDPKVYKLGGNDWKKVKTKVEKSVQDIADDLIKLYAEREASKGYAYTPDTAEQQEF 616
S38_Mfd/1-1177 529 KDYLNIKYQGNDKLYVPIEQIDQVQKYVGSEGKDPKVYKLGGNDWKKVKTKVEKSVQDIADDLIKLYAEREASKGYAYTPDTAEQQEF 616
S11_Mfd/1-1177 529 KDYLNIKYQGNDKLYVPIEQIDQVQKYVGSEGKEPKVYKLGGNDWKKVKTKVEKSVQDIADDLIKLYAEREASKGYAYTPDTAEQQEF 616
S52_Mfd/1-1177 529 KDYLNIKYQGNDKLYVPIEQIDQVQKYVGSEGKEPKVYKLGGNDWKKVKTKVEKSVQDIADDLIKLYAEREASKGYAYTPDTAEQQEF 616
S44_Mfd/1-1177 529 KDYLNIKYQGNDKLYVPIEQIDQVQKYVGSEGKDPKVYKLGGNDWKKVKTKVEKSVQDIADDLIKLYAEREASKGYAYTPDTAEQQEF 616
S13_Mfd/1-1177 529 KDYLNIKYQGNDKLYVPIEQIDQVQKYVGSEGKDPKVYKLGGNDWKKVKTKVEKSVQDIADDLIKLYAEREASKGYAYTPDTAEQQEF 616
S12_Mfd/1-1177 529 KDYLNIKYQGNDKLYVPIEQIDQVQKYVGSEGKDPKVYKLGGNDWKKVKTKVEKSVQDIADDLIKLYAEREASKGYAYTPDTAEQQEF 616
S46_Mfd/1-1177 529 KDYLNIKYQGNDKLYVPIEQIDQVQKYVGSEGKDPKVYKLGGNDWKKVKTKVEKSVQDIADDLIKLYAEREASKGYAYTPDTAEQQGF 616
S50_Mfd/1-1177 529 KDYLNIKYQGNDKLYVPIEQIDQVQKYVGSEGKDPKVYKLGGNDWKKVKTKVEKSVQDIADDLIKLYAEREASKGYAYTPDTAEQQGF 616
Conservation
620 630 640 650 660 670 680 690 700
S53_Mfd/1-1177 617 ESSFPYQETEDQLRSIEEIKKDMERGRPMDRLLCGDVGYGKTEVAIRAAFKAIMDEKQVAILVPTTILAQQHYETIRERFQDYPINIG 704
S62_Mfd/1-1177 617 ESSFPYQETEDQLRSIEEIKKDMERGRPMDRLLCGDVGYGKTEVAIRAAFKAIMDEKQVAILVPTTILAQQHYETIRERFQDYPINIG 704
S61_Mfd/1-1177 617 ESSFPYQETEDQLRSIEEIKKDMERGRPMDRLLCGDVGYGKTEVAIRAAFKAIMDEKQVAILVPTTILAQQHYETIRERFQDYPINIG 704
S8_Mfd/1-1177 617 ESSFPYQETEDQLRSIEEIKKDMERGRPMDRLLCGDVGYGKTEVAIRAAFKAIMDEKQVAILVPTTILAQQHYETIRERFQDYPINIG 704
S16_Mfd/1-1177 617 ESSFPYQETEDQLRSIEEIKKDMERGRPMDRLLCGDVGYGKTEVAIRAAFKAIMDEKQVAILVPTTILAQQHYETIRERFQDYPINIG 704
S17_Mfd/1-1177 617 ESSFPYQETEDQLRSIEEIKKDMERGRPMDRLLCGDVGYGKTEVAIRAAFKAIMDEKQVAILVPTTILAQQHYETIRERFQDYPINIG 704
S55_Mfd/1-1177 617 ESSFPYQETEDQLRSIEEIKKDMERGRPMDRLLCGDVGYGKTEVAIRAAFKAIMDEKQVAILVPTTILAQQHYETIRERFQDYPINIG 704
S14_Mfd/1-1177 617 ESSFPYQETEDQLRSIEEIKKDMERGRPMDRLLCGDVGYGKTEVAIRAAFKAIMDEKQVAILVPTTILAQQHYETIRERFQDYPINIG 704
S15_Mfd/1-1177 617 ESSFPYQETEDQLRSIEEIKKDMERGRPMDRLLCGDVGYGKTEVAIRAAFKAIMDEKQVAILVPTTILAQQHYETIRERFQDYPINIG 704
S59_Mfd/1-1177 617 ESSFPYQETEDQLRSIEEIKKDMERGRPMDRLLCGDVGYGKTEVAIRAAFKAIMDEKQVAILVPTTILAQQHYETIRERFQDYPINIG 704
S9_Mfd/1-1177 617 ESSFPYQETEDQLRSIEEIKKDMERGRPMDRLLCGDVGYGKTEVAIRAAFKAIMDEKQVAILVPTTILAQQHYETIRERFQDYPINIG 704
S7_Mfd/1-1177 617 ESSFPYQETEDQLRSIEEIKKDMERGRPMDRLLCGDVGYGKTEVAIRAAFKAIMDEKQVAILVPTTILAQQHYETIRERFQDYPINIG 704
S10_Mfd/1-1177 617 ESSFPYQETEDQLRSIDEIKKDMERGRPMDRLLCGDVGYGKTEVAIRAAFKAIMDEKQVAILVPTTILAQQHYETIRERFQDYPINIG 704
S6_Mfd/1-1177 617 ESSFPYQETEDQLRSIDEIKKDMERGRPMDRLLCGDVGYGKTEVAIRAAFKAIMDEKQVAILVPTTILAQQHYETIRERFQDYPINIG 704
S38_Mfd/1-1177 617 ESSFPYQETEDQLRSIDEIKKDMERGRPMDRLLCGDVGYGKTEVAIRAAFKAIMDEKQVAILVPTTILAQQHYETIRERFQDYPINIG 704
S11_Mfd/1-1177 617 ESLFPYQETEDQLRSIEEIKKDMERGRPMDRLLCGDVGYGKTEVAIRAAFKAIMDEKQVAILVPTTILAQQHYETIRERFQDYPINIG 704
S52_Mfd/1-1177 617 ESLFPYQETEDQLRSIEEIKKDMERGRPMDRLLCGDVGYGKTEVAIRAAFKAIMDEKQVAILVPTTILAQQHYETIRERFQDYPINIG 704
S44_Mfd/1-1177 617 ESLFPYQETEDQLRSIEEIKKDMERGRPMDRLLCGDVGYGKTEVAIRAAFKAIMDEKQVAILVPTTILAQQHYETIRERFQDYPINIG 704
S13_Mfd/1-1177 617 ESSFPYQETEDQLRSIEEIKKDMERGRPMDRLLCGDVGYGKTEVAIRAAFKAIMDEKQVAILVPTTILAQQHYETIRERFQDYPINIG 704
S12_Mfd/1-1177 617 ESSFPYQETEDQLRSIEEIKKDMERGRPMDRLLCGDVGYGKTEVAIRAAFKAIMDEKQVAILVPTTILAQQHYETIRERFQDYPINIG 704
S46_Mfd/1-1177 617 ESSFPYQETEDQLRSIEEIKKDMERGRPMDRLLCGDVGYGKTEVAIRAAFKAIMDEKQVAILVPTTILAQQHYETIRERFQDYPINIG 704
S50_Mfd/1-1177 617 ESSFPYQETEDQLRSIEEIKKDMERGRPMDRLLCGDVGYGKTEVAIRAAFKAIMDEKQVAILVPTTILAQQHYETIRERFQDYPINIG 704
Conservation

Fig 1

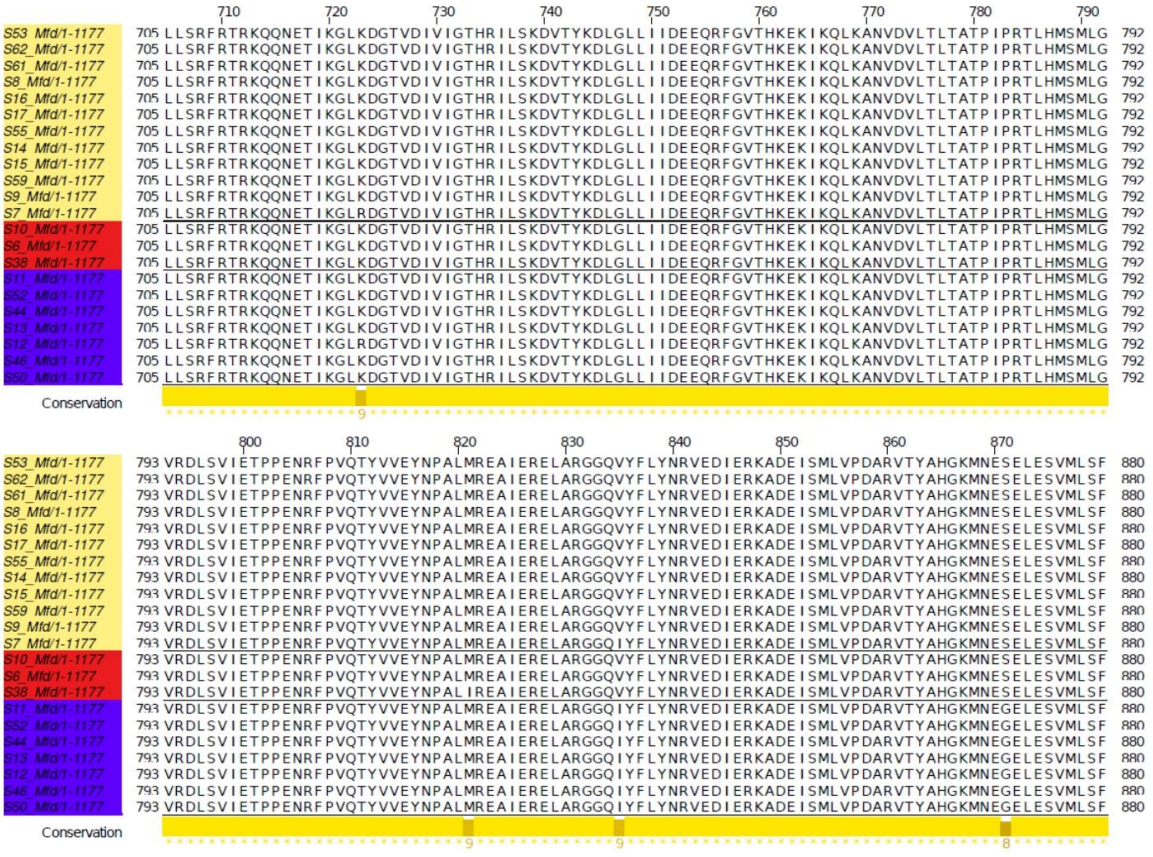
710 720 730 740 750 760 770 780 790
S53_Mfd/1-1177 705 LLSRFRTRKQQNETIKGLKDGTVDIVIGTHRILSKDVTYKDLGLLIIDEEQRFGVTHKEKIKQLKANVDVLTLTATPIPRTLHMSMLG 792
S62_Mfd/1-1177 705 LLSRFRTRKQQNETIKGLKDGTVDIVIGTHRILSKDVTYKDLGLLIIDEEQRFGVTHKEKIKQLKANVDVLTLTATPIPRTLHMSMLG 792
S61_Mfd/1-1177 705 LLSRFRTRKQQNETIKGLKDGTVDIVIGTHRILSKDVTYKDLGLLIIDEEQRFGVTHKEKIKQLKANVDVLTLTATPIPRTLHMSMLG 792
S8_Mfd/1-1177 705 LLSRFRTRKQQNETIKGLKDGTVDIVIGTHRILSKDVTYKDLGLLIIDEEQRFGVTHKEKIKQLKANVDVLTLTATPIPRTLHMSMLG 792
S16_Mfd/1-1177 705 LLSRFRTRKQQNETIKGLKDGTVDIVIGTHRILSKDVTYKDLGLLIIDEEQRFGVTHKEKIKQLKANVDVLTLTATPIPRTLHMSMLG 792
S17_Mfd/1-1177 705 LLSRFRTRKQQNETIKGLKDGTVDIVIGTHRILSKDVTYKDLGLLIIDEEQRFGVTHKEKIKQLKANVDVLTLTATPIPRTLHMSMLG 792
S55_Mfd/1-1177 705 LLSRFRTRKQQNETIKGLKDGTVDIVIGTHRILSKDVTYKDLGLLIIDEEQRFGVTHKEKIKQLKANVDVLTLTATPIPRTLHMSMLG 792
S14_Mfd/1-1177 705 LLSRFRTRKQQNETIKGLKDGTVDIVIGTHRILSKDVTYKDLGLLIIDEEQRFGVTHKEKIKQLKANVDVLTLTATPIPRTLHMSMLG 792
S15_Mfd/1-1177 705 LLSRFRTRKQQNETIKGLKDGTVDIVIGTHRILSKDVTYKDLGLLIIDEEQRFGVTHKEKIKQLKANVDVLTLTATPIPRTLHMSMLG 792
S59_Mfd/1-1177 705 LLSRFRTRKQQNETIKGLKDGTVDIVIGTHRILSKDVTYKDLGLLIIDEEQRFGVTHKEKIKQLKANVDVLTLTATPIPRTLHMSMLG 792
S9_Mfd/1-1177 705 LLSRFRTRKQQNETIKGLKDGTVDIVIGTHRILSKDVTYKDLGLLIIDEEQRFGVTHKEKIKQLKANVDVLTLTATPIPRTLHMSMLG 792
S7_Mfd/1-1177 705 LLSRFRTRKQQNETIKGLRDGTVDIVIGTHRILSKDVTYKDLGLLIIDEEQRFGVTHKEKIKQLKANVDVLTLTATPIPRTLHMSMLG 792
S10_Mfd/1-1177 705 LLSRFRTRKQQNETIKGLKDGTVDIVIGTHRILSKDVTYKDLGLLIIDEEQRFGVTHKEKIKQLKANVDVLTLTATPIPRTLHMSMLG 792
S6_Mfd/1-1177 705 LLSRFRTRKQQNETIKGLKDGTVDIVIGTHRILSKDVTYKDLGLLIIDEEQRFGVTHKEKIKQLKANVDVLTLTATPIPRTLHMSMLG 792
S38_Mfd/1-1177 705 LLSRFRTRKQQNETIKGLKDGTVDIVIGTHRILSKDVTYKDLGLLIIDEEQRFGVTHKEKIKQLKANVDVLTLTATPIPRTLHMSMLG 792
S11_Mfd/1-1177 705 LLSRFRTRKQQNETIKGLKDGTVDIVIGTHRILSKDVTYKDLGLLIIDEEQRFGVTHKEKIKQLKANVDVLTLTATPIPRTLHMSMLG 792
S52_Mfd/1-1177 705 LLSRFRTRKQQNETIKGLKDGTVDIVIGTHRILSKDVTYKDLGLLIIDEEQRFGVTHKEKIKQLKANVDVLTLTATPIPRTLHMSMLG 792
S44_Mfd/1-1177 705 LLSRFRTRKQQNETIKGLKDGTVDIVIGTHRILSKDVTYKDLGLLIIDEEQRFGVTHKEKIKQLKANVDVLTLTATPIPRTLHMSMLG 792
S13_Mfd/1-1177 705 LLSRFRTRKQQNETIKGLKDGTVDIVIGTHRILSKDVTYKDLGLLIIDEEQRFGVTHKEKIKQLKANVDVLTLTATPIPRTLHMSMLG 792
S12_Mfd/1-1177 705 LLSRFRTRKQQNETIKGLRDGTVDIVIGTHRILSKDVTYKDLGLLIIDEEQRFGVTHKEKIKQLKANVDVLTLTATPIPRTLHMSMLG 792
S46_Mfd/1-1177 705 LLSRFRTRKQQNETIKGLKDGTVDIVIGTHRILSKDVTYKDLGLLIIDEEQRFGVTHKEKIKQLKANVDVLTLTATPIPRTLHMSMLG 792
S50_Mfd/1-1177 705 LLSRFRTRKQQNETIKGLKDGTVDIVIGTHRILSKDVTYKDLGLLIIDEEQRFGVTHKEKIKQLKANVDVLTLTATPIPRTLHMSMLG 792
Conservation
800 810 820 830 840 850 860 870
S53_Mfd/1-1177 793 VRDLSVIETPPENRFPVQTYVVEYNPALMREAIERELARGGQVYFLYNRVEDIERKADEISMLVPDARVTYAHGKMNESELESVMLSF 880
S62_Mfd/1-1177 793 VRDLSVIETPPENRFPVQTYVVEYNPALMREAIERELARGGQVYFLYNRVEDIERKADEISMLVPDARVTYAHGKMNESELESVMLSF 880
S61_Mfd/1-1177 793 VRDLSVIETPPENRFPVQTYVVEYNPALMREAIERELARGGQVYFLYNRVEDIERKADEISMLVPDARVTYAHGKMNESELESVMLSF 880
S8_Mfd/1-1177 793 VRDLSVIETPPENRFPVQTYVVEYNPALMREAIERELARGGQVYFLYNRVEDIERKADEISMLVPDARVTYAHGKMNESELESVMLSF 880
S16_Mfd/1-1177 793 VRDLSVIETPPENRFPVQTYVVEYNPALMREAIERELARGGQVYFLYNRVEDIERKADEISMLVPDARVTYAHGKMNESELESVMLSF 880
S17_Mfd/1-1177 793 VRDLSVIETPPENRFPVQTYVVEYNPALMREAIERELARGGQVYFLYNRVEDIERKADEISMLVPDARVTYAHGKMNESELESVMLSF 880
S55_Mfd/1-1177 793 VRDLSVIETPPENRFPVQTYVVEYNPALMREAIERELARGGQVYFLYNRVEDIERKADEISMLVPDARVTYAHGKMNESELESVMLSF 880
S14_Mfd/1-1177 793 VRDLSVIETPPENRFPVQTYVVEYNPALMREAIERELARGGQVYFLYNRVEDIERKADEISMLVPDARVTYAHGKMNESELESVMLSF 880
S15_Mfd/1-1177 793 VRDLSVIETPPENRFPVQTYVVEYNPALMREAIERELARGGQVYFLYNRVEDIERKADEISMLVPDARVTYAHGKMNESELESVMLSF 880
S59_Mfd/1-1177 793 VRDLSVIETPPENRFPVQTYVVEYNPALMREAIERELARGGQVYFLYNRVEDIERKADEISMLVPDARVTYAHGKMNESELESVMLSF 880
S9_Mfd/1-1177 793 VRDLSVIETPPENRFPVQTYVVEYNPALMREAIERELARGGQVYFLYNRVEDIERKADEISMLVPDARVTYAHGKMNESELESVMLSF 880
S7_Mfd/1-1177 793 VRDLSVIETPPENRFPVQTYVVEYNPALMREAIERELARGGQIYFLYNRVEDIERKADEISMLVPDARVTYAHGKMNESELESVMLSF 880
S10_Mfd/1-1177 793 VRDLSVIETPPENRFPVQTYVVEYNPALMREAIERELARGGQVYFLYNRVEDIERKADEISMLVPDARVTYAHGKMNESELESVMLSF 880
S6_Mfd/1-1177 793 VRDLSVIETPPENRFPVQTYVVEYNPALMREAIERELARGGQVYFLYNRVEDIERKADEISMLVPDARVTYAHGKMNESELESVMLSF 880
S38_Mfd/1-1177 793 VRDLSVIETPPENRFPVQTYVVEYNPALIREAIERELARGGQVYFLYNRVEDIERKADEISMLVPDARVTYAHGKMNESELESVMLSF 880
S11_Mfd/1-1177 793 VRDLSVIETPPENRFPVQTYVVEYNPALMREAIERELARGGQIYFLYNRVEDIERKADEISMLVPDARVTYAHGKMNEGELESVMLSF 880
S52_Mfd/1-1177 793 VRDLSVIETPPENRFPVQTYVVEYNPALMREAIERELARGGQIYFLYNRVEDIERKADEISMLVPDARVTYAHGKMNEGELESVMLSF 880
S44_Mfd/1-1177 793 VRDLSVIETPPENRFPVQTYVVEYNPALMREAIERELARGGQIYFLYNRVEDIERKADEISMLVPDARVTYAHGKMNEGELESVMLSF 880
S13_Mfd/1-1177 793 VRDLSVIETPPENRFPVQTYVVEYNPALMREAIERELARGGQIYFLYNRVEDIERKADEISMLVPDARVTYAHGKMNEGELESVMLSF 880
S12_Mfd/1-1177 793 VRDLSVIETPPENRFPVQTYVVEYNPALMREAIERELARGGQIYFLYNRVEDIERKADEISMLVPDARVTYAHGKMNEGELESVMLSF 880
S46_Mfd/1-1177 793 VRDLSVIETPPENRFPVQTYVVEYNPALMREAIERELARGGQIYFLYNRVEDIERKADEISMLVPDARVTYAHGKMNEGELESVMLSF 880
S50_Mfd/1-1177 793 VRDLSVIETPPENRFPVQTYVVEYNPALMREAIERELARGGQIYFLYNRVEDIERKADEISMLVPDARVTYAHGKMNEGELESVMLSF 880
Conservation

Fig 1

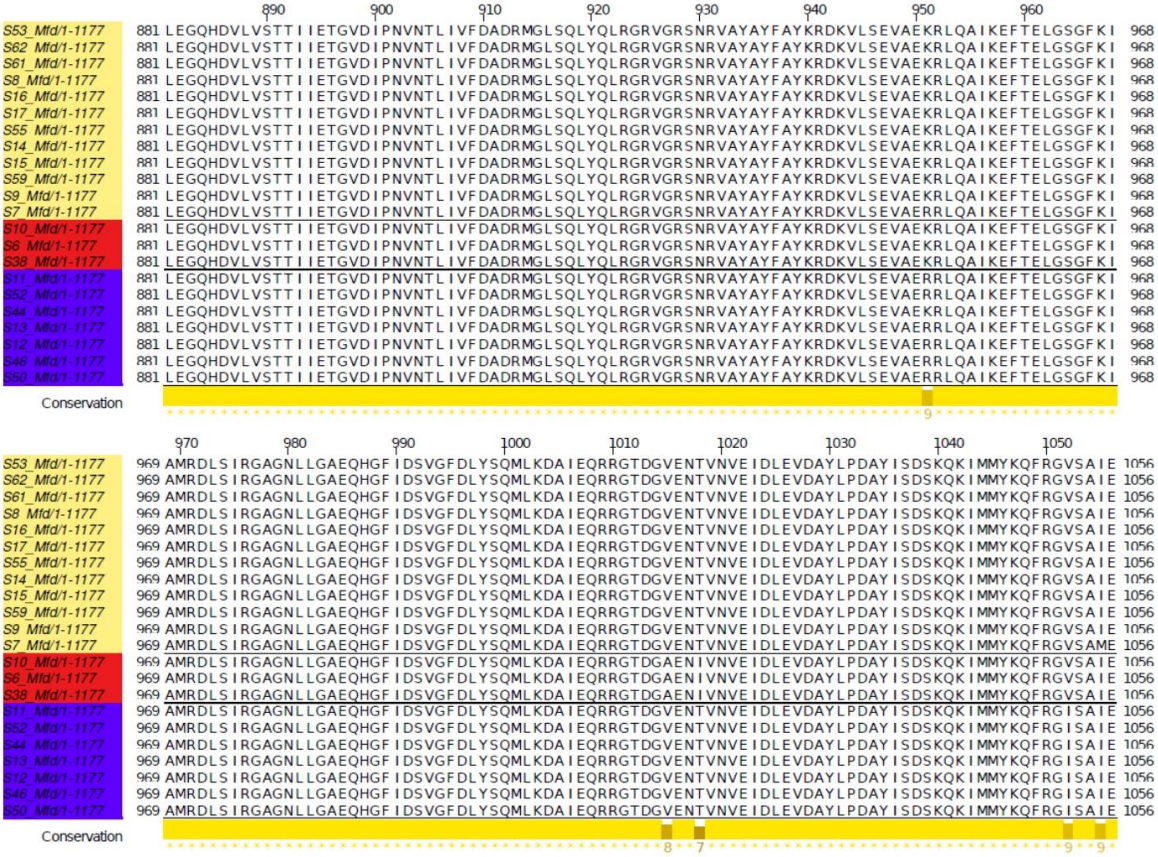
890 900 910 920 930 940 950 960
S53_Mfd/1-1177 881 LEGQHDVLVSTTIIETGVDIPNVNTLIVFDADRMGLSQLYQLRGRVGRSNRVAYAYFAYKRDKVLSEVAEKRLQAIKEFTELGSGFKI 968
S62_Mfd/1-1177 881 LEGQHDVLVSTTIIETGVDIPNVNTLIVFDADRMGLSQLYQLRGRVGRSNRVAYAYFAYKRDKVLSEVAEKRLQAIKEFTELGSGFKI 968
S61_Mfd/1-1177 881 LEGQHDVLVSTTIIETGVDIPNVNTLIVFDADRMGLSQLYQLRGRVGRSNRVAYAYFAYKRDKVLSEVAEKRLQAIKEFTELGSGFKI 968
S8_Mfd/1-1177 881 LEGQHDVLVSTTIIETGVDIPNVNTLIVFDADRMGLSQLYQLRGRVGRSNRVAYAYFAYKRDKVLSEVAEKRLQAIKEFTELGSGFKI 968
S16_Mfd/1-1177 881 LEGQHDVLVSTTIIETGVDIPNVNTLIVFDADRMGLSQLYQLRGRVGRSNRVAYAYFAYKRDKVLSEVAEKRLQAIKEFTELGSGFKI 968
S17_Mfd/1-1177 881 LEGQHDVLVSTTIIETGVDIPNVNTLIVFDADRMGLSQLYQLRGRVGRSNRVAYAYFAYKRDKVLSEVAEKRLQAIKEFTELGSGFKI 968
S55_Mfd/1-1177 881 LEGQHDVLVSTTIIETGVDIPNVNTLIVFDADRMGLSQLYQLRGRVGRSNRVAYAYFAYKRDKVLSEVAEKRLQAIKEFTELGSGFKI 968
S14_Mfd/1-1177 881 LEGQHDVLVSTTIIETGVDIPNVNTLIVFDADRMGLSQLYQLRGRVGRSNRVAYAYFAYKRDKVLSEVAEKRLQAIKEFTELGSGFKI 968
S15_Mfd/1-1177 881 LEGQHDVLVSTTIIETGVDIPNVNTLIVFDADRMGLSQLYQLRGRVGRSNRVAYAYFAYKRDKVLSEVAEKRLQAIKEFTELGSGFKI 968
S59_Mfd/1-1177 881 LEGQHDVLVSTTIIETGVDIPNVNTLIVFDADRMGLSQLYQLRGRVGRSNRVAYAYFAYKRDKVLSEVAEKRLQAIKEFTELGSGFKI 968
S9_Mfd/1-1177 881 LEGQHDVLVSTTIIETGVDIPNVNTLIVFDADRMGLSQLYQLRGRVGRSNRVAYAYFAYKRDKVLSEVAEKRLQAIKEFTELGSGFKI 968
S7_Mfd/1-1177 881 LEGQHDVLVSTTIIETGVDIPNVNTLIVFDADRMGLSQLYQLRGRVGRSNRVAYAYFAYKRDKVLSEVAERRLQAIKEFTELGSGFKI 968
S10_Mfd/1-1177 881 LEGQHDVLVSTTIIETGVDIPNVNTLIVFDADRMGLSQLYQLRGRVGRSNRVAYAYFAYKRDKVLSEVAEKRLQAIKEFTELGSGFKI 968
S6_Mfd/1-1177 881 LEGQHDVLVSTTIIETGVDIPNVNTLIVFDADRMGLSQLYQLRGRVGRSNRVAYAYFAYKRDKVLSEVAEKRLQAIKEFTELGSGFKI 968
S38_Mfd/1-1177 881 LEGQHDVLVSTTIIETGVDIPNVNTLIVFDADRMGLSQLYQLRGRVGRSNRVAYAYFAYKRDKVLSEVAEKRLQAIKEFTELGSGFKI 968
S11_Mfd/1-1177 881 LEGQHDVLVSTTIIETGVDIPNVNTLIVFDADRMGLSQLYQLRGRVGRSNRVAYAYFAYKRDKVLSEVAERRLQAIKEFTELGSGFKI 968
S52_Mfd/1-1177 881 LEGQHDVLVSTTIIETGVDIPNVNTLIVFDADRMGLSQLYQLRGRVGRSNRVAYAYFAYKRDKVLSEVAERRLQAIKEFTELGSGFKI 968
S44_Mfd/1-1177 881 LEGQHDVLVSTTIIETGVDIPNVNTLIVFDADRMGLSQLYQLRGRVGRSNRVAYAYFAYKRDKVLSEVAEKRLQAIKEFTELGSGFKI 968
S13_Mfd/1-1177 881 LEGQHDVLVSTTIIETGVDIPNVNTLIVFDADRMGLSQLYQLRGRVGRSNRVAYAYFAYKRDKVLSEVAERRLQAIKEFTELGSGFKI 968
S12_Mfd/1-1177 881 LEGQHDVLVSTTIIETGVDIPNVNTLIVFDADRMGLSQLYQLRGRVGRSNRVAYAYFAYKRDKVLSEVAERRLQAIKEFTELGSGFKI 968
S46_Mfd/1-1177 881 LEGQHDVLVSTTIIETGVDIPNVNTLIVFDADRMGLSQLYQLRGRVGRSNRVAYAYFAYKRDKVLSEVAERRLQAIKEFTELGSGFKI 968
S50_Mfd/1-1177 881 LEGQHDVLVSTTIIETGVDIPNVNTLIVFDADRMGLSQLYQLRGRVGRSNRVAYAYFAYKRDKVLSEVAERRLQAIKEFTELGSGFKI 968
Conservation
970 980 990 1000 1010 1020 1030 1040 1050
S53_Mfd/1-1177 969 AMRDLSIRGAGNLLGAEQHGFIDSVGFDLYSQMLKDAIEQRRGTDGVENTVNVEIDLEVDAYLPDAYISDSKQKIMMYKQFRGVSAIE 1056
S62_Mfd/1-1177 969 AMRDLSIRGAGNLLGAEQHGFIDSVGFDLYSQMLKDAIEQRRGTDGVENTVNVEIDLEVDAYLPDAYISDSKQKIMMYKQFRGVSAIE 1056
S61_Mfd/1-1177 969 AMRDLSIRGAGNLLGAEQHGFIDSVGFDLYSQMLKDAIEQRRGTDGVENTVNVEIDLEVDAYLPDAYISDSKQKIMMYKQFRGVSAIE 1056
S8_Mfd/1-1177 969 AMRDLSIRGAGNLLGAEQHGFIDSVGFDLYSQMLKDAIEQRRGTDGVENTVNVEIDLEVDAYLPDAYISDSKQKIMMYKQFRGVSAIE 1056
S16_Mfd/1-1177 969 AMRDLSIRGAGNLLGAEQHGFIDSVGFDLYSQMLKDAIEQRRGTDGVENTVNVEIDLEVDAYLPDAYISDSKQKIMMYKQFRGVSAIE 1056
S17_Mfd/1-1177 969 AMRDLSIRGAGNLLGAEQHGFIDSVGFDLYSQMLKDAIEQRRGTDGVENTVNVEIDLEVDAYLPDAYISDSKQKIMMYKQFRGVSAIE 1056
S55_Mfd/1-1177 969 AMRDLSIRGAGNLLGAEQHGFIDSVGFDLYSQMLKDAIEQRRGTDGVENTVNVEIDLEVDAYLPDAYISDSKQKIMMYKQFRGVSAIE 1056
S14_Mfd/1-1177 969 AMRDLSIRGAGNLLGAEQHGFIDSVGFDLYSQMLKDAIEQRRGTDGVENTVNVEIDLEVDAYLPDAYISDSKQKIMMYKQFRGVSAIE 1056
S15_Mfd/1-1177 969 AMRDLSIRGAGNLLGAEQHGFIDSVGFDLYSQMLKDAIEQRRGTDGVENTVNVEIDLEVDAYLPDAYISDSKQKIMMYKQFRGVSAIE 1056
S59_Mfd/1-1177 969 AMRDLSIRGAGNLLGAEQHGFIDSVGFDLYSQMLKDAIEQRRGTDGVENTVNVEIDLEVDAYLPDAYISDSKQKIMMYKQFRGVSAIE 1056
S9_Mfd/1-1177 969 AMRDLSIRGAGNLLGAEQHGFIDSVGFDLYSQMLKDAIEQRRGTDGVENTVNVEIDLEVDAYLPDAYISDSKQKIMMYKQFRGVSAIE 1056
S7_Mfd/1-1177 969 AMRDLSIRGAGNLLGAEQHGFIDSVGFDLYSQMLKDAIEQRRGTDGVENTVNVEIDLEVDAYLPDAYISDSKQKIMMYKQFRGVSAME 1056
S10_Mfd/1-1177 969 AMRDLSIRGAGNLLGAEQHGFIDSVGFDLYSQMLKDAIEQRRGTDGAENIVNVEIDLEVDAYLPDAYISDSKQKIMMYKQFRGVSAIE 1056
S6_Mfd/1-1177 969 AMRDLSIRGAGNLLGAEQHGFIDSVGFDLYSQMLKDAIEQRRGTDGAENIVNVEIDLEVDAYLPDAYISDSKQKIMMYKQFRGVSAIE 1056
S38_Mfd/1-1177 969 AMRDLSIRGAGNLLGAEQHGFIDSVGFDLYSQMLKDAIEQRRGTDGAENIVNVEIDLEVDAYLPDAYISDSKQKIMMYKQFRGVSAIE 1056
S11_Mfd/1-1177 969 AMRDLSIRGAGNLLGAEQHGFIDSVGFDLYSQMLKDAIEQRRGTDGVENTVNVEIDLEVDAYLPDAYISDSKQKIMMYKQFRGISAIE 1056
S52_Mfd/1-1177 969 AMRDLSIRGAGNLLGAEQHGFIDSVGFDLYSQMLKDAIEQRRGTDGVENTVNVEIDLEVDAYLPDAYISDSKQKIMMYKQFRGISAIE 1056
S44_Mfd/1-1177 969 AMRDLSIRGAGNLLGAEQHGFIDSVGFDLYSQMLKDAIEQRRGTDGVENTVNVEIDLEVDAYLPDAYISDSKQKIMMYKQFRGISAIE 1056
S13_Mfd/1-1177 969 AMRDLSIRGAGNLLGAEQHGFIDSVGFDLYSQMLKDAIEQRRGTDGVENTVNVEIDLEVDAYLPDAYISDSKQKIMMYKQFRGISAIE 1056
S12_Mfd/1-1177 969 AMRDLSIRGAGNLLGAEQHGFIDSVGFDLYSQMLKDAIEQRRGTDGVENTVNVEIDLEVDAYLPDAYISDSKQKIMMYKQFRGISAIE 1056
S46_Mfd/1-1177 969 AMRDLSIRGAGNLLGAEQHGFIDSVGFDLYSQMLKDAIEQRRGTDGVENTVNVEIDLEVDAYLPDAYISDSKQKIMMYKQFRGISAIE 1056
S50_Mfd/1-1177 969 AMRDLSIRGAGNLLGAEQHGFIDSVGFDLYSQMLKDAIEQRRGTDGVENTVNVEIDLEVDAYLPDAYISDSKQKIMMYKQFRGISAIE 1056
Conservation

Fig 1

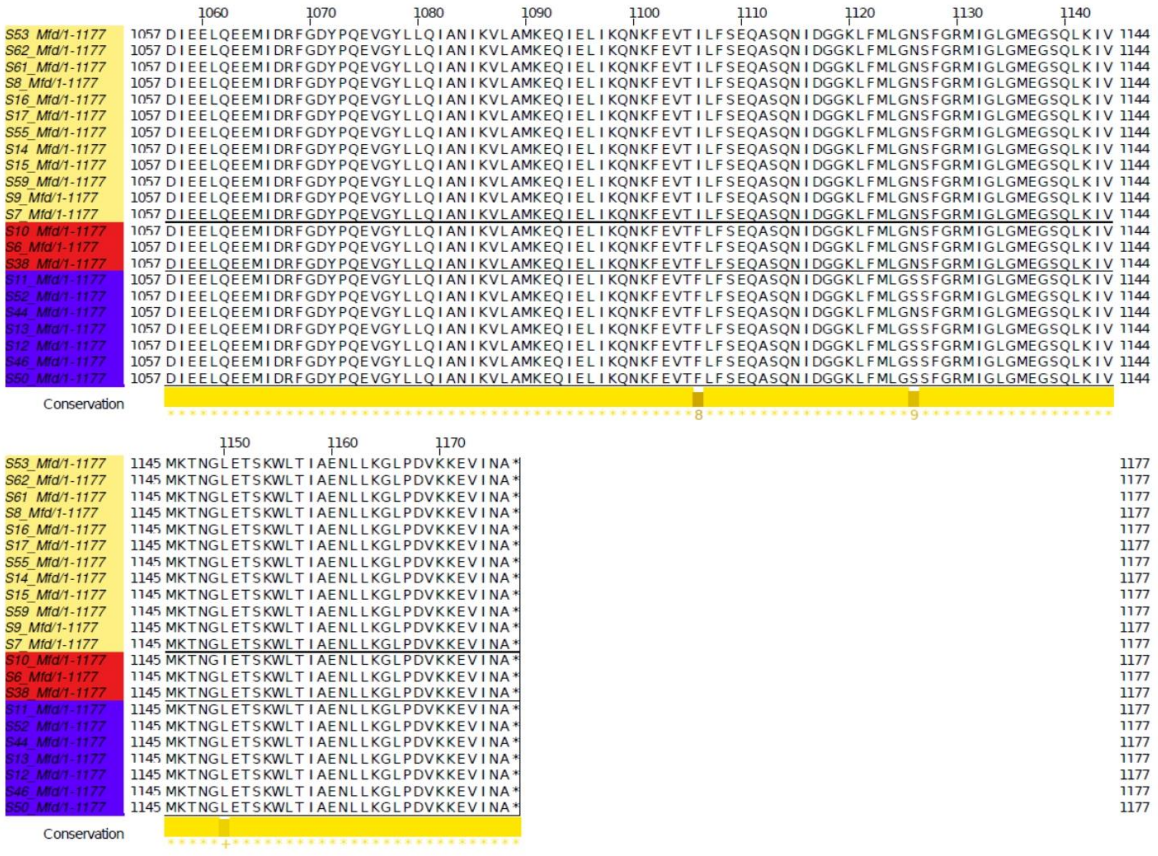
1060 1070 1080 1090 1100 1110 1120 1130 1140
S53_Mfd/1-1177 1057 DIEELQEEMIDRFGDYPQEVGYLLQIANIKVLAMKEQIELIKQNKFEVTILFSEQASQNIDGGKLFMLGNSFGRMIGLGMEGSQLKIV 1144
S62_Mfd/1-1177 1057 DIEELQEEMIDRFGDYPQEVGYLLQIANIKVLAMKEQIELIKQNKFEVTILFSEQASQNIDGGKLFMLGNSFGRMIGLGMEGSQLKIV 1144
S61_Mfd/1-1177 1057 DIEELQEEMIDRFGDYPQEVGYLLQIANIKVLAMKEQIELIKQNKFEVTILFSEQASQNIDGGKLFMLGNSFGRMIGLGMEGSQLKIV 1144
S8_Mfd/1-1177 1057 DIEELQEEMIDRFGDYPQEVGYLLQIANIKVLAMKEQIELIKQNKFEVTILFSEQASQNIDGGKLFMLGNSFGRMIGLGMEGSQLKIV 1144
S16_Mfd/1-1177 1057 DIEELQEEMIDRFGDYPQEVGYLLQIANIKVLAMKEQIELIKQNKFEVTILFSEQASQNIDGGKLFMLGNSFGRMIGLGMEGSQLKIV 1144
S17_Mfd/1-1177 1057 DIEELQEEMIDRFGDYPQEVGYLLQIANIKVLAMKEQIELIKQNKFEVTILFSEQASQNIDGGKLFMLGNSFGRMIGLGMEGSQLKIV 1144
S55_Mfd/1-1177 1057 DIEELQEEMIDRFGDYPQEVGYLLQIANIKVLAMKEQIELIKQNKFEVTILFSEQASQNIDGGKLFMLGNSFGRMIGLGMEGSQLKIV 1144
S14_Mfd/1-1177 1057 DIEELQEEMIDRFGDYPQEVGYLLQIANIKVLAMKEQIELIKQNKFEVTILFSEQASQNIDGGKLFMLGNSFGRMIGLGMEGSQLKIV 1144
S15_Mfd/1-1177 1057 DIEELQEEMIDRFGDYPQEVGYLLQIANIKVLAMKEQIELIKQNKFEVTILFSEQASQNIDGGKLFMLGNSFGRMIGLGMEGSQLKIV 1144
S59_Mfd/1-1177 1057 DIEELQEEMIDRFGDYPQEVGYLLQIANIKVLAMKEQIELIKQNKFEVTILFSEQASQNIDGGKLFMLGNSFGRMIGLGMEGSQLKIV 1144
S9_Mfd/1-1177 1057 DIEELQEEMIDRFGDYPQEVGYLLQIANIKVLAMKEQIELIKQNKFEVTILFSEQASQNIDGGKLFMLGNSFGRMIGLGMEGSQLKIV 1144
S7_Mfd/1-1177 1057 DIEELQEEMIDRFGDYPQEVGYLLQIANIKVLAMKEQIELIKQNKFEVTILFSEQASQNIDGGKLFMLGNSFGRMIGLGMEGSQLKIV 1144
S10_Mfd/1-1177 1057 DIEELQEEMIDRFGDYPQEVGYLLQIANIKVLAMKEQIELIKQNKFEVTFLFSEQASQNIDGGKLFMLGNSFGRMIGLGMEGSQLKIV 1144
S6_Mfd/1-1177 1057 DIEELQEEMIDRFGDYPQEVGYLLQIANIKVLAMKEQIELIKQNKFEVTFLFSEQASQNIDGGKLFMLGNSFGRMIGLGMEGSQLKIV 1144
S38_Mfd/1-1177 1057 DIEELQEEMIDRFGDYPQEVGYLLQIANIKVLAMKEQIELIKQNKFEVTFLFSEQASQNIDGGKLFMLGNSFGRMIGLGMEGSQLKIV 1144
S11_Mfd/1-1177 1057 DIEELQEEMIDRFGDYPQEVGYLLQIANIKVLAMKEQIELIKQNKFEVTFLFSEQASQNIDGGKLFMLGSSFGRMIGLGMEGSQLKIV 1144
S52_Mfd/1-1177 1057 DIEELQEEMIDRFGDYPQEVGYLLQIANIKVLAMKEQIELIKQNKFEVTFLFSEQASQNIDGGKLFMLGSSFGRMIGLGMEGSQLKIV 1144
S44_Mfd/1-1177 1057 DIEELQEEMIDRFGDYPQEVGYLLQIANIKVLAMKEQIELIKQNKFEVTFLFSEQASQNIDGGKLFMLGNSFGRMIGLGMEGSQLKIV 1144
S13_Mfd/1-1177 1057 DIEELQEEMIDRFGDYPQEVGYLLQIANIKVLAMKEQIELIKQNKFEVTFLFSEQASQNIDGGKLFMLGSSFGRMIGLGMEGSQLKIV 1144
S12_Mfd/1-1177 1057 DIEELQEEMIDRFGDYPQEVGYLLQIANIKVLAMKEQIELIKQNKFEVTFLFSEQASQNIDGGKLFMLGSSFGRMIGLGMEGSQLKIV 1144
S46_Mfd/1-1177 1057 DIEELQEEMIDRFGDYPQEVGYLLQIANIKVLAMKEQIELIKQNKFEVTFLFSEQASQNIDGGKLFMLGSSFGRMIGLGMEGSQLKIV 1144
S50_Mfd/1-1177 1057 DIEELQEEMIDRFGDYPQEVGYLLQIANIKVLAMKEQIELIKQNKFEVTFLFSEQASQNIDGGKLFMLGSSFGRMIGLGMEGSQLKIV 1144
Conservation
1150 1160 1170
S53_Mfd/1-1177 1145 MKTNGLETSKWLTIAENLLKGLPDVKKEVINA* 1177
S62_Mfd/1-1177 1145 MKTNGLETSKWLTIAENLLKGLPDVKKEVINA* 1177
S61_Mfd/1-1177 1145 MKTNGLETSKWLTIAENLLKGLPDVKKEVINA* 1177
S8_Mfd/1-1177 1145 MKTNGLETSKWLTIAENLLKGLPDVKKEVINA* 1177
S16_Mfd/1-1177 1145 MKTNGLETSKWLTIAENLLKGLPDVKKEVINA* 1177
S17_Mfd/1-1177 1145 MKTNGLETSKWLTIAENLLKGLPDVKKEVINA* 1177
S55_Mfd/1-1177 1145 MKTNGLETSKWLTIAENLLKGLPDVKKEVINA* 1177
S14_Mfd/1-1177 1145 MKTNGLETSKWLTIAENLLKGLPDVKKEVINA* 1177
S15_Mfd/1-1177 1145 MKTNGLETSKWLTIAENLLKGLPDVKKEVINA* 1177
S59_Mfd/1-1177 1145 MKTNGLETSKWLTIAENLLKGLPDVKKEVINA* 1177
S9_Mfd/1-1177 1145 MKTNGLETSKWLTIAENLLKGLPDVKKEVINA* 1177
S7_Mfd/1-1177 1145 MKTNGLETSKWLTIAENLLKGLPDVKKEVINA* 1177
S10_Mfd/1-1177 1145 MKTNGIETSKWLTIAENLLKGLPDVKKEVINA* 1177
S6_Mfd/1-1177 1145 MKTNGLETSKWLTIAENLLKGLPDVKKEVINA* 1177
S38_Mfd/1-1177 1145 MKTNGLETSKWLTIAENLLKGLPDVKKEVINA* 1177
S11_Mfd/1-1177 1145 MKTNGLETSKWLTIAENLLKGLPDVKKEVINA* 1177
S52_Mfd/1-1177 1145 MKTNGLETSKWLTIAENLLKGLPDVKKEVINA* 1177
S44_Mfd/1-1177 1145 MKTNGLETSKWLTIAENLLKGLPDVKKEVINA* 1177
S13_Mfd/1-1177 1145 MKTNGLETSKWLTIAENLLKGLPDVKKEVINA* 1177
S12_Mfd/1-1177 1145 MKTNGLETSKWLTIAENLLKGLPDVKKEVINA* 1177
S46_Mfd/1-1177 1145 MKTNGLETSKWLTIAENLLKGLPDVKKEVINA* 1177
S50_Mfd/1-1177 1145 MKTNGLETSKWLTIAENLLKGLPDVKKEVINA* 1177
Conservation

Fig 1

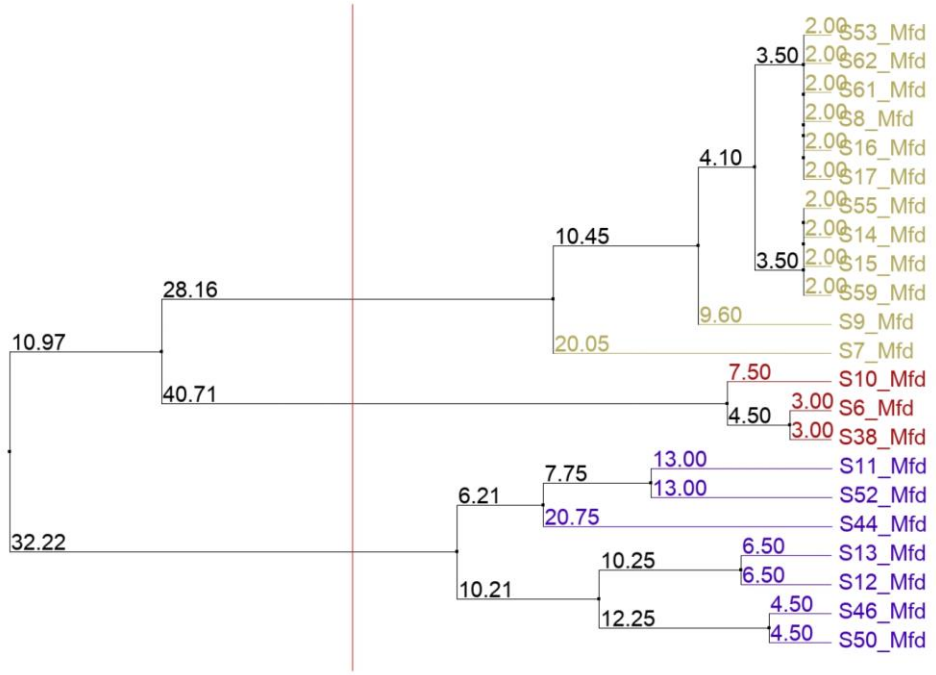
2.00 S53_Mfd
2.00 S62_Mfd
2.00 S61_Mfd
2.00 S8_Mfd
2.00 S16_Mfd
2.00 S17_Mfd
2.00 S55_Mfd
2.00 S14_Mfd
2.00 S15_Mfd
2.00 S59_Mfd
S9_Mfd
S7_Mfd
S10_Mfd
S6_Mfd
S38_Mfd
S11_Mfd
S52_Mfd
S44_Mfd
S13_Mfd
S12_Mfd
S46_Mfd
S50_Mfd
3.50
4.10
10.45
3.50
28.16
9.60
10.97
20.05
7.50
40.71
4.50
3.00
3.00
13.00
7.75
13.00
6.21
20.75
32.22
6.50
10.25
6.50
10.21
4.50
12.25
4.50

Fig 2

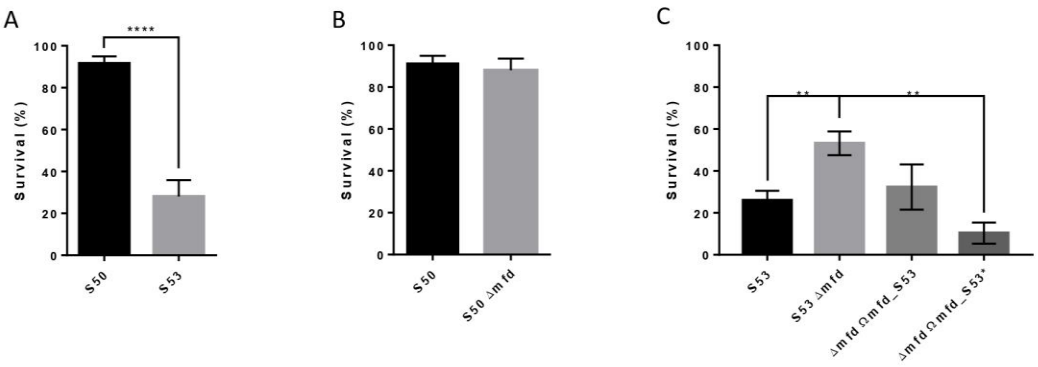
A
****
Survival (%)
100
80
60
40
20
0
S50
S53
B
Survival (%)
100
80
60
40
20
0
S50
S50 Δmfd
C
**
**
Survival (%)
100
80
60
40
20
0
S53
S53 Δmfd
Δmfd Ωmfd_S53
Δmfd Ωmfd_S53*

Fig 3

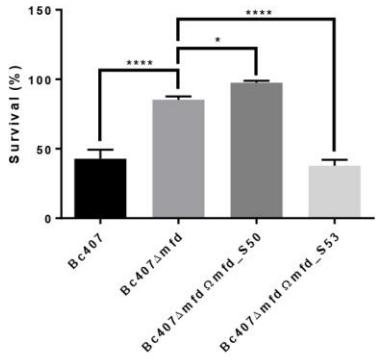
Survival (%)
150
100
50
0
****
*
****
Bc407
Bc407Δmfd
Bc407Δmfd Ωmfd_S50
Bc407Δmfd Ωmfd_S53

Fig 4

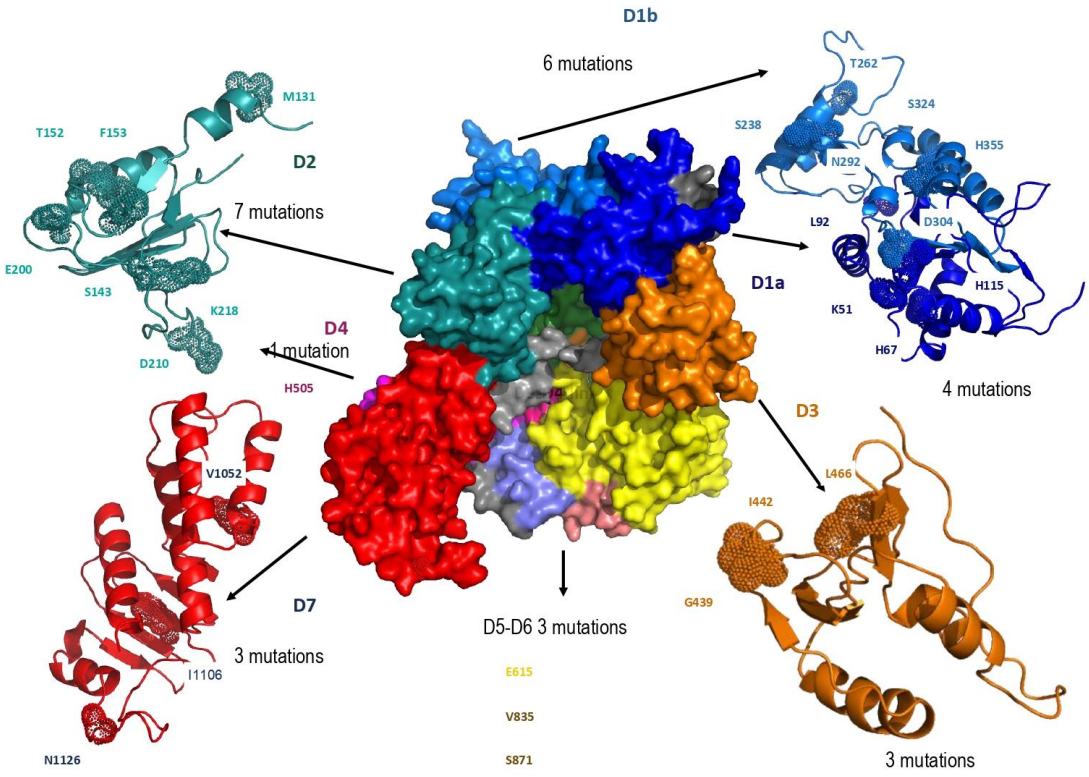
D1b
6 mutations
T262
S324
S238
H355
N292
L92
D304
D1a
H115
K51
H67
4 mutations
M131
T152
F153
D2
7 mutations
E200
S143
K218
D210
D4
1 mutation
H505
D3
L466
I442
G439
V1052
D7
3 mutations
I1106
N1126
D5-D6 3 mutations
E615
V835
S871
3 mutations

Fig 5

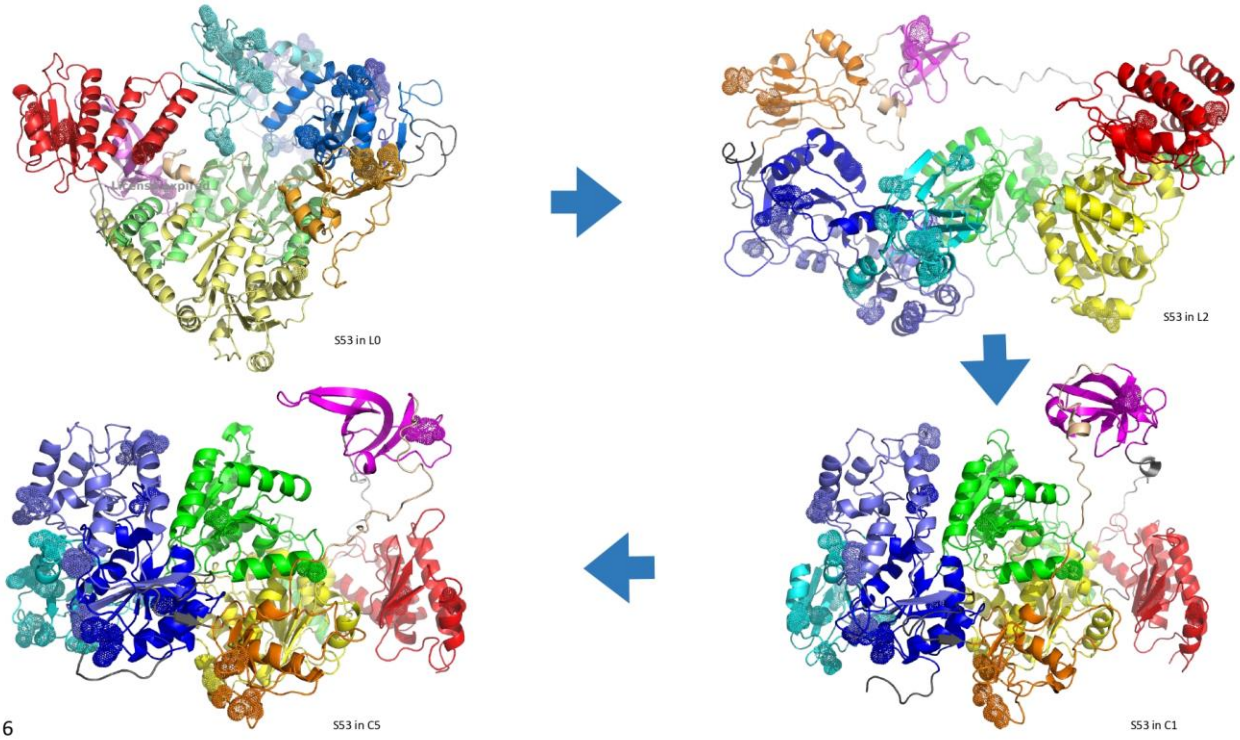

Fig 6

Tab. 3 : *In sillico* analysis of Mfd sequences

	S50	S53	S50_S53 Mutations/domain	Mutation ratio
D1a 1-127	Q51 Y67 V92 N115	K51 (l) H67 (h) L92 (l) H115 (l)	4/127	0.03
D2 128-228	I131 N143 **A152** **L153** Q200 E210 R218	M131 (l) S143 (l) **T152 (h)** **F153 (h)** E200 (l) D210 (l) K218 (b)	7/100	0.07
D1b 229-366	**L238** **A262** **K292** N304 T324 N355	**S238 (h)** **T262 (l)** **N292 (l)** D304 (l) S324 (h) H355 (h)	6/137	0.04
D3 378-478	**A439** V442 **F466**	**G439 (l)** I442 (l) **L466 (b)**	3/100	0.03
D4 RID 502-568	H505	Y505 (l)	1/166	0.006
D5 601-804	**G615**	**E615 (h)**	1/203	0.005
D6 804-948	I835 **G871**	V835 (l) **S871 (h)**	2/144	0.01
linker 949-988	R951	K951 (h)	1/40	0.025
D7 1022-1076	I1052 **F1106** S1126	V1052 (l) **I1106 (b)** N1126 (l)	3/154	0.02

17/28 concentrated on UvrB homology module less than 400 aa residues

11/28 on the remaining 700 aa residues

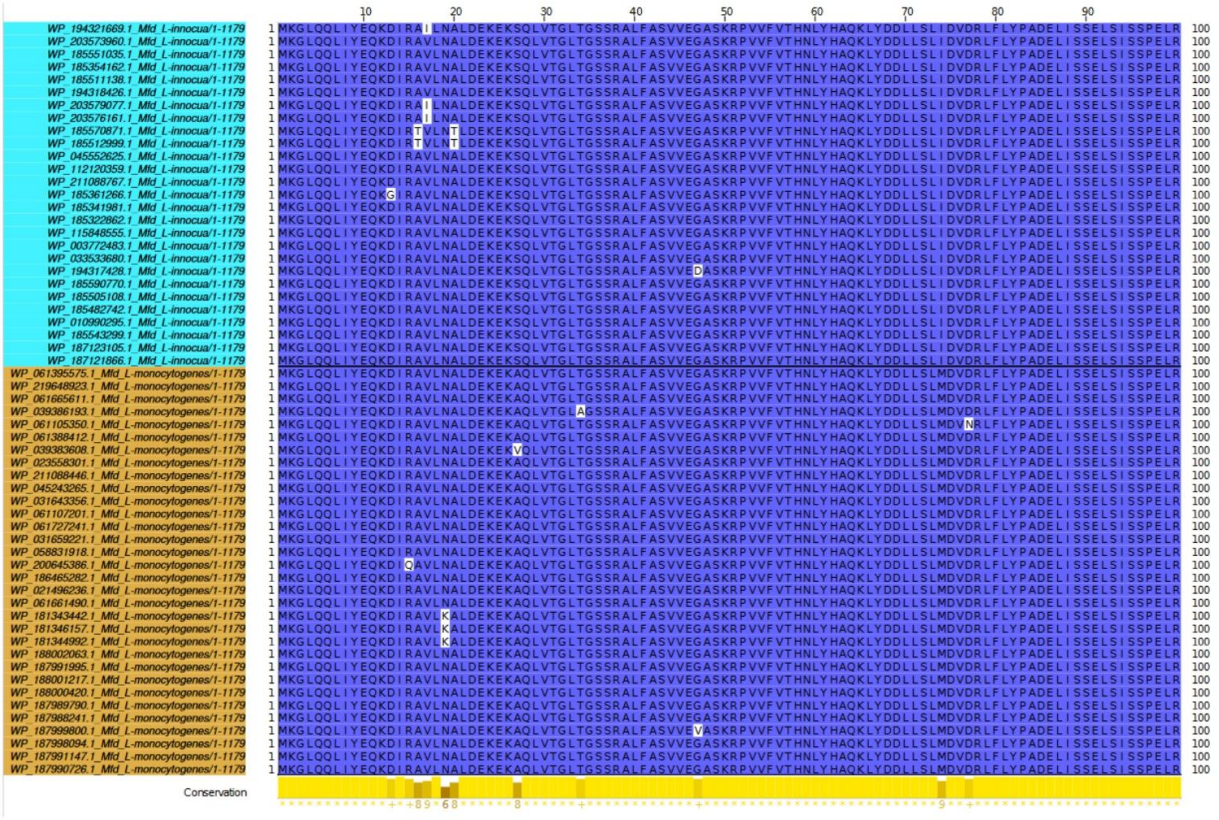

Supp fig. 1

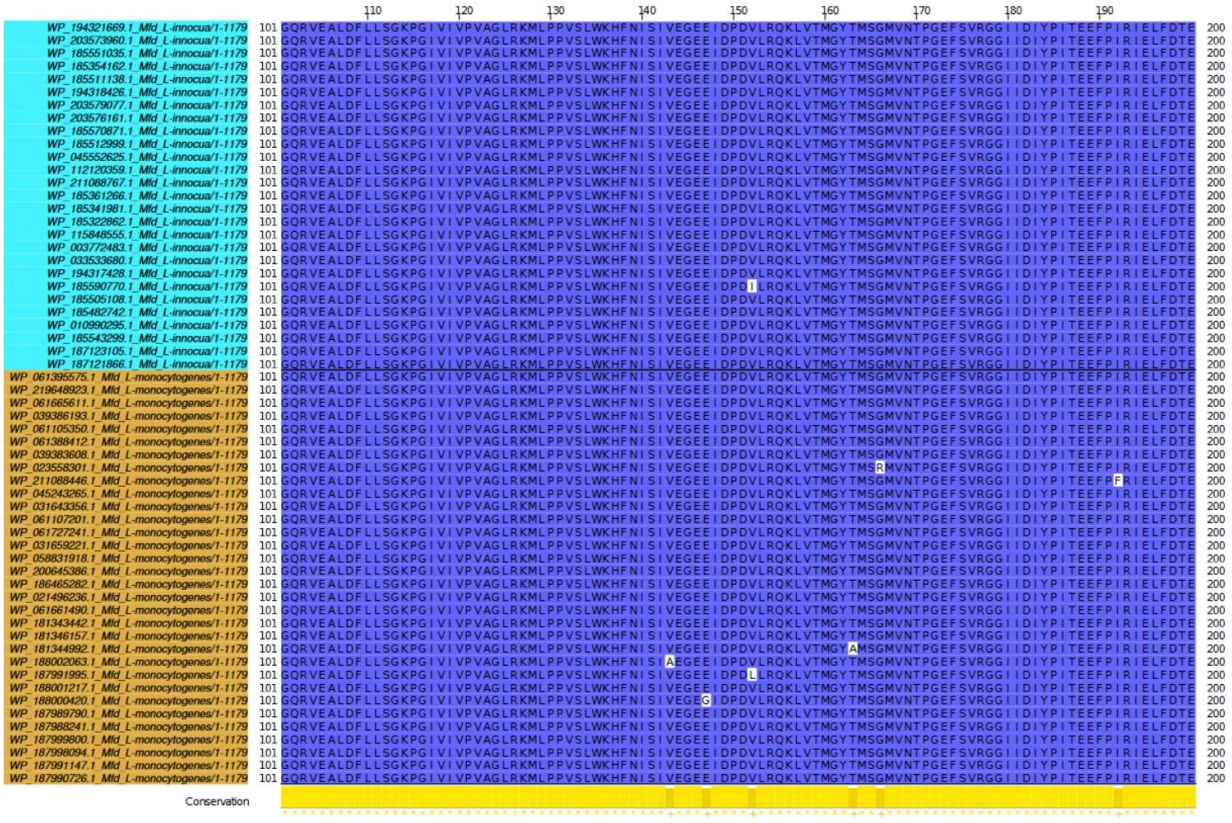

Supp fig. 1

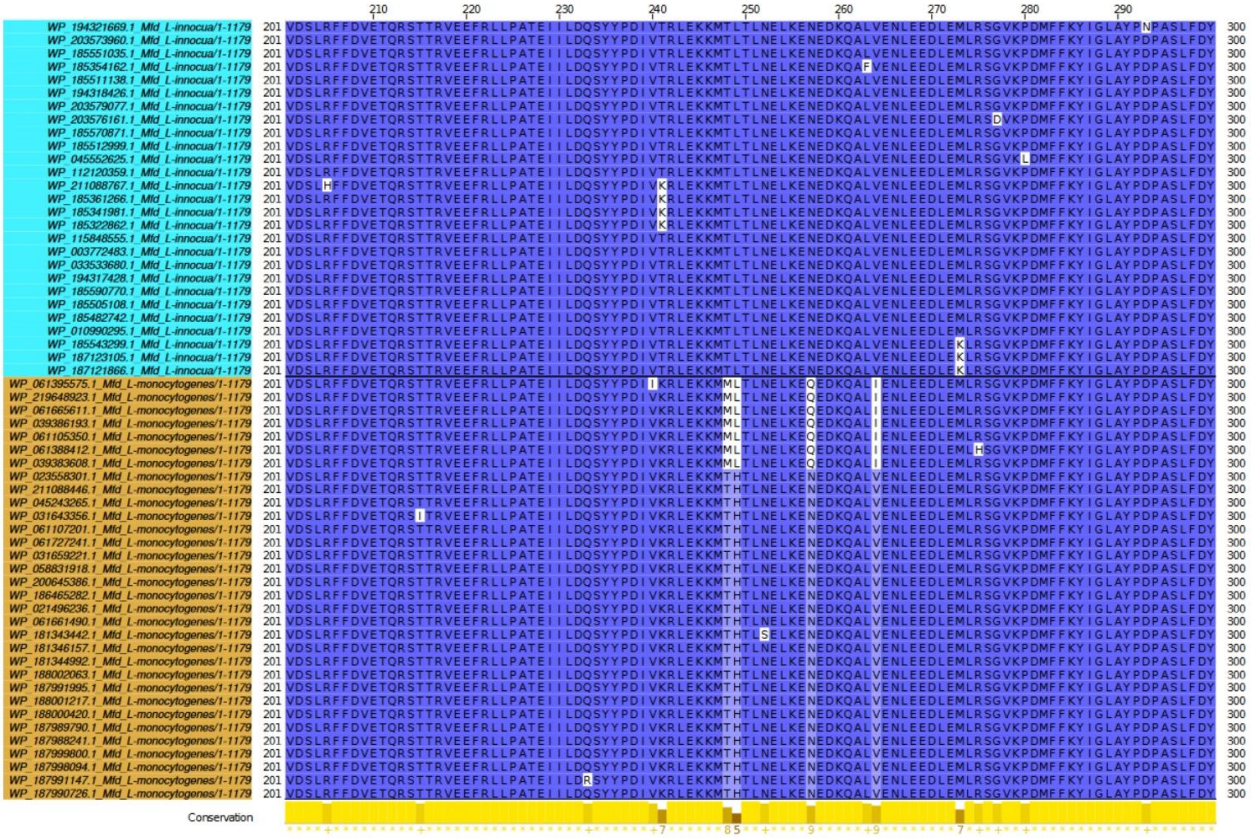

Supp fig. 1

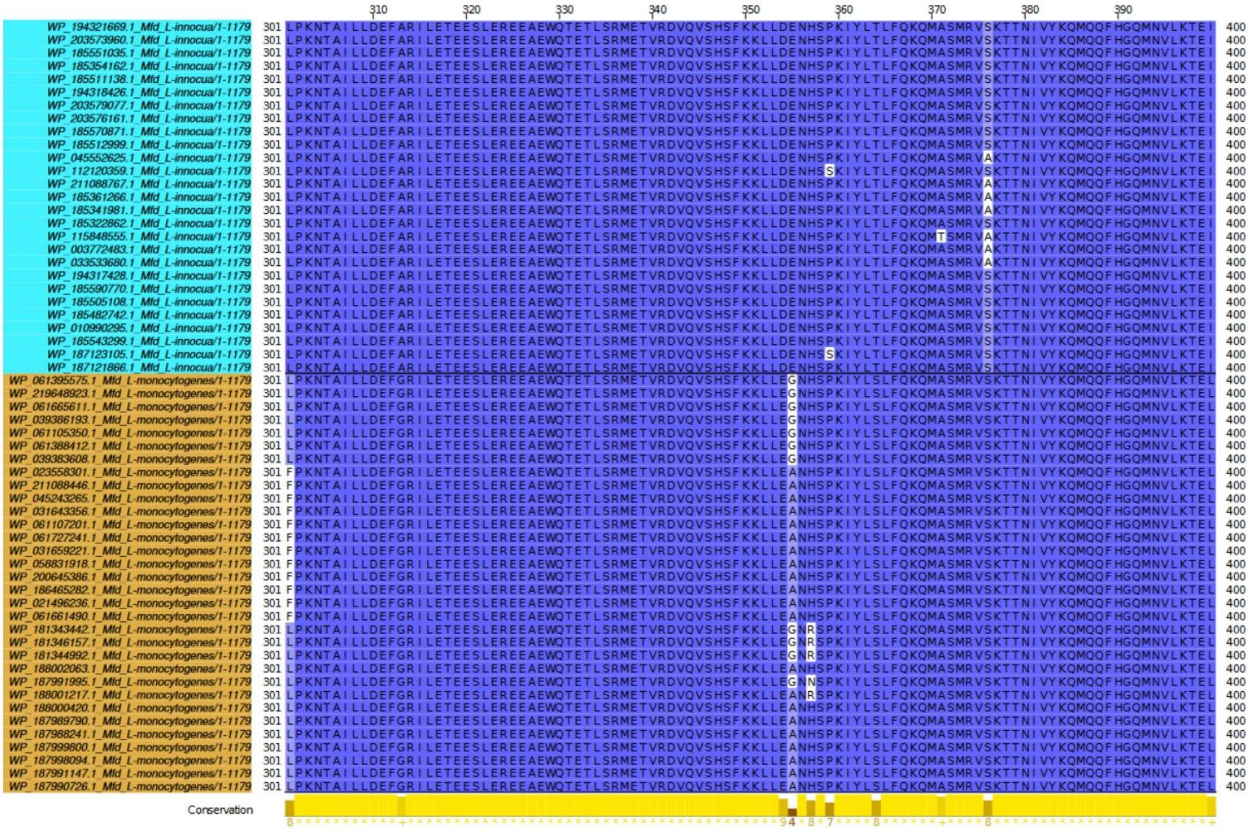

Supp fig. 1

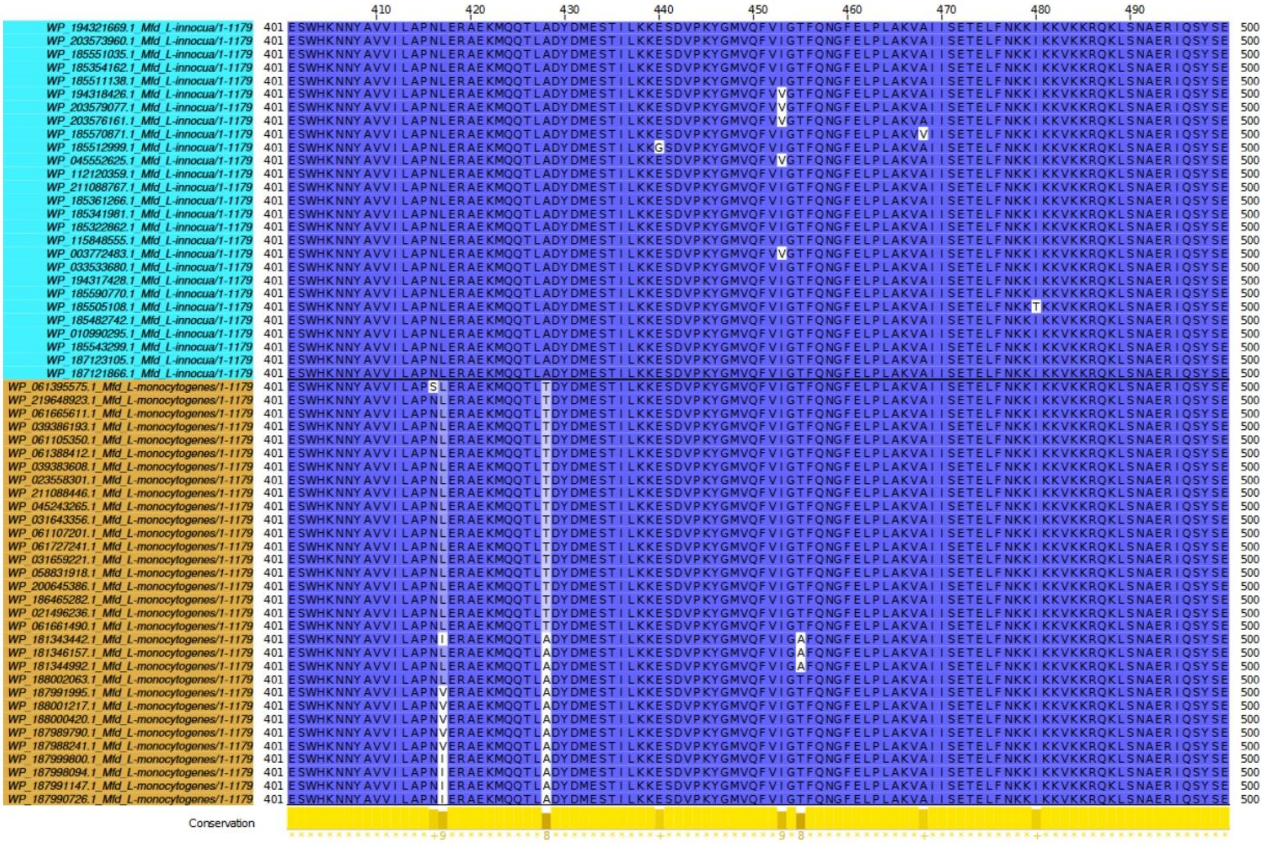

Supp fig. 1

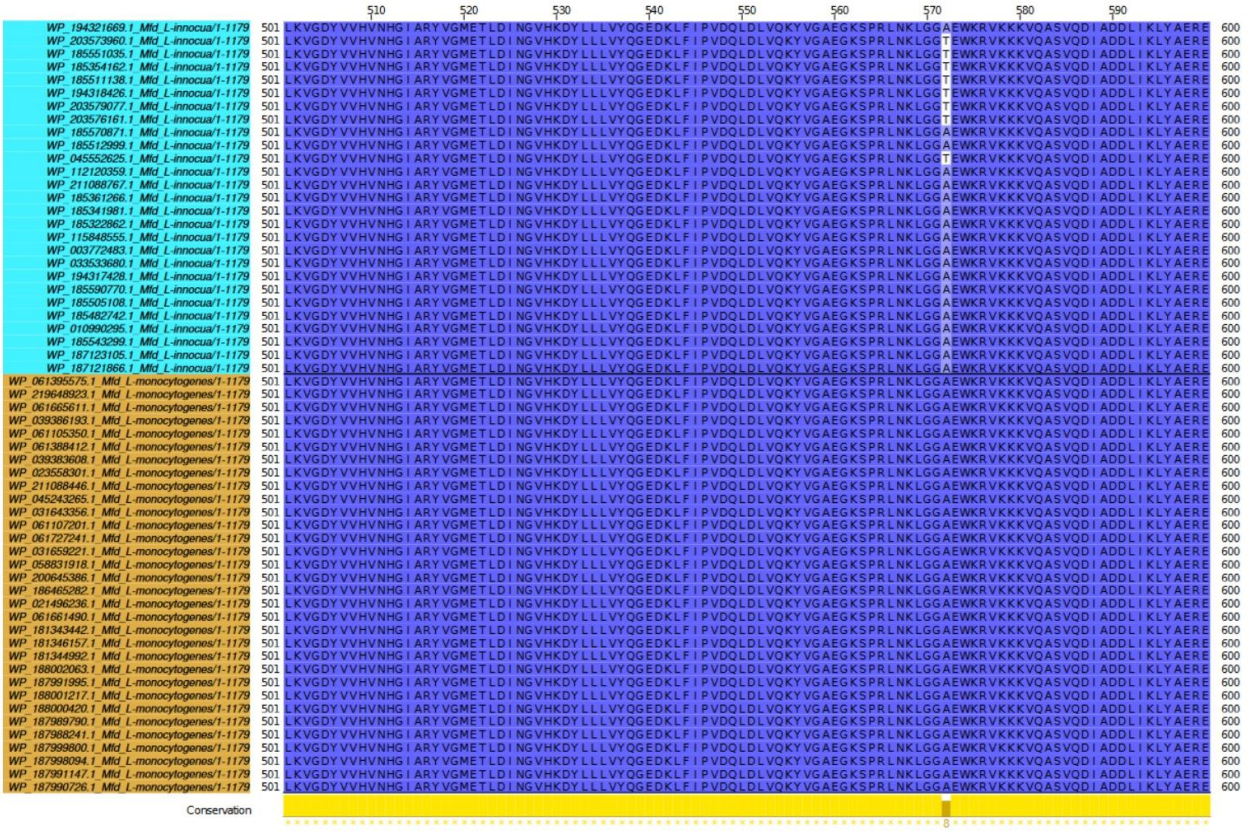

Supp fig. 1

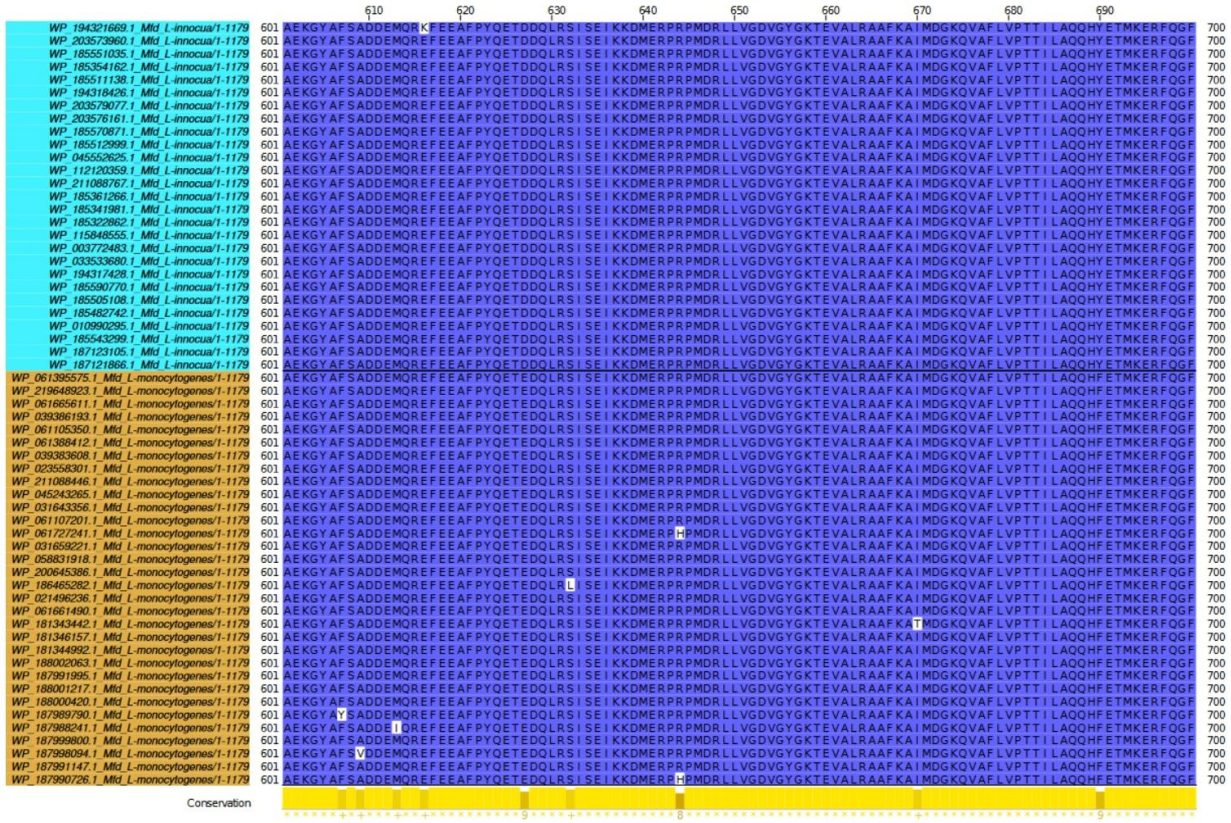

Supp fig. 1

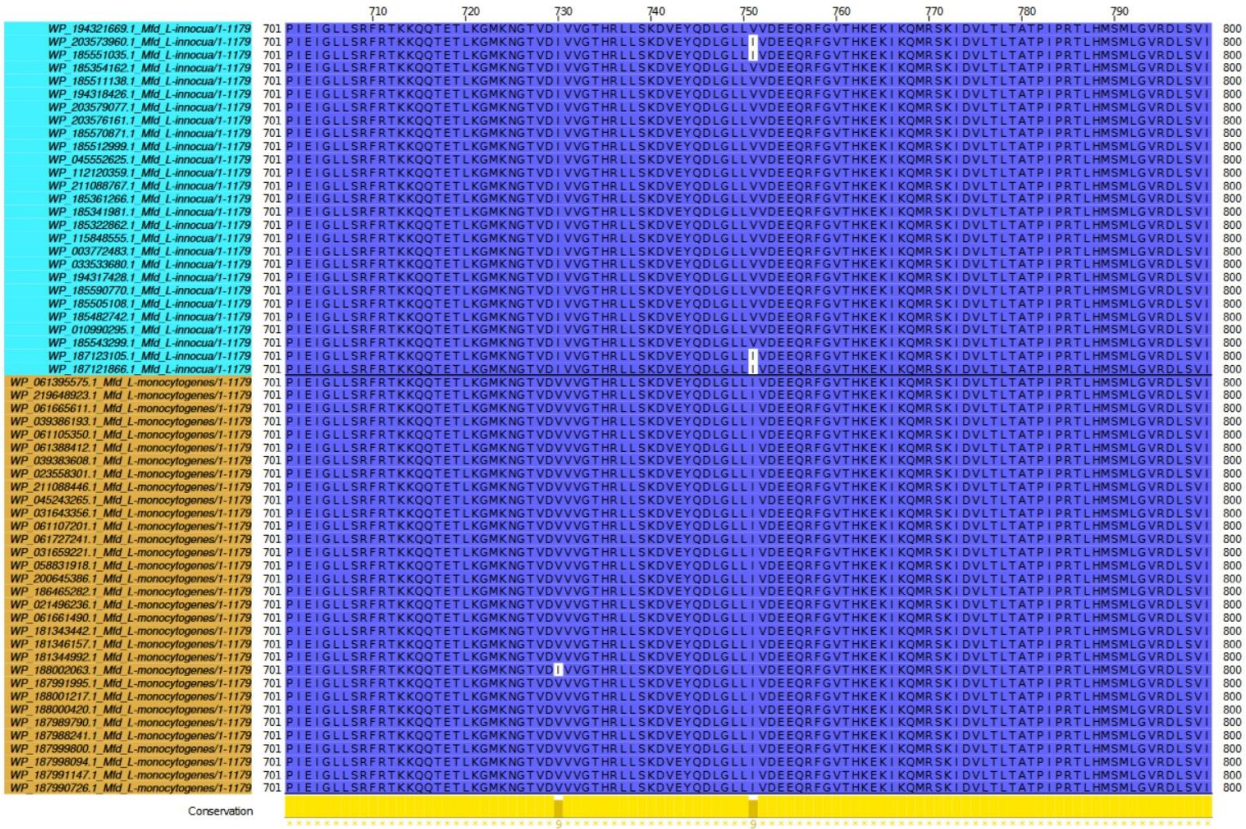

Supp fig. 1

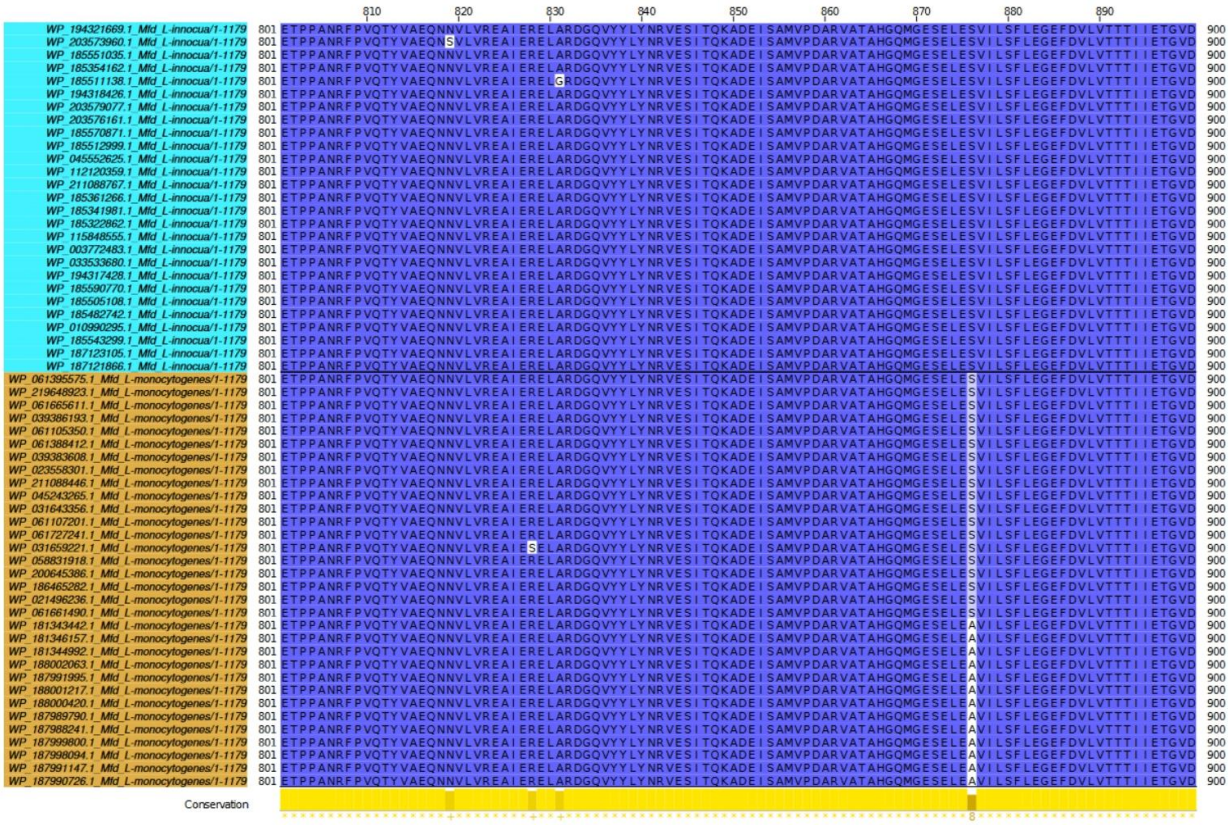

Supp fig. 1

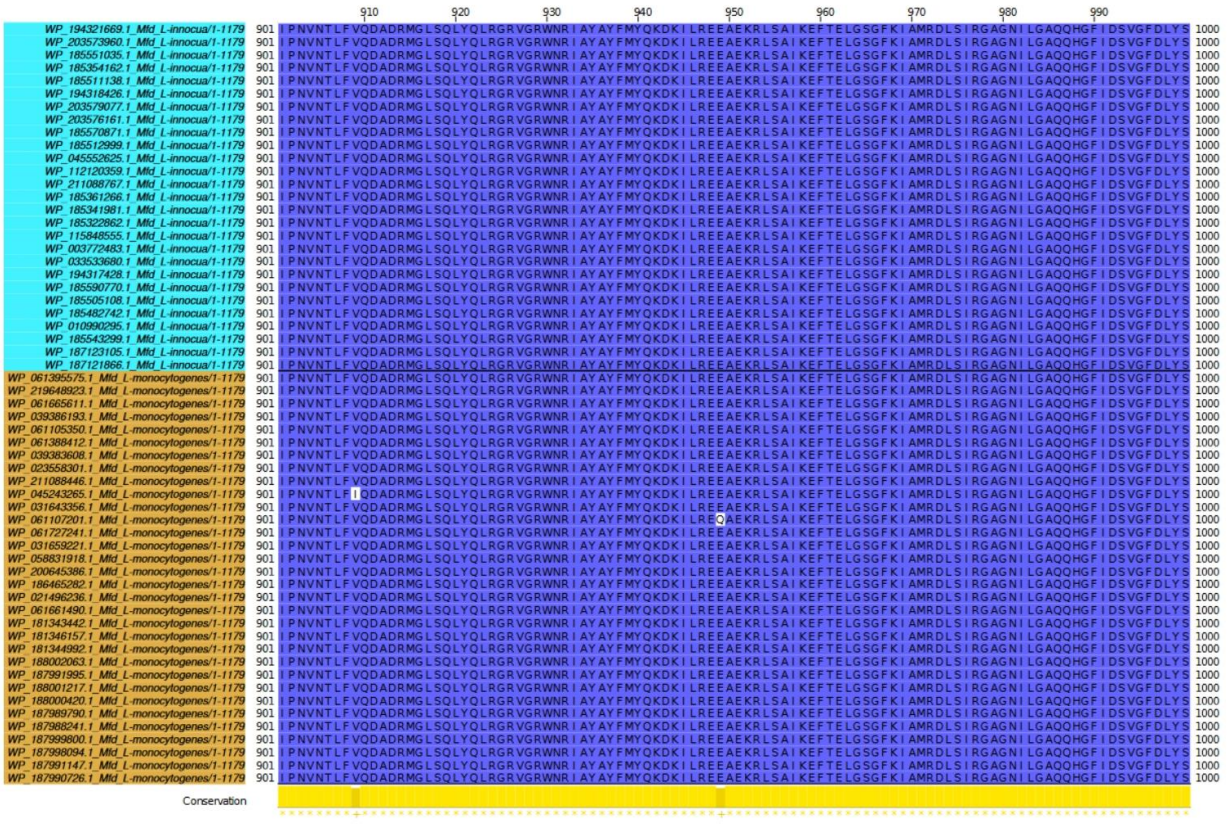

Supp fig. 1

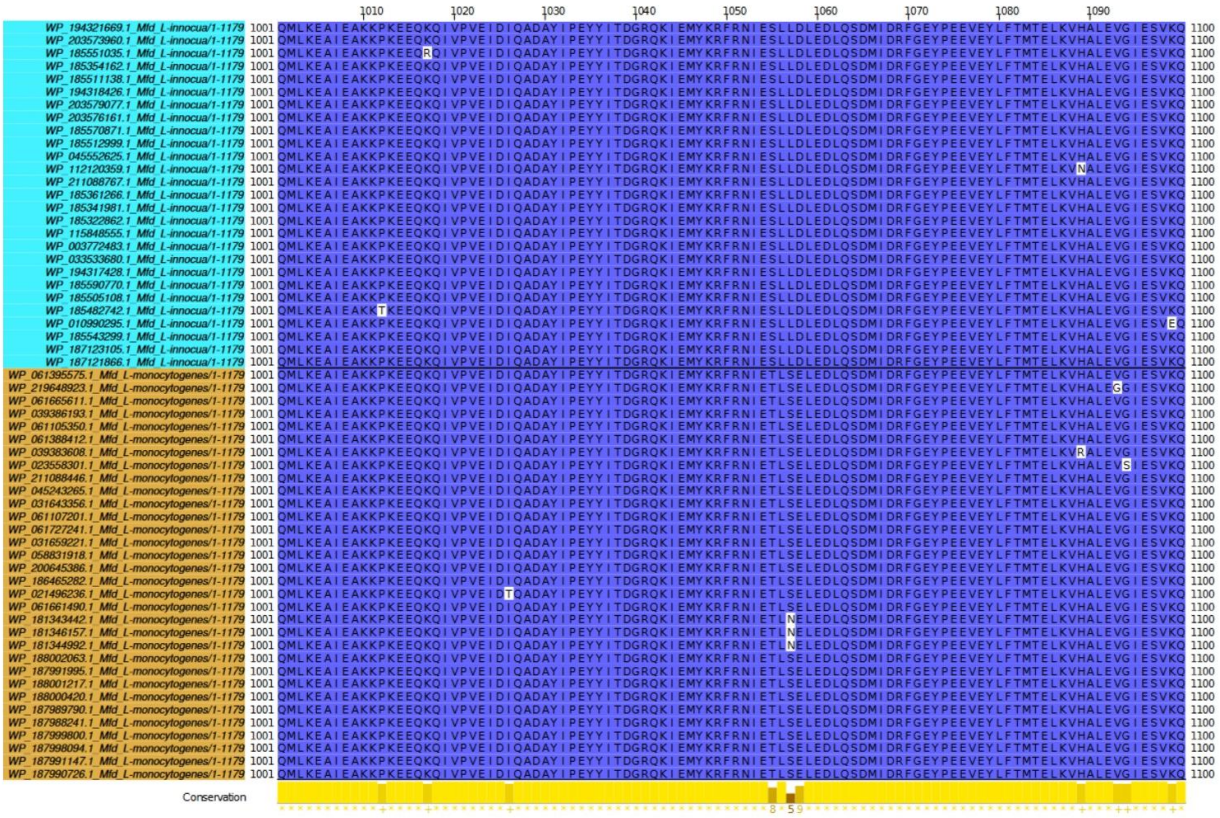

Supp fig. 1

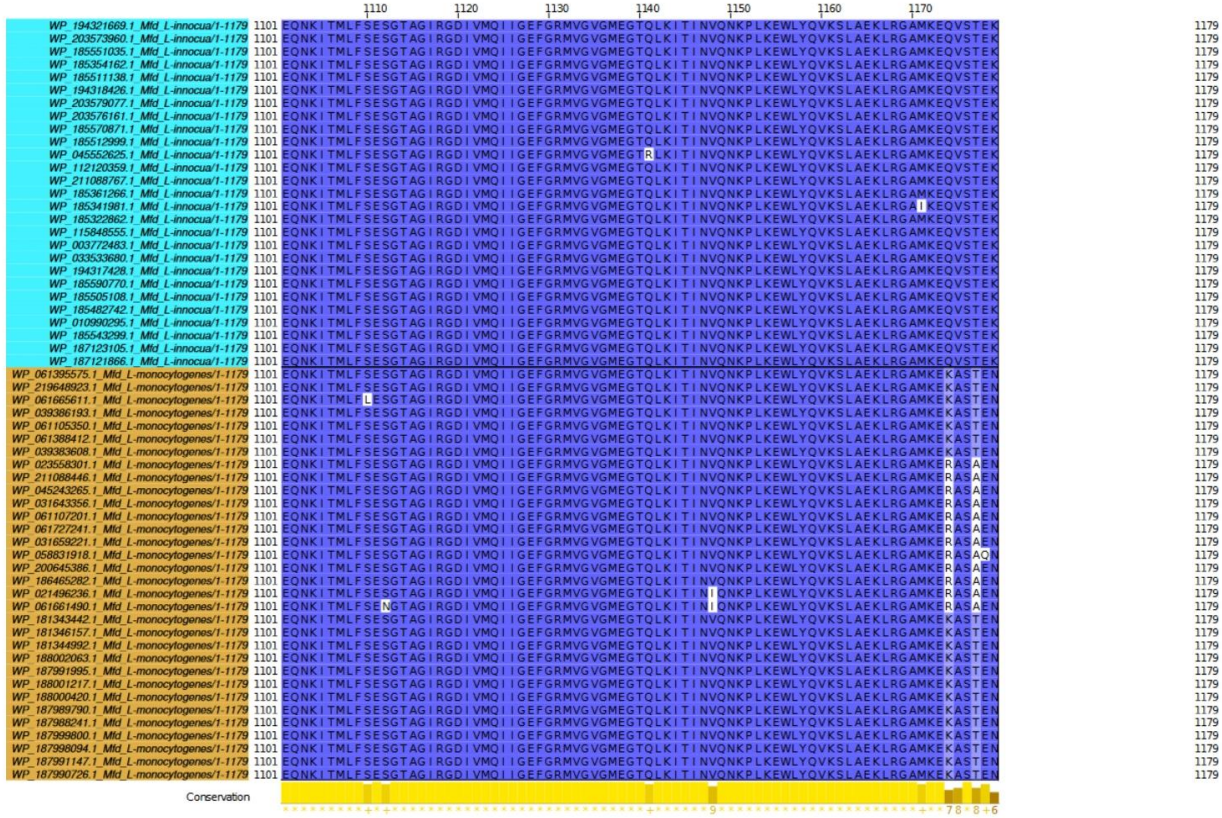

Supp fig. 1

3. Étude complémentaire sur le rôle de Mfd en réponse à divers processus cellulaires

Lors de ma thèse, j'ai eu l'opportunité de partir deux mois en Allemagne, à Tübingen, au sein de l'unité « Microbiome-Host-Interactions » de Lisa Maier qui étudie le microbiome dans différentes conditions de stress qu'il peut rencontrer. Grâce à une plateforme automatisée et à haut débit, ils sont capables de tester des librairies de molécules afin de mesurer leur impact sur différentes espèces et communautés bactériennes retrouvées dans le microbiome humain.

Avec cette collaboration, j'ai eu l'opportunité de tester 21 composés pour voir leur impact sur la croissance bactérienne de souches sauvage ou mutante pour *mfd*. Parmi les composés testés, 13 ont été sélectionnés pour leur capacité à induire des dommages sur l'ADN et les 8 restants sont des molécules utilisées dans différents traitements de maladies humaines et pour lesquels l'équipe de Lisa Maier a observé un impact sur la croissance bactérienne. J'ai cherché à observer l'implication de Mfd dans la réponse bactérienne dans différents types de stress. Grâce à leur plateforme automatisée, j'ai pu effectuer ces tests en condition aérobie et anaérobie.

Expérimentalement, j'ai utilisé *K. pneumoniae* et son mutant pour *mfd*, notre souche de laboratoire de *B. cereus* Bc407 et son mutant *Δmfd*, la souche clinique de *B. cereus* S53 et son mutant et enfin la souche environnementale S50 a été rajoutée pour voir si S53 Δ*mfd* présente des résultats similaires à celle-ci. En condition anaérobie, j'ai aussi rajouté la souche *E. coli* UTI89 comme contrôle puisqu'elle est utilisée dans les tests du laboratoire. Des plaques 96 puits ont été préparées en amont contenant 50 µL de LB dans lesquels les composés sont dilués pour obtenir une gamme de concentration finale à 160 ; 80 ; 40 ; 20 ; 10 ; 5 ; 2,5 et 1,25 µM et avec une ligne contrôle dans chacune des plaques contenant 1 % de DMSO ou de H_2O final selon les milieux de re-suspension utilisés pour les composés. Ces plaques sont conservées à -20 °C jusqu'à leur utilisation. Que ce soit en condition aérobie ou anaérobie, je suis partie d'une culture de nuit qui est diluée à DO = 0,04 en milieu LB où 50 µL sont ajoutés dans chaque puits des plaques 96 puits préparées précédemment. En condition aérobie, les plaques ont été incubées à 37 °C pendant 24 h dans un TECAN prenant des mesures d'absorbance toutes les heures. En condition anaérobie, les plaques ont été placées dans un lecteur de plaque pouvant contenir jusqu'à 18 plaques en même temps. Celles-ci ont aussi été incubées pendant 24 h à 37 °C avec une mesure de l'absorbance toutes les heures. Les analyses ont été effectuées sur R afin de calculer les concentrations inhibant différents pourcentages de la croissance. Pour ces analyses, seulement les sept premières heures de croissance ont été sélectionnées et je vais présenter les résultats pour une inhibition moyenne (50 % de la croissance) et une inhibition forte (90 % de la croissance).

En condition aérobie, pour 50 % d'inhibition (Figure 18), on voit que la souche Bc407 Δ*mfd* est plus sensible que la souche sauvage à l'étoposide, le clomiphène, la streptozotocine et la phléomycine. À l'opposé, la souche sauvage est plus sensible à la félopidine. L'étoposide, la phléomycine et la streptozotine entrainent des dommages sur l'ADN tandis que le clomiphène et la félodine sont utilisés dans le traitement de l'infertilité chez la femme et de l'hypertension respectivement. Néanmoins, aucune de ces différences n'est significative. Pour *K. pneumoniae*, la seule différence notable se trouve lors d'une exposition au NQO, un composé induisant la production d'espèces réactives de l'oxygène. Le mutant est plus sensible que la souche sauvage mais encore une fois, cela n'est pas significatif. Lorsque l'on s'intéresse à 90 % d'inhibition, on ne retrouve aucune différence entre notre souche sauvage et mutante (Figure 19). Entre les souches S50 et S53, nous retrouvons des différences d'inhibition mais cela ne corrèle pas avec les résultats obtenus entre Bc407 sauvage et Bc407 *Δmfd*.
En condition anaérobie, pour 50 % d'inhibition (Figure 20), il n'y a aucune différence entre la souche S53 et le mutant S53 *Δmfd*. Entre la souche Bc407 sauvage et la souche Bc407 *Δmfd*, on peut voir que le mutant semble plus sensible au nitrofurazone, au clomiphène, à l'étoposide et à la félopidine. La seule différence qui pourrait être significative est celle au nitrofurazone, un antibiotique entraînant la production de NO (oxyde nitrique) et de dommages sur l'ADN. Néanmoins, cette différence n'est pas retrouvée pour la souche S53 et *K. pneumoniae*. Entre *K. pneumoniae* sauvage et mutant, il y a une différence de MIC pour la streptozotocine, le NQO et la floxuridine mais cette différence est trop légère pour être significative. À 90 % d'inhibition (Figure 21), le mutant de la souche S53 est plus sensible à l'ofloxacine, à la diacerine, à l'acide nalidixic, et au NQO. Seule la différence à l'ofloxacine, un antibiotique de la famille des fluoroquinoles, pourrait être significative mais cela est difficile à juger avec les résultats actuels puisque l'on ne trouve pas cette différence à des concentrations d'inhibition plus basses, la valeur de la MIC étant en dessous de la gamme utilisée. Contrairement à ce qu'on a pu voir précédemment, cette fois-ci nous avons une souche mutante de *mfd* qui est moins sensible au clomiphène que la souche sauvage. Alors que nous avons observé ce résultat chez la souche S53, c'est le contraire chez Bc407 où le mutant reste toujours plus faible. L'effet du clomiphène, bien que prometteur, semble être souche- dépendant chez *B. cereus*. Pour S53 comme pour Bc407, les souches sauvages sont plus sensibles au tiratricol, un médicament utilisé dans le traitement de cancer de la tyroïde, que la souche mutante. Néanmoins, aucun impact du tiratricol n'a été observé à des pourcentages d'inhibition inférieurs alors que le calcul d'une MIC a pu être effectué. Pour Bt407, on peut voir que le mutant est plus sensible la floxuridine, ce que nous ne pouvions pas observer précédemment car la MIC est en dessous de notre gamme à 50 % d'inhibition. Dans le cas opposé, nous avons la ciprofloxacine pour laquelle la souche sauvage est plus sensible que la souche mutante pour Bc407 et *K. pneumoniae*. Lorsque l'on s'intéresse à *K. pneumoniae*, aucune des différences calculées n'est assez importante pour être significative. En condition anaérobie, nous avions aussi testé

sur deux composés qui semblaient les plus prometteurs, l'impact du NM102 sur la croissance de *K. pneumoniae*. Nous avons sélectionné le NQO et la streptozocine mais pour chacun, aucune action du NM102 n'a été observée.

À l'issue de l'analyse de ces résultats, on peut voir que certains composés ressortent comme ayant potentiellement un impact sur la croissance liée à la présence de Mfd. Néanmoins, cet impact est la plupart du temps trop faible pour être significatif. Même si j'ai pu voir des différences dans les MIC en condition anaérobie, cette expérience pourrait être améliorée avec l'utilisation d'un milieu plus approprié que le LB pour la croissance en anaérobie.

Dans les rares cas où nous avons des différences qui sont significatives, cela semble être spécifique à une souche. Il aurait été intéressant de poursuivre les études sur quelques-uns de ces composés comme le NQO, le nitrofurazone (qui a montré des résultats intéressants mais non significatifs à 10 %, 25 %, 50 %, et 75 % d'inhibition en condition anaérobie) ou encore le clomiphène. L'ofloxacine et la floxuridine, qui sont respectivement un antibiotique de la famille des fluoroquinolones et une molécule utilisée dans le traitement de cancers en inhibant la synthèse d'ADN et d'ARN, pourraient être prometteurs en utilisant une gamme de concentration allant plus bas.

Malheureusement, par manque de temps en Allemagne, je n'ai pas pu poursuivre cette étude. Néanmoins, j'ai eu l'opportunité d'apprendre de nouvelles techniques dans le criblage à haut débit de molécules avec l'utilisation d'un robot capable de contenir plusieurs plaques 96 puits en même temps et d'effectuer les mesures d'absorbance pour chacune. J'ai eu aussi l'opportunité d'apprendre à travailler en conditions anaérobies qui était quelque chose que je n'avais pas encore eu la possibilité d'effectuer auparavant. Ce fut une expérience enrichissante scientifiquement parlant mais aussi humainement parlant avec la rencontre et l'échange de savoirs et de culture.

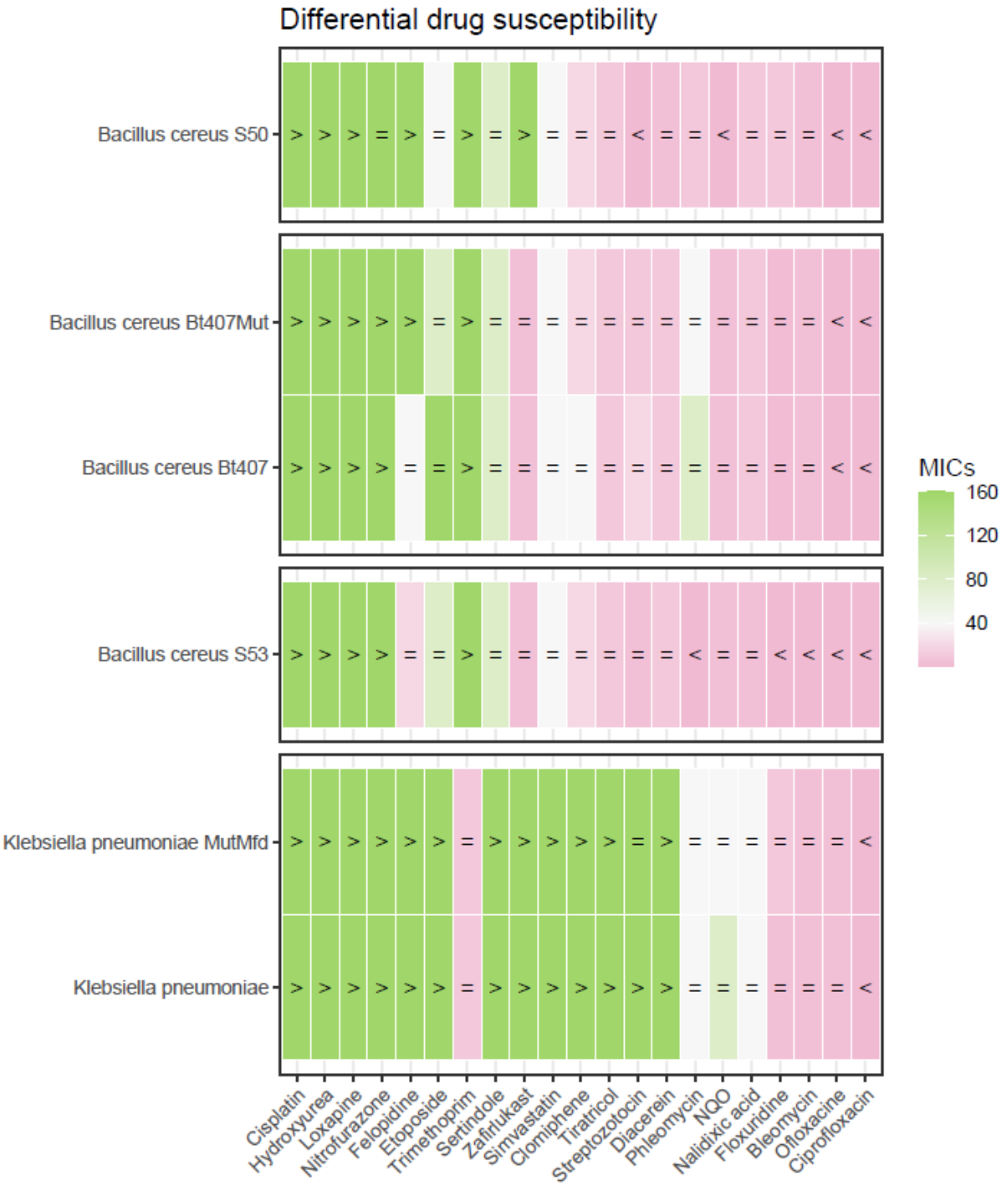

Figure 18 : CMI calculée pour obtenir 50 % d'inhibition de la croissance en condition aérobie (> : CMI supérieure à ; = CMI calculée ; < CMI inférieure au minimum de la gamme).
Les CMI sont calculées en µM et N = 3.

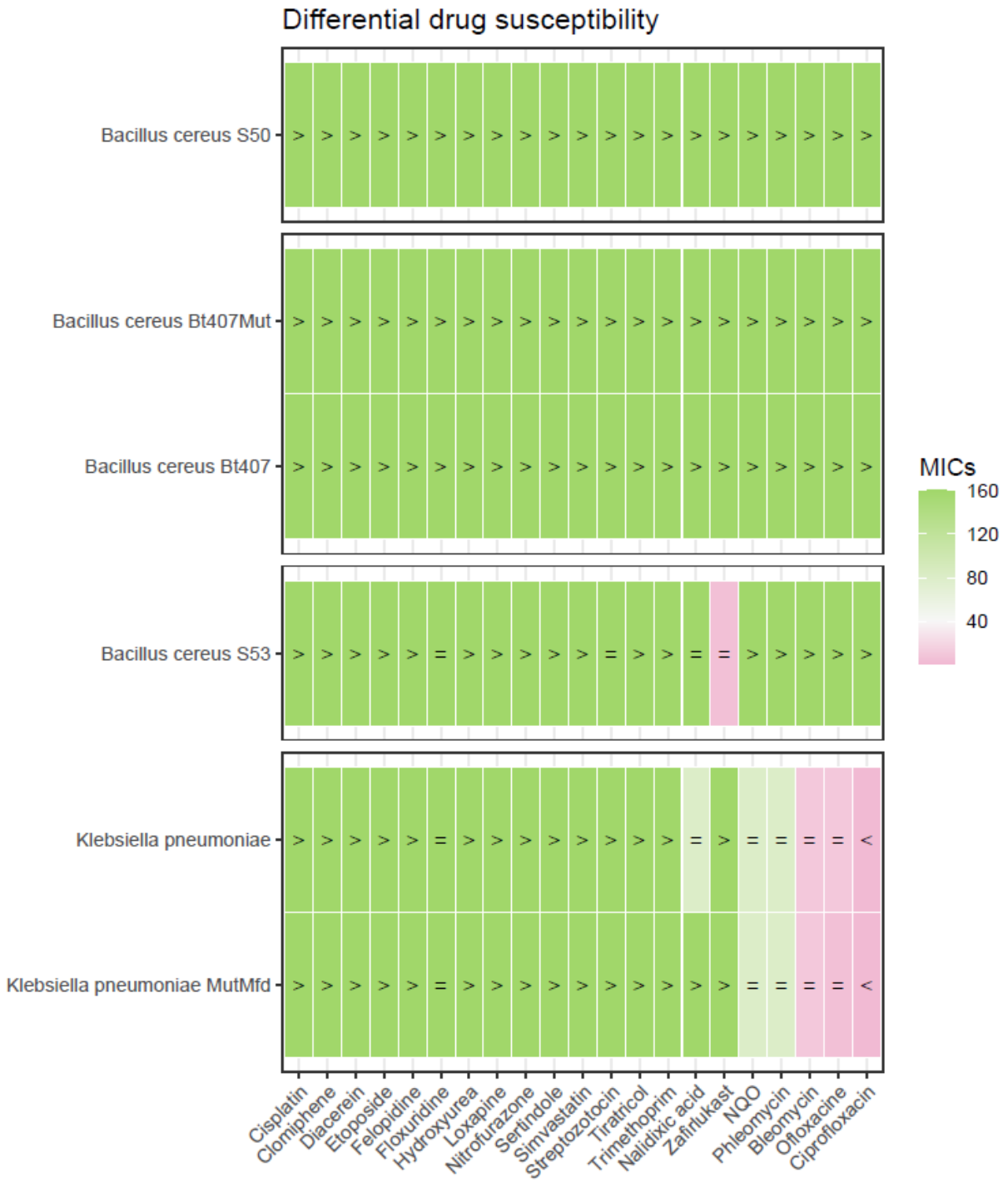

Figure 19 : CMI calculée pour obtenir 90 % d'inhibition de la croissance en condition aérobie (> : CMI supérieure à ; = CMI calculée ; < CMI inférieure au minimum de la gamme).
Les CMI sont calculées en µM et N = 3.

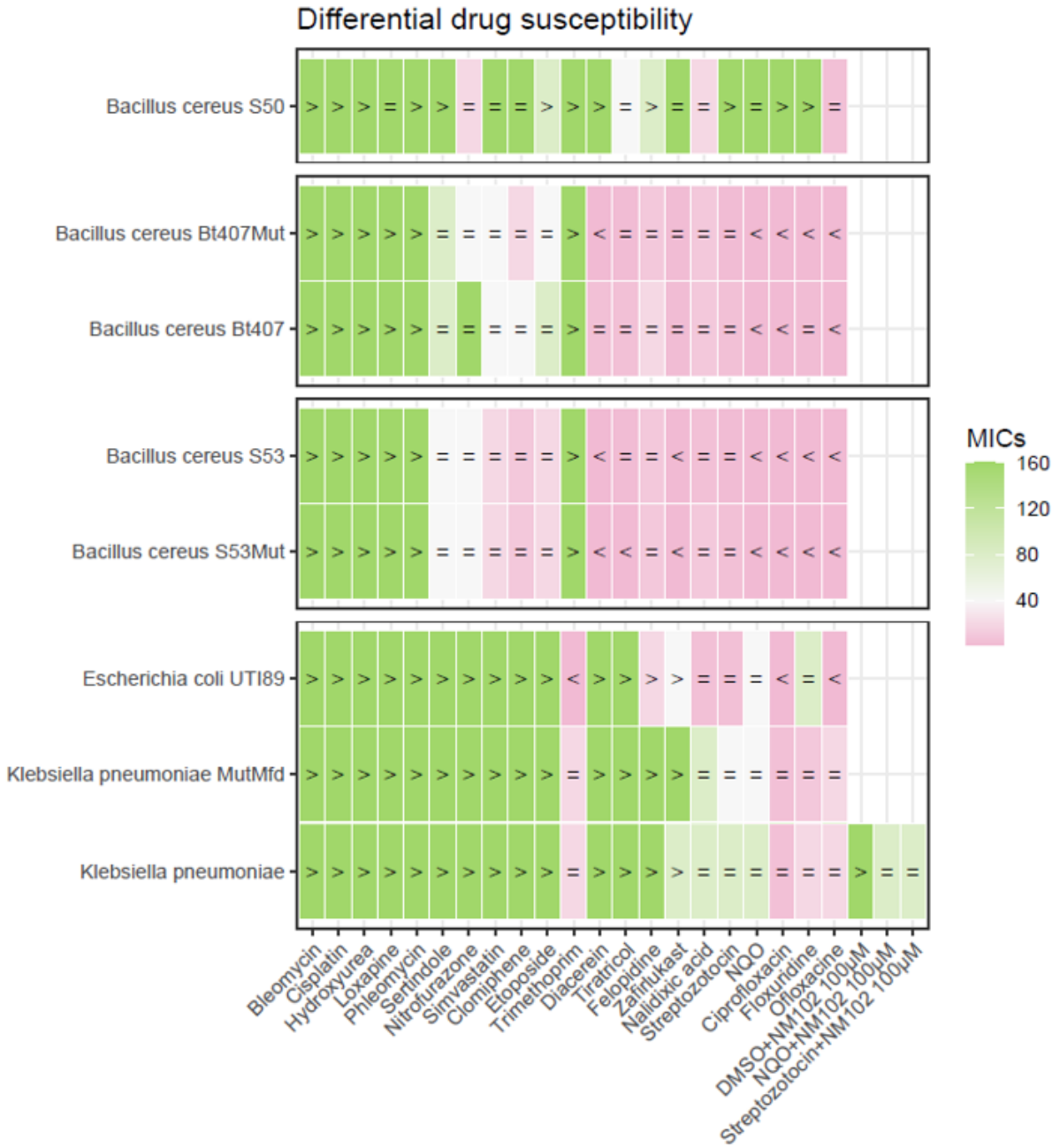

Figure 20 : CMI calculée pour obtenir 50 % d'inhibition de la croissance en condition anaérobie (> : CMI supérieure à ; = CMI calculée ; < CMI inférieure au minimum de la gamme).
Les CMI sont calculées en µM et N = 3.

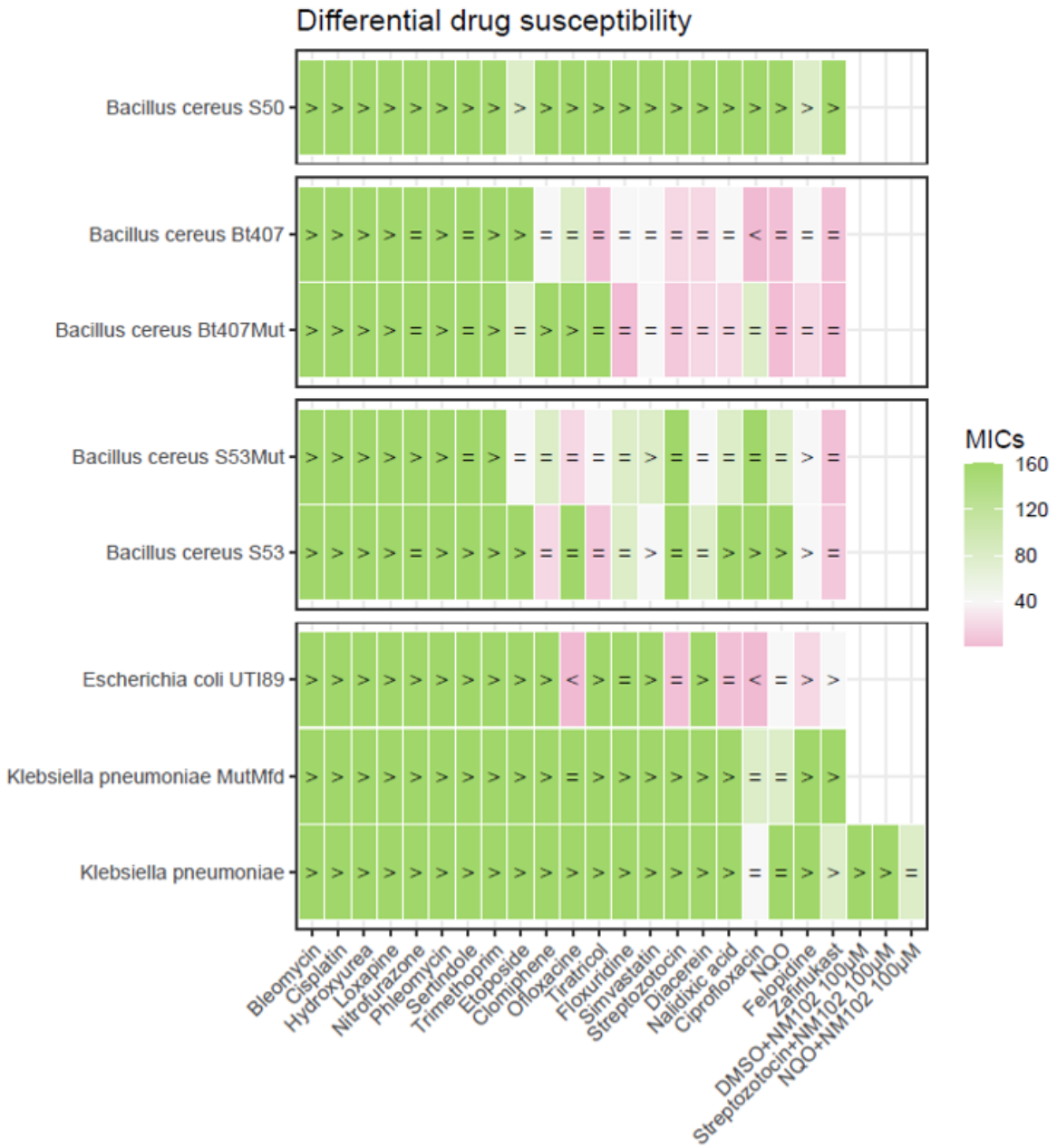

Figure 21 : CMI calculée pour obtenir 90 % d'inhibition de la croissance en condition anaérobie (> : CMI supérieure à ; = CMI calculée ; < CMI inférieure au minimum de la gamme).
Les CMI sont calculées en µM et N = 3

Partie 2 : Mfd en tant que cible pour le développement de nouveaux antimicrobiens

1. Résumé article 2

La lutte contre les infections bactériennes est redevenue un challenge avec l'émergence et la propagation de souches résistantes aux antibiotiques actuellement utilisés. A l'heure actuelle, 700 000 personnes décèdent d'infections causées par des bactéries résistantes et ce nombre pourrait passer à 10 millions d'ici 2050, devenant alors la première cause de mortalité dans le monde. Un groupe de bactéries, appelé ESKAPE (*Enterococcus faecium, Staphylococcus aureus, Klebsiella pneumoniae, Acinetobacter baumannii, Pseudomonas aeruginosa* et *Enterobacter spp*), est constitué des bactéries considérées par l'OMS comme présentant une menace majeure et pour lesquelles il est urgent de développer de nouveaux antibiotiques.

Avec cette crise en cours, la recherche et le développement d'antibiotiques ont eu un regain d'intérêt ces dernières années. De nombreuses pistes dans le développement de nouvelles solutions thérapeutiques restent encore à explorer. Dans l'article qui va suivre, nous nous sommes intéressés à une nouvelle cible innovante : la protéine Mfd. Cette protéine est non essentielle, ubiquitaire, conservée et absente chez les eucaryotes et est impliquée dans la réparation de l'ADN, la mutagénèse ou encore la transcription. Des études réalisées dans notre équipe ont montré que Mfd était impliquée dans la virulence de *B. cereus* et *S. flexneri* en conférant une résistance au stress nitrique généré lors de la réponse immunitaire. De plus, Mfd a été associée au développement de résistances via son rôle dans la mutagénèse. Une molécule inhibant Mfd ne serait pas bactéricide mais limiterait la capacité des bactéries à résister au système immunitaire et à développer des résistances aux antibiotiques. Etant donné que notre stratégie thérapeutique repose sur la réponse immunitaire, l'action du composé serait spécifique au site de l'inflammation. Cela réduirait la pression pour le développement de résistances et ne toucherait pas les bactéries du microbiome si celui-ci n'est pas le lieu d'inflammation.

Avant mon arrivée au laboratoire, afin de trouver un inhibiteur de Mfd, l'équipe a effectué un criblage à haut débit *in silico* au niveau de la poche ATPase de Mfd pour identifier des molécules qui pourraient rentrer en compétition avec l'ATP et donc bloquer l'activité de la protéine. Un modèle 3D de Mfd d'*E. coli* a été utilisé pour cribler une bibliothèque contenant 4,8 millions de composés. 95 molécules ont été sélectionnées comme potentiels inhibiteurs et l'étude de leur impact sur l'activité de Mfd a été poursuivie *in vitro*. Le taux d'inhibition a été mesuré sur une Mfd de *E. coli* grâce à un test ATPase et une gamme d'inhibition entre 10 % et 85 % a été obtenu. Une dose réponse a été réalisée sur le meilleur inhibiteur, appelé NM102, qui présente un IC_{50} à 29 µM et un K_i à 27 µM. Par ailleurs, l'effet

de la molécule est spécifique à Mfd puisqu'elle n'inhibe pas l'activité ATPase de la protéine eucaryote yUpf1.

Une étude *in silico* menée en parallèle a montré que le NM102 est capable de se positionner dans les poches ATPase des bactéries du groupe ESKAPE et que l'énergie de liaison nécessaire est plus faible que celle de l'ATP. L'affinité du NM102 pour se placer dans la poche ATPase de Mfd est donc plus importante que l'ATP. Cela suggère que le NM102 pourrait être un inhibiteur universel de Mfd.

Mfd, en absence de stress, est non essentielle à la survie de la bactérie. Le NM102 a été montré comme ne présentant pas d'activité antimicrobienne sur *K. pneumoniae* et *P. aeruginosa*, deux membres du groupe ESKAPE. Pour mesurer l'efficacité du NM102, il faut donc mimer les conditions dans lesquelles la protéine devient nécessaire. Pour cela nous avons effectué un stress nitrique *in vitro* dans lequel Mfd joue un rôle majeur. La molécule entraine une forte inhibition de la survie de *K. pneumoniae* en condition de stress avec une IC_{50} à 7.5 µM. Le NM102 est aussi capable d'inhiber la survie d'*E. coli* et de *P. aeruginosa* mais nécessite des doses plus fortes avec de IC_{50} calculées respectivement à 61,2 µM et 94,2 µM. Cette efficacité en condition de stress est aussi visible sur des souches cliniques résistantes aux antibiotiques de *K. pneumoniae* même si cela nécessite une dose plus forte par rapport à une souche sensible. Ces tests *in vitro* ont permis de montrer que le NM102 est capable d'agir sur des bactéries à coloration Gram négative et que cela inclut même des bactéries résistantes difficiles à traiter.

Dans ce projet, je me suis occupée de tester l'activité du NM102 par des tests *in vivo* en utilisant des larves d'insectes *Bombyx eri*. J'ai mis en place le modèle d'infection avec *P. aeruginosa* et testé différents schémas de traitements afin de déterminer lequel était le plus efficace. Le NM102 étant une molécule très peu soluble, son milieu de re-suspension est le DMSO qui est toxique et qui aggrave les infections. Cela a entrainé une limitation dans la quantité de NM102 injectable dans les larves. Afin de contrer la limitation induite par la présence du DMSO et maximiser nos chances d'obtenir une efficacité de la molécule, j'ai mis en place un traitement impliquant deux rappels après infection. En suivant ce schéma de traitement, j'ai pu voir que les insectes infectés par *P. aeruginosa* et traités avec le NM102 contiennent significativement moins de bactéries que les insectes non traités. J'ai pu aussi confirmer que la cible du NM102 était bien Mfd puisque le traitement n'a aucun effet sur la quantité de bactéries retrouvée dans les insectes infectés avec la souche de *P. aeruginosa* Δ*mfd*. Le NM102 présente donc bien une efficacité *in vivo* qui est spécifique à la présence de Mfd.

Pour tester l'efficacité du NM102 *in vivo* dans un modèle murin, il a fallu trouver une solution au problème du DMSO. L'alternative choisie a été l'établissement d'une nanoformulation de NM102 par sonication de PLGA (poly(D-L lactide-co-glycolide)) en présence de NM102, en collaboration avec l'institut Galien. Dans sa nanoformulation le NM102 est capable de se re-suspendre dans un milieu aqueux et peut donc être injecté dans la souris. Le traitement au NM102 dans des souris infectées avec

K. pneumoniae a induit une diminution de la charge bactérienne dans les poumons. Lorsque l'on compare l'efficacité du NM102 avec le méropénème, un antibiotique couramment utilisé, nous observons une efficacité similaire à une concentration moins importante. L'efficacité du méropénème est visible à 10 mg/kg tandis que pour le NM102 celle-ci est visible à 6 mg/kg. Nous avons pu voir aussi que comme pour les insectes, cette efficacité est spécifique à une inhibition de Mfd puisqu'une infection réalisée avec un mutant Δ*mfd* et traitée avec le NM102 n'induit pas de diminution de la charge bactérienne dans les poumons. Lors de tests sur une souche résistante de *K. pneumoniae*, celle-ci est aussi sensible à un traitement au NM102 alors qu'elle est résistante au traitement avec le méropénème. Sur *P. aeruginosa*, on observe un effet synergique avec un traitement combiné de NM102 et méropénème. En conclusion, le NM102 est efficace contre *K. pneumoniae* et *P. aeruginosa* et il peut aussi être utilisé dans un traitement en combinaison avec un autre antibiotique pour améliorer son efficacité.

En plus de mon rôle dans l'établissement d'un modèle insecte et les tests d'efficacité qui ont suivis, j'ai aussi été impliquée dans la caractérisation des souches sensibles et résistantes aux antibiotiques utilisées dans cette étude en réalisant les CMI pour chacune d'entre elles (Supp Table2).

En parallèle des tests d'efficacité, des tests de toxicité sur cellules ont été effectués, ainsi qu'une étude sur l'impact du NM102 sur le microbiome en collaboration avec l'équipe allemande de Lisa Maier. Les résultats indiquent que le NM102 n'a pas d'effet toxique sur l'hôte et son microbiote.

Pour finir, nous avons mis en évidence que le NM102 diminue la fréquence de mutations de *E. coli* et réduit la vitesse d'apparition de résistances à la rifampicine et la streptomycine. Le NM102 permet donc d'inhiber le rôle de Mfd dans la mutagénèse.

En conclusion, nous avons montré que Mfd est une nouvelle cible prometteuse pour le développement de nouveaux antibiotiques avec un mode de fonctionnement innovant. En effet, nous avons développé une stratégie d'antivirulence qui n'entraine pas d'inhibition de la croissance bactérienne ou qui n'est pas bactéricide. Nous inhibons la capacité des bactéries à échapper au système immunitaire de l'hôte. De cette façon, en ciblant une protéine non essentielle, nous diminuons la pression pour le développement de résistances et l'impact d'un traitement sur les microbiomes de l'hôte. Par le choix de notre cible, nous avons aussi la particularité de pouvoir potentiellement toucher un large panel de bactérie étant donné que Mfd est ubiquitaire et conservée, ce qui est rare pour de l'antivirulence. De plus, nous n'avons pas seulement un impact sur la survie bactérienne mais aussi sur le développement de résistances. Cela veut dire qu'un inhibiteur de Mfd, en traitement seul ou combiné, permettrait de limiter l'apparition de nouvelles souches résistantes.

2. Article 2 : An anti-virulence drug targeting the evolvability protein Mfd protects against infections with antimicrobial resistant ESKAPE pathogens

En révision pour Cell Host and Microbes

An anti-virulence drug targeting the evolvability protein Mfd protects against infections with antimicrobial resistant ESKAPE pathogens

SL. Tran[1], L. Lebreuilly[1], D. Cormontagne[1], S. Samson[1,2], TB. Tô[1,3], R. Dervyn[1], A. Grießhammer[4,5], N. Akduman[4,5], J. de la Cuesta-Zuluaga[4,5], L. Maier[4,5], T. Naas[6], S. Mura[3], J. Nicolas[3], D. Rognan[7], G. André[2] and N. Ramarao[1]*

[1]Université Paris-Saclay, INRAE, Micalis Institute, 78350, Jouy-en-Josas, France

[2]Université Paris-Saclay, INRAE, MaIAGE, 78350, Jouy-en-Josas, France

[3]Université Paris-Saclay, CNRS, Institut Galien Paris-Saclay, 92296, Châtenay-Malabry, France

[4]Interfaculty Institute of Microbiology and Infection Medicine, University of Tübingen, Tübingen, Germany

[5]Cluster of Excellence 'Controlling Microbes to Fight Infections', University of Tübingen, Tübingen, Germany

[6]Team ReSIST, INSERM U1184, School of Medicine Université Paris-Saclay, LabEx LERMIT, Assistance Publique/Hôpitaux de Paris, French NRC for Carbapenemase-producing Enterobacterales, Bicêtre Hospital, 94270 Le Kremlin-Bicêtre, France

[7]Université de Strasbourg, CNRS, UMR 7200, LIT, 67400 Illkirch, France

*Correspondance to nalini.ramarao@inrae.fr

Highlight

- NM102 is a “first in class” molecule specifically targeting the active site of the bacterial Mfd protein
- NM102 has a new mode of action: it inhibits Mfd function during immune stress response
- NM102 also inhibits Mfd evolvability function and thereby decreases bacterial resistance to known antibiotics
- NM102 effectively treats Gram-negative infections in animal models
- NM102 is efficient against clinically relevant resistant bacteria and provides an increased efficacy in combination with the β-lactam meropenem
- NM102 is neither toxic for the host nor its microbiota

Key words

Mutation Frequency Decline; new target; high-throughput screening; *in silico* modeling; antimicrobials; clinical pathogens; immune stress; *in vivo* efficacy; antimicrobial resistance; antivirulence drug.

Abstract

The increased incidence of antibiotic resistance and declining discovery of new antibiotics have created a global health crisis, especially for the treatment of infections caused by Gram-negative bacteria. Here, we identify and characterize a molecule, NM102, that displays antimicrobial activity exclusively in the context of infection, thus avoiding resistance and collateral damage to the host and its microbiome. NM102 inhibits the activity of the non-essential Mutation Frequency Decline (Mfd) protein by competing with ATP binding to its active site. Inhibition of Mfd by NM102 sensitizes pathogenic bacteria to the host immune response and blocks infections due to clinically-relevant *K. pneumoniae* and *P. aeruginosa*, without inducing host toxicity. Finally, NM102 inhibits the function of Mfd as a mutation and evolvability factor, thus reducing the bacterial capacity to induce antimicrobial resistance. These data provide a potential roadmap for antibiotic discovery to expand the arsenal of drugs to combat antimicrobial resistance.

Introduction

The fight against pathogenic bacteria is turning again into one of the greatest challenges faced by our societies, especially with the spread of multi- and extensively-drug resistant bacteria, that seriously imperil the use of traditional antibiotics (Cook and Wright, 2022). Estimates suggest that at least 700,000 people die annually from drug-resistant infections and, in the absence of measures, this number could rise up to 10 million by 2050, by far surpassing cancer as the major cause of death worldwide (Collaborators, 2022). In particular, infections caused by the ESKAPE pathogens, namely, *Enterococcus faecium, Staphylococcus aureus, Klebsiella pneumoniae, Acinetobacter baumannii, Pseudomonas aeruginosa* and *Enterobacter* spp., are increasingly associated with therapeutic dead-ends. As such, they constitute the top World Health Organization's priority list of bacteria for which novel therapeutics are urgently needed. Identification and characterization of antibiotics with novel molecular scaffolds, innovative targets and/or original mechanisms of action, associated with a low potential of resistance induction, are an emergency, especially towards Gram-negative pathogens. Indeed, in the last decades, only six new classes of antibiotics have been approved (Butler et al., 2017). Recent efforts have begun to reactivate antibiotics research, and compounds are explored either through drug repositioning or through molecular mechanisms that are usually redundant with those of traditional antibiotics. For example, finafloxacin, a fluoroquinolone antibiotic, was recently approved to treat ear infections with *P. aeruginosa* (McKeage, 2015). Nevertheless, it is still susceptible to induce the same resistance mechanisms that affect other fluoroquinolones (Randall et al., 2016). Darobactin was recently shown to specifically target Gram-negative bacteria, but the latter are easily prone to develop resistance to this drug (Imai et al., 2019). By contrast, the recent discovery of teixobactin, which was isolated from soil bacteria and targets the cell wall, suggests that it is possible to find compounds that selectively kill bacteria without being prone to resistance (Ling et al., 2015). Still, teixobactin is only functional against Gram-positive bacteria. A new compound, irresistin-16, was recently described to be bactericidal towards both Gram-negative and Gram-positive bacteria. This molecule acts on two independent cellular targets and impacts both membrane integrity and folate biosynthesis without inducing any resistance, so far (Martin et al., 2020). These data pave the way to the discovery of new molecules, a mandatory step to provide efficient antibiotics acting on novel targets, thus avoiding any cross resistances.

In this context, this study focuses on an innovative bacterial target, the Mutation Frequency Decline protein (Mfd), and its inhibition by novel small molecules. Mfd is a non-essential transcription repair coupling factor, ubiquitous in bacteria and absent in eukaryotes (Deaconescu, 2021). Mfd recognizes the RNA polymerase (RNAP) stalled at non-coding lesions and utilizes ATP to translocate along DNA, most likely forcing RNAP forward and ultimately dissociating it from the bulky DNA template (Roberts and Park, 2004). Mfd then stimulates DNA repair by recruiting components of the Nucleic Excision

Repair system (Deaconescu et al., 2006; Million-Weaver et al., 2015; Pomerantz and O'Donnell, 2010; Smith and Savery, 2008). The structure of Mfd has been solved revealing the presence of an ATP-ase motor module, highly conserved among bacteria and functionally mandatory (Brugger et al., 2020; Deaconescu et al., 2006). Stress-induced mutagenesis can assist pathogens in generating drug-resistant cells during antibiotic therapy. Mfd has been associated with the development of antibiotic resistance in *Campylobacter jejuni* and *Helicobacter pylori* (Han et al., 2008; Lee et al., 2009) and suggested as an evolvability factor that promotes hypermutation in bacteria, thus accelerating the evolution of antimicrobial resistance (AMR) (Ragheb et al., 2019). These data strongly suggest that blocking Mfd could hamper molecular evolution, hence inhibiting resistance development in many bacterial pathogens.

Furthermore, Mfd is critical for virulence in the Gram-positive *Bacillus cereus* and in the Gram-negative *Shigella flexneri* species and confers resistance to nitric oxide (NO) stress (Darrigo et al., 2016; Guillemet et al., 2016). Production of reactive nitrogen species is a key step in the immune response following infections (Porrini et al., 2020). NO induces lesions to bacterial DNA, thus limiting bacterial growth within hosts. Mfd is involved in the DNA repair following NO-induced DNA damages and is thus required for bacterial resistance to the host-NO-response. Consequently, in both species, a mutant lacking Mfd is severely impaired in its virulence capacity in cell and animal models. As Mfd is widely conserved in the bacterial kingdom, these data highlight a mechanism possibly ubiquitous in bacteria to overcome the host immune response and tackle the mutagenic properties of NO.

The function of Mfd in the bacterial bypass of host immunity, its role as an evolvability factor during antimicrobial resistance, its ubiquity in the prokaryotic world and its absence in higher eukaryotes, all support the selection of this protein as an innovative bacterial target for anti-infective therapies. Molecules that inhibit Mfd activity would neither directly inhibit nor kill bacteria, but instead curb bacterial evolution while impeding their ability to resist to the host immune response. Thereby, Mfd inhibitory compounds should boost the immune system response against pathogenic bacteria, while acting exclusively within the inflammation site, thus reducing resistance pressure and collateral damages to the host microbiota.

Here we report a targeted and structure-based high throughput *in silico* screening on the druggable ATP-binding site of Mfd to identify molecules capable to act as competitors of the cognate ligand ATP, thus inhibiting Mfd activity. One molecule, NM102, was identified as a potent molecule that specifically targets the ATP binding site of Mfd. *In silico* molecular analysis and *in vivo* assays revealed that NM102 displays antimicrobial activity, specifically in a context of infection, even against clinically relevant Gram-negative bacterial pathogens such as resistant *K. pneumonia*, *P. aeruginosa* and pathogenic *E. coli*. In animal models, NM102 blocked infections with these pathogens, without inducing toxicity

either to the host or to its microbiota. Finally, NM102 blocked the function of Mfd as an evolvability factor, thus reducing the bacterial capacity to induce antimicrobial resistance.

As a whole, our findings identify and characterize a promising antimicrobial candidate that could be used either alone as a helper to the host immune system or in combination with other antibiotics by inhibiting Mfd evolvability activity.

Results

Identification of promising hits targeting Mfd in silico

In order to identify antimicrobials with a novel mechanism of action, we performed a rational, targeted and structure-based high throughput *in silico* screening of small molecules to challenge their efficiency to accommodate to the ATP binding site of the bacterial protein Mfd. A 3D modeling of Mfd of *E. coli* in an active conformation was designed (Supp Fig.1). Using this template, a large library of 4.8 million compounds was screened for their capacity to virtually bind the ATP-ase site of Mfd. The virtual screening led to the selection of 95 molecules for subsequent experimental validation (Supp Fig.1).

Inhibition of Mfd activity in vitro

The 95 molecules were challenged to inhibit the ATP-ase function of *E. coli* Mfd *in vitro* (Fig. 1A). The inhibition rates of Mfd activity ranged from 10% to 85%. The best hit, called NM102, showed an inhibition rate above 80% and was therefore selected for further analysis. Dose-response assays on ATP-ase activity (Fig. 1B) and Lineweaver Burk plot (Fig. 1C) revealed a competitive mode of inhibition of NM102 to ATP with an IC_{50} of 29 µM and a K_i of 27 µM.

NM102 is a small molecule with a chemical scaffold relatively closed to ATP as it is composed of an indole-like ring close to the adenosine ring followed by a ribose-like ring and eventually polar sulfur groups that coul mimic phosphate moities (Fig 1D).

To assess the specificity of the NM102 inhibitor towards the ATP-ase activity of Mfd, we evaluated its capacity to decrease the ATP-ase activity in the eukaryotic ATP-ase yUpf1 protein (Fig 2A). NM102 sharply inhibited Mfd ATP-ase activity, while it showed no effect on yUpf1 activity.

NM102 binds Mfd of E. coli in silico with a better affinity as compared to ATP

In parallel with the experimental evaluation of the specificity of NM102, docking was computed in the ATP pocket of Mfd of *E. coli* and the binding affinity was evaluated (Fig 2B). NM102 showed a marked enhanced affinity for Mfd as compared to its cognate ATP ligand, with a binding energy of -9.8 $kcal.mol^{-1}$ *vs* -6.5 $kcal.mol^{-1}$, respectively. The docking highlighted that Mfd accommodates NM102 in its ATP binding site, within the same binding pocket encompassing most of the walker A motif (residues from Asp629 to Glu636), especially including the catalytic Lys634 and involving similar residues such as

Phe597 and Phe599 through conserved π-stacking interactions, and Thr635 as well as Glu636 plus Arg905 for polar and charged interactions, respectively (Fig 2C). Markedly, we were able to define 21 conserved positions of close interactions involved in the binding of ATP and NM102 (Supp Table 1). Because NM102 is a slightly longer molecule as compared to ATP, its accommodation extends towards residues that are remote from the very catalytic nexus, namely Gln664, His665, Asn668 and even Glu730 of walker B motif, and D876 of motif V. This feature could explain the computed increase in affinity for NM102 as compared to ATP.

Furthermore, to confirm this specificity, NM102 was docked in the ATP pocket of the yUpf1 protein of *S. cerevisiae* and the binding affinity was measured (Fig 2B). In contrast to Mfd binding, NM102 shows a lower binding affinity to the eukaryotic yUpf1 protein as compared to the ATP control (-8.7 *vs* -11.2 kcal.mol^{-1} respectively), further suggesting the specificity of NM102 towards Mfd, which is consistently with our experimental data.

In silico, NM102 binds to the Mfd active site of the ESKAPE bacteria

Mfd is widely conserved in the bacterial kingdom (Roberts and Park, 2004). To assess whether NM102 could more generally bind and inhibit the function of Mfd from a wide range of bacteria implicated in AMR, multiple sequence alignment and homology modeling of Mfd were performed for one strain of each species of the ESKAPE bacteria (Supp Fig 2 and 3). The alignment revealed that Mfds cluster distinctly into Gram-positive and Gram-negative bacteria but overall share 38% of sequence similarity along 1200 amino acid residues of the ESKAPE bacteria. Markedly, this average on Mfd full length sequence does not reflect the trend observed for each functional module. Indeed, modules composed of domains D1a-D2-D1b, D3, D4, D5-D6 and D7 show 21%, 14%, 47%, 66% and 26% of sequence similarity, respectively. Particularly, the ATP-ase motor module, composed of D5 and D6 domains, is by far the most conserved. It shares 66% and 36% sequence similarity and identity within the ESKAPE strains, respectively. Furthermore, the ATP binding site, which locates at the interface between D5 and D6, shows fairly high to strict conservation of the catalytic motifs, the so-called I to VI patterns as well as walker A & B boxes (black squared in Supp Fig 2).

To profile the affinity of NM102 towards Mfds from the ESKAPE bacteria and identify the probable conserved features of binding, NM102 was docked into each 3D homology model Mfd and its binding energy was measured (Fig 2D, E, Supp Fig 3). Molecular binding revealed that both ATP and NM102 engage in conserved interactions in the ATP binding site for all the modeled Mfds. Indeed, 21 residues were identified as positions always involved in the coordination sphere. All are strictly conserved except P2, P3, P9 and P19 which are nevertheless higly conserved (Suppl Table 1). The positions describe an hydrophobic pattern of interactions with Phe597 and Phe599 located around the adenine moiety, polar interaction with Thr634 and charged interaction with Glu636 and R905 around the

phosphate groups of the ATP, respectively. The ATP binding ranges from -5.5 to -8.4 kcal.mol^{-1}, whilst NM102 binding ranges from -8.5 to -10.5 kcal.mol^{-1}, suggesting that NM102 binds to all Mfd from the ESKAPE group with a significantly better affinity as compared to the physiological ATP. Noticeably, this could indicate a putative universal inhibition power for NM102 towards this ATP-ase motor.

Taken together, our results strongly suggest that NM102 targets the ATP binding site of Mfd protein of all ESKAPE bacteria, competing with physiological ATP, hence specifically inhibiting Mfd ATP-ase activity. As the challenging urgency is to identify molecules efficient against Gram-negative pathogenic bacteria of the ESKAPE group, the rest of the study is focused on clinically relevant *K. pneumoniae*, *P. aeruginosa* and *E. coli* strains.

NM102 has antimicrobial activity in the context of nitric oxide stress

Mfd is a non-essential protein in unstressed conditions. However, we have previously shown that Mfd is essential to resist NO stress during infection (Darrigo et al., 2016; Guillemet et al., 2016). Our innovative antimicrobial strategy is to identify inhibitors with no antibiotic activity in unstressed conditions and active only in stressed conditions when Mfd is required. NM102 was thus first tested for its antimicrobial activity in the absence of stress. Under these conditions, no antimicrobial activity on *K. pneumoniae* was observed (Fig 3A). Conversely, NM102 strongly inhibited *K. pneumoniae* survival under NO stress conditions (Fig 3B) with an IC_{50} of 7.5 µM. These results highlight that NM102 has an antimicrobial activity against *K. pneumoniae* under NO stress conditions.

When further tested towards other important bacterial pathogens, NM102 inhibited bacterial survival of clinical *E. coli* under NO stress conditions compared to unstressed conditions (IC_{50} of 61.2 µM, Fig 3C) and, although to a lesser extent, of *P. aeruginosa* (IC_{50} of 94.2 µM, Fig 3D). These data show that NM102 acts against Gram-negative pathogenic bacteria under conditions that mimic immune stress.

NM102 is efficient against clinically-relevant pathogenic bacteria

NM102 was then tested for its activity under NO stress conditions against bacteria that are resistant to some or most usual antibiotics (Supp Table 2). Strikingly, NM102 has an antimicrobial activity against resistant *K. pneumoniae* strains DOU (Fig 3E) and ALE (Fig 3F), although with an increased IC_{50} (78.8 µM and 97.2 µM, respectively) compared to the non-resistant *K. pneumoniae* strain (7.5 µM). NM102 was also active against the resistant *E. coli* strain GUE (Fig 3G) (IC_{50} of 68.2 µM).

Overall, NM102 proved to be a potent antimicrobial molecule active against clinically-relevant pathogens, including multidrug-resistant bacteria that may be associated with diificult to treat infections and sometimes to therapeutic failure.

NM102 is effective *in vivo*

To assess the activity of NM102 as an antimicrobial *in vivo*, two different animal models were used. First, *Bombyx eri* larvae were injected with *P. aeruginosa* CIP27853 and treated with NM102 (Fig 4A). The insects were then crushed and Colony-Forming Units (CFU) were counted by plating. Treatment with NM102 led to a drastic shift in the bacterial load showing that NM102 is effective against *P. aeruginosa in vivo*.

To confirm that NM102 was targeting Mfd *in vivo*, the effect of NM102 was investigated on the survival of the *P. aeruginosa* mutant *Δmfd*. First, the amount of CFU of the *Δmfd* mutant was lower compared to the CFU recovered following insect infection with the wild-type strain, showing that Mfd is a critical virulence factor for *P. aeruginosa*. Second, NM102 did not decrease the bacterial load of the Δ*mfd* mutant, confirming that NM102 is specifically active on Mfd *in vivo*.

NM102 nanoformulation is a potent antimicrobial agent active in vivo against clinically-relevant pathogens

To further investigate the potential of NM102 *in vivo*, a mouse lung model of infection by *K. pneumoniae* and *P. aeruginosa* was chosen (Liu et al., 2019). Due to its poor solubility in most common solvents (Supp Table 3), the above studies were performed using a solution of NM102 in DMSO. However, DMSO is known to be toxic to mice at high concentrations (Yi et al., 2017). Thus, an alternative to the DMSO vehicle was developped to further assess the therapeutic effect of NM102. Herein, a DMSO-free nanoformulation was prepared *via* a sonication assisted-nanoprecipitation method in the presence of poly(D-L lactide-*co*-glycolide) (PLGA) (Supp Fig 4A-D). The resulting NM102 nanoformulation (drug content = 0.6 mg/mL) exhibited an average diameter = 180 nm, with narrow particle size distribution (polydispersity index, PDI = 0.2) and a neutral surface charge (ζ potential = -2 ± 1 mV). An empty nanoformulation was prepared according to the same protocol but without the drug (average diameter = 136 nm ± 7, PDI = 0.08 ± 0.04, ζ potential = -4 ± 1 mV) to serve as a control. NM102 nanoformulation showed colloidal stability for up to 2 weeks both at 4°C and at room temperature (Supp Fig 4E, F).

Mice were infected intranasally with *K. pneumoniae* and treated *via* the intraperitoneal route with the NM102 nanoformulation. After 24 h the CFU in the lung were assessed (Fig 4B). The NM102 nanoformulation significantly reduced the bacterial burden in lungs compared to control group treated with empty nanoformulation, showing that NM102 acts as an efficient antimicrobial against *K. pneumoniae* infection *in vivo*. The efficacy of the NM102 molecule was compared in the same conditions with that of meropenem (MPN), a beta-lactam antibiotic commonly used in the treatment of various infections including *K. pneumoniae* and *P. aeruginosa* (Liu et al., 2019). NM102 showed

similar efficacy to MPN at 6 and 10 mg/kg, respectively in reducing the *K. pneumoniae* CFU in the lung of the infected mice (Fig 4B).

To confirm that NM102 targets Mfd *in vivo*, mice were also infected with the *K. pneumoniae* mutant *Δmfd*. NM102 nanoformulation showed no effect on the bacterial burden of the Δ*mfd* mutant, further highlighting the inhibitor specificity (Fig 4C).

The efficacy of NM102 was further investigated on the clinical *K. pneumoniae* ALE strain, which is resistant to several antibiotics including MPN (Fig 4D). NM102 nanoformulation at 6 mg/kg drastically decreased the bacterial load in the lung. Strikingly, MPN at 10 mg/kg had no significant effect on the resistant *K. pneumoniae* ALE, highlighting the potential of the NM102 molecule on resistant Gram-negative bacteria *in vivo*.

For *P. aeruginosa*, NM102 formulation at 6 mg/kg had no significant impact on the bacterial load, whereas MPN at 10 mg/ml decreased the bacterial load (Fig 4E). The combination of the two treatments was more efficient against *P. aeruginosa* in an NM102-dose dependent manner compared to single treatments. These data suggest the possible uses of NM102 as an antimicrobial drug during combination therapy.

NM102 was also tested on the clinical strain *P. aeruginosa* VED (Fig. 4F) that did not show *in vitro* resistance to MPN. *P. aeruginosa* VED was sensitive to NM102 formulation and to MPN *in vivo*, showing that the *P. aeruginosa* CIP 27853 strain was less sensitive to MPN and NM102 treatment than the *P. aeruginosa* VED strain.

NM102 is not toxic for the host

An important feature in the development of antiinfectives is to assess their impact on the host. When tested for toxicity towards human cells (Fig 5A, B), NM102 and NM102 nanoformulation did not induce cytotoxicity neither to HeLa nor to Vero cells at the highest doses used in insect and mouse experiments, respectively. MPN showed no toxicity to HeLa cells, but induced cytotoxicity on Vero cells at 10 and 100 µM.

Treatment with NM102 had no impact on insect or mouse survival nor on the mice weight (Fig 5C). Importantly, PLGA, which was used for the nanoformulation of NM102, is an FDA-approved copolymer for which no systemic or organ toxicity has been reported in animal models (Rong et al., 2014; Semete et al., 2010).

NM102 is a microbiome-friendly drug

As NM102 is active on bacteria only in the context of a stress like inflammation, we hypothesized that NM102 treatment should not affect microbiota species, in contrast to treatment with conventional antibiotics. To test this, we selected 20 species that are representative of the oropharyngeal and lung

microbiome of healthy individuals (Supp Table 4). We assessed growth inhibition of all species in monoculture in the presence of up to 100 µM of NM102 (Fig 6A). In sharp contrast to MPN, NM102 had no or very low effect on the bacterial growth of these human-associated bacterial species, suggesting its innocuity to the host microbiome.

To assess the innocuity of NM102 towards the gut microbiome *in vivo*, mice were treated with NM102 and feces were recovered after treatment. The state of the microbiome was assessed by quantifying the overall quantity of bacteria in the feces by qPCR (Supp Fig 5A). NM102 did not impact the overall quantity of bacteria in the feces after 1 and 7 days of treatment.

We further assessed the composition of the gut microbiome following infection by *K. pneumoniae* and NM102 formulation treatment. We did not detect changes in gut microbiome diversity between untreated and NM102-treated mice. The Shannon index of NF and NF-MN102-treated mice was similar to untreated mice (Fig 6B). Similarly, we did not detect significant differences in beta-diversity between treatments using weigted and unweigted UniFrac distances (Supp Fig 5B). In addition, the family-level microbiome profile following NM102 treatment largely resembled that of untreated mice (Fig 6C. These results indicate that the NM102 treatment does not induce changes in the richness or structure of the microbiome, further supporting that it is a microbiome-friendly drug.

NM102 is an anti-evolvability drug to combat AMR

Mfd has been shown to play a critical role in promoting bacterial resistance to commonly used antibiotics and has been proposed as a target for the development of anti-evolvability drugs (Ragheb et al., 2019). We thus assessed whether NM102 could also inhibit Mfd evolvability activity. First, the mutation rate of *E. coli* wild type and *Δmfd* mutant was assessed following exposure to Rifampicin (Fig 7A). The mutation frequency of the *Δmfd* mutant was significantly reduced compared to that of the wild type strain, confirming the role of Mfd in the induction of mutations. Second, the strains were treated with NM102 resulting in a drastic reduction in the mutation frequency of the wild type strain to a level similar to that of the Δ*mfd* strain. NM102 had no impact on the mutation frequency of the mutant strain.

Then, the impact of NM102 on the evolution rate was evaluated following treatment of *E. coli* with several antibiotics. NM102 significantly decreased the evolution rate of *E. coli* following treatment with Rifampicin (Fig 7B) or streptomycin (Fig 7C) treatments by 8 and 2 folds, respectively. These data strongly suggest that NM102 targets the evolvability activity of Mfd and could thus be used as a combinatory drug to decrease antimicrobial resistance.

Discussion

To address the need of novel bacterial drug targets and the design and synthesis of innovative anti-infectives with new mechanisms of action, especially towards Gram-negative bacteria, we have identified and characterized an innovative bacterial target, the Mutation Frequency Decline protein, Mfd, and promoted its inhibition by a novel therapeutic molecule. Mfd is a non-essential transcription repair coupling factor that is ubiquitous and conserved in bacteria, but absent in eukaryotes. In this study, we identified a promising molecule, NM102, as an inhibitor of Mfd activity and showed its dual capacity to first display antimicrobial activity in animals against *K. pneumoniae* and *P. aeruginosa*, two major nosocomial Gram-negative bacteria of the ESKAPE group, and second, to inhibit Mfd evolvability function, thus reducing the frequency of antibiotic resistance appearance. As such, NM102 is active on its own to prevent bacterial infections. At the same time, it is also predicted to strongly reinforce the efficacy of existing antibiotics and prevent the emergence of resistance, an aspect rather unique and essential in the field of drug development and antibiotic therapy.

As Mfd is not an essential protein, standard MIC assays to identify inhibitory molecules could not be used. Thus, for the identification of the promising NM102 molecule, we developed a targeted approach based on the 3D structure of the active site of Mfd. This rational approach allowed to rapidly screen a large bank of molecules to identify potential hit inhibitory molecules. Hence, we propose a strategy that can be applied to other non-essential bacterial targets and provide a rapid and efficient pathway to screen small molecule potential without the development of laborious and specific *in vitro* activity tests. This structure-based method allowed us to predict the target druggability based on the 3D structural descriptors (i.e. polarity, hydrophobicity, volume) of ligand-bound cavities in the Mfd ATP binding druggable site (Rognan, 2017). The main advantage of such methods is their high interpretability in terms of pocket properties. In addition, once a potentially druggable pocket has been identified, it can be screened using various *in silico* tools to propose potential ligands for experimental validation and further optimization.

We chose to target the ATP binding domain of Mfd for the identification of inhibitory molecules because: i) ATP plays a central role in Mfd activity; ii) the 3D-structure of the ATP binding site structure in Mfd is known; iii) ATP-binding sites, despite their large structural diversity, are notoriously known to be druggable, as evidenced by inhibitors of many targets (protein kinases, HSP-90a for example) (Kahraman et al., 2007) and iv) although a large proportion of proteins carry ATP-binding sites, these sites present a large structural diversity and thus distinct specificity and selectivity towards ligands (Kahraman et al., 2007).

We report that NM102 is a potent ATP-like competitive inhibitor *in silico* and *in vitro*. *In silico*, its molecular mode of interaction grounds how NM102 is competitive and accommodates into the ATP pocket with a greater affinity than ATP. Markedly, its length could reinforce the bilobal binding

between D5 and D6 domains, expected for ATP-ase activity, through direct and closer interaction with the Q664-H665 stretch and through ancillary salt bridge between D876 and R905. Consistently, NM102 showed *in vitro* a competitive activity to ATP. In addition, such interaction could trap Mfd in its ATP-ase conformation and preclude any chance to engage into the ensuing DNA translocation step. Indeed, Mfd undergoes a functional cycle to couple ATP-ase to DNA translocation and then to UvrA recruitment. NM102 interacts strongly through polar interaction with the catalytic residue E730, which mutation into a glutamine is defective in ATP hydrolysis. Besides, E730 is sandwiched between R733 and R953, and R953A has been reported to result in loss of DNA translocation (Deaconescu, 2021). Any modification of interaction at E730 nexus, which connects both ATP-ase and DNA translocation activities, could impact the coordination of the two activities that must be exquisitely tuned. Markedly, the pseudo-adenine part of NM102 conserves a π-stacking with F597, as seen for the adenine of ATP. Taken together, this work suggests that NM102 not only occludes the ATP site but may also freeze the ATP-ase domain into a conformation that is unable to expel it as it does for ADP, thus blocking the functional cycle. These data provide mechanistic and molecular insights into NM102 binding to its target and specificity.

Regarding specificity, NM102 did not bind to nor inhibit the ATP-ase activity of the unrelated eukaryotic ATPase protein, yUpf1, further suggesting that the ATP pockets of ATP-ase proteins present structural diversity allowing distinct specificity towards ligands. The absence of toxicity of NM102 towards bacteria (in the absence of exogenous stress) and eukaryotic cells provided further hints that NM102 did not affect general ATP-ase proteins activity.

By conferring resistance to nitric oxide (NO), a major toxic component of the host innate immune system, Mfd activity enables the bacteria to overcome the host defense responses (Guillemet et al., 2016). The host defense against bacteria is predominantly mediated by cellular immune mechanisms. Various cells, such as macrophages, neutrophils and epithelial cells produce toxic species, including NO, during most types of infections. NO can severely damage biological molecules, such as proteins and nucleic acids, thereby inducing DNA damage and strand breaks (Akuta et al., 2006). NO is cytotoxic and mutagenic for various pathogens and host cells (Yoshitake et al., 2004; Zaki et al., 2005; Zhuang et al., 1998) and plays an important role during infections by limiting microbial proliferation (Porrini et al., 2020). Bacteria express sensor proteins that are able to detect NO and, accordingly, to switch on the expression of enzymes that detoxify NO before it reaches lethal levels (Porrini et al., 2021)(Laver et al., 2010). In addition, we previously demonstrated a link between NO-induced bacterial DNA damage and DNA repair by Mfd (Darrigo et al., 2016). Mfd is ubiquitous in bacteria, and almost all bacteria induce a NO response from the host, so the Mfd-targeted inhibitor is expected to have a broad spectrum of activity. We have consistently shown that NM102 docks *in silico* to the Mfd of all ESKAPE pathogens and that it has antibacterial activity in the context of NO stress on Gram-negative bacteria.

As a proof of concept of efficacy against Gram-positive bacteria, we also confirmed NM102 antimicrobial activity during NO stress against *B. cereus*, for which we had initially identified Mfd function during immune stress (Supp Fig 6).

Nevertheless, Mfd activity is not restricted to NO stress. It has indeed been shown that Mfd protects against oxidative stress in *Bacillus subtilis* (Martin et al., 2019). The ability to evolve is critical for bacterial survival especially in the context of pathogenesis, where escaping host immunity is essential and requires constant adaptation. Thus, Mfd may be involved in bacterial virulence, likely by preventing the DNA damages induced by the host through its overall immune response and/or stress conditions encountered *in vivo*. This question is difficult to technically address *in vivo* since bacteria encounter a lot of various stresses during infection. However, we could speculate that blocking Mfd activity by the inhibitory molecule hampers the bacterial capacity to cope with the host response, allowing the immune system to be efficient against the invading pathogens.

This anti-virulence therapy constitutes a promising alternative to the classical antibiotic approach as it neither leads to bacterial growth inhibition nor to bacterial death. Instead, an anti-virulence therapy blocks the bacterial pathogenicity by counteracting the ability of pathogens to resist to the host immune system. As a consequence, such compounds do not target essential bacterial pathways and are thus expected to reduce resistance pressure and consequently decrease the rate of resistance development. It was not possible to address the potential resistance to NM102 *in vitro* as it did not induce direct bacterial death. In the context of NO stress, this would require a prolonged exposure to NO+NM102 and the NO stress by itself could eventually be toxic and/or induce bacterial resistance. Terefore, we focused our study on the impact of NM102 on the mutagenic property of Mfd to assess its role on antibioresistance. Indeed, Mfd has been demonstrated as a general evolvability factor promoting bacterial mutagenesis during infections (Deaconescu, 2021). It has been suggested that Mfd is required for developing high levels of drug resistance upon primary exposure to sub-inhibitory concentrations of antibiotics, accelerating AMR development (Ragheb et al., 2019) and that stress-induced mutagenesis can assist pathogens in generating drug-resistant cells during antibiotic therapy (Suzuki et al., 2018). Here we show that NM102 inhibits Mfd function as a mutation and evolvability factor during antibiotic stress. This decreases the ability of bacteria to develop resistance to classical antibiotics. As such, NM102 can be proposed as a new class of drug targeting the evolvability property of Mfd. By decreasing the resistance pressure, the drugs will have a longer efficacy and this will in turn contribute to limit the spread of antibiotic resistance.

For clinical treatment, combination therapies have had and will still play an important role. We have shown that NM102 is efficient as antimicrobial *in vivo* alone and during combination treatment with meropenem, and that NM102 treatment can kill bacteria in contexts where other therapies fail due to resistant strains. Thus, a combination treatment including an inhibitor of Mfd coupled with a classical

antibiotic could constitute a promising strategy with an increased antimicrobial efficacy combined with a reduced likelihood of resistance development at the onset of treatment. As recently proposed, targeting the evolutionary capacity of bacteria could also have wide-ranging implications outside of AMR development, from reducing cancer evolution to limiting pathogenic diversity in the context of host immunity (Ragheb et al., 2019).

Drug loaded into nanocarriers has been largely proposed for the delivery of poorly soluble drugs, allowing not only to overcome the physicochemical limitation of the drug, but also to ensure enhanced accumulation at the site of action and sustained drug release (Anselmo and Mitragotri, 2021; Hwang et al., 2020; Lee, 2020; Tibbitt et al., 2016). The design of a NM102 nanoformulation helped overcome the issues related to the low solubility of the drug molecule, allowing its administration in a clinically acceptable solvent. Herein, we provided a first proof of efficacy of the aqueous nanoformulation of NM102 opening the way to the development of a novel antibiotic formulation suitable for widespread use.

Classical antibiotics target essential bacterial pathways and as such are highly efficient but not specific, thus also affecting commensal members of the microbiome (Maier et al., 2021). In particular, the microbiome is essential in human and animal health as it is involved in a variety of health associated processes, including digestion, metabolism, immune development, and also protects against invading pathogens. As Mfd is not an essential protein, its inhibition by NM102 should not have an impact on the host microbiome in the absence of inflammatory stress. We tested this hypothesis in several contexts. First, NM102 activity was assessed on species of the human upper respiratory tract microbiome. In monoculture, NM102 does not interfere with the growth of any of the tested bacteria. Second, the gut microbiome composition was assessed after treatment with NM102 on healthy mice and on mice infected with *K. pneumoniae*. NM102 had no detectable effect on the diversity of the gut microbiome, that might be collaterally damaged during classical, non-selective antibiotic treatment. This is a rather unique feature and may help to develop microbiome-friendly molecules that will not only heal the infectious diseases but also contribute to the general better health of the patients. This could, however, not be applied to treat gut infections and/or inflammation as the local gut inflammation will probably render Mfd essential for the survival of bacterial commensals as well.

As a whole, new drugs targeting the non-essential, evolvability and virulence factor Mfd could be used alone or as supplemental drugs during the treatment of infections to improve the potency of current antibiotics and reduce the appearance of resistance. These novel molecules could provide a new therapeutic option and expand the arsenal of drugs available to combat AMR and potentially other diseases.

Ethic statement

All animals were handled in strict accordance with good animal practice as defined by the local animal welfare bodies (Unité IERP, INRAE Jouy en Josas, France, Agreement No. 78120) and all experiments were approved by the ethics committee COMETHEA and by the French Ministry of Higher Education and Research (APAFIS#10124-2017040413027917 v12). All animal experiments were performed in accordance with European directive 2010/63/EU. All efforts were undertaken to minimize animal suffering and to follow the 3R rules (Reduce, Refine, Reuse).

Declaration of interests

A patent application describing the use of NM102 as an antibiotic, as well as the use as antibiotic of derivatives is published EP3868376, 2021.

Acknowledgments

We thank Antoine Allier for his help with R, Andrea Villarino for her input on the *in vitro* assay and Isabelle Barbosa for her input in the yUpf1 assay. We thank all members of the IERP animal facility (INRAE, Jouy en Josas) and Catherine Cailleau (Institut Galien, Châtenay-Malabry) for their technical help for animal studies. We thank Marion Leclerc for the qPCR experirments. We warmly thank Erwin Bohn and his team at the University of Tübingen for their help, advice and biological material for the construction of the *P. aeruginosa* Δ*mfd* mutant strain. We thank Cordula Gekeler for excellent technical assistance, Constance Porrini for her participation in the NO assay experimental design and Saoussen Oueslati for her help during the MIC tests. We thank the NCCT of Tübingen for sequencing. We warmly thank Dr. Libera Lo Presti for proofreading the manuscript.

This work was supported by *r*esearch grants from: SATT PARIS-SACLAY (CM2016-0067), Postdoctoral research Fellowship Prestige, Campus France (Prestige-2016-2-0011), Prematuration IDEX 2018 (CDE-2018-002324/IRE 2018-0022), DIM One health region Ile de France (R19104DD), Procope Campus France (46651WA), TWB biosciences and bioproduction, the Interdisciplinary Action "Health and Therapeutic Innovation" (HEALTHI) of the Université Paris-Saclay and DFG (CMFI Cluster of Excellence EXC 2124).

Figure legends

Fig 1- NM102 identification as ATP competitor for Mfd activity. (A) *In vitro* high throughput screening for inhibitors of Mfd-C ATP-ase activity. The indicated compounds were tested at a final concentration of 100 mg/mL. The data were normalized to those of the DMSO control. MfdC ATP-ase activity was measured at 0.35 µM at an ATP concentration of 1 mM. The results are the average of two independent experiments done in duplicate with standard deviation. (B) Michaelis Menten plot for inhibitory activity of NM102 (0 to 100 µM) on *E. coli* Mfd-C (0.35 µM) ATP-ase activity with ATP (0 to 0.3 mM). The results are the average of three independent experiments done in duplicate with standard deviation. The IC_{50} was computed using Graph Pad 7.05. (C) Lineweaver-Burk plot showing NM102 inhibition of Mfd-C ATP-ase activity through a competitive mode of action. (D) Chemical structure of the NM102 compound.

Fig 2. NM102 specifically binds the ATP binding site of Mfd. (A) NM102 inhibition of bacterial Mfd and eukaryotic yUpf1 ATP-ase activity. ATP-ase activity of Mfd and yUpf1 in the absence and presence of 100 µM of NM102 as assessed by using BIOMOL® Green reagent microtiter-plate assay. Data were normalized to that of the DMSO control. The graph shows the mean ± SD of three independent experiments. (B) Binding energy measured *in silico* in kcal/mol between Mfd and ATP or NM102 (left), and between yUpf1 and ATP or NM102 (right). (C) Left side: 3D structure of modelized full-length Mfd from *E. coli* in complex with NM102 and ATP at the active site. Right side: close view of ATP (upper panel, yellow stick) and NM102 (lower panel, pink stick) poses. The positions identified as conserved and involved in the binding of ligands are indicated: residues hydrophobic, acidic, polar, basic and glycine are colored in green, salmon, cyan, wheat and marine, respectively. (D) Binding energy measured *in silico* in kcal/mol between Mfd and ADP (left), ATP (middle) and NM102 (right) for the homology modeled Mfds from ESKAPE bacteria. (E) Close-view of ATP (yellow stick) and NM102 (pink stick) docked in Mfd of *K. pneumoniae*.

Fig 3. Antimicrobial effect of NM102 on Gram-negative bacteria during NO-stress. Strains were grown to exponential phase in LB medium. Bacteria solution was prepared in RPMI medium and dispatched in 96-wells plate. Bacteria were exposed for 4 h at 37°C to 50 µL of increasing concentrations of NM102 alone (A: *K. pneumoniae* ATCC 700603) or with NOC5 as a NO donor (B: *K. pneumoniae* ATCC 700603, C: *E. coli* ATCC 25922, D: *P. aeruginosa* CIP27853, and resistant strains E: *K. pneumonia* DOU, F: *K. pneumonia* ALE and G: *E. coli* GUE). Bacteria survival rate was calculated by normalizing bacteria load against control without NM102. The results reported are mean ± SD of four independent experiments each in triplicates, P values are calculated against the condition without NM102, using One Way ANOVA (**** P<0.0001, *** P<0.001, ** P<0.01, * P<0.05). IC_{50} were computed using Graph Pad 7.05.

Fig 4. Antimicrobial effect of NM102 *in vivo* in insects and mice. (A) *P. aeruginosa* CIP27853 wt and Δ*mfd* strains were grown to late exponential phase in LB medium at 37°C and injected into forth instar silkworm larvae without or with NM102 (2.78 µg/larvae). Boosts of NM102 (6.97 µg/larvae) were administrated at 4 h and 8 h post infection. At 24 h post infection larvae were crushed and the content of each tube was serially diluted on LB plates for CFU numeration. Each point represents one larva. P values are calculated against the condition wild type-strain without NM102, using Mann-Whitney test (**** $p < 0,0001$).

For mice experiments, *K. pneumoniae* ATCC 700603 wt (B) and Δ*mfd* (C), *K. pneumoniae* ALE (D), *P. aeruginosa* CIP27853 (E) and *P. aeruginosa* VED (F) were grown to late exponential phase and diluted in PBS. Intranasal (i.n.) bacterial administration was performed through slow instillation of 20 µL of bacterial suspension (1x 10^7 CFU). 200 µL of NM102 formulation (NF-NM102, 6 mg/kg) or empty formulation (control) were administrated in mice via the i.p. route (B, C). Alternatively, 20 µl of a mixture containing bacterial suspension (1x 10^7 CFU) and NM102 formulation (1.5 or 6 mg/kg) or empty formulation was administred via the i.n. route (D, E, F). MPN (10 mg/kg) was inoculated via the i.p. route. Mice were sacrified by cervical dislocation after 24 h and the log CFU in the lung was calculated per gram of organ. Each dot represents a mouse. P values are calculated using Mann-Whitney test (*** $p < 0,0005$; ** $p < 0, 001$; * $p < 0, 005$).

Fig 5. NM102 is not toxic to the host. HeLa (A) and Vero (B) cells were cultured in DMEM at 37°C and 5% CO_2. Cells were treated for 1 h with MPN at 10 and 100 µM, NM102 at 10 and 300 µM, NM102 formulation at 1.29 and 5.16 mM or their respective control 10% DMSO or empty formulation. Cytotoxicity was assessed using CellTiter96®AQ_{ueous}. Values for treated cells were normalized to the untreated control. The results reported are mean ± SD of three independent experiments each in triplicates (B) Mice were i.p. treated with NM102 (6 mg/kg) or control. Changes in the mice body weight were assessed for 7 days.

Fig 6. NM102 does not impact the microbiome. (A) Growth of representative species of the human oropharyngeal and lung microbiome is unaffected by NM102. Monocultures were grown in the presence of different concentrations (0 to 100 µM) of MPN (upper panel) or NM102 (lower panel). Heatmap depicts the area under the growth curve (AUC) normalized to steady growth. AUC values of 1 indicate no growth inhibition in comparison to the DMSO control. Tiles depict the mean of three biological replicates. (B, C) Gut microbiome diversity is unaffected by NM102. Mice were infected with *K. pneumoniae* and left untreated or treated with NM102 formulation (NF-NM102) or the empty formulation (NF) as control. After 24 h, the feces were collected and the diversity of the microbiome

was analyzed by 16S rRNA sequencing. The Shannon index (B) and the relative abundance of the bacterial families (C) were determined. The bar colors represent bacterial families with mean abundance > 1%. Each dot (B) and each column (C) represents the value obtained for one mouse.

Fig 7. NM102 inhibits Mfd evolvability activity. (A) The mutation rate of *E. coli* wt and Δ*mfd* strains were measured following exposition to NM102 (100 μM) or the DMSO control, using the frequency of spontaneous accumulation of resistant mutants towards Rifampicin as measurement reference. Data in this figure are representative of at least three biological replicates. Error bars show SEM. Turkey's multiple comparisons test was used to determine significance ($*p < 0.02$; $**p < 0.008$). Resistance evolution of *E. coli* to Rifampicin (B) and Streptomycin (C) was measured following exposure to NM102 (100 μM) or the DMSO control. Line plots show median antibiotic concentration at each sampled time point for at least three independent experiments.

Material and Methods

***E. coli* Mfd modelling**

As we aimed to explore the capacity of Mfd to bind ligands possibly competitive to ATP, a prerequisite was to design Mfd in a conformation prone to accommodate a ligand, meaning that the ATP binding site must adopt an opened and accessible conformation. At the time of computation, all the available crystal coordinates of Mfd from *E. coli* were in an inactive form because of the so-called walker A motif that closed over the active site, hence precluding any binding (pdb id 2EYQ) (Deaconescu et al., 2006). The D2 domain of RecG helicase from *Thermotoga maritima* (pdb id 1GM5) is a structural homolog of Mfd, solved in active conformation complexed to ADP (Singleton et al., 2001). Thus, the nucleotide-bound active form of *E. coli* Mfd (K578-P780, UniProt identifier P30958) was obtained by morphing the inactive form of *E. coli* Mfd into the active form of RecG using standard settings of the Yale Morph2 server (http://morph2.molmovdb.org/submit.html).

High-throughput *in silico* screening

The Bioinfo-DB database (http://bioinfo-pharma.u-strasbg.fr/bioinfo) is an in-house developed database of 4.8 million commercially available compounds as powder (1-50 mg) and filtered according to internal rules to contain drug-like compounds only. The database was first filtered to keep compounds grossly resembling to nucleotides and fulfilling the following properties: (i) at least one hydrogen-bond donor, (ii) at least two hydrogen-bond acceptors, (iii) at least one aromatic ring, (iv) predicted aqueous solubility higher than 50 μM (predicted with PipelinePilot v.9.5, Dassault Systèmes, Paris), (v) topological polar surface area lower than 120 $Å^2$. The filtered set of 1.2 million compounds was then converted into three-dimensional (3D) space using Corina v3.40 (Molecular Networks,

Erlangen, Germany). Up to 4 stereoisomers were created in case of the presence of undefined stereocenters. When the stereocenter was explicitly defined, it was kept unchanged. Altogether, 3D atomic coordinates were defined for 1 874 034 compounds, constituting the docking set.

The docking set was anchored to the above-described nucleotide-binding site of *E.coli* Mfd (Phe599, Thr602, Gln605, Gly631, Phe632, Gly633, Lys634, Thr635) with the Surflex-Dock v.3066 program (Jain, 2003). A prototyping molecular dynamics object or "protomol" was first generated from the list of binding site residues. Compounds were then docked with default settings (excepted for the -pgeom option) of the docking engine, keeping the best 10 poses according to the native Surflex-Dock scoring function.

Potential hits were selected according to the following two strategies (Supp Fig.1):

Strategy A: The 178 best scoring poses (Surflex-Dock score > 10) from the docking set were retained. Then, compound redundancy was removed (highest score retained if more than two poses originate from the same compounds) to yield 91 compounds. A chemical diversity selection by maximum common substructures was performed using the LibMCS algorithm (ChemAxon Ltd., Budapest, Hungary) to retain a first set (SET1) of 23 chemically diverse compounds.

Strategy B: All poses from the docking set were submitted to an interaction-based filter (Marcou and Rognan, 2007) to select 206 non-redundant compounds verifying absolutely the following interactions: hydrogen bond to Gln605.OE1 atom, hydrogen bond to Gln605.NE2 atom, hydrogen-bond to Gly631.N atom, π-π aromatic stacking to Phe599. In case of multiple poses from the same compound verifying the interaction similarity filter, the top scored posed (best Surflex-Dock score) was kept. A chemical diversity selection by maximum common substructures was performed using the LibMCS algorithm (ChemAxon Ltd., Budapest, Hungary) to retain a second set (SET2) of 74 chemically diverse compounds. Previously defined SET1 and SET2 were merged to yield a final selection of 95 unique hits (two hits were common to both sets) that were further purchased in 5 mg quantities.

Homology modelling of Mfd from the ESKAPE species

Mfd sequences from the ESKAPE pathogens were retrieved from NCBI (https://www.ncbi.nlm.nih.gov/). They were aligned using the multiple sequence alignment (msa) MAFFT algorithm with default parameters (Katoh et al., 2002). The alignment visualization was done using Jalview 2 (Waterhouse et al., 2009).

For homology modelling, a chimeric Mfd was modeled to mimic full length Mfd from ESKAPE bacteria in a conformation compatible with ligand binding. During this study, the structure of Mfd from *Mycobacterium smegmatis* in complex with ADP (pdb id 6ACX) was solved in an active opened conformation. The structures of Mfd full length from *E. coli* in its apo form and Mfd full length from *M. smegmatis* in its holo form served as 3D templates. For the former, its ATP-ase center was excised and

replaced by RecG helicase D2 domain to reinforce the coordinates of an active ATP-ase center. Then, homology modeling of the Mfds from the ESKAPE bacteria was performed by inserting their corresponding Mfd sequences into the building software Modeller (version 9.18) (Sali and Blundell, 1993) and by using our Mfd chimera as 3D template. For each Mfd, hundred models were computed and ranked according to the score function of Modeller. Eventually, the final one was selected upon this lowest score as it had the highest probability to satisfy the spatial contraints. Last, the stereochemistry of the model was checked using Procheck (Laskowski et al., 2018).

NM102 docking

ATP and NM102 were docked individually into the active site of each modelled Mfd. AutoDock Tools 4.2 (ADT4) was used with a cubic grid box centered onto the active site of the ATP-ase, with the algorithm of Lamarck and the default parameters for 20 runs (22). ATP and NM102 coordinates were obtained from the ZINC database (https://zinc.docking.org/substances/home/) in mol2 format, converted into ADT4's PDBQT format with their dihedrals set free to rotate. The crystal coordinates of the ADP molecule were first extracted from Mfd of *M. smegmatis* and redocked into this site, following the protocol described above. As the method docks it similarly to the coordinates of the solved structure, it serves as positive control, and subsequently the protocol was approved for docking of ATP and NM102 molecules in all homology modeled Mfds. ATP and NM102 ligands were also docked into the crystal structure of the eukaryotic protein yUpf1 (PDB ID: 2XZL) (Chakrabarti et al., 2011). For each run of each complex, an affinity score was calculated. Regarding this score, the most probable pose of ligand, that corresponds to the lowest interaction energy computed between protein and ligand, was selected. The binding energy was measured in kcal.mol^{-1}. Finally, holo models were visually inspected using PyMOL 2.0.7. (Schrödinger, LLC) and protein-ligand interactions were characterized using the Protein-Ligand Interaction Profiler (PLIP) program (Adasme et al., 2021).

Bacteria

Klebsiella pneumoniae ATCC 700603 was purchased from ATCC. *K. pneumoniae* DOU CTXM-15, ALE CTXM-15+, *P. aeruginosa* CIP27853, *P. aeruginosa VED*, *E. coli* ATCC25922 and *E. coli* GUE ST131 were provided by Dr. Thierry Naas (CHU de Bicêtre, Le Kremlin-Bicêtre, France) (Supp Table 1). The minimum inhibitory concentration (MIC) of antibiotics was realized on those strains. Briefly, a bacterial solution of 0.5 McFarland was prepared in physiological water and then diluted 1/1000 in Mueller Hinton broth (MHB) medium. 50 µL of bacterial solution were added in 96 well plates containing 100 µL of various concentration ranges of antibiotics (Penicillin, Ampicillin, Ceftriaxone, Meropenem, Cefotaxin, Oxacillin, Streptomycin, Ciprofloxacin). The plates were incubated over night at 37°C. Bacterial growth was measured in each well to determine the MIC.

E. coli Keio wild type (BW25113) and Δ*mfd* mutant strains were kindly provided by Ivan Matic.
Twenty species (covering 5 phyla and 14 genera) representative for the oropharyngeal and lung microbiome of healthy individuals were previously descibed (Maier et al., 2018) and are listed in Supp Table 2.
All Strains were stored at −80 °C as 20% (v/v) glycerol cultures.

Construction of Δ*mfd* mutants

The *P. aeruginosa* CIP27853 Δ*mfd* mutant strain was constructed by double-crossover region deletion. Briefly, using the available sequencing information of *P. aeruginosa* CIP27853 strain, around 1-kb regions upstream (region 3360879 to 3361826) and downstream (region 3363535 to 3364310) of the targeted *mfd* gene were synthesized by the Genecust company (Boynes, France). The two fragments were cloned and juxtaposed into the (suicide) pEXTK vector by the Genecust company. The constructed plasmid was named pPa001 and transformed into electro competent *E. coli* SM10 λpir and then, by conjugation into *P. aeruginosa* CIP27853 strain as previously described (Hmelo et al., 2015). Briefly, the donor and receptor strains were mixed at a 1:2 ratio on a sterile membrane filter with a pore size of 0.05 µm (VMWP02500 Milipore) deposited on LB agar plates supplemented with irgasan 25 µg/ml and gentamicin 75 µg/ml for 18 h at 37°C. After mating, bacteria were resuspended from filter with LB-IPTG 1 mM, incubated for 3 h at 37°C and plated on LB agar plates with AZT 100 µg/ml and IPTG 1mM for 18 h at 37°C. The trans-conjugates were selected for loss of gentamicin resistance by picking individual colonies on LB agar plates and on LB supplemented with 75 µg/mL of gentamicin at 37°C. The deletion of the *mfd* gene by double recombination event was verified by PCR using primers located upstream (GAACACCACCAGTTCCACCTG) and downstream (GGTAGAGCTGGCCAATCAGC) of the cloned region and by sequencing. The corresponding mutant was named *P. aeruginosa* Δ*mfd*.

The *K. pneumoniae* ATCC 700603 Δ*mfd* mutant strain was constructed by double-crossover region deletion. Briefly, around 1-kb region upstream (region 2056347 to 2057137) and downstream (region 2060189 to 2060810) of the targeted *mfd* gene were synthesized using the available sequencing information of *K. pneumoniae* ATCC700603 strain, by the Genecust company (Boynes, France). The two fragments upstream and downstream of the *mfd* gene were cloned at each side of the chloramphenicol cassette (CatR) from the pDK3 plasmid (Addgene) into the pUC57 vector (Addgene) by the Genecust company. The synthesized DNA fragments and the CatR cassette were digested with the appropriate enzymes and assembled by ligation to produce a "*mfd*-upstream"-"CatR"-"*mfd*-downstream" *Kpn*I-*EcoR*I fragment, which was then inserted between the *Kpn*I and *EcoR*I sites of the pDG704 vector (Addgene). The constructed plasmid was named pKp002 and transformed into electro competent *E. coli* SM10 λpir and then by conjugation into *K. pneumoniae* ATCC700603 strain. Briefly,

the donor strain and receptor strains were mixed at a 2:1 ratio on a sterile membrane filter with a pore size of 0.05 µm (VMWP02500Milipore) and deposited on LB agar plates for 4 h at 37°C. After mating, bacteria were resuspended from filter with 1.5 mL of LB medium. The trans-conjugates were selected on LB agar plates supplemented with 25 µg/mL of chloramphenicol at 37°C. The deletion of the *mfd* gene by double recombination event was verified by PCR using primers located upstream (CCCCAGGATGTTGTTTTGCA) and downstream (CCGTTATCCTGCACCACATG) of the cloned region and by sequencing. The corresponding mutant was named *K. pneumoniae* Δmfd.

Chemicals

The 95 molecules were sourced from commercial vendors: Enamine, Chembridge, Chemspace, AbamaChem, Asinex, Chemdiv, Interbioscreen, BCH research and Specs. Each compound was dissolved in DMSO (Sigma-Aldrich) and stored at room temperature until further use. The Roswell Park Memorial Institute (RPMI) 1640 GlutaMAXTM medium was purchased from Gibco. The Nitric Oxide (NO) donor, 3-[2-hydroxy-1-(1-methylethyl)-2-nitrosohydrazino]-1-propanamine NOC-5, was purchased from Calbiochem, Sigma-Aldrich. NOC-5 was dissolved in NaOH 0.01 N at a final concentration of 200 mM. NOC-5 has a half-life time of NO release of 25 min at 37 °C. Under these conditions, a stable NO-amine complex can spontaneously release two NO equivalents (Porrini et al., 2020). Meropenem (MPN) was purchased from Sigma-Aldrich and dissolved in water at a stock concentration of 25 mM. Poly(lactide-co-glycolide) (PLGA) (Resomer® RG502 H, acid terminated, M_W = 7-17 kDa), poly(vinyl alcohol) (PVA) (87–89% hydrolysed, MW = 30–70 kDa), trehalose and all other reagents and solvents were supplied by Sigma-Aldrich (France).

Protein purification

E. coli MG1655 His6-tagged MfdC (residues 451-1148 Uniprot accession code P30958) was synthesized and purified by BioBasic Inc. (Markham, ON, Canada) with a purity >90%. Briefly, expression plasmid PET21a containing *mfdC*, was transformed into *E.coli* BL21(DE3) and expression of His6-tagged MfdC was induced by 0.5 mM IPTG at 37℃ for 4 h. Cells were lysed and protein was purified with the Ni-IDA column. Elution fractions were dialyzed with dialysis buffer (2 mM DTT, 50 mM Tris, 300 mM NaCl, pH 8.0) overnight at 4℃.

Saccharomyces cerevisiae protein yUpf1 HD (residues 221–851 Uniprot accession code P30771, which corresponds to the helicase domain) was kindly provided by Dr Hervé Le Hir (Institut de biologie de l'Ecole normale supérieure (IBENS), Paris, France) and described in (Kanaan et al., 2018).

Inhibition of ATP-ase activity *in vitro*

MfdC enzyme activity was evaluated by measuring the quantity of inorganic phosphate (PO4i) released using BIOMOL® Green reagent microtiter-plate assay (Enzo Life Sciences). For the initial drug screening, MfdC (0.35 µM) was incubated with DMSO (2% (v/v)) or with the 95 compounds (100 mg/mL) and 1 mM ATP for 10 min at 37°C. To further evaluate NM102 activity, MfdC (0.35 µM) was incubated with NM102 at the indicated concentration (0 to 100 µM). ATPase reaction was measured in Tris buffer 0,05M at pH 8, in the presence of ATP (0 µM to 0.3 mM) for 30 min at 37°C. yUpf1 HD ATPase activity was measured in reaction buffer (20 mM MES pH 6.0, 100 mM potassium acetate, 1 mM DTT, 0.1 mM EDTA, 1 mM magnesium acetate, 1 mM zinc sulfate, and 5% (v/v) glycerol). 0.127 µM of protein was incubated with 2% DMSO or 100 µM NM102. ATPase reaction was quantified after 30 min incubation at 30°C. For MfdC and yUpf1 HD, 50 µL of each reaction medium was transferred into clear, flat-bottom 96-well plates and the reaction was terminated by the addition of 100 µL of BIOMOL® Green reagent. The absorbance at 620 nm was measured in a microplate reader (Tecan). The absorbance values were then transformed into nmols of released PO4i based on a PO4i standard curve prepared as recommended by the supplier. The potency of each compound was calculated relative to the DMSO control.

The z' factor of the ATP-ase test was calculated by using the formulae $Z'=1-(3\sigma c+ + 3\sigma c-)/(|\mu c+ - \mu c-|)$ where (σc+) and (σc−) are the data standard deviation for the high and low reference control, respectively, and |µc+—µc−| is the absolute value of the difference of the two control signal means.

Plot of MfdC ATPase activity versus ATP concentration (0.002-0.3 mM) in the presence of various concentrations of NM102 inhibitor was used to measure the IC_{50}. Data analysis and IC_{50} computing were performed using the Graph Pad Prism 7.05 software (San Diego, CA). Lineweaver-Burk plots were obtained by using Sigma Plot Software.

Nitric Oxid (NO) cell free assay

Bacteria were grown in LB medium at 37°C under agitation at 200 rpm until late exponential phase. Bacterial suspensions were prepared in RPMI medium at concentrations between 5 x 10^4 and 1 x 10^5 CFU/mL and 150 µL were dispatched into a 96-well plate. Bacteria were exposed to NO through the addition of 50 µL of NOC-5 at final concentrations ranging from 0 to 1000 µM. Bacterial survival rate was quantified by plating on LB agar after 4 h at 37°C and by normalizing bacterial load in NOC-5-treated samples against control untreated samples (0 µM of NOC5). NOC-5 concentrations (Log10-transformed) were plotted and a non-linear fit with a variable Hill slope was made using Graph Pad Prism 7.05 to obtain NO dose-response curves. NOC-5 concentrations required to induce 10 and 20% of mortality of the strain were calculated using R and the drc package (Christian Ritz and Jens C. Strebig).

For efficacy assays, bacterial solutions were prepared as described above. Bacteria were exposed to 50 µL of NOC5 at a concentration inducing a survival of around 80 - 90 % compared to the untreated condition (*K. pneumoniae*: 9 µM, Kp DOU 14 µM, Kp ALE 23 µM, *P. aeruginosa* 5 µM, *E. coli* ATCC 42 µM, *E. coli* GUE 26 µM), in absence (0 µM) or in the presence (from 5 to 80 µM) of NM102. Bacterial survival rate was quantified by plating on LB agar after 4 h at 37°C and by normalizing bacterial load in NM102-treated samples against control samples. Toxicity of the inhibitor in the absence of NO was assessed by exposure of bacterial suspension to NM102 at a concentration ranging from 0 to 80 µM of NM102 as described above, but without NOC5. NM102 concentration required to induce 50% of mortality of the strain (IC_{50}) was calculated using R and the drc package.

Nanoformulation of NM102 and characterization

NM102 was formulated in the presence of poly(D-L lactide-*co*-glycolide) (PLGA) according to a previously described method with some modifications (Van de Ven et al., 2012). It consists of an ultrasonic emulsification process, followed by dialysis to remove the organic solvent. First, 120 mg of PLGA and 28 mg of NM102 were dissolved in 4 mL of DMSO and then the organic phase was injected through a 23 G-needle into 50 mL of a 0.5% w/v aqueous solution of PVA under sonication in ice (5 min, amplitude 20%, cycle of sonication: 10 s ON and 10 s OFF) using a tip sonicator (Vibra-cellTM–75041, Fisher Bioblock Scientific, Belgium). The organic phase was then removed by dialysis (24 h, room temperature) using a 100 kDa MW cut-off cellulose ester membrane (Thermo Fisher Scientific, France). Empty nanoformulation was prepared according to the same protocol but in absence of drug in the organic phase. Nanoformulations were stored at 4°C. Intensity-averaged diameters (D_z) and particle size distributions were measured at 25°C by dynamic light scattering (DLS) using a Nano ZS instrument (173° scattering angle, Malvern, France) after 1/20 dilution in Milli-Q water (Millipore, France). The surface charge of the nanoformulations was determined by measuring the ζ-potential at 25°C using the same instrument after 1/10 NP dilution in 1 mM NaCl. All measurements were performed in triplicate. Colloidal stability of the nanoformulations was assessed by measuring the evolution of the mean diameter and the particle size distribution for up to two weeks at 4°C and room temperature.

For conservation, 20-mL flat bottom glass vials were filled with 2 mL of nanoformulation supplemented with 5% w/v of trehalose as a cryoprotectant. Samples were frozen at -20°C for 12 h and then freeze-dried (24 h) using an Alpha 2–4 LD plus freeze-drier (Martin Christ, Germany) (condenser temperature < 70°C, vacuum < 0.1 mbar). Freeze-dried samples were capped, weighted and stored at 4°C. Samples were reconstituted immediately before use by addition of Milli-Q water, followed by gentle homogenization by pipetting and vortexing.

The drug content was determined by direct quantification of NM102 in freeze-dried NM102 nanoformulation samples (without cryoprotectant). Briefly, one sample was dissolved in DMSO (1 mL) by vortexing. The amount of NM102 was then quantified by UV spectroscopy at 282 nm (Perkin-Elmer UV/VIS spectrophotometer, Germany). The drug concentration was calculated using a NM102 calibration curve in DMSO (correlation coefficient >0.999), as follows: drug content (mg/mL) = weight of drug/volume of nanoformulation dispersion.

Insect assay

Fourth instar silkworm larvae *Bombyx eri* were purchased from *« L'office pour les insectes et leur environnement »* (OPIE), Guyancourt, France. Larvae were reared with *Ligustrum vulgare* or *Ligustrum japonicum* until they reached a weight of [0,6 – 0,9] g. Prior to assays, *Bombyx eri* larvae were kept under starvation overnight and randomly distributed in groups of 30. *P. aeruginosa* wt and Δmfd strains were grown in LB medium at 37°C under agitation at 180 rpm until late exponential growth phase. Bacterial cultures were then diluted in Phosphate Saline Buffer (PBS). The last dilution to obtain the desired concentration was done in PBS with 10% DMSO with or without NM102. Bacteria were plated right before infection to determine the quantity injected. Larvae were injected with 20 µL of bacterial suspension (3 x 10^3 CFU/injection in 10% DMSO) containing NM102 (2.78 µg/larvae) or 10% DMSO in the haemolymph via the last pro-leg. Larvae were placed at 27°C. At 4 h and 8 h post first injection, larvae were injected with 50 µL of: (i) PBS, 10% DMSO or (ii) PBS, 10% DMSO with NM102 (6.97 µg/larvae) *via* the last pro-leg on the other side of the larvae. All injections were performed using a 1 mL hypodermic syringe with a 0.5 x 25 mm needle and an automated syringe pump (KD Scientific KDS 100). 24 h post infection, insects were placed in 2 mL sterile tubes containing 500 µL of PBS and 1.4 mm ceramic lysing beads (MP Biomedicals, Solon, OH, USA) and crushed using a Fast Prep instrument (MP Biomedicals, Solon, OH, USA). The bacterial content in each tube was assessed by serial dilutions on LB plates and CFU numeration. The log CFU was calculated per gram of larvae.

Mice infections

Nine-week-old, specific-pathogen-free, female C56BL/6J mice were purchased from Janvier Labs (Le Genest-Saint-Isle, France). They were housed with a maximum of five animals per cage and had *ad libidum* access to food and water. Mice were adapted to the environment of the facility (IERP, INRAE, Jouy-en-Josas, France) one week before experiments.

Prior to infection, mice were mildly anaesthetized by intra peritoneal (i.p.) injection of ketamine (79 mg/kg) and xylazine (9 mg/kg). Bacterial strains were grown to late exponential phase and diluted in PBS. Intranasal (i.n.) bacterial administration was performed through slow instillation of 20 µL of bacterial suspension (1x 10^7 CFU) with a micropipette (10 µL in each naris). Inoculated suspensions

were plated on LB agar for CFU determination prior to injection. Empty and NM102-containing formulations were administrated in mice either: (i) *via* the i.p. route with 200 µL of suspension containing 1.5 or 6 mg/kg (1.29 and 5.16 mM, respectively) of drug or (ii) *via* the i. n. route with 20 µl of a mixture containing bacterial suspension (1x 10^7 CFU) and NM102 formulation (1.5 or 6 mg/kg) or empty formulation. MPN (10 mg/kg) was inoculated *via* the i.p. route. For combination therapy studies, NM102 formulation and MPN were inoculated *via* the i.n. and the i.p. route, respectively.

Mice were sacrified by cervical dislocation after 24 h and the left lung was placed in 2 mL sterile tubes containing 600 µL of PBS and 1.4 mm ceramic lysing beads (MP Biomedicals, Solon, OH, USA). Organs were homogenized using a FastPrep instrument (MP Biomedicals, Solon, OH, USA) and aliquots from each tube were serially diluted on LB plates for CFU enumeration. The log CFU was calculated per g of organ.

For the toxicity study, mice were treated (i.p., 200L/injection) with NM102 (6 mg/kg) or DMSO as control and mice weight was monitored for 7 days.

Cytotoxicity

HeLa (human cervical epithelial cell line) and Vero (monkey kidney epithelial cell line) cells were cultured in Dulbecco's Modified Eagles Medium (DMEM), supplemented with 10% heat inactivated fetal bovine serum (FBS) and 1 U/mL penicillin, and 1 µg/mL streptomycin at 37°C and 5% CO_2. Once reaching a confluency of 70%, cells were washed with Dulbeccos Phosphate Buffered Saline (DPBS) and detached by treatment with 0,05% Trypsin-EDTA. Total cell number was determined by using a Neubauer Cell chamber and cells were seeded at a concentration of 4x10^4 cells/well in a flat-bottom Tissue Culture 96-well plate. Cells were then incubated at 37°C and 5% CO_2 overnight before starting the cytotoxicity assay. Two hours before the assay, medium in each well was replaced by an antibiotic-free DMEM medium. Cells were washed and treated with the respective chemical (MPN at 10 and 100 µM; NM102 at 10 and 300 µM; NM102 formulation at 1.29 and 5.16 mM) or their respective control (10% DMSO or empty formulation) in a total volume of 100 µL in Hanks' Balanced Salt Solution (HBSS) medium (ThermoFischer). After one hour of incubation, 20 µL of CellTiter96®AQ_{ueous} was added to each well and cells were incubated again for one hour. Absorbance was measured at 490 nm after 5 seconds of shaking to determine cytotoxicity. The background of CellTiter96®AQ_{ueous} in HBSS and the background of each chemical was subtracted of the respective values. Treated cells were compared and normalized to the untreated control.

Susceptibility testing on commensals in monoculture

Stock solutions of compound NM102 and MPN were prepared in DMSO. Drug master plates were prepared from these stock solutions at 100X final concentration in DMSO, arranged in 96-well format

and stored at -30 °C until use. The master plates were diluted to 2X drug concentration in species-specific growth medium (Supp Table 2). All media, materials, and 96-well drug plates were pre-reduced in the anaerobic chamber (Coy Laboratory Products Inc., 2% H_2, 12% CO_2, and the balance N_2) for at least one day before use, and all growth experiments were performed under anaerobic conditions at 37°C. Each strain was streaked on BHIs agar (Brain Heart Infusion Medium, Oxoid CM1135, 5% sheep blood, 1.2% Iso Vitalex enrichment) O/N at 37°C. Single colonies were then inoculated into the appropriate liquid media (Supp Table 2) and cultured O/N at 37°C. First, the O/N cultures were diluted to an OD578 of 0.02 in the respective media. Then, 50 µL of the diluted culture was added to each well already containing 50 µL of the 2X drug solution, resulting in a starting $OD_{578\ nm}$ of 0.01 and a 1X drug concentration. After inoculation, plates were sealed with breathable membranes (Breathe-Easy) to prevent evaporation and cross-contamination between wells. $OD_{578\ nm}$ was measured hourly for 24 h after 30 s of linear shaking using a microplate spectrophotometer (Epoch2, BioTek, Gen5 software, version 3.05) and an automated microplate stacker (BioStack 4, BioTek) installed in a custom-built incubator (EMBL Mechanical Workshop). At least three biological replicates of each compound/strain combination were tested. Data analysis was performed as previously described (Maier et al., 2018). Briefly, growth curves were blanked, truncated at stationary phase entry, AUCs calculated and normalized to control growth curves (1% DMSO, no compound).

Analysis of microbiome diversity

Mice were treated (i.p., 200 µL/injection) with DMSO or NM102 (6 mg/kg). Feces were collected (day 1 and day 7) and the quantity of bacteria was assessed by qPCR as previously described (Mayeur et al., 2013). In addition, microbiota diversity was assessed by 16S rRNA sequencing. Mice were treated (i.p., 200 µL/injection) with DMSO or NM102 (6 mg/kg) after i.n. infection with *K. pneumoniae*. Feces of untreated and treated mice were collected and stored at -80°C. Microbial DNA was extracted using the DNeasy PowerSoil Pro Kit following the provider's instructions (Qiagen, Hilden, Germany). DNA samples were sent to the NGS Competence Center Tübingen (Tübingen, Germany) for quantification, library construction and sequencing. DNA concentration was quantified using a Qubit fluorometer (Thermo Fischer, Waltham, MA). The V4 hypervariable region of the 16S rRNA gene was amplified using primers F515 (5'-GTGCCAGCMGCCGCGGTAA-3') and R806 (5'-GGACTACHVGGGTWTCTAAT-3') (Caporaso et al., 2011) and sequenced with the Illumina MiSeq sequencing platform with v2 chemistry. To process 16S rRNA amplicon sequences, we used the dada2 v.1.21.0 package of R (v.4.2.0) (Callahan et al., 2016) following its standard operating procedure as available at https://benjjneb.github.io/dada2/bigdata.html. Briefly, after inspecting the quality profiles of the raw sequences, we trimmed and filtered the paired-end reads using the following parameters: trimLeft: 23, 24; truncLen: 240, 200; maxEE: 2, 2; truncQ: 11. The filtered forward and reverse reads were

dereplicated separately and used for inference of the amplicon sequence variants (ASVs) with default parameters, after which they were merged in a per-sample basis. We next filtered the merged reads to retain only those with a length between 250 and 256 bp and carried out chimera removal.

We then performed the taxonomic assignment on the final set of ASVs using a curated dada2-formated database based on the genome taxonomy database (GTDB) release R06-RS202 (Parks et al., 2018). A maximum-likelihood tree of the ASVs was obtained using the R packages DECIPHER v.2.24.0 and phangorn v.2.8.1 (Schliep, 2011) after performing a multiple sequence alignment with each of the representative sequences. We used the PERFect v.1.10 package of R (Smirnova et al., 2019) to identify spurious ASVs, defined as those that made insignificant contributions to the total covariance of the microbiome dataset.

For alpha- and beta-diversity analyses, samples were rarefied to 21300 reads/sample to account for differences in library size. To compare alpha-diversity between samples, we used the Shannon index as implemented in the vegan v.2.6-2 package of R (https://CRAN.R-project.org/package=vegan). Global differences in Shannon index between treatments were assessed using the Kruskal-Wallis-Test and pairwise contrasts between treatments were performed using the Wilcoxon signed-rank test. We used the ASV-level abundance profile to obtain matrices of the weighted and unweighted UniFrac distances with the GUniFrac v.1.6 package of R (Chen et al., 2012). We assessed differences in beta-diversity estimates using the adonis function (analysis of variance using distance matrices) of the permutational multivariate analysis of variance (PERMANOVA) on the distance matrices with 9999 permutations, as implemented in the vegan v.2.6-2 package of R. For pairwise PERMANOVA tests, we used the pairwiseAdonis v.0.4 package of R (available at https://github.com/pmartinezarbizu/pairwiseAdonis). P values were adjusted for multiple comparisons using the Benjamini-Hochberg method.

Mutation rate

E. coli Keio WT and Δ*mfd* strains were grown onto LB agar O/N at 37°C. Cultures in LB broth were started from a single colony at 37°C at 200 rpm until an $OD_{600\ nm}$ at around 0.005. Each culture was then divided in two with one culture exposed to 100 µM NM102 and the other to 2% final DMSO as control. Bacteria were incubated until the culture reached $OD_{600\ nm}$ of 2, which corresponds to the early stationary phase. Bacteria were plated onto LB agar plates with 50 µg/mL rifampicin and incubated for 24 h at 37°C. The number of colonies was counted and used to determine the mutation frequency. Total number of bacteria were determined following serial dilution and plating onto LB agar plate.

Evolvability assays

A serial passage broth microdilution protocol was performed based on previously described methods (Ragheb et al., 2019) to identify the effect of NM102 on the evolution of antibiotic resistance. Briefly, culture of *E. coli* Keio WT started from a single colony was diluted to $OD_{600\ nm}$ = 0.005. Bacterial suspension was subsequently transferred into a 96-well microplate (180 µL/well) and incubated with NM102, DMSO 2% or left untreated. Treated and untreated bacteria were grown in LB with a gradient of concentrations of the indicated antibiotic to select for resistance for 18 h-24 h at 37°C under stationary conditions. The $OD_{600\ nm}$ was measured and MICs were determined. Serial passage was performed using cells growing (defined by an $OD_{600\ nm}$ at a minimum of 50% of the untreated condition) in the highest concentration of antibiotic. Antimicrobial concentrations were adjusted during the process to compensate for the rise in MIC values. This process was repeated for 4 or 5 passages. Results were expressed as the median MIC of the 3 replicates.

References

Adasme, M.F., Linnemann, K.L., Bolz, S.N., Kaiser, F., Salentin, S., Haupt, J., and Schroeder, M. (2021). PLIP 2021: expanding the scope of the protein–ligand interaction profiler to DNA and RNA. Nucleic Acids Res *49*, 530-534.

Anselmo, A.C., and Mitragotri, S. (2021). Nanoparticles in the clinic: An update post COVID-19 vaccines. Bioeng Transl Med *6*, e10246.

Brugger, C., Zhang, C., Suhanovsky, M.M., Kim, D.D., Sinclair, A.N., Lyumkis, D., and Deaconescu, A.M. (2020). Molecular determinants for dsDNA translocation by the transcription-repair coupling and evolvability factor Mfd. Nat Commun *11*, 3740.

Butler, M., Blaskovich, M., and Cooper, M. (2017). Antibiotics in the clinical pipeline at the end of 2015. J Antibiot *70*, 3-24.

Callahan, B.J., McMurdie, P.J., Rosen, M.J., Han, A.W., Johnson, A.J., and Holmes, S.P. (2016). DADA2: High-resolution sample inference from Illumina amplicon data. Nat Methods *13*, 581-583.

Caporaso, J.G., Lauber, C.L., Walters, W.A., Berg-Lyons, D., Lozupone, C.A., Turnbaugh, P.J., Fierer, N., and Knight, R. (2011). Global patterns of 16S rRNA diversity at a depth of millions of sequences per sample. Proc Natl Acad Sci U S A *108 Suppl 1*, 4516-4522.

Chakrabarti, S., Jayachandran, U., Bonneau, F., Fiorini, F., Basquin, C., Domcke, S., Le Hir, H., and Conti, E. (2011). Molecular mechanisms for the RNA-dependent ATPase activity of Upf1 and its regulation by Upf2. Mol Cell *41*, 693-703.

Chen, J., Bittinger, K., Charlson, E.S., Hoffmann, C., Lewis, J., Wu, G.D., Collman, R.G., Bushman, F.D., and Li, H. (2012). Associating microbiome composition with environmental covariates using generalized UniFrac distances. Bioinformatics *28*, 2106-2113.

Collaborators, A.R. (2022). Global burden of bacterial antimicrobial resistance in 2019: a systematic analysis. Lancet *20*, 2724.

Cook, M.A., and Wright, G.D. (2022). The past, present, and future of antibiotics. Sci Transl Med *14*, eabo7793.

Darrigo, C., Guillemet, E., Dervyn, R., and Ramarao, N. (2016). The Bacterial Mfd Protein Prevents DNA Damage Induced by the Host Nitrogen Immune Response in a NER-Independent but RecBC-Dependent Pathway. PLoS ONE *11*, e0163321.

Deaconescu, A.M. (2021). Mfd - at the crossroads of bacterial DNA repair, transcriptional regulation and molecular evolvability. Transcription *12*, 156-170.

Deaconescu, A.M., Chambers, A.L., Smith, A.J., Nickels, B.E., Hochschild, A., Savery, N.J., and Darst, S.A. (2006). Structural basis for bacterial transcription-coupled DNA repair. Cell *124*, 507-520.

Guillemet, E., Leréécc, A., Royer, C., Tran, S., Barbosa, I., Sansonetti, P., Lereclus, D., and Ramarao, N. (2016). The bacterial repair protein Mfd confers resistance to the host nitric-oxide response. Scientific Reports *6*, 29349.

Han, J., Sahin, O., Barton, Y.W., and Zhang, Q. (2008). Key role of Mfd in the development of fluoroquinolone resistance in Campylobacter jejuni. PLoS Pathog *4*, e1000083.

Hwang, D., Ramsey, J.D., and Kabanov, A.V. (2020). Polymeric micelles for the delivery of poorly soluble drugs: From nanoformulation to clinical approval. Adv Drug Deliv Rev *156*, 80-118.

Imai, Y., Meyer, K.J., Iinishi, A., Favre-Godal, Q., Green, R., Manuse, S., Caboni., and al., e. (2019). A new antibiotic selectively kills Gram-negative pathogens. Nature *576*, 459-464.

Jain, A.N. (2003). Surflex: fully automatic flexible molecular docking using a molecular similarity-based search engine. J Med Chem *46*, 499-511.

Kahraman, A., Morris, R.J., Laskowski, R.A., and Thornton, J.M. (2007). Shape variation in protein binding pockets and their ligands. J Mol Biol *368*, 283-301.

Kanaan, J., Raj, S., Decourty, L., Saveanu, C., Croquette, V., and Le Hir, H. (2018). UPF1-like helicase grip on nucleic acids dictates processivity. Nat Commun *9*, 3752.

Katoh, K., Misawa, K., Kuma, K., and Miyata, T. (2002). MAFFT: a novel method for rapid multiple sequence alignment based on fast Fourier transform Nucleic Acid Res *30*, 3059-3066.

Laskowski, R.A., Jablonska, J., Pravda, L., Varekova, R.S., and Thornton, J.M. (2018). PDBsum: Structural summaries of PDB entries. Protein Sci *27*, 129-134.

Laver, J.R., Stevanin, T.M., Messenger, S.L., Lunn, A.D., Lee, M.E., Moir, J.W., Poole, R.K., and Read, R.C. (2010). Bacterial nitric oxide detoxification prevents host cell S-nitrosothiol formation: a novel mechanism of bacterial pathogenesis. FASEB J *24*, 286-295.

Lee, G.H., Jeong, J.Y., Chung, J.W., Nam, W.H., Lee, S.M., Pak, J.H., Choi, K.D., Song, H.J., Jung, H.Y., and Kim, J.H. (2009). The Helicobacter pylori Mfd protein is important for antibiotic resistance and DNA repair. Diagn Microbiol Infect Dis *65*, 454-456.

Lee, M.K. (2020). Liposomes for Enhanced Bioavailability of Water-Insoluble Drugs: In Vivo Evidence and Recent Approaches. Pharmaceutics *12*.

Ling, L.L., Schneider, T., Peoples, A.J., and Spoering, A.L. (2015). A new antibiotic kills pathogens without detectable resistance. Nature *517*, 455-459.

Liu, S., Zhang, J., Zhou, Y., Hu, N., Li, J., Wang, Y., Niu, X., Deng, X., and Wang, J. (2019). Pterostilbene restores carbapenem susceptibility in New Delhi metallo-beta-lactamase-producing isolates by inhibiting the activity of New Delhi metallo-beta-lactamases. Br J Pharmacol *176*, 4548-4557.

Maier, L., Goemans, C.V., Wirbel, J., Kuhn, M., Eberl, C., Pruteanu, M., Muller, P., Garcia-Santamarina, S., Cacace, E., Zhang, B., *et al.* (2021). Unravelling the collateral damage of antibiotics on gut bacteria. Nature *599*, 120-124.

Maier, L., Pruteanu, M., Kuhn, M., Zeller, G., Telzerow, A., Anderson, E.E., Brochado, A.R., Fernandez, K.C., Dose, H., Mori, H., *et al.* (2018). Extensive impact of non-antibiotic drugs on human gut bacteria. Nature *555*, 623-628.

Marcou, G., and Rognan, D. (2007). Optimizing fragment and scaffold docking by use of molecular interaction fingerprints. J Chem Inf Model *47*, 195-207.

Martin, H.A., Porter, K.E., Vallin, C., Ermi, T., Contreras, N., Pedraza-Reyes, M., and Robleto, E.A. (2019). Mfd protects against oxidative stress in Bacillus subtilis independently of its canonical function in DNA repair. BMC Microbiol *19*, 26.

Martin, J.K., Sheehan, J.P., Bratton, B.P., Moore, G.M., Mateus, A., Li, S.H., Kim, H.I., Rabinowitz, J.D., Typass, A., Savitski, M.M., *et al.* (2020). A dual-mechanism antibiotik kills Gram-negative bacteria and avoids drug resistance. Cell *181*, 1518-1532.

Mayeur, C., Gratadoux, J.J., Bridonneau, C., Chegdani, F., Larroque, B., Kapel, N., Corcos, O., Thomas, M., and Joly, F. (2013). Faecal D/L lactate ratio is a metabolic signature of microbiota imbalance in patients with short bowel syndrome. PLoS One *8*, e54335.

McKeage, K. (2015). Finafloxacin: first global approval. Drugs *75*, 687-693.

Million-Weaver, S., Samadpour, A.N., Moreno-Habel, D.A., Nugent, P., Brittnacher, M.J., Weiss, E., Hayden, H.S., Miller, S.I., Liachko, I., and Merrikh, H. (2015). An underlying mechanism for the increased mutagenesis of lagging-strand genes in Bacillus subtilis. Proc Natl Acad Sci U S A *112*, E1096-1105.

Parks, D.H., Chuvochina, M., Waite, D.W., Rinke, C., Skarshewski, A., Chaumeil, P.A., and Hugenholtz, P. (2018). A standardized bacterial taxonomy based on genome phylogeny substantially revises the tree of life. Nat Biotechnol *36*, 996-1004.

Pomerantz, R.T., and O'Donnell, M. (2010). Direct restart of a replication fork stalled by a head-on RNA polymerase. Science.

Porrini, C., Guerin, C., Tran, S.L., Dervyn, R., Nicolas, P., and Ramarao, N. (2021). Implication of a Key Region of Six Bacillus cereus Genes Involved in Siroheme Synthesis, Nitrite Reductase Production and Iron Cluster Repair in the Bacterial Response to Nitric Oxide Stress. Int J Mol Sci *22*.

Porrini, C., Ramarao, N., and Tran, S.L. (2020). Dr. NO and Mr. Toxic - the versatile role of nitric oxide. Biol Chem *401*, 547-572.

Ragheb, M.N., Thomason, M.K., Hsu, C., Nugent, P., Gage, J., Samadpour, A.N., Kariisa, A., Merrikh, C.N., Miller, S.I., Sherman, D.R., *et al.* (2019). Inhibiting the Evolution of Antibiotic Resistance. Mol Cell *73*, 157-165 e155.

Randall, L.B., Georgi, E., Genzel, G.H., and Schweizer, H.P. (2016). Finafloxacin overcomes Burkholderia pseudomallei efflux-mediated fluoroquinolone resistance. Curr Opin Microbiol *7*, 120-125.

Roberts, J., and Park, J.S. (2004). Mfd, the bacterial transcription repair coupling factor: translocation, repair and termination. Curr Opin Microbiol *7*, 120-125.

Rognan, D. (2017). The impact of in silico screening in the discovery of novel and safer drug candidates. Pharmacol Ther *175*, 47-66.

Rong, X., Yuan, W., Lu, Y., and Mo, X. (2014). Safety evaluation of poly(lactic-co-glycolic acid)/poly(lactic-acid) microspheres through intravitreal injection in rabbits. Int J Nanomedicine *9*, 3057-3068.

Sali, A., and Blundell, T.L. (1993). Comparative protein modelling by satisfaction of spatial restraints. J Mol Biol *234*, 779-815.

Schliep, K.P. (2011). phangorn: phylogenetic analysis in R. Bioinformatics *27*, 592-593.

Semete, B., Booysen, L., Lemmer, Y., Kalombo, L., Katata, L., Verschoor, J., and Swai, H.S. (2010). In vivo evaluation of the biodistribution and safety of PLGA nanoparticles as drug delivery systems. Nanomedicine *6*, 662-671.

Singleton, M.R., Scaife, S., and Wigley, D.B. (2001). Structural analysis of DNA replication fork reversal by RecG. Cell *107*, 79-89.

Smirnova, E., Huzurbazar, S., and Jafari, F. (2019). PERFect: PERmutation Filtering test for microbiome data. Biostatistics *20*, 615-631.

Smith, A.J., and Savery, N.J. (2008). Effects of the bacterial transcription-repair coupling factor during transcription of DNA containing non-bulky lesions. DNA Repair (Amst) *7*, 1670-1679.

Suzuki, H., Taketani, T., Kobayashi, J., and Ohshiro, T. (2018). Antibiotic resistance mutations induced in growing cells of Bacillus-related thermophiles. J Antibiot (Tokyo) *71*, 382-389.

Tibbitt, M.W., Dahlman, J.E., and Langer, R. (2016). Emerging Frontiers in Drug Delivery. J Am Chem Soc *138*, 704-717.

Van de Ven, H., Paulussen, C., Feijens, P.B., Matheeussen, A., Rombaut, P., Kayaert, P., Van den Mooter, G., Weyenberg, W., Cos, P., Maes, L., *et al.* (2012). PLGA nanoparticles and nanosuspensions with amphotericin B: Potent in vitro and in vivo alternatives to Fungizone and AmBisome. J Control Release *161*, 795-803.

Waterhouse, A.M., Procter, J.B., Martin, D.M., Clamp, M., and Barton, G.J. (2009). Jalview Version 2--a multiple sequence alignment editor and analysis workbench. Bioinformatics *25*, 1189-1191.

Yi, X., Liu, M., Luo, Q., Zhuo, H., Cao, H., Wang, J., and Han, Y. (2017). Toxic effects of dimethyl sulfoxide on red blood cells, platelets, and vascular endothelial cells in vitro. FEBS Open Bio *7*, 485-494.

Yoshitake, J., Akaike, T., Akuta, T., Tamura, F., Ogura, T., Esumi, H., and Maeda, H. (2004). Nitric oxide as an endogenous mutagen for Sendai virus without antiviral activity. J Virol *78*, 8709-8719.

Zaki, M.H., Akuta, T., and Akaike, T. (2005). Nitric oxide-induced nitrative stress involved in microbial pathogenesis. J Pharmacol Sci *98*, 117-129.
Zhuang, J.C., Lin, C., Lin, D., and Wogan, G.N. (1998). Mutagenesis associated with nitric oxide production in macrophages. Proc Natl Acad Sci U S A *95*, 8286-8291.

Figure

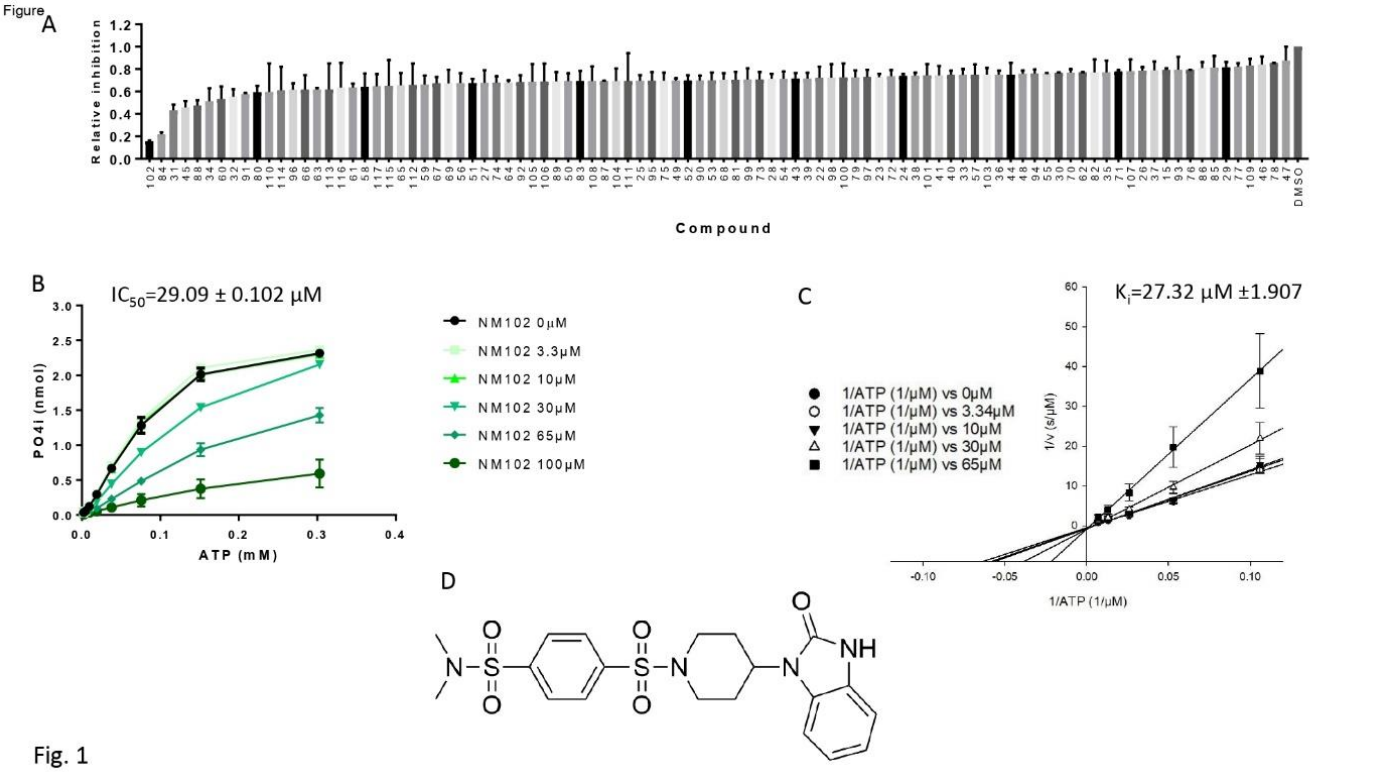

Fig. 1

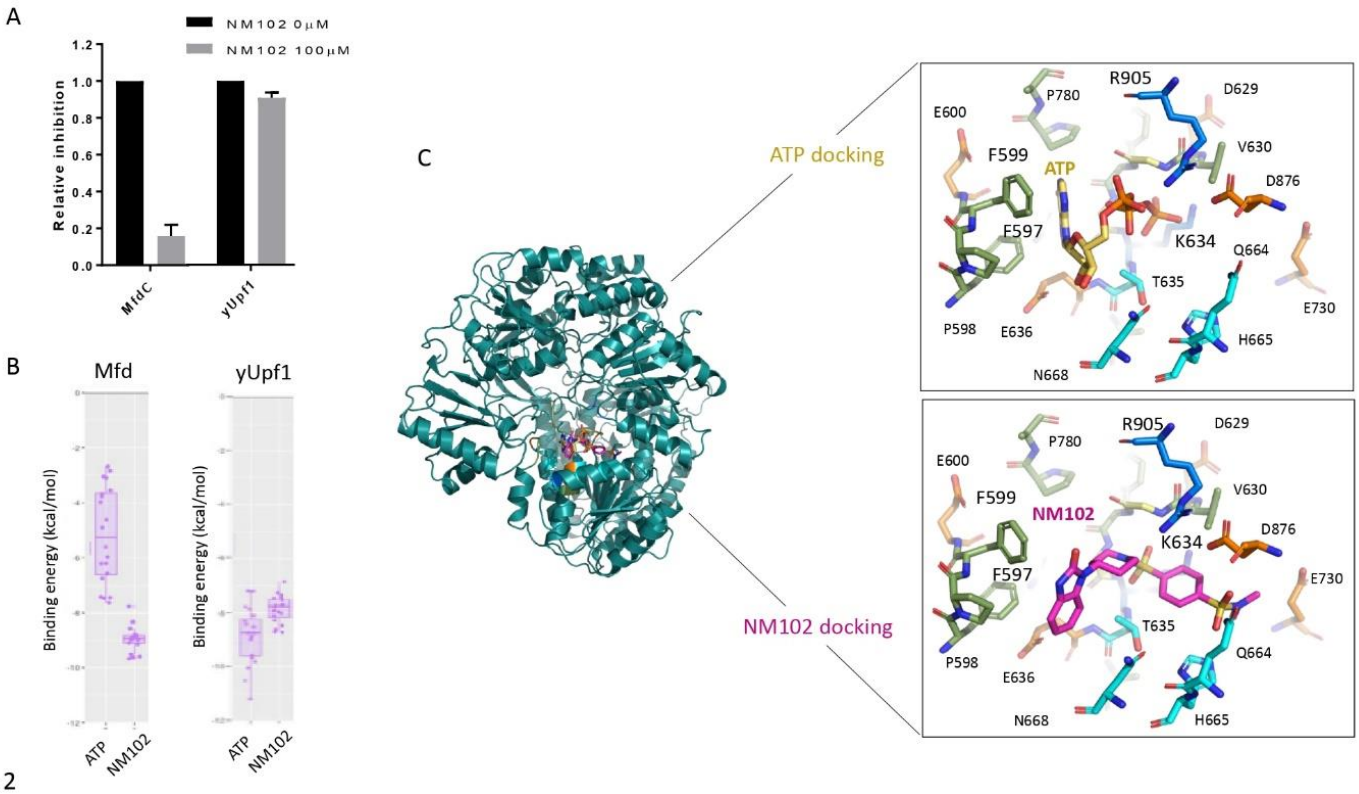

Fig 2

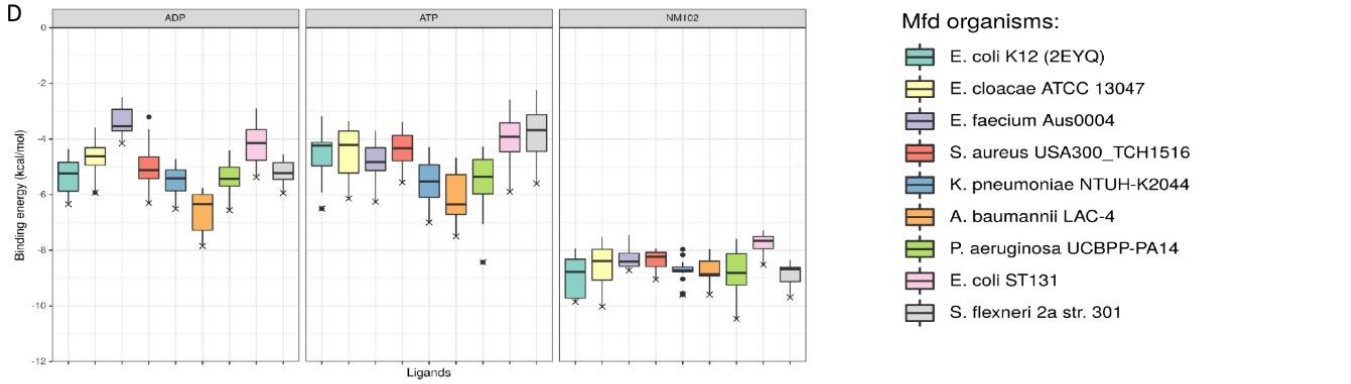
D
ADP
ATP
NM102
Binding energy (kcal/mol)
Ligands
Mfd organisms:
E. coli K12 (2EYQ)
E. cloacae ATCC 13047
E. faecium Aus0004
S. aureus USA300_TCH1516
K. pneumoniae NTUH-K2044
A. baumannii LAC-4
P. aeruginosa UCBPP-PA14
E. coli ST131
S. flexneri 2a str. 301

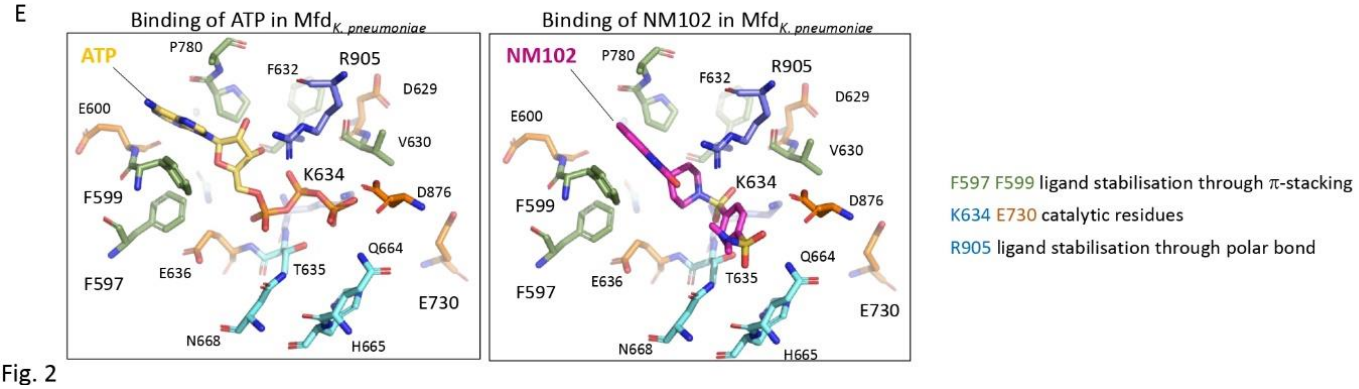
E
Binding of ATP in Mfd K. pneumoniae
Binding of NM102 in Mfd K. pneumoniae
ATP
NM102
P780
F632
R905
D629
E600
V630
K634
D876
F599
Q664
T635
E636
F597
E730
N668
H665
F597 F599 ligand stabilisation through π-stacking
K634 E730 catalytic residues
R905 ligand stabilisation through polar bond

Fig. 2

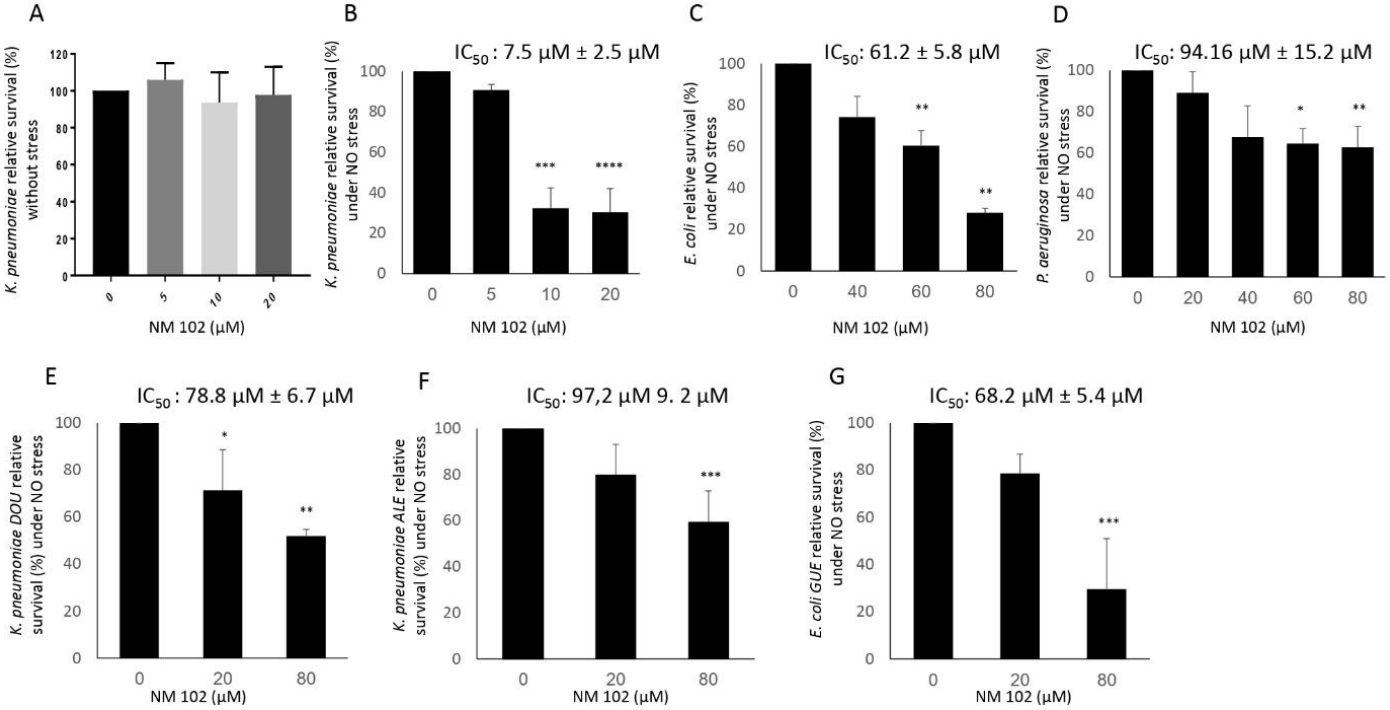
A
K. pneumoniae relative survival (%) without stress
NM 102 (µM)
B
K. pneumoniae relative survival (%) under NO stress
IC50 : 7.5 µM ± 2.5 µM
NM 102 (µM)
C
E. coli relative survival (%) under NO stress
IC50: 61.2 ± 5.8 µM
NM 102 (µM)
D
P. aeruginosa relative survival (%) under NO stress
IC50: 94.16 µM ± 15.2 µM
NM 102 (µM)
E
K. pneumoniae DOU relative survival (%) under NO stress
IC50 : 78.8 µM ± 6.7 µM
NM 102 (µM)
F
K. pneumoniae ALE relative survival (%) under NO stress
IC50: 97,2 µM 9. 2 µM
NM 102 (µM)
G
E. coli GUE relative survival (%) under NO stress
IC50: 68.2 µM ± 5.4 µM
NM 102 (µM)

Fig. 3

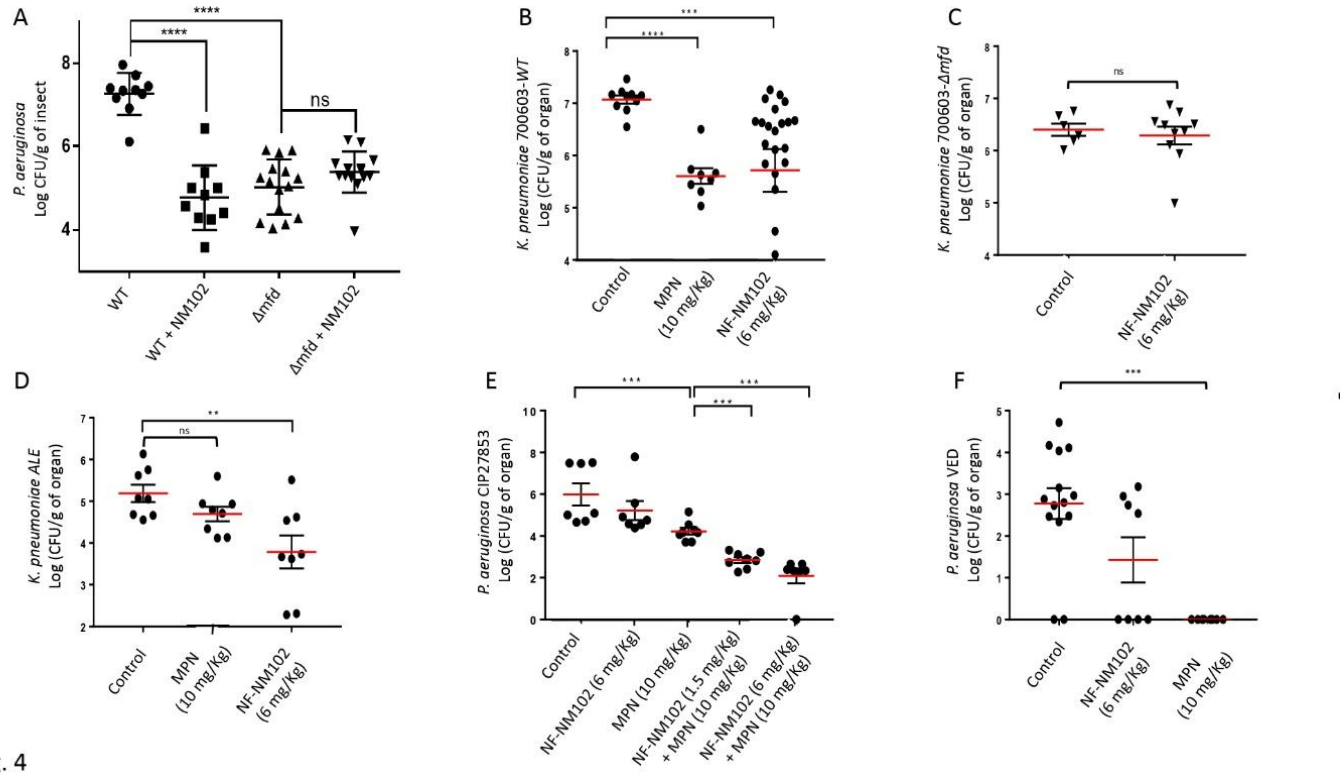
A
P. aeruginosa
Log CFU/g of insect
****
****
ns
WT
WT + NM102
Δmfd
Δmfd + NM102
B
K. pneumoniae 700603-WT
Log (CFU/g of organ)
***
****
Control
MPN (10 mg/Kg)
NF-NM102 (6 mg/Kg)
C
K. pneumoniae 700603-Δmfd
Log (CFU/g of organ)
ns
Control
NF-NM102 (6 mg/Kg)
D
K. pneumoniae ALE
Log (CFU/g of organ)
**
ns
Control
MPN (10 mg/Kg)
NF-NM102 (6 mg/Kg)
E
P. aeruginosa CIP27853
Log (CFU/g of organ)
***
***
***
Control
NF-NM102 (6 mg/Kg)
MPN (10 mg/Kg)
NF-NM102 (1.5 mg/Kg) + MPN (10 mg/Kg)
NF-NM102 (6 mg/Kg) + MPN (10 mg/Kg)
F
P. aeruginosa VED
Log (CFU/g of organ)
***
Control
NF-NM102 (6 mg/Kg)
MPN (10 mg/Kg)

Fig. 4

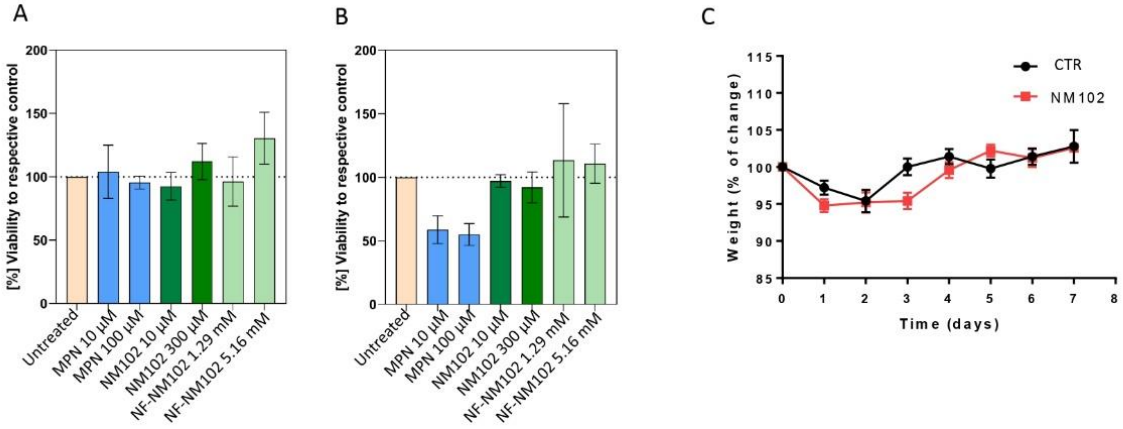
A
[%] Viability to respective control
Untreated
MPN 10 μM
MPN 100 μM
NM102 10 μM
NM102 300 μM
NF-NM102 1.29 mM
NF-NM102 5.16 mM
B
[%] Viability to respective control
Untreated
MPN 10 μM
MPN 100 μM
NM102 10 μM
NM102 300 μM
NF-NM102 1.29 mM
NF-NM102 5.16 mM
C
CTR
NM102
Weight (% of change)
Time (days)

Fig. 5

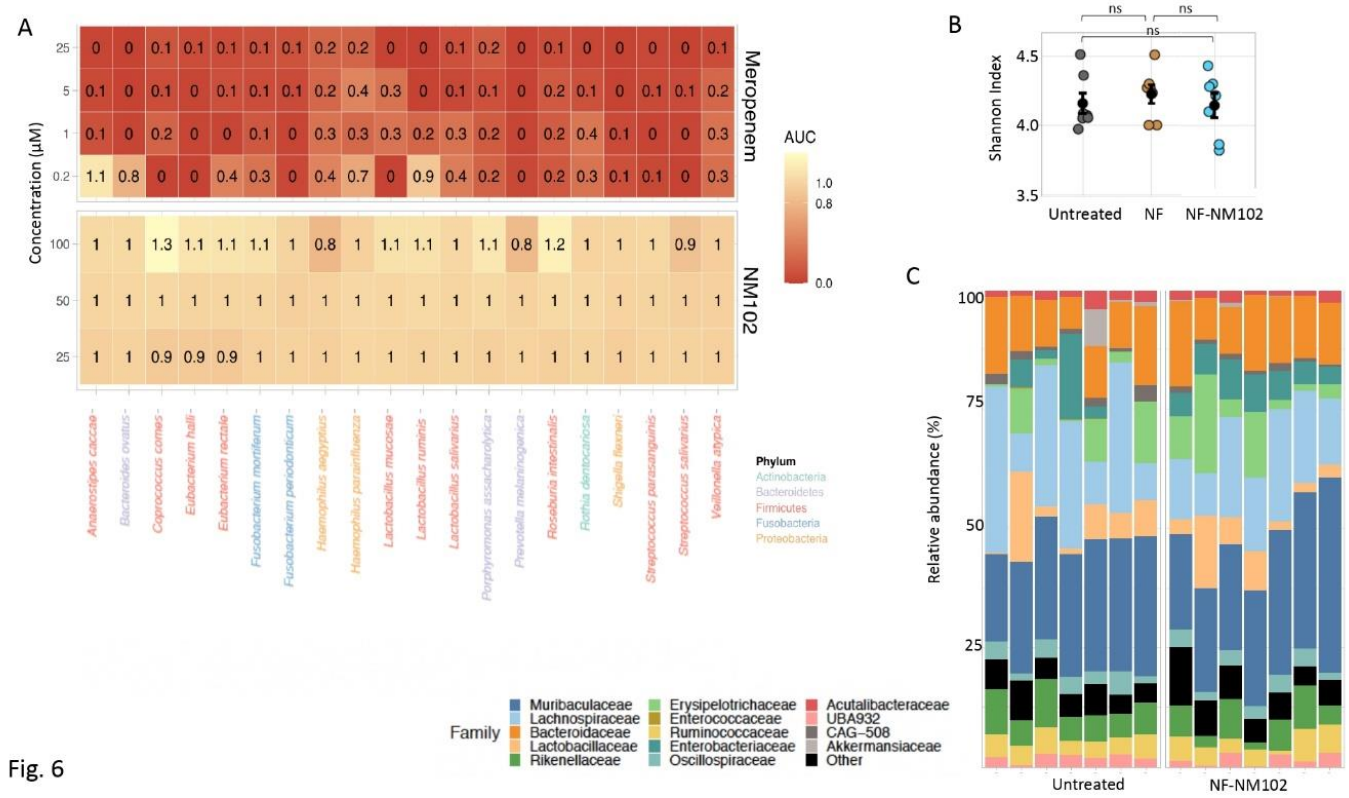
A
Concentration (μM)
Meropenem
NM102
AUC
Phylum
Actinobacteria
Bacteroidetes
Firmicutes
Fusobacteria
Proteobacteria
Family
Muribaculaceae
Lachnospiraceae
Bacteroidaceae
Lactobacillaceae
Rikenellaceae
Erysipelotrichaceae
Enterococcaceae
Ruminococcaceae
Enterobacteriaceae
Oscillospiraceae
Acutalibacteraceae
UBA932
CAG−508
Akkermansiaceae
Other
B
Shannon Index
ns
Untreated
NF
NF-NM102
C
Relative abundance (%)
Untreated
NF-NM102

Fig. 6

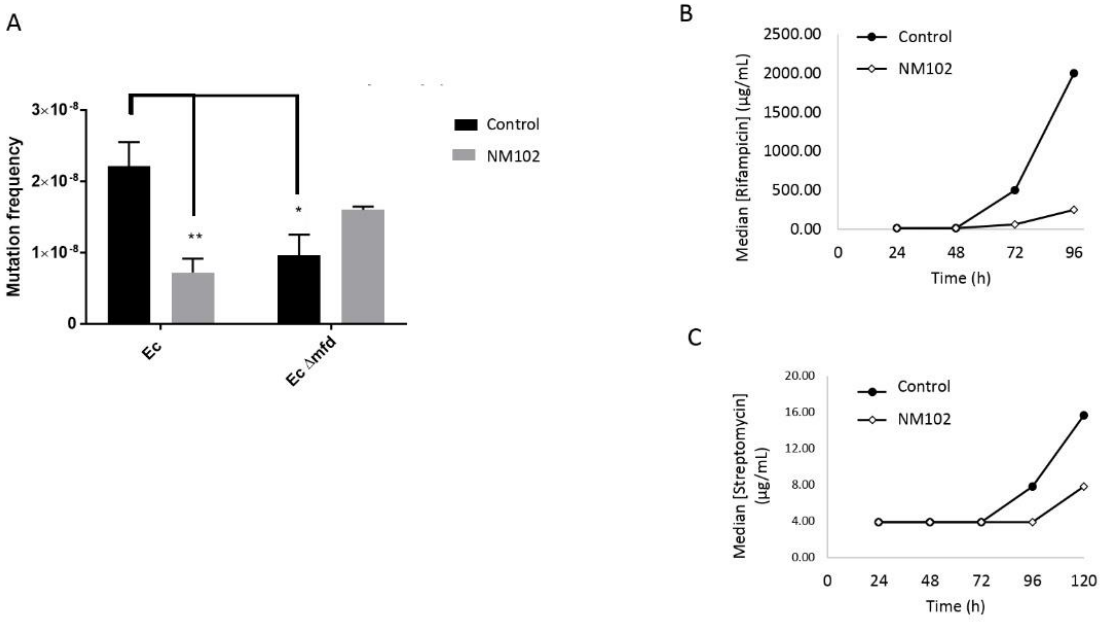
A
Mutation frequency
Control
NM102
Ec
Ec Δmfd
B
Median [Rifampicin] (μg/mL)
Control
NM102
Time (h)
C
Median [Streptomycin] (μg/mL)
Control
NM102
Time (h)

Fig. 7

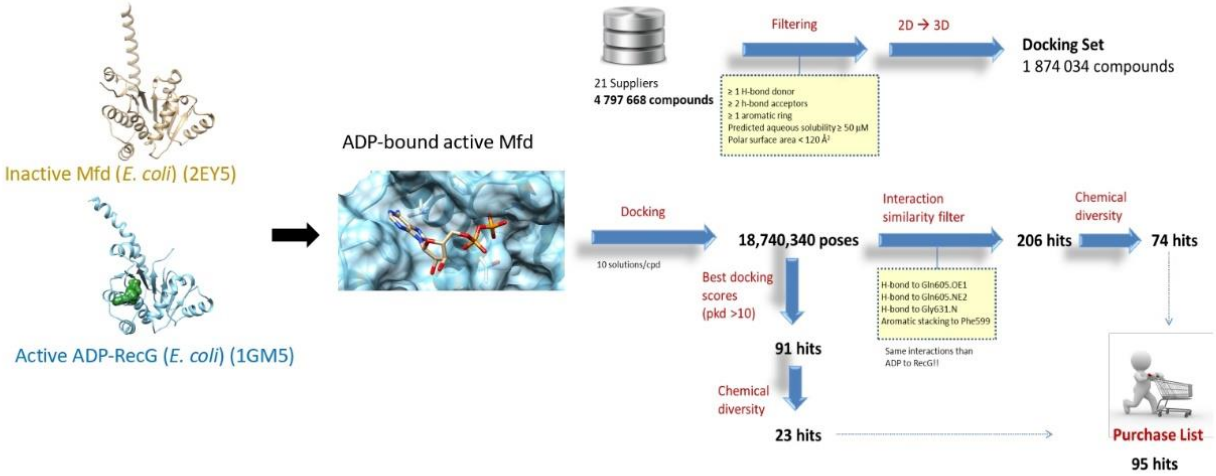

Supp Fig 1

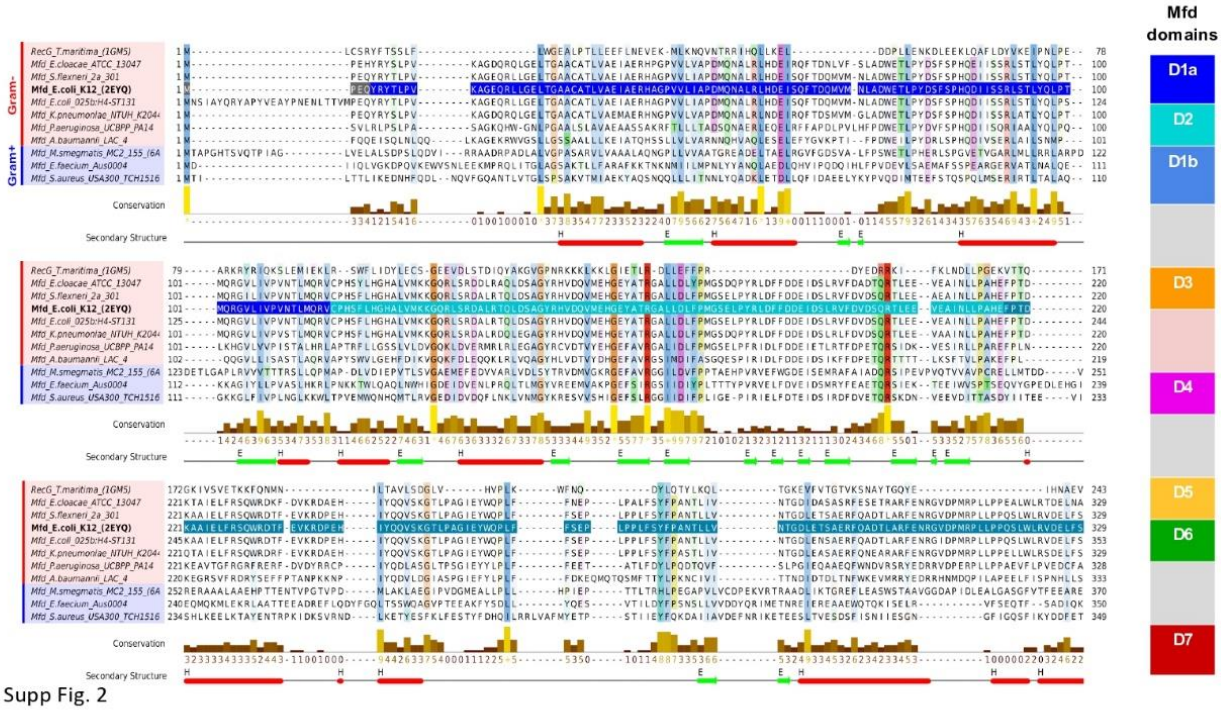

Supp Fig. 2

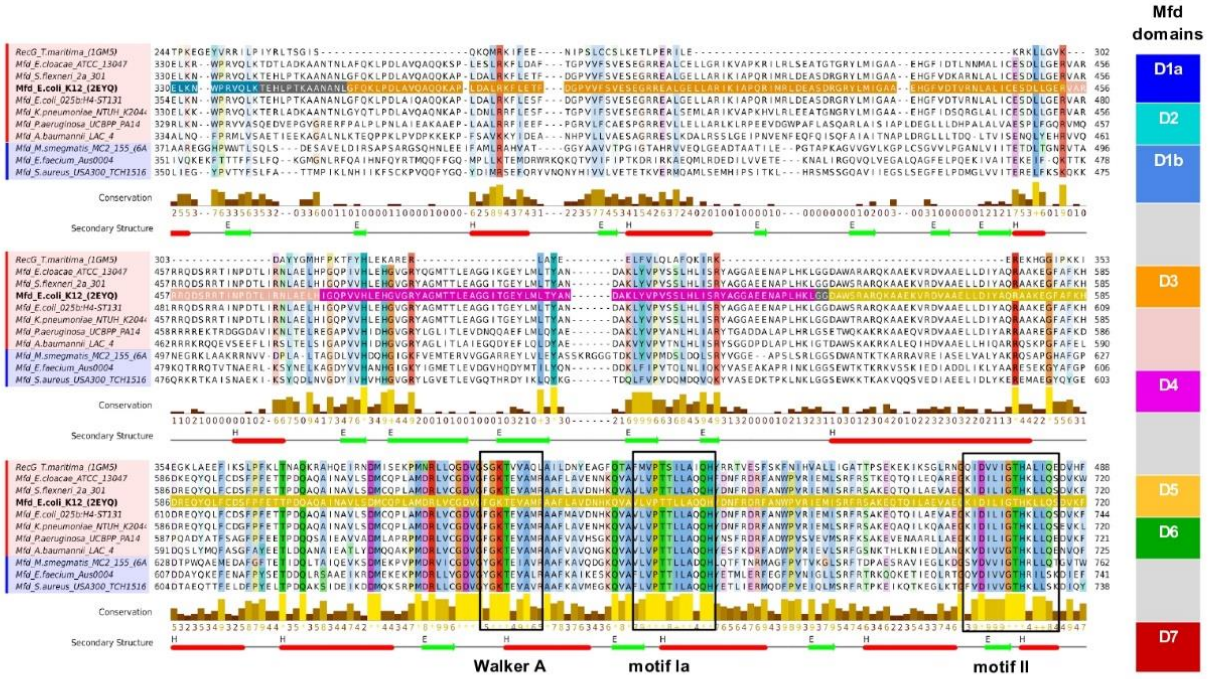

Supp Fig. 2

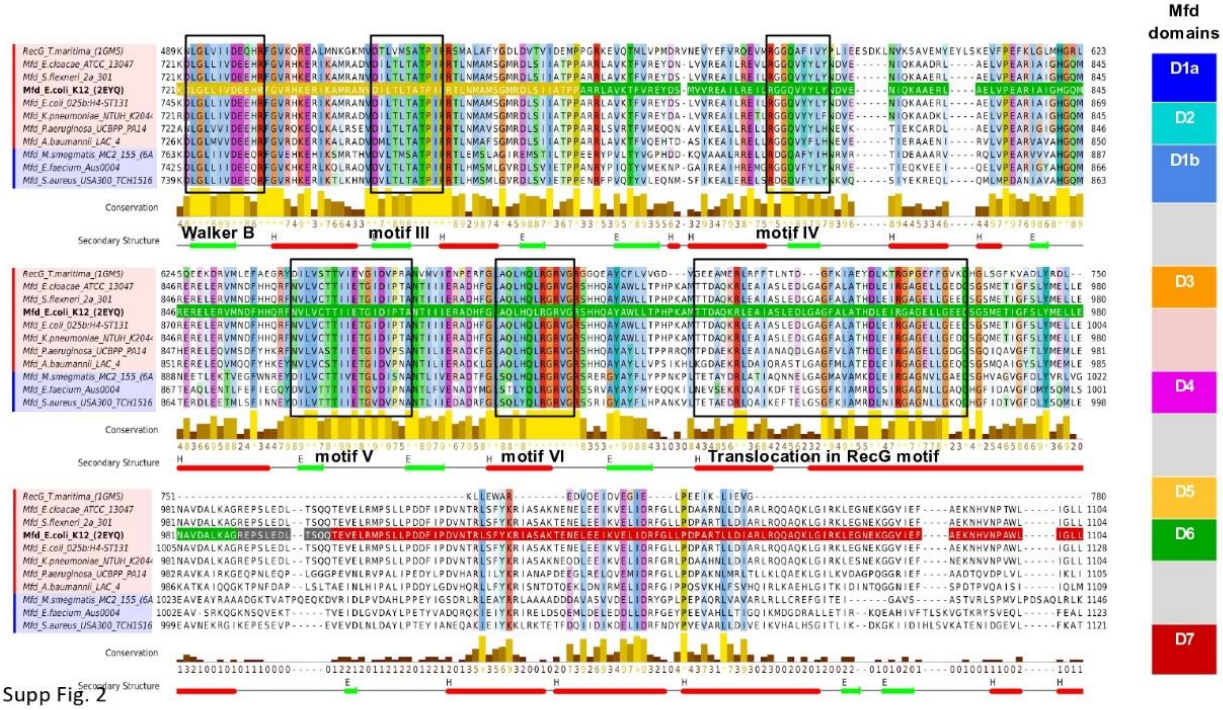

Supp Fig. 2

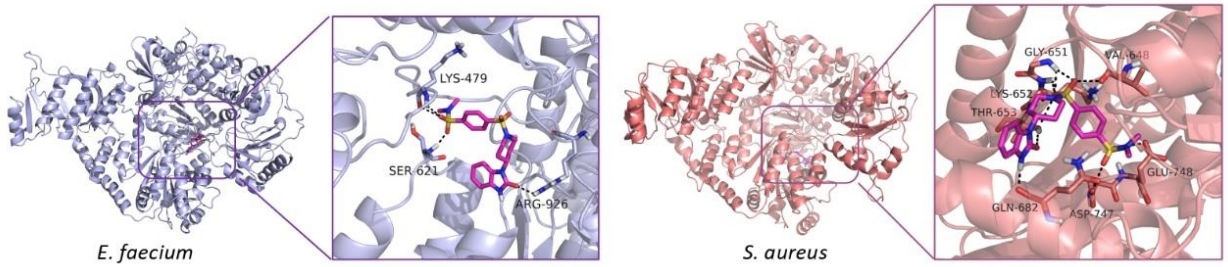

E. faecium *S. aureus*

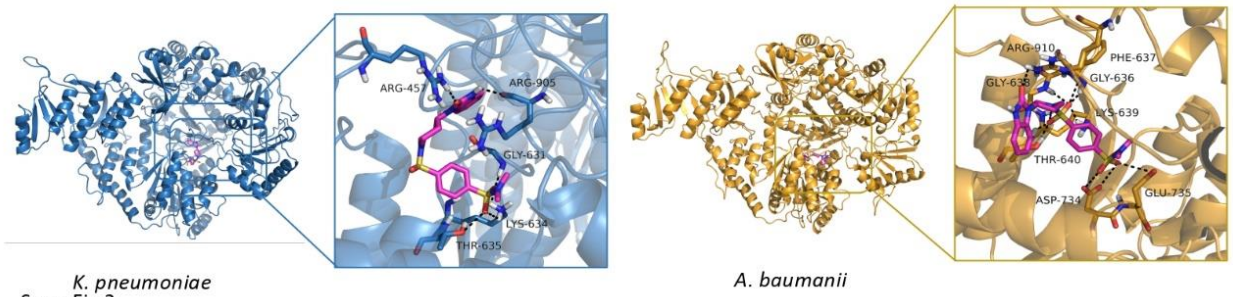

K. pneumoniae *A. baumanii*

Supp Fig 3

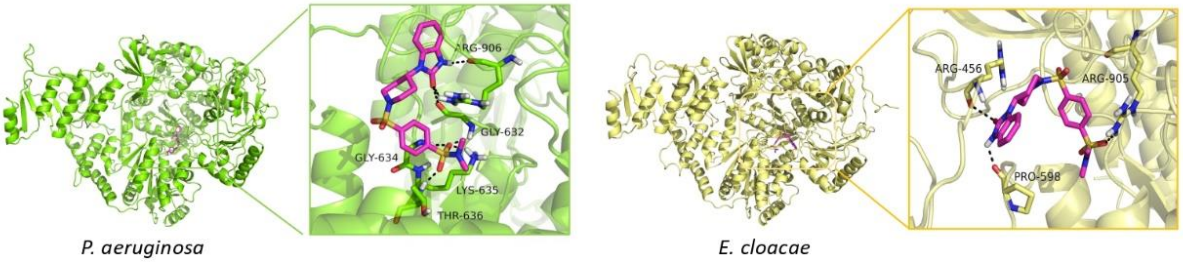

P. aeruginosa *E. cloacae*

Supp Fig 3

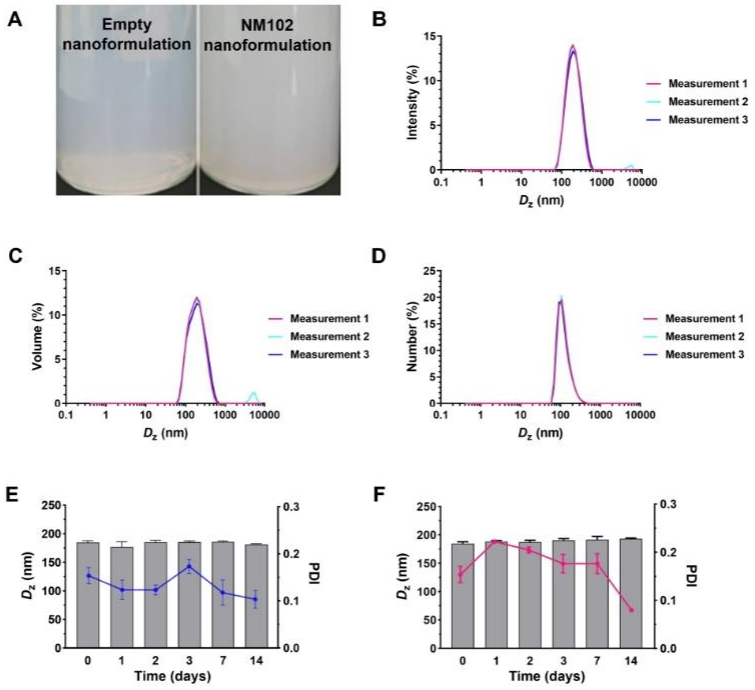

Supp Fig. 4

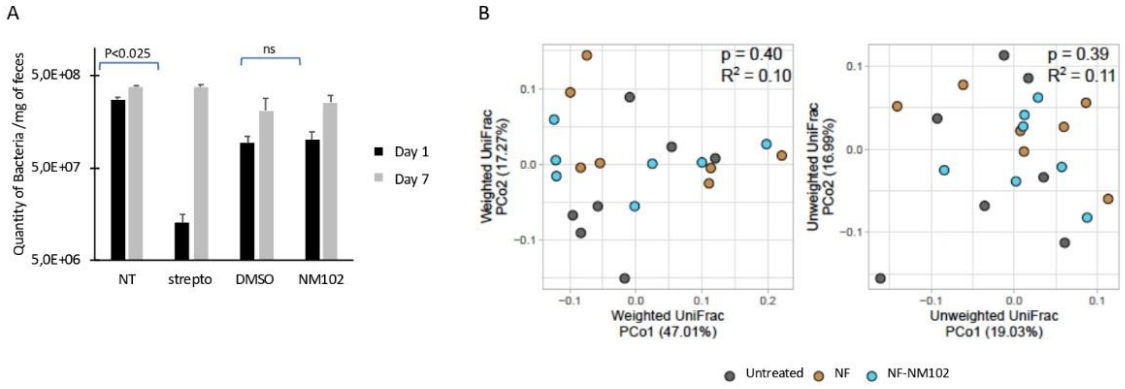

Supp Fig 5

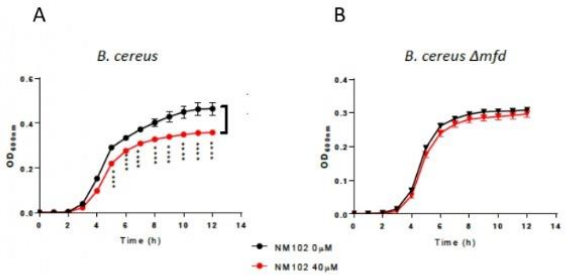

Supp Fig 6

Supp Fig. 1. Modelling of active Mfd of *E. coli* and high throughput screening of compounds library. Left: 3D model of active *E. coli* Mfd allows the docking of ADP and molecules. Right: Virtual screening workflow to select 95 commercially-available potential Mfd inhibitors.

Supp Fig 2. Mfd alignment. Multiple sequence alignment of Mfd from ESKAPE and RecG from *T. maritima* using MAFFT. The vertical stripe gives the color code of the multiple domains of Mfd. This color code is highlighted in the multiple alignment sequence along $Mfd_{E.\ coli}$ sequence. The typical functional motifs of an ATP-ase protein exclusively located in domains D5 and D6 are annotated and highlighted in black.

Supp Fig 3 Homology models of Mfd from ESKAPE bacteria and NM102 docking. Inserted are close-views of their respective active site with residues involved in the binding. The NM102 is shown as pink stick.

Supp Fig.4. NM102 nanoformulation. (A) Represenative images of empty and NM102 nanoformulations. Size distribution of NM102 nanoformulation by (B) intensity, (C) volume and (D) number. Evolution with time of intensity-averaged diameter of NM102 nanoformulation at (E) 4°C and (F) room temperature up to 14 days.

Supp Fig.5. NM102 does not impact the host microbiome. (A) The quantity of total bacteria present in the mice feces was quantified by qPCR at day 1 and day 7 post-administration of NM102. The graph shows the mean ± SD of two independent samples. (B) Mice were infected with *K. pneumoniae* and left untreated or treated with NM102 formulation (NF-NM102) or the empty formulation (NF) as control. After 24 h, the feces were collected and the diversity of the microbiome was analyzed by profiling the weighted and unweighted UniFrac distances. Each dot represents the value obtained for one mouse.

Supp Fig.6. NM102 decreases *B. cereus* survival in the context of NO-stress. *B. cereus* wt and Δ*mfd* strains were exposed to NM102 (40 µM) and NOC 5 and bacterial growth was followed by measuring the $OD_{600\ nm}$ for 12 h. The results reported are mean ± SD of three independent experiments each in triplicates, P values are calculated against the condition without NM102, using One Way ANOVA (**** P<0.0001).

Supp Table 1. ESKAPE strains used in this study and their resistance to antibiotics. The MIC for each antibiotic tested is in µg/mL.

	K. pneumoniae ATCC 700603	K. pneumoniae ALE CTXM-15+	K. pneumoniae DOU CTXM-15	P. aeruginosa CIP 27853	P. aeruginosa VED AmpC hyp	E. coli ATCC 25922	E. coli GUE ST131
Penicillin	16	>512	>512	32	16	1	>512
Ampicillin	8	4	>512	64	64	4	>512
Ceftriaxone	>512	>512	>512	>512	>512	16	>512
Meropenem	2	>512	>512	16	8	<0.5	128
Cefotaxin	<0.5	8	8	<0.5	<0.5	<0.5	4
Oxacillin	8	>512	>512	16	8	<0.5	512
Streptomycin	>512	>512	>512	>512	64	2	>512
Ciprofloxacin	>512	>512	>512	>512	128	4	>512

Supp Table 2. The solubility of NM102 in some common solvents

Excipient	Maximal solubility of NM102 after 24 h at 20°C, quantified by HPLC (mg/mL)
Water	≤ 0.001
Tween 80	0.09
Intralipid 20%	0.05
Soya oil	< 0.002
Corn oil	< 0.002
Capmul® MCM	0.01
Mygliol 912	0.002
NMP	≥ 10
DMSO	≈ 6.7

Supp Table 3. Commensal bacterial strains tested in this study

Lab code	Species	Strain name/source	Liquid medium
NT5038	*Streptococcus salivarius*	DSM 20560	BHI (Brain Heart infusion medium, Oxoid CM1135)
NT5072	*Streptococcus parasanguinis*	DSM 6778	BHI (Brain Heart infusion medium, Oxoid CM1135)
LM0306	*Haemophilus aegypticus*	DSM 21187	BHI++ (Brain Heart medium, Oxoid CM1135, 15 mg NAD and 15 mg hemine per L)
NT5018	*Haemophilus parainfluenzae*	DSM 8978	BHI++ (Brain Heart medium, Oxoid CM1135, 15 mg NAD and 15 mg hemine per L)
LM0305	*Veillonella atypica*	DSM 20739	BHI+Na-Lactate (Brain Heart medium, Oxoid CM1135, 1.25 % Sodium DL-Lactate , TCI Deutschland, S0928)
LM0308	*Porphyromonas asaccharolytica*	DSM-20707	LYBHI (Brain Heart medium, Oxoid CM1135, 0.5 % Yeast extract, 0.05% Cellobiose, 0.05% Maltose, 0.05% L-cysteine)
LM0310	*Rothia dentocariosa*	DSM 43762	LYBHI (Brain Heart medium, Oxoid CM1135, 0.5 % Yeast extract, 0.05% Cellobiose, 0.05% Maltose, 0.05% L-cysteine)
NT5054	*Bacteroides ovatus*	ATCC 8483	mGAM (Gifu Anaerobic Medium (GAM) Broth, Modified)
NT5020	*Prevotella melaninogenica*	DSM 7089	mGAM (Gifu Anaerobic Medium (GAM) Broth, Modified)
NT14114	*Shigella flexneri*	DSM 4782	mGAM (Gifu Anaerobic Medium (GAM) Broth, Modified)
NT5009	*Eubacterium rectale*	DSM 17629	mGAM (Gifu Anaerobic Medium (GAM) Broth, Modified)
LM0323	*Lactobacillus mucosae*	DSM 13345	MRS (Lactobacillus MRS broth, Neolab 69966-500G)
NT14072	*Lactobacillus salivarius*	DSM 20555	MRS (Lactobacillus MRS broth, Neolab 69966-500G)
NT14073	*Lactobacillus ruminis*	DSM 20403	MRS (Lactobacillus MRS broth, Neolab 69966-500G)
LM0321	*Fusobacterium mortiferum*	DSM 19809	PYG (modified Peptone Yeast Extract Glucose Broth, DSMZ media 104)
LM0325	*Anaerostipes caccae*	DSM 14662	PYG (modified Peptone Yeast Extract Glucose Broth, DSMZ media 104)
NT5011	*Roseburia intestinalis*	DSM 14610	PYG (modified Peptone Yeast Extract Glucose Broth, DSMZ media 104)
NT5048	*Coprococcus comes*	ATCC 27758	PYG (modified Peptone Yeast Extract Glucose Broth, DSMZ media 104)
NT24011	*Fusobacterium periodonticum*	HM-41 (BEI Resources) (HMP ID 0399)	PYG (modified Peptone Yeast Extract Glucose Broth, DSMZ media 104)
NT5067	*Eubacterium halii*	DSM 3353	PYG (modified Peptone Yeast Extract Glucose Broth, DSMZ media 104)

2.1. Résultats complémentaires

Depuis l'étude de la molécule NM102 en tant qu'inhibiteur, nous essayons d'optimiser celle-ci chimiquement afin d'en augmenter l'efficacité, la solubilité ou améliorer le rendement d'encapsulation dans les nanoformulations.

Pour cela, une librairie de 80 analogues présentant des similarités structurales avec le NM102 nous a été fournie par nos collaborateurs chimistes du CEA. J'ai réalisé des tests ATPase préliminaires pour chacun de ces composés afin de mesurer leur impact sur l'activité ATPase de Mfd de *E. coli* (Figure 22). Les tests ont été effectués avec différentes doses d'ATP afin d'observer si l'inhibition des analogues est compétitive, c'est-à-dire si l'augmentation de la concentration d'ATP provoque une diminution du taux d'inhibition. Nous avons pu identifier des molécules présentant un fort potentiel dans l'inhibition de l'activité de Mfd. Une trentaine de composés induisent une inhibition meilleure ou similaire au NM102 en compétition avec 0,035 mM d'ATP. En augmentant la dose d'ATP à 0,07 mM, ce nombre passe à 19. Sur les analogues les plus prometteurs, nos collaborateurs ont pu nous en re-synthétiser huit : A2, A3, A11, A15, A25, A45, A66 et A71. Avec ces molécules, j'ai continué les tests ATPases afin de valider la valeur d'inhibition obtenue lors du test préliminaire (Figure 23). À l'exception de A2, j'ai confirmé que ces analogues sont capables d'inhiber l'activité ATPase de Mfd. A3 et A45 sont les plus prometteurs.

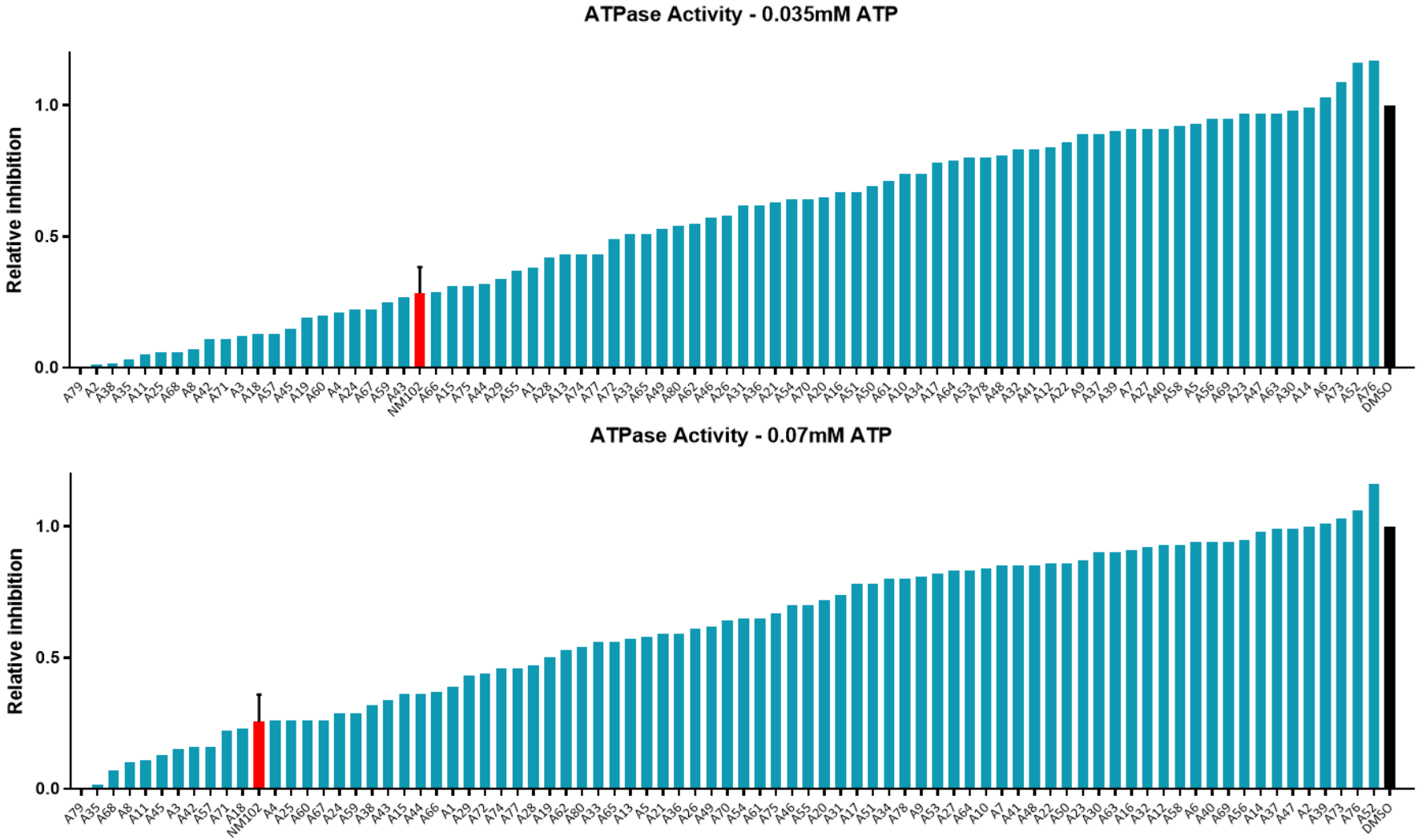

Figure 22 : Classement des analogues en fonction de leur taux d'inhibition de l'activité ATPase de Mfd de E. coli en présence de 0,035 mM d'ATP ou 0,07 mM d'ATP
Les composés ont été testés à une concentration de 100 µM. Les données sont normalisées par rapport au contrôle DMSO.

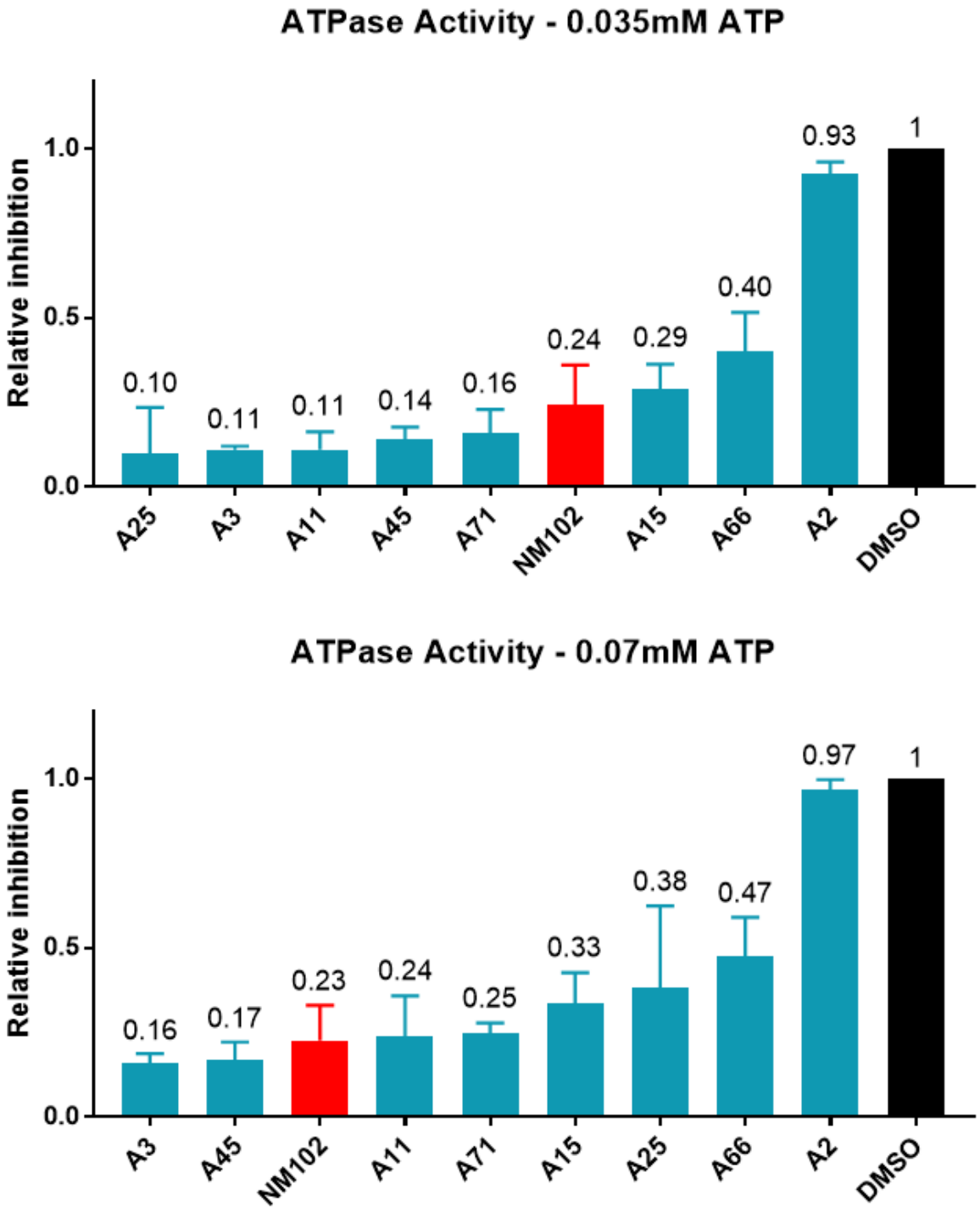

Figure 23 : Classement des huit analogues sélectionnés en fonction de leur taux d'inhibition de l'activité ATPase de Mfd de E. coli en présence de 0,035 mM d'ATP ou 0,07 mM d'ATP

Les composés ont été testés à une concentration de 100 µM. Les données sont normalisées par rapport au contrôle DMSO.

Pour déterminer si l'inhibition est compétitive, j'ai réalisé des doses réponses sur le NM012, A3 et A45 (Figure 24). Pour le NM102, j'ai obtenu une concentration inhibitrice de 50 % de l'activité de Mfd (IC_{50}) de 35,71 µM à 0,07 mM d'ATP et une constance d'inhibition (K_i) de 16,31. Pour A3 et A45, j'ai pu calculer respectivement une IC_{50} de 43,76 µM et 91,99 µM et un K_i de 39,6 et 58,67. Pour les deux

molécules, leur IC_{50} et leur K_i est plus haut que pour le NM102. Cela veut dire qu'elles sont moins efficaces que le NM102 même si A3 en est proche et que leur compétitivité avec l'ATP est plus faible. En effet, plus un K_i est bas, plus la molécule est compétitive avec l'ATP. À l'issue de ces tests, A3 est ressortie comme une molécule proche du NM102 en terme d'efficacité mais moins compétitive. Pour A45, même si elle présente une activité prometteuse, celle-ci est inférieure au NM102.

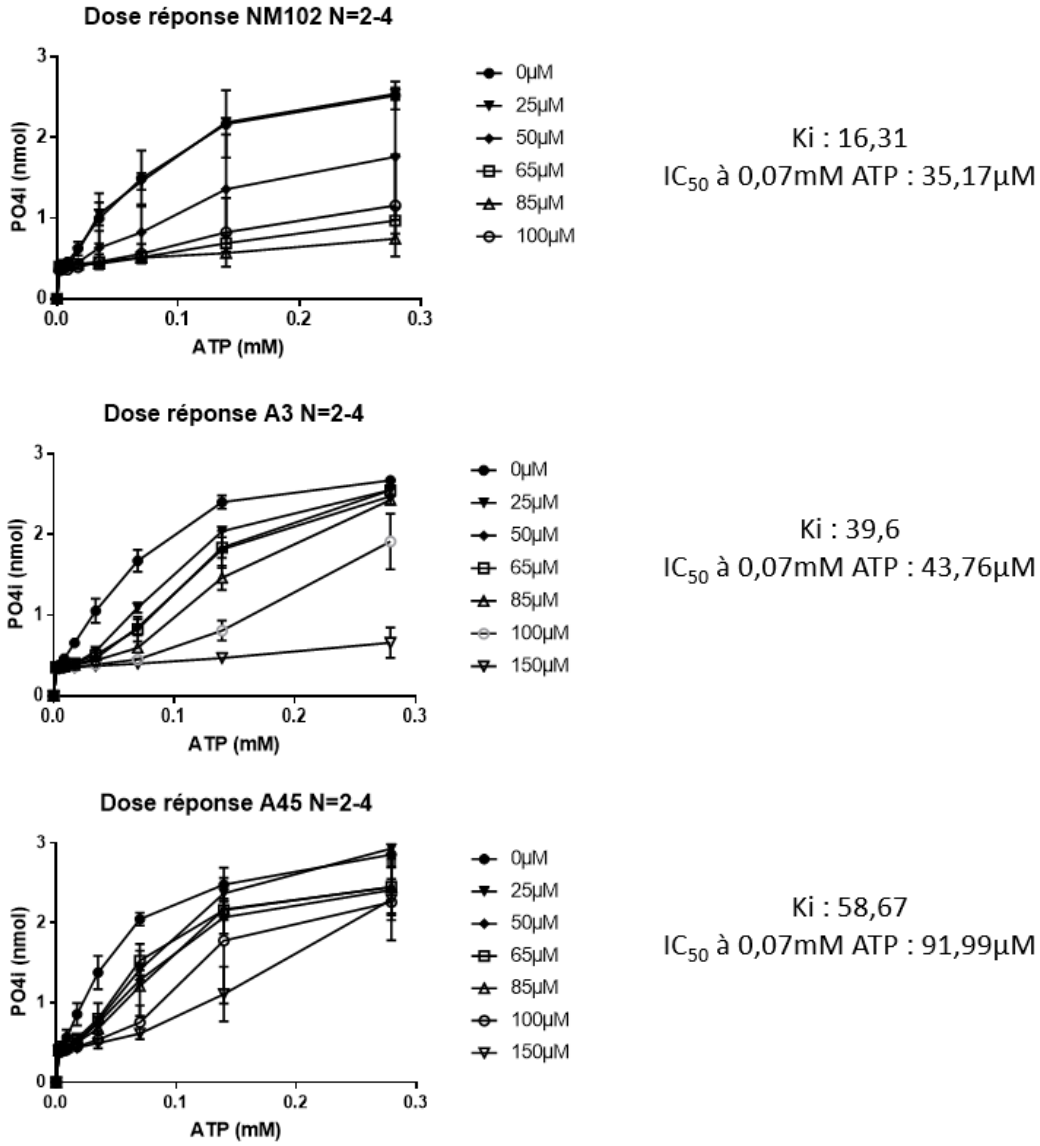

Figure 24 : Dose-réponses ATPase du NM102, A3 et A45 avec la valeur de leur constante d'inhibition (Ki) et leur concentration inhibant 50 % de l'activité de Mfd (IC_{50}).

Bien que A3 et A45 soient un peu moins efficaces que le NM102, elles présentent en contrepartie l'avantage d'être plus solubles. Nous avons donc voulu tester l'efficacité de ces molécules en condition de stress nitrique *in vitro*. Or, pour *K. pneumoniae*, dès 2 µM de molécule nous observons un effet bactéricide sur les bactéries pour A3 et A45 en absence de stress (Figure 25A et B). Par contre, nous observons tout de même une efficacité de A3 à 1 µM en condition de stress tandis que A45 n'induit

pas de mortalité bactérienne spécifique à la présence de stress (Figure 25C et D). Alors que ces composés sont bactéricides pour *K. pneumoniae*, cela n'est pas le cas pour *P. aeruginosa* où même 200 µM de composé n'induit pas de mortalité (Figure 26A et B). Néanmoins, bien que non toxiques, elles ne sont pas efficaces en condition de stress (Figure 26C et D).

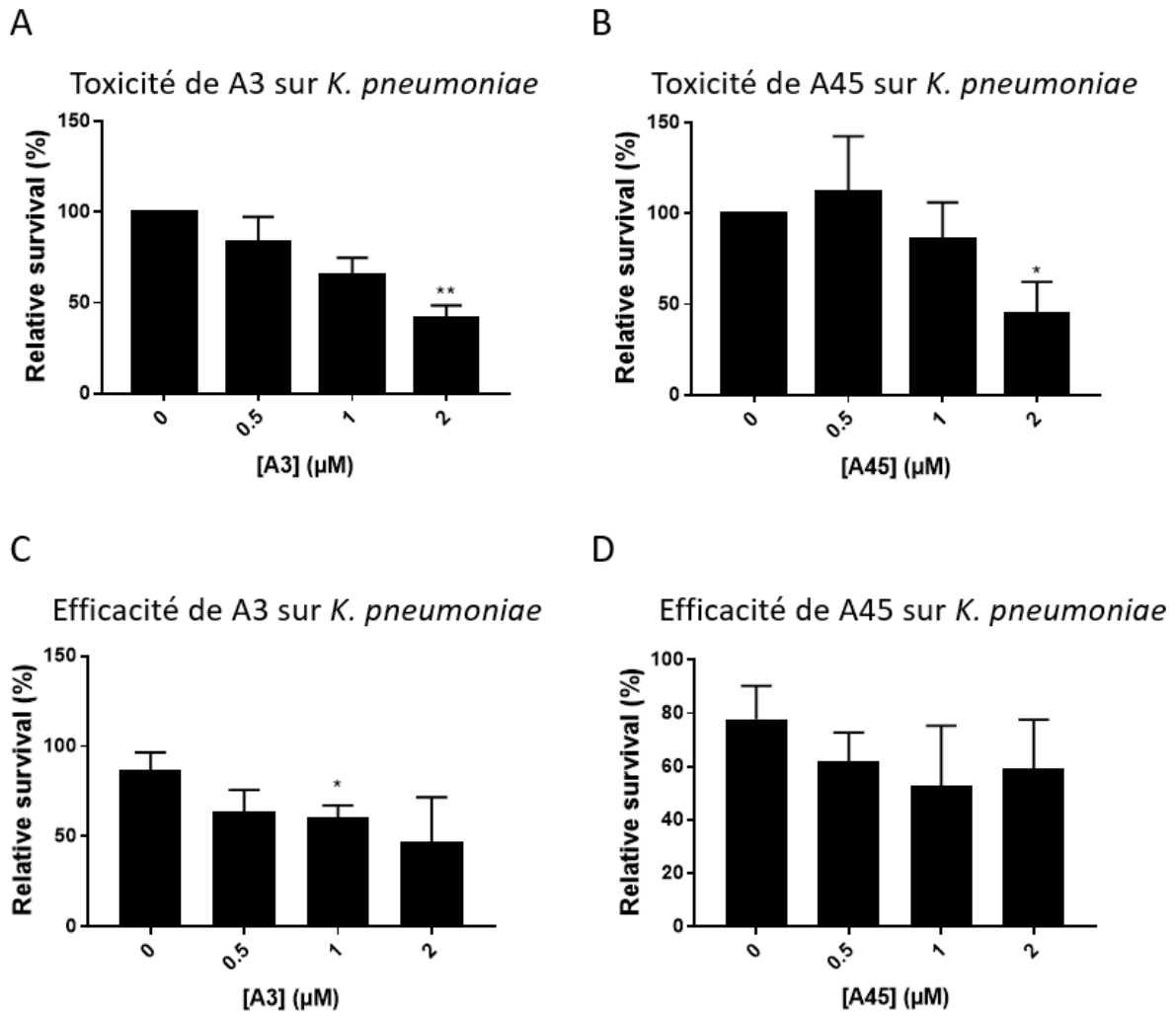

Figure 25 : Toxicité in vitro de A3 (A) et A45 (B) et efficacité en condition de stress nitrique de A3 (C) et A45 (D) sur K. pneumoniae

*Les bactéries ont été prises en phase exponentielle de croissance et ont été incubées pendant 4 h à 37 °C dans du RPMI en présence de NOC-5, un donneur de NO. La survie des bactéries a été calculée en normalisant par rapport au contrôle sans analogue. Les P-values ont été calculées par ANOVA (** p<0,01 ; * p<0,05)*

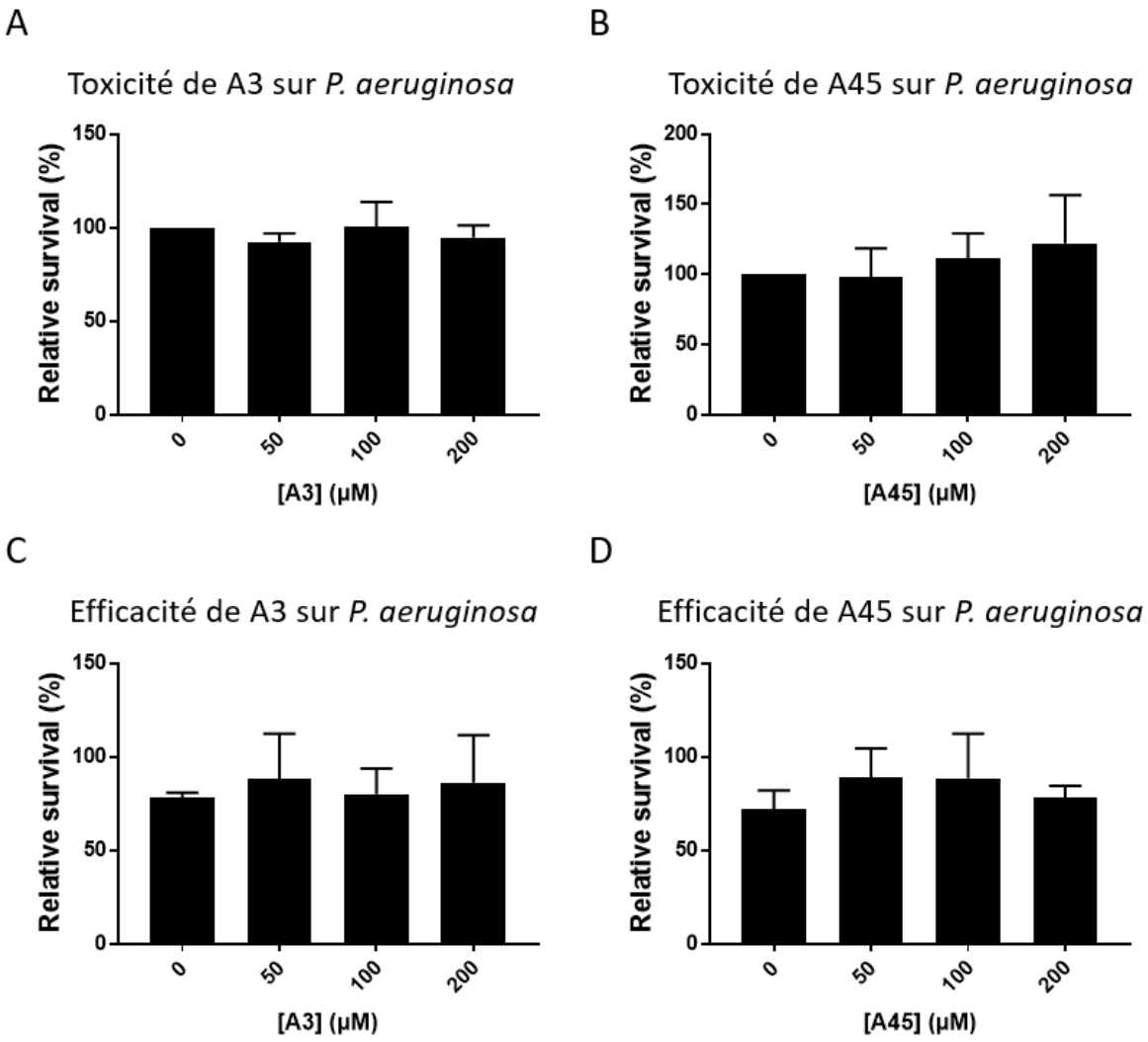

Figure 26 : Toxicité in vitro de A3 (A) et A45 (B) et efficacité en condition de stress nitrique de A3 (C) et A45 (D) sur P. aeruginosa

Les bactéries ont été prises en phase exponentielle de croissance et ont été incubées pendant 4h à 37°C dans du RPMI en présence de NOC-5, un donneur de NO. La survie des bactéries a été calculée en normalisant par rapport au contrôle sans analogue

En parallèle des stress nitriques, j'ai réalisé des premiers tests d'efficacité *in vivo* contre *P. aeruginosa* chez l'insecte (*B. eri*). Avec un traitement en une injection, je n'ai pas observé d'effet ni sur la quantité de bactéries présentes dans l'insecte, qui varie énormément d'un individu à l'autre (Figure 27A), ni sur la survie des insectes (Figure 27B).

Avec un traitement en trois injections successives, il n'y a pas d'effet significatif sur le nombre de bactéries (Figure 27C), mais le traitement avec A3 permet de remonter la survie des insectes de 67 % à 87 % (Figure 27D).

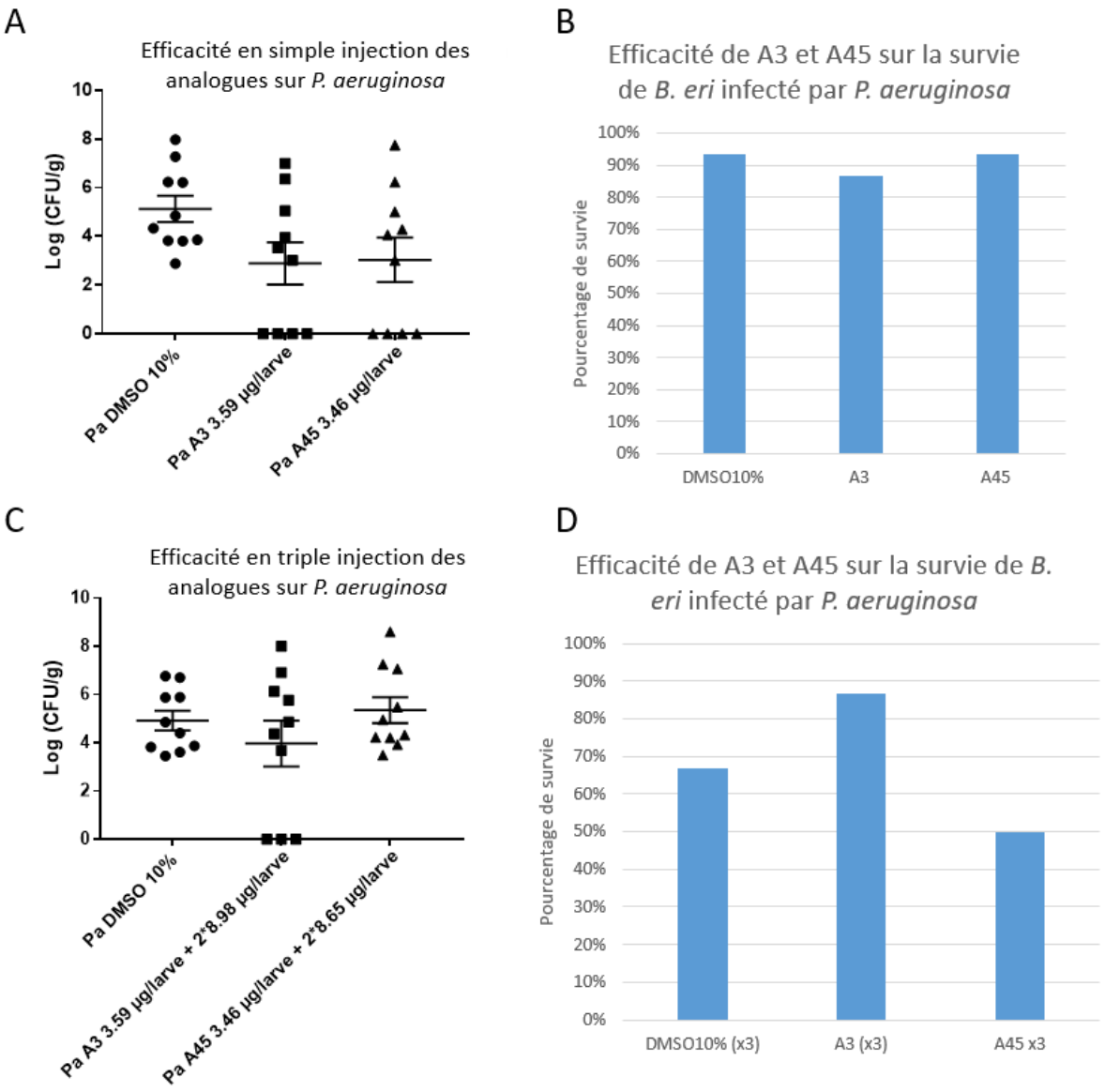

Figure 27 : Efficacité in vivo chez B. eri de A3 et A45 en simple injection sur la charge bactérienne (A) et la survie des insectes (B) ou en injection multiple sur la charge bactérienne (C) et la survie des insectes (D) lors d'une infection par P. aeruginosa
Des larves de B. eri ont été infectées par P. aeruginosa en milieu de phase exponentielle. La survie et les bactéries ont été récupérées 24h après l'infection. Les barres d'erreurs sont des SEM.

En prenant en compte tous ces résultats, nous voyons que ces deux analogues ne montrent pas un potentiel thérapeutique plus important que le NM102. Bien que capable d'inhiber l'activité ATPase de Mfd et leur solubilité supérieure au NM102, leur toxicité *in vitro* sur *K. pneumoniae* et leur faible efficacité *in vitro* et *in vivo* nous montrent que A3 et A45 ne sont pas les meilleurs candidats pour améliorer notre stratégie thérapeutique.

À l'issue de ces tests, nous avons décidé de poursuivre l'amélioration de la molécule NM102 avec d'autres analogues plus ciblés afin de déterminer quel est le noyau structural primordial pour l'activité inhibitrice de Mfd. Nous sommes actuellement en train de tester de nouveaux analogues pour trouver

une molécule présentant une efficacité similaire ou meilleure au NM102 couplée à une meilleure solubilité.

3. Résumé article 3

Dans le but de lutter contre l'antibiorésistance, de nouvelles stratégies thérapeutiques sont en développement, l'une d'entre elle est l'antivirulence qui vise à diminuer la virulence des bactéries plutôt que les voies essentielles à leur survie. De ce fait, il est impossible d'effectuer des MICs standards sur des composés non bactéricides. Pour tester l'efficacité de ces composés, il est primordial de développer de nouveaux outils *in vitro* et *in vivo* pour mimer une infection.

L'utilisation d'insectes pour effectuer des tests d'efficacité *in vivo* est une alternative très intéressante par rapport à la souris. Les insectes possèdent une réponse immunitaire innée similaire aux mammifères. Leur utilisation n'entraine pas de contrainte éthique et leur prix est plus faible que la souris. J'ai donc testé dans deux modèles insectes, la larve du ver à soie *Bombyx mori* et la larve de la fausse teigne de la cire *Galleria mellonella*, cinq souches du groupe ESKAPE et *B. cereus* en tant que contrôle car cette bactérie infecte naturellement des insectes. Pour chaque bactérie et chaque modèle, la LD_{50} (dose létale pour 50 % de mortalité) et la LD_{90} (dose létale pour 90 % de mortalité) ont été calculées. Pour *B. mori*, la survie des insectes a été observée 24 h à 28 °C après l'infection. Sur ce modèle, il y a une grande variabilité dans la virulence entre les différentes souches testées. *K. pneumoniae, A. baumannii* et *E. coli* ne sont pas virulents même à fortes doses. Par contre, *S. aureus* et *P. aeruginosa* sont tous deux capables d'infecter la larve. À l'intérieur du groupe ESKAPE, *P. aeruginosa* est la bactérie montrant la plus haute virulence. *B. cereus* est quant à lui la bactérie la plus virulente comme attendu. Avec *G. mellonella*, la survie a aussi été observée après 24 h d'infection mais ce modèle permet d'incuber les larves à 37 °C. Les cinq souches du groupe ESKAPE sont capables d'infecter ces larves. Les moins virulentes sont *K. pneumoniae* et *A. baumannii* et les plus virulents sont *E. coli* et *P. aeruginosa*. Ces derniers surpassent même la virulence de *B. cereus*. *G. mellonella* et *B. mori* sont donc tous les deux des modèles pouvant être utilisés pour tester l'efficacité de composés contre des bactéries du groupe ESKAPE.

Afin de vérifier le modèle dans un contexte de traitement thérapeutique, j'ai infecté *Bombyx* avec *P. aeruginosa* et j'ai effectué un traitement avec soit du méropénème, soit le composé que nous développons au laboratoire, le NM102. J'ai pu montrer qu'un traitement avec l'un ou l'autre permettait de diminuer la charge bactérienne dans les insectes après 24 h d'infection. Ces données nous permettent de dire que le modèle insecte peut être utilisé pour déterminer l'efficacité d'un composé antimicrobien.

Nous avons aussi mis en place un test *in vitro* permettant de mimer la réponse immunitaire et plus particulièrement la production de NO. Le NO est capable d'endommager des protéines, des lipides mais aussi l'ADN. Dans notre test, nous utilisons le NOC-5, un donneur de NO qui dépend de la dose

de NOC-5 et du temps pendant lequel il le relâche. Plus on augmente la concentration de NOC-5 plus nous relâchons du NO et si nous laissons trop longtemps le NOC-5 dans son milieu, la quantité de NO relargué va diminuer. Pour nos tests, nous utilisons une concentration maximale de 1000 µM de NOC-5 avec un temps expérimental de 4 h pendant lequel le relargage est stable. Grâce à ce donneur, nous sommes capables de mimer l'induction d'un stress nitrique présent dans la réponse immunitaire.

Nous avons effectué des doses réponses pour chacune des cinq bactéries du groupe ESKAPE testées précédemment. Pour toutes les bactéries, l'augmentation de la quantité de NOC-5 entraine une diminution de leur survie. Néanmoins, leur sensibilité est différente. Pour *S. aureus* et *A. baumannii*, une faible concentration entraine une augmentation de la survie ce qui n'est pas le cas pour *K. pneumoniae, E. coli* et *P. aeruginosa*. Les IC_{10} (concentration inhibitrice pour 10 % de mortalité) et IC_{50} (concentration inhibitrice pour 50 % de mortalité) ont été calculées pour chaque bactérie. *A. baumannii* et *P. aeruginosa* sont les plus sensibles tandis que *E. coli* est la plus résistante du groupe.

Nous avons testé l'utilisation de ce modèle pour déterminer l'efficacité du composé antimicrobien, NM102. Nous avons validé la capacité du NM102 à diminuer la survie bactérienne en condition de stress immunitaire. Ce modèle nous permet donc de pouvoir tester l'efficacité de composés antivirulents ciblant les voies résistantes au système immunitaire.

Dans l'antivirulence, le système immunitaire peut jouer un rôle crucial dans l'efficacité d'un médicament antivirulent. L'un des acteurs de cette réponse est l'oxyde nitrique. Nous avons établi un test *in vitro* facile à réaliser malgré le faible temps de vie de l'oxyde nitrique. Notre format, l'utilisation des plaques 96 puits, permet de réaliser un criblage haut débit de potentiels composés antimicrobiens. Le NO relâché dans notre test est stable sur plusieurs heures et sa concentration peut être ajustée en fonction des bactéries utilisées.

4. Article 3: Comparative analysis of different infection models to characterize new anti-virulence drugs

Soumission prochaine à Pathogens

Comparative analysis of different infection models to characterize new anti-virulence drugs

Delphine Cormontagne[a+], Lucie Lebreuilly[a+], Constance Porrini[a+], Fairouz Gzara[a], Nalini Ramarao[a*] and Seav-Ly Tran[a*]

[a]Université Paris-Saclay, INRAE, AgroParisTech, Micalis Institute, 78350, Jouy-en-Josas, France.
+These authors contributed equally to the work
*correspondings authors

Abstract

Bacterial infections by human pathogens are a considerable and still to-date health issue. In addition, bacterial resistance to antimicrobials is becoming alarming, and the WHO has classified bacteria according to the risk that their resistance capacities represent for human health. In particular, the so called ESKAPE pathogens are classified as high-risk bacteria. Anti-virulence therapeutics are alternative approaches to antibiotics that aim to attenuate virulence rather than targeting bacterial essential functions. To assess the efficacy of such anti-virulence drugs, it is essential to develop appropriate physiological model. In particular, the development of models reflecting the complex host/pathogen interactions is a challenging issue. In this work, we developed complementary *in vitro* and *in vivo* models to better understand the infectious process of relevant pathogenic bacteria and design appropriate model to test anti-virulence drugs. We developed an *in vitro* assay that assesses bacterial resistance to an essential anti-infective component of the host immune response, the nitric oxide. The microplate and easy to perform assay could be further used for high-throughput screening of antimicrobials. We showed that bacteria present different sensitivity to nitric oxide. We then tested the virulence of the strains in two insect models. We demonstrated that correlation between *in vivo* pathogenicity and resistance to the host immune response is strain dependant. Our data provide complementary *in vitro* and invertebrate models that can be used to decipher the bacterial mechanism of pathogenicity and fight antibioresistance of clinically relevant pathogens such as the ESKAPE bacteria, for a better health care.

Keywords

Anti-virulence drugs, Infection model, ESKAPE, Insect model, Mice model, Nitric oxide, Host-pathogen interaction, Alternative models

Introduction

Pathogenic organisms have always had tremendous impacts on civilization. Even nowadays, we are still facing old diseases such as tuberculosis and have to deal with the emergence of new virulent pathogens such as SARS-CoV-2. Human infectious and parasitic diseases are estimated to have caused over 5 million deaths in 2019 and the death toll will likely continue to increase in the following years ("Projections of mortality and causes of death, 2016 to 2060," n.d.). While numerous infectious diseases can now be controlled through appropriate therapeutic treatment, other global health threats are rising such as antibiotics resistance. Antimicrobial resistance (AMR) increases the global incidence of infectious disease and has a devastating clinical and economical cost. AMR kills 700 000 people each year (Ferri et al., 2017; Zhen et al., 2019). In 2017, the World Health Organization (WHO) published its first ever list of antibiotic-resistant "priority pathogens", a catalogue of twelve families of bacteria that pose the greatest threat to human health (Tacconelli, 2017; Tacconelli et al., 2018). A group of them was highlighted as being the leading cause of healthcare-acquired infections as well as associated with high level of multidrug resistance. This group includes *Enterococcus faecium*, *Staphylococcus aureus*, *Klebsiella pneumoniae*, *Acinetobacter baumannii*, *Pseudomonas aeruginosa* and Enterobacter spp., and are acronymically termed the "ESKAPE" pathogens (da Rosa et al., 2020; Santajit and Indrawattana, 2016). Carbapenem resistant *A. baumannii* and *P. aeruginosa* along with extended spectrum β-lactamase (ESBL) or carbapenem resistant *K. pneumoniae* and Enterobacter spp. are listed in the critical priority list of pathogens. Vancomycin resistant *E. faecium* and methicillin/vancomycin resistant *S. aureus* are in the list of high priority category.

Recent efforts have begun to reactivate antibiotics research, and compounds are explored either through drug repositioning or through molecular mechanisms that are usually redundant with those of traditional antibiotics thus keeping the issue that bacteria already have or will likely develop broad resistance to these antibiotics.

Recent drug research and development have increasingly turned to alternative therapeutic strategies, which target bacterial pathogens through mechanisms distinct from existing antibiotics. Anti-virulence therapeutics are alternative approaches to antibiotics that aim to attenuate virulence rather than targeting bacterial essential functions, while minimizing microbiota perturbation and the risk of AMR development. This constitutes a promising alternative to the classical antibiotic approach as it neither leads to bacterial growth inhibition nor to bacterial death. Instead, an anti-virulence therapy blocks the bacterial pathogenicity by counteracting the ability of pathogens to induce virulence and/or to resist to the host immune system. As a consequence, such compounds are expected to reduce resistance pressure and consequently decrease the rate of resistance development.

Increasing number of publications are relating innovative bacterial targets as new anti-virulence strategies. For instance, *P. aeruginosa* pathogenesis is due to an arsenal of cell-associated and secreted

virulence factors and disarming *P. aeruginosa* by reducing its virulence *in v*ivo is a logical and promising therapeutic strategy that is gaining momentum (Chadha et al., 2023; Wood et al., 2023). Similarly, the development of anti-virulence drug therapy against *A. baumannii* infections as an alternative to traditional antibacterial therapy is studied and it has been shown that inhibition of a transcriptional regulator that plays a pivotal role in the pathogenesis of diverse *A. baumannii* clinical strains in multiple murine and *G. mellonella* invertebrate infection models will facilitate future drug discovery programs (Trebosc et al., 2022).

We have recently identified the non-essential protein Mfd (Mutation Frequency Decline) as a new bacterial target and identified a small inhibitory molecule, NM102, as an innovative anti-virulence drug, which is efficient against bacteria of the ESKAPE group (Tran et al., n.d.). NM102 inhibits the activity of Mfd protein by competing with ATP binding to its active site. Inhibition of Mfd by NM102 sensitizes pathogenic bacteria to the host immune response and blocks infections due to clinically-relevant *K. pneumoniae* and *P. aeruginosa*, without inducing host toxicity (Tran et al., n.d.).

Anti-virulence therapeutics to date largely focus on the inhibition of well-studied virulence factors associated with toxins, secretion systems and quorum sensing (Chadha et al., 2023). While there are a handful of new anti-virulence therapies being developed, there is a need to increase the repertoire of possible drug targets and drug candidates. The expansion of genomics data has enabled the development of genomics-based and metagenomics-based virulence factor predictors (Lau et al., 2023). However, these powerful tools alone are not sufficient to characterize virulence factors. Experimental validation is required to determine whether the candidates have a role in virulence and how to inhibit their function. Moreover, as classical antibiotics target essential bacterial pathways, their identification require to assess bacterial survival during standardized MIC (Minimum Inhibitory Concentration) assays, by contrast to anti-virulence drugs for which virulence tests are to be used, and/or specific activity tests need to be developed, if the bacterial target is known.

Deciphering the mechanisms by which bacterial pathogens penetrate and proliferate in a specific host, resist to the host's immune system and induce pathogenicity while also resisting antimicrobial compounds is crucial for the prevention and treatment of infectious diseases. But, advances in research on infectious diseases and anti-virulence strategies depend largely on the availability of physiological relevant models. Host-pathogen interaction is very complex and even for a given pathogen, the ideal model may vary. Models can be diverse and can be used to mimic immunological responses *in vitro*, *ex-vivo* or at the level of an entire living organism.

Thus, the development of *in vitro* and *in vivo* infection models is necessary to characterize potential virulence functions and whether these factors can serve as targets for subsequent anti-virulence drug development.

Animal models have been extremely useful in advancing our understanding of bacterial pathogenesis and for the development and the therapeutic assessment of new antibiotics or novel biologicals to control the pathogens. But these models pose ethical and cost issues. In order to minimize them, alternative models can be used that could mimic the conditions encountered *in vivo*. In particular, the innate immune system possesses powerful cellular (e.g., neutrophils and macrophages) components that destroy pathogens via many mechanisms such as phagocytosis, bursts of reactive oxygen and nitrogen species (ROS and RNS).

The aim of this study was to establish multiple models that could be jointly used to study clinically relevant pathogenic bacteria and test classical antibiotics as well as new anti-virulence drugs. We particularly focused on five bacteria that belong to the ESKAPE group: *S. aureus*, *K. pneumonia*, *A. baumanii*, *P. aeruginosa* and *E. coli*. We established an easy to perform, new and innovative *in vitro* model to study bacterial resistance to the host's immune response, and demonstrate that pathogens have different sensitivity towards NO. This model can also be used to assess new compounds efficacy in an *in vitro* model mimicking the host NO-response. We also describe *in vivo* insect models of infection for each bacterial strain. While a perfect model system may not always be available, we developed three complementary models, which can be used to decipher the bacterial mechanisms of pathogenicity and test new anti-virulence drugs for which a classical test of minimum inhibitory concentration is not possible. These models may help in the search and development of new and innovative therapeutic options to fight the current alarming and worldwide AMR issue.

Materials and Methods

Bacterial strains

Gram-negative *Klebsiella pneumoniae* (ATCC700603), *Pseudomonas aeruginosa* (CIP27853 and PaVED), pathogenic *Escherichia coli* (ATCC25922), *Acinetobacter baumannii* (CIP7034) strains and the Gram-positive *Staphylococcus aureus* (CIP658) strain were kindly provided by Dr. Thierry Naas (CHU de Bicêtre, Le Kremlin-Bicêtre, France). The Gram-positive *Bacillus cereus* 407 Cry- (Bc 407) was also used in this study. This strain, cured of its plasmid, is acrystalliferous and shows high phylogenic similarity with the *B. cereus* reference strain ATCC 14579 (Lapidus et al., 2008). Strains were stored at −80 °C as 20% (v/v) glycerol cultures.

Medium and reagents

The Roswell Park Memorial Institute (RPMI) 1640 GlutaMAX™ medium was purchased from Gibco, Thermo Fisher Scientific, Waltham, MA, USA. The Nitric Oxide (NO) donor, 3-[2-hydroxy-1-(1-methylethyl)-2-nitrosohydrazino]-1-propanamine NOC-5 was purchased from Calbiochem, Sigma-Aldrich, Saint-Louis, MO, USA. NOC-5 was dissolved in NaOH 0.01 M (Chem-Lab, Zedelgem, Belgium)

at a final concentration of 200 mM. NOC-5 has a half-life time of NO release of 25 min at 37 °C (Cruz-Ramos et al., 2002). Under these conditions, a stable NO-amine complex can spontaneously release two equivalents of NO (Poole, 2011). The NM102 molecule was purchased from Enamine. Meropenem (MPN) was purchased from Sigma-Aldrich

Determination of nitric oxide (NO) concentration

NO concentrations were evaluated using 2', 7'-dichlorodihydrofluorescein diacetate (DCF-DA) (Sigma-Aldrich, Saint-Louis, MO, USA) and the Griess Reagent System (Promega, Madison, WI). DCF-DA was dissolved in DMSO to generate a stock solution at 20 mM.

DCF-DA is a peroxinitrite indicator capable of detecting both nitric oxide (NO) and hydrogen peroxide present inside and outside cells (Possel et al., 1997). DCF-DA is first hydrolysed into the non-fluorescent 2,7-dihydrodichlorofluorescein (DCF-H) in alkaline condition. Then, NO converts DCF-H into the highly fluorescent product dichlorofluorescein (DCF) through oxidation. Solutions of NOC-5 at final concentrations from 0 µM to 1000 µM were prepared in RPMI and 50 µL of each concentration were dispatched into 96-well plate in triplicate. DCF-DA was added to the NOC-5 solutions at a final concentration of 50 µM and the plate was incubated for 4 h at 37 °C. Fluorescence emission at 523 nm was measured every hour using an infinite M200 fluorescent reader (TECAN, Germany) with an excitation at 503 nm. Relative fluorescence was calculated by normalizing fluorescence in NOC-5 samples against control samples (0 µM of NOC-5).

In addition, NO released by NOC-5 was estimated using the Griess method according to manufacturer's instructions. The Griess Reagent System measures nitrite (NO2–), a stable and non-volatile breakdown product of NO. The nitrite concentration was calculated by comparison with standard solutions of sodium nitrite $NaNO_2$ prepared in RPMI.

Absorbance was measured at 540 nm using a microplate reader (TECAN, Germany).

NO cell free assay

Bacteria were grown in LB medium at 37 °C under agitation at 200 rpm until late exponential phase. Bacterial solutions were prepared in RPMI medium at concentrations between 5 x 10^4 and 1 x 10^5 CFU/mL and 150 µL were dispatched into 96-well plate. Bacteria were exposed to NO through the addition of 50 µL of NOC-5 at final concentrations from 0 µM to 1000 µM. Bacterial survival rate was quantified by plating on LB agar after 4 h at 37 °C and by normalizing bacterial load in NOC-5-treated samples against control samples (0 µM of NOC5). NOC-5 concentrations were transformed into Log10 and a non-linear fit with a variable Hill slope was made using GraphPad Prism 7 (GraphPad Software, San Diego, CA) to obtain NO dose-response curves. NOC-5 concentrations required to induce 10 and

50% of mortality of each strain (IC10 and IC50, respectively) were calculated using R and the drc package (Christian Ritz and Jens C. Strebig).

For efficacy assays, bacterial solutions were prepared as described above. Bacteria were exposed to 50 µL of NOC5 at a concentration inducing a survival of around 80 - 90 % compared to the untreated condition (*K. pneumoniae*: 9 µM, *P. aeruginosa* 5 µM, *E. coli* ATCC 42 µM), in absence (0 µM) or in the presence (from 5 to 80 µM) of NM102. Bacterial survival rate was quantified by plating on LB agar after 4 h at 37°C and by normalizing bacterial load in NM102-treated samples against control samples. Toxicity of the inhibitor in the absence of NO was assessed by exposure of bacterial suspension to NM102 at a concentration ranging from 0 to 80 µM of NM102 as described above, but without NOC5. NM102 concentration required to induce 50% of mortality of the strain (IC_{50}) was calculated using R and the drc package.

Insect infections

Fifth instar wax moth *Galleria mellonella* larvae weighting approximately 0.25 g were used. Insects were provided by INRAE-Micalis, Jouy en Josas, France and reared as described previously (Buisson et al., 2019). Silkworm larvae *Bombyx mori* and *Bombyx eri* were purchased from La Magnanerie de Saillans, Saillans, France and Silkworm store, Chelmsford, UK. Larvae were reared with an artificial diet (cooked mulberry chow) and fifth instar larvae with a weight of [0,7-1,0] g were used for the infection as previously described (Guillemet et al., 2016a). Briefly, prior to assays, the *Galleria* and *Bombyx* larvae were stored under starvation conditions for 4 h to 24 h and randomly distributed in experimental groups of 10 or 20. Bacteria were grown in LB medium at 37 °C under agitation at 200 rpm until late exponential or early stationary growth phases. Bacterial cultures were then diluted in Phosphate Saline Buffer (PBS) to obtain the targeted final concentrations. Bacteria were plated on LB agar before and after infection to determine the quantity injected. Larvae were infected with 20 µL of solutions (bacterial suspension at various doses ranging from 1×10^1 to 2×10^8 CFU/injection, PBS) injected into the haemolymph via the last pro-leg using a 1 mL hypodermic syringe with a 0.5 x 25 mm needle. Injections were done using an automated syringe pump (KD Scientific KDS 100). Larvae mortality were recorded after 24 h at 37 °C for *G. mellonella* and 24 h at 27 °C for *B. mori*. Insects were considered dead if they displayed no movement in response to touch. Mortality data were analyzed with the Log-Probit program which tests the linearity of dose-mortality curves and provides lethal doses 50 and 90 (LD50 and LD90), which correspond to the bacterial dose that kill 50% and 90% of the larvae population, respectively.

For efficacy assay, *P. aeruginosa* was grown in LB medium at 37°C under agitation at 180 rpm until late exponential growth phase. Bacterial cultures were then diluted in Phosphate Saline Buffer (PBS). The last dilution to obtain the desired concentration was done in PBS with 10% DMSO with or without NM102. Bacteria were plated right before infection to determine the quantity injected. *Bombyx eri* larvae were injected with 20 µL of bacterial suspension (3 x 10^3 CFU/injection in 10% DMSO) containing NM102 (2.78 µg/larvae) or MPN (10 µg/mL) or 10% DMSO in the haemolymph via the last pro-leg. Larvae were placed at 27°C. At 4 h and 8 h post first injection, larvae were injected with 50 µL of: (i) PBS, 10% DMSO or (ii) PBS, 10% DMSO with NM102 (6.97 µg/larvae) or iii) PBS, 10%DMSO with MPN (10 µg/mL) 10 *via* the last pro-leg on the other side of the larvae. All injections were performed using a 1 mL hypodermic syringe with a 0.5 x 25 mm needle and an automated syringe pump (KD Scientific KDS 100). 24 h post infection, insects were placed in 2 mL sterile tubes containing 500 µL of PBS and 1.4 mm ceramic lysing beads (MP Biomedicals, Solon, OH, USA) and crushed using a Fast Prep instrument (MP Biomedicals, Solon, OH, USA). The bacterial content in each tube was assessed by serial dilutions on LB plates and CFU numeration. The log CFU was calculated per gram of larvae.

Results

Establishment of insect infection models against clinically relevant bacteria

Mouse models still represent one of the best and most popular approaches for studying infection by bacterial pathogens. However, these models raise cost, time and ethical issues. Insects are a promising alternative to murine models. They possess an innate immune response relatively similar to mammals. They present the advantage to be cost friendly, they can be used without ethical agreements and are relatively easy to rear. We thus tested the virulence of five ESKAPE bacterial strains in two insect infection models. As insects are not the natural hosts of those bacteria, we added the pathogenic bacteria *Bacillus cereus* as a reference strain to validate our experimental model. *B. cereus* is an important agent responsible for gastrointestinal and nosocomial infections in humans (Bottone, 2010) but also capable of naturally infecting insects (Stenfors Arnesen et al., 2008). Two insect models were used in this study, the silkworm larvae *B. mori* (Fig 1, Table 1) and the wax moth larvae *G. mellonella* (Fig 2, Table 2).

We first examined whether injection of bacteria that are pathogenic to humans could kill *B. mori* larvae. Infections were done using increasing doses of bacteria and silkworm survival was assessed 24 h post-infection at 27 °C. Data demonstrated a differential virulence among the pathogenic bacteria. LD50 was determined by logistic regression to assess difference in virulence (Table 1). *K. pneumoniae*, *A. baumannii* and *E. coli* ATCC25922 did not show major virulence towards silkworm and even the injection of high doses of bacteria, up to 10^8 CFU/larvae, did not induce a significant death (Fig 1.A, B and C). Consequently, the estimated LD50 were either not defined or high and with a large confidence

interval (Table 1). In contrast, *S. aureus* and *P. aeruginosa* were both highly capable of killing the silkworm (Fig 1D, E). The LD50 data ranking among the ESKAPE group identified *P. aeruginosa* as having the most potent virulence, with a LD50 a thousand times lower than the *S. aureus*'s one. As expected, *B. cereus* was the most virulent strain overall towards the silkworm, with a LD50 of only 4 CFU/larvae (Fig. 1F) which is consistent with previous publications (Fedhila et al., 2004, 2002).

In order to establish a virulence model for the bacterial strains that were not strongly virulent in the silkworm model, we used *G. mellonella* larvae as a second insect model. Administration was performed by injection of increasing doses of bacteria and *G. mellonella* survival was assessed 24 h post infection at 37 °C. The survival rates presented in Fig. 2 show that all five ESKAPE bacterial strains were virulent towards *G. mellonella*. Unlike what was observed for *B. mori*, *K. pneumonia* and *A. baumannii* were able to kill *G. mellonella* with LD50 of 2.59×10^6 and 1.32×10^5 CFU/larvae, respectively (Table 2). Our data also demonstrated that *E. coli* was highly virulent towards *G. mellonella* compared to *B. mori*. Interestingly, *E. coli* ATCC25922 *and P. aeruginosa* are even more potent than *B. cereus* in killing *G. mellonella*. *B. cereus* LD50 was consistent with previous data (Fedhila et al., 2004; Tran et al., 2010).
Taken together, we compared the virulence of five strains representative of the ESKAPE group towards the insect larvae *B. mori* and *G. mellonella*. We demonstrated that *G. mellonella* is overall a suitable model to examine the virulence of different Gram-positive and Gram-negative ESKAPE bacteria. We also established that *B. mori* is particularly relevant to analyze *P. aeruginosa* and can also be used to assess the virulence of *S. aureus*.

Use of the insect models to assess impact of new anti-virulence drugs

We have previously shown that Mfd is a new virulence factor allowing *K. pneumoniae* and *P. aeruginosa* to resist to the host immune system (Tran et al., n.d.). We have also identified a new compound NM102 as an anti-virulence drug that inhibits Mfd activity, thus reducing the capacity of bacteria to resist the host immune system. In a mice model of infection, this molecule reduces the bacterial load of *K. pneumoniae* and *P. aeruginosa* in the lung to the same level as obtained with MPN (Tran et al., n.d.).
We assessed whether our insect model could be used to measure antibiotics and anti-virulence drugs activity. *Bombyx* were infected with *P. aeruginosa* and then crushed to estimate the remaining cfu post infection following treatment with MPN (Fig. 3A) or NM102 (Fig. 3B). In both cases, MPN and NM102 decreased significantly the cfu recovered post infection.
These data show that the insects can be used to assess virulence of the bacteria of the ESKAPE group and that this virulence model can be used to determine anti-virulence drug efficacy *in vivo*.

Development and characterisation of a nitric oxide assay model

The host defense against bacteria is predominantly mediated by cellular immune mechanisms. Various cells, such as macrophages, neutrophils and epithelial cells produce toxic species, including NO, during most types of infections. NO can severely damage biological molecules, such as proteins and nucleic acids, thereby inducing DNA damage and strand breaks (Akuta et al., 2006). NO is cytotoxic and mutagenic for various pathogens and host cells (Yoshitake et al., 2004; Zaki et al., 2005; Zhuang et al., 1998) and plays an important role during infections by limiting microbial proliferation (Porrini et al., 2020). We developed a NO assay that could mimic pathogen exposition to nitrosative stress *in vivo* during inflammation by using the NO donor NOC-5. First, several NO donors were tested (data not shown) and NOC-5 was selected as the best compound for our NO stress assay because of its capacity to form an aqueous solution under physiological pH and due to its NO temporal release profiles. NOC-5 half-life time at pH 7,4 is 93 min at 22 °C and 25 min at 37 °C (Bradley and Steinert, 2015; *Globins and Other Nitric Oxide-Reactive Proteins, Part A, Volume 436 - 1st Edition*, 2008). NOC-5 is a diazeniumdiolate compound that spontaneously decomposes into a solution with first order kinetics, yielding two moles of NO per mole of NOC-5.

Several methods exist to quantify NO directly or indirectly and each method has its advantages and disadvantages. It is thus often recommended to use at least two methods to quantify NO (Gupta and Igamberdiev, 2013). Measuring NO can be really challenging as it is a free radical with an extremely short half-life (less than 1 second in circulating blood). We measured the NO released by NOC-5 at concentrations between 0 and 1000 µM in a cell-free system (Fig. 4). We used the fluorescent probe 2', 7'-dichlorodihydrofluorescein diacetate (DCF-DA) to measure the NOC-5 generated NO. First, DCF-DA was loaded at final concentrations of 200, 100 and 50 µM into various solutions of NOC-5 in order to select the optimal non-saturating probe concentration (data not shown). Our data demonstrated that 50 µM of DCF-DA allowed for a non-saturating signal at 1000 µM of NOC-5 and for a significant signal detection at 2 µM of NOC-5. This concentration of DCF-DA was therefore selected. Next, DCF-DA at 50 µM was used to identify the kinetics of NO release by NOC-5 for 4 h (Fig. 4A). Our data show that NO release was detected in a dose- and time-dependant manner.

In order to have a better assessment of the NO released under our conditions, quantification was also performed using the Griess method. Using a nitrate standard curve, we estimated the NO release immediately, and after 4 h of incubation (Fig. 4B). We confirmed that release of NO is NOC-5-dose dependent. Moreover, we could show that the NO concentration is stable during the 4 h of incubation. Altogether, we demonstrated that in the conditions of our NO assay, NO is produced and that measuring nitrite, its stable breakdown product, allows a precise measure of the initial NO concentration. We next used the NO assay to evaluate the sensitivity of bacterial pathogens towards NO.

Establishment of an NO assay to assess bacterial sensitivity to the human immune response

The NO donor NOC-5 was used to investigate the direct antibacterial effects of NO against five bacteria of the ESKAPE group. The bacterial survival was assessed in the presence of increasing concentrations of NO (Fig. 5, Table 3). All bacteria showed a decrease in their survival capacity with increasing NO concentration. However, the resistance profile to NO varies according to the bacterial model, but also according to the NO concentrations. Indeed, we observed that although NO demonstrates a strong antibacterial effect towards *A. baumannii* and *S. aureus*, presence of sublethal doses of NO may stimulate the growth of those bacteria. In order to better understand bacterial behaviour towards NO, IC10 and IC50, which correspond to NO concentration inducing 10% and 50% mortality respectively, were evaluated (Table 3). IC10 values highlight the minimal concentration of NO that decreased bacterial survival and characterised *P. aeruginosa* (IC10 of 3 µM), *A. baumannii* (IC10 of 4 µM) and *S. aureus* (IC10 of 7 µM) as having the lower resistances to NO. Both IC10 and IC50 values showed a higher resistance towards NO for clinical *E. coli strain and K. pneumoniae,* compared to *S. aureus*, *P. aeruginosa* and *A. baumannii*.

We conclude that our NO assay is suitable to evaluate resistance towards NO of clinically, human relevant bacterial strains.

NO assay to measure the impact of anti-virulence drugs

Mfd is a non-essential protein in unstressed conditions. However, we have previously shown that Mfd is essential to resist NO stress during infection (Darrigo et al., 2016; Guillemet et al., 2016b). We have previously identified an innovative anti-virulence drug that has no antimicrobial activity in unstressed conditions and active only in stressed conditions when Mfd is required. Under NO stress, NM102 strongly inhibits *K. pneumoniae* survival (Fig. 6A) with an IC_{50} of 7.5 µM. NM102 also inhibits bacterial survival of clinical *E. coli* under NO stress conditions compared to unstressed conditions (IC_{50} of 61.2 µM, Fig. 6B) and, although to a lesser extent, of *P. aeruginosa* (IC_{50} of 94.2 µM, Fig. 6C). Additionally, using this model, we could show that the anti-virulence drug NM102 affected *K. pneumoniae* growth following NO exposure over time (Fig. 6D).

These data show that this model can be used to mimic immune stress and assess the impact of innovative anti-virulence drugs targeting the bacterial capacity to counteract the host immune response.

Discussion

Studying bacteria from the ESKAPE group is a crucial challenge for the future, as resistance to antibiotics keeps growing and the need for novel therapeutics is vital. In this study, we developed

complementary *in vitro* and *in vivo* models that could be used to better understand the pathophysiology of relevant pathogenic bacteria and to evaluate more thoroughly the efficacy of anti-infective agents towards infection caused by ESKAPE bacteria. We selected five clinical representative strains of the ESKAPE group that belong to the Gram-negative and -positive organisms, and we showed that their pathogenicity can be effectively studied using our combined models.

The most commonly used model in research on human diseases is the mouse, probably because of its high degree of anatomically, physiologically and genetically resemblance with humans. Although very performant, this model poses ethical issues. Because of this, the tendency is to find alternative *in vivo* and *ex vivo* models. As such, a large variety of insects has been used as model to study virulence of medically relevant pathogens and the host's defense mechanism against them (Cox and Gilmore, 2007; Frankel and Schroeder, 2019; Kaito, 2016; Rakic Martinez et al., 2020). They have advantages compared to mammalian model: they are cheap, easy to raise, do not require ethical approval or trained staff and most of them have had their genome sequenced.

The silkworm *Bombyx* has been domesticated for ages to maximize silk fiber productivity to the point that no population remains in the wild. Due to its relatively large size, ease of rearing and sequenced genome, it became an important model for research on pathogen virulence, host immunity and the evaluation of antimicrobial compounds (Kawamoto et al., 2019; Yang et al., 2018). Also, its large size makes the injection of large volumes feasible. Moreover, *Bombyx* anatomy allows a differentiation between intra-haemolymph and intra-midgut administration to mimic systemic or oral infections, respectively (Matsumoto and Sekimizu, 2019).

The greater wax moth *Galleria mellonella* has also been widely used to study human pathogens (Champion et al., 2016; Cools et al., 2019; González et al., 2020; Mukherjee et al., 2020; Rakic Martinez et al., 2020; Ramarao et al., 2012; Sheehan et al., 2020; Whelan et al., 2019; Willcocks et al., 2020) and some studies have shown a strong correlation between virulence of a pathogen in *G. mellonella* and in mammalian (Brennan et al., 2002; Jander et al., 2000; Malmquist et al., 2019; Olsen et al., 2011). At the fifth instar, a stage that is typically used for infection, *G. mellonella* larvae have an average length of 2 cm and diameter around 6 mm. Therefore, injection is attributed to an intra-haemolymph route of administration, and oral administration can be achieved through force feeding, although this technique is less frequently used. One major advantage is that compared to *Bombyx*, *G. mellonella* larvae are less susceptible to variation of environmental conditions and to viral diseases (Kato et al., 1998; Kobayashi et al., 1981; Sarkhel and Shrivastava, 2017) and can be raised at up to 37°C, thus mimicking the human body temperature.

The immune system's role is to protect against pathogens, and toxins, and to eliminate senescent or deregulated (tumor) cells. The human immune system is divided into two types of responses: innate and adaptive immunity. Innate immunity is the first to answer when it finds an invader and generates

a fast response, while adaptive immunity can differentiate one particular antigenic determinant and is associated with long-term protective memory (Nicholson, 2016). While insects lack an adaptive immune system, insects and humans share similarities in their innate immune system with both systems including humoral and cellular responses (Sheehan et al., 2018). Insects possess several classes of hemocytes (equivalent to human blood cells) that capture pathogens through phagocytosis, encapsulation and nodulation for larger intruders. The humoral response consists in the secretion of antimicrobial peptides (AMPs) and free radicals into the haemolymph, melanisation and clotting (Chen and Lu, 2018; Chen et al., 2019; Cutuli et al., 2019; Keehnen et al., 2017; Pereira et al., 2018; Wang et al., 2020). *B. mori* and *G. mellonella* have already been used as infection models to study Gram-positive and Gram-negative human pathogenic bacteria including *Vibrio cholerae* (Bokhari et al., 2017; Kaito et al., 2002), *Listeria monocytogenes* (Castillo et al., 2016; Rakic Martinez et al., 2017), *Porphyromonas gingivalis* (Dos Santos et al., 2017; Ishii et al., 2010) or even some yeasts such as *Candida albicans* (Cotter et al., 2000; Hanaoka et al., 2008). In the present study, systemic infections were established by administration of ESKAPE bacteria via injection into the insect haemolymph, which corresponds to an intra-venous injection in a mammalian model. Furthermore, *B. cereus* was added as control for our insect models. Indeed *B. cereus* has been shown to infect both *G. mellonella* and *B. mori* (Guillemet et al., 2016b; Ramarao et al., 2012). *B. cereus* is also a human pathogen that induces nosocomial infection (Bottone, 2010; Ramarao et al., 2014; Tran et al., 2011, 2010). As such, finding the appropriate models to study this pathogen is also an important health issue. Our lethal doses 50 and 90 for *B. cereus* were consistent with previous studies (Abi Khattar et al., 2009; Guillemet et al., 2016b). Interestingly, the virulence potential of the strains varied between the two insect models. *K. pneumoniae* and *A. baumanii* were able to kill *G. mellonella* but not *B. mori.* Consistently, no previous reports were found on *B. mori* infection with *K. pneumoniae*. On average, all bacteria were more infectious for *G. mellonella* than for *B. mori,* with the exception of *B. cereus,* which was very virulent to *B. mori*. This difference may be explained by the incubation temperature of 37°C for *G. mellonella* and 27°C for *B. mori*. It has been shown for several bacteria that the incubation temperature has an impact on the expression of several virulence factors, which may be overexpressed at 37°C, corresponding to the human body temperature (Kouse et al., 2013; Weber et al., 2014). On the opposite, *S. aureus* and *P. aeruginosa* were able to kill both insects. These two bacteria have already been studied using *G. mellonella* and *B. mori* as models and we found similar lethal doses 50 and 90 (Desbois and Coote, 2011; Hernandez et al., 2019; Kaito et al., 2002; Silva et al., 2017; Siriyong et al., 2018).

Taken together, insects appear as great alternative models to study bacterial pathogenesis and can be further used to screen novel antibiotics. The models developed in this study allow to assess the pathogenicity of ESKAPE bacteria and their inhibition by classical antibiotics as well as by novel anti-virulence drugs. It is interesting to note that bacteria behave differently in the two insect models. This

discrepancy highlights the need of confirming data using several models and being cautious with data interpretation. Nevertheless, insects can be used to refine scientific questions before going to mammalian models, which require additional ethical considerations.

The impact of the host's immune system on bacterial pathogenesis is a critical issue. One essential actor of the innate response is nitric oxide (NO). NO is a free radical synthesized via the action of specific enzymes, the NO synthase (NOS). Three NOS have been identified in humans: the two isoforms nNOS (neuronal NOS) and eNOS (endothelial NOS) are constitutively expressed and essential for physiological functions, while iNOS's (inducible NOS) expression is triggered following specific signals such as inflammation (Porrini et al., 2020). NO generates highly toxic byproducts during inflammation that have deleterious effect on pathogens. NO has been shown to participate in the control of infection by various pathogens including *Mycobacterium*, *Listeria* and *Pseudomonas* (Darling and Evans, 2003; Ito et al., 2005; MacMicking et al., 1997; Porrini et al., 2020; Reece et al., 2018; Wink et al., 2011). It has also been demonstrated that following infection, NO production increases in *B. mori* leading to an activation of AMPs production (Chen and Lu, 2018). Despite the importance of NO in the host defense against infection, only few tests have been developed to study the impact of NO on bacterial virulence (Feura et al., 2020; Friedman et al., 2011; Hall et al., 2020; Jensen et al., 2020; Jones et al., 2010; Neidrauer et al., 2014; Nurhasni et al., 2015; Pegalajar-Jurado et al., 2015). In those studies, NO was delivered as gas, was associated with nanomaterial, biopolymers, or was topically delivered using patches and ointments, which required specific material or technically trained staff.

Because of the NO's short life, evidence of the antimicrobial effect of NO have mainly been demonstrated using macrophage-derived NO or *in vivo* models (Chakravortty et al., 2002; Guillemet et al., 2016a; Waters et al., 2004; Yadav et al., 2018). For instance, we have previously shown that the two human pathogens *B. cereus* and *Shigella flexneri* have increased virulence in NOS2-deficient mice (Guillemet et al., 2016a). Here, we established, using the NO donor NOC-5, a robust and easy to perform cell free method to induce a stress that mimics the NO production during the host's immune response. In our model, the absence of cells for the production of NO enables the comparison of resistance of intra- or extracellular bacteria. Moreover, the miniaturized 96-wells microliter-based format allows a high-throughput approach to drug screening. We demonstrated that the NO released in our assay is stable and can be used with a large range of NO concentrations. Using this model, we showed that ESKAPE bacteria present different sensitivities to NO. Interestingly, bacteria survival to NO is finely tuned, with NO being beneficial or deleterious depending on the concentration. For all the strains, we observed a correlation between survival and the amount of NO delivered under our experimental condition. Our data are consistent with previous studies using cell free technologies to deliver NO and assess its antimicrobial activity against bacteria from the ESKAPE group (Friedman et al., 2011; Jensen et al., 2020; Neidrauer et al., 2014; Nurhasni et al., 2015; Pegalajar-Jurado et al.,

2015). For instance, the release of NO by the enzyme S-nitrosated dextran-cysteamine (Pegalajar-Jurado et al., 2015) or from NO–zeolite ointment (Neidrauer et al., 2014) impaired the growth of *E. coli*, *A. baumannii* and *S. aureus*. Consistently with our data, the decrease of the CFU over time was also dose-dependent. However, as the bactericidal effect of NO varies depending on the delivery system, experimental set up and delivery time, a direct comparison of resistance for a given strain across literatures is not straightforward. In addition, it was previously shown that when *S. aureus*, *P. aeruginosa* and *A. baumannii* are treated with antibiotics in the presence or absence of an atmosphere containing gaseous NO, bacteria showed less resistance to the antibiotic when NO was present (Jensen et al., 2020). As such, our model could also be used to assess antimicrobial resistance in the context of NO stress. To allow a precise measure of NO stress resistance, we used two parameters, IC50 and IC10, to compare resistance to NO between strains and we showed that resistance to NO is superior for *E. coli* and *K. pneumoniae* compared to *S. aureus*, *P. aeruginosa* and *A. baumannii*. Although most bacteria are sensitive to the bactericidal effect of NO, some like *E. coli* are more resistant. This is consistent with the fact that NO resistance is an important feature of *E. coli* pathogenicity (Shimizu et al., 2012). Resistance to NO does not always fully explain the virulence of a bacterial stain, however it might help decipher the mechanism of virulence and design drug specific to each step of infection. We conclude that our NO assay is suitable to evaluate resistance towards NO of clinically relevant human bacterial strains, and can be used to efficiently assess the potency of antimicrobials drugs in conditions that mimic an exposition to innate immune response.

Complexity of the pathogenicity mechanisms highlight the need for combined models to obtain a complete view of pathogens' virulence. Here, we have established three models varying from *in vitro* to *in vivo* and covering a large panel of clinically relevant bacteria including Gram negative and Gram positive that can be used for the development of new therapeutics to fight antimicrobial resistance.

Acknowledgments

We are grateful to Thierry Naas for the gift of strains. We thank Antoine Allier for his help with R and Margot Draveny for her implication in insect experiment. We thank all members of the IERP animal facility (INRAE, Jouy en Josas) for their technical help for animal studies. We also thank Christina Nielson-LeRoux and Christophe Buisson for *Galleria Mellonella* rearing.

Funding

This work was supported by the AAP Prematuration IDEX 2018 (CDE-2018-002324/IRE 2018-0022), DIM One health region Ile de France (R19104DD) and the Interdisciplinary Action "Health and Therapeutic Innovation" (HEALTHI) of the Université Paris-Saclay.

Author contributions

NR and ST conceived the study; ST, DC, LL, CP and FG performed experiments; ST, DC and LL wrote the manuscript; NR, ST and DC contributed to editing and revisions.

Disclosure statement

No potential conflict of interest was reported by the authors.

References

Abi Khattar, Z., Rejasse, A., Destoumieux-Garzón, D., Escoubas, J.M., Sanchis, V., Lereclus, D., Givaudan, A., Kallassy, M., Nielsen-Leroux, C., Gaudriault, S., 2009. The dlt operon of Bacillus cereus is required for resistance to cationic antimicrobial peptides and for virulence in insects. J. Bacteriol. 191, 7063–7073. https://doi.org/10.1128/JB.00892-09

Akuta, T., Zaki, M.H., Yoshitake, J., Okamoto, T., Akaike, T., 2006. Nitrative stress through formation of 8-nitroguanosine: insights into microbial pathogenesis. Nitric Oxide 14, 101–108. https://doi.org/10.1016/j.niox.2005.10.004

Bokhari, H., Ali, A., Noreen, Z., Thomson, N., Wren, B.W., 2017. Galleria mellonella is low cost and suitable surrogate host for studying virulence of human pathogenic Vibrio cholerae. Gene 628, 1–7. https://doi.org/10.1016/j.gene.2017.07.019

Bottone, E.J., 2010. Bacillus cereus, a volatile human pathogen. Clin. Microbiol. Rev. 23, 382–398. https://doi.org/10.1128/CMR.00073-09

Bradley, S.A., Steinert, J.R., 2015. Characterisation and comparison of temporal release profiles of nitric oxide generating donors. J Neurosci Methods 245, 116–124. https://doi.org/10.1016/j.jneumeth.2015.02.024

Brennan, M., Thomas, D.Y., Whiteway, M., Kavanagh, K., 2002. Correlation between virulence of Candida albicans mutants in mice and Galleria mellonella larvae. FEMS Immunol. Med. Microbiol. 34, 153–157. https://doi.org/10.1111/j.1574-695X.2002.tb00617.x

Browne, N., Heelan, M., Kavanagh, K., 2013. An analysis of the structural and functional similarities of insect hemocytes and mammalian phagocytes. Virulence 4, 597–603. https://doi.org/10.4161/viru.25906

Buisson, C., Gohar, M., Huillet, E., Nielsen-LeRoux, C., 2019. Bacillus thuringiensis Spores and Vegetative Bacteria: Infection Capacity and Role of the Virulence Regulon PlcR Following Intrahaemocoel Injection of Galleria mellonella. Insects 10. https://doi.org/10.3390/insects10050129

Castillo, Y., Suzuki, J., Watanabe, K., Shimizu, T., Watarai, M., 2016. Effect of Vitamin A on Listeria monocytogenes Infection in a Silkworm Model. PLoS ONE 11, e0163747. https://doi.org/10.1371/journal.pone.0163747

Chadha, J., Ravi, null, Singh, J., Harjai, K., 2023. α-Terpineol synergizes with gentamicin to rescue Caenorhabditis elegans from Pseudomonas aeruginosa infection by attenuating quorum sensing-regulated virulence. Life Sci 313, 121267. https://doi.org/10.1016/j.lfs.2022.121267

Chakravortty, D., Hansen-Wester, I., Hensel, M., 2002. Salmonella pathogenicity island 2 mediates protection of intracellular Salmonella from reactive nitrogen intermediates. J. Exp. Med. 195, 1155–1166. https://doi.org/10.1084/jem.20011547

Champion, O.L., Wagley, S., Titball, R.W., 2016. Galleria mellonella as a model host for microbiological and toxin research. Virulence 7, 840–845. https://doi.org/10.1080/21505594.2016.1203486
Chen, K., Lu, Z., 2018. Immune responses to bacterial and fungal infections in the silkworm, Bombyx mori. Developmental & Comparative Immunology, Insect innate immunity in China 83, 3–11. https://doi.org/10.1016/j.dci.2017.12.024
Chen, S., Dong, Z., Ren, X., Zhao, D., Zhang, Y., Tang, M., Han, J., Ye, L., Zhao, P., 2019. Proteomic Identification of Immune-Related Silkworm Proteins Involved in the Response to Bacterial Infection. J. Insect Sci. 19. https://doi.org/10.1093/jisesa/iez056
Cools, F., Torfs, E., Aizawa, J., Vanhoutte, B., Maes, L., Caljon, G., Delputte, P., Cappoen, D., Cos, P., 2019. Optimization and Characterization of a Galleria mellonella Larval Infection Model for Virulence Studies and the Evaluation of Therapeutics Against Streptococcus pneumoniae. Front Microbiol 10, 311. https://doi.org/10.3389/fmicb.2019.00311
Cotter, G., Doyle, S., Kavanagh, K., 2000. Development of an insect model for the in vivo pathogenicity testing of yeasts. FEMS Immunol. Med. Microbiol. 27, 163–169. https://doi.org/10.1111/j.1574-695X.2000.tb01427.x
Cox, C.R., Gilmore, M.S., 2007. Native microbial colonization of Drosophila melanogaster and its use as a model of Enterococcus faecalis pathogenesis. Infect. Immun. 75, 1565–1576. https://doi.org/10.1128/IAI.01496-06
Cruz-Ramos, H., Crack, J., Wu, G., Hughes, M.N., Scott, C., Thomson, A.J., Green, J., Poole, R.K., 2002. NO sensing by FNR: regulation of the Escherichia coli NO-detoxifying flavohaemoglobin, Hmp. EMBO J 21, 3235–3244. https://doi.org/10.1093/emboj/cdf339
Cutuli, M.A., Petronio Petronio, G., Vergalito, F., Magnifico, I., Pietrangelo, L., Venditti, N., Di Marco, R., 2019. Galleria mellonella as a consolidated in vivo model hosts: New developments in antibacterial strategies and novel drug testing. Virulence 10, 527–541. https://doi.org/10.1080/21505594.2019.1621649
da Rosa, T.F., Coelho, S.S., Foletto, V.S., Bottega, A., Serafin, M.B., Machado, C. de S., Franco, L.N., de Paula, B.R., Hörner, R., 2020. Alternatives for the treatment of infections caused by ESKAPE pathogens. J Clin Pharm Ther 45, 863–873. https://doi.org/10.1111/jcpt.13149
Darling, K.E.A., Evans, T.J., 2003. Effects of nitric oxide on Pseudomonas aeruginosa infection of epithelial cells from a human respiratory cell line derived from a patient with cystic fibrosis. Infect. Immun. 71, 2341–2349. https://doi.org/10.1128/iai.71.5.2341-2349.2003
Darrigo, C., Guillemet, E., Dervyn, R., Ramarao, N., 2016. The Bacterial Mfd Protein Prevents DNA Damage Induced by the Host Nitrogen Immune Response in a NER-Independent but RecBC-Dependent Pathway. PLoS ONE 11, e0163321. https://doi.org/10.1371/journal.pone.0163321
Desbois, A.P., Coote, P.J., 2011. Wax moth larva (Galleria mellonella): an in vivo model for assessing the efficacy of antistaphylococcal agents. J. Antimicrob. Chemother. 66, 1785–1790. https://doi.org/10.1093/jac/dkr198
Dos Santos, J.D., de Alvarenga, J.A., Rossoni, R.D., García, M.T., Moraes, R.M., Anbinder, A.L., Cardoso Jorge, A.O., Junqueira, J.C., 2017. Immunomodulatory effect of photodynamic therapy in Galleria mellonella infected with Porphyromonas gingivalis. Microb. Pathog. 110, 507–511. https://doi.org/10.1016/j.micpath.2017.07.045
Fedhila, S., Guillemet, E., Nel, P., Lereclus, D., 2004. Characterization of two Bacillus thuringiensis genes identified by in vivo screening of virulence factors. Appl. Environ. Microbiol. 70, 4784–4791. https://doi.org/10.1128/AEM.70.8.4784-4791.2004

Fedhila, S., Nel, P., Lereclus, D., 2002. The InhA2 metalloprotease of Bacillus thuringiensis strain 407 is required for pathogenicity in insects infected via the oral route. J. Bacteriol. 184, 3296–3304. https://doi.org/10.1128/jb.184.12.3296-3304.2002

Ferri, M., Ranucci, E., Romagnoli, P., Giaccone, V., 2017. Antimicrobial resistance: A global emerging threat to public health systems. Crit Rev Food Sci Nutr 57, 2857–2876. https://doi.org/10.1080/10408398.2015.1077192

Feura, E.S., Yang, L., Schoenfisch, M.H., 2020. Antibacterial activity of nitric oxide-releasing carboxymethylcellulose against periodontal pathogens. J Biomed Mater Res A. https://doi.org/10.1002/jbm.a.37056

Frankel, G., Schroeder, G.N., 2019. The Galleria mellonella Infection Model for Investigating the Molecular Mechanisms of Legionella Virulence. Methods Mol. Biol. 1921, 333–346. https://doi.org/10.1007/978-1-4939-9048-1_22

Friedman, A., Blecher, K., Sanchez, D., Tuckman-Vernon, C., Gialanella, P., Friedman, J.M., Martinez, L.R., Nosanchuk, J.D., 2011. Susceptibility of Gram-positive and -negative bacteria to novel nitric oxide-releasing nanoparticle technology. Virulence 2, 217–221. https://doi.org/10.4161/viru.2.3.16161

Globins and Other Nitric Oxide-Reactive Proteins, Part A, Volume 436 - 1st Edition, 2008. . Academic Press.

González, G.M., Andrade, A., Villanueva-Lozano, H., Campos-Cortés, C.L., Becerril-García, M.A., Montoya, A.M., Sánchez-González, A., Bonifaz, A., Franco-Cendejas, R., López-Jácome, L.E., Treviño-Rangel, R. de J., 2020. Comparative Analysis of Virulence Profiles of Serratia marcescens Isolated from Diverse Clinical Origins in Mexican Patients. Surg Infect (Larchmt). https://doi.org/10.1089/sur.2020.029

Guillemet, E., Leréec, A., Tran, S.-L., Royer, C., Barbosa, I., Sansonetti, P., Lereclus, D., Ramarao, N., 2016a. The bacterial DNA repair protein Mfd confers resistance to the host nitrogen immune response. Sci Rep 6, 29349. https://doi.org/10.1038/srep29349

Guillemet, E., Leréec, A., Tran, S.-L., Royer, C., Barbosa, I., Sansonetti, P., Lereclus, D., Ramarao, N., 2016b. The bacterial DNA repair protein Mfd confers resistance to the host nitrogen immune response. Sci Rep 6, 29349. https://doi.org/10.1038/srep29349

Gupta, K.J., Igamberdiev, A.U., 2013. Recommendations of using at least two different methods for measuring NO. Front Plant Sci 4, 58. https://doi.org/10.3389/fpls.2013.00058

Hall, J.R., Rouillard, K.R., Suchyta, D.J., Brown, M.D., Ahonen, M.J.R., Schoenfisc, M.H., 2020. Mode of nitric oxide delivery affects antibacterial action. ACS Biomater Sci Eng 6, 433–441. https://doi.org/10.1021/acsbiomaterials.9b01384

Hanaoka, N., Takano, Y., Shibuya, K., Fugo, H., Uehara, Y., Niimi, M., 2008. Identification of the putative protein phosphatase gene PTC1 as a virulence-related gene using a silkworm model of Candida albicans infection. Eukaryotic Cell 7, 1640–1648. https://doi.org/10.1128/EC.00129-08

Hernandez, R.J., Hesse, E., Dowling, A.J., Coyle, N.M., Feil, E.J., Gaze, W.H., Vos, M., 2019. Using the wax moth larva Galleria mellonella infection model to detect emerging bacterial pathogens. PeerJ 6, e6150. https://doi.org/10.7717/peerj.6150

Ishii, K., Hamamoto, H., Imamura, K., Adachi, T., Shoji, M., Nakayama, K., Sekimizu, K., 2010. Porphyromonas gingivalis peptidoglycans induce excessive activation of the innate immune system in silkworm larvae. J. Biol. Chem. 285, 33338–33347. https://doi.org/10.1074/jbc.M110.112987

Ito, S., Ishii, K.J., Ihata, A., Klinman, D.M., 2005. Contribution of Nitric Oxide to CpG-Mediated Protection against Listeria monocytogenes. Infection and Immunity 73, 3803–3805. https://doi.org/10.1128/IAI.73.6.3803-3805.2005

Jander, G., Rahme, L.G., Ausubel, F.M., 2000. Positive correlation between virulence of Pseudomonas aeruginosa mutants in mice and insects. J. Bacteriol. 182, 3843–3845. https://doi.org/10.1128/jb.182.13.3843-3845.2000

Jensen, J., Packert, D., Miller, C., Packert, G., Hanft, J., Jensen, S., 2020. Discovery and Development of Gaseous Nitric Oxide Under Increased Atmospheric Pressure as an Antimicrobial: In Vitro and In Vivo Testing of Nitric Oxide Against Multidrug-Resistant Organisms. Clin Podiatr Med Surg 37, 231–246. https://doi.org/10.1016/j.cpm.2019.11.001

Jones, M.L., Ganopolsky, J.G., Labbé, A., Prakash, S., 2010. A novel nitric oxide producing probiotic patch and its antimicrobial efficacy: preparation and in vitro analysis. Appl. Microbiol. Biotechnol. 87, 509–516. https://doi.org/10.1007/s00253-010-2490-x

Kaito, C., 2016. Understanding of bacterial virulence using the silkworm infection model. Drug Discov Ther 10, 30–33. https://doi.org/10.5582/ddt.2016.01020

Kaito, C., Akimitsu, N., Watanabe, H., Sekimizu, K., 2002. Silkworm larvae as an animal model of bacterial infection pathogenic to humans. Microb. Pathog. 32, 183–190. https://doi.org/10.1006/mpat.2002.0494

Kato, M., Nagayasu, K., Hara, W., Ninagi, O., 1998. Effect of Exposure of the Silkworm, Bombyx mori, To High Temperature on Survival Rate and Cocoon characters. Japan Agricultural Research Quarterly 32, 61–64.

Kawamoto, M., Jouraku, A., Toyoda, A., Yokoi, K., Minakuchi, Y., Katsuma, S., Fujiyama, A., Kiuchi, T., Yamamoto, K., Shimada, T., 2019. High-quality genome assembly of the silkworm, Bombyx mori. Insect Biochem. Mol. Biol. 107, 53–62. https://doi.org/10.1016/j.ibmb.2019.02.002

Keehnen, N.L.P., Rolff, J., Theopold, U., Wheat, C.W., 2017. Chapter One - Insect Antimicrobial Defences: A Brief History, Recent Findings, Biases, and a Way Forward in Evolutionary Studies, in: Ligoxygakis, P. (Ed.), Advances in Insect Physiology, Insect Immunity. Academic Press, pp. 1–33. https://doi.org/10.1016/bs.aiip.2017.02.003

Kobayashi, M., Inagaki, S., Kawase, S., 1981. Effect of high temperature on the development of nuclear polyhedrosis virus in the silkworm, Bombyx mori. Journal of Invertebrate Pathology 38, 386–394. https://doi.org/10.1016/0022-2011(81)90106-3

Kouse, A.B., Righetti, F., Kortmann, J., Narberhaus, F., Murphy, E.R., 2013. RNA-mediated thermoregulation of iron-acquisition genes in Shigella dysenteriae and pathogenic Escherichia coli. PLoS ONE 8, e63781. https://doi.org/10.1371/journal.pone.0063781

Lange, A., Beier, S., Huson, D.H., Parusel, R., Iglauer, F., Frick, J.-S., 2018. Genome Sequence of Galleria mellonella (Greater Wax Moth). Genome Announc 6. https://doi.org/10.1128/genomeA.01220-17

Lapidus, A., Goltsman, E., Auger, S., Galleron, N., Ségurens, B., Dossat, C., Land, M.L., Broussolle, V., Brillard, J., Guinebretiere, M.-H., Sanchis, V., Nguen-The, C., Lereclus, D., Richardson, P., Wincker, P., Weissenbach, J., Ehrlich, S.D., Sorokin, A., 2008. Extending the Bacillus cereus group genomics to putative food-borne pathogens of different toxicity. Chem. Biol. Interact. 171, 236–249. https://doi.org/10.1016/j.cbi.2007.03.003

Lau, W.Y.V., Taylor, P.K., Brinkman, F.S.L., Lee, A.H.Y., 2023. Pathogen-associated gene discovery workflows for novel antivirulence therapeutic development. EBioMedicine 88, 104429. https://doi.org/10.1016/j.ebiom.2022.104429

MacMicking, J.D., North, R.J., LaCourse, R., Mudgett, J.S., Shah, S.K., Nathan, C.F., 1997. Identification of nitric oxide synthase as a protective locus against tuberculosis. Proc. Natl. Acad. Sci. U.S.A. 94, 5243–5248. https://doi.org/10.1073/pnas.94.10.5243

Malmquist, J.A., Rogan, M.R., McGillivray, S.M., 2019. Galleria mellonella as an Infection Model for Bacillus anthracis Sterne. Front Cell Infect Microbiol 9, 360. https://doi.org/10.3389/fcimb.2019.00360

Matsumoto, Y., Sekimizu, K., 2019. Silkworm as an experimental animal for research on fungal infections. Microbiol. Immunol. 63, 41–50. https://doi.org/10.1111/1348-0421.12668

Mukherjee, K., Amsel, D., Kalsy, M., Billion, A., Dobrindt, U., Vilcinskas, A., 2020. MicroRNAs regulate innate immunity against uropathogenic and commensal-like Escherichia coli infections in the surrogate insect model Galleria mellonella. Sci Rep 10, 2570. https://doi.org/10.1038/s41598-020-59407-3

Neidrauer, M., Ercan, U.K., Bhattacharyya, A., Samuels, J., Sedlak, J., Trikha, R., Barbee, K.A., Weingarten, M.S., Joshi, S.G., 2014. Antimicrobial efficacy and wound-healing property of a topical ointment containing nitric-oxide-loaded zeolites. J. Med. Microbiol. 63, 203–209. https://doi.org/10.1099/jmm.0.067322-0

Nicholson, L.B., 2016. The immune system. Essays Biochem. 60, 275–301. https://doi.org/10.1042/EBC20160017

Nurhasni, H., Cao, J., Choi, M., Kim, I., Lee, B.L., Jung, Y., Yoo, J.-W., 2015. Nitric oxide-releasing poly(lactic-co-glycolic acid)-polyethylenimine nanoparticles for prolonged nitric oxide release, antibacterial efficacy, and in vivo wound healing activity. Int J Nanomedicine 10, 3065–3080. https://doi.org/10.2147/IJN.S82199

Olsen, R.J., Watkins, M.E., Cantu, C.C., Beres, S.B., Musser, J.M., 2011. Virulence of serotype M3 Group A Streptococcus strains in wax worms (Galleria mellonella larvae). Virulence 2, 111–119. https://doi.org/10.4161/viru.2.2.14338

Pegalajar-Jurado, A., Wold, K.A., Joslin, J.M., Neufeld, B.H., Arabea, K.A., Suazo, L.A., McDaniel, S.L., Bowen, R.A., Reynolds, M.M., 2015. Nitric oxide-releasing polysaccharide derivative exhibits 8-log reduction against Escherichia coli, Acinetobacter baumannii and Staphylococcus aureus. J Control Release 217, 228–234. https://doi.org/10.1016/j.jconrel.2015.09.015

Pereira, T.C., de Barros, P.P., Fugisaki, L.R. de O., Rossoni, R.D., Ribeiro, F. de C., de Menezes, R.T., Junqueira, J.C., Scorzoni, L., 2018. Recent Advances in the Use of Galleria mellonella Model to Study Immune Responses against Human Pathogens. J Fungi (Basel) 4. https://doi.org/10.3390/jof4040128

Poole, R.K., 2011. Globins and Other Nitric Oxide-Reactive Proteins, Part B. Academic Press.

Porrini, C., Ramarao, N., Tran, S.-L., 2020. Dr. NO and Mr. Toxic - the versatile role of nitric oxide. Biol. Chem. 401, 547–572. https://doi.org/10.1515/hsz-2019-0368

Possel, H., Noack, H., Augustin, W., Keilhoff, G., Wolf, G., 1997. 2,7-Dihydrodichlorofluorescein diacetate as a fluorescent marker for peroxynitrite formation. FEBS Letters 416, 175–178. https://doi.org/10.1016/S0014-5793(97)01197-6

Projections of mortality and causes of death, 2016 to 2060 [WWW Document], n.d. . World Health Organization. URL https://www.who.int/healthinfo/global_burden_disease/projections/en/

Rakic Martinez, M., Ferguson, M., Datta, A.R., 2020. Virulence assessment of Listeria monocytogenes grown in different foods using a Galleria mellonella model. PLoS ONE 15, e0232485. https://doi.org/10.1371/journal.pone.0232485

Rakic Martinez, M., Wiedmann, M., Ferguson, M., Datta, A.R., 2017. Assessment of Listeria monocytogenes virulence in the Galleria mellonella insect larvae model. PLoS ONE 12, e0184557. https://doi.org/10.1371/journal.pone.0184557

Ramarao, N., Belotti, L., Deboscker, S., Ennahar-Vuillemin, M., de Launay, J., Lavigne, T., Koebel, C., Escande, B., Guinebretière, M.H., 2014. Two unrelated episodes of Bacillus cereus bacteremia in a neonatal intensive care unit. Am J Infect Control 42, 694–695. https://doi.org/10.1016/j.ajic.2014.01.025

Ramarao, N., Nielsen-Leroux, C., Lereclus, D., 2012. The insect Galleria mellonella as a powerful infection model to investigate bacterial pathogenesis. J Vis Exp e4392. https://doi.org/10.3791/4392

Reece, S.T., Vogelzang, A., Tornack, J., Bauer, W., Zedler, U., Schommer-Leitner, S., Stingl, G., Melchers, F., Kaufmann, S.H.E., 2018. Mycobacterium tuberculosis-Infected Hematopoietic Stem and Progenitor Cells Unable to Express Inducible Nitric Oxide Synthase Propagate Tuberculosis in Mice. J. Infect. Dis. 217, 1667–1671. https://doi.org/10.1093/infdis/jiy041

Santajit, S., Indrawattana, N., 2016. Mechanisms of Antimicrobial Resistance in ESKAPE Pathogens. Biomed Res Int 2016, 2475067. https://doi.org/10.1155/2016/2475067

Sarkhel, S., Shrivastava, S., 2017. The Effective Influence of Temperature on the Varied Characteristic of Silkworm: A Review. Asian J. Exp. Sci. 31, 31–37.

Sheehan, G., Garvey, A., Croke, M., Kavanagh, K., 2018. Innate humoral immune defences in mammals and insects: The same, with differences ? Virulence 9, 1625–1639. https://doi.org/10.1080/21505594.2018.1526531

Sheehan, G., Tully, L., Kavanagh, K.A., 2020. Candida albicans increases the pathogenicity of Staphylococcus aureus during polymicrobial infection of Galleria mellonella larvae. Microbiology (Reading, Engl.) 166, 375–385. https://doi.org/10.1099/mic.0.000892

Shimizu, T., Tsutsuki, H., Matsumoto, A., Nakaya, H., Noda, M., 2012. The nitric oxide reductase of enterohaemorrhagic Escherichia coli plays an important role for the survival within macrophages. Mol. Microbiol. 85, 492–512. https://doi.org/10.1111/j.1365-2958.2012.08122.x

Silva, L.N., Da Hora, G.C.A., Soares, T.A., Bojer, M.S., Ingmer, H., Macedo, A.J., Trentin, D.S., 2017. Myricetin protects Galleria mellonella against Staphylococcus aureus infection and inhibits multiple virulence factors. Sci Rep 7, 2823. https://doi.org/10.1038/s41598-017-02712-1

Siriyong, T., Voravuthikunchai, S.P., Coote, P.J., 2018. Steroidal alkaloids and conessine from the medicinal plant Holarrhena antidysenterica restore antibiotic efficacy in a Galleria mellonella model of multidrug-resistant Pseudomonas aeruginosa infection. BMC Complement Altern Med 18, 285. https://doi.org/10.1186/s12906-018-2348-9

Stenfors Arnesen, L.P., Fagerlund, A., Granum, P.E., 2008. From soil to gut: Bacillus cereus and its food poisoning toxins. FEMS Microbiol. Rev. 32, 579–606. https://doi.org/10.1111/j.1574-6976.2008.00112.x

Tacconelli, E., 2017. Global priority list of antibiotic-resistant bacteria to guide research, discovery, and development of new antibiotics.

Tacconelli, E., Carrara, E., Savoldi, A., Harbarth, S., Mendelson, M., Monnet, D.L., Pulcini, C., Kahlmeter, G., Kluytmans, J., Carmeli, Y., Ouellette, M., Outterson, K., Patel, J., Cavaleri, M., Cox, E.M., Houchens, C.R., Grayson, M.L., Hansen, P., Singh, N., Theuretzbacher, U., Magrini, N., WHO Pathogens Priority List Working Group, 2018. Discovery, research, and development of new antibiotics: the WHO priority list of antibiotic-resistant bacteria and tuberculosis. Lancet Infect Dis 18, 318–327. https://doi.org/10.1016/S1473-3099(17)30753-3

Tran, S.-L., Guillemet, E., Gohar, M., Lereclus, D., Ramarao, N., 2010. CwpFM (EntFM) is a Bacillus cereus potential cell wall peptidase implicated in adhesion, biofilm formation, and virulence. J. Bacteriol. 192, 2638–2642. https://doi.org/10.1128/JB.01315-09

Tran, S.-L., Guillemet, E., Ngo-Camus, M., Clybouw, C., Puhar, A., Moris, A., Gohar, M., Lereclus, D., Ramarao, N., 2011. Haemolysin II is a Bacillus cereus virulence factor that induces apoptosis of macrophages. Cell. Microbiol. 13, 92–108. https://doi.org/10.1111/j.1462-5822.2010.01522.x

Tran, S.-L., Lebreuilly, L., Cormontagne, D., Samson, S., Tô, T.B., Dervyn, R., Grießhammer, A., Akduman, N., Cuesta-Zuluaga, J.D.L., Maier, L., Naas, T., Mura, S., Nicolas, J., Rognan, D., André, G., Ramarao, N., n.d. An anti-virulence drug targeting the evolvability protein Mfd protects against infections with antimicrobial resistant ESKAPE pathogens (in revision). Cell Host and Microbes.

Trebosc, V., Lucchini, V., Narwal, M., Wicki, B., Gartenmann, S., Schellhorn, B., Schill, J., Bourotte, M., Frey, D., Grünberg, J., Trauner, A., Ferrari, L., Felici, A., Champion, O.L., Gitzinger, M., Lociuro, S., Kammerer, R.A., Kemmer, C., Pieren, M., 2022. Targeting virulence regulation to disarm Acinetobacter baumannii pathogenesis. Virulence 13, 1868–1883. https://doi.org/10.1080/21505594.2022.2135273

Wang, R.-J., Chen, K., Xing, L.-S., Lin, Z., Zou, Z., Lu, Z., 2020. Reactive oxygen species and antimicrobial peptides are sequentially produced in silkworm midgut in response to bacterial infection. Developmental & Comparative Immunology 110, 103720. https://doi.org/10.1016/j.dci.2020.103720

Waters, W.R., Palmer, M.V., Nonnecke, B.J., Whipple, D.L., Horst, R.L., 2004. Mycobacterium bovis infection of vitamin D-deficient NOS2-/- mice. Microb. Pathog. 36, 11–17. https://doi.org/10.1016/j.micpath.2003.08.008

Weber, G.G., Kortmann, J., Narberhaus, F., Klose, K.E., 2014. RNA thermometer controls temperature-dependent virulence factor expression in Vibrio cholerae. Proc. Natl. Acad. Sci. U.S.A. 111, 14241–14246. https://doi.org/10.1073/pnas.1411570111

Whelan, M.V.X., Ardill, L., Koide, K., Nakajima, C., Suzuki, Y., Simpson, J.C., Ó Cróinín, T., 2019. Acquisition of fluoroquinolone resistance leads to increased biofilm formation and pathogenicity in Campylobacter jejuni. Sci Rep 9, 18216. https://doi.org/10.1038/s41598-019-54620-1

Willcocks, S.J., Denman, C., Cia, F., McCarthy, E., Cuccui, J., Wren, B.W., 2020. Virulence of the emerging pathogen, Burkholderia pseudomallei, depends upon the O-linked oligosaccharyltransferase, PglL. Future Microbiol 15, 241–257. https://doi.org/10.2217/fmb-2019-0165

Wink, D.A., Hines, H.B., Cheng, R.Y.S., Switzer, C.H., Flores-Santana, W., Vitek, M.P., Ridnour, L.A., Colton, C.A., 2011. Nitric oxide and redox mechanisms in the immune response. J. Leukoc. Biol. 89, 873–891. https://doi.org/10.1189/jlb.1010550

Wood, S.J., Kuzel, T.M., Shafikhani, S.H., 2023. Pseudomonas aeruginosa: Infections, Animal Modeling, and Therapeutics. Cells 12, 199. https://doi.org/10.3390/cells12010199

Yadav, S., Pathak, S., Sarikhani, M., Majumdar, S., Ray, S., Chandrasekar, B.S., Adiga, V., Sundaresan, N.R., Nandi, D., 2018. Nitric oxide synthase 2 enhances the survival of mice during Salmonella Typhimurium infection-induced sepsis by increasing reactive oxygen species, inflammatory cytokines and recruitment of neutrophils to the peritoneal cavity. Free Radic. Biol. Med. 116, 73–87. https://doi.org/10.1016/j.freeradbiomed.2017.12.032

Yang, Y., Tang, H., Zhang, Y., Zhu, F., Lü, P., Yao, Q., Chen, K., 2018. Research progress on the immune mechanism of the silkworm Bombyx mori. Physiological Entomology 43, 159–168. https://doi.org/10.1111/phen.12241

Yoshitake, J., Akaike, T., Akuta, T., Tamura, F., Ogura, T., Esumi, H., Maeda, H., 2004. Nitric oxide as an endogenous mutagen for Sendai virus without antiviral activity. J Virol 78, 8709–8719. https://doi.org/10.1128/JVI.78.16.8709-8719.2004

Zaki, M.H., Akuta, T., Akaike, T., 2005. Nitric oxide-induced nitrative stress involved in microbial pathogenesis. J Pharmacol Sci 98, 117–129. https://doi.org/10.1254/jphs.crj05004x

Zhen, X., Lundborg, C.S., Sun, X., Hu, X., Dong, H., 2019. Economic burden of antibiotic resistance in ESKAPE organisms: a systematic review. Antimicrob Resist Infect Control 8, 137. https://doi.org/10.1186/s13756-019-0590-7

Zhuang, J.C., Lin, C., Lin, D., Wogan, G.N., 1998. Mutagenesis associated with nitric oxide production in macrophages. Proc Natl Acad Sci U S A 95, 8286–8291. https://doi.org/10.1073/pnas.95.14.8286

Figure and table legends

Table 1. Lethal doses of bacterial strains towards *Bombyx mori*

*ND=Not determined, because probabilities cannot be computed

Mortality data were analyzed with the Log-Probit program which tests the linearity of dose-mortality curves and provides lethal doses 50 and 90 (LD50 and LD90), which correspond to the bacterial dose that kill 50% and 90% of the larvae population, respectively.

Table 2. Lethal doses of bacterial strains towards *Galleria mellonella*

Mortality data were analyzed with the Log-Probit program which tests the linearity of dose-mortality curves and provides lethal doses 50 and 90 (LD50 and LD90), which correspond to the bacterial dose that kill 50% and 90% of the larvae population, respectively.

Table 3. Comparison of nitric oxide resistance of five clinical relevant pathogens

NO concentration that induced 50% (IC50) and 10% (IC10) of bacterial mortality, and the standard error (SE) were determined from the dose response curves using R.

Figure 1. Dose-dependent survival of silkworm larvae *Bombyx mori*

K. pneumoniae (A), *A. baumanii* (B), *E. coli* ATCC25922 (C), *S. aureus* (D), *P. aeruginosa* (E), *B. cereus* (F) were grown to late exponential growth phase and injected into fifth instar silkworm larvae at various doses (n=10/dose). Insect survival was recorded after 24 h and each culture of bacteria were plated before and after injection on LB agar to determine the real dose injected. Survival plot per dose (Log (CFU/larvae)) and the lethal doses 90 (LD_90) were determined using Log-Probit program. Data shown for each strain correspond to at least four independent experiments.

Figure 2. Dose-dependent survival of wax moth larvae *Galleria mellonella*

The survival rates of larvae infected by exponential growth phase *K. pneumoniae* (A), *A. baumanii* (B), *E. coli* ATCC25922 (C), *S. aureus* (D), *P. aeruginosa* (E), *B. cereus* (F) were measured (n=10 or 20/dose) 24 h after injection. Each culture of bacteria was plated before and after injection on LB agar to determine the real dose injected. Survival plot per dose (Log (CFU/larvae)) and the lethal doses 90 (LD_90) were determined using Log-Probit program. Data shown for each strain correspond to at least three independent experiments.

Figure 3. Efficacity assay of drugs in insects

P. aeruginosa CIP27853 was grown to late exponential phase in LB medium at 37°C and injected into forth instar silkworm larvae without or with meropenem (A) or NM102 (B). At 24 h post infection larvae were crushed and the content of each tube was serially diluted on LB plates for CFU numeration. Each

point represents one larva. P values are calculated against the condition wild type-strain without NM102, using Mann-Whitney test (**** $p < 0,0001$).

Figure 4. Measure of NO released by NOC-5 in a cell-free system

Dose range of NOC-5 (1000, 200, 250, 125, 63, 31, 16, 8, 4, 2µM) were added to RPMI and incubated for 4 h at 37 °C. Nitric oxide (NO) release were evaluated using 2 methods.

(A) The release of NO by NOC-5 was estimated using the fluorescent dye DCF-DA during 4 h. Values were expressed relative to the fluorescence signal of the control (0µM NOC-5). The data were presented as mean ± SD of at least four independent experiments.

(B) Formed nitrite was quantified as indicator of NO release using Griess assay. Accumulated nitrite formation was assessed at the beginning and 4 h after addition of NOC-5. For each time point, Abs540nm were normalized to the control sample (0 µM NOC-5). The quantitative data were presented as mean (µM) ± SD of four independent experiments.

Figure 5. Effect of increasing concentrations of NO on bacterial survival

K. pneumoniae (A), *A. baumannii* (B), *E. coli* ATCC25922 (C), *S. aureus* (D), *P. aeruginosa* (E) in exponential growth phase were exposed to increasing concentrations of NOC-5 generated-NO for 4 h at 37 °C (NOC-5 at 0, 2, 4, 8, 16, 31, 62, 125, 250, 1000 µM). Bacteria survival rate was quantified after plating on LB agar and by normalizing bacterial load in NOC-5-treated samples against control samples (0 µM of NOC-5). The results are reported as mean ± SD of at least four independent experiments.

(F) Comparison of bacterial survival for the 5 species with increasing concentrations of NO. NOC-5 concentration was transformed into Log10, and a non-linear fit with variable Hill slope was made using GraphPad Prism to obtain the NO dose response curves. Data are presented as means for at least four independent experiments.

Figure 6: Efficacy test in NO stress

Strains were grown to exponential phase in LB medium. Bacteria solution was prepared in RPMI medium and dispatched in 96-wells plate. Bacteria (A: *K. pneumoniae* ATCC 700603, B: *E. coli* ATCC 25922, C: *P. aeruginosa* CIP27853) were exposed for 4 h at 37°C to NOC5 as a NO donor. Bacteria survival rate was calculated by normalizing bacteria load against control without NM102. The results reported are mean ± SD of four independent experiments each in triplicates, P values are calculated against the condition without NM102, using One Way ANOVA (**** $P<0.0001$, *** $P<0.001$, ** $P<0.01$, * $P<0.05$). IC_{50} were computed using Graph Pad 7.05. (D) *K. pneumoniae* ATCC 700603 was exposed to NM102 (40 µM) and NOC 5 and bacterial growth was followed by measuring the $OD_{600\ nm}$ for 24 h. The results reported are mean ± SD of three independent experiments each in triplicates.

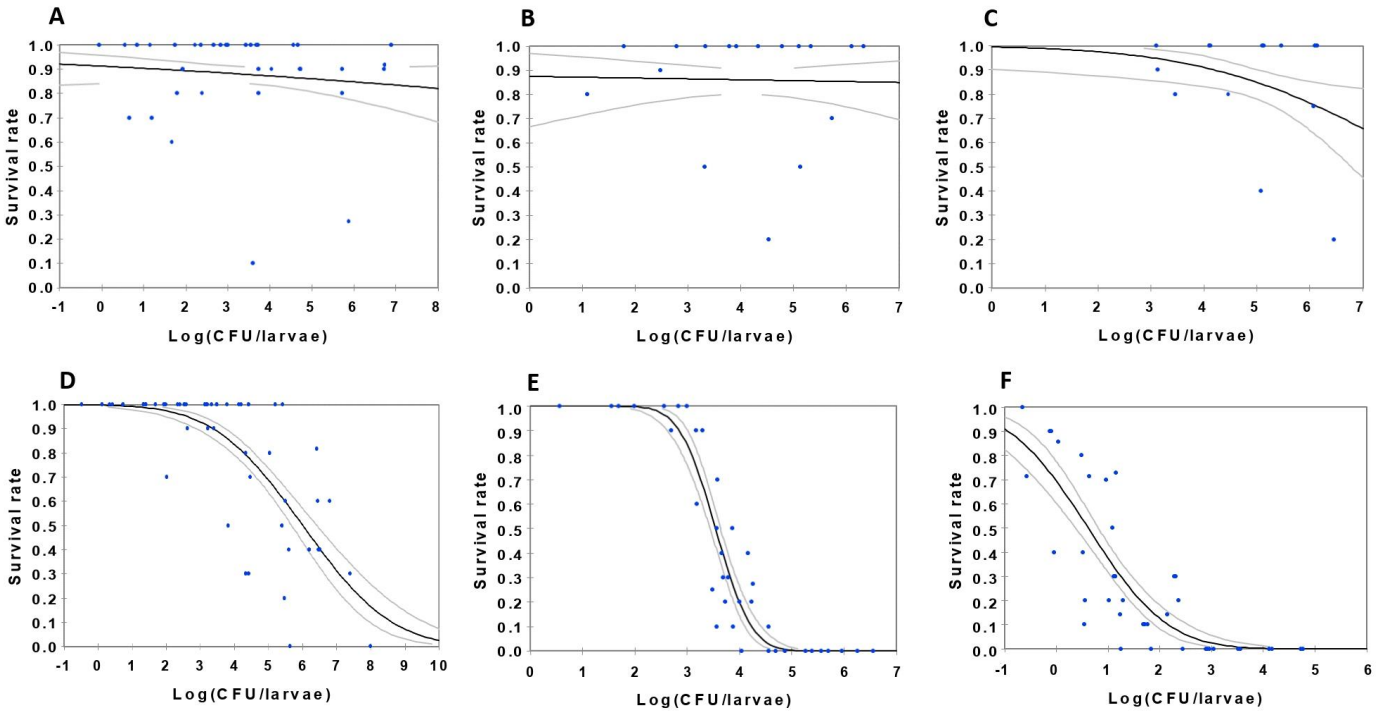
A
B
C
D
E
F
Survival rate
Log(CFU/larvae)

Fig 1

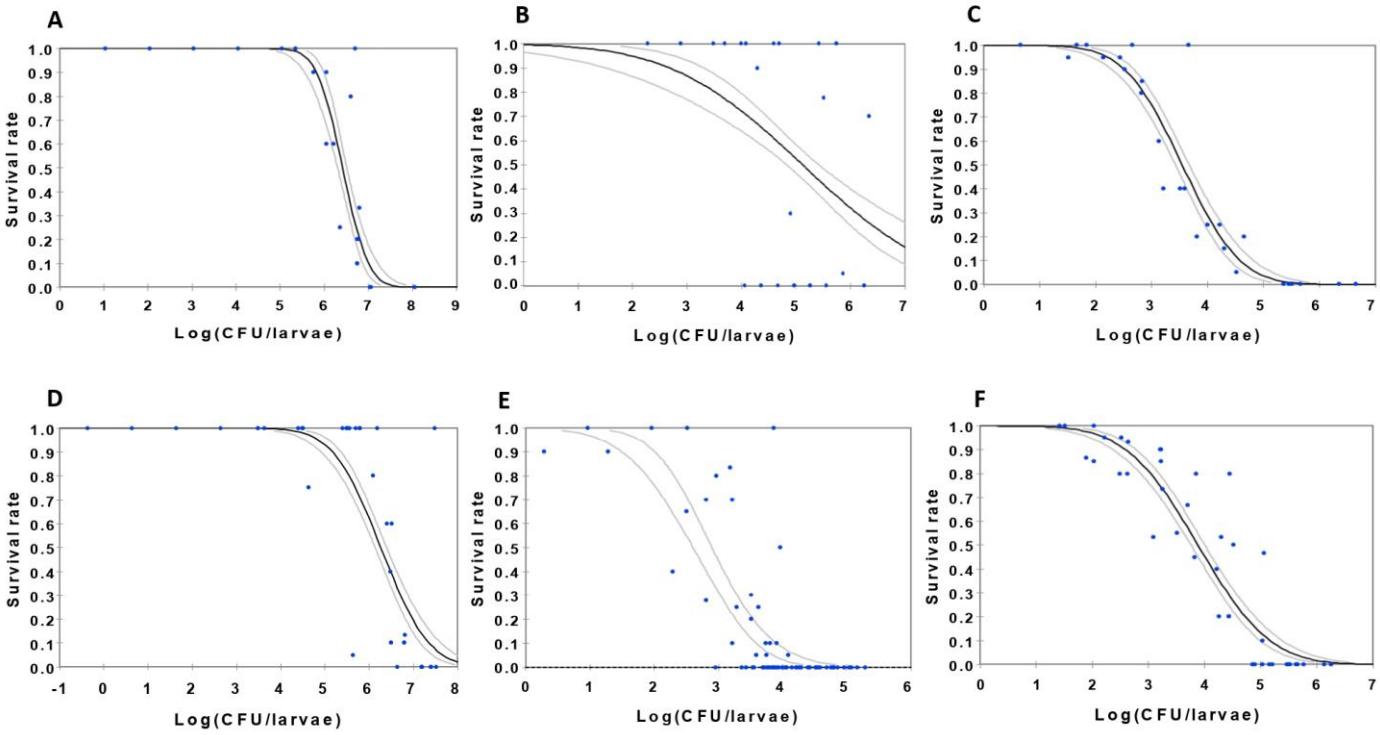
A
B
C
D
E
F
Survival rate
Log(CFU/larvae)

Fig 2

A

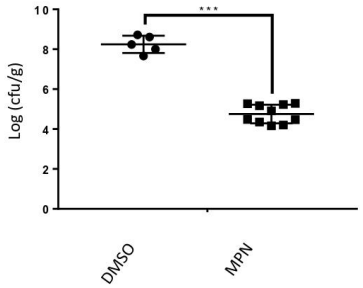

B

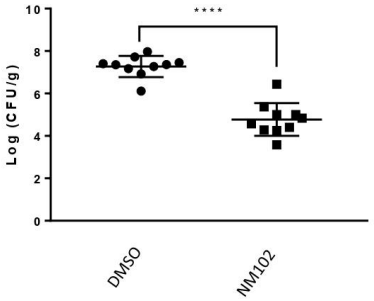

Fig 3

A

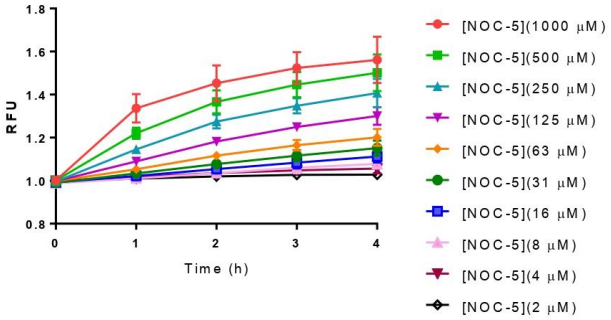

B

	T0		T4	
NOC-5 (μM)	Mean	SD	Mean	SD
1000	1778.21	234.319	1429.81	146.474
500	476.30	44.235	356.67	52.981
250	256.61	11.222	196.95	17.872
125	121.94	5.981	94.00	6.398
63	61.33	2.313	44.43	4.712
31	29.76	1.508	21.08	2.104
16	14.32	1.515	9.52	1.344
8	5.92	1.098	4.06	0.667
4	2.87	0.832	2.40	0.691
2	1.41	0.848	1.52	0.557

Fig 4

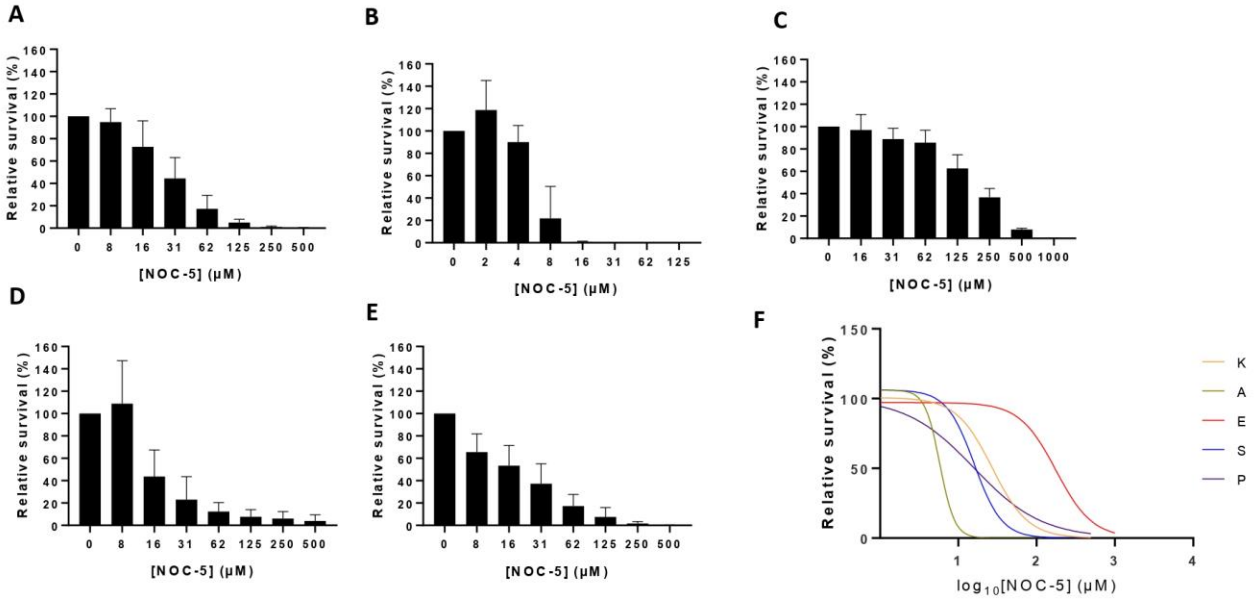
A
B
C
D
E
F
Relative survival (%)
[NOC-5] (µM)
log10[NOC-5] (µM)
K
A
E
S
P

Fig 5

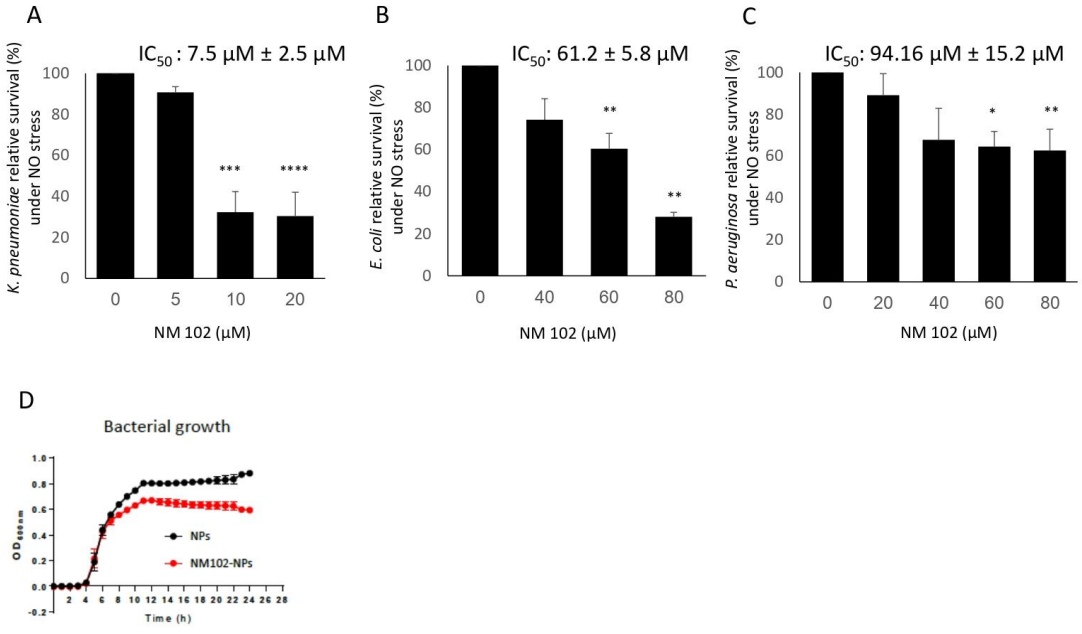
A
B
C
D
IC50 : 7.5 µM ± 2.5 µM
IC50: 61.2 ± 5.8 µM
IC50: 94.16 µM ± 15.2 µM
K. pneumoniae relative survival (%) under NO stress
E. coli relative survival (%) under NO stress
P. aeruginosa relative survival (%) under NO stress
NM 102 (µM)
Bacterial growth
NPs
NM102-NPs
Time (h)

Fig. 6

Bacterial strain	LD50 (CFU/larvae)	95% Confidence Interval	LD90 (CFU/larvae)	95% Confidence Interval
K. pneumoniae	ND	ND	ND	ND
A. baumannii	ND	ND	ND	ND
E. coli	1.97×10^{8}	[6.05×10^{6} ; 8.48×10^{19}]	2.40×10^{12}	[1.39×10^{9} ; 8.49×10^{38}]
S. aureus	1.00×10^{6}	[4.71×10^{5} ; 2.58×10^{6}]	4.22×10^{8}	[9.26×10^{7} ; 3.74×10^{9}]
P. aeruginosa	3.48×10^{3}	[2.74×10^{3} ; 4.23×10^{3}]	1.71×10^{4}	[1.26×10^{4} ; 2.60×10^{4}]
B. cereus	4.1	[2.35 ; 6.46]	1.45×10^{2}	[7.83×10^{1} ; 3.48×10^{2}]

Table 1 : Lethal doses of bacterial strains towards *Bombyx mori*
*ND=Not determined, because probabilities cannot be computed

Bacterial strain	LD50 (CFU/larvae)	95% Confidence Interval	LD90 (CFU/larvae)	95% Confidence Interval
K. pneumoniae	2.59×10^{6}	[2.00×10^{6} ; 3.23×10^{6}]	1.01×10^{7}	[7.41×10^{6} ; 1.62×10^{7}]
A. baumannii	1.32×10^{5}	[6.76×10^{4} ; 2.62×10^{5}]	3.57×10^{7}	[8.10×10^{6} ; 5.69×10^{8}]
E. coli	3.52×10^{3}	[2.66×10^{3} ; 4.69×10^{3}]	3.83×10^{4}	[2.49×10^{4} ; 6.66×10^{4}]
S. aureus	1.82×10^{6}	[1.36×10^{6} ; 2.46×10^{6}]	2.26×10^{7}	[1.43×10^{7} ; 4.17×10^{7}]
P. aeruginosa	5.79×10^{2}	[4.04×10^{2} ; 7.93×10^{2}]	5.42×10^{3}	[3.87×10^{3} ; 8.1×10^{3}]
B. cereus	7.64×10^{3}	[5.76×10^{3} ; 1.01×10^{4}]	1.48×10^{5}	[9.80×10^{4} ; 2.45×10^{5}]

Table 2 : Lethal doses of bacterial strains towards *Galleria mellonella*

	IC50 (µM)	SE	IC10 (µM)	SE
K. pneumoniae	27	2.24	8	1.55
A. baumanii	6	0.53	4	0.66
E. coli	176	15.19	54	11.32
S. aureus	16	1.87	7	1.69
P. aeruginosa	17	2.13	3	0.73

Table 3 : Comparison of nitric oxide resistance of five clinical relevant pathogens

4.1. Données supplémentaires

En plus de l'établissement des modèles présentés dans l'article, nous avons développé des modèles d'infections murins pour les cinq bactéries (*K. pneumoniae, A. baumannii, E. coli, S. aureus* et *P. aeruginosa*) du groupe ESKAPE. Nous avons utilisé la voie d'injection intra-péritonéale pour chacune des bactéries et nous avons pu voir que nous mimions une septicémie. Pour *K. pneumoniae* et *P. aeruginosa*, nous avons aussi effectué une infection par voie intranasale afin de mimer une pneumonie. Les organes des souris infectées ont été récupérés 24 h après infection afin de mesurer la charge bactérienne. Dans le modèle d'infection par voie intra-péritonéale, nous retrouvons des bactéries dans tous les organes prélevés (foie, rate, cœur, poumon et rein) (Figure 28). Et pour notre modèle d'infection par voie intranasale, nous ne retrouvons des bactéries que dans le poumon (Figure 28). Nous avons donc pu développer des modèles d'infections différents pour les bactéries du groupe ESKAPE. En comptant les modèles précédemment décris dans l'article, nous avons mis en place tout un panel d'outils permettant l'étude et le développement de nouveaux composés antimicrobiens.

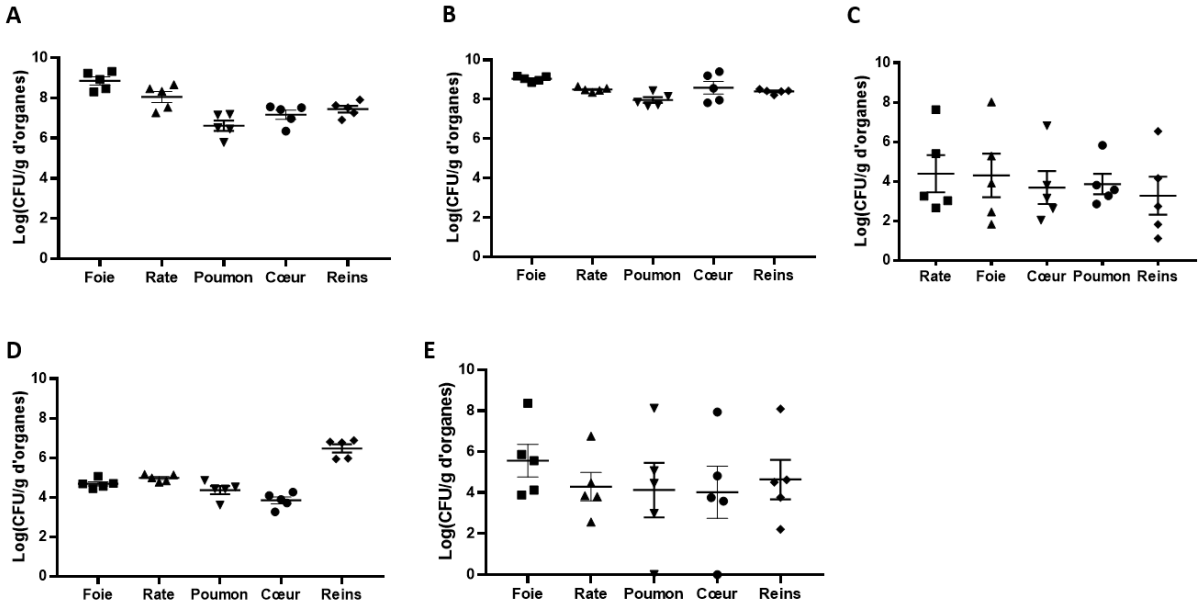

Figure 28 : Charge bactérienne dans des organes de souris C56BL/6J lors d'infections systémiques.
Des souris C56BL/6J âgées de 9 semaines ont été infectées par voie intra-péritonéale avec 2 x 10^8 CFU de K. pneumoniae (A), 1 x 10^8 CFU de A. baumannii (B), 4 x 10^6 CFU de E. coli ATCC25922 (C), 1 x 10^7 CFU de S. aureus (D) et 6 x 10^6 CFU de P. aeruginosa (E). Les organes ont été récupérés 24 h après l'infection. Les barres d'erreurs sont des SEM.

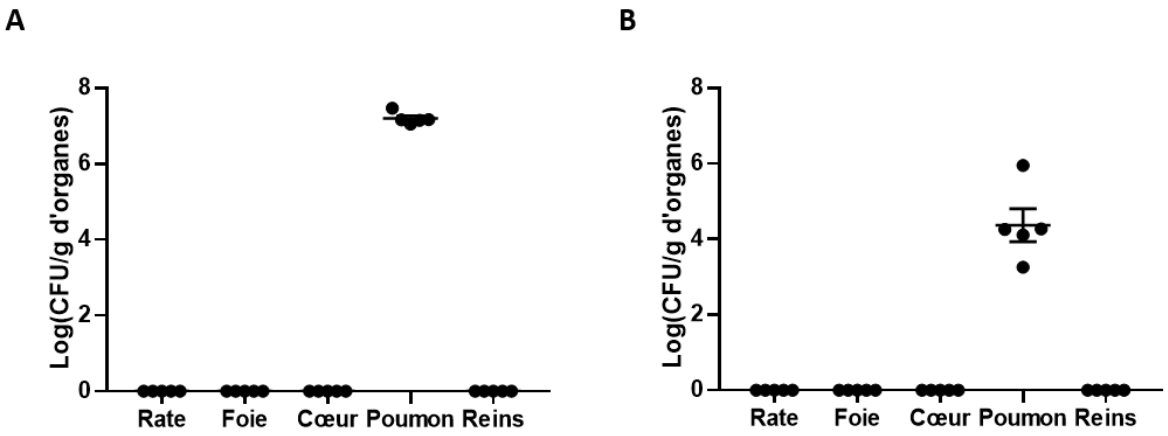

Figure 29 : Charge bactérienne dans des organes de souris C56BL/6J lors de pneumonie.
Des souris C56BL/6J âgées de 9 semaines ont été infectées par voie intra-nasale avec 1 x 10^7 CFU de K. pneumoniae (A), 1 x 10^6 CFU de P. aeruginosa (B). Les organes ont été récupérés 24 h après l'infection. Les barres d'erreurs sont des SEM.

CONCLUSION
&
DISCUSSION

Mfd est une protéine bactérienne conservée et impliquée dans de nombreux processus cellulaires tels que la réparation de l'ADN, la régulation de la transcription, la mutagénèse et la virulence. Ma thèse s'est déroulée autour de cette protéine où d'un côté j'ai voulu mieux comprendre son implication dans la virulence et de l'autre j'ai utilisé Mfd comme cible pour le développement de nouveaux composés anti-microbiens.

L'importance de *B. cereus* comme pathogène d'origine alimentaire et comme pathogène opportuniste a entrainé un besoin dans la compréhension de sa virulence. En effet, *B. cereus* est le 2ème agent responsable de TIAC en France et est responsable d'infections non gastro intestinales pouvant être asymptomatiques mais aussi provoquer des infections plus graves causant des lésions cérébrales ou encore des chocs septiques aboutissant au décès du patient. Ces infections graves sont principalement retrouvées chez les nouveau-nés et les personnes immunodéprimées qui sont particulièrement sensibles. Étant donné la variabilité de *B. cereus* en tant que pathogène, il est primordial de connaitre et d'étudier les facteurs qui rentrent en jeu dans sa virulence. Il existe déjà actuellement de nombreux facteurs identifiés qui lui sont associés. Néanmoins, ils n'expliquent pas toujours la totalité de la pathogénicité de *B. cereus*. Des souches présentant ces facteurs ne sont pas forcément virulentes. L'un des facteurs très peu étudié est la protéine Mfd. Notre équipe étudie Mfd en tant que tel et a pu montrer son importance dans la pathogénicité d'une souche de laboratoire de *B. cereus*. Je me suis focalisée sur l'étude de souches ayant une origine environnementale ou clinique afin de savoir si leur Mfd pourrait expliquer leur différence de pathogénicité. Sur les 22 souches étudiées, chacune d'entre elles possède le gène *mfd* et les deux présentant le plus de différences dans la séquence protéique de leur Mfd ont été sélectionnées pour étudier la virulence associée à Mfd : la souche S50 et la souche S53 (respectivement une souche environnementale et une souche clinique). J'ai pu montrer qu'il existait une différence de virulence entre ces deux souches et que cette virulence était bien liée à la séquence/structure de leur Mfd. Une étude *in silico* a été effectuée dans le but de comparer plus en détails les séquences protéiques des Mfd des souches S50 et S53. Il n'existe que 28 différences entre leurs séquences, ce qui nous laisse penser que la variation de la virulence entre les deux souches liées à Mfd se porterait sur quelques différences spécifiques. Sur ces 28 différences, quatre se sont montrées comme étant particulièrement intéressantes puisqu'elles pourraient induire une modification de la conformation ou une modification de l'activité de Mfd. J'ai cherché à savoir si ces quatre différences ont une importance dans la virulence de *B. cereus* associée à Mfd. Pour le moment, les résultats obtenus ne permettent pas de définir si elles sont bien à l'origine des différents niveaux de virulence des souches. Néanmoins, nous continuons actuellement à tester des mutants ayant des séquences hybrides entre S50 et S53 afin de mieux comprendre quelle partie de Mfd rentre en jeu

dans la virulence de *B. cereus*. Par ailleurs, une meilleure compréhension de la séquence de Mfd et des éléments associés à la virulence pourrait nous servir en tant que marqueur supplémentaire pour distinguer les souches non pathogènes des souches pathogènes. En plus de la compréhension de la séquence, il nous est important de comprendre aussi par quel moyen Mfd agi pour augmenter la virulence ou non d'une souche. On sait que Mfd est impliquée dans de nombreux processus cellulaires. Plusieurs d'entre eux pourraient avoir un impact sur la virulence d'une souche. La réparation de l'ADN est un processus essentiel pour la survie des bactéries lors d'une infection. Mfd a déjà été montrée comme étant importante dans la survie de *B. cereus* lors d'un stress nitrique en promouvant la réparation des dégâts causés par le NO (Guillemet et al. 2016). Est-ce qu'il y aurait donc une différence d'activité de Mfd entre les deux souches ? Est-il alors possible que la protéine Mfd de la souche S53 soit plus active que la protéine Mfd de la souche S50 ? Il serait intéressant de regarder par exemple l'activité ATPase de chacune des protéines afin de savoir s'il y a une différence entre les deux souches. Parmi les quatre différences auxquelles nous nous intéressons pour le moment, l'une d'entre elle se trouve au niveau du domaine D5. Il s'agit de la seule différence retrouvée sur ce domaine très conservé qui contient le motif ATPase. Il est donc possible que selon l'acide aminé présent en position 615, l'activité de la poche ATPase soit accrue ou diminuée. Nous savons aussi que le domaine D7 de Mfd sert de régulateur pour l'activité de la protéine. Dans le cycle fonctionnel de Mfd, lorsque le domaine D7 est en interaction avec le domaine D2, cela entraine un changement de conformation de la protéine rendant impossible son interaction avec UvrA et ainsi bloquant le recrutement des facteurs impliqués dans la voie de réparation de l'ADN par excision de nucléotides (Deaconescu, Savery, and Darst 2007). D'après notre étude des séquences de Mfd des souches S50 et S53, il y a trois différences présentes sur le domaine D7 et sept sur le domaine D2 (dont deux que nous avons sélectionnées comme pouvant entrainer une modification de la conformation de Mfd) entre les souches S50 et S53. Il n'est donc pas impossible qu'un changement de conformation de Mfd entraine une diminution ou une augmentation de son activité.

On peut aussi se demander si l'implication de Mfd dans la virulence est uniquement due à son rôle dans la réparation de l'ADN ou si elle agit sur différents niveaux. Par son rôle en tant que facteur de transcription, il est possible que, par des forces d'interactions différentes, le taux de transcription de certains gènes soit modifié entre les deux souches. Par exemple, CodY est un régulateur global de la transcription et il a été montré que Mfd permettrait de réduire la répression de ce facteur (Belitsky and Sonenshein 2011). Chez *B. cereus,* CodY a été montré comme régulant la transcription de certains gènes codant pour des facteurs de virulence comme *nhe*, *plcB* et *inhA2* qui sont sous-exprimés dans un mutant Δ*codY* par rapport au niveau d'expression de la souche sauvage. La virulence même de *B. cereus* est affectée par ce mutant puisque celui-ci est moins virulent dans un modèle d'infection

insecte (*G. mellonella*) que la souche sauvage (Frenzel et al. 2012). Etant donné que Mfd joue un rôle dans la régulation de l'expression de facteurs de virulence, il est possible que selon l'activité ou la conformation de la protéine, son impact de manière générale sur les processus cellulaires diffère d'une souche à une autre.

Le gène *mfd* est présent chez nos souches environnementales et cliniques, pourtant son impact sur la virulence n'est pas le même. Bien que son rôle dans la virulence soit visible, la relation séquence/structure/virulence reste encore un mystère. Il ne s'agit pas d'une présence ou d'une absence du gène. Il semblerait que son rôle dans la virulence soit plus complexe et jouerait sur une variation de son activité ou/et de sa conformation. Mfd est impliquée dans tellement de processus cellulaires qu'un changement sur la protéine pourrait avoir des conséquences sur des facteurs de virulence déjà identifiés et caractérisés. De plus, cela ne se restreint pas à *B. cereus* puisque j'ai pu aussi mettre en évidence le rôle de Mfd dans la virulence de *P. aeruginosa* dans un modèle d'infection d'insectes (*B. eri*) dans lequel un mutant est moins virulent qu'une souche sauvage. Mfd semble avoir aussi une fonction universelle dans la résistance au système immunitaire puisqu'elle est nécessaire à la survie de *B. cereus*, *K. pneumoniae* et *P. aeruginosa* lors d'un stress nitrique *in vitro*. Etant donné que Mfd est retrouvée chez toutes les bactéries, comprendre le fonctionnement de la protéine en détail est important pour comprendre un facteur de virulence qui pourrait être global et universel.

Le second aspect de ma thèse a été l'utilisation de Mfd en tant que cible pour le développement de composés antimicrobiens. Comme cité juste au-dessus, cette protéine est ubiquitaire et semble être un facteur de virulence universel en augmentant la résistance des bactéries au système immunitaire. Elle présente en plus l'avantage d'être absente chez les eucaryotes. L'inhibition de Mfd, par son rôle dans la mutagénèse, permettrait une diminution de la fréquence d'apparition de résistances aux antibiotiques et par son rôle dans la résistance au stress nitrique permettrait d'augmenter l'efficacité de la réponse immunitaire. Un inhibiteur de Mfd pourrait donc aussi être utilisé en combinaison avec des antibiotiques pré-existants pour renforcer leur efficacité en limitant l'émergence de résistances. Dans ce projet pluridisciplinaire impliquant de nombreux collaborateurs, de potentiels inhibiteurs ont été identifiés *in silico* et *in vitro*. *In silico*, un criblage a sélectionné des molécules interagissant avec la poche ATPase de Mfd qui est la partie de la protéine la plus conservée et est centrale à son activité. De plus, de manière générale, les poches ATPase sont connues comme pouvant être inhibées de manière spécifique (Kahraman et al. 2007). Ces molécules candidates ont ensuite été validées *in vitro* en mesurant leur pouvoir inhibant sur la poche ATPase de Mfd. Une molécule, le NM102, est ressortie comme ayant un fort potentiel inhibiteur. Mfd étant très conservée, on s'attend à ce qu'un inhibiteur de Mfd puisse agir contre de nombreuses espèces bactériennes. Des analyses *in silico* ont confirmé

que le NM102 était capable de se placer dans la poche ATPase des bactéries du groupe ESKAPE. Afin d'étudier l'effet de cette molécule sur ces pathogènes, il a fallu mettre en place différents modèles *in vitro* et *in vivo*. En effet, Mfd n'étant pas une protéine essentielle, il ne nous était pas possible d'établir une concentration minimale inhibitrice en suivant un protocole standard pour mesurer l'impact du NM102 sur la survie bactérienne. Nous avons donc mis en place un modèle *in vitro* où nous exposons les bactéries à un stress nitrique lors duquel nous savons que Mfd devient alors essentielle à leur survie (Darrigo et al. 2016). Le NO est une molécule produite lors de la réponse immunitaire qui est toxique pour les bactéries et induit notamment des dommages sur l'ADN (Porrini, Ramarao, and Tran 2020). Grâce à un donneur de NO nous avons pu mettre en place une expérience mimant un stress nitrique en utilisant des plaques 96 puits, ce qui facilite le criblage de multiples molécules en même temps, avec plusieurs doses de molécules et/ou d'oxyde nitrique. Ce modèle ne nécessite de plus pas l'utilisation de cellules, il nous est donc possible de comparer la résistance de bactéries à un stress nitrique sur des bactéries intra et extracellulaires. Nous avons testé l'effet du stress nitrique sur des bactéries ESKAPE et aucune d'entre elles ne présentent la même sensibilité à celui-ci mais dans tous les cas nous observons un effet dose. Plus nous ajoutons d'oxyde nitrique, moins les bactéries survivent. Grâce à cet effet dose, il est possible de calculer des concentrations inhibitrices adaptées pour tester l'efficacité de molécules d'intérêt. Nous avons donc testé l'effet du NM102 sur la survie bactérienne en condition de stress nitrique et celui-ci s'avère être efficace contre *K. pneumonia*, *E. coli* et *P. aeruginosa*. La molécule est même efficace contre des souches cliniques résistantes aux antibiotiques de *K. pneumoniae* et *E. coli*. En plus d'être efficace contre des bactéries ayant un intérêt clinique fort, le NM102 est aussi capable d'agir sur des souches difficiles à traiter actuellement. L'effet de notre molécule est uniquement visible en condition de stress nitrique. Sans ce stress, le NM102 n'induit pas de mortalité bactérienne. Le composé ne devrait pas cibler les bactéries localisées en dehors de la zone d'inflammation.

En plus de ce test *in vitro*, j'ai mis en place différents modèles *in vivo* d'infection d'insectes pour les bactéries du groupe ESKAPE. Ce modèle est intéressant à utiliser car les insectes ont une réponse immunitaire innée. Par exemple, *G. mellonella* a des hémocytes présentant des similarités avec les phagocytes des mammifères (Browne, Heelan, and Kavanagh 2013). Les insectes sont un bon modèle intermédiaire pour étudier la pathogénicité des bactéries sans avoir les contraintes éthiques rencontrées lors de l'utilisation des souris. Bien que ce modèle ne permette pas de remplacer le modèle murin, il présente plusieurs avantages dans le criblage de composés antimicrobiens. Avec ce modèle, nous pouvons plus facilement (1) tester plusieurs composés sur une gamme de doses plus importante, (2) effectuer différents modèles de traitement, (3) les insectes peuvent être infectés par l'intégralité du groupe ESKAPE selon l'espèce d'insecte choisie et (4) les expériences peuvent être

réalisées sur plus d'individus avant de passer chez la souris. Nous avons montré que chez *B. eri* infecté par *P. aeruginosa,* le NM102 est capable de réduire la charge bactérienne et que son effet est bien dû à une inhibition de Mfd puisque nous n'observons pas d'efficacité du composé chez un mutant Δ*mfd*.
Afin de confirmer l'efficacité et l'innocuité de nos molécules dans un modèle murin, nous avons mis en place des modèles d'infection chez la souris par voie intrapéritonéale pour quatre bactéries du groupe ESKAPE (*K. pneumoniae*, *A. baumannii*, *S. aureus* et *P. aeruginosa*) et des modèles d'infection par voie intranasale pour deux d'entre elles (*K. pneumoniae* et *P. aeruginosa*) afin de provoquer une pneumonie. La quantité de bactéries retrouvée dans les organes est corrélée avec la quantité de bactéries injectée et la voie d'administration utilisée. En effet, par voie intrapéritonéale, on retrouve des bactéries dans tous les organes récupérés (rate, foie, cœur, poumons et reins) tandis qu'avec la voie intranasale, on ne retrouve des bactéries que dans les poumons. Nous sommes donc capables d'ajuster le modèle murin pour différents types de pathologies.
L'efficacité du NM102 a ensuite été confirmée *in vivo* chez la souris dans ces modèles d'infection. Néanmoins, pour effectuer nos tests chez la souris, il nous a fallu trouver une solution concernant la faible solubilité du NM102. Jusqu'à présent, le solvant de re-suspension de la molécule était le DMSO mais pour la souris, celui-ci est toxique et aggrave les infections. Pour remédier à ce problème, nous avons établi une collaboration avec l'Institut Galien afin de procéder à une encapsulation du NM102 dans des nanoparticules. Il s'agit d'un vecteur d'administration largement proposé pour les composés très peu solubles qui est de plus en plus approuvé cliniquement (Anselmo and Mitragotri 2021). Ces nanoparticules peuvent être re-suspendues dans un milieu aqueux et donc utilisables dans notre modèle murin. Grace à cette encapsulation, nous avons pu montrer l'efficacité du NM102 chez la souris lors d'une infection par voie intranasale de *K. pneumoniae*. Par ailleurs, l'efficacité du NM102 est retrouvée pour la souche sauvage de *K. pneumoniae* mais pas lors d'une infection par la souche Δ*mfd*, montrant à nouveau la spécificité de notre molécule pour sa cible.
Avec une infection de *P. aeruginosa* par la même voie, nous avons aussi observé une efficacité de notre molécule, ainsi qu'une synergie lors d'un traitement combiné avec du méropénème. Il semblerait donc qu'un inhibiteur de Mfd puisse améliorer les traitements actuels avec un traitement en combinaison.
La molécule est en outre efficace contre des souches de *K. pneumoniae* et *P. aeruginosa* résistantes aux antibiotiques classiques. Cela ouvre un nouvel espoir de traitement contre les bactéries pathogènes multirésistantes et qui peuvent actuellement conduire à des impasses de traitements.
Les antibiotiques actuels ciblent les voies essentielles bactériennes ce qui les rendent très efficaces mais peu spécifiques. De ce fait, ils affectent même les bactéries de notre microbiome (Maier et al. 2021) qui est essentiel pour notre santé (digestion, métabolisme…) et qui nous protège contre des bactéries invasives. Etant donné que Mfd n'est pas essentielle à la survie bactérienne hors stress, son

inhibition ne devrait pas avoir d'impact sur le microbiome, sauf dans le cas d'une infection localisée au niveau de celui-ci. Pour vérifier cette hypothèse, nous nous sommes intéressés à l'impact du NM102 sur le microbiome des voies respiratoires supérieures et sur le microbiome intestinal. Le NM102 n'affecte pas la survie des bactéries testées et il n'affecte pas non plus la composition du microbiome intestinal. Les fèces de souris infectées par *K. pneumoniae* par voie nasale ont aussi été analysés et aucune différence dans la composition du microbiome intestinal n'a été retrouvée entre les souris non traitées et celles ayant reçu le NM012. Cela suggère qu'en dehors de la zone d'infection, les bactéries du microbiome ne devraient pas être impactées par le traitement. Cela constitue une nouveauté par rapport aux traitements classiquement utilisés en antibiothérapie et pourrait constituer une avancée majeure dans le développement de traitements qui prendraient en compte la santé globale du patient.
Outre son effet antimicrobien, nous avons testé l'impact du NM102 sur l'apparition de résistances aux antibiotiques. En effet, Mfd est connue pour jouer un rôle dans la mutagénèse des bactéries et notamment dans le développement de résistances aux antibiotiques auxquels elles sont exposées en concentration non létale (Ragheb et al. 2019). La diminution de la fréquence d'apparition de résistances à la rifampicine chez *E. coli* nous indique qu'un traitement par NM102 est capable d'inhiber la fonction de Mfd dans la mutagénèse.
D'après nos résultats, un inhibiteur de Mfd pourrait être utilisé seul ou en combinaison avec d'autres antibiotiques afin d'améliorer leur efficacité tout en réduisant l'apparition de résistance et en limitant l'impact sur le microbiome. Notre stratégie d'antivirulence est une alternative prometteuse à l'antibiothérapie classiquement utilisée puisque nous n'inhibons pas la croissance bactérienne, ni ne provoquons directement la mort de bactéries. À la place, l'antivirulence permet de bloquer la pathogénicité des bactéries ainsi que leur résistance au système immunitaire. De cette manière, les composés développés ne vont pas cibler des voies essentielles diminuant ainsi la pression sur l'apparition de résistance et leur impact sur le microbiome. L'antivirulence est une piste déjà utilisée dans le développement de nouveaux antibiotiques mais ceux-ci vont être efficaces sur une famille de bactéries spécifiques voire une seule espèce. Notre inhibiteur présenterait les avantages de la stratégie thérapeutique utilisant l'antivirulence tout en étant efficace sur un large panel de bactéries.
Actuellement, nous cherchons à améliorer le NM102 chimiquement afin d'obtenir une molécule plus efficace, plus soluble et pouvant plus facilement être encapsulée. Pour cela, nous avons testé une librairie d'analogues du NM102 par test ATPase afin de savoir s'ils étaient capables d'inhiber l'activité ATPase de Mfd. À l'issue de ces tests de nouveaux candidats sont ressortis. Lors de tests préliminaires, nous avons pu voir une efficacité chez l'insecte infecté par *P. aeruginosa* pour deux des analogues prometteurs et seulement l'un des deux a été efficace *in vitro* lors d'un stress nitrique sur *K. pneumoniae*. Néanmoins, on observe aussi en parallèle un effet bactéricide de ces molécules. C'est

pourquoi nous continuons de tester des analogues du NM102 afin de savoir quelle est la structure chimique essentielle à son efficacité et quelles sont les parties que nous pouvons modifier pour améliorer son effet, sa solubilité et qui permettrait une meilleure encapsulation.

En plus des tests que nous avons déjà effectués pour le NM102, il nous faudrait également regarder sa toxicité sur les cellules eucaryotes et sur un organisme vivant, la fréquence d'apparition de résistance au composé, son absorption, sa distribution dans l'organisme, comment il est métabolisé et éliminé. Il reste donc encore de nombreux tests à réaliser dans cette phase. C'est uniquement après toutes ces données qu'une molécule peut passer ou non en test clinique afin d'étudier la toxicité sur l'humain, la dose à administrer et les effets indésirables qu'elle pourrait provoquer. Même après les trois phases cliniques, il faut obtenir l'autorisation de mise sur le marché. Le développement d'un médicament est un processus long et qui n'aboutit pas forcément. Néanmoins, avec la crise de l'antibiorésistance en cours, il est nécessaire d'étudier et de développer de nouvelles solutions. De nombreuses molécules ne passeront jamais la phase pré-clinique mais le besoin en nouveaux antibiotiques est tellement important qu'il faut tout de même effectuer cette recherche et étudier toutes les pistes possibles afin de proposer des solutions dans cette crise. Il s'agit d'une de ces pistes que nous investiguons actuellement en prenant Mfd, une nouvelle cible ubiquitaire pour une nouvelle classe d'antibiotiques à large spectre. Les nouvelles molécules sur lesquelles nous travaillons pourraient être une arme supplémentaire dans le combat contre les bactéries sensibles ou résistantes aux antibiotiques.

BIBLIOGRAPHIE

. 1999. *The Use of Drugs in Food Animals: Benefits and Risks* (Washington (DC)).

Agaisse, H., M. Gominet, O. A. Okstad, A. B. Kolsto, and D. Lereclus. 1999. 'PlcR is a pleiotropic regulator of extracellular virulence factor gene expression in Bacillus thuringiensis', *Mol Microbiol*, 32: 1043-53.

Agata, N., M. Mori, M. Ohta, S. Suwan, I. Ohtani, and M. Isobe. 1994. 'A novel dodecadepsipeptide, cereulide, isolated from Bacillus cereus causes vacuole formation in HEp-2 cells', *FEMS Microbiol Lett*, 121: 31-4.

Agata, N., M. Ohta, M. Mori, and M. Isobe. 1995. 'A novel dodecadepsipeptide, cereulide, is an emetic toxin of Bacillus cereus', *FEMS Microbiol Lett*, 129: 17-20.

Akanbi, O. E., H. A. Njom, J. Fri, A. C. Otigbu, and A. M. Clarke. 2017. 'Antimicrobial Susceptibility of Staphylococcus aureus Isolated from Recreational Waters and Beach Sand in Eastern Cape Province of South Africa', *Int J Environ Res Public Health*, 14.

Akesson, A., S. A. Hedstrom, and T. Ripa. 1991. 'Bacillus cereus: a significant pathogen in postoperative and post-traumatic wounds on orthopaedic wards', *Scand J Infect Dis*, 23: 71-7.

Alonzo, D. A., N. A. Magarvey, and T. M. Schmeing. 2015. 'Characterization of cereulide synthetase, a toxin-producing macromolecular machine', *PLoS One*, 10: e0128569.

Andreeva, Z. I., V. F. Nesterenko, I. S. Yurkov, Z. I. Budarina, E. V. Sineva, and A. S. Solonin. 2006. 'Purification and cytotoxic properties of Bacillus cereus hemolysin II', *Protein Expr Purif*, 47: 186-93.

Anselmo, A. C., and S. Mitragotri. 2021. 'Nanoparticles in the clinic: An update post COVID-19 vaccines', *Bioeng Transl Med*, 6: e10246.

Antimicrobial Resistance, Collaborators. 2022. 'Global burden of bacterial antimicrobial resistance in 2019: a systematic analysis', *Lancet*, 399: 629-55.

'AR-301 (Tosatoxumab)' https://www.aridispharma.com/ar-301/.

Arnaout, M. K., R. F. Tamburro, S. M. Bodner, J. T. Sandlund, G. K. Rivera, C. H. Pui, and R. C. Ribeiro. 1999. 'Bacillus cereus causing fulminant sepsis and hemolysis in two patients with acute leukemia', *J Pediatr Hematol Oncol*, 21: 431-5.

Assenmacher, N., K. Wenig, A. Lammens, and K. P. Hopfner. 2006. 'Structural basis for transcription-coupled repair: the N terminus of Mfd resembles UvrB with degenerate ATPase motifs', *J Mol Biol*, 355: 675-83.

Aubry Damon H, Carlet J, Courvalin P, Desenclos J C, Drucker J, Guillemot D, Jarlier V, Régnier B, Schlemmer B. 2000. 'La résistance bactérienne aux antibiotiques en France : une priorité en santé publique', *Euro Surveill*.

Auger, S., N. Ramarao, C. Faille, A. Fouet, S. Aymerich, and M. Gohar. 2009. 'Biofilm formation and cell surface properties among pathogenic and nonpathogenic strains of the Bacillus cereus group', *Appl Environ Microbiol*, 75: 6616-8.

Avashia, S. B., W. S. Riggins, C. Lindley, A. Hoffmaster, R. Drumgoole, T. Nekomoto, P. J. Jackson, K. K. Hill, K. Williams, L. Lehman, M. C. Libal, P. P. Wilkins, J. Alexander, A. Tvaryanas, and T. Betz. 2007. 'Fatal pneumonia among metalworkers due to inhalation exposure to Bacillus cereus Containing Bacillus anthracis toxin genes', *Clin Infect Dis*, 44: 414-6.

Barbara H. Knowles, David J. Ellar. 1987. 'Colloid-osmotic lysis is a general feature of the mechanism of action of Bacillus thuringiensis δ-endotoxins with different insect specificity

', *Biochimica et Biophysica Acta (BBA)*, 924: 509-18.

Bargabus, R. L., N. K. Zidack, J. E. Sherwood, and B. J. Jacobsen. 2003. 'Oxidative burst elicited by Bacillus mycoides isolate Bac J, a biological control agent, occurs independently of hypersensitive cell death in sugar beet', *Mol Plant Microbe Interact*, 16: 1145-53.

Barrie, D., P. N. Hoffman, J. A. Wilson, and J. M. Kramer. 1994. 'Contamination of hospital linen by Bacillus cereus', *Epidemiol Infect*, 113: 297-306.

Beecher, D. J., and J. D. MacMillan. 1990. 'A novel bicomponent hemolysin from Bacillus cereus', *Infect Immun*, 58: 2220-7.

Beecher, D. J,. and J. D. Macmillan. 1991. 'Characterization of the components of hemolysin BL from Bacillus cereus', *Infect Immun*, 59: 1778-84.
Beecher, D. J., J. S. Pulido, N. P. Barney, and A. C. Wong. 1995. 'Extracellular virulence factors in Bacillus cereus endophthalmitis: methods and implication of involvement of hemolysin BL', *Infect Immun*, 63: 632-9.
Beecher, D. J., and A. C. Wong. 1997. 'Tripartite hemolysin BL from Bacillus cereus. Hemolytic analysis of component interactions and a model for its characteristic paradoxical zone phenomenon', *J Biol Chem*, 272: 233-9.
Beecher, D. J., and A. C. L. Wong. 2000. 'Tripartite haemolysin BL: isolation and characterization of two distinct homologous sets of components from a single Bacillus cereus isolate', *Microbiology (Reading)*, 146 (Pt 6): 1371-80.
Belitsky, B. R., and A. L. Sonenshein. 2011. 'Roadblock repression of transcription by Bacillus subtilis CodY', *J Mol Biol*, 411: 729-43.
Beloor Suresh, A., A. Rosani, and R. Wadhwa. 2022. 'Rifampin.' in, *StatPearls* (Treasure Island (FL)).
Blondeau, J. M. 2004. 'Fluoroquinolones: mechanism of action, classification, and development of resistance', *Surv Ophthalmol*, 49 Suppl 2: S73-8.
Bordeaux, Université de. 2019. 'Antibiotique', *Université de Bordeaux*.
Bottone, E. J. 2010. 'Bacillus cereus, a volatile human pathogen', *Clin Microbiol Rev*, 23: 382-98.
Bravo, A., S. S. Gill, and M. Soberon. 2007. 'Mode of action of Bacillus thuringiensis Cry and Cyt toxins and their potential for insect control', *Toxicon*, 49: 423-35.
Bravo, A., S. Likitvivatanavong, S. S. Gill, and M. Soberon. 2011. 'Bacillus thuringiensis: A story of a successful bioinsecticide', *Insect Biochem Mol Biol*, 41: 423-31.
Browne, N., M. Heelan, and K. Kavanagh. 2013. 'An analysis of the structural and functional similarities of insect hemocytes and mammalian phagocytes', *Virulence*, 4: 597-603.
Brunel, J. 1951. 'Antibiosis from Pasteur to Fleming', *J Hist Med Allied Sci*, 6: 287-301.
Bryce, E. A., J. A. Smith, M. Tweeddale, B. J. Andruschak, and M. R. Maxwell. 1993. 'Dissemination of Bacillus cereus in an intensive care unit', *Infect Control Hosp Epidemiol*, 14: 459-62.
Bush, K., and G. A. Jacoby. 2010. 'Updated functional classification of beta-lactamases', *Antimicrob Agents Chemother*, 54: 969-76.
Callegan, M. C., M. C. Booth, B. D. Jett, and M. S. Gilmore. 1999. 'Pathogenesis of gram-positive bacterial endophthalmitis', *Infect Immun*, 67: 3348-56.
Caron, P. R., S. R. Kushner, and L. Grossman. 1985. 'Involvement of helicase II (uvrD gene product) and DNA polymerase I in excision mediated by the uvrABC protein complex', *Proc Natl Acad Sci U S A*, 82: 4925-9.
Carroll, L. M., R. A. Cheng, M. Wiedmann, and J. Kovac. 2022. 'Keeping up with the Bacillus cereus group: taxonomy through the genomics era and beyond', *Crit Rev Food Sci Nutr*, 62: 7677-702.
Cars, O. 2014. 'Securing access to effective antibiotics for current and future generations. Whose responsibility?', *Ups J Med Sci*, 119: 209-14.
Cegelski, L., G. R. Marshall, G. R. Eldridge, and S. J. Hultgren. 2008. 'The biology and future prospects of antivirulence therapies', *Nat Rev Microbiol*, 6: 17-27.
Ceuppens, S., N. Boon, and M. Uyttendaele. 2013. 'Diversity of Bacillus cereus group strains is reflected in their broad range of pathogenicity and diverse ecological lifestyles', *FEMS Microbiol Ecol*, 84: 433-50.
Chakroun, M., N. Banyuls, Y. Bel, B. Escriche, and J. Ferre. 2016. 'Bacterial Vegetative Insecticidal Proteins (Vip) from Entomopathogenic Bacteria', *Microbiol Mol Biol Rev*, 80: 329-50.
Chambers, A. L., A. J. Smith, and N. J. Savery. 2003. 'A DNA translocation motif in the bacterial transcription--repair coupling factor, Mfd', *Nucleic Acids Res*, 31: 6409-18.
Charlton, S., A. J. Moir, L. Baillie, and A. Moir. 1999. 'Characterization of the exosporium of Bacillus cereus', *J Appl Microbiol*, 87: 241-5.

Chayot, R., B. Montagne, D. Mazel, and M. Ricchetti. 2010. 'An end-joining repair mechanism in Escherichia coli', *Proc Natl Acad Sci U S A*, 107: 2141-6.

Chitlaru, T., O. Gat, Y. Gozlan, N. Ariel, and A. Shafferman. 2006. 'Differential proteomic analysis of the Bacillus anthracis secretome: distinct plasmid and chromosome CO2-dependent cross talk mechanisms modulate extracellular proteolytic activities', *J Bacteriol*, 188: 3551-71.

Chopra, I., and M. Roberts. 2001. 'Tetracycline antibiotics: mode of action, applications, molecular biology, and epidemiology of bacterial resistance', *Microbiol Mol Biol Rev*, 65: 232-60 ; second page, table of contents.

Chung, M. C., T. G. Popova, B. A. Millis, D. V. Mukherjee, W. Zhou, L. A. Liotta, E. F. Petricoin, V. Chandhoke, C. Bailey, and S. G. Popov. 2006. 'Secreted neutral metalloproteases of Bacillus anthracis as candidate pathogenic factors', *J Biol Chem*, 281: 31408-18.

Clavel, T., F. Carlin, D. Lairon, C. Nguyen-The, and P. Schmitt. 2004. 'Survival of Bacillus cereus spores and vegetative cells in acid media simulating human stomach', *J Appl Microbiol*, 97: 214-9.

Cohen, M. L. 2000. 'Changing patterns of infectious disease', *Nature*, 406: 762-7.

Collignon, P. J., and S. A. McEwen. 2019. 'One Health-Its Importance in Helping to Better Control Antimicrobial Resistance', *Trop Med Infect Dis*, 4.

Colmer, J. A., J. A. Fralick, and A. N. Hamood. 1998. 'Isolation and characterization of a putative multidrug resistance pump from Vibrio cholerae', *Mol Microbiol*, 27: 63-72.

Cormontagne, D., V. Rigourd, J. Vidic, F. Rizzotto, E. Bille, and N. Ramarao. 2021. 'Bacillus cereus Induces Severe Infections in Preterm Neonates: Implication at the Hospital and Human Milk Bank Level', *Toxins (Basel)*, 13.

Cornaglia, G., A. Mazzariol, R. Fontana, and G. Satta. 1996. 'Diffusion of carbapenems through the outer membrane of enterobacteriaceae and correlation of their activities with their periplasmic concentrations', *Microb Drug Resist*, 2: 273-6.

Cusumano, C. K., J. S. Pinkner, Z. Han, S. E. Greene, B. A. Ford, J. R. Crowley, J. P. Henderson, J. W. Janetka, and S. J. Hultgren. 2011. 'Treatment and prevention of urinary tract infection with orally active FimH inhibitors', *Sci Transl Med*, 3: 109ra15.

Dalhammar, G., and H. Steiner. 1984. 'Characterization of inhibitor A, a protease from Bacillus thuringiensis which degrades attacins and cecropins, two classes of antibacterial proteins in insects', *Eur J Biochem*, 139: 247-52.

Dalhus, B., J. K. Laerdahl, P. H. Backe, and M. Bjoras. 2009. 'DNA base repair--recognition and initiation of catalysis', *FEMS Microbiol Rev*, 33: 1044-78.

Darrigo, C., E. Guillemet, R. Dervyn, and N. Ramarao. 2016. 'The Bacterial Mfd Protein Prevents DNA Damage Induced by the Host Nitrogen Immune Response in a NER-Independent but RecBC-Dependent Pathway', *PLoS One*, 11: e0163321.

Deaconescu, A. M., A. L. Chambers, A. J. Smith, B. E. Nickels, A. Hochschild, N. J. Savery, and S. A. Darst. 2006. 'Structural basis for bacterial transcription-coupled DNA repair', *Cell*, 124: 507-20.

Deaconescu, A. M., N. Savery, and S. A. Darst. 2007. 'The bacterial transcription repair coupling factor', *Curr Opin Struct Biol*, 17: 96-102.

Delmas G, Gallay A, Espie E, Haeghebaert S, Pihier N, Weill FX, de Valk H, Vaillant V, Desenclos JC. 2006. 'Les toxi-infections alimentaires collectives en France entre 1996 et 2005', *Bulletin Epidémiologique Hebdomadaire*, 51-51: 418-22.

Dervyn, R., D. W. Kavanaugh, D. Cormontagne, B. Glasset, and N. Ramarao. 2021. 'Identification of a New Pathogenicity Island Within the Large pAH187_270 Plasmid Involved in Bacillus cereus Virulence', *Front Cell Infect Microbiol*, 11: 788757.

Dierick, K., E. Van Coillie, I. Swiecicka, G. Meyfroidt, H. Devlieger, A. Meulemans, G. Hoedemaekers, L. Fourie, M. Heyndrickx, and J. Mahillon. 2005. 'Fatal family outbreak of Bacillus cereus-associated food poisoning', *J Clin Microbiol*, 43: 4277-9.

DiGiandomenico, A., A. E. Keller, C. Gao, G. J. Rainey, P. Warrener, M. M. Camara, J. Bonnell, R. Fleming, B. Bezabeh, N. Dimasi, B. R. Sellman, J. Hilliard, C. M. Guenther, V. Datta, W. Zhao, C. Gao, X.

Q. Yu, J. A. Suzich, and C. K. Stover. 2014. 'A multifunctional bispecific antibody protects against Pseudomonas aeruginosa', *Sci Transl Med*, 6: 262ra155.
Dillingham, M. S., and S. C. Kowalczykowski. 2008. 'RecBCD enzyme and the repair of double-stranded DNA breaks', *Microbiol Mol Biol Rev*, 72: 642-71, Table of Contents.
Dixon, T. C., M. Meselson, J. Guillemin, and P. C. Hanna. 1999. 'Anthrax', *N Engl J Med*, 341: 815-26.
Drobniewski, F. A. 1993. 'Bacillus cereus and related species', *Clin Microbiol Rev*, 6: 324-38.
Ebomah, K. E., and A. I. Okoh. 2020. 'Detection of Carbapenem-Resistance Genes in Klebsiella Species Recovered from Selected Environmental Niches in the Eastern Cape Province, South Africa', *Antibiotics (Basel)*, 9.
ECDC. 2022. 'Antimicrobial Resistance in the EU/EEA - A One Health response'.
Ehling-Schulz, M., M. Fricker, and S. Scherer. 2004. 'Bacillus cereus, the causative agent of an emetic type of food-borne illness', *Mol Nutr Food Res*, 48: 479-87.
Ehling-Schulz, M., M. H. Guinebretiere, A. Monthan, O. Berge, M. Fricker, and B. Svensson. 2006. 'Toxin gene profiling of enterotoxic and emetic Bacillus cereus', *FEMS Microbiol Lett*, 260: 232-40.
Fagerlund, A., J. Brillard, R. Furst, M. H. Guinebretiere, and P. E. Granum. 2007. 'Toxin production in a rare and genetically remote cluster of strains of the Bacillus cereus group', *BMC Microbiol*, 7: 43.
Fagerlund, A., O. Ween, T. Lund, S. P. Hardy, and P. E. Granum. 2004. 'Genetic and functional analysis of the cytK family of genes in Bacillus cereus', *Microbiology (Reading)*, 150: 2689-97.
Faille, C., T. Benezech, G. Midelet-Bourdin, Y. Lequette, M. Clarisse, G. Ronse, A. Ronse, and C. Slomianny. 2014. 'Sporulation of Bacillus spp. within biofilms: a potential source of contamination in food processing environments', *Food Microbiol*, 40: 64-74.
Fawcett, P., P. Eichenberger, R. Losick, and P. Youngman. 2000. 'The transcriptional profile of early to middle sporulation in Bacillus subtilis', *Proc Natl Acad Sci U S A*, 97: 8063-8.
Fedhila, S., N. Daou, D. Lereclus, and C. Nielsen-LeRoux. 2006. 'Identification of Bacillus cereus internalin and other candidate virulence genes specifically induced during oral infection in insects', *Mol Microbiol*, 62: 339-55.
Filippov, V. D., and E. E. Zagoruiko. 1978. 'Study of MFD in Bacillus subtilis', *Mutat Res*, 52: 49-56.
Fleming, A. 2001. 'On the antibacterial action of cultures of a penicillium, with special reference to their use in the isolation of B. influenzae. 1929', *Bull World Health Organ*, 79: 780-90.
Flemming, H. C., and J. Wingender. 2010. 'The biofilm matrix', *Nat Rev Microbiol*, 8: 623-33.
France, Santé publique. 2021. 'Surveillance des toxi-infections alimentaires collectives (TIAC). Données de la déclaration obligatoire, 2019'.
Frenzel, E., V. Doll, M. Pauthner, G. Lucking, S. Scherer, and M. Ehling-Schulz. 2012. 'CodY orchestrates the expression of virulence determinants in emetic Bacillus cereus by impacting key regulatory circuits', *Mol Microbiol*, 85: 67-88.
Fujita, M., J. E. Gonzalez-Pastor, and R. Losick. 2005. 'High- and low-threshold genes in the Spo0A regulon of Bacillus subtilis', *J Bacteriol*, 187: 1357-68.
Galperin, M. Y., S. L. Mekhedov, P. Puigbo, S. Smirnov, Y. I. Wolf, and D. J. Rigden. 2012. 'Genomic determinants of sporulation in Bacilli and Clostridia: towards the minimal set of sporulation-specific genes', *Environ Microbiol*, 14: 2870-90.
Gelpi, A., A. Gilbertson, and J. D. Tucker. 2015. 'Magic bullet: Paul Ehrlich, Salvarsan and the birth of venereology', *Sex Transm Infect*, 91: 68-9.
Gill, M. J., S. Simjee, K. Al-Hattawi, B. D. Robertson, C. S. Easmon, and C. A. Ison. 1998. 'Gonococcal resistance to beta-lactams and tetracycline involves mutation in loop 3 of the porin encoded at the penB locus', *Antimicrob Agents Chemother*, 42: 2799-803.
Gilmore, M. S., A. L. Cruz-Rodz, M. Leimeister-Wachter, J. Kreft, and W. Goebel. 1989. 'A Bacillus cereus cytolytic determinant, cereolysin AB, which comprises the phospholipase C and sphingomyelinase genes: nucleotide sequence and genetic linkage', *J Bacteriol*, 171: 744-53.

Glasset, B., S. Herbin, L. Guillier, S. Cadel-Six, M. Vigaud, J. Grout, S. Pairaud, V. Michel, J. Hennekinne, N. Ramarao and A. Brisabois. 2016. ' Bacillus cereus-induced food-borne outbreaks in France, 2007 to 2014: epidemiology and genetic characterisation', *Euro surveillance : bulletin Europeen sur les maladies transmissibles = European communicable disease bulletin,* 21(48), 30413.

Gohar, M., K. Faegri, S. Perchat, S. Ravnum, O. A. Okstad, M. Gominet, A. B. Kolsto, and D. Lereclus. 2008. 'The PlcR virulence regulon of Bacillus cereus', *PLoS One*, 3: e2793.

Gohar, M., O. A. Okstad, N. Gilois, V. Sanchis, A. B. Kolsto, and D. Lereclus. 2002. 'Two-dimensional electrophoresis analysis of the extracellular proteome of Bacillus cereus reveals the importance of the PlcR regulon', *Proteomics*, 2: 784-91.

Gomez-Marroquin, M., H. A. Martin, A. Pepper, M. E. Girard, A. A. Kidman, C. Vallin, R. E. Yasbin, M. Pedraza-Reyes, and E. A. Robleto. 2016. 'Stationary-Phase Mutagenesis in Stressed Bacillus subtilis Cells Operates by Mfd-Dependent Mutagenic Pathways', *Genes (Basel)*, 7.

Gopal, N., C. Hill, P. R. Ross, T. P. Beresford, M. A. Fenelon, and P. D. Cotter. 2015. 'The Prevalence and Control of Bacillus and Related Spore-Forming Bacteria in the Dairy Industry', *Front Microbiol*, 6: 1418.

Granum, P. E., and T. Lund. 1997. 'Bacillus cereus and its food poisoning toxins', *FEMS Microbiol Lett*, 157: 223-8.

Granum, P. E., K. O'Sullivan, and T. Lund. 1999. 'The sequence of the non-haemolytic enterotoxin operon from Bacillus cereus', *FEMS Microbiol Lett*, 177: 225-9.

Grau, R. R., P. de Ona, M. Kunert, C. Lenini, R. Gallegos-Monterrosa, E. Mhatre, D. Vileta, V. Donato, T. Holscher, W. Boland, O. P. Kuipers, and A. T. Kovacs. 2015. 'A Duo of Potassium-Responsive Histidine Kinases Govern the Multicellular Destiny of Bacillus subtilis', *mBio*, 6: e00581.

Grundmann, H., M. Aires-de-Sousa, J. Boyce, and E. Tiemersma. 2006. 'Emergence and resurgence of meticillin-resistant Staphylococcus aureus as a public-health threat', *Lancet*, 368: 874-85.

Guerin, A., H. T. Ronning, C. Dargaignaratz, T. Clavel, V. Broussolle, J. Mahillon, P. E. Granum, and C. Nguyen-The. 2017. 'Cereulide production by Bacillus weihenstephanensis strains during growth at different pH values and temperatures', *Food Microbiol*, 65: 130-35.

Guidi-Rontani, C., M. Weber-Levy, E. Labruyere, and M. Mock. 1999. 'Germination of Bacillus anthracis spores within alveolar macrophages', *Mol Microbiol*, 31: 9-17.

Guillemet, E., C. Cadot, S. L. Tran, M. H. Guinebretiere, D. Lereclus, and N. Ramarao. 2010. 'The InhA metalloproteases of Bacillus cereus contribute concomitantly to virulence', *J Bacteriol*, 192: 286-94.

Guillemet, E., A. Lereec, S. L. Tran, C. Royer, I. Barbosa, P. Sansonetti, D. Lereclus, and N. Ramarao. 2016. 'The bacterial DNA repair protein Mfd confers resistance to the host nitrogen immune response', *Sci Rep*, 6: 29349.

Guinebretiere, M. H., S. Auger, N. Galleron, M. Contzen, B. De Sarrau, M. L. De Buyser, G. Lamberet, A. Fagerlund, P. E. Granum, D. Lereclus, P. De Vos, C. Nguyen-The, and A. Sorokin. 2013. 'Bacillus cytotoxicus sp. nov. is a novel thermotolerant species of the Bacillus cereus Group occasionally associated with food poisoning', *Int J Syst Evol Microbiol*, 63: 31-40.

Ha, K. P., and A. M. Edwards. 2021. 'DNA Repair in Staphylococcus aureus', *Microbiol Mol Biol Rev*, 85: e0009121.

Haas, L. F. 1999. 'Papyrus of Ebers and Smith', *J Neurol Neurosurg Psychiatry*, 67: 578.

Hakemi Vala, M., M. Hallajzadeh, A. Hashemi, H. Goudarzi, M. Tarhani, M. Sattarzadeh Tabrizi, and F. Bazmi. 2014. 'Detection of Ambler class A, B and D ss-lactamases among Pseudomonas aeruginosa and Acinetobacter baumannii clinical isolates from burn patients', *Ann Burns Fire Disasters*, 27: 8-13.

Hamon, M. A., and B. A. Lazazzera. 2001. 'The sporulation transcription factor Spo0A is required for biofilm development in Bacillus subtilis', *Mol Microbiol*, 42: 1199-209.

Han, J., O. Sahin, Y. W. Barton, and Q. Zhang. 2008. 'Key role of Mfd in the development of fluoroquinolone resistance in Campylobacter jejuni', *PLoS Pathog*, 4: e1000083.

Hardy, S. P., T. Lund, and P. E. Granum. 2001. 'CytK toxin of Bacillus cereus forms pores in planar lipid bilayers and is cytotoxic to intestinal epithelia', *FEMS Microbiol Lett*, 197: 47-51.

Haydar, A., S. L. Tran, E. Guillemet, C. Darrigo, S. Perchat, D. Lereclus, L. Coquet, T. Jouenne, and N. Ramarao. 2018. 'InhA1-Mediated Cleavage of the Metalloprotease NprA Allows Bacillus cereus to Escape From Macrophages', *Front Microbiol*, 9: 1063.

Helgason, E., O. A. Okstad, D. A. Caugant, H. A. Johansen, A. Fouet, M. Mock, I. Hegna, and A. B. Kolsto. 2000. 'Bacillus anthracis, Bacillus cereus, and Bacillus thuringiensis--one species on the basis of genetic evidence', *Appl Environ Microbiol*, 66: 2627-30.

Hemady, R., M. Zaltas, B. Paton, C. S. Foster, and A. S. Baker. 1990. 'Bacillus-induced endophthalmitis: new series of 10 cases and review of the literature', *Br J Ophthalmol*, 74: 26-9.

Hernaiz, C., A. Picardo, J. I. Alos, and J. L. Gomez-Garces. 2003. 'Nosocomial bacteremia and catheter infection by Bacillus cereus in an immunocompetent patient', *Clin Microbiol Infect*, 9: 973-5.

Ho, H. N., A. M. van Oijen, and H. Ghodke. 2018. 'The transcription-repair coupling factor Mfd associates with RNA polymerase in the absence of exogenous damage', *Nat Commun*, 9: 1570.

Hoffmaster, A. R., K. K. Hill, J. E. Gee, C. K. Marston, B. K. De, T. Popovic, D. Sue, P. P. Wilkins, S. B. Avashia, R. Drumgoole, C. H. Helma, L. O. Ticknor, R. T. Okinaka, and P. J. Jackson. 2006. 'Characterization of Bacillus cereus isolates associated with fatal pneumonias: strains are closely related to Bacillus anthracis and harbor B. anthracis virulence genes', *J Clin Microbiol*, 44: 3352-60.

Hoton, F. M., N. Fornelos, E. N'Guessan, X. Hu, I. Swiecicka, K. Dierick, E. Jaaskelainen, M. Salkinoja-Salonen, and J. Mahillon. 2009. 'Family portrait of Bacillus cereus and Bacillus weihenstephanensis cereulide-producing strains', *Environ Microbiol Rep*, 1: 177-83.

Houry, A., R. Briandet, S. Aymerich, and M. Gohar. 2010. 'Involvement of motility and flagella in Bacillus cereus biofilm formation', *Microbiology (Reading)*, 156: 1009-18.

Houry, A., M. Gohar, J. Deschamps, E. Tischenko, S. Aymerich, A. Gruss, and R. Briandet. 2012. 'Bacterial swimmers that infiltrate and take over the biofilm matrix', *Proc Natl Acad Sci U S A*, 109: 13088-93.

Hrenovic, J., G. Durn, M. S. Music, S. Dekic, T. Troskot-Corbic, and D. Skoric. 2017. 'Extensively and multi drug-resistant Acinetobacter baumannii recovered from technosol at a dump site in Croatia', *Sci Total Environ*, 607-608: 1049-55.

Hsueh, P. R., L. J. Teng, P. C. Yang, H. L. Pan, S. W. Ho, and K. T. Luh. 1999. 'Nosocomial pseudoepidemic caused by Bacillus cereus traced to contaminated ethyl alcohol from a liquor factory', *J Clin Microbiol*, 37: 2280-4.

Hu, X., G. Van der Auwera, S. Timmery, L. Zhu, and J. Mahillon. 2009. 'Distribution, diversity, and potential mobility of extrachromosomal elements related to the Bacillus anthracis pXO1 and pXO2 virulence plasmids', *Appl Environ Microbiol*, 75: 3016-28.

Huovinen, P., L. Sundstrom, G. Swedberg, and O. Skold. 1995. 'Trimethoprim and sulfonamide resistance', *Antimicrob Agents Chemother*, 39: 279-89.

Hussain, M. A., and C. O. Dawson. 2013. 'Economic Impact of Food Safety Outbreaks on Food Businesses', *Foods*, 2: 585-89.

Hutchings, M. I., A. W. Truman, and B. Wilkinson. 2019. 'Antibiotics: past, present and future', *Curr Opin Microbiol*, 51: 72-80.

Imai, Y., K. J. Meyer, A. Iinishi, Q. Favre-Godal, R. Green, S. Manuse, M. Caboni, M. Mori, S. Niles, M. Ghiglieri, C. Honrao, X. Ma, J. J. Guo, A. Makriyannis, L. Linares-Otoya, N. Bohringer, Z. G. Wuisan, H. Kaur, R. Wu, A. Mateus, A. Typas, M. M. Savitski, J. L. Espinoza, A. O'Rourke, K. E. Nelson, S. Hiller, N. Noinaj, T. F. Schaberle, A. D'Onofrio, and K. Lewis. 2019. 'A new antibiotic selectively kills Gram-negative pathogens', *Nature*, 576: 459-64.

Jensen, G. B., B. M. Hansen, J. Eilenberg, and J. Mahillon. 2003. 'The hidden lifestyles of Bacillus cereus and relatives', *Environ Microbiol*, 5: 631-40.

Jimenez, G., A. R. Blanch, J. Tamames, and R. Rossello-Mora. 2013. 'Complete Genome Sequence of Bacillus toyonensis BCT-7112T, the Active Ingredient of the Feed Additive Preparation Toyocerin', *Genome Announc*, 1.

Kahraman, A., R. J. Morris, R. A. Laskowski, and J. M. Thornton. 2007. 'Shape variation in protein binding pockets and their ligands', *J Mol Biol*, 368: 283-301.

Kapoor, G., S. Saigal, and A. Elongavan. 2017. 'Action and resistance mechanisms of antibiotics: A guide for clinicians', *J Anaesthesiol Clin Pharmacol*, 33: 300-05.

Kato, K., Y. Matsumura, M. Yamamoto, M. Nagao, Y. Ito, S. Takakura, and S. Ichiyama. 2016. 'Erratum to: Seasonal trend and clinical presentation of Bacillus cereus bloodstream infection: association with summer and indwelling catheter', *Eur J Clin Microbiol Infect Dis*, 35: 875-83.

Kavanaugh, D. W., B. Glasset, R. Dervyn, C. Guerin, S. Plancade, S. Herbin, A. Brisabois, P. Nicolas, and N. Ramarao. 2022. 'New genetic biomarkers to differentiate non-pathogenic from clinically relevant Bacillus cereus strains', *Clin Microbiol Infect*, 28: 137 e1-37 e8.

Kawatani, E., Y. Kishikawa, C. Sankoda, N. Kuwahara, D. Mori, K. Osoegawa, E. Matsuishi, and H. Gondo. 2009. '[Bacillus cereus sepsis and subarachnoid hemorrhage following consolidation chemotherapy for acute myelogenous leukemia]', *Rinsho Ketsueki*, 50: 300-3.

Kemnic, T. R., and M. Coleman. 2022. 'Trimethoprim Sulfamethoxazole.' in, *StatPearls* (Treasure Island (FL)).

Krause, K. M., A. W. Serio, T. R. Kane, and L. E. Connolly. 2016. 'Aminoglycosides: An Overview', *Cold Spring Harb Perspect Med*, 6.

Kumar, A., and H. P. Schweizer. 2005. 'Bacterial resistance to antibiotics: active efflux and reduced uptake', *Adv Drug Deliv Rev*, 57: 1486-513.

Kumar, S., M. M. Mukherjee, and M. F. Varela. 2013. 'Modulation of Bacterial Multidrug Resistance Efflux Pumps of the Major Facilitator Superfamily', *Int J Bacteriol*, 2013.

Kuroda, T., and T. Tsuchiya. 2009. 'Multidrug efflux transporters in the MATE family', *Biochim Biophys Acta*, 1794: 763-8.

Kuroki, R., K. Kawakami, L. Qin, C. Kaji, K. Watanabe, Y. Kimura, C. Ishiguro, S. Tanimura, Y. Tsuchiya, I. Hamaguchi, M. Sakakura, S. Sakabe, K. Tsuji, M. Inoue, and H. Watanabe. 2009. 'Nosocomial bacteremia caused by biofilm-forming Bacillus cereus and Bacillus thuringiensis', *Intern Med*, 48: 791-6.

Kutima, P. M., and P. M. Foegeding. 1987. 'Involvement of the spore coat in germination of Bacillus cereus T spores', *Appl Environ Microbiol*, 53: 47-52.

Kuzminov, A. 1999. 'Recombinational repair of DNA damage in Escherichia coli and bacteriophage lambda', *Microbiol Mol Biol Rev*, 63: 751-813, table of contents.

Lam, S. J., N. M. O'Brien-Simpson, N. Pantarat, A. Sulistio, E. H. Wong, Y. Y. Chen, J. C. Lenzo, J. A. Holden, A. Blencowe, E. C. Reynolds, and G. G. Qiao. 2016. 'Combating multidrug-resistant Gram-negative bacteria with structurally nanoengineered antimicrobial peptide polymers', *Nat Microbiol*, 1: 16162.

Lambert, P. A. 2002. 'Cellular impermeability and uptake of biocides and antibiotics in Gram-positive bacteria and mycobacteria', *J Appl Microbiol*, 92 Suppl: 46S-54S.

Lapidus, A., E. Goltsman, S. Auger, N. Galleron, B. Segurens, C. Dossat, M. L. Land, V. Broussolle, J. Brillard, M. H. Guinebretiere, V. Sanchis, C. Nguen-The, D. Lereclus, P. Richardson, P. Wincker, J. Weissenbach, S. D. Ehrlich, and A. Sorokin. 2008. 'Extending the Bacillus cereus group genomics to putative food-borne pathogens of different toxicity', *Chem Biol Interact*, 171: 236-49.

Le, T. T., Y. Yang, C. Tan, M. M. Suhanovsky, R. M. Fulbright, Jr., J. T. Inman, M. Li, J. Lee, S. Perelman, J. W. Roberts, A. M. Deaconescu, and M. D. Wang. 2018. 'Mfd Dynamically Regulates Transcription via a Release and Catch-Up Mechanism', *Cell*, 173: 1823.

Lechner, S., R. Mayr, K. P. Francis, B. M. Pruss, T. Kaplan, E. Wiessner-Gunkel, G. S. Stewart, and S. Scherer. 1998. 'Bacillus weihenstephanensis sp. nov. is a new psychrotolerant species of the Bacillus cereus group', *Int J Syst Bacteriol*, 48 Pt 4: 1373-82.

Lee, G. H., J. Y. Jeong, J. W. Chung, W. H. Nam, S. M. Lee, J. H. Pak, K. D. Choi, H. J. Song, H. Y. Jung, and J. H. Kim. 2009. 'The Helicobacter pylori Mfd protein is important for antibiotic resistance and DNA repair', *Diagn Microbiol Infect Dis*, 65: 454-6.

Lereclus, D., H. Agaisse, C. Grandvalet, S. Salamitou, and M. Gominet. 2000. 'Regulation of toxin and virulence gene transcription in Bacillus thuringiensis', *Int J Med Microbiol*, 290: 295-9.

Li, X. Z., H. Nikaido, and K. Poole. 1995. 'Role of mexA-mexB-oprM in antibiotic efflux in Pseudomonas aeruginosa', *Antimicrob Agents Chemother*, 39: 1948-53.

Lindsay, D., V. S. Brozel, and A. Von Holy. 2006. 'Biofilm-spore response in Bacillus cereus and Bacillus subtilis during nutrient limitation', *J Food Prot*, 69: 1168-72.

Ling, L. L., T. Schneider, A. J. Peoples, A. L. Spoering, I. Engels, B. P. Conlon, A. Mueller, T. F. Schaberle, D. E. Hughes, S. Epstein, M. Jones, L. Lazarides, V. A. Steadman, D. R. Cohen, C. R. Felix, K. A. Fetterman, W. P. Millett, A. G. Nitti, A. M. Zullo, C. Chen, and K. Lewis. 2015. 'A new antibiotic kills pathogens without detectable resistance', *Nature*, 517: 455-9.

Liu, X., Y. Jiang, X. Chen, J. Li, D. Shi, and D. Xin. 2014. 'Drug resistance mechanisms of Mycoplasma pneumoniae to macrolide antibiotics', *Biomed Res Int*, 2014: 320801.

Lodge, J. M., S. D. Minchin, L. J. Piddock, and S. J. Busby. 1990. 'Cloning, sequencing and analysis of the structural gene and regulatory region of the Pseudomonas aeruginosa chromosomal ampC beta-lactamase', *Biochem J*, 272: 627-31.

Lopez, A. C., J. Minnaard, P. F. Perez, and A. M. Alippi. 2015. 'A case of intoxication due to a highly cytotoxic Bacillus cereus strain isolated from cooked chicken', *Food Microbiol*, 46: 195-99.

Lund, T., M. L. De Buyser, and P. E. Granum. 2000. 'A new cytotoxin from Bacillus cereus that may cause necrotic enteritis', *Mol Microbiol*, 38: 254-61.

Mah, T. F. 2012. 'Biofilm-specific antibiotic resistance', *Future Microbiol*, 7: 1061-72.

Mahler, H., A. Pasi, J. M. Kramer, P. Schulte, A. C. Scoging, W. Bar, and S. Krahenbuhl. 1997. 'Fulminant liver failure in association with the emetic toxin of Bacillus cereus', *N Engl J Med*, 336: 1142-8.

Maier, L., C. V. Goemans, J. Wirbel, M. Kuhn, C. Eberl, M. Pruteanu, P. Muller, S. Garcia-Santamarina, E. Cacace, B. Zhang, C. Gekeler, T. Banerjee, E. E. Anderson, A. Milanese, U. Lober, S. K. Forslund, K. R. Patil, M. Zimmermann, B. Stecher, G. Zeller, P. Bork, and A. Typas. 2021. 'Unravelling the collateral damage of antibiotics on gut bacteria', *Nature*, 599: 120-24.

Marrone, Pamela G. 1994. 'Present and future use of Bacillus thuringiensis in integrated pest management systems: An industrial perspective', *Biocontrol Science and Technology*, 4: 517-26.

Martin, H. A., M. Pedraza-Reyes, R. E. Yasbin, and E. A. Robleto. 2011. 'Transcriptional de-repression and Mfd are mutagenic in stressed Bacillus subtilis cells', *J Mol Microbiol Biotechnol*, 21: 45-58.

Martin, H. A., A. Sundararajan, T. S. Ermi, R. Heron, J. Gonzales, K. Lee, D. Anguiano-Mendez, F. Schilkey, M. Pedraza-Reyes, and E. A. Robleto. 2021. 'Mfd Affects Global Transcription and the Physiology of Stressed Bacillus subtilis Cells', *Front Microbiol*, 12: 625705.

Martin, J. K., 2nd, J. P. Sheehan, B. P. Bratton, G. M. Moore, A. Mateus, S. H. Li, H. Kim, J. D. Rabinowitz, A. Typas, M. M. Savitski, M. Z. Wilson, and Z. Gitai. 2020. 'A Dual-Mechanism Antibiotic Kills Gram-Negative Bacteria and Avoids Drug Resistance', *Cell*, 181: 1518-32 e14.

Mercer, A. 2021. 'Protection against severe infectious disease in the past', *Pathog Glob Health*, 115: 151-67.

Messelhausser, U., E. Frenzel, C. Blochinger, R. Zucker, P. Kampf, and M. Ehling-Schulz. 2014. 'Emetic Bacillus cereus are more volatile than thought: recent foodborne outbreaks and prevalence studies in Bavaria (2007-2013)', *Biomed Res Int*, 2014: 465603.

Michael, I., L. Rizzo, C. S. McArdell, C. M. Manaia, C. Merlin, T. Schwartz, C. Dagot, and D. Fatta-Kassinos. 2013. 'Urban wastewater treatment plants as hotspots for the release of antibiotics in the environment: a review', *Water Res*, 47: 957-95.

Mikkola, R., N. E. Saris, P. A. Grigoriev, M. A. Andersson, and M. S. Salkinoja-Salonen. 1999. 'Ionophoretic properties and mitochondrial effects of cereulide: the emetic toxin of B. cereus', *Eur J Biochem*, 263: 112-7.

Milla, C. E., J. F. Chmiel, F. J. Accurso, D. R. VanDevanter, M. W. Konstan, G. Yarranton, D. E. Geller, and K. B. Study Group. 2014. 'Anti-PcrV antibody in cystic fibrosis: a novel approach targeting Pseudomonas aeruginosa airway infection', *Pediatr Pulmonol*, 49: 650-8.

Miller, J. M., J. G. Hair, M. Hebert, L. Hebert, F. J. Roberts, Jr., and R. S. Weyant. 1997. 'Fulminating bacteremia and pneumonia due to Bacillus cereus', *J Clin Microbiol*, 35: 504-7.

Miller, W. R., J. M. Munita, and C. A. Arias. 2014. 'Mechanisms of antibiotic resistance in enterococci', *Expert Rev Anti Infect Ther*, 12: 1221-36.

Million-Weaver, S., A. N. Samadpour, D. A. Moreno-Habel, P. Nugent, M. J. Brittnacher, E. Weiss, H. S. Hayden, S. I. Miller, I. Liachko, and H. Merrikh. 2015. 'An underlying mechanism for the increased mutagenesis of lagging-strand genes in Bacillus subtilis', *Proc Natl Acad Sci U S A*, 112: E1096-105.

Miyoshi, S., and S. Shinoda. 2000. 'Microbial metalloproteases and pathogenesis', *Microbes Infect*, 2: 91-8.

Moayeri, M., D. Haines, H. A. Young, and S. H. Leppla. 2003. 'Bacillus anthracis lethal toxin induces TNF-alpha-independent hypoxia-mediated toxicity in mice', *J Clin Invest*, 112: 670-82.

Mock, M., and A. Fouet. 2001. 'Anthrax', *Annu Rev Microbiol*, 55: 647-71.

Molle, V., M. Fujita, S. T. Jensen, P. Eichenberger, J. E. Gonzalez-Pastor, J. S. Liu, and R. Losick. 2003. 'The Spo0A regulon of Bacillus subtilis', *Mol Microbiol*, 50: 1683-701.

Moolenaar, G. F., M. F. Herron, V. Monaco, G. A. van der Marel, J. H. van Boom, R. Visse, and N. Goosen. 2000. 'The role of ATP binding and hydrolysis by UvrB during nucleotide excision repair', *J Biol Chem*, 275: 8044-50.

Moravek, M., R. Dietrich, C. Buerk, V. Broussolle, M. H. Guinebretiere, P. E. Granum, C. Nguyen-The, and E. Martlbauer. 2006. 'Determination of the toxic potential of Bacillus cereus isolates by quantitative enterotoxin analyses', *FEMS Microbiol Lett*, 257: 293-8.

Moyer, A. L., R. T. Ramadan, B. D. Novosad, R. Astley, and M. C. Callegan. 2009. 'Bacillus cereus-induced permeability of the blood-ocular barrier during experimental endophthalmitis', *Invest Ophthalmol Vis Sci*, 50: 3783-93.

Murphy, M. N., P. Gong, K. Ralto, L. Manelyte, N. J. Savery, and K. Theis. 2009. 'An N-terminal clamp restrains the motor domains of the bacterial transcription-repair coupling factor Mfd', *Nucleic Acids Res*, 37: 6042-53.

Murphy, P. B., K. G. Bistas, and J. K. Le. 2022. 'Clindamycin.' in, *StatPearls* (Treasure Island (FL)).

Naranjo, M., S. Denayer, N. Botteldoorn, L. Delbrassinne, J. Veys, J. Waegenaere, N. Sirtaine, R. B. Driesen, K. R. Sipido, J. Mahillon, and K. Dierick. 2011. 'Sudden death of a young adult associated with Bacillus cereus food poisoning', *J Clin Microbiol*, 49: 4379-81.

Ngamwongsatit, P., W. Buasri, P. Pianariyanon, C. Pulsrikarn, M. Ohba, A. Assavanig, and W. Panbangred. 2008. 'Broad distribution of enterotoxin genes (hblCDA, nheABC, cytK, and entFM) among Bacillus thuringiensis and Bacillus cereus as shown by novel primers', *Int J Food Microbiol*, 121: 352-6.

Nishikawa, T., Y. Okamoto, T. Tanabe, Y. Kodama, Y. Shinkoda, and Y. Kawano. 2009. 'Critical illness polyneuropathy after Bacillus cereus sepsis in acute lymphoblastic leukemia', *Intern Med*, 48: 1175-7.

O'Neill, Jim. 2016. 'Tackling Drug-Resistant Infections Globally: final report and recommendations'.

Organization, World Health. 1998. 'Emerging and other communicable diseases: antimicrobial resistance', *World Health Assembly, 51.*

Otten, H. 1986. 'Domagk and the development of the sulphonamides', *J Antimicrob Chemother*, 17: 689-96.

Paananen, A., R. Mikkola, T. Sareneva, S. Matikainen, M. Hess, M. Andersson, I. Julkunen, M. S. Salkinoja-Salonen, and T. Timonen. 2002. 'Inhibition of human natural killer cell activity by cereulide, an emetic toxin from Bacillus cereus', *Clin Exp Immunol*, 129: 420-8.

Pages, J. M. 2004. '[Bacterial porin and antibiotic susceptibility]', *Med Sci (Paris)*, 20: 346-51.

Palma, L., D. Munoz, C. Berry, J. Murillo, and P. Caballero. 2014. 'Bacillus thuringiensis toxins: an overview of their biocidal activity', *Toxins (Basel)*, 6: 3296-325.

Park, J. S., M. T. Marr, and J. W. Roberts. 2002. 'E. coli Transcription repair coupling factor (Mfd protein) rescues arrested complexes by promoting forward translocation', *Cell*, 109: 757-67.

Patel, P. H., and M. F. Hashmi. 2022. 'Macrolides.' in, *StatPearls* (Treasure Island (FL)).

Patrick J. Piggot, Richard Losick. 2002. 'Sporulation Genes and Intercompartmental Regulation'.

Paul, S., S. Million-Weaver, S. Chattopadhyay, E. Sokurenko, and H. Merrikh. 2013. 'Accelerated gene evolution through replication-transcription conflicts', *Nature*, 495: 512-5.

Payne, D. J., M. N. Gwynn, D. J. Holmes, and D. L. Pompliano. 2007. 'Drugs for bad bugs: confronting the challenges of antibacterial discovery', *Nat Rev Drug Discov*, 6: 29-40.

Perchat, S., T. Dubois, S. Zouhir, M. Gominet, S. Poncet, C. Lemy, M. Aumont-Nicaise, J. Deutscher, M. Gohar, S. Nessler, and D. Lereclus. 2011. 'A cell-cell communication system regulates protease production during sporulation in bacteria of the Bacillus cereus group', *Mol Microbiol*, 82: 619-33.

Perchat, S., A. Talagas, S. Poncet, N. Lazar, I. Li de la Sierra-Gallay, M. Gohar, D. Lereclus, and S. Nessler. 2016. 'How Quorum Sensing Connects Sporulation to Necrotrophism in Bacillus thuringiensis', *PLoS Pathog*, 12: e1005779.

Piano, S., V. Singh, P. Caraceni, R. Maiwall, C. Alessandria, J. Fernandez, E. C. Soares, D. J. Kim, S. E. Kim, M. Marino, J. Vorobioff, R. C. R. Barea, M. Merli, L. Elkrief, V. Vargas, A. Krag, S. P. Singh, L. A. Lesmana, C. Toledo, S. Marciano, X. Verhelst, F. Wong, N. Intagliata, L. Rabinowich, L. Colombato, S. G. Kim, A. Gerbes, F. Durand, J. P. Roblero, K. R. Bhamidimarri, T. D. Boyer, M. Maevskaya, E. Fassio, H. S. Kim, J. S. Hwang, P. Gines, A. Gadano, S. K. Sarin, P. Angeli, and Group International Club of Ascites Global Study. 2019. 'Epidemiology and Effects of Bacterial Infections in Patients With Cirrhosis Worldwide', *Gastroenterology*, 156: 1368-80 e10.

Piggot, P. J., and D. W. Hilbert. 2004. 'Sporulation of Bacillus subtilis', *Curr Opin Microbiol*, 7: 579-86.

Pilo, P., and J. Frey. 2011. 'Bacillus anthracis: molecular taxonomy, population genetics, phylogeny and patho-evolution', *Infect Genet Evol*, 11: 1218-24.

Piret, J., and G. Boivin. 2020. 'Pandemics Throughout History', *Front Microbiol*, 11: 631736.

Podschun, R., and U. Ullmann. 1998. 'Klebsiella spp. as nosocomial pathogens: epidemiology, taxonomy, typing methods, and pathogenicity factors', *Clin Microbiol Rev*, 11: 589-603.

Porrini, C., N. Ramarao, and S. L. Tran. 2020. 'Dr. NO and Mr. Toxic - the versatile role of nitric oxide', *Biol Chem*, 401: 547-72.

Pybus, C., M. Pedraza-Reyes, C. A. Ross, H. Martin, K. Ona, R. E. Yasbin, and E. Robleto. 2010. 'Transcription-associated mutation in Bacillus subtilis cells under stress', *J Bacteriol*, 192: 3321-8.

Ragheb, M. N., C. Merrikh, K. Browning, and H. Merrikh. 2021. 'Mfd regulates RNA polymerase association with hard-to-transcribe regions in vivo, especially those with structured RNAs', *Proc Natl Acad Sci U S A*, 118.

Ragheb, M. N., M. K. Thomason, C. Hsu, P. Nugent, J. Gage, A. N. Samadpour, A. Kariisa, C. N. Merrikh, S. I. Miller, D. R. Sherman, and H. Merrikh. 2019. 'Inhibiting the Evolution of Antibiotic Resistance', *Mol Cell*, 73: 157-65 e5.

Ramarao, N., and D. Lereclus. 2005. 'The InhA1 metalloprotease allows spores of the B. cereus group to escape macrophages', *Cell Microbiol*, 7: 1357-64.

Ramarao, N., and D. Lereclus. 2006. 'Adhesion and cytotoxicity of Bacillus cereus and Bacillus thuringiensis to epithelial cells are FlhA and PlcR dependent, respectively', *Microbes Infect*, 8: 1483-91.

Ramirez, M. S., and M. E. Tolmasky. 2010. 'Aminoglycoside modifying enzymes', *Drug Resist Updat*, 13: 151-71.

Rasko, D. A., M. J. Rosovitz, O. A. Okstad, D. E. Fouts, L. Jiang, R. Z. Cer, A. B. Kolsto, S. R. Gill, and J. Ravel. 2007. 'Complete sequence analysis of novel plasmids from emetic and periodontal Bacillus cereus isolates reveals a common evolutionary history among the B. cereus-group plasmids, including Bacillus anthracis pXO1', *J Bacteriol*, 189: 52-64.

Redgrave, L. S., S. B. Sutton, M. A. Webber, and L. J. Piddock. 2014. 'Fluoroquinolone resistance: mechanisms, impact on bacteria, and role in evolutionary success', *Trends Microbiol*, 22: 438-45.

Rice, L. B. 2008. 'Federal funding for the study of antimicrobial resistance in nosocomial pathogens: no ESKAPE', *J Infect Dis*, 197: 1079-81.

Rima, M., M. Rima, Z. Fajloun, J. M. Sabatier, B. Bechinger, and T. Naas. 2021. 'Antimicrobial Peptides: A Potent Alternative to Antibiotics', *Antibiotics (Basel)*, 10.

Roberts, J., and J. S. Park. 2004. 'Mfd, the bacterial transcription repair coupling factor: translocation, repair and termination', *Curr Opin Microbiol*, 7: 120-5.

Roberts, M. C. 2004. 'Resistance to macrolide, lincosamide, streptogramin, ketolide, and oxazolidinone antibiotics', *Mol Biotechnol*, 28: 47-62.

Robicsek, A., J. Strahilevitz, G. A. Jacoby, M. Macielag, D. Abbanat, C. H. Park, K. Bush, and D. C. Hooper. 2006. 'Fluoroquinolone-modifying enzyme: a new adaptation of a common aminoglycoside acetyltransferase', *Nat Med*, 12: 83-8.

Ross, C., C. Pybus, M. Pedraza-Reyes, H. M. Sung, R. E. Yasbin, and E. Robleto. 2006. 'Novel role of mfd: effects on stationary-phase mutagenesis in Bacillus subtilis', *J Bacteriol*, 188: 7512-20.

Ryan, P. A., J. D. Macmillan, and B. A. Zilinskas. 1997. 'Molecular cloning and characterization of the genes encoding the L1 and L2 components of hemolysin BL from Bacillus cereus', *J Bacteriol*, 179: 2551-6.

SantéCanada. 2017. 'Lutter contre la résistance aux antimicrobiens et optimiser leur utilisation : un cadre d'action pancanadien', *L'agence de la santé publique du Canada*.

Sanz, P., L. D. Teel, F. Alem, H. M. Carvalho, S. C. Darnell, and A. D. O'Brien. 2008. 'Detection of Bacillus anthracis spore germination in vivo by bioluminescence imaging', *Infect Immun*, 76: 1036-47.

Schalow, B. J., C. T. Courcelle, and J. Courcelle. 2012. 'Mfd is required for rapid recovery of transcription following UV-induced DNA damage but not oxidative DNA damage in Escherichia coli', *J Bacteriol*, 194: 2637-45.

Schnepf, E., N. Crickmore, J. Van Rie, D. Lereclus, J. Baum, J. Feitelson, D. R. Zeigler, and D. H. Dean. 1998. 'Bacillus thuringiensis and its pesticidal crystal proteins', *Microbiol Mol Biol Rev*, 62: 775-806.

Schwarz, S., C. Kehrenberg, B. Doublet, and A. Cloeckaert. 2004. 'Molecular basis of bacterial resistance to chloramphenicol and florfenicol', *FEMS Microbiol Rev*, 28: 519-42.

Selby, C. P. 2017. 'Mfd Protein and Transcription-Repair Coupling in Escherichia coli', *Photochem Photobiol*, 93: 280-95.

Selby, C. P., and A. Sancar. 1993. 'Molecular mechanism of transcription-repair coupling', *Science*, 260: 53-8.

Selby, C. P., and A. Sancar. 1994. 'Mechanisms of transcription-repair coupling and mutation frequency decline', *Microbiol Rev*, 58: 317-29.

Setlow, P. 2006. 'Spores of Bacillus subtilis: their resistance to and killing by radiation, heat and chemicals', *J Appl Microbiol*, 101: 514-25.

Shatri, G., and P. Tadi. 2022. 'Polymyxin.' in, *StatPearls* (Treasure Island (FL)).

Shinagawa, K., J. Sugiyama, T. Terada, N. Matsusaka, and S. Sugii. 1991. 'Improved methods for purification of an enterotoxin produced by Bacillus cereus', *FEMS Microbiol Lett*, 64: 1-5.

Shinagawa, K., Y. Ueno, D. Hu, S. Ueda, and S. Sugii. 1996. 'Mouse lethal activity of a HEp-2 vacuolation factor, cereulide, produced by Bacillus cereus isolated from vomiting-type food poisoning', *J Vet Med Sci*, 58: 1027-9.

Silver, L. L. 2011. 'Challenges of antibacterial discovery', *Clin Microbiol Rev*, 24: 71-109.

Sinev, M. A., I. Budarina Zh, I. V. Gavrilenko, AIu Tomashevskii, and N. P. Kuz'min. 1993. '[Evidence of the existence of hemolysin II from Bacillus cereus: cloning the genetic determinant of hemolysin II]', *Mol Biol (Mosk)*, 27: 1218-29.

Slamti, L., and D. Lereclus. 2002. 'A cell-cell signaling peptide activates the PlcR virulence regulon in bacteria of the Bacillus cereus group', *EMBO J*, 21: 4550-9.

Smith, A. J., M. D. Szczelkun, and N. J. Savery. 2007. 'Controlling the motor activity of a transcription-repair coupling factor: autoinhibition and the role of RNA polymerase', *Nucleic Acids Res*, 35: 1802-11.

Solveig Langsrud, Maan Singh Sidhu, Even Heir, Askild L. Holck. 2003. 'Bacterial disinfectant resistance—a challenge for the food industry', *International Biodeterioration & Biodegradation*, 51: 283-90.

Soto, S. M. 2013. 'Role of efflux pumps in the antibiotic resistance of bacteria embedded in a biofilm', *Virulence*, 4: 223-9.

Stenfors Arnesen, L., P. E. Granum, C. Buisson, J. Bohlin, and C. Nielsen-LeRoux. 2011. 'Using an insect model to assess correlation between temperature and virulence in Bacillus weihenstephanensis and Bacillus cereus', *FEMS Microbiol Lett*, 317: 196-202.

Stenfors Arnesen, L. P., A. Fagerlund, and P. E. Granum. 2008. 'From soil to gut: Bacillus cereus and its food poisoning toxins', *FEMS Microbiol Rev*, 32: 579-606.

Stenfors, L. P., and P. E. Granum. 2001. 'Psychrotolerant species from the Bacillus cereus group are not necessarily Bacillus weihenstephanensis', *FEMS Microbiol Lett*, 197: 223-8.

Stewart, P. S., J. Rayner, F. Roe, and W. M. Rees. 2001. 'Biofilm penetration and disinfection efficacy of alkaline hypochlorite and chlorosulfamates', *J Appl Microbiol*, 91: 525-32.

Storz, M. P., C. K. Maurer, C. Zimmer, N. Wagner, C. Brengel, J. C. de Jong, S. Lucas, M. Musken, S. Haussler, A. Steinbach, and R. W. Hartmann. 2012. 'Validation of PqsD as an anti-biofilm target in Pseudomonas aeruginosa by development of small-molecule inhibitors', *J Am Chem Soc*, 134: 16143-6.

Sulakvelidze, A., Z. Alavidze, and J. G. Morris, Jr. 2001. 'Bacteriophage therapy', *Antimicrob Agents Chemother*, 45: 649-59.

Summers, W. C. 2012. 'The strange history of phage therapy', *Bacteriophage*, 2: 130-33.

Thompson, N. E., M. J. Ketterhagen, M. S. Bergdoll, and E. J. Schantz. 1984. 'Isolation and some properties of an enterotoxin produced by Bacillus cereus', *Infect Immun*, 43: 887-94.

Timmins, G. S., and V. Deretic. 2006. 'Mechanisms of action of isoniazid', *Mol Microbiol*, 62: 1220-7.

Titball, R. W. 1998. 'Bacterial phospholipases', *Symp Ser Soc Appl Microbiol*, 27: 127S-37S.

Tran, S. L., D. Cormontagne, J. Vidic, G. Andre-Leroux, and N. Ramarao. 2020. 'Structural Modeling of Cell Wall Peptidase CwpFM (EntFM) Reveals Distinct Intrinsically Disordered Extensions Specific to Pathogenic Bacillus cereus Strains', *Toxins (Basel)*, 12.

Tran, S. L., E. Guillemet, M. Gohar, D. Lereclus, and N. Ramarao. 2010. 'CwpFM (EntFM) is a Bacillus cereus potential cell wall peptidase implicated in adhesion, biofilm formation, and virulence', *J Bacteriol*, 192: 2638-42.

Tran, S. L., E. Guillemet, D. Lereclus, and N. Ramarao. 2013. 'Iron regulates Bacillus thuringiensis haemolysin hlyII gene expression during insect infection', *J Invertebr Pathol*, 113: 205-8.

Tran, S. L., E. Guillemet, M. Ngo-Camus, C. Clybouw, A. Puhar, A. Moris, M. Gohar, D. Lereclus, and N. Ramarao. 2011. 'Haemolysin II is a Bacillus cereus virulence factor that induces apoptosis of macrophages', *Cell Microbiol*, 13: 92-108.

Tran, S. L., and N. Ramarao. 2013. 'Bacillus cereus immune escape: a journey within macrophages', *FEMS Microbiol Lett*, 347: 1-6.

UE. 2019. 'RÈGLEMENT (UE) 2019/6 DU PARLEMENT EUROPÉEN ET DU CONSEIL du 11 décembre 2018 relatif aux médicaments vétérinaires et abrogeant la directive 2001/82/CE', *Journal officiel de l'Union européenne*.

Vachon, V., R. Laprade, and J. L. Schwartz. 2012. 'Current models of the mode of action of Bacillus thuringiensis insecticidal crystal proteins: a critical review', *J Invertebr Pathol*, 111: 1-12.

Van Acker, H., P. Van Dijck, and T. Coenye. 2014. 'Molecular mechanisms of antimicrobial tolerance and resistance in bacterial and fungal biofilms', *Trends Microbiol*, 22: 326-33.

Van Der Zwet, W. C., G. A. Parlevliet, P. H. Savelkoul, J. Stoof, A. M. Kaiser, A. M. Van Furth, and C. M. Vandenbroucke-Grauls. 2000. 'Outbreak of Bacillus cereus infections in a neonatal intensive care unit traced to balloons used in manual ventilation', *J Clin Microbiol*, 38: 4131-6.

van Gestel, J., M. A. Nowak, and C. E. Tarnita. 2012. 'The evolution of cell-to-cell communication in a sporulating bacterium', *PLoS Comput Biol*, 8: e1002818.

Verraes, C., S. Van Boxstael, E. Van Meervenne, E. Van Coillie, P. Butaye, B. Catry, M. A. de Schaetzen, X. Van Huffel, H. Imberechts, K. Dierick, G. Daube, C. Saegerman, J. De Block, J. Dewulf, and L. Herman. 2013. 'Antimicrobial resistance in the food chain: a review', *Int J Environ Res Public Health*, 10: 2643-69.

Vilas-Boas, G. T., A. P. Peruca, and O. M. Arantes. 2007. 'Biology and taxonomy of Bacillus cereus, Bacillus anthracis, and Bacillus thuringiensis', *Can J Microbiol*, 53: 673-87.

Waksman, S. A., A. Schatz, and D. M. Reynolds. 2010. 'Production of antibiotic substances by actinomycetes', *Ann N Y Acad Sci*, 1213: 112-24.

Wassenaar, T. M., and W. Gaastra. 2001. 'Bacterial virulence: can we draw the line?', *FEMS Microbiol Lett*, 201: 1-7.

Weiner, L. M., A. K. Webb, B. Limbago, M. A. Dudeck, J. Patel, A. J. Kallen, J. R. Edwards, and D. M. Sievert. 2016. 'Antimicrobial-Resistant Pathogens Associated With Healthcare-Associated Infections: Summary of Data Reported to the National Healthcare Safety Network at the Centers for Disease Control and Prevention, 2011-2014', *Infect Control Hosp Epidemiol*, 37: 1288-301.

Weir, C. B., and J. K. Le. 2022. 'Metronidazole.' in, *StatPearls* (Treasure Island (FL)).

WHO. 2022. '2021 ANTIBACTERIAL AGENTS IN CLINICAL AND PRECLINICAL DEVELOPMENT: an overview and analysis', *Geneva: World Health Organization*.

Wijman, J. G., P. P. de Leeuw, R. Moezelaar, M. H. Zwietering, and T. Abee. 2007. 'Air-liquid interface biofilms of Bacillus cereus: formation, sporulation, and dispersion', *Appl Environ Microbiol*, 73: 1481-8.

Wilcox, M. H., D. N. Gerding, I. R. Poxton, C. Kelly, R. Nathan, T. Birch, O. A. Cornely, G. Rahav, E. Bouza, C. Lee, G. Jenkin, W. Jensen, Y. S. Kim, J. Yoshida, L. Gabryelski, A. Pedley, K. Eves, R. Tipping, D. Guris, N. Kartsonis, M. B. Dorr, I. Modify, and Modify Ii Investigators. 2017. 'Bezlotoxumab for Prevention of Recurrent Clostridium difficile Infection', *N Engl J Med*, 376: 305-17.

Witkin, E. M. 1994. ' Mutation frequency decline revisited', *BioEssays : news and reviews in molecular, cellular and developmental biology,* 16(6), 437–444.

Yerushalmi, H., M. Lebendiker, and S. Schuldiner. 1995. 'EmrE, an Escherichia coli 12-kDa multidrug transporter, exchanges toxic cations and H+ and is soluble in organic solvents', *J Biol Chem*, 270: 6856-63.

Yi, Y., Z. Li, C. Song, and O. P. Kuipers. 2018. 'Exploring plant-microbe interactions of the rhizobacteria Bacillus subtilis and Bacillus mycoides by use of the CRISPR-Cas9 system', *Environ Microbiol*, 20: 4245-60.

Yocum, R. R., J. R. Rasmussen, and J. L. Strominger. 1980. 'The mechanism of action of penicillin. Penicillin acylates the active site of Bacillus stearothermophilus D-alanine carboxypeptidase', *J Biol Chem*, 255: 3977-86.

Yokoyama, K., M. Ito, N. Agata, M. Isobe, K. Shibayama, T. Horii, and M. Ohta. 1999. 'Pathological effect of synthetic cereulide, an emetic toxin of Bacillus cereus, is reversible in mice', *FEMS Immunol Med Microbiol*, 24: 115-20.

Zalieckas, J. M., L. V. Wray, Jr., A. E. Ferson, and S. H. Fisher. 1998. 'Transcription-repair coupling factor is involved in carbon catabolite repression of the Bacillus subtilis hut and gnt operons', *Mol Microbiol*, 27: 1031-8.

Zhanel, G. G., A. J. Walkty, and J. A. Karlowsky. 2015. 'Fidaxomicin: A novel agent for the treatment of Clostridium difficile infection', *Can J Infect Dis Med Microbiol*, 26: 305-12.

ANNEXES

Annexe I

Revue : "*Bacillus cereus* Induces Severe Infections in Preterm Neonates: Implication at the Hospital and Human Milk Bank Level

toxins

MDPI

Review

Bacillus cereus Induces Severe Infections in Preterm Neonates: Implication at the Hospital and Human Milk Bank Level

Delphine Cormontagne [1,†], Virginie Rigourd [2,†], Jasmina Vidic [1], Francesco Rizzotto [1], Emmanuelle Bille [3,4] and Nalini Ramarao [1,*]

[1] Micalis Institute, INRAE, AgroParisTech, Université Paris-Saclay, 78350 Jouy-en-Josas, France; delphine.cormontagne@inrae.fr (D.C.); jasmina.vidic@inrae.fr (J.V.); francesco.rizzotto@inrae.fr (F.R.)
[2] Région Île-de-France Human Milk Bank, Hôpital Necker-Enfants Malades, Assistance Publique-Hôpitaux de Paris, 75015 Paris, France; virginie.rigourd@aphp.fr
[3] Department of Clinical Microbiology, Necker Enfants-Malades Hospital, AP-HP, 75015 Paris, France; emmanuelle.bille@aphp.fr
[4] INSERM U1151-CNRS UMR 8253, Institut Necker-Enfants Malades, Université de Paris, 75015 Paris, France
* Correspondence: nalini.ramarao@inrae.fr
† These authors contributed equally to this work.

Abstract: Human breast milk (HBM) is a source of essential nutrients for infants and is particularly recommended for preterm neonates when their own mother's milk is not available. It provides protection against infections and decreases necrotizing enterocolitis and cardiovascular diseases. Nevertheless, HBM spoilage can occur due to contamination by pathogens, and the risk of a shortage of HBM is very often present. *B. cereus* is the most frequent ubiquitous bacteria responsible for HBM being discarded. It can contaminate HBM at all stages, from its collect point to the storage and delivery. *B. cereus* can induce severe infection in newborns with very low birth weight, with sometimes fatal outcomes. Although the source of contamination is rarely identified, in some cases, HBM was suspected as a potential source. Even if the risk is low, as infection due to *B. cereus* in preterm infants should not be overlooked, human milk banks follow strict procedures to avoid contamination, to accurately identify remaining bacteria following pasteurization and to discard non-compliant milk samples. In this review, we present a literature overview of *B. cereus* infections reported in neonates and the suspected sources of contamination. We highlight the procedures followed by the human milk banks from the collection of the milk to its microbiological characterization in Europe. We also present improved detection and decontamination methods that might help to decrease the risk and to preserve the public's confidence in this vital biological product for infants whose mothers cannot breastfeed.

Keywords: *Bacillus cereus*; human breast milk; preterm neonates

Key Contribution: *B. cereus* is responsible for severe infection in newborns, and although the source of contamination is rarely identified, the human breast milk was suspected as a potential source. *B. cereus* spores resist milk pasteurization and human milk banks follow strict procedures to avoid contamination.

Citation: Cormontagne, D.; Rigourd, V.; Vidic, J.; Rizzotto, F.; Bille, E.; Ramarao, N. *Bacillus cereus* Induces Severe Infections in Preterm Neonates: Implication at the Hospital and Human Milk Bank Level. *Toxins* **2021**, *13*, 123. https://doi.org/10.3390/toxins13020123

Received: 15 December 2020
Accepted: 2 February 2021
Published: 7 February 2021

1. Introduction

Very premature infants cannot be breastfed directly by their mothers, but when possible, will receive their own mother's milk by enteral nutrition. As an alternative, human milk collected, qualified and pasteurized by human milk banks must be used to enhance nutrition or to complete the mother's milk production. Human milk contains many biologic factors that improve the global outcome of preterm neonates, and formula-fed infants are reported to have 6 to 20 times the risk of experiencing necrotizing enterocolitis compared with breast milk-fed infants. However, despite the obvious beneficial role of human milk, it could also contain bacteria and viruses originating from the milk itself, or from the

environment of collection, transport, storage, treatment and administration. Because of the fragility and the high susceptibility of these newborns to infections (prematurity and/or pathology), one of the questions of interest for health professionals is to reduce the risk of bacterial and viral contamination [1]. For a mother's own raw milk, this question is a direct concern for the neonatal intensive care units. For pasteurized human milk, a human milk bank is the first actor for preventive actions with two aims: (i) prevent milk contamination to avoid preterm infection, and (ii) control the milk process to limit bacteriological rejection and prevent milk shortage [2,3]. During these processes, the main concern is milk contamination by the bacteria *Bacillus cereus*. Indeed, *B. cereus* is the most frequent bacteria found in milk following pasteurization, and it is responsible for a high rate of bacteriologic rejection in human milk banks [4]. Ninety percent of the milk is rejected due to *B. cereus*, which represents 10% of the total volume collected. *B. cereus* is responsible for severe diseases in preterm neonates and the milk has been regularly suspected as the source of contamination [5,6].

The *Bacillus cereus sensu lato* group is composed of seven bacterial species, of which the four best known due to their pathogenicity are *B. cereus sensu stricto*, *B. thuringiensis*, *B. cytotoxicus* and *B. anthracis*. They are Gram-positive, facultative aerobic or anaerobic, sporulating bacteria. These bacteria, which display similar properties, have specific toxins which allow them to colonize hosts as diverse as insects and mammals. *B. cereus* is a saprophytic bacterium, which can be found in a large number of environments, in particular at all stages of the food production chain in hospitals and in human milk banks. The survival of these bacteria along the lines is explained by their ability to produce spores that are resistant to high temperatures, but also able to firmly adhere to materials such as polymers or stainless steels [7]. The presence of bacteria in food is also due to their ability to multiply at low temperatures. *B. cereus* is dangerous from 10^5–10^6 bacteria ingested [8]. When ingested, *B. cereus* can cause gastrointestinal infections of varying severity, from mild diarrhea to death due to liver failure or other complications of those infected. *B. cereus* is thus placed in second place of the agents responsible for collective food borne poisoning (FBO) in France and third in Europe [9].

In addition, *B. cereus* is also associated with rare but also more serious non-gastrointestinal pathologies, such as eye infections, pneumonia or meningitis, with sometimes fatal outcomes [10]. In addition, a strain of *B. cereus* carrying a plasmid similar to pXO1 and a plasmid carrying capsule genes, which are known as factors specific to *B. anthracis*, has been responsible for severe anthrax-like infections [11]. *B. cereus* can induce severe pathologies especially in vulnerable children, such as septicemia, respiratory tract infection, enterocolitis, hepatitis, endocarditis, endophthalmitis, encephalitis with cerebral abscess [12–16].

Case reports often focus on individual cases from one hospital only. The overall incidence of local and systemic infections by *B. cereus* is unknown and the characterization of the strains is scarce. A recent study analyzed a survey of infection cases by *B. cereus* from nine different hospitals and proposed a scheme based on biochemical and genetic properties [17]. This revealed that *B. cereus* can be maintained in the hospital environment for up to two years, despite cleaning procedures, and can contaminate unrelated patients, promoting uncontrolled nosocomial infections. Furthermore, in 38% of the cases studied, *B. cereus* was discarded as a simple contaminant. This underlines the fact that not every case of infection is reported and that *B. cereus* incidence is likely underestimated.

Nevertheless, premature infant infection due to *B. cereus* is extremely rare, but neonatal sepsis related to this bacterium remains particularly severe and can be fatal [18–20].

2. *B. cereus* Induces Severe Pathologies in Preterm Neonates

Cases of infections due to *B. cereus* have previously been reported in immunosuppressed patients. In particular, premature infants and Very Low Birth Weight Infant neonates are highly susceptible to infections because of their immature immune systems and their prolonged exposure to invasive procedures, such as mechanical ventilation and the frequent use of intravascular catheters. However, the pathophysiology of these in-

fections remains poorly understood, with a relatively small number of published cases. Table 1 resumes different clinical forms of *B. cereus* infections reported in the literature. Table 2 relates 42 cases of post-natal infection of *B. cereus* that occurred since December 2016 in Île-de-France (IDF) with the percentages of severe forms and favorable cases. In most of the cases reported in Table 1, the neonates were premature, born before 30 weeks of gestation and, by their young age, had a very low weight: the mean birth was only 27 gestational weeks and the mean baby weight was 1344 g. The sex of the patient was not reported in 76% of the cases and an assessment of a correlation between the sex of the child and infection by *B. cereus* is not possible. Except for the prematurity, a common trait shared by 82% of the cases is low weight at birth (57% for the neonates and 70% for the premature infants, although 24% of the premature cases did not disclose the weight at birth). The patients did not have any other underlying disorders in common.

Table 1. *B. cereus* infection in neonates. Literature review (NS: Not specified; ND: Not determined; F: Female; M: Male; ET: Endotracheal tube; CSF: Cerebrospinal fluid; HBM: Human breast milk).

Ref	Sex	Birth Weight (g)	Gestational Age, Weeks + Days	Age at First Positive Culture, Days	Predisposing Factors	Treatment	Outcome	Suspected or Proven Source of Infection	First *B. cereus* Identification	Toxin Identified
[21]	NS	750	30 +2	3	Premature, low weight	NS	Died	Pasteurized milk, packs of diapers, linen, baby bath, benches (suspected)	Blood culture	ND
	NS	3000	40	1		NS	Survived		Cavum	ND
	NS	1075	29 + 2	5	Premature, low weight	NS	Died		Blood culture	ND
	NS	2815	37 + 2	2		NS	Survived		Blood culture	ND
	NS	3515	38 + 6	6		NS	Survived		Blood culture	ND
	NS	3240	39	9		NS	Survived		Blood culture	ND
	NS	1380	31	9	Premature, low weight	NS	Survived		Blood culture	ND
	NS	1025	29 + 4	11	Premature, low weight	NS	Survived		Blood culture	ND
	NS	750	27 + 5	76	Premature, low weight	NS	Died		Blood culture	ND
	NS	1720	31	10	Premature, low weight	NS	Survived		Blood culture	ND
[18]	F	880	27 + 2	4	Premature, low weight	Cefotaxime, gentamicin, vancomycin, fluoroquinolone	Died	Incubator, ultrasonographic probe, bench used for bottle feeding (suspected)	Tracheobronchial aspiration	CytK2, Nhe
	M	1480	29 + 4	4	Premature, low weight	Cefotaxime, gentamicin, vancomycin	Died		Blood culture	

Table 1. *Cont.*

Ref	Sex	Birth Weight (g)	Gestational Age, Weeks + Days	Age at First Positive Culture, Days	Predisposing Factors	Treatment	Outcome	Suspected or Proven Source of Infection	First *B. cereus* Identification	Toxin Identified
[22]	NS	1650	31	70	Premature, low weight	Vancomycin	Survived	Bioaerosol and surface contamination. Work stations, storage room, linens (suspected)	Blood culture	ND
	NS	1148	29	58	Premature, low weight	Vancomycin	Survived		Blood culture	ND
	NS	1515	28	23	Premature, low weight	Vancomycin	Survived		Blood culture	ND
	NS	710	24	14	Premature, low weight	Vancomycin	Survived		Blood culture	ND
	NS	945	25	59	Premature, low weight	Vancomycin	Survived		Blood culture	ND
[23]	M	1580	26	30	Premature, low weight	Ampicillin, cefotaxime then amikacin and vancomycin	Died	ND	Blood culture	ND
[5]	NS	960	29	3	Premature, low weight	Vancomycin, cefotaxime and metronidazole	Survived	Food-related origin: milk (suspected)	Gastric fluid culture	ND
	NS	1500	30	3	Premature, low weight	Vancomycin, cefotaxime and metronidazole	Survived		Gastric fluid culture	ND
[24]	F	1670	31	28	Premature, low weight	Cefotaxime, amoxicillin, metronidazole, amikacin	Died	ND	Blood culture and central catheter	ND

Table 1. *Cont.*

Ref	Sex	Birth Weight (g)	Gestational Age, Weeks + Days	Age at First Positive Culture, Days	Predisposing Factors	Treatment	Outcome	Suspected or Proven Source of Infection	First *B. cereus* Identification	Toxin Identified
[25]	NS	880	27	1	Premature, low weight	Vancomycin	Survived	Water from washing machine chamber (proven)	ET aspirates	ND
	NS	880	28	1	Premature, low weight	Vancomycin	Died		ET aspirates	ND
	NS	720	27	3	Premature, low weight	ND	Survived		ET aspirates	ND
	NS	880	29	3	Premature, low weight	ND	Survived		ET aspirates	ND
	NS	640	28	2	Premature, low weight	Vancomycin	Died	Vial of pulmonary surfactant used for both of them (but no growth)	ET aspirates	ND
	NS	530	26	3	Premature, low weight	Vancomycin	Died		ET aspirates	ND
[26]	F	800	NS	1	Premature, low weight	Vancomycin, meropenem and for meningitis: linezolid, meropenem and clindamycin	Survived	Ventilator equipment, intravascular catheters and linen (suspected)	Blood culture	ND
[27]	F	830	26	8	Premature, low weight	Vancomycin, amikacin	Died	ND	Blood culture	ND
[19]	NS	650	24 + 5	32	Premature, low weight	Cefotaxime, vancomycin and amikacin	Survived	Arterial catheter (suspected)	Blood culture	Nhe
	NS	615	26 + 5	5	Premature, low weight	NS	Died	Catheter (suspected)	Peripheral catheter and central catheter	Nhe

Table 1. *Cont.*

Ref	Sex	Birth Weight (g)	Gestational Age, Weeks + Days	Age at First Positive Culture, Days	Predisposing Factors	Treatment	Outcome	Suspected or Proven Source of Infection	First *B. cereus* Identification	Toxin Identified
[28]	M	NS	NS	1	NS	Cefozopran	Died	Hospital linens (proven)		ND
	F	NS	NS	19	NS	Ampicillin, meropenem, vancomycin, panipenem	Died			ND
[29]	F	3764	37	6	Premature	Ampicillin, gentamicin	Died	Peripheral vein catheter (suspected)	CSF and blood culture	ND
	F	1506	36	9	Premature, low weight	Ampicillin, cefotaxime	Died	Nasal feeding tube (suspected)	CSF culture	ND
[20]	M	895	28 + 5	5	Premature, low weight	Amoxicillin and cefotaxime	Died	Balloons of manual ventilation, person to person transmission (health care workers hands) (suspected)	Blood culture, CSF, trachea aspirate, necrotic Skin lesion at insertion site of arterial catheter	ND
	F	1000	26 + 4	5	Premature, low weight	Meropenem, vancomycin	Survived		Blood, aspirate from left knee	ND
	M	2780	37 + 3	14	Premature	Meropenem, vancomycin	Survived		Blood, CSF, tip of peripheral catheter	ND
[30]	M	585	24	19	Premature, low weight	Vancomycin, tobramycin	Survived	ND	Blood culture	ND
[31]	NS	590	25	10	Premature, low weight	Linezolid, meropenem, vancomycin	Died	Batches of HBM but the strains from the baby are different (suspected)	Blood culture	ND

Table 1. *Cont.*

Ref	Sex	Birth Weight (g)	Gestational Age, Weeks + Days	Age at First Positive Culture, Days	Predisposing Factors	Treatment	Outcome	Suspected or Proven Source of Infection	First *B. cereus* Identification	Toxin Identified
	NS	560	24	6	Premature, low weight	Ampicillin, tobramycin, vancomycin, meropenem, piperacillin-tazobactam, fluconazole, amphotericin and trimethoprim-sulfamethoxazole	Died	HBM (suspected)	Blood culture	ND
[32]	NS	NS	NS	NS	Premature		Died	ND	Blood culture and cerebrospinal fluid	Nhe
	NS	NS	NS	NS	Premature	Vancomycin, cefotaxime	Survived	ND	Blood culture	Nhe, Hbl
	NS	NS	NS	NS	Premature	Vancomycin	Survived	ND	Blood culture	Nhe
	NS	NS	NS	NS		Vancomycin	Survived	ND	Neonatal gastric liquid	Nhe
	NS	NS	NS	NS		Cefotaxime, amoxicillin, amikacin	Survived	ND	Umbilical	Nhe
	NS	NS	NS	NS		Ceftriaxone	Survived	ND	Axilla later feces	Nhe
	NS	NS	NS	NS	Premature	Cefotaxime, amoxicillin, amikacin	Survived	ND	Stomach tube feeding	Nhe
	NS	NS	NS	NS	Premature	Vancomycin	Survived	ND	Gastric acid	Nhe

Table 1. *Cont.*

Ref	Sex	Birth Weight (g)	Gestational Age, Weeks + Days	Age at First Positive Culture, Days	Predisposing Factors	Treatment	Outcome	Suspected or Proven Source of Infection	First *B. cereus* Identification	Toxin Identified
	NS	NS	NS	NS	Premature	Amoxicillin, amikacin, vancomycin	Survived	ND	Central venous catheter	Nhe
	NS	NS	NS	NS	Premature	Vancomycin, cefotaxime, amikacin	Survived	ND	Blood culture	Nhe
	NS	NS	NS	NS	Premature		Died	ND	Blood culture	Nhe
	NS	NS	NS	NS	Premature	Vancomycin, cefotaxime, metronidazole	Survived	ND	Stomach tube feeding	ND
	NS	NS	NS	NS	Premature	Vancomycin, cefotaxime, metronidazole	Survived	ND	Stomach tube feeding	ND
	NS	NS	NS	NS		Ceftriaxone, gentamicin	Survived	ND	Blood culture	ND
	NS	NS	NS	NS	Premature	Vancomycin	Died	ND	Blood culture from umbilical venous catheter and peripheral veins	Nhe, Hbl
	NS	NS	NS	NS	Premature	Vancomycin	Died	ND	Bronchial aspiration (lung)	Nhe

Table 2. *B. cereus* infection cases reported in Île-de-France since 2016 (WA: Week of amenorrhea; UVC: Umbilical venous catheter; LS: lipids in parenteral solution; MB: milk from Human Milk Bank; OMM: own mother's milk; HL: artificial milk type hydrolysate).

Term and Birth Weight	Hours or Days After Birth	Bacteriological Analyses	Symptoms	Evolution
25 WA 675 g	D14	Blood (+) UVC(+) LS (+) MB (-)	Diffuse multiple abscess 2 hemispheres	Death
39 WA + 1 2500 g	D22	Blood (+) OMM (-) HL	Respiratory breaks	Favorable
25 WA + 1 665 g	D134	Blood (+) OMM(-)	Respiratory breaks	Favorable
25 WA 600 g	D15	Blood (+) OMM (-)	No symptom	Favorable
38 WA 2700 g	D32	Blood (+) HL	No symptom	Favorable
26 WA 675 g	D26	Blood (+) MB (-)	No symptom	Favorable
ND		Blood (+) Parenteral	No symptom	Favorable
28 WA + 5 585 g	D13	Blood (+) Incubator (+)	No symptom	Favorable
32 WA 1530 g	D3	Blood (+) MB (-)	No symptom	Favorable
ND		Blood (+) MB (-)		Favorable
29 WA + 5 1240 g	D20	Blood (+)	No symptom	Favorable
31 WA 1410 g	D4	Blood (+) MB (-)	No symptom	Favorable
25 WA 635 g	D6	Blood (+) MB (-)	Respiratory breaks	Favorable
29 WA 1260 g	D18	Blood (+)	Respiratory breaks	Favorable
31 WA + 2 1940 g	D16	Blood (+) MB(-)	No symptom	Favorable
25 WA + 6 855 g	D6	Blood (+) Peritonitis MB (-)	Increase needs in 0_2	Favorable
37 WA + 2 2035 g	D16	Blood (+)	No symptom	Favorable
28 WA + 2 865 g	D16	Blood (+) MB (-)		Favorable
4 premature babies		Blood (+) MB (-)	One with a brain abscess	1 Death/4
1 premature baby		MB (-)		Favorable

Table 2. *Cont.*

Term and Birth Weight	Hours or Days After Birth	Bacteriological Analyses	Symptoms	Evolution
1 premature baby		Blood (+) LS (+) MB (-)		Death
29 WA 1210 g	D21	Electric ramp (+) Blood (+ *Bacillus pumilus*) MB (-)	Bone localization	Favorable
29 WA + 5 1285 g	D6	Blood (+) MB (-)	Extensive periventricular hemorrhage and cytotoxic Involvement of the cortex and central gray nuclei	Death
1 premature baby		Blood (+) MB (-)		Favorable
31 WA + 2 1430 g	D29	Blood (+) MB (+ 10^3 *Bc*)		Favorable
		Blood (+)		Favorable
Near born		Blood (+) Incubator (+)		
25 WA	D19	2 Blood (+) *Bacillus subtilis* MB (-)		Favorable
ND		Tracheal suction (+) MB (-)		
ND		MB (-)		
1 premature baby		Blood (+) MB(-)		
1 premature baby		Blood (+) MB (-)		
29 WA 550 g	D3	Blood (+) Parenteral (+)	Brain abscess	Death
30 WA 740 g	H50	Blood (+)	Brain abscess	Death
36 WA 2000 g	D1	Nasopharynx (+)		Favorable

The preterm neonates were often born without any sign of infection. Nonetheless, because of their premature state, their immune system is not yet mature and they are particularly prone to infection. Most infections developed during the first 10 days of life and the state of the patient quickly declined following the first signs of infection.

Infection was revealed by septic syndromes with positive blood culture (60% of cases) and more or less severe symptomatology, ranging from near-asymptomatic cases to respiratory pauses and cases with extensive and irreversible brain lesions with abscess. Many symptoms were observed, such as respiratory distress with the neonate doing apnea or not breathing by themselves, cardiologic distress with tachycardia and bradycardia, hypotension, increase in leukocytes, which is to be expected during an infection, abdominal distension and, in the worst cases, septic shock, meningitis or cerebral edemas. When sepsis occurred, the mortality was high and frequently led to spontaneous death or medical decision of palliative demarches. In 40% of the cases, an infection by *B. cereus* resulted in the death of the neonate. Histological examination of tissues collected at autopsies of

fatal cases of neonatal *B. cereus* infection have demonstrated that tissue invasion with the multiplication of organisms in various organs can also occur [10].

Luckily, *B. cereus* can also cause asymptomatic infections. In the cases identified since 2016 in Île-de-France (Table 2), many patients did not present any symptoms, even though *B. cereus* was found in their blood.

As a whole, newborn neonate infection by *B. cereus* can develop into a multitude of diverse symptoms, which makes it complicated to easily differentiate from other bacteria inducing similar symptoms. The symptoms may indeed be attributed to other bacteria such as *Streptococcus* spp., *Escherichia coli* and *Listeria monocytogenes*, responsible for early bacterial infection disease, or *Staphylococcus aureus* and *Clostridioides* spp., responsible for secondary infectious diseases. In addition, as *B. cereus* was long considered a hospital environment bacterium, a proper diagnosis is sometimes missing or done too late.

Usually, as soon as the symptoms appear, the preterm neonates start an antibiotic treatment, mostly with a combination of antibiotics. Most *B. cereus* are resistant to penicillin and cephalosporin, but they are reported to be susceptible to aminoglycosides, clindamycin, vancomycin, carbapanems, chloramphenicol and erythromycin. Combination therapy with vancomycin and aminoglycoside given empirically has been recommended for systemic infection while awaiting susceptibility data. The efficacy of a treatment of 6 to 8 weeks with an association of vancomycin and carbapenem or ciprofloxacin has also been shown in case of cerebral abscess [17]. Unfortunately, when the first symptoms appear before the eighth day of life, the usual first treatment is ampicillin and/or cephalosporin, which is not efficient against *B. cereus*. Since the infection by *B. cereus* may be rapidly deadly, early recognition of the organism is key for the accurate treatment of the neonates. The pathology of *B. cereus* is serious and needs to be considered more often in predisposed patients. When Gram-positive bacilli are found in blood culture or in the cerebrospinal fluid (CSF), the risks of septicemia or meningitis cannot be overlooked, and an infection by *B. cereus* needs to be considered, especially in preterm neonates.

3. Toxins Potentially Involved in *B. cereus* Infection

Clinical manifestations of *B. cereus* have been ascribed to the production of various exotoxins, including the enterotoxin responsible for food borne disease, lecithinase, phospholipase, protease and hemolysins that produce extensive damage and liquefactive necrosis of infected tissues [32].

Diarrheal syndrome is caused by toxins synthesized directly in the intestine by vegetative bacteria. The bacteria are ingested in dairy products, mashed vegetables, or meat dishes, presumably most often in the form of spores [33], which reach the intestine where they germinate, multiply, and produce enterotoxins. The enterotoxins destroy the intestinal barrier, thus causing diarrhea. The contamination is therefore revealed several hours after ingestion, and is manifested by abdominal pain and profuse diarrhea. Currently, three enterotoxins, haemolysin BL (Hbl), non haemolytic enterotoxin (Nhe) and cytotoxin K (CytK), have been described and may play a role in diarrheal symptoms.

Hbl and Nhe are both tripartite toxins. Hbl has three components, the proteins L1, L2 and B. This toxin induces an accumulation of fluid in rabbit ileal loops [34], dermonecrotic activity, vascular permeability [35], cytotoxic activity towards Vero cells and retinal tissues [36,37] and haemolytic activity towards erythrocytes from several species [38,39].

Nhe is a three-protein complex, NheA, NheB and NheC, encoded by the *nhe*ABC operon [40]. This toxin was first characterized in 1995 during a food poisoning outbreak in Norway [41]. Nhe causes cell death through colloid osmotic lysis by provoking a disruption of the plasma membrane and inducing pores in planar lipid bilayers [42]. The *nhe* operon has been found in every *B. cereus* strain so far.

CytK is a single component toxin which is part of the β-barrel pore-forming toxin family. It has cytotoxic and haemolytic activities and demonstrates a similar cytotoxic potency towards cell cultures as Hbl and Nhe [43]. There are two variants of the protein (CytK1 and CytK2), the first one being more toxic than the second [44,45].

The measurement of the level of production of the two enterotoxins Nhe and Hbl in the laboratory environment by immunological kits provides an indication of the pathogenicity of the isolated strains. However, it is not possible to determine a threshold of expression of these enterotoxins discriminating pathogenic strains from non-pathogenic strains. At present, the investigation and epidemiology of toxi-infections with *B. cereus* is difficult due to the lack of a known marker of pathogenesis. Regulatory tests only allow the detection and enumeration of bacteria in suspected foods.

Emetic syndrome results from poisoning; the cereulide toxin is synthesized by *B. cereus* present in food, and quickly (between 30 min and 6 h after ingestion) causes nausea and vomiting. The dishes that cause emetic syndrome are usually based on floury foods such as rice and pasta, prepared in advance, kept at room temperature or poorly refrigerated, and then quickly reheated before tasting. *B. cereus* spores, still present in the food after its initial preparation, germinate during storage and produce the emetic toxin [46]. This toxin is very heat resistant and therefore is not destroyed when reheating food. It is also not broken down by the acidic pH of the stomach or by digestive enzymes, so it can reach the intestine intact. The dose of cereulide sufficient to induce emetic symptoms is estimated to be in the range of 5 to 10 μg/kg body weight, according to tests in monkeys and after analysis of contaminated food. Such a quantity of cereulide can be found in food when a strain of *B. cereus* reaches a concentration greater than or equal to 10^6 CFU/g. However, no dose-response curve has been established. The strains of *B. cereus* capable of producing the emetic toxin represent a minority (less than 1%) of isolates obtained from food or the environment, but represent 15% of the strains isolated from food that have caused gastrointestinal infections.

In the case of emetic syndrome, it may be necessary to test for cereulide in the offending food, especially if no bacteria are recovered from the food. The detection of cereulide requires the implementation of cell cytotoxicity tests followed by confirmation by mass spectrometry [47]. Cereulide is very stable and can remain in the food after inactivation of the bacteria, for example, by heat treatment. The number of *B. cereus* in food at the stage of its consumption is therefore not a sufficient indicator of the risk of poisoning.

In addition, *B. cereus* produces several other proteins that are toxic *in vitro* or on animal models, which could also contribute to pathologies. For example, the HlyII toxin allows bacteria to resist the host's immune system by inducing death by apoptosis of macrophages [48–51]. The proteases InhA1 and NprA allow *B. cereus* spores to escape macrophages after phagocytosis [52,53]. The Mfd protein repairs damage to bacterial DNA caused by nitrogen stress during the host's immune response to infection [54,55]. CwpFM is involved in the adhesion to epithelial cells and biofilm formation, and CwpFM from pathogenic strains possess structural specificities [56,57].

The role of all these toxins in newborn neonate infections has not been described. The potential roles of these toxins have been studied in vitro and in animal models, but they cannot be considered alone as markers of pathogenicity, and the virulence potential of a strain is likely multifactorial. In addition, as the contamination routes of the newborns are usually unknown, it is difficult to speculate on the impact of one specific toxin on the outcome of the disease.

4. Contamination Sources

The sources of patient contamination by *B. cereus* are often suspected but not confirmed. In the case of clinical non-gastrointestinal pathologies, the bacteria can be found in the catheter, in a blood culture or in a wound. Sources of *Bacillus* are not always evaluated, and in less than half of the cases, an environmental or material origin is confirmed (incubator/bed, ventilator equipment, lipids, layers, parenteral solute) [10]. After investigation, the main suspected sources of contamination are the ventilation system, the catheters, but also the feeding tubes, the linens or the benches. Since *B. cereus* is ubiquitous in the environment, the investigations often lead to the discovery of several possible sources of contamination for the patients. *B. cereus* or its spores are even present on collection

material considered sterile (in particular, on the wooden stems of swabs) or in antiseptic solutions (alcohol at 95 °C). The isolation of a strain of *B. cereus* from an infection therefore needs to be critically interpreted. Its responsibility for an infection can only be established insofar as *B. cereus* is isolated, in pure culture or in large numbers, several times in the same individual. Furthermore, the strains of *B. cereus* found in the patient's environment are often different from the isolate of the patient.

In the past few years, advances in neonate care have made the survival of low weight preterm babies possible thanks to invasive equipment. However, this equipment can become a source of infection. The use of mechanical ventilation systems or intravascular catheters during a long period of time make the risks of infections by environmental organisms jump for a vulnerable population. For instance, in 1998, an outbreak of *B. cereus* infection occurred in Amsterdam. Three neonates developed a serious infection, while 35 others were colonized [20]. Approximately one-third of the neonates became infected during their stay. The source of contamination was identified when the interior of balloons used for manual ventilation were positive for *B. cereus*. The isolates from the balloons were the same as the ones infecting the neonates. It is possible that the patients were infected by a direct inoculation of *B. cereus* in the respiratory tract while being manually ventilated. Even though the balloons are often cleaned, the interior is not reached. Furthermore, *B. cereus* has been shown to survive when exposed to cleaning products such as ethanol [58].

The hospital environment as a potential source of *B. cereus* contamination has been reported in many studies. However, the fact that *B. cereus* remaining in the hospital environment can infect unrelated patients as a consequence of nosocomial infections was only recently proven [17]. We indeed performed an extensive study of *B. cereus* strains isolated from patients and hospital environments from nine hospitals during a 5-year study, giving an overview of the consequences, sources and pathogenic patterns of *B. cereus* clinical infections. We demonstrated the occurrence of several hospital-cross-contaminations. Identical *B. cereus* strains were recovered from different patients and hospital environments for up to 2 years. We also clearly revealed the occurrence of inter hospital contaminations by the same strain (Figure 1). These cases represent the first documented events of nosocomial epidemy by *B. cereus* responsible for intra and inter hospital contaminations. The contamination of different patients with the same strain of *B. cereus* was so far never shown. However, for each single case, the actual source of infection remains unknown.

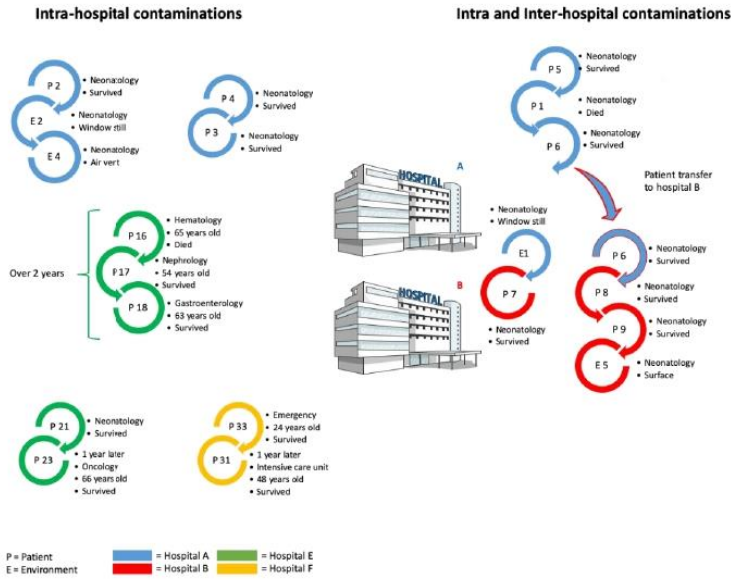

Figure 1. Nosocomial *B. cereus* infections (adapted from [17]).

Foodborne outbreaks caused by *B. cereus* in neonates are mainly suspected to occur by the ingestion of contaminated dairy products [59–62]. For instance, *B. cereus* was detected in 27% of pasteurized milk samples collected from major cities in China [59]. Although it is still not directly demonstrated, milk contamination may occur through soil and air that contain a high concentration of *B. cereus* spores: soil contains 50–380,000 CFU/g and air contains <100 CFU/m^3 of *B. cereus* spores. The production of powered infant formula and the preservation of human milk involve procedures such as pasteurization, which efficiently eliminate vegetative cells of pathogenic bacteria, but not *B. cereus* spores that are resistant to heat, dryness and disinfectants [63]. Besides, the environments for milk production, handling and processing could introduce *B. cereus* into milk. Some studies reported that the storage temperature of dairy products also affected the number and toxicity of *B. cereus*, as toxic strains could produce toxins even at +8 °C [64].

The concomitant occurrence of several cases, and the common nutrition practices with human breast milk (HBM), pointed to the supplied pasteurized human milk as a possible source of contamination. As a first example, we reported a cluster of severe intestinal infections due to *B. cereus* in two very low birth weight neonates. Pooled breast milk was suspected as a source of contamination. However, the strains isolated from the neonates differed from the strains isolated in the milk and in the hospital environment [5]. As another example, in 2016, HBM was suspected as a possible source of *B. cereus* infection in three premature neonates admitted in intensive care units in two hospitals in Île-de-France [21]. Milk batch recall procedure was launched and banked milk production was stopped during the investigation. Five hundred liters of HBM were discarded in regard to commonly used guidelines. The putative role of HBM was raised and microbiological investigation was performed on batches that were used to feed the infants. Despite the absence of bacteria with standard post-pasteurization bacteriological testing, a *B. cereus* isolate was found in an implicated batch upon large sample culture (i.e., 25 mL sampling) and 16 s RNA sequencing for bacterial confirmation. However, after thorough microbiological investigations on retained batches of HBM, no molecular epidemiological relationship and causality could be established between the ingestion of contaminated HBM and neonatal infections, as strains found in HBM and in infected neonates were distinct [21]. Numerous preterm infants have received milk from the same concerned batches without any infectious disease. Finally, additional investigations failed to identify the source of infection. Despite the absence of proven causality, one cannot rule out that the strains that remain on the milk following pasteurization might be dangerous. Thus, *Bacillus* detection and milk controls were reinforced in the two biggest human milk banks of France: the milk bank of Île-de-France and the milk bank of Marmande.

5. Food Safety Regulation

B. cereus is not subject to food safety criteria according to European regulations. However, since infants are a high-risk category, the products intended for their consumption are subjected to particularly restrictive safety criteria. The amended Regulation No. 2073/2005 defines a process hygiene criterion applicable to *B. cereus* in the case of dehydrated preparations intended for children under 6 months. EU legislation requires the systematic screening of powered infant formula for *B. cereus* contamination (Commission regulation (EC) No 1441/2007). The safety limit for *B. cereus* in foods for children under age of 6 months is established to be 50 CFU/g. Globally, the maximum acceptable number of *B. cereus* is 10^2 CFU/mL according to the Codex Alimentarius Commission of the Food and Agriculture Organization of the United Nations (FAO) and the World Health Organization (WHO). Such low values are fixed because the *B. cereus* infective dose is 10^3 CFU/g of food.

In addition, the NF EN ISO 7932 and 21,871 standards allow the identification and enumeration of presumptive *B. cereus* which can be revived.

Especially powdered infant formula, as an effective breast milk substitute, causes a potential safety risk to newborns and infants' health because it is not a sterile product. In 2014, Brandl et al. [65] showed the presence of about fifty different aerobic culturable

microorganisms in the air of Swiss milk processing facilities. Among them, *B. cereus* was one of the most frequent and most harmful bacterial groups affecting the safety of powdered milk. Their spores strongly resist stress conditions encountered in the production of powdered products. The detection of spores is an even longer procedure than that for vegetative cell detection because spores firstly need to germinate, and only formed vegetative cells are detected using standard procedure for *B. cereus* bacteria. In addition, spores may germinate directly in milk, forming vegetative cells productive of toxins or spoilage enzymes [66]. Currently, the genes *hbl*, *nhe*, *cwpFM*, *cytK* and *hlyII* encoding toxins are targeted in powdered milk by PCR, RT-PCR or multiplex-PCR [59].

Emetic strains have been isolated from raw milk, and the isolated emetic toxin, cereulide, showed high toxicity, highlighting the importance of detecting and eliminating emetic toxins and strains from raw milk [67]. Progress has been made in the detection of the emetic toxin, cereulide [68]. These methods include mass spectrometry, allowing for cereulide detection in milk [69]. In addition, emetic *B. cereus* strains possess specific growth characteristics, and this should be taken into account to prevent the risk of emetic food poisoning [70].

The large number of potential toxin genes related to *B. cereus* virulence strongly limits the efficiency of existing techniques and official diagnostic methods for *B. cereus*, and virulence factors still have to be developed. Similarly, an efficient method for the direct detection of *B. cereus* spores in milk and infant formula (without the need for a germination step) is still missing. We have recently reviewed analytical methods under development for *B. cereus* spores and toxin detection [60,71]. The time needed for their validation and subsequent adaptation by hospitals is uncertain.

6. Human Milk Banks—Methods, Practices and Issues

The Île-de-France milk bank collects, pasteurizes, qualifies and distributes approximately 12,000 L of human milk necessary to feed approximately 3500 preterm neonates annually in complement to their own mother's milk. Production procedures, such as collection, preparation and post-pasteurization microbiological analyses for human milk bank qualification, follow ADLF's (Association Française Des Lactariums de France (http://association-des-lactariums-de-france.fr)) standards.

6.1. General Hygiene Procedure and Milk Treatment

The regulation regarding preventive hygiene practices is specific to each country [2,3] (https://www.edqm.eu/en/organs-tissues-and-cells-technical-guides, Chapter 33). In France, for instance, the reference legislation is the article L. 2323-1 of the public health code (https://www.legifrance.gouv.fr/codes/article_lc/LEGIARTI000025104626/). It defines the quality management and control system to be applied, from staff training to the use of rooms and equipment. The procedures for the collection, control, processing and storage of donated milk are defined as well. All materials used by donors and staff are sterilized and provided by the institution. Any material in contact with the skin or milk is systematically washed and decontaminated. The transport of milk, from collection to its distribution, is carried out in strict compliance with the cold chain. Figure 2 resumes the different steps of human milk treatment from the breast pump to the administration to the preterm neonates.

Process	Location	Procedure
Breast pump milk 	At home or at hospital Specific approved milk donor	Hygienic measures for hand and breast Sterile bottles One used device or clean and decontaminate breast pump Storage in fridge (+4 °C) max 48 h in freezer (−18 °C) max 4 months
Milk collection 	By HMB team or hospital team	Respect of the cold chain Estimate the volume of milk, Discard when cold chain is broken
Storage of frozen milk 	By HMB team or hospital team	At −18 °C Serologic exams Anonymization—donor milk ID number assignment
Defrosting milk **Logging of incoming milk**	By HMB team or hospital team	At +4 °C one night Bottle decontamination Integrity control and labeling of each bottle
Pooling milk 	By HMB team	Pooling milk in iso 8 clean room at +4 °C Sample of each pool for bacteriologic screening before pasteurization
Aliquoting milk 		Pooled milk is aliquoted in clean containers tractability Labeling milk (batch number expiration date)
Heat processing 	By HMB team	Holder pasteurization 62.5 °C 30 min Temperature monitored and recorded Rapid cooling below +10 °C in less than 1 h Sample of each pool for bacteriologic screening after pasteurization
Chilling and storage 	By HMB team	Freezer cell at −18 °C Cold chamber Quarantine pending bacteriology
Milk dispensing 	By HMB team or hospital team	Compliant milk is dispensed to NICU Contaminated milk discarded

Figure 2. Standard procedure for milk collection and handling. HMB: Human Milk Bank; NICU: Neonatal Intensive Care Unit.

As a first step, regular cleaning and disinfection of surfaces and material used for breast milk pumps with an ordinary household disinfectant containing a 1% dilute chlorinated solution appears as an essential barrier measure. As recommended by the Centers for Disease Control of Prevention (2020), World Health Organization (2020) and Milk Banking Association (2020), "after each pumping session, all pump part that come into contact with breast milk should be appropriately disinfected". It was also demonstrated that steam decontamination using a microwavable bag after washing resulted in a lower proportion of discarded HBM (1.3% vs. 18% $p < 0.001$). The French Food Safety Agency recommended sterile single-use or autoclavable sterilized or bacteriological clean breast pump milk collection kits for mothers in hospital. An important step is the bio-cleaning of the pump and its accessories with a detergent/disinfectant followed by boiling in water for 20 min, pressure cooker for 10 min, steam or microwave sterilizers, which constitutes by far the most widespread method of decontamination; or, less common but also less time consuming and probably easier to apply, using chlorine solution (CS) [72]. CS would provide a simple solution to numerous mothers to improve the safety of their maternal milk, and we have recently published that it is safe for the infant [73]. This could especially apply to women living in precarious conditions or women who breast pump their milk at work and do not have access to boiling water for decontamination. The second step is to prevent milk contamination with skin flora. Usually *B. cereus* is not concerned, unlike *Staphylococcus*, and an easy process such as hand and breast washing with soap before pumping breast milk is sufficient.

Strict respect of the cold chain temperature of the milk at all the stages of its management must be guaranteed. This concerns the donor at home, the storage of milk at the human milk bank and its transport during delivery. For transport between 30 min and 2 h, the milk must remain refrigerated (between 0 °C and 8 °C) or frozen (below −10 °C) according to its initial state of preservation. For transport exceeding 2 h, breast milk must be transported frozen and stored at a temperature between −10 °C and −30 °C.

Milk treatments after microbiological analysis usually consist of a pasteurization (at 62.5 °C for 30 min) and a fast refrigeration [74]. Other thermal pasteurization conditions (72–75 °C) and a few non-thermal processes (high pressure processing, microwave irradiation) have also been investigated [75]. In any case, a new microbiological analysis has to be performed and the results must be negative for each lot. Milk is kept in quarantine before being analyzed for microbiological safety. The milk must therefore be frozen and kept in special storage compartments for the entire storage period prior to use. A freeze-drying process can optionally be carried out as an alternative to freezing. Finally, the appearance of the product, the integrity of the container and the labeling must be checked during distribution and dispensing.

6.2. B. cereus in HBM

At arrival at the human milk bank (HMB), the raw HBM is firstly analyzed by bacteriological analysis. Then, post-pasteurization of the milk, a mandatory second bacteriological analysis, is carried out. Milk banks have established safety standards that define the acceptance or rejection criteria prior to distributing pasteurized milk. For the pre-pasteurized milk, an aerobic total flora count on blood agar and a coagulase-positive *Staphylococci* count on a specific medium after 48 h of incubation at 37 °C have to be performed. Batches shall be declared non-compliant if the aerobic flora is equal to or greater than 10^6 CFU/mL, or if the number of coagulase-positive *Staphylococci* is equal to or greater than 10^4 CFU/mL. For a pasteurized milk sample, a 0.5 mL volume is spread onto a rich medium and incubated aerobically at 37 °C for 48 h. Following pasteurization, any batch with quantitative culture $\geq$2 CFU/mL is destroyed. For *B. cereus*, all currently available milk bank guidelines recommend the release of milk only once cultures are completely negative. A negative result for *Bacillus* in a post-pasteurization culture does not mean that this micro-organism is absent, but only that it is under the detection limit by the technique (e.g., 10^2 CFU/mL if 10 mL of milk was cultured). To be compliant and used, the HBM should respect the three criteria:

total flora below 10^6 CFU/mL and coagulase-positive *Staphylococci* below 10^4 CFU/mL before pasteurization, as well as total flora below 2 CFU/mL post pasteurization (Figure 3).

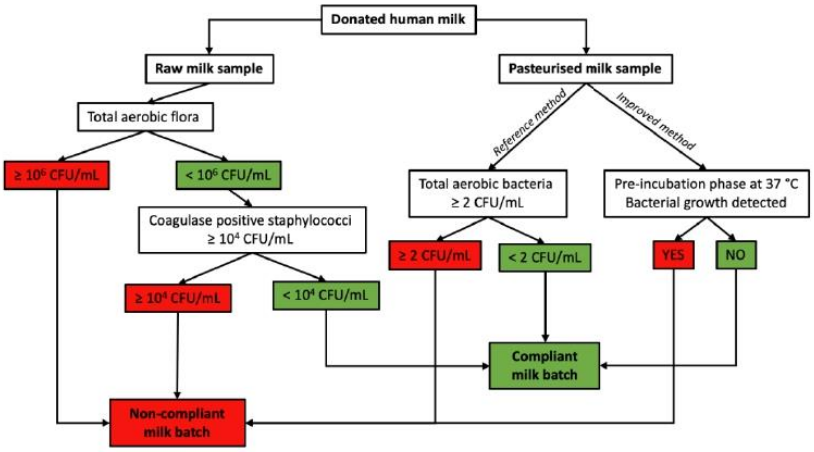

Figure 3. Good practice rules according to paragraph 3 of article L. 2323-1 of the French Public Health with reference and improved method.

Following these methods and recommendations, the analysis revealed that, on average, 7 to 25% of the samples are still contaminated following pasteurization treatments (Figure 4a). Interestingly, we can also notice a variation in contamination according to the season. Identification of the bacteria surviving the pasteurization process shows that *B. cereus* and *Streptococcus thermophilus* are almost the unique remaining bacteria (Figure 4a). This is not surprising as *B. cereus* spores have been shown to resist heat treatments up to 70 °C [76].

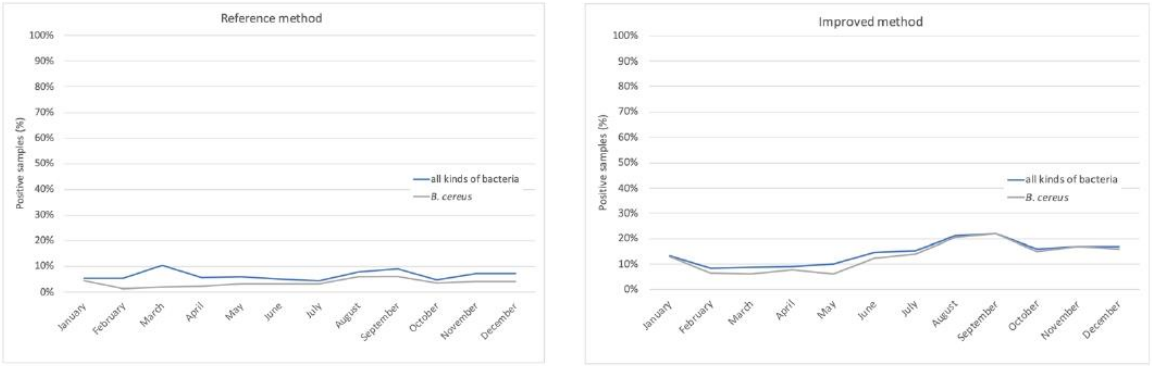

(**a**) (**b**)

Figure 4. Contaminated milk samples post-pasteurization detected with reference method (**a**) and improved method (**b**).

As said previously, HBM has been suspected in some cases as a potential source of *B. cereus* contamination of preterm neonates, although a causality has never been proven. Nevertheless, as *B. cereus* is a major HBM contaminant surviving the pasteurization process, it is of paramount importance to perform risk assessment of *B. cereus* in pasteurized milk. Consistently, and following the 2016 incidents, the Necker human milk bank has decided to use an even sensitized post-pasteurization analysis for *B. cereus* (Figure 3). On arrival at the laboratory, 20 mL of the sample is incubated for 18 h at 37 °C under aerobic conditions

(pre-incubation or enrichment stage). This step encourages any spores present in the milk to enter the vegetative cycle. At the end of the pre-incubation period, 50 µL of milk is used to seed a Petri dish containing Colombia-horse blood medium, incubated for at least 18 h at 37 °C under aerobic conditions. Each type of colony present on the agar plates is then identified by MALDI-TOF mass spectrometry. With this "improved" method, 71% of the positive batches with *B. cereus* were negative with the reference method, but identification of the germs allowed the determination of whether the isolated germs were non-pathogenic and/or known to be destroyed by pasteurization, suggesting a contamination of the sample during analysis, but not a contamination of the milk lot. The improved method thus avoids false positive samples.

Historically (Figure 4a, Table 3), 7% of the milk batches produced by our milk bank have been disqualified because of microbial contamination; half for pre-pasteurization contamination (total flora >10^6 CFU/mL or coagulase-positive *Staphylococci* >10^4 CFU/mL) and the other half for post-pasteurization contamination (thermal resistant bacteria or sporulated bacteria). A modification of bacteriologic control of post-pasteurized milk has unsurprisingly increased the rate to 15% and even 21% in 2019 post-pasteurization non-conformity (Table 3). *B. cereus* was the microorganism found in 80–90% of the batches that were disqualified (Figure 3B). Thus, we have developed a bacteriological analysis method more sensitive than the reference method for the research of *B. cereus* in pasteurized woman's milk delivered by the human milk bank. This analysis also allows us to limit discharges for bacteriological nonconformities due to contamination (when handling the sample or in the laboratory) or the presence of non-pathogenic thermophilic germs, such as *S. thermophilus*.

Table 3. Volume of human milk unfit for consumption as % of total volume collected.

Year	Bacteriologic Contamination Liters (%)
2000	192 (3.3%)
2001	174 (3.4%)
2002	172 (3.2%)
2003	155 (2.5%)
2004	256 (4%)
2005	215 (3.3%)
2006	249 (3.4%)
2007	293 (4.2%)
2008 *	524 (8.1%)
2009	401 (6.4%)
2010	465 (7.2%)
2011	541 (8.1%)
2012 **	628 (11.3%)
2013	515 (8.1%)
2014 ***	1221 (14.5%)
2015	815 (9.6%)
2016 ****	1097 (13.9%)
2017 ■	1851(19.45%)
2018	2018 (19%)
2019	2463 (21.2%)

* Hardening of bacteriological standards official guidelines. ** Necker transfer. *** Significant raw milk session by other Human Milk Banks with a bacteriological rejection rate of 20%. **** Introduction of the enhanced method following the *B. cereus* crisis. ■ Generalization of the strengthening of post-pasteurization bacteriology, sensitization towards *B. cereus*.

A Canadian analysis has evaluated the number of cases prevented by an improved method versus the number of discarded liters of milk [31]. They have estimated the potential risk of *B. cereus* infection in preterm infants caused by the ingestion of contaminated pasteurized HBM using different post-pasteurization release criteria (i.e., 9 samplings of 100 microliters versus the human milk bank association of north America (HMBANA) guideline of 1 sampling of 100 µL per pool). A simulation highlights the very small risk

of *B. cereus* infection following the ingestion of pasteurized HBM, even in the worst cases scenarios, and suggests that a 100-µL sample for post-pasteurization culture is sufficient to mitigate this risk. A larger sampling volume would only lead to a higher rate of disqualification for this important health-care resource, without having any significant positive impact on safety.

To decrease *B. cereus* milk contamination, a new process of pasteurization was also developed. It was determined that heating for 32 min at 48 °C, 20 min at 50 °C, 4 min at 54 °C, and 0.4 min at 60 °C would be sufficient for a 6 log10 CFU/mL reduction (t-6 log(T)) in vegetative cells of the most heat-resistant among the six psychrotolerant strains tested. These results suggest that the reheating of food products before consumption could rapidly eliminate psychrotolerant *B. cereus* vegetative cells, if storage conditions had permitted their multiplication in the food products. However, reheating would not inactivate cereulide, the heat stable emetic toxin produced by some rare psychrotolerant strains of *B. cereus*, but will also more drastically deprive the milk of its anti-infection properties such as IgA (Secretory Immunoglobuline A), lactoferrin and lysozyme.

Deep freeze is also a way to minimize post-pasteurization contamination by making the hypothesis that thermal shock prevents the multiplication of aerobic spores [2]. Furthermore, deep freezing does not alter the milk nutritional quality [2,77,78]. The acceleration of the freezing procedure certainly has a beneficial role by limiting the time when the milk temperature is between 30 °C and 37 °C and preventing the risk of entry into the vegetative cycle effective between +10 °C and +4 °C.

We conducted a comparative study using the improved detection protocol on post-deep freeze versus post-pasteurization milk. Thirty-four samples were analyzed. Table 4 resumes the results of bacteriology post-pasteurization and post pasteurization-deep freezing. Thirty-two percent of non-compliant milk after pasteurization was compliant after pasteurization/deep freezing. The implementation of this new pasteurization/deep freezing method on these samples, which have become compliant, shows that they correspond to concentrations of less than 0.07 CFU/mL. This interesting approach could be widely used by neonatalogy services. This would reduce losses while pursuing a strengthened method of detecting *B. cereus*, therefore achieving maximum safety for the final product.

Table 4. Impact of pasteurization and fast freezing on *B. cereus* contamination.

Date	Culture Post Pasteurization	Culture Post Pasteurization/Fast-Freezing
21-Feb	*Bacillus cereus*	Negative
16-Apr	*Bacillus cereus*	*Bacillus cereus*
28-May	*Bacillus cereus*	Negative
11-Apr	*Bacillus cereus*	*Streptococcus thermophilus*
29-May	*Bacillus cereus*	*Bacillus cereus*
05-Apr	*Bacillus cereus*	*Bacillus cereus*
13-May	*Bacillus cereus*	Negative
29-Mar	*Bacillus cereus*	Negative
10-Apr	*Bacillus cereus*	Negative
05-Apr	*Bacillus cereus*	Negative
07-Mar	*Bacillus cereus*	*Bacillus cereus*
04-Mar	*Bacillus cereus*	Negative
12-Mar	*Bacillus cereus*	*Bacillus cereus*
21-Mar	*Bacillus cereus*	*Bacillus cereus*
18-Mar	*Bacillus cereus*	*Bacillus cereus*

Table 4. *Cont.*

Date	Culture Post Pasteurization	Culture Post Pasteurization/Fast-Freezing
16-Apr	*Bacillus cereus*	Negative
03-Jun	*Bacillus cereus*	*Bacillus cereus*
28-Feb	*Bacillus cereus*	*Enterococcus faecalis*
20-Feb	*Bacillus cereus*	Negative
14-May	*Bacillus cereus*	*Bacillus cereus*
22-May	*Bacillus cereus*	Negative
27-Feb	*Bacillus cereus*	*Bacillus cereus*
27-Feb	*Bacillus cereus*	*Bacillus cereus*
04-Feb	*Bacillus cereus*	Negative
08-Feb	*Bacillus cereus*	*Bacillus cereus*
05-Feb	*Bacillus cereus*	*Bacillus cereus*
15-Feb	*Bacillus cereus*	*Bacillus cereus*
27-Feb	*Bacillus cereus*	*Bacillus cereus*
06-May	*Bacillus cereus*	*Bacillus cereus*
12-Feb	*Bacillus cereus*	*Bacillus cereus*
27-Feb	*Bacillus cereus*	*Bacillus spp.*
07-Feb	*Bacillus cereus*	*Bacillus cereus*
12-Feb	*Bacillus cereus*	*Bacillus cereus*
01-Mar	*Bacillus cereus*	*Bacillus cereus*

Taken together, improved detection and decontamination methods might help decreasing the risk and help to preserve the public's confidence in this vital biological product for infants whose mothers cannot breastfeed.

7. Conclusions

In this review, we have gathered information on various *B. cereus* cases and outcomes in preterm neonates. These data clearly indicate that newborn infections by *B. cereus* should not be overlooked. The range of symptoms is wide and it is difficult to associate a particular disease to *B. cereus*. The infection can be asymptomatic to severe, with brain lesions and septic shock, to lethal. It is key to identify as quickly as possible the agent responsible for the infection in order to pursue a line of treatment adapted to *B. cereus*. As such, *B. cereus* should not be discarded as a contaminant and appropriate antibiotic treatment needs to be given promptly.

The contamination sources of *B. cereus* are often found to be in the hospital equipment—in particular, the ventilation system and the catheters. The spores are highly resistant and can be found in sterile material and even in antiseptic solutions. Even though the strains found in the environment of the patient are often different from the strain infecting them, the identification of the source is often lacking. In a few cases, HBM has been suspected to be the source of contamination, but no correlation between the strain found in the milk and the one infecting the patients could be found. Nonetheless, since HBM could be a potential source of contamination, the detection and the control in the milk are sometimes reinforced and follow a strict protocol. As such, the risk appears extremely low and is mitigated by post-pasteurization microbiological criteria applied to define HBM acceptance for distribution. New technology applied in human milk banks such as high pressure could be a real improvement as it totally destroys *B. cereus* spores. It could reduce discarding human milk while preserving a maximum of anti-infectious properties. Before high pressure

becomes available, bacteriology post deep-freezing seems to be a good opportunity to reduce residual *B. cereus* in pasteurized human milk.

Given the widespread dissemination of *B. cereus* in hospital, and the important risks for preterm neonate children, more emphasis should be given to the immediate Intensive Care Unit environment, such as invasive care equipment, linens, ventilation and air conditioning systems.

Author Contributions: D.C., V.R.: writing of the first draft, designed figures; J.V., F.R.: writing of the first draft; E.B.: designed figures, final drafting of the manuscript; N.R.: overall supervision, writing first draft and final version of the manuscript. All authors have read and agreed to the published version of the manuscript.

Funding: This research received no external funding.

Institutional Review Board Statement: Not applicable.

Informed Consent Statement: Not applicable.

Data Availability Statement: No new data were created or analyzed in this study. Data sharing is not applicable to this article.

Conflicts of Interest: The authors declare no conflict of interest.

References

1. Picaud, J.C.; Buffin, R.; Gremmo-Feger, G.; Rigo, J.; Putet, G.; Casper, C.; Working group of the French Neonatal Society on fresh human milk use in preterm infants. Review concludes that specific recommendations are needed to harmonise the provision of fresh mother's milk to their preterm infants. *Acta Paediatr.* **2018**, *107*, 1145–1155. [CrossRef]
2. Moro, G.E.; Billeaud, C.; Rachel, B.; Calvo, J.; Cavallarin, L.; Christen, L.; Escuder-Vieco, D.; Gaya, A.; Lembo, D.; Wesolowska, A.; et al. Processing of donor human milk: Update and recommendations from the european milk bank association (EMBA). *Front. Pediatr.* **2019**, *7*, 49. [CrossRef] [PubMed]
3. Weaver, G.; Bertino, E.; Gebauer, C.; Grovslien, A.; Mileusnic-Milenovic, R.; Arslanoglu, S.; Barnett, D.; Boquien, C.-Y.; Buffin, R.; Gaya, A.; et al. Recommendations for the establishment and operation of human milk banks in Europe: A consensus statement from the european milk bank association (EMBA). *Front. Pediatr.* **2019**, *7*, 53. [CrossRef]
4. Lewin, A.; Quach, C.; Rigourd, V.; Picaud, J.-C.; Perreault, T.; Frange, P.; Domingo, M.-C.; Lalancette, C.; Delage, G.; Germain, M. *Bacillus cereus* infection in neonates and the absence of evidence for the role of banked human milk: Case reports and literature review. *Infect. Control. Hosp. Epidemiol.* **2019**, *40*, 787–793. [CrossRef]
5. Decousser, J.-W.; RamaRao, N.; Duport, C.; Dorval, M.; Bourgeois-Nicolaos, N.; Guinebretière, M.-H.; Razafimahefa, H.; Doucet-Populaire, F. *Bacillus cereus* and severe intestinal infections in preterm neonates: Putative role of pooled breast milk. *Am. J. Infect. Control* **2013**, *41*, 918–921. [CrossRef] [PubMed]
6. Lin, S.; Schraft, H.; Odumeru, J.A.; Griffiths, M.W. Identification of contamination sources of *Bacillus cereus* in pasteurized milk. *Int. J. Food Microbiol.* **1998**, *43*, 159–171. [CrossRef]
7. Stenfors Arnesen, L.; Fagerlund, A.; Granum, P. From soil to gut: *Bacillus cereus* and its food poisoning toxins. *FEMS Microbiol. Rev.* **2008**, *32*, 579–606. [CrossRef]
8. Glasset, B.; Herbin, S.; Guillier, L.; Cadel-Six, S.; Vignaud, M.L.; Grout, J.; Pairaud, S.; Michel, V.; Hennekinne, J.-A.; Ramarao, N.; et al. Large-scale survey of *Bacillus cereus*-induced food-borne outbreaks: Epidemiologic and genetic characterization. *Eurosurveillance* **2016**, *21*, 30413.
9. European Food Safety Authority ECfDPaC. The European Union summary report on trends and sources of zoonoses, zoonotic agents and food-borne outbreaks in 2016. *EFSa J.* **2018**, *13*.
10. Bottone, E.J. *Bacillus cereus*, a volatile human pathogen. *Clin. Microbiol. Rev.* **2010**, *23*, 382–398. [CrossRef] [PubMed]
11. Baldwin, V.M. You Can't B. cereus-A review of *Bacillus cereus* strains that cause anthrax-like disease. *Front. Microbiol.* **2020**, *11*, 1731. [CrossRef] [PubMed]
12. Lequin, M.H.; Vermeulen, J.R.; Van Elburg, R.M.; Barkhof, F.; Kornelisse, R.F.; Swarte, R.; Govaert, P.P. *Bacillus cereus* meningoencephalitis in preterm infants: Neuroimaging characteristics. *AJNR Am. J. Neuroradiol.* **2005**, *26*, 2137–2143. [PubMed]
13. Heep, A.; Schaller, C.; Rittmann, N.; Himbert, U.; Bartmann, P. Multiple brain abscesses in an extremely preterm infant: Treatment surveillance with interleukin-6 in the CSF. *Eur. J. Nucl. Med. Mol. Imaging* **2003**, *163*, 44–45. [CrossRef] [PubMed]
14. Jevon, G.P.; Dunne, W.M., Jr.; Hicks, M.J.; Langston, C. *Bacillus cereus pneumonia* in premature neonates: A report of two cases. *Pediatr. Infect. Dis. J.* **1993**, *12*, 251–253. [CrossRef] [PubMed]
15. Steen, M.K.; Bruno-Murtha, L.A.; Chaux, G.; Lazar, H.; Bernard, S.; Sulis, C. *Bacillus cereus endocarditis*: Report of a Case and Review. *Clin. Infect. Dis.* **1992**, *14*, 945–946. [CrossRef]
16. David, D.B.; Kirkby, G.R.; Noble, B.A. *Bacillus cereus* endophthalmitis. *Br. J. Ophthalmol.* **1994**, *78*, 577–580. [CrossRef]

17. Glasset, B.; Herbin, S.; Granier, S.A.; Cavalié, L.; Lafeuille, E.; Guérin, C.; Ruimy, R.; Casagrande-Magne, F.; Levast, M.; Chautemps, N.; et al. *Bacillus cereus*, a serious cause of nosocomial infections: Epidemiologic and genetic survey. *PLoS ONE* **2018**, *13*, e0194346. [CrossRef]
18. Lotte, R.; Hérissé, A.L.; Berrouane, Y.; Lotte, L.; Casagrande, F.; Landraud, L.; Herbin, S.; Ramarao, N.; Boyer, L.; Ruimy, R.; et al. Virulence analysis of *Bacillus cereus* isolated after death of preterm neonates, Nice, France. *Emerg. Infect. Dis.* **2017**, *23*, 845–848. [CrossRef]
19. RamaRao, N.; Belotti, L.; Deboscker, S.; Ennahar-Vuillemin, M.; De Launay, J.; Lavigne, T.; Koebel, C.; Escande, B.; Guinebretière, M.H. Two unrelated episodes of *Bacillus cereus bacteremia* in a neonatal intensive care unit. *Am. J. Infect. Control.* **2014**, *42*, 694–695. [CrossRef]
20. Van Der Zwet, W.C.; Parlevliet, G.A.; Savelkoul, P.H.; Stoof, J.; Kaiser, A.M.; Van Furth, A.M.; Vandenbroucke-Grauls, C.M. Outbreak of *Bacillus cereus* infections in a neonatal intensive care unit traced to balloons used in manual ventilation. *J. Clin. Microbiol.* **2000**, *38*, 4131–4136. [CrossRef]
21. Fournier, S.; Faraut-Derouin, V.; Casetta, A.; Frange, P.; Doit, C.; Fortineau, N.; Romain, O.; Patkai, J.; de Chillaz, C.; Rigourd, V.; et al. Bactériémies à *Bacillus cereus* en réanimation néonatale à l'ap-hp en 2016. *Bull. Epidémiol. Hebd. BEH* **2018**, *25*, 536–540.
22. Campbell, J.R.; Hulten, K.; Baker, C.J. Cluster of *Bacillus species bacteremia* cases in neonates during a hospital construction project. *Infect. Control. Hosp. Epidemiol.* **2011**, *32*, 1035–1038. [CrossRef] [PubMed]
23. Chu, W.P.; Que, T.L.; Lee, W.K.; Wong, S.N. Meningoencephalitis caused by *Bacillus cereus* in a neonate. *Hong Kong Med. J.* **2001**, *7*.
24. Evreux, F.; Delaporte, B.; Leret, N.; Buffet-Janvresse, C.; Morel, A. A case of fatal neonatal *Bacillus cereus* meningitis. *Arch. Pediatr.* **2007**, *14*, 365–368. [CrossRef] [PubMed]
25. Gray, J.; George, R.; Durbin, G.; Ewer, A.; Hocking, M.; Morgan, M. An outbreak of *Bacillus cereus* respiratory tract infections on a neonatal unit due to contaminated ventilator circuits. *J. Hosp. Infect.* **1999**, *41*, 19–22. [CrossRef]
26. Horii, T.; Tamai, K.; Notake, S.; Yanagisawa, H. *Bacillus cereus* bloodstream infection in a preterm neonate complicated by late meningitis. *Case Rep. Infect. Dis.* **2012**, *2012*, 1–3.
27. Patrick, C.C.; Langston, C.; Baker, C.J. *Bacillus Species* infections in neonates. *Clin. Infect. Dis.* **1989**, *11*, 612–615. [CrossRef]
28. Sasahara, T.; Hayashi, S.; Morisawa, Y.; Sakihama, T.; Yoshimura, A.; Hirai, Y. *Bacillus cereus bacteremia* outbreak due to contaminated hospital linens. *Eur. J. Clin. Microbiol. Infect. Dis.* **2010**, *30*, 219–226. [CrossRef]
29. Tokieda, K.; Morikawa, Y.; Maeyama, K.; Mori, K.; Ikeda, K. Clinical manifestations of *Bacillus cereus* meningitis in newborn infants. *J. Paediatr. Child Health* **1999**, *35*, 582–584. [CrossRef]
30. Hilliard, N.J.; Schelonka, R.L.; Waites, K.B. *Bacillus cereus bacteremia* in a preterm neonate. *J. Clin. Microbiol.* **2003**, *41*, 3441–3444. [CrossRef]
31. Lewin, A.; Delage, G.; Bernier, F.; Germain, M. Banked human milk and quantitative risk assessment of *Bacillus cereus* infection in premature infants: A simulation study. *Can. J. Infect. Dis. Med Microbiol.* **2019**, *2019*, 6348281. [CrossRef]
32. Ramarao, N.; Sanchis, V. The pore-forming haemolysins of *Bacillus cereus*: A review. *Toxins* **2013**, *5*, 1119–1139. [CrossRef]
33. Guinebretiere, M.; Girardin, H.; Dargaignaratz, C.; Carlin, F.; Nguyen, C. Contamination flows of *Bacillus cereus* and spore-forming aerobic bacteria in a cooked, pasteurized and chilled zucchini purée processing line. *Int. J. Food Microbiol.* **2003**, *82*, 223–232. [CrossRef]
34. Beecher, D.J.; Schoeni, J.L.; Wong, A.C. Enterotoxic activity of hemolysin BL from *Bacillus cereus*. *Infect. Immun.* **1995**, *63*, 4423–4428. [CrossRef] [PubMed]
35. Beecher, D.J.; Wong, A.C. Identification of hemolysin BL-producing *Bacillus cereus* isolates by a discontinuous hemolytic pattern in blood agar. *Appl. Environ. Microbiol.* **1994**, *60*, 1646–1651. [CrossRef] [PubMed]
36. Beecher, D.J.; Pulido, J.S.; Barney, N.P.; Wong, A.C. Extracellular virulence factors in *Bacillus cereus* endophthalmitis: Methods and implication of involvement of hemolysin BL. *Infect. Immun.* **1995**, *63*, 632–639. [CrossRef] [PubMed]
37. Lund, T.; Granum, P.E. Comparison of biological effect of the two different enterotoxin complexes isolated from three different strains of *Bacillus cereus*. *Microbiology* **1997**, *143*, 3329–3336. [CrossRef] [PubMed]
38. Beecher, D.J.; Macmillan, J.D. A novel bicomponent hemolysin from *Bacillus cereus*. *Infect. Immun.* **1990**, *58*, 2220–2227. [CrossRef]
39. Beecher, D.J.; Wong, A.C.L. Tripartite haemolysin BL: Isolation and characterization of two distinct homologous sets of components from a single *Bacillus cereus* isolate. *Microbiology* **2000**, *146*, 1371–1380. [CrossRef]
40. Granum, P.E.; O'Sullivan, K.; Lund, T. The sequence of the non-haemolytic enterotoxin operon from *Bacillus cereus*. *FEMS Microbiol. Lett.* **1999**, *177*, 225–229. [CrossRef]
41. Granum, P.E.; Tomas, J.M.; Alouf, J.E. A survey of bacterial toxins involved in food poisoning: A suggestion for bacterial food poisoning toxin nomenclature. *Int. J. Food Microbiol.* **1995**, *28*, 129–144. [CrossRef]
42. Fagerlund, A.; Lindback, T.; Storset, A.K.; Granum, P.E.; Hardy, S.P. *Bacillus cereus* Nhe is a pore-forming toxin with structural and functional properties similar to the ClyA (HlyE, SheA) family of haemolysins, able to induce osmotic lysis in epithelia. *Microbiology* **2008**, *154*, 693–704. [CrossRef]
43. Lund, T.; De Buyser, M.-L.; Granum, P.E. A new cytotoxin from *Bacillus cereus* that may cause necrotic enteritis. *Mol. Microbiol.* **2000**, *38*, 254–261. [CrossRef]
44. Fagerlund, A.; Brillard, J.; Fürst, R.; Guinebretière, M.-H.; Granum, P.E. Toxin production in a rare and genetically remote cluster of strains of the *Bacillus cereus* group. *BMC Microbiol.* **2007**, *7*, 43. [CrossRef]

45. Fagerlund, A.; Ween, O.; Lund, T.; Hardy, S.P.; Granum, P.E. Genetic and functional analysis of the cytK family of genes in Bacillus cereus. *Microbiology* **2004**, *150*, 2689–2697. [CrossRef]
46. Ehling-Schulz, M.; Guinebretiere, M.-H.; Monthã¡n, A.; Berge, O.; Fricker, M.; Svensson, B. Toxin gene profiling of enterotoxic and emetic *Bacillus cereus*. *FEMS Microbiol. Lett.* **2006**, *260*, 232–240. [CrossRef] [PubMed]
47. Ehling-Schulz, M.; Svensson, B.; Guinebretiere, M.-H.; Lindbäck, T.; Andersson, M.; Schulz, A.; Fricker, M.; Christiansson, A.; Granum, P.E.; Märtlbauer, E.; et al. Emetic toxin formation of *Bacillus cereus* is restricted to a single evolutionary lineage of closely related strains. *Microbiology* **2005**, *151*, 183–197. [CrossRef] [PubMed]
48. Tran, S.L. *Bacillus cereus* immune escape: A journey within macrophages. *FEMS Microbiol. Lett.* **2013**, *347*, 1–6. [CrossRef]
49. Tran, S.L.; Puhar, A.; Ngo-Camus, M.; Ramarao, N. Trypan blue dye enters viable cells incubated with the pore-forming toxin HlyII of *Bacillus cereus*. *PLoS ONE* **2011**, *6*, e22876. [CrossRef] [PubMed]
50. Tran, S.L.; Guillemet, E.; Ngo-Camus, M.; Clybouw, C.; Puhar, A.; Moris, A.; Gohar, M.; Lereclus, D.; Ramarao, N. Hemolysin II is a *Bacillus cereus* virulence factor that induces apoptosis of macrophages. *Cell Microbiol.* **2011**, *13*, 92–108. [CrossRef]
51. Cadot, C.; Tran, S.-L.; Vignaud, M.-L.; de Buyser, M.-L.; Kolstø, A.-B.; Brisabois, A.; Nguyen, C.; Lereclus, D.; Guinebretière, M.-H.; Ramarao, N. InhA1, NprA and HlyII as candidates to differentiate pathogenic from non-pathogenic *Bacillus cereus* strains. *J. Clin. Microbiol.* **2010**, *3*, 1358–1365. [CrossRef] [PubMed]
52. RamaRao, N.; Lereclus, D. The InhA1 metalloprotease allows spores of the *B. cereus* group to escape macrophages. *Cell. Microbiol.* **2005**, *7*, 1357–1364.
53. Haydar, A.; Tran, S.L.; Guillemet, E.; Darrigo, C.; Perchat, S.; Lereclus, D.; Coquet, L.; Jouenne, T.; Ramarao, N. InhA1-mediated cleavage of the metalloprotease NprA allows *Bacillus cereus* to escape from macrophages. *Front Microbiol.* **2018**, *23*, 1063. [CrossRef] [PubMed]
54. Guillemet, E.; Leréec, A.; Tran, S.-L.; Royer, C.; Barbosa, I.; Sansonetti, P.; Lereclus, D.; RamaRao, N. The bacterial DNA repair protein Mfd confers resistance to the host nitrogen immune response. *Sci. Rep.* **2016**, *6*, 29349. [CrossRef]
55. Darrigo, C.; Guillemet, E.; Dervyn, R.; Ramarao, N. The bacterial Mfd protein prevents DNA damage induced by the host nitrogen immune response in a NER-independent but RecBC-dependent pathway. *PLoS ONE* **2016**, *11*, e0163321. [CrossRef]
56. Tran, S.-L.; Guillemet, E.; Gohar, M.; Lereclus, D.; RamaRao, N. CwpFM (EntFM) is a *Bacillus cereus* potential cell wall peptidase implicated in adhesion, biofilm formation, and virulence. *J. Bacteriol.* **2010**, *192*, 2638–2642. [CrossRef]
57. Tran, S.-L.; Cormontagne, D.; Vidic, J.; André-Leroux, G.; RamaRao, N. Structural modeling of cell wall peptidase CwpFM (EntFM) reveals distinct intrinsically disordered extensions specific to pathogenic *Bacillus cereus* strains. *Toxins* **2020**, *12*, 593. [CrossRef] [PubMed]
58. Hsueh, P.-R.; Teng, L.-J.; Yang, P.-C.; Pan, H.-L.; Ho, S.-W.; Luh, K.-T. Nosocomial pseudoepidemic caused by *Bacillus cereus* traced to contaminated ethyl alcohol from a liquor factory. *J. Clin. Microbiol.* **1999**, *37*, 2280–2284. [CrossRef] [PubMed]
59. Liu, X.; Hu, Q.; Xu, F.; Ding, S.; Zhu, K. Characterization of *Bacillus cereus* in dairy products in China. *Toxins* **2020**, *12*, 454. [CrossRef]
60. Vidic, J.; Chaix, C.; Manzano, M.; Heyndrickx, M. Food sensing: Detection of *Bacillus cereus* spores in dairy products. *Biosensors* **2020**, *10*, 15. [CrossRef]
61. Egopal, N.; Ehill, C.; Ross, P.R.; Beresford, T.P.; Fenelon, M.A.; Cotter, P.D. The prevalence and control of *Bacillus* and related spore-forming bacteria in the dairy industry. *Front. Microbiol.* **2015**, *6*, 1418.
62. Machado, S.G.; Baglinière, F.; Marchand, S.; Van Coillie, E.; Vanetti, M.C.D.; De Block, J.; Heyndrickx, M. The biodiversity of the microbiota producing heat-resistant enzymes responsible for spoilage in processed bovine milk and dairy products. *Front. Microbiol.* **2017**, *8*, 302. [CrossRef]
63. Sarita Kumari, P.K.S. *Bacillus cereus* hazard and control in industrial dairy processing environment. *Food Control.* **2016**, *69*, 20–29. [CrossRef]
64. Saleh-Lakha, S.; Leon-Velarde, C.G.; Chen, S.; Lee, S.; Shannon, K.; Fabri, M.; Downing, G.; Keown, B. A study to assess the numbers and prevalence of *Bacillus cereus* and its toxins in pasteurized fluid milk. *J. Food Prot.* **2017**, *80*, 1085–1089. [CrossRef] [PubMed]
65. Brandl, H.; Fricker-Feer, C.; Ziegler, M.; Mandal, J.; Stephan, R.; Lehner, A. Distribution and identification of culturable airborne microorganisms in a Swiss milk processing facility. *J. Dairy Sci.* **2014**, *97*, 240–246. [CrossRef] [PubMed]
66. Esteban, M.-D.; Huertas, J.-P.; Fernández, P.; Palop, A. Effect of the medium characteristics and the heating and cooling rates on the nonisothermal heat resistance of *Bacillus sporothermodurans* IC4 spores. *Food Microbiol.* **2013**, *34*, 158–163. [CrossRef]
67. Cui, Y.; Liu, Y.; Liu, X.; Xia, X.; Ding, S.; Zhu, K. Evaluation of the toxicity and toxicokinetics of *Cereulide* from an *Emetic Bacillus cereus* strain of milk origin. *Toxins* **2016**, *8*, 156. [CrossRef]
68. Ehling-Schulz, M.; Vukov, N.; Schulz, A.; Shaheen, R.; Andersson, M.; Märtlbauer, E.; Scherer, S. Identification and partial characterization of the nonribosomal peptide synthetase gene responsible for cereulide production in emetic *Bacillus cereus*. *Appl. Environ. Microbiol.* **2005**, *71*, 105–113. [CrossRef]
69. Ducrest, P.J.; Pfammatter, S.; Stephan, D.; Vogel, G.; Thibault, P.; Schnyder, B. Rapid detection of *Bacillus ionophore cereulide* in food products. *Sci. Rep.* **2019**, *9*, 5814. [CrossRef]
70. Carlin, F.; Fricker, M.; Pielaat, A.; Heisterkamp, S.; Shaheen, R.; Salonen, M.S.; Svensson, B.; Nguyen, C.; Ehling-Schulz, M. Emetic toxin-producing strains of *Bacillus cereus* show distinct characteristics within the *Bacillus cereus* group. *Int. J. Food Microbiol.* **2006**, *109*, 132–138. [CrossRef]

71. RamaRao, N.; Tran, S.-L.; Marin, M.; Vidic, J. Advanced methods for detection of *Bacillus cereus* and its pathogenic factors. *Sensors* **2020**, *20*, 2667. [CrossRef] [PubMed]
72. Price, E.; Weaver, G.; Hoffman, P.; Jones, M.; Gilks, J.; O'Brien, V.; Ridgway, G. Decontamination of breast pump milk collection kits and related items at home and in hospital: Guidance from a joint working group of the healthcare infection society and infection prevention society. *J. Hosp. Infect.* **2016**, *92*, 213–221. [CrossRef] [PubMed]
73. Rigourd, V.; Barnier, J.P.; Ferroni, A.; Nicloux, M.; Hachem, T.; Magny, J.F.; Lapillonne, A.; Frange, P.; Nassif, X.; Bille, E. Recent actuality about *Bacillus cereus* and human milk bank: A new sensitive method for microbiological analysis of pasteurized milk. *Eur. J. Clin. Microbiol. Infect. Dis.* **2018**, *37*, 1297–1303. [CrossRef]
74. Peila, C.; Emmerik, N.E.; Giribaldi, M.; Stahl, B.; Ruitenberg, J.E.; Van Elburg, R.M.; Cavallarin, L. Human milk processing: A systematic review of innovative techniques to ensure the safety and quality of donor milk. *J. Pediatr. Gastroenterol. Nutr.* **2017**, *64*, 353–361. [CrossRef]
75. Wesolowska, A.; Sinkiewicz-Darol, E.; Barbaska, O.; Bernatowicz-Lojko, U.; Borszewska-Kornacka, M.; van Goudoever, J. Innovative techniques of processing human milk to preserve key components. *Nutrients* **2019**, *11*, 1169. [CrossRef] [PubMed]
76. Ramarao, N. *Bacillus cereus*: Caractéristiques et pathogénicité. *EMC Biol. Medic.* **2020**, *7*, 1–11. [CrossRef]
77. Arslanoglu, S.; Moro, G.E.; Ziegler, E.E.; the WAPM Working Group on Nutrition. Optimization of human milk fortification for preterm infants: New concepts and recommendations. *J. Périnat. Med.* **2010**, *38*, 233–238.
78. Moro, G.E.; Arslanoglu, S. Heat treatment of human milk. *J. Pediatr. Gastroenterol. Nutr.* **2012**, *54*, 165–166. [CrossRef]

Annexe II

Article : “Structural Modeling of Cell Wall Peptidase CwpFM (EntFM) Reveals Distinct Intrinsically Disordered Extensions Specific to Pathogenic *Bacillus cereus* Strains”

toxins

MDPI

Article

Structural Modeling of Cell Wall Peptidase CwpFM (EntFM) Reveals Distinct Intrinsically Disordered Extensions Specific to Pathogenic *Bacillus cereus* Strains

Seav-Ly Tran [1], Delphine Cormontagne [1], Jasmina Vidic [1], Gwenaëlle André-Leroux [2,*] and Nalini Ramarao [1,*]

[1] Micalis Institute, INRAE, AgroParisTech, Université Paris-Saclay, 78350 Jouy-en-Josas, France; seav-ly.tran@inrae.fr (S.-L.T.); delphine.cormontagne@inrae.fr (D.C.); jasmina.vidic@inrae.fr (J.V.)

[2] MaIAGE, INRAE, AgroParisTech, Université Paris-Saclay, 78350 Jouy-en-Josas, France

* Correspondence: gwenaelle.andre-leroux@inrae.fr (G.A.-L.); nalini.ramarao@inrae.fr (N.R.)

Received: 10 August 2020; Accepted: 9 September 2020; Published: 14 September 2020

Abstract: The emergence of *B. cereus* as an opportunistic food-borne pathogen has intensified the need to distinguish strains of public health concern. The heterogeneity of the diseases associated with *B. cereus* infections emphasizes the versatility of these bacteria strains to colonize their host. Nevertheless, the molecular basis of these differences remains unclear. Several toxins are involved in virulence, particularly in gastrointestinal disorders, but there are currently no biological markers able to differentiate pathogenic from harmless strains. We have previously shown that CwpFM is a cell wall peptidase involved in *B. cereus* virulence. Here, we report a sequence/structure/function characterization of 39 CwpFM sequences, chosen from a collection of *B. cereus* with diverse virulence phenotypes, from harmless to highly pathogenic strains. CwpFM is homology-modeled in silico as an exported papain-like endopeptidase, with an N-terminal end composed of three successive bacterial Src Homology 3 domains ($SH3b_{1-3}$) likely to control protein–protein interactions in signaling pathways, and a C-terminal end that contains a catalytic NLPC_P60 domain primed to form a competent active site. We confirmed in vitro that CwpFM is an endopeptidase with a moderate peptidoglycan hydrolase activity. Remarkably, CwpFMs from pathogenic strains harbor a specific stretch of twenty residues intrinsically disordered, inserted between the $SH3b_3$ and the catalytic NLPC_P60 domain. This strongly suggests this linker as a marker of differentiation between *B. cereus* strains. We believe that our findings improve our understanding of the pathogenicity of *B. cereus* while advancing both clinical diagnosis and food safety.

Keywords: *Bacillus cereus*; cell wall peptidase; disordered extensions; homology modeling

Key Contribution: CwpFM as an exported papain-like endopeptidase with PG hydrolase activity; CwpFMs from pathogenic *B. cereus* strains harbor a specific disordered linker; the CwpFM linker is a new marker of pathogenic *B. cereus* strains.

1. Introduction

The cell wall (CW) of bacteria is an intricate mesh of macromolecules composed of peptidoglycan (PG), a complex polymer formed by linear glycan chains cross-linked by peptide stems. The glycan chains are usually long and alternate N-acetylglucosamine (NAG) with N-acetylmuramic acid (NAM) residues through β-(1, 4) bonds. In most Gram-positive bacteria like *Bacillus cereus*, the core structure of a non-cross-linked stem attached is L-Ala-γ-D-Glu-L-Lys-D-Ala-D-Ala. Due to environmental adaptation, the PG core can undergo chemical modification like O-acetylation, N-deacetylation amidation or can incorporate Gly and non-canonical D-amino acids [1]. Additionally, the CW accommodates macromolecular components such as teichoic acid, lipoteichoic acids, polysaccharides and complex proteins like export secretion systems. CW integrity and plasticity need to be tuned to adapt readily to the bacterial cell cycle or to the changing environment, and its biosynthesis must be also highly regulated as CW disruption leads to bacterial cell death [2]. Accordingly, PG metabolism requires an exquisite and timely remodeling, organized by bacterial cell wall hydrolases (CWHs) [3]. CWHs play an essential physiological role in cell wall integrity. Additionally, they are implicated in bacterial adhesion and invasiveness [4], persistence in the host [5] and in the initiation step of biofilm formation [6], therefore contributing to bacterial pathogenicity. Moreover, the resulting cell wall fragments are recycled as signaling molecules to trigger bacterial communication, immune response or antibiotics resistance [5,7]. Finally, they also prime the insertion of supramolecular structures like secretion, flagella or pili systems [8]. Three types of CWH exist, each displaying a specificity towards PG: (i) cell wall amidase (CWA) catalyzes the hydrolysis of the amide bond between NAM and L-Ala at the N-terminal of the stem peptide; (ii) cell wall glycosidase (CWG) cleaves the glycosidic linkages; and (iii) cell wall peptidase (CWP) hydrolyses the amide bonds with the PG chains [8]. Recent structural data evidence that CWHs show modularity, with a catalytic domain combined to one or several CW binding domains (CBDs) located at the N- or C-terminal ends. This modular organization associated with CBD repeats is highly suspected to engage these hydrolases as a platform responsible for CW integrity. Interestingly, due to their inherent flexibility and lack of structural characterization, the linker regions that connect the binding domains to the catalytic one have received little attention until now. Nevertheless, interest is increasing as they are shown to play a role in domains orientation or swapping, and dynamics that result in substrate specificity and affinity [1–3].

The *Bacillus cereus* group is composed of rod-shaped, spore-forming, aerobic or facultative anaerobic species [9], among which the most noticeable members are species from *B. cereus sensu stricto* (usually referred to as *B. cereus*), *B. mycoides*, *B. pseudomycoides*, *B. weihenstephanensis*, *B. anthracis*, *B. thuringiensis*, *B. cytotoxicus* and *B. toyonensis*. The genetic proximity of the species within the *B. cereus* group has not permitted their distinction from a phylogenetic point of view; nevertheless, species can be differentiated through phenotypic characteristics, host species predilection and clinical manifestation [10,11]. Four members are pathogens, namely *B. thuringiensis, B. anthracis, B. cytotoxicus* and *B. cereus*. Despite being long considered as nonpathogenic to humans, *B. thuringiensis* has been occasionally identified as responsible for human infections including food poisoning-associated diarrheas, ocular infections, periodontitis, burn and wound infections or bacteremia [12]. In addition, *B. thuringiensis* can produce potent insecticidal crystal proteins and has been used since a decade ago as a bio-insecticide [13]. *B. anthracis* is the agent responsible for anthrax disease in animals and humans, and is an important biological warfare agent [14]. *B. cytotoxicus* is a human pathogen associated with occasional fatal food poisoning [15]. *B. cereus* is a major food-borne human pathogen (FBO), responsible for two types of food poisoning, the emetic and gastrointestinal syndromes [16]. The emetic syndrome is caused by an emetic toxin called cereulide, and results in vomiting [17–20]. The diarrheal syndrome is associated with three pore-forming enterotoxins, called Cytotoxin K (CytK1 and CytK2), Enterotoxin Nhe (non-hemolytic enterotoxin) and Enterotoxin Hbl (Hemolysin BL) [20,21]. Recently, the non-redundant Nhe and Hbl toxins were shown to share the same mode of action and to operate synergistically to activate the NLRP3 inflammasome, which is a critical component of host innate immune defense [22]. Other factors have also been implicated in *B. cereus* virulence. In particular

hemolysins, proteases and repair factors have been shown to be involved in the resistance of *B. cereus* to the host immune system [23–27]. Furthermore, we have shown that EntFM, formerly isolated after purification from *B. cereus* strain FM-1 and identified as an enterotoxin [28], is in fact a cell wall peptidase. Accordingly, EntFM was renamed CwpFM [29]. CwpFM is a 45-kDa protein, responsible for characteristic enterotoxin symptoms in animal models, increases in vascular permeability in rabbits, infiltration into the ligated loops of rabbits and toxicity towards Vero epithelial cells, whereas it did not show either hemolytic or lecithinase activities [30,31]. Consistently, we have evidenced that CwpFM of *B. cereus* is involved in bacterial motility and morphology, adhesion to epithelial cells and biofilm formation and is essential to promote *B. cereus* virulence in an insect model of infection [27]. Prevalence studies have shown that the *cwpFM* gene is present on the chromosome as a single copy and restricted to almost all members of the *B. cereus* group [32–34].

Here, we report a sequence/structure/function characterization, following the subsequent bioinformatic analysis of 39 CwpFM sequences, chosen from a collection of *B. cereus* with a diverse virulence phenotype, from harmless to highly pathogenic strains. We also homology-modeled the 3D structure of the CwpFM protein from *B. cereus*. We show that CwpFM is an exported papain-like endopeptidase with, at the N-terminal end, three successive bacterial Src Homology 3 domains ($SH3b_{1-3}$), and at the C-terminal end, a catalytic NLPC_P60 domain (New lipoprotein C/Protein of 60 KDa), that involves a competent active site. We confirmed in vitro that CwpFM is an endopeptidase despite a moderate peptidoglycan hydrolase activity. Additionally, we predicted that each of the three linkers connecting $SH3b_{1-2}$, $SH3b_{2-3}$ or $SH3b_3$ to NLPC_P60 modules associates low-complexity with an intrinsically disordered pattern. Remarkably, CwpFMs from pathogenic strains harbor a specific stretch of intrinsically disordered linkers, particularly long, located between $SH3b_3$ and catalytic NLPC_P60 domains. This pattern exquisitely discriminates pathogenic from non-pathogenic strains. Thus, we propose that it could define a marker of differentiation between the *B. cereus* strains.

2. Results

2.1. CwpFM is Present and Highly Conserved within the Members of the B. cereus Group

We have previously shown that CwpFM is only detected within the members of the *B. cereus* group [26]. Here, we did a comparative analysis of CwpFM from 10 strains representative of the *B. cereus* group (Table 1). A Blastn search with the complete published sequence of *cwpFM* from *B. cereus* isolate A6 (AY789084.1) was performed to identify CwpFM homologues in the selected genome (Table 2).

Only one copy of the gene was detected in each *Bacillus* genome. All the proteins encoded by the identified CwpFM homologues belong to the C40 family peptidase. Our bioinformatic analysis revealed that CwpFM is highly conserved among the *B. cereus* group. Sequence identities, when compared to CwpFM of the A6 strain, range from 72% for *B. pseudomycoides* DSM 12442 to 99% for *B. cereus* ATCC 14579. The most closely related sequences are between *B. cereus* and *B. thuringiensis* species with identities above 95.5%.

Table 1. Distribution of CwpFM within the *Bacillus cereus* group. Characteristics of representative strains of the *Bacillus cereus* group.

Species	Strain	Origin/Description	PanC Group	Ref Genome
B. cereus	ATCC 14579	Isolated from a farmhouse in the United States, 1916	IV	NC_004722.1
B. cereus	ATCC 10987	Isolated from dairy cheese in Canada, 1930	III	NC_003909.8
B. thuringiensis	Bt407 cry-	Soil isolate that has been cured of the plasmid that encodes the intesticidal crystalline toxin	IV	NC_018877.1
B. thuringiensis	serovar konkukian str. 97–27	Soil organism isolated from a severe tissue necrosis of a soldier severely wounded by a land mine explosion in former Yugoslavia, 1995	III	NC_005957.1
B. mycoides	ATCC 6462	Also known as DSM 2048; isolated from soil	VI	NZ_CP009692.1
B. pseudomycoides	DSM 12442	Also known as NRRL B617; isolated from soil in Ghana, 1998	I	NZ_CM000745.1
B. weihenstephanensis	KBAB4	Psychrotolerant soil isolate isolated in forest soil in France, 2000	VI	NC_010184.1
B. anthracis	Ames	Isolated from a dead cow in Texas, 1981	III	NC_007530.2
B. cytotoxicus	NVH 391-98	Isolated from a food poisoning outbreak (vegetable puree) in a nursing home for elderly people in France, 1998	VII	NC_009674.1
B. toyonensis	BCT-7112	Isolated for use as probiotics in animal nutrition in Japan, 1966	V	NC_022781.1

Table 2. Blastn of *B. cereus* isolate A6 *cwpFM* nucleotide sequence (AY789084.1) against the genome of representative strains of the *Bacillus cereus* group.

Species	Strain	Identities	Gaps	Strand	Gene Identification	Protein Name	Protein Reference	Max Score	Total Scorer	Query Cover	E Value	Per. Ident.
B. cereus	ATCC 14579	1277/1293 (99%)	12/1293 (0%)	Plus/Plus	BC_RS09755	C40 family peptidase	WP_000755498.1	838	838	1.00	0.0	99.07%
B. cereus	ATCC 10987	1238/1281 (97%)	0/1281 (0%)	Plus/Plus	BCE_RS10070	C40 family peptidase	WP_000755518.1	828	828	1.00	0.0	97.89%
B. thuringiensis	Bt407 cry-	1268/1293 (98%)	12/1293 (0%)	Plus/Plus	BTB_RS09950	C40 family peptidase	WP_000755523.1	836	836	1.00	0.0	98.84%
B. thuringiensis	serovar konkukian str. 97-27	1215/1281 (95%)	18/1281 (1%)	Plus/Plus	BT9727_RS09585	C40 family peptidase	WP_000755548.1	800	800	1.00	0.0	95.54%
B. mycoides	ATCC 6462	1178/1312 (90%)	32/1312 (2%)	Plus/Minus	BG05_RS21755	C40 family peptidase	WP_003188709.1	667	667	1.00	0.0	88.99%
B. pseudomycoides	DSM 12442	997/1324 (75%)	47/1324 (3%)	Plus/Plus	BPMYX0001_RS08705	C40 family peptidase	WP_006094561.1	582	582	0.99	0.0	72.27%
B. weihenstephanensis	KBAB4	1168/1296 (90%)	18/1296 (1%)	Plus/Plus	BCERKBAB4_RS09410	C40 family peptidase	WP_002012346.1	672	672	1.00	0.0	91.44%
B. anthracis	Ames	1211/1281 (95%)	18/1281 (1%)	Plus/Plus	GBAA_RS09755	C40 family peptidase	WP_000755532.1	796	796	1.00	0.0	95.07%
B. cytotoxicus	NVH 391-98	1050/1290 (81%)	39/1290 (3%)	Plus/Plus	BCER98_RS07835	C40 family peptidase	WP_012093983.1	644	644	0.99	0.0	81.65%
B. toyonensis	BCT-7112	1200/1309 (92%)	35/1309 (2%)	Plus/Plus	BTOYO_RS22750	C40 family peptidase	WP_016513917.1	711	711	1.00	0.0	91.45%

2.2. Domain Organization of the CwpFM Homologues from the B. cereus Group Indicates the Presence of Cell Wall Degradation Domains

All the CwpFM amino acid sequences from strains representative of the *B. cereus* group were aligned and domains were identified using both Clustal Omega (clustalo 1.2.4) and InterPro online tools. A conserved signal peptide composed of 26 amino acid residues was predicted to translocate using the Sec translocon, and to be cleaved by Signal peptidase I at the cleavage site AH/QA_QV, located between positions 26 and 27. The prediction of secondary domains for CwpFMs indicated a modular topology combining three protein–protein interaction SH3b domains and one catalytic NLPC_P60 family for all the strains (Figure 1). This topology is predicted to be strictly conserved for all the strains, even for CwpFM from *B. pseudomycoides* that shows a sensitively lower identity with the other members of the *B. cereus* group. More largely, the topology is fully consistent with the modular architecture highlighted for CWPs in bacterial CWHs because it associates several cell wall binding domains to a catalytic domain [8].

Sequence alignment of CwpFM homologues from *B. cereus* isolate A6 (AAX14641.1), *B. cereus* ATCC 14579 (WP_000755498.1), *B. cereus ATCC* 10987 (WP_000755518.1), *B. thuringiensis* 407 cry- (WP_000755523.1), *B. thuringiensis* serovar konkukian str. 97–27 (WP_000755548.1), *B. mycoides* ATCC 6462 (WP_003188709.1), *B. pseudomycoides* DSM 12442 (WP_006094561.1), *B. weihenstephanensis KBAB4* (WP_002012346.1), *B. anthracis* str Ames (WP_000755532.1), *B. cytotoxicus* NVH 391–98 (WP_012093983.1) and *B. toyonensis* BCT-7112 (WP_016513917.1) show a similar domain organization (Figure 1). LytF of *B. subtilis* (NP_388818.2) was also aligned. Sequences were aligned using Clustal Omega (1.2.4) and domains were predicted using Interproscan (InterPro 78.1). The black box indicates the signal peptide, the blue boxes highlight SH3b domains and the red box shows the NLPC_P60 domain characteristic of the cell wall peptidases.

To gain further insights into the potential functions of CwpFM, the domain organization of CwpFM was compared with known NLPC_P60 proteins of *B. cereus* and *B. subtilis* (Figure 2). In all cases, a single NLPC_P60 domain is located at the C-terminus of the proteins. According to our domain prediction analysis, CwpFM and YkfC from *B. cereus* contain three and one SH3b domains, respectively, in addition to their catalytic domain NLPC_P60. However, the crystal structure of YkfC from *B. cereus* revealed that it actually contains two N-terminal SH3b domains [35]. By contrast, YkfC of *B. subtilis* has an NLPC_P60 domain, but neither any defined SH3b nor LysM Cell wall binding domain. Despite the strong biochemical characterization of YkfC in *B. cereus* and *B. subtilis*, there is no description of their physiological role in the bacteria. *B. subtilis* LytF shares 25% identity and 36% similarity with CwpFM of the ATCC 14579 *B. cereus* strain. When compared to CwpFM of the *B. cereus* group members, the LytF sequence differs in domain organization, evidencing a conserved NLPC_P60 domain at the C-terminus as in CwpFM, but no SH3b domain (Figures 1 and 2). By contrast, LytF possesses five LysM domains. LytE, CwlO and CwlS of *B. subtilis* contain one NLPC_P60 domain and three, zero and four LysM domains, respectively. In any case, no SH3b domain was defined. This is consistent with the fact that the majority of cell wall peptidases display, in addition to their catalytic site, at least one domain necessary for the interaction with peptides, carbohydrates and lipids of the cell wall, such as SH3b or LysM domains. The endolysins BlyA (YomC) and LytD (CwlG) of *B. subtilis* also possess SH3b domains, but no NLPC_P60 domains. BlyA carries two SH3b domains linked to an N-acetylmuramoyl-L-alanine amidase catalytic domain. For the sake of clarity, the domain organization for known NLPC_P60 proteins of *B. cereus* and *B. subtilis* is resumed in Figure 2 below. Markedly, these differences in domain organization may reflect substrate specificities of the proteins, and functional and synergistic differences between *B. cereus* and *B. subtilis* CWHs.

Figure 1. Multiple sequence alignment and domain organization of CwpFM homologues.

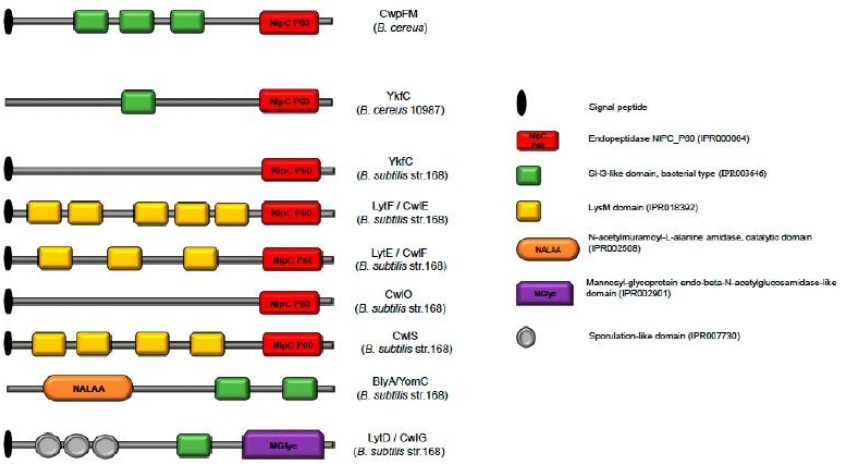

Figure 2. Schematic representation of cell wall hydrolases of *B. cereus* and *B. subtilis*. Domain organization of seven cell wall hydrolases from *B. subtilis* and two from *B. cereus*. InterProScan protein domain prediction analysis indicates the presence of a short signal peptide domain (black ellipse) at the N-terminus of every enzyme, except for YkfC (*B. cereus*) and BlyA (*B. subtilis*). Catalytic domains of three types can be distinguished: NLPC_P60 domain (red rectangle), N-acetylmuramoyl-L-alanine amidase, catalytic domain (orange rectangle) and Mannosyl-glycoprotein endo-beta-N-acetylglucosamidase-like domain (purple rectangle). The two cell-wall binding domains SH3b and LysM are shown in green and yellow squares, respectively. LytD has three sporulation-like domains specifically found in bacterial proteins involved in sporulation and cell division.

2.3. Homology Modeling of CwpFM 3D Structure Highlights a Conserved Modular Topology Composed of Three SH3b Domains Connected to an NLPC_P60 Cysteine Peptidase Domain, and Emphasizes the Presence of Disordered Connecting Domains that Could Play a Role in Specificity and Affinity towards PG and Proteins

To highlight the main sequence/structure/function features of CwpFM within the *B. cereus* group, we focused on CwpFM full-length from *B. cereus* ATCC 14579 that contains 420 residues, the first 26 of which were confirmed to be a signal peptide by the Phobius server [35]. The mature sequence, i.e., the endopeptidase with the signal peptide excised, was predicted to be 37% similar to the putative dipeptidyl-peptidase VI from *Bacteroides ovatus* by HHpred (pdb id 3NPF). In addition, the N-terminal segment of CwpFM from *B. cereus* (amino acid residues 14–73) was predicted by HHpred to be 37% sequence-similar to the SH3b part of the putative endopeptidase from *Anabena variabilis* ATCC29413 (pdb id 2HBW) [36]. Since the similarity scores were high enough, we homology-modeled CwpFM from *B. cereus* with the above-cited templates. Expectedly, the homology model evidences a classical endopeptidase topology with three SH3b domains, named $SH3b_1$, $SH3b_2$ and $SH3b_3$, located at the N-terminal-end, and the NLPC_P60 endopeptidase domain, located at the C-terminal end (Figure 3A,B). Both $SH3b_2$ and NLPC_P60 contribute clearly to the formation of the active site, and possibly $SH3b_1$, of which orientation varies most, up to 13 Å, according to the 100 models computed by the homology modeling. Interestingly, this could give a hint on the flexibility amplitude of this domain, with respect to the other domains (Figure 3B). However, modeling cannot infer on the possible swapping of SH3b domains, known to exist in CWPs, but hard to predict in silico. Thus, at this stage, one cannot thus exclude or certify any close interaction between $SH3b_1$, $SH3b_2$ and NLPC_P60. The NLPC_P60 domain harbors a typical papain catalytic dyad, composed of strictly conserved Cys328 and His379 residues (Figure 3A). Additionally, it displays the strictly conserved Tyr316, known to act as the oxyanion hole, mandatory for endopeptidases. Further, sequence analysis evidences that both Tyr316 and Cys328 belong to the conserved catalytic motif $YX_{10}DCS$. Thus, according to papain-like endopeptidases, the catalytic site of CwpFM is complete and prone to be active. Markedly, the sequence reveals large

insertions from 17 to 34 residues, located at the N-terminus of each SH3b and between $SH3b_3$ and NLPC_P60 domains (Figure 3C). Those insertions display low complexity with a large prevalence of polar Gln, Thr and Asn residues, and they are also highly susceptible to post-translational modifications and likely to be partially or completely unfolded. Accordingly, they have been named intrinsically disordered linkers and numbered from IDL_1 to IDL_4 (Figure 3C). Their role could be to adjust the positioning of each SH3b, either close to the active site for a functional role in specificity or remotely positioned to bind to the PG matrix or other cognate partners.

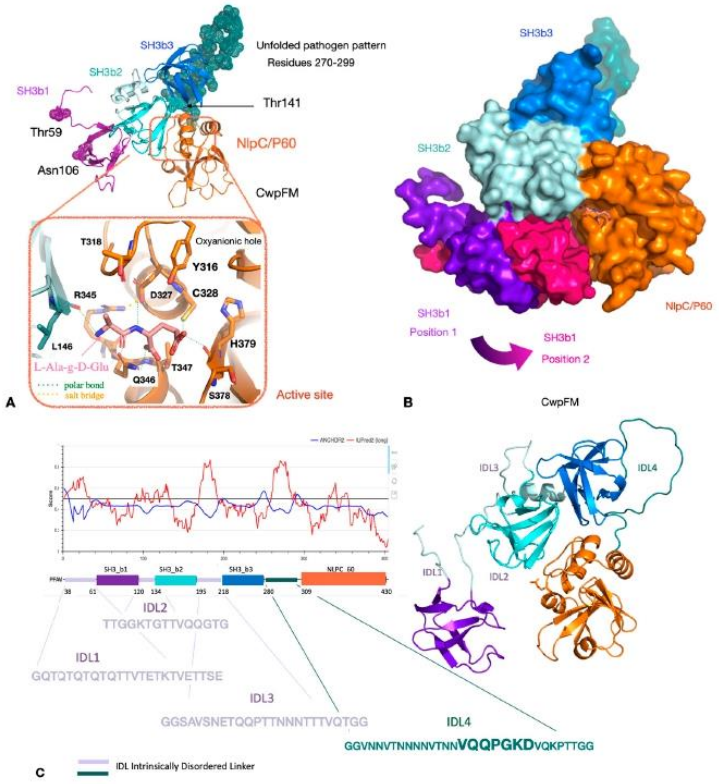

Figure 3. 3D model of CwpFM from *B. cereus* ATCC 14579. Panel **A** upper view: the homology model of mature CwpFM highlights its modular topology with $SH3b_1$ in purple (N-terminal end), $SH3b_2$ in light blue, $SH3b_3$ in marine blue and the catalytic NLPC_P60 domain in orange (C-terminal end). Panel A lower view: close view of the active site. The L-Ala-γ-D-Glu ligand, accommodated in the active site, is shown as salmon sticks, and the residues of the active site are shown in light blue ($SH3b_2$) and orange (NLPC_P60). Panel **B**: surface of CwpFM with the same color code as in A. The catalytic pocket is highlighted and the flexibility of $SH3b_1$ is emphasized with two extreme positions, one in purple and the other in hot magenta, coming from two distinct homology models, and were superimposed on the catalytic domain. Panel **C**: details on the position, sequence and conformation of the insertions numbered IDL1, IDL2, IDL3 and IDL4. Figures were made by PyMOL, LLC, Schrödinger.

2.4. CwpFM Structure Is Able to Accommodate a PG Fragment

To ascertain, more precisely, the function of CwpFM, a L-Ala-γ-D-Glu PG fragment, which corresponds to the reaction product performed by CWPs, was docked into the binding site formed at the interface between $SH3b_2$ and NLPC_P60 domains (Figure 3B). The redocking of the L-Ala-γ-D-Glu moiety inside YkfC shows a strictly similar accommodation, with respect to its crystal position, and a binding energy of −2.8 kcal/mol. The structure of *B. cereus* YkfC in complex with L-Ala-γ-D-Glu was

the first structural representative of an NLPC_P60 enzyme with a bound ligand. The enzyme releases L-Ala-γ-D-Glu dipeptides from cell wall peptides via cleavage of an L-Ala-γ-D-Glu-|-L-Lys bond.

The docking of L-Ala-γ-D-Glu inside CwpFM gives an interaction energy of −3.7 kcal/mol, which is in the same range as in YkfC, thus suggesting that a short substrate with a free alanine residue could be accommodated in the active site of CwpFM. Additionally, the substrate accommodation highlights Tyr316, Asp327, Cys328, Ser329, Arg345, Gln346 and His379 (CwpFM numbering), as binding residues (Figure 3A). Interestingly, they are conserved in dipeptidyl-peptidase from *B. ovatus* and dipeptidyl-peptidase from *Anabaea variables* ATCC 29413. Particularly, Asp327 and Arg345 form a salt bridge strictly conserved in the three enzymes and involved in the hydrogen bonds network that connects many residues of the active site. Nevertheless, the binding shows a moderate affinity and the IDL extensions, which are difficult to model, could participate in reshaping the binding groove while enhancing the affinity. In short, CwpFM is able to accommodate the L-Ala- γ-D-Glu product fragment of the peptidase reaction, but it is likely that a longer substrate with the L-Ala extremity, free or not, could also bind.

2.5. B. cereus CwpFM Shows a Weak PG Hydrolase Activity

Our modeling of CwpFM identified a catalytic domain typical of cysteine papain peptidase and computed a reasonable affinity towards a PG moiety, so we aimed to characterize CwpFM PG hydrolase activity. We expressed and purified *B. cereus* CwpFM with a GST tag on the N-terminal end of the protein. Next, purified CwpFM enzyme activity was examined by zymography analysis using the *Micrococcus* cell wall as a substrate (Figure 4). The results showed a small clearance band in the zymogram. No clearing zones were observed when the same amount of purified GST was subjected to zymography. These results demonstrate that the CwpFM protein exhibits a weak CW degrading activity, which is consistent with our 3D model that illustrated a low binding affinity with PG.

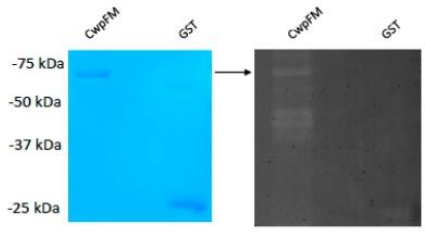

Figure 4. SDS-12%PAGE and zymography of CwpFM-GST. CwpFM-GST was overexpressed in the *E. coli* M15 strain. Lane M, protein standard; left panel: SDS-PAGE; right panel: zymography. The arrow indicates the position of the purified CwpFM-GST.

2.6. CwpFM Distribution in B. cereus Strains of Various Pathogenic Potentials

We have shown that CwpFM is present and conserved amongst the *B. cereus* group members. However, within *B. cereus sensu stricto* strains, the pathologies vary from harmless to highly toxic strains. We thus studied CwpFM from *B. cereus* strains causing different pathologies: FBO, clinical non-gastrointestinal infections and non-pathogenic strains. We performed a homology search using the nucleotide sequence of *cwpFM* from *B. cereus* isolate A6 (AY789084.1) and we identified homologues of *cwpFM* as a single copy in every genome (Table 3), the result of which correlates with the high prevalence of the gene described in the literature. Despite being prevalent, these ORFs are variously annotated Peptidase P60, C40 family peptidase, putative endopeptidase LytE or Enterotoxin, in the databases. On average, the *cwpFM* genes showed between 89% and 99% identity. For the FBO and clinical strains, the *cwpFM* genes showed above 94% identity with the reference strain A6. The identity was, on average, lower for the non-pathogenic strains ranging from 89% to 92% identity, with two exceptions. These exceptions belong to the strains INRA PF (97% identity) and INRA A3 (99% identity).

Table 3. Characterization of *B. cereus* strains used in this study and their corresponding CwpFM proteins.

Strain	Collection	Origin/Description	Ref Genome	Identities	Gaps	Strand	Gene Identification	Protein Name	Protein Reference
NVH 0075/95	FBO	Stew with vegetables, food poisoning outbreak of diarrheal syndrome in Norway, 1995	LABM00000000.1	1236/1281(96%)	0/1281(0%)	Plus/Plus	TU63_19225	peptidase P60	KMP84856.1
G9842	FBO	Human stool, outbreak that involved three individuals in the USA, 1996	NC_011772.1	1273/1299(98%)	18/1299(1%)	Plus/Plus	BCG9842_RS09225	C40 family peptidase	WP_000755522.1
AH187	FBO	Human vomit of a person having previously eaten cooked rice in London, emetic outbreak in UK, 1972	NC_011658.1	1236/1281(96%)	0/1281(0%)	Plus/Plus	BCAH187_RS10030	C40 family peptidase	WP_000755553.1
NC7401	FBO	Feces/vomit, food poisoning in Japan, 1994	NC_016771.1	1234/1281(96%)	0/1281(0%)	Plus/Plus	BCN_RS09705	C40 family peptidase	WP_014297774.1
NVH_141/1-01_V_C53	FBO	Vegetarian pasta, diarrheal food poisoning outbreak in Norway, 2001	FMJK00000000.1	1191/1299(92%)	27/1299(2%)	Plus/Plus	BC141101_01248	Enterotoxin	SCN16078.1
NVH 0674-98	FBO	Mashed swedes/scrambled eggs, diarrheal food poisoning in Norway, 1998	FMJM00000000.1	1231/1281(96%)	6/1281(0%)	Plus/Plus	BC067498_01849	Enterotoxin	SCN44411.1
HN001	FBO	Human vomit, food poisoning in China, 2000	NZ_CP011155.1	1272/1287(99%)	6/1287(0%)	Plus/Plus	WR52_RS09190	C40 family peptidase	WP_063536128.1
NVH 0861-00	FBO	Ice scream, diarrheal food poisoning in Norway, 2000	FMBJ00000000.1	1221/1305(94%)	27/1305(2%)	Plus/Plus	BC0861_01953	Enterotoxin	SCC09072.1

Table 3. *Cont.*

Strain	Collection	Origin/Description	Ref Genome	Identities	Gaps	Strand	Gene Identification	Protein Name	Protein Reference
RIVM_BC120	FBO	Human feces, diarrheal food poisoning in Netherlands	FMIJ00000000.1	1237/1281(97%)	0/1281(0%)	Plus/Plus	BCRIVMBC120_02096	Enterotoxin FM	SCL92408.1
RIVM_BC126	FBO	Human feces, diarrheal food poisoning in Netherlands	FMJJ00000000.1	1238/1287(96%)	6/1287(0%)	Plus/Plus	BCRIVMBC126_01928	Enterotoxin	SCN07222.1
F2404B-79	FBO	Diarrheal food poisoning outbreak in the UK	FMJG00000000.1	1231/1287(96%)	6/1287(0%)	Plus/Plus	BCF24048_01956	Enterotoxin	SCM94734.1
6/27/S	FBO	Human feces, diarrheal	NZ_LABV00000000.1	1278/1281(99%)	0/1281(0%)	Plus/Plus	TU48_RS34500	C40 family peptidase	WP_000755525.1
F3175/03(D7)	FBO	Human feces, diarrheal	NZ_JYPI00000000.1	1214/1289(94%)	13/1289(1%)	Plus/Plus	TU54_28630	peptidase P60	KMP31545.1
F528/94	FBO	Poisoning outbreak from beef and chow rice in the UK, 1994	NZ_JYPH00000000.1	1207/1290(94%)	27/1290(2%)	Plus/Plus	TU52_12565	peptidase P60	KMP35524.1
F4429/71	FBO	Vanilla pudding, diarrheal	NZ_JYPJ00000000.1	1214/1281(95%)	18/1281(1%)	Plus/Minus	TU55_10935	peptidase P60	KMP45116.1
RIVM BC 90	FBO	Human feces, diarrheal, 1999	LABN00000000.1	1236/1281(96%)	0/1281(0%)	Plus/Plus	TU64_27355	peptidase P60	KMP79201.1
7/27/S	FBO	Human feces, diarrheal	NZ_LABW00000000.1	1232/1287(96%)	6/1287(0%)	Plus/Plus	TU49_15830	peptidase P60	KMP18977.1
FORC_005	FBO	Korean side dish, food-borne illness in South Korea	NZ_CP009686.1	1215/1301(93%)	25/1301(1%)	Plus/Plus	FORC5_RS09925	C40 family peptidase	WP_044307235.1
F4430/73	FBO	Peas soup, diarrheal syndrome in Belgium, 1973	JYPK00000000.1	1278/1281(99%)	0/1281(0%)	Plus/Minus	TU56_09675	peptidase P60	KMP71144.1
F837/76	FBO	Food-borne outbreak in the UK, 1976	NC_016779.1	1214/1281(95%)	18/1281(1%)	Plus/Plus	BCF_RS09455	C40 family peptidase	WP_000755546.1
09–13	Clinical	Premature newborn, blood culture, 2009	this study	1277/1287 (99%)	6/1287 (0%)	Plus/Plus		putative peptidoglycan endopeptidase LytE	

Table 3. *Cont.*

Strain	Collection	Origin/Description	Ref Genome	Identities	Gaps	Strand	Gene Identification	Protein Name	Protein Reference
09–14	Clinical	Premature newborn, blood culture, 2009	this study	1235/1293 (96%)	12/1293 (0%)	Plus/Plus		putative peptidoglycan endopeptidase LytE	
09–33	Clinical	New born, axilla, 2009	ERS1507218	1215/1287 (94%)	24/1287 (1%)	Plus/Plus		putative peptidoglycan endopeptidase LytE	
12–31	Clinical	Premature newborn, blood culture, 2011	this study	1236/1281 (96%)	0/1281 (0%)	Plus/Plus		putative peptidoglycan endopeptidase LytE	
13–06	Clinical	Intensive care unit, blood culture from catheter, 2011	this study	1236/1281 (96%)	0/1281 (0%)	Plus/Plus		putative peptidoglycan endopeptidase LytE	
09–11	Clinical	Premature newborn, blood culture, 2009	ERS1493302	1215/1293 (94%)	30/1293 (2%)	Plus/Plus		putative peptidoglycan endopeptidase LytE	
09–16	Clinical	New born, Umbilicus, 2009	ERS1494027	1215/1293 (94%)	30/1293 (2%)	Plus/Plus		putative peptidoglycan endopeptidase LytE	
09–12	Clinical	Premature newborn, cerebrospinal fluid, 2009	ERS1494026	1215/1293 (94%)	30/1293 (2%)	Plus/Plus		putative peptidoglycan endopeptidase LytE	
09–17	Clinical	Surface of neonatology ward (window sill), 2009	ERS1494028	1236/1281 (96%)	0/1281 (0%)	Plus/Plus		putative peptidoglycan endopeptidase LytE	
09–34	Clinical	Premature newborn, stomach tube feeding, 2009	ERS1494031	1236/1281 (96%)	0/1281 (0%)	Plus/Plus		putative peptidoglycan endopeptidase LytE	

Table 3. *Cont.*

Strain	Collection	Origin/Description	Ref Genome	Identities	Gaps	Strand	Gene Identification	Protein Name	Protein Reference
INRA PF	Non-pathogenic	Milk protein	this study	1237/1281 (97%)	0/1281 (0%)	Plus/Plus		putative peptidoglycan endopeptidase LytE	
INRA 5	Non-pathogenic	Pasteurized zucchini puree	FLZU01000000	1187/1309 (91%)	29/1309 (2%)	Plus/Plus		putative peptidoglycan endopeptidase LytE	
INRA C64	Non-pathogenic	Pasteurized vegetables	this study	1157/1294 (89%)	29/1294 (2%)	Plus/Plus		putative peptidoglycan endopeptidase LytE	
ADRIA I3	Non-pathogenic	Cooked foods	this study	1156/1300 (89%)	35/1300 (2%)	Plus/Plus		putative peptidoglycan endopeptidase LytE	
INRA A3	Non-pathogenic	Starch	LABH01000000	1277/1287 (99%)	6/1287 (0%)	Plus/Plus		putative peptidoglycan endopeptidase LytE	
INRA SL′	Non-pathogenic	Soil	this study	1184/1290 (92%)	21/1290 (1%)	Plus/Plus		putative peptidoglycan endopeptidase LytE	
I21	Non-pathogenic	Unknown	this study	1170/1293 (90%)	30/1293 (2%)	Plus/Plus		putative peptidoglycan endopeptidase LytE	
ADRIA I21	Non-pathogenic	Cooked foods	FMJF01000000	1170/1293 (90%)	30/1293 (2%)	Plus/Plus		putative peptidoglycan endopeptidase LytE	
WSBC 10204	Non-pathogenic	Pasteurized milk	PRJNA258373	1187/1306 (91%)	26/1306 (1%)	Plus/Plus		putative peptidoglycan endopeptidase LytE	

2.7. Analysis of the Differences at the 2D and 3D Levels

Since we aimed to extract significant differences that could discriminate pathogenic from non-pathogenic strains, we align series of strain sequences using MAFFT. The first alignment is between FBO and non-pathogenic strains (Figure 5A), whilst the second is between clinical and non-pathogenic ones (Figure 5B).

The sequences of CwpFM cluster according to the origin of their *B. cereus* strain, with only two exceptions. Indeed, the CwpFM from the pathogenic strains, either FBO or clinical, are clearly separated from the non-pathogenic strains. The outsider strains INRA-PF and INRA-A3 clustered within the pathogenic strains group. Three point-mutations, Asp/Glu31, Thr/Asn106 and Thr/Ile141, and, more importantly, a 20-residues segment (276–296) located between $SH3b_3$ and NLPC_P60 could be noted as significantly different between non-pathogenic strains and pathogenic strains. Glu31 is positioned at the N-terminal end, close to the excised peptide. Glu31 is substituted by an aspartic acid in non-pathogenic strains. Its substitution could not be mapped onto the CwpFM 3D structure because the protein was homology-modeled starting from residue 53. Thr/Asn106 in pathogenic strains is replaced by a serine, whilst Thr/Ile141 is substituted by an alanine, in non-pathogenic strains. In our homology model, Thr/Asn106 in $SH3b_1$ and Thr/Ile151 in $SH3b_2$ are positioned too far from each other to be in contact together (Figure 3A). Nevertheless, one can hypothesize that domain swapping or a close interaction between the two SH3b domains could favor the polar interaction between the two residues, the possibility of which cannot be excluded as domain swapping of SH3bs has been already mentioned for CWPs. Correspondingly, this feature could be claimed for the covariation of residues. Reversely, if we consider those residues as not engaged in mutual interaction, they could be largely accessible to any binding or post-translational modification. Markedly, the most significant difference is a segment, called IDL4, an intrinsically disordered linker, located between residues 280 and 309, that is clearly distinct in sequence when compared between non-pathogenic and pathogenic strains. Clearly, this segment could not be modeled (i) because it is partly an insertion as compared to our 3D templates, and (ii) because it is very low in complexity, and thus largely unstructured. Accordingly, in both non-pathogenic and pathogenic strains, we expect these segments of CwpFM to be natively unfolded. Notably, IDL4 displays a significant difference in sequences between non-pathogenic and pathogenic strains as VTGG(X)NQGTNQ (X being-, T or NQGTNQGT) is replaced by $T(N)_{0–6}$VTNNVQQPGKD (Figures 3C and 5).

The pathogenic strains harbor a significant amount of Asn residues, while the non-pathogenic ones display more Gly and Gln residues. Asn residues are highly susceptible to hydroxylation which is a post-translational modification shown recently as reversible [37]. Therefore, one cannot exclude the hydroxylation of Asn residues, which could contribute to protein modification, flexibility and anchoring at the PG. This is fully consistent with the linker role of IDL4 that connects $SH3b_3$ to the catalytic NLPC_P60. Such modifications could tune the adequate positioning of $SH3b_3$ towards protein partners, including $SH3b_1$ and $SH3b_2$, and adapt the exquisite mobility of the catalytic domain towards the PG. Due to the length and prevalence of Asn in all pathogenic strains, this segment could be considered as a pattern signature for *B. cereus* virulent strains.

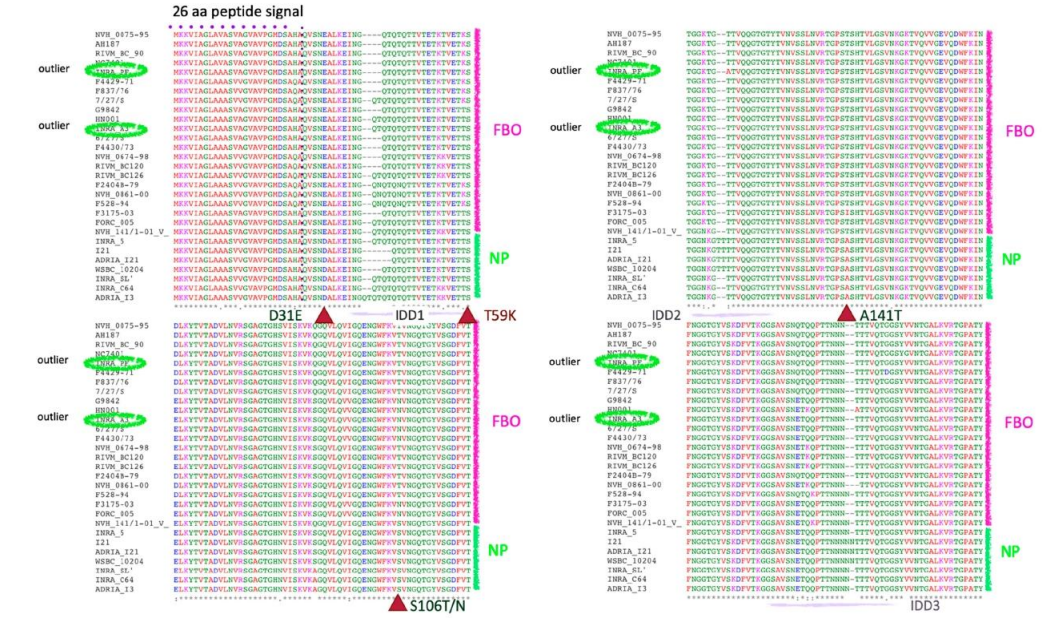

Figure 5. *Cont.*

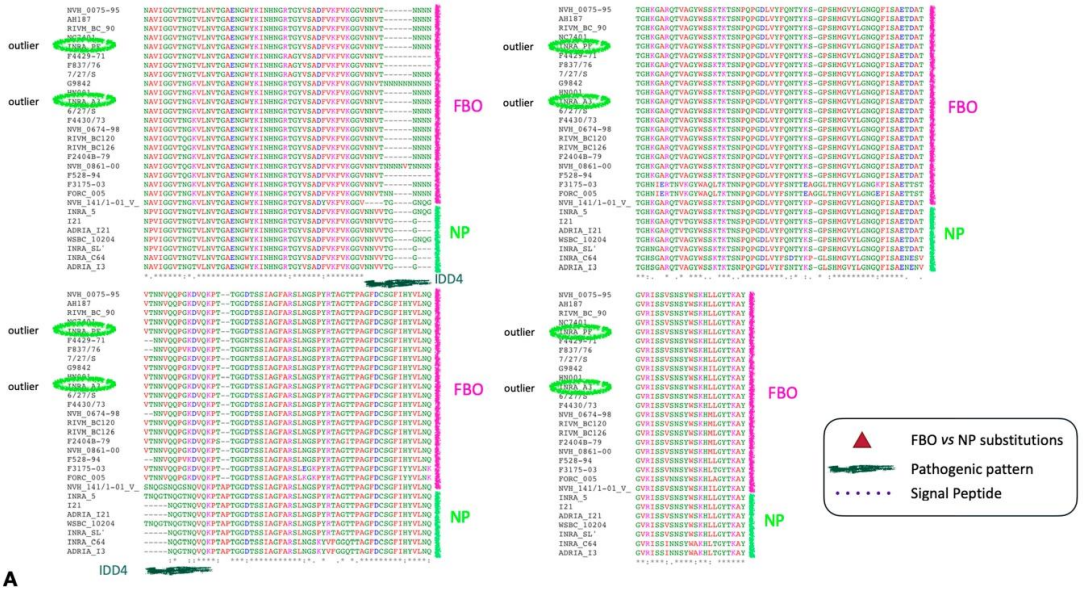

Figure 5. *Cont.*

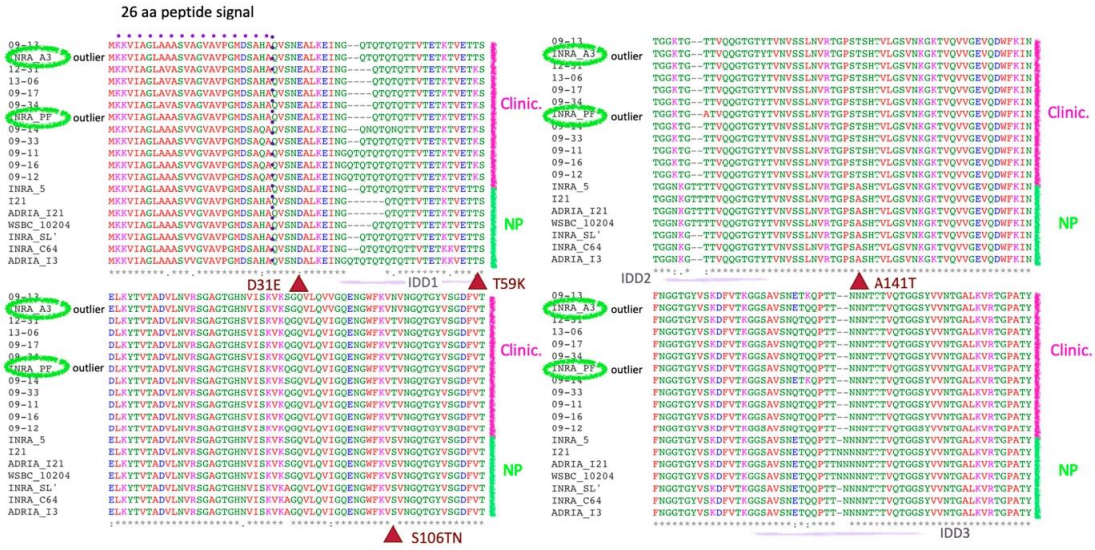

Figure 5. *Cont.*

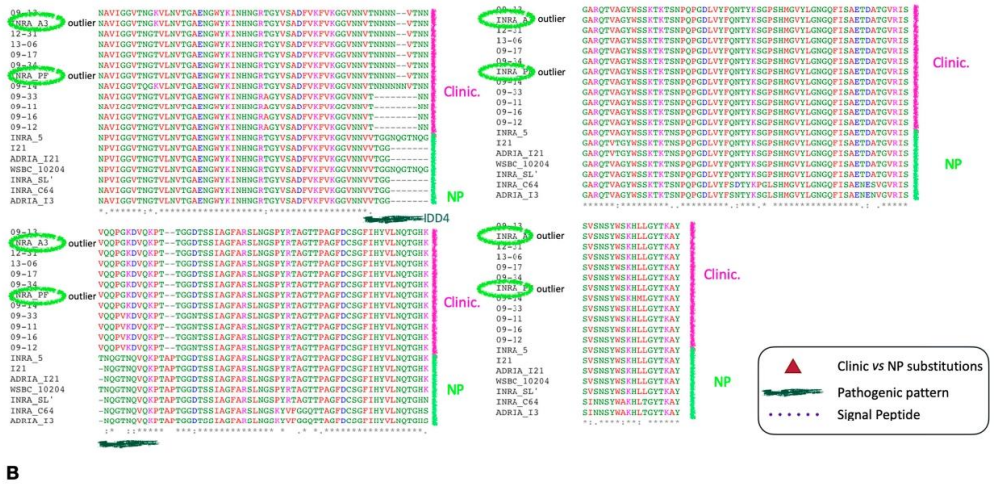

Figure 5. Alignment of CwpFM sequences of (**A**) NP vs. FBO strains and (**B**) NP vs. clinical strains. Panel **A**: CwpFM protein sequences of 9 non-pathogenic strains (NP) were aligned with those of 20 FBO strains and, in panel **B**: with 10 clinical strains. Alignments were performed using MAFFT. Amino acid substitutions strictly distinct between FBO or clinical and NP are indicated as red arrows.

3. Discussion

B. cereus is a serious cause of food poisoning. It is largely known that the emetic toxin and the enterotoxins Nhe, Hbl and CytK are responsible for vomiting and diarrhea syndromes, respectively [21,38]. Many other putative virulence factors have been described in *B. cereus*. However, their precise role in bacterial pathogenesis is still uncertain, although their involvement in virulence has been suggested due to their toxic effects on cellular models, insects or mammals. Unlike *B. anthracis*, *B. thuringiensis* and the specific *B. cereus* emetic strains, whose toxin genes are carried by plasmids, *B. cereus* virulence factors are specified by genes located on the chromosome and the virulence is probably multifactorial [20,38,39]. Among them, CwpFM, formerly identified as an enterotoxin, is in fact a cell wall peptidase of the NLPC_P60 family of peptidases, which is one of the most abundant secreted cell wall peptidase CWP families. Nevertheless, the CwpFM family lacks distribution, prevalence, sequence characterization and a molecular description of its mode of action.

Here, we report for the first time a distribution analysis of CwpFM within the *Bacillus* group. To infer the sequence/structure/function of CwpFM within the *B. cereus* group and gain molecular consistency, the features observed from bioinformatics analysis were mapped onto a 3D structure of CwpFM from *B. cereus* ATCC1479 modeled in silico. We highlight that CwpFM from *B. cereus* is a papain-like cysteine endopeptidase that displays the emblematic catalytic motif $Y_{316}X_{10}DCS_{329}$ associated with the strictly conserved histidine residue H_{379} of the NLPC_P60 family. Cys_{328} of this motif and His_{379} residues form the catalytic dyad, while Y_{316} of the motif frames the oxyanionic hole, expected to occur in every peptidase protein. Thus, CwpFM displays a competent active site. Additionally, docking computation evidences that a PG moiety is able to bind to the active site. In line with that, structural bioinformatics analysis highlights that the binding site is composed of residues strictly conserved and located in both $SH3b_2$ and NLPC_P60 domains. Only Gly_{172} in CwpFM replaces the bulky Tyr_{118} or Tyr_{80}, and Gln_{356} replaces Asp_{256} or Asp_{221}, in the YkfC of *B. cereus* and in the putative dipeptidyl-peptidase VI from *Bacteroides ovatus*, respectively. Since tyrosine and aspartate residues are known to interact together to fix the free amine group of the Alanine peptido-glycan moiety, the absence of a side chain in Gly_{172} could preclude the close interaction with Gln_{346} and result in an enlargement of the binding site while allowing the accommodation of substrates with an attached fragment at the Alanine extremity. Those structural features, key in the specific recognition of murein peptides by the subfamily of the NLPC_P60 protein, interrogate the substrate specificity and affinity. Accordingly, we could only detect in vitro a weak peptidoglycan hydrolase activity from purified CwpFM. One could argue that the PG from *Micrococcus lysodeikticus* ATCC M3770 may not be the cognate substrate, neither in PG length nor in molecular characteristics. One can also explain that the post-translational modification profile of CwpFM has not reached its optimum activity, due to its production in *E. coli*, that is unable to perform the hydroxylation of asparagine or phosphorylation of serine and threonine residues [40]. Still, the optimum substrate(s), the activation and the toxin target mode of action of CwpFM are open questions. We can also speculate that CwpFM activity is dependent of another enzyme/activator. As an example, it has been demonstrated that the amidase LytH of *Staphylococcus aureus* is only active in the presence of its membrane partner ActH [41]. With respect to the modular topology of CwpFM, the SH3b and catalytic domains could synergize to attain full endopeptidase activity. Further work is needed to identify the other substrates and/or activator allowing *B. cereus* CwpFM to be fully active, and to decipher the toxin mode of action.

B. cereus CwpFM contains three SH3b domains. Thus, despite its homology with *B. subtilis* LytF, the role of CwpFM probably differs from LytF. Indeed, the binding domains ensure the localization and the proper function of the CWH, particularly in CWPs [8]. Nine SH3b domains have been described ($SH3b_{-1}$ to $SH3b_{-9}$) so far and domains can be found at the two terminal ends of CWPs. Of note, cell wall binding domains that can be found along the mono-polypeptide chain generally improve the efficiency of the enzymatic activity, either by increasing the concentration of the ligand at the active site or by anchoring properly onto the enzyme, or even by reshaping the active site [1,8]. In line with that, the SH3b domains demonstrate a selective affinity for pentaglycine cross-bridges [42].

Additionally, it has been shown that loops from the SH3b domain can dock into the ends of the catalytic groove, remodel the substrate binding site and thus modulate substrate specificity [43]. This specificity can be driven by a single mutation. In line with that, two out of three mutations, that have been identified between non-pathogenic and pathogenic strains, are positioned on loops that could participate in substrate affinity or binding site reshaping. Further, it has recently been demonstrated that recognition is shared by two independent SH3bs, tightly engaged to each other, allowing protein clusterization [44,45]. Their interaction potentiates and compensates for the weak affinity of individual SH3b towards pentaglycine [42,46].

In *B. subtilis*, numerous CWPs such as LytF (CwlE), LytE (CwlF) and CwlS are known to work in synergy to ensure cell separation during vegetative growth, and deletion of these genes results in a long filament-like bacteria phenotype [47,48]. They all display an NLPC_P60 domain and a variable number of LysM (Lysin M) domains comprised between zero and five. LysM is amongst the most frequent CW binding motifs and has been shown to recognize the N-acetylglucosamine (GlcNac) polymers (NAG-X-NAG motif) of PG [49,50]. Particularly, LysM is involved in the specific localization of LytF at the separation sites and poles of *B. subtilis* [51]. LytE, in combination with CwlO, has also been associated with cell growth and morphogenesis as they both participate in breaking the PG cross-links along the lateral side of bacteria to support the process of elongation. Although domain prediction analysis reveals no presence of CW-binding domains within CwlO, it is most likely that a domain recognizing a specific fragment of the PG (probably LysM) is present to dictate the enzyme specificity of action. *B. subtilis* BlyA has three SH3b domains. To date, no physiological function has been linked to *B. subtilis* BlyA, however, BlyA from *Borrelia Burgdorferi* is a bacteriophage-encoded holin which, if expressed in *E. coli*, can induce damage to the *E. coli* cell envelope and allows the release of intracellular cytotoxin ClyA, inducing hemolysis on blood agar [52]. LytD (CwlG) was predicted to harbor one SH3b domain and a sporulation-like domain that may indicate a role during sporulation. Finally, LytD (CwlG) is an N-acetylglucosaminidase that has been implicated but is not essential in cell separation and motility [53]. Therefore, the exact role of LytD (CwlG) remains unclear.

CwpFM is present in all strains of our collection of *B. cereus*, gathering strains of various origins and causing different pathologies. CwpFM is a major *B. cereus* toxin that is involved in virulence. We have previously shown that CwpFM is involved in the bacterial shape and division, in adhesion to eukaryotic cells and in promoting virulence. Presence of the gene is now routinely assessed in combination with other diarrheal toxins-encoded genes such as *ces*, *nhe* and *hbl* to determine the potential pathogenicity of a strain. Data show that *cwpFM* is widely distributed (detection rate of 68–98%) in *B. cereus* isolated from diverse food matrices [53–57]. *cwpFM* is also detected in strains associated with food-borne illnesses [33,58] and is even present in emetic strains [59]. Due to the high distribution of *cwpFM* in pathogenic but also non-pathogenic strains, it is hard to use the detection of the *cwpFM* gene as a biomarker of pathogenicity. However, an accurate bioinformatics comparison between the sequences of our strain collection was performed, and then the residues distinct between non-pathogenic, FBO and clinical strains were mapped onto the homology model of CwpFM to check if the sequence and 3D structure could correlate with the pathogenicity of a strain [60]. All CwpFMs from *B. cereus* display four intrinsically disordered linkers (IDL) as connectors between SH3b and/or NLPC_P60 domains. Particularly, the IDL4 that connects $SH3b_3$ to the catalytic domain is particularly long and displays a significant difference that both aggregates pathogenic FBO and clinical strains, while it segregates non-pathogenic strains. The stretch is NQGTNQVQ in non-pathogenic sequences that is replaced by the VQQPGKD patch in pathogenic ones. Additionally, one can observe an extra stretch of up to 10 additional asparagine residues found to be inserted in all pathogenic strains (FBO and clinical) and strictly absent in non-pathogenic ones. Such differences observed not only in length but also in the low complexity with a high prevalence of Asn (for pathogenic strains) vs Gly/Gln (for non-pathogenic strains) can have conformational and functional consequences. Interestingly, as this specific pattern defines the IDL4 junction domain between SH3b and NLPC_P60 domains, we suspect that this domain, natively unfolded, could play a role in the recruitment of binding partners, putatively

through glycosylated Asn residues. The disordered part of CwpFM may possibly be involved in bacterial pathogenicity. Indeed, although deficient in stable secondary and tertiary structures under physiological conditions of pH and salinity, disordered parts in proteins may function as dynamic ensembles of interconverting conformers. Unstructured parts of CwpFM are depleted in hydrophobic amino acid residues, but enriched in polar and charged residues. It was shown that disordered proteins, enriched in polar/charged residues, are highly hydrated compared to ordered ones and as such, they behave distinctly in bulk and air/water or lipid/water interfaces [61]. For instance, α-synuclein, amyloid-β peptide and PB1-F2 influenza protein are disordered monomeric peptides in aqueous solution, but may adopt a β-sheet conformation that further aggregates into toxic amyloid fibrils in contact with negatively charged phospholipids and induces membrane morphological changes and disruption [62–64]. We previously reported the morphological changes of a mammalian cell membrane exposed to recombinant CwpFM [31], which may be linked to this region.

The precise role of CwpFM in pathogenic and non-pathogenic strains remains to be studied. The differences in sequences may have a direct or indirect role during virulence, possibly on the protein partners or post-translational modifications. This is a challenging question to address because many hydrolases, produced by the bacteria, may have a redundant function and take over in the case of a mutation. In addition, some have different functions and can even have more than one function [65]. For instance, in *Enterococcus faecalis*, the SagA protein is a secreted endopeptidase, which has an antibiotic role against enteric pathogens such as *Clostridium difficle* [66]. *Nocardia seriolae* protein NLPC_P60 is a cell wall peptidase also identified as a virulence factor [67]. In *Mycobacterium tuberculosis*, the protein Rv0024 has been shown to be involved in biofilm formation. Those biofilms have been found to be resistant to cell wall-acting anti-TB drugs [68]. Still, *M. tuberculosis*, a mutant lacking the NLPC_P60 protein, is more sensitive to antibiotics and lysozymes, leading to a decrease in the survival in macrophages [69], and the Rv2190c protein is required not only for cell wall maintenance but also for virulence since a mutant is less virulent in a mice model of infection in vivo [70]. Furthermore, NLPC_P60 was described as a virulence factor in *Bacillus anthracis* as it is part of its secretome and can be found in the blood of infected animals [71]. The function of CWP can also indirectly contribute to bacterial virulence. A recent work has demonstrated that the PG hydrolase Cwp19 contributes to *Clostridium difficile* autolysis, which induces the release of bacterial toxins [72]. Markedly, PG fragments released by CWPs can also act as signaling molecules to promote the presence of antimicrobial agents or to interact with the component of the host [73,74].

The versatility of these endopeptidases in the virulence of multiple bacteria towards the host could be explained by their modular architecture that also integrates intrinsically disordered segments and point mutations, both possibly subjected to post-translational modification. These data pave the way for further in silico and in vitro studies because they explore beyond the chromosomal gene presence and ground the first description of a pattern within *B. cereus* CwpFM sequences capable of discriminating pathogenic from non-pathogenic strains.

4. Materials and Methods

4.1. Bacterial Strain Sequences

The genome and *cwpFM* sequences of 10 strains belonging to the *B. cereus* group were retrieved from NCBI (Table 1). The genome and *cwpFM* sequences of 20 *B. cereus* strains isolated from food or human samples and associated with food poisoning were also retrieved from NCBI (Table 2). In addition, this study includes ten strains isolated from human samples following systemic or local infections [75] and nine non-pathogenic strains, isolated from food that did not cause infection in humans or animals [76,77]. The corresponding genome sequences were retrieved from the European Nucleotide Archive (ENA) or obtained in this study (Table 2).

4.2. Sequence Alignment, Conserved Motifs and Domain Analysis of the Proteins

Multiple nucleotide sequence alignments were conducted using the BLASTn interface. Multiple amino acid sequence alignments of the CwpFM proteins were performed using Clustal Omega v1.2.4 (https://www.ebi.ac.uk/Tools/msa/clustalo/). Signal peptide sequences were predicted using Phobius [36] and SignalP 5.0 [78] servers. The potential protein domains were identified using InterProScan protein domain prediction analysis (www.ebi.ac.uk/Tools/pfa/iprscan/).

4.3. D Alignments and Clustering of the Strains

Alignments were performed with MAFFT—Multiple Alignment using Fast Fourier Transform—v6.861b, with the default options [79]. It is a high-speed multiple alignment program which implements fast Fourier transform (FFT) to optimize protein alignments based on the physical properties of the amino acids. The program uses progressive and iterative alignment and is implemented at the ebi (https://www.ebi.ac.uk/Tools/msa/mafft/).

4.4. Molecular Modeling

CwpFM from the *B. cereus* ATCC 14579 strain (CwpFM_BC) was homology-modeled using the model-building software Modeller (mod9v18) [80]. The crystal structures of the apo putative dipeptidyl-peptidase VI from *Bacteroides ovatus* (pdb id 3NPF), and the SH3b domain of the putative endopeptidase from *Anabena variabilis* ATCC 29413 (pdb id 2HBW amino acid residues 14–73) served as 3D templates (10.2210/pdb3NPF/pdb; 10.2210/pdb2HBW/pdb) [35]. The 3D templates were previously chosen from the HHpred webserver, dedicated to structural homology detection. They were sorted as the two first hits. One hundred homology models of CwpFM were generated, and one was eventually chosen from a selection of the five best models with respect to the lowest values of the Modeller score function, best stereochemistry, as checked by Molprobity (http://molprobity.biochem.duke.edu/), and visual inspection, using PyMOL 2.0.7 (Schrödinger, LLC, New York, NY, USA). The selected model was then minimized using the Biologic suite of Schrödinger, LLC, New York, NY, USA. The sequences were also analyzed using IUPred to characterize disordered segments and identify molecular recognition features (https://iupred2a.elte.hu/) [81].

4.5. Docking

As a prerequisite before performing our docking of the L-Ala-γ-D-Glu ligand in our model of CwpFM, we validated our protocol by redocking the ligand in the active site of YkfC (pdb id 3H41) because it is a structural and functional homologue in a holo configuration. Formerly, the ligand was discarded from YkfC to get the apo form and the tri-oxidized Cys238 of the crystal structure was reduced into a Cys residue to mimic the active site, with respect to the papain family of cysteine peptidases (pdb 3H41) [35]. Docking was performed using Autodock4 with the following parameters: a grid box centered on L-Ala-γ-D-Glu bound to the catalytic site, encompassing all the residues involved in the interaction, a genetic algorithm of Lamarck, ten runs of computation with a final ranking and clustering of the docked peptide. The best pose computed for L-Ala-γ-D-Glu superimposes very well to the L-Ala- γ-D-Glu crystal position, so the protocol was validated and used for subsequent docking of L-Ala-γ-D-Glu, in the apo form of a 3D template of dipeptidyl-peptidase VI from *Bacteroides ovatus* (pdb id 3NPF) and the homology-modeled CpwFM, after superimposition of their NLPC_P60 domains. The analysis of the complexes and figures were generated with PyMOL 2.0.7. (Schrödinger, LLC., New York, NY, USA).

4.6. Expression and Purification of the CwpFM-GST-Tagged Protein

The plasmid pGEX6P1-GST-CwpFM was constructed as follows. The *cwpFM* gene was amplified from the *B. thuringiensis 407* cry- chromosome by PCR using the primer pairs CwpFM-GST-1 (5′-CGGGATCCC AAGTTTCAAATGAAGCGCTAA-3′) and CwpFM-GST-2 (5′-CCGCTCGAGTCCCA

AGTTTCCTTGGAAAGCC-3′). The DNA fragment was inserted between the BamHI and XhoI sites of plasmid pGEX6P1 (GE Healthcare), and the resulting plasmid was introduced into *E. coli M15* [pREP4] (Qiagen). Additionally, *E. coli BL21* bacteria were transformed with pGEX6P1–GST plasmid. Strains were grown at 37 °C for 8 h in 100 mL of LB containing ampicillin (100 µg/mL) for the strain BL21 or ampicillin and kanamycin (40 µg/mL) for the strain M15. Protein expression was induced by adding 100 µg/mL isopropyl-β-d-thio-galactoside for 4h at 30 °C. For the purification of the recombinant GST and CwpFM-GST fusion, bacterial pellets were re-suspended in lysis buffer (50 mm Tris-HCl, pH 7.8, 60 mm NaCl, 1 mm EDTA, 2 mm DTT, 0.2% Triton X-100) supplemented with complete Protease Inhibitor mixture (Roche), and incubated for 1 h on ice. Cells were then disrupted using a BAZIC Z cell disruptor (Constant Systems Ltd., Daventry, UK) at a pressure of 1600 bars, and centrifuged at 4 °C for 30 min at 10,000× *g*. GSH-Sepharose 4B beads (GE Healthcare) were added to clarified supernatants and incubated at 4 °C for 3 h. Beads were then washed two times in lysis buffer and three times in 20 mM Tris buffer, pH 8. Purity was assessed by 12% (*v*/*v*) SDS-PAGE with Coomassie blue staining. Protein concentration was measured using a Bradford assay (Sigma France, Lezennes, France).

4.7. Zymogram

CwpFM cell wall hydrolyzing activity was assessed using zymogram analysis. An amount of 3.5 µg of purified GST and CwpFM-GST was loaded onto SDS-PAGE using 12% (*v*/*v*) polyacrylamide separating gels containing 0·2% (*v*/*v*) *Micrococcus lysodeikticus* ATCC M3770 (Sigma) as the enzyme substrate. Micrococci were suspended in water and heat-inactivated at 120 °C for 10 min before they were mixed into the resolving gel. After sample migration, gels were washed with deionized water for 1 h at room temperature and incubated in 50 mM Tris-HCl pH 8 containing 1% Triton X100 (*v*/*v*) for 24 h at 37 °C. The total amount of proteins was detected by staining of the SDS-PAGE gel with Coomassie blue staining. The CwpFM hydrolyzing activity was characterized by a lysis plague visible as a halo on the gel at the level of the protein.

Author Contributions: Conceptualization: J.V., S.-L.T., N.R., G.A.-L.; validation: S.-L.T., N.R., G.A.-L.; formal analysis: S.-L.T., G.A.-L.; methodology/investigation: J.V., S.-L.T., D.C., G.A.-L.; writing—original draft preparation: J.V., S.-L.T., N.R., G.A.-L., D.C.; writing—review and editing: J.V., S.-L.T., N.R., G.A.-L., funding acquisition: N.R. All authors have read and agreed to the published version of the manuscript.

Funding: This research received no particular funding.

Acknowledgments: We thank Simon Palussière and Marie-Pierre Chapot-Chartier for their helpful assistance with zymogram assays.

Conflicts of Interest: The authors declare no conflict of interest.

References

1. Alcorlo, M.; Martinez-Caballero, S.; Molina, R.; Hermoso, J.A. Carbohydrate recognition and lysis by bacterial peptidoglycan hydrolases. *Curr. Opin. Struct. Biol.* **2017**, *44*, 87–100. [CrossRef]
2. Do, T.; Page, J.E.; Walker, S. Uncovering the activities, biological roles, and regulation of bacterial cell wall hydrolases and tailoring enzymes. *J. Biol. Chem.* **2020**, *295*, 3347–3361. [CrossRef]
3. Dorr, T.; Moynihan, P.J.; Mayer, C. Editorial: Bacterial Cell Wall Structure and Dynamics. *Front. Microbiol.* **2019**, *10*, 2051. [CrossRef]
4. He, J.; Fu, W.; Zhao, S.; Zhang, C.; Sun, T.; Jiang, T. Lack of MSMEG_6281, a peptidoglycan amidase, affects cell wall integrity and virulence of *Mycobacterium smegmatis*. *Microb. Pathog.* **2019**, *128*, 405–413. [CrossRef]
5. Healy, C.; Gouzy, A.; Ehrt, S. Peptidoglycan Hydrolases RipA and Ami1 Are Critical for Replication and Persistence of *Mycobacterium tuberculosis* in the Host. *MBio* **2020**, *11*, e03315-19. [CrossRef]
6. Mahasenan, K.V.; Batuecas, M.T.; De Benedetti, S.; Kim, C.; Rana, N.; Lee, M.; Hesek, D.; Fisher, J.F.; Sanz-Aparicio, J.; Hermoso, J.A.; et al. Catalytic Cycle of Glycoside Hydrolase BglX from Pseudomonas aeruginosa and Its Implications for Biofilm Formation. *ACS Chem. Biol.* **2020**, *15*, 189–196. [CrossRef]
7. Lonergan, Z.R.; Nairn, B.L.; Wang, J.; Hsu, Y.P.; Hesse, L.E.; Beavers, W.N.; Chazin, W.J.; Trinidad, J.C.; VanNieuwenhze, M.S.; Giedroc, D.P.; et al. An *Acinetobacter baumannii*, Zinc-Regulated Peptidase Maintains

Cell Wall Integrity during Immune-Mediated Nutrient Sequestration. *Cell Rep.* **2019**, *26*, 2009–2018.e6. [CrossRef]
8. Vermassen, A.; Leroy, S.; Talon, R.; Provot, C.; Popowska, M.; Desvaux, M. Cell Wall Hydrolases in Bacteria: Insight on the Diversity of Cell Wall Amidases, Glycosidases and Peptidases Toward Peptidoglycan. *Front. Microbiol.* **2019**, *10*, 331. [CrossRef]
9. Ramarao, N.; Lereclus, D.; Sorokin, A. The *Bacillus cereus* group. In *Molecular Medical Microbiology*, 2nd ed.; Academic Press: Cambrige, MA, USA, 2015; Volume III, pp. 1041–1078.
10. Kolsto, A.B.; Tourasse, N.J.; Okstad, O.A. What sets *Bacillus anthracis* apart from other *Bacillus* species? *Annu. Rev. Microbiol.* **2009**, *63*, 451–476. [CrossRef]
11. Jessberger, N.; Krey, V.M.; Rademacher, C.; Bohm, M.E.; Mohr, A.K.; Ehling-Schulz, M.; Scherer, S.; Martlbauer, E. From genome to toxicity: A combinatory approach highlights the complexity of enterotoxin production in *Bacillus cereus*. *Front. Microbiol.* **2015**, *6*, 560.
12. Celandroni, F.; Salveti, S.; Senesi, S.; Ghelardi, E. *Bacillus thuringiensis* membrane-damaging toxins acting on mammalian cells. *FEMS* **2014**, *361*, 95–103.
13. Carlson, C.R.; Caugant, D.A.; Kolstø, A.-B. Genotypic diversity among *Bacillus cereus* and *Bacillus thuringiensis* strains. *Appl. Environ. Microbiol.* **1994**, *60*, 1719–1725. [CrossRef] [PubMed]
14. Mock, M.; Fouet, A. Anthrax. *Annu. Rev. Microbiol.* **2001**, *55*, 647–671. [CrossRef]
15. Stevens, M.J.A.; Tasara, T.; Klumpp, J.; Stephan, R.; Ehling-Schulz, M.; Johler, S. Whole-genome-based phylogeny of Bacillus cytotoxicus reveals different clades within the species and provides clues on ecology and evolution. *Sci. Rep.* **2019**, *9*, 1984. [CrossRef]
16. Glasset, B.; Herbin, S.; Guillier, L.; Cadel-Six, S.; Vignaud, M.L.; Grout, J.; Pairaud, S.; Michel, V.; Hennekinne, J.A.; Ramarao, N.; et al. Bacillus cereus-induced food-borne outbreaks in France, 2007 to 2014: Epidemiology and genetic characterisation. *Eurosurveillance* **2016**, *21*, 30413. [CrossRef]
17. Agata, N.; Ohta, M.; Mori, M.; Isobe, M. A novel dodecadepsipeptide, cereulide, is an emetic toxin of *Bacillus cereus*. *FEMS Microbiol. Lett.* **1995**, *129*, 17–20.
18. Mahler, H.; Pasa, A.; Kramer, J.; Schulte, P.; Scoging, A.; Bar, W.; Krahenbuhl, S. Fulminant liver failure in association with the emetic toxin of Bacillus cereus. *N. Engl. J. Med.* **1997**, *336*, 1142–1148. [CrossRef]
19. Naranjo, M.; Denayer, S.; Botteldoorn, N.; Delbrassinne, L.; Veys, J.; Waegenaere, J.; Sirtaine, N.; Driesen, R.B.; Sipido, K.R.; Mahillon, J.; et al. Sudden death of a young adult associated with Bacillus cereus food poisoning. *J. Clin. Microbiol.* **2011**, *49*, 4379–4381. [CrossRef]
20. Ramarao, N.; Sanchis, V. The pore-forming hemolysins of Bacillus cereus: A review. *Toxins* **2013**, *5*, 1119–1139. [CrossRef]
21. Granum, E.; Lund, T. *Bacillus cereus* and its food poisoning toxins. *FEMS Microbiol. Lett.* **2006**, *157*, 223–228. [CrossRef]
22. Fox, D.; Mathur, A.; Xue, Y.; Liu, Y.; Tan, W.H.; Feng, S.; Pandey, A.; Ngo, C.; Hayward, J.A.; Atmosukarto, I.I.; et al. *Bacillus cereus* non-haemolityc enterotoxin activates the NLRP3 inflammasome. *Nat. Commun.* **2020**, *11*, 760–775. [CrossRef] [PubMed]
23. Haydar, A.; Tran, S.L.; Guillemet, E.; Darrigo, C.; Perchat, S.; Lereclus, D.; Coquet, L.; Jouenne, T.; Ramarao, N. InhA1-Mediated Cleavage of the Metalloprotease NprA Allows *Bacillus cereus* to Escape From Macrophages. *Front. Microbiol.* **2018**, *9*, 1063. [CrossRef] [PubMed]
24. Tran, S.L.; Guillemet, E.; Ngo-Camus, M.; Clybouw, C.; Puhar, A.; Moris, A.; Gohar, M.; Lereclus, D.; Ramarao, N. Hemolysin II is a *Bacillus cereus* virulence factor that induces apoptosis of macrophages. *Cell Microbiol.* **2011**, *13*, 92–108. [CrossRef]
25. Guillemet, E.; Lereec, A.; Tran, S.L.; Royer, C.; Barbosa, I.; Sansonetti, P.; Lereclus, D.; Ramarao, N. The bacterial DNA repair protein Mfd confers resistance to the host nitrogen immune response. *Sci. Rep.* **2016**, *6*, 29349. [CrossRef]
26. Guillemet, E.; Cadot, C.; Tran, S.L.; Guinebretiere, M.H.; Lereclus, D.; Ramarao, N. The InhA metalloproteases of *Bacillus cereus* contribute concomitantly to virulence. *J. Bacteriol.* **2010**, *192*, 286–294. [CrossRef]
27. Darrigo, C.; Guillemet, E.; Dervyn, R.; Ramarao, N. The Bacterial Mfd Protein Prevents DNA Damage Induced by the Host Nitrogen Immune Response in a NER-Independent but RecBC-Dependent Pathway. *PLoS ONE* **2016**, *11*, e0163321. [CrossRef]
28. Asano, S.; Nukumizu, Y.; Bando, H.; Iizuka, T.; Yamamoto, T. Cloning of novel enterotoxin genes from *Bacillus cereus* and *Bacillus thuringiensis*. *Appl. Environ. Microbiol.* **1997**, *63*, 1054–1057. [CrossRef]

29. Tran, S.L.; Guillemet, E.; Gohar, M.; Lereclus, D.; Ramarao, N. CwpFM (EntFM) is a *Bacillus cereus* potential cell wall peptidase implicated in adhesion, biofilm formation and virulence. *J. Bacteriol.* **2010**, *192*, 2638–2642. [CrossRef]
30. Shinagawa, K.; Sugiyama, J.; Terada, T.; Matsusaka, N.; Sugii, S. Improved methods for purification of an enterotoxin produced by *Bacillus cereus*. *FEMS Microbiol. Lett.* **1991**, *80*, 1–6. [CrossRef]
31. Boonchai, N.; Asano, S.; Bando, H.; Wiwat, C. Study on cytotoxicity and nucleotide sequences of Enterotoxin FM of *Bacillus cereus* isolated from various food sources. *J. Med. Assoc. Thail.* **2008**, *91*, 1425–1432.
32. Chon, J.W.; Yim, J.H.; Kim, H.S.; Kim, D.H.; Kim, H.; Oh, D.H.; Kim, S.K.; Seo, K.H. Quantitative Prevalence and Toxin Gene Profile of Bacillus cereus from Ready-to-Eat Vegetables in South Korea. *Foodborne Pathog. Dis.* **2015**, *12*, 795–799. [CrossRef] [PubMed]
33. Kim, J.B.; Kim, J.M.; Cho, S.H.; Oh, H.S.; Choi, N.J.; Oh, D.H. Toxin genes profiles and toxin production ability of *Bacillus cereus* isolated from clinical and food samples. *J. Food Sci.* **2011**, *76*, T25–T29. [CrossRef] [PubMed]
34. Ngamwongsatit, P.; Buasri, W.; Puianariyanon, P.; Pulsrikarn, C.; Ohba, M.; Assavanig, A.; Panbangreb, W. Broad distribution of enterotoxin genes (hblCDA, nheABC, cytK, and entFM) among *Bacillus thuringiensis* and *Bacillus cereus* as shown by novel primers. *Int. J. Food Microbiol.* **2008**, *121*, 352–356. [CrossRef]
35. Kall, L.; Krogh, A.; Sonnhammer, E.L. Advantages of combined transmembrane topology and signal peptide prediction–the Phobius web server. *Nucleic Acids Res.* **2007**, *35*, W429–W432. [CrossRef] [PubMed]
36. Xu, Q.; Abdubek, P.; Astakhova, T.; Axelrod, H.L.; Bakolitsa, C.; Cai, X.; Carlton, D.; Chen, C.; Chiu, H.J.; Chiu, M.; et al. Structure of the gamma-D-glutamyl-L-diamino acid endopeptidase YkfC from *Bacillus cereus* in complex with L-Ala-gamma-D-Glu: Insights into substrate recognition by NlpC/P60 cysteine peptidases. *Acta Crystallogr. Sect. F Struct. Biol. Cryst. Commun.* **2010**, *66 Pt 10*, 1354–1364. [CrossRef]
37. Rodriguez, J.; Haydinger, C.D.; Peet, D.J.; NGuyen, L.K.; von Kriegsheim, A. Asparagine hydroxylation is likely to be a reversible post-translational modification. *BioRxiv* **2020**. [CrossRef]
38. Ehling-SChulz, M.; Lereclus, D.; Koehler, T. The *Bacillus cereus* group-*Bacillus* species with pathogenic potential. *Microbiol. Spect.* **2019**, *7*, 10.
39. Ramarao, N.; Tran, S.L.; Marin, M.; Vidic, J. Advanced method for detection of *Bacillus cereus* and its pathogenic factors. *Sensors* **2020**, *20*, 2667. [CrossRef]
40. Martinez, M.; Alzari, P.M.; André-Leroux, G. Signalling mechanism in Procaryotes. In *Bacterial Membranes: Structural and Molecular Biology*; Remaut, H., Fronzes, R., Eds.; Honrizon Scientific Press: Poole, UK, 2014.
41. Do, T.; Schaefer, K.; Santiago, A.G.; Coe, K.A.; Fernandes, P.B.; Kahne, D.; Pinho, M.G.; Walker, S. *Staphylococcus aureus* cell growth and division are regulated by an amidase that trims peptides from uncrosslinked peptidoglycan. *Nat. Microbiol.* **2020**, *5*, 291–303. [CrossRef]
42. Mitkowski, P.; Jagielska, E.; Nowak, E.; Bujnicki, J.M.; Stefaniak, F.; Niedzialek, D.; Bochtler, M.; Sabala, I. Structural bases of peptidoglycan recognition by lysostaphin SH3b domain. *Sci. Rep.* **2019**, *9*, 5965. [CrossRef]
43. Xu, Q.; Mengin-Lecreulx, D.; Liu, X.W.; Patin, D.; Farr, C.L.; Grant, J.C.; Chiu, H.J.; Jaroszewski, L.; Knuth, M.W.; Godzik, A.; et al. Insights into Substrate Specificity of NlpC/P60 Cell Wall Hydrolases Containing Bacterial SH3 Domains. *MBio* **2015**, *6*, e02327-14. [CrossRef] [PubMed]
44. Gonzalez-Delgado, L.S.; Walters-Morgan, H.; Salamaga, B.; Robertson, A.J.; Hounslow, A.M.; Jagielska, E.; Sabala, I.; Williamson, M.P.; Lovering, A.L.; Mesnage, S. Two-site recognition of *Staphylococcus aureus* peptidoglycan by lysostaphin SH3b. *Nat. Chem. Biol.* **2020**, *16*, 24–30. [CrossRef] [PubMed]
45. Lee, K.O.; Kong, M.; Kim, I.; Bai, J.; Cha, S.; Kim, B.; Ryu, K.S.; Ryu, S.; Suh, J.Y. Structural Basis for Cell-Wall Recognition by Bacteriophage PBC5 Endolysin. *Structure* **2019**, *27*, 1355–1365.e4. [CrossRef] [PubMed]
46. Benesik, M.; Novacek, J.; Janda, L.; Dopitova, R.; Pernisova, M.; Melkova, K.; Tisakova, L.; Doskar, J.; Zidek, L.; Hejatko, J.; et al. Role of SH3b binding domain in a natural deletion mutant of Kayvirus endolysin LysF1 with a broad range of lytic activity. *Virus Genes* **2018**, *54*, 130–139. [CrossRef] [PubMed]
47. Margot, P.; Pagni, M.; Karamata, D. *Bacillus subtilis* 168 gene lytF encodes a gamma-D-glutamate-meso-diaminopimelate muropeptidase expressed by the alternative vegetative sigma factor, sigmaD. *Microbiology* **1999**, *145 Pt 1*, 57–65. [CrossRef]
48. Fukushima, T.; Afkham, A.; Kurosawa, S.; Tanabe, T.; Yamamoto, H.; Sekiguchi, J. A new D,L-endopeptidase gene product, YojL (renamed CwlS), plays a role in cell separation with LytE and LytF in *Bacillus subtilis*. *J. Bacteriol.* **2006**, *188*, 5541–5550. [CrossRef]

49. Mesnage, S.; Dellarole, M.; Baxter, N.J.; Rouget, J.B.; Dimitrov, J.D.; Wang, N.; Fujimoto, Y.; Hounslow, A.M.; Lacroix-Desmazes, S.; Fukase, K.; et al. Molecular basis for bacterial peptidoglycan recognition by LysM domains. *Nat. Commun.* **2014**, *5*, 4269. [CrossRef]
50. Wong, J.E.; Alsarraf, H.M.; Kaspersen, J.D.; Pedersen, J.S.; Stougaard, J.; Thirup, S.; Blaise, M. Cooperative binding of LysM domains determines the carbohydrate affinity of a bacterial endopeptidase protein. *FEBS J.* **2014**, *281*, 1196–1208. [CrossRef]
51. Carballido-Lopez, R.; Formstone, A.; Li, Y.; Ehrlich, S.D.; Noirot, P.; Errington, J. Actin homolog MreBH governs cell morphogenesis by localization of the cell wall hydrolase LytE. *Dev. Cell* **2006**, *11*, 399–409. [CrossRef]
52. Damman, C.J.; Eggers, C.H.; Samuels, D.S.; Oliver, D.B. Characterization of *Borrelia burgdorferi* BlyA and BlyB proteins: A prophage-encoded holin-like system. *J. Bacteriol.* **2000**, *182*, 6791–6797. [CrossRef]
53. Blackman, S.A.; Smith, T.J.; Foster, S.J. The role of autolysins during vegetative growth of *Bacillus subtilis* 168. *Microbiology* **1998**, *144 Pt 1*, 73–82. [CrossRef] [PubMed]
54. Sanchez Chica, J.; Correa, M.M.; Aceves-Diez, A.E.; Rasschaert, G.; Heyndrickx, M.; Castaneda-Sandoval, L.M. Genomic and Toxigenic Heterogeneity of *Bacillus cereus sensu lato* Isolated from Ready-to-Eat Foods and Powdered Milk in Day Care Centers in Colombia. *Foodborne Pathog. Dis.* **2020**, *17*, 340–347. [CrossRef] [PubMed]
55. Zhao, S.; Chen, J.; Fei, P.; Feng, H.; Wang, Y.; Ali, M.A.; Li, S.; Jing, H.; Yang, W. Prevalence, molecular characterization, and antibiotic susceptibility of *Bacillus cereus* isolated from dairy products in China. *J. Dairy Sci.* **2020**, *103*, 3994–4001. [CrossRef] [PubMed]
56. Park, K.M.; Kim, H.J.; Jeong, M.; Koo, M. Enterotoxin Genes, Antibiotic Susceptibility, and Biofilm Formation of Low-Temperature-Tolerant *Bacillus cereus* Isolated from Green Leaf Lettuce in the Cold Chain. *Foods* **2020**, *9*, 249. [CrossRef]
57. Gao, T.; Ding, Y.; Wu, Q.; Wang, J.; Zhang, J.; Yu, S.; Yu, P.; Liu, C.; Kong, L.; Feng, Z.; et al. Prevalence, Virulence Genes, Antimicrobial Susceptibility, and Genetic Diversity of *Bacillus cereus* Isolated From Pasteurized Milk in China. *Front. Microbiol.* **2018**, *9*, 533. [CrossRef]
58. Chon, J.W.; Kim, J.H.; Lee, S.J.; Hyeon, J.Y.; Song, K.Y.; Park, C.; Seo, K.H. Prevalence, phenotypic traits and molecular characterization of emetic toxin-producing *Bacillus cereus* strains isolated from human stools in Korea. *J Appl Microbiol* **2012**, *112*, 1042–1049. [CrossRef]
59. Yang, Y.; Gu, H.; Yu, X.; Zhan, L.; Chen, J.; Luo, Y.; Zhang, Y.; Lu, Y.; Jiang, J.; Mei, L. Genotypic heterogeneity of emetic toxin producing *Bacillus cereus* isolates from China. *FEMS Microbiol. Lett.* **2017**, *364*, fnw237. [CrossRef]
60. Appadurai, R.; Uversky, V.N.; Srivastava, A. The Structural and Functional Diversity of Intrinsically Disordered Regions in Transmembrane Proteins. *J. Membr. Biol.* **2019**, *252*, 273–292. [CrossRef]
61. Li, Q.; Chevalier, C.; Henry, C.; Richard, C.-A.; Moudjou, M.; Vidic, J. Shadoo binds lipid membranes and undergoes aggregation and fibrillization. *Biochem. Biophys. Res. Commun.* **2013**, *438*, 519–525. [CrossRef]
62. Chevalier, C.; Al Bazzal, A.; Vidic, J.; Février, V.; Bourdieu, C.; Bouguyon, E.; Le Goffic, R.; Vautherot, J.-F.; Bernard, J.; Moudjou, M. PB1-F2 influenza A virus protein adopts a β-sheet conformation and forms amyloid fibers in membrane environments. *J. Biol. Chem.* **2010**, *285*, 13233–13243. [CrossRef]
63. Vidic, J.; Richard, C.-A.; Péchoux, C.; Da Costa, B.; Bertho, N.; Mazerat, S.; Delmas, B.; Chevalier, C. Amyloid assemblies of influenza A virus PB1-F2 protein damage membrane and induce cytotoxicity. *J. Biol. Chem.* **2016**, *291*, 739–751. [CrossRef] [PubMed]
64. Galvagnion, C.; Brown, J.W.; Ouberai, M.M.; Flagmeier, P.; Vendruscolo, M.; Buell, A.K.; Sparr, E.; Dobson, C.M. Chemical properties of lipids strongly affect the kinetics of the membrane-induced aggregation of α-synuclein. *Proc. Natl. Acad. Sci. USA* **2016**, *113*, 7065–7070. [CrossRef] [PubMed]
65. Vollmer, W.; Joris, B.; Charlier, P.; Foster, S. Bacterial peptidoglycan (murein) hydrolases. *FEMS Microbiol. Rev.* **2008**, *32*, 259–286. [CrossRef] [PubMed]

66. Mohamed, J.A.; Teng, F.; Nallapareddy, S.R.; Murray, B.E. Pleiotrophic effects of 2 *Enterococcus faecalis* sagA-like genes, salA and salB, which encode proteins that are antigenic during human infection, on biofilm formation and binding to collagen type i and fibronectin. *J. Infect. Dis.* **2006**, *193*, 231–240. [CrossRef] [PubMed]
67. Hou, S.; Chen, G.; Wang, W.; Xia, L.; Wang, Z.; Lu, Y. Identification of a cell-wall peptidase (NlpC/P60) from *Nocardia seriolae* which induces apoptosis in fathead minnow cells. *J. Fish Dis.* **2020**, *43*, 571–581. [CrossRef]
68. Padhi, A.; Naik, S.K.; Sengupta, S.; Ganguli, G.; Sonawane, A. Expression of *Mycobacterium tuberculosis* NLPC/p60 family protein Rv0024 induce biofilm formation and resistance against cell wall acting anti-tuberculosis drugs in *Mycobacterium smegmatis*. *Microbes Infect.* **2016**, *18*, 224–236. [CrossRef]
69. Gao, L.Y.; Pak, M.; Kish, R.; Kajihara, K.; Brown, E.J. A mycobacterial operon essential for virulence in vivo and invasion and intracellular persistence in macrophages. *Infect. Immun.* **2006**, *74*, 1757–1767. [CrossRef]
70. Parthasarathy, G.; Lun, S.; Guo, H.; Ammerman, N.C.; Geiman, D.E.; Bishai, W.R. Rv2190c, an NlpC/P60 family protein, is required for full virulence of *Mycobacterium tuberculosis*. *PLoS ONE* **2012**, *7*, e43429. [CrossRef]
71. Sela-Abramovich, S.; Chitlaru, T.; Gat, O.; Grosfeld, H.; Cohen, O.; Shafferman, A. Novel and unique diagnostic biomarkers for *Bacillus anthracis* infection. *Appl. Environ. Microbiol.* **2009**, *75*, 6157–6167. [CrossRef]
72. Wydau-Dematteis, S.; El Meouche, I.; Courtin, P.; Hamiot, A.; Lai-Kuen, R.; Saubamea, B.; Fenaille, F.; Butel, M.J.; Pons, J.L.; Dupuy, B.; et al. Cwp19 Is a Novel Lytic Transglycosylase Involved in Stationary-Phase Autolysis Resulting in Toxin Release in *Clostridium difficile*. *MBio* **2018**, *9*, e00648-18. [CrossRef]
73. Boudreau, M.A.; Fisher, J.F.; Mobashery, S. Messenger functions of the bacterial cell wall-derived muropeptides. *Biochemistry* **2012**, *51*, 2974–2990. [CrossRef] [PubMed]
74. Schaub, R.E.; Perez-Medina, K.M.; Hackett, K.T.; Garcia, D.L.; Dillard, J.P. *Neisseria gonorrhoeae* PBP3 and PBP4 Facilitate NOD1 Agonist Peptidoglycan Fragment Release and Survival in Stationary Phase. *Infect. Immun.* **2019**, *87*, e00833-18. [CrossRef] [PubMed]
75. Glasset, B.; Herbin, S.; Granier, S.; Cavalié, L.; Lafeuille, E.; Guérin, C.; Ruimy, R.; Casagrande, F.; Levast, M.; Chautemps, N.; et al. *Bacillus cereus*, a serious cause of nosocomial infections: Epidemiologic and genetic survey. *PLoS ONE* **2018**, *13*, e0194346. [CrossRef] [PubMed]
76. Guinebretière, M.H.; Broussolle, V.; Nguyen-The, C. Enterotoxigenic profiles of food-poisoning and food-borne *Bacillus cereus* strains. *J. Clin. Microbiol.* **2002**, *40*, 3053–3056. [CrossRef] [PubMed]
77. Kamar, R.; Gohar, M.; Jehanno, I.; Rejasse, A.; Kallassy, M.; Lereclus, D.; Sanchis, V.; Ramarao, N. Pathogenic potential of *Bacillus cereus* strains as revealed by phenotypic analysis. *J. Clin. Microbiol.* **2013**, *51*, 320–323. [CrossRef]
78. Armenteros, J.J.A.; Tsirigos, K.D.; SØnderby, C.K.; Petersen, T.N.; Winther, O.; Brunak, S.; von Heijne, G.; Nielsen, H. SignalP5.0 improves signal peptide predictions using deep neural networks. *Nat. Biotechnol.* **2019**, *37*, 420–423. [CrossRef] [PubMed]
79. Katoh, K.; Standley, D.M. MAFFT multiple sequence alignment software version 7: Improvements in performance and usability. *Mol. Biol. Evol.* **2013**, *30*, 772–780. [CrossRef]
80. Webb, B.; Salí, A. Protein Structure Modeling with MODELLER. *Methods Mol. Biol.* **2017**, *1654*, 39–54.
81. Mészáros, B.; Erdös, G.; Dostányi, Z. IUPred2A: Context-dependent prediction of protein disorder as a function of redox state and protein binding. *Nucleic Acid Res.* **2018**, *46*, 329–337. [CrossRef]

Annexe III

Article : “Identification of a New Pathogenicity Island Within the Large pAH187_270 Plasmid Involved in *Bacillus cereus* Virulence”

frontiers in Cellular and Infection Microbiology

ORIGINAL RESEARCH
published: 20 January 2022
doi: 10.3389/fcimb.2021.788757

Identification of a New Pathogenicity Island Within the Large pAH187_270 Plasmid Involved in *Bacillus cereus* Virulence

Rozenn Dervyn†, *Devon W. Kavanaugh*†, *Delphine Cormontagne*, *Benjamin Glasset and Nalini Ramarao**

Université Paris-Saclay, INRAE, Micalis Institute, Jouy-en-Josas, France

Objectives: *Bacillus cereus* is responsible for food poisoning and rare but severe clinical infections. The pathogenicity of *B. cereus* strains varies from harmless to lethal strains. The objective of this study was to characterize three *B. cereus* isolates isolated from the same patient and identify their virulence potentials.

Methods: Three isolates of *B. cereus* were isolated from various blood samples from a patient who developed sepsis following a central venous catheter infection. The three isolates were compared by WGS, genotyping and SNP analysis. Furthermore, the isolates were compared by phenotypical analysis including bacterial growth, morphology, germination efficacy, toxin production, antibiotic susceptibility and virulence in an insect model of infection.

Results: According to WGS and genotyping, the 3 isolates were shown to be identical strains. However, the last recovered strain had lost the mega pAH187_270 plasmid. This last strain showed different phenotypes compared to the first isolated strain, such as germination delay, different antibiotic susceptibility and a decreased virulence capacity towards insects. A 50- kbp region of pAH187_270 plasmid was involved in the virulence potential and could thus be defined as a new pathogenicity island of *B. cereus*.

Conclusions: These new findings help in the understanding of *B. cereus* pathogenic potential and complexity and provide further hints into the role of large plasmids in the virulence of *B. cereus* strains. This may provide tools for a better assessment of the risks associated with *B. cereus* hospital contamination to improve hygiene procedure and patient health.

Keywords: ***Bacillus cereus*, clinical infection, virulence, mega-plasmid, pathogenicity island**

OPEN ACCESS

Edited by:
Costas C. Papagiannitsis, University of Thessaly, Greece

Reviewed by:
Ibrahim Bitar, Charles University, Czechia
Alberto Antonelli, University of Florence, Italy

***Correspondence:**
Nalini Ramarao
nalini.ramarao@inrae.fr

†*These authors have contributed equally to this work*

Specialty section:
This article was submitted to Clinical Microbiology, a section of the journal Frontiers in Cellular and Infection Microbiology

Received: *03 October 2021*
Accepted: *21 October 2021*
Published: *20 January 2022*

Citation:
Dervyn R, Kavanaugh DW, Cormontagne D, Glasset B and Ramarao N (2022) Identification of a New Pathogenicity Island Within the Large pAH187_270 Plasmid Involved in Bacillus cereus Virulence. Front. Cell. Infect. Microbiol. 11:788757. doi: 10.3389/fcimb.2021.788757

INTRODUCTION

Bacillus cereus is a Gram positive, spore-forming bacterium found in nearly all environments. The pathogenic potential of the strains of *B. cereus* ranges from beneficial to benign to pathogenic (Stenfors Arnesen et al., 2008). *B. cereus* is the 3rd most frequent bacterial agent responsible for food-borne outbreaks in Europe (Journal, 2009). In addition, infection with *B. cereus* is associated with

non-gastrointestinal diseases and can potentially result in pneumonia, septicaemia, endocarditis, and meningitis, with immunocompromised individuals and neonates being particularly susceptible (Bottone, 2010; Cormontagne et al., 2021). *B. cereus* is able to persist in the environment over long periods and can cause recurrent nosocomial infections (Glasset et al., 2018).

Among the most widely studied toxins of *B. cereus* are those related to the diarrheal syndrome, which include non-haemolytic enterotoxin (Nhe), Haemolysin BL (Hbl), and Cytotoxins K (CytK1 and CytK2), all of which are pore-forming toxins (Granum and Lund, 1997; Fagerlund et al., 2008; Guinebretiere et al., 2013; Ramarao and Sanchis, 2013). Additionally, enzymatic proteins have been identified, which contribute to *B. cereus* toxicity, such as InhAs and CwpFM (Haydar et al., 2018; Tran et al., 2020). Furthermore, the causative agent of emesis, the dodecadepsipeptide cereulide, is restricted to strains carrying pXO-1-like megaplasmids (Carlin et al., 2006). Although these factors are involved in *B. cereus* pathogenicity, the differentiation of pathogenic from non-pathogenic strains has proven difficult, even with molecular methods (Ramarao et al., 2020).

We have recently identified a subset of genes, not previously associated with virulence, which presence helps to discern clinical from harmless strains (Kavanaugh et al., 2021). Considering the difficulty in discerning strains as well as the time required for phenotypic tests, it is anticipated that future methodologies will focus on risk-orientated differential diagnostics, through inclusion of methods for detection of toxins, toxin genes and markers of virulence (Fricker et al., 2007).

In the present study, 3 strains were isolated from the same patient over an 87-day period. The first two strains were virtually identical with the third having lost a mega plasmid that contains several of the recently identified biomarkers. This last isolated strain had a decreased capacity to germinate and to induce virulence in an insect model, strongly suggesting that the pAH187_270 plasmid promotes virulence.

MATERIALS AND METHODS

Bacterial Strains and Growth Conditions

A 63-year-old male patient was admitted at a French University Hospital with Crohn's disease and chronic renal failure. The patient further developed sepsis and a central venous catheter infection. *B. cereus* isolates were isolated from various blood samples from this patient.

The patient underwent intensive rounds of antibiotic treatment including amoxicillin, ciprofloxacin (21 days), gentamycin (3 days), imipenem (18 days) followed by ciprofloxacin and vancomycin (10 days) (Glasset et al., 2018). Three positive blood cultures yielding *B. cereus* isolates (12CEB42BAC_S94, 12CEB40BAC_S20, 12CEB43BAC_S95, further named S94, S20 and S95, respectively) were obtained during a span of 87 days. The first sample (S94) was collected before the patient received antibiotic treatments, the second sample (S20) was collected after 23 days of treatment, and the last sample (S95) was collected 64 days after the previous one. The isolated strains were confirmed as being *B. cereus* by MALDI-TOF and no other bacteria were isolated in the blood cultures. The patient was later released from hospital, presenting no further signs of infection.

DNA Extraction, Genome Sequencing, and Assembly

The bacterial strains were grown overnight in BHI medium at 37°C, 200 rpm until mid-exponential growth phase and bacteria were pelleted. Total DNA was extracted as previously described (Cadot et al., 2010; Kavanaugh et al., 2021) and quantified with the Qubit® Fluorimeter. DNA concentrations were adjusted to 30 ng/ml and sequenced by the MiSeq Illumina platform hosted at the Pasteur Institute, giving 2x150 bp paired-end reads.

Sequencing analysis was performed as previously described (Kavanaugh et al., 2021) and included quality control using FastQC and MultiQC, *de novo* assembly of draft genomes with SPAdes version 3.13.0. Raw WGS data are accessible through https://www.ebi.ac.uk/ena/ (accession number PRJEB46455).

The genome sequences of the 3 strains were aligned against the pAH187_270 plasmid from the strain *B. cereus* AH187 using NUCmer for sequence alignment and MUMmer/MUMmerplot for visualisation/coverage plots. Further analysis was performed using the Proksee server (https://beta.proksee.ca/) to create circular alignments of reads to the reference plasmid.

Genotyping, Genome Annotation, and SNPs Analysis

MLST was determined for the 3 strains using the online MLST tool available from the Centre for Genomic Epidemiology (Larsen et al., 2012). Genome annotation was carried out using the Prokka automatic annotation tool v [1.13] (Seemann, 2014). Core and accessory genomes were determined by Roary with default settings, with the core genome defined as genes present in at least 3 of 4 samples, including *B. cereus* AH187 as reference strain.

SNPs were identified using Snippy (Seemann, 2014), which infers polymorphisms at the nucleotide level by aligning the sequencing reads against the reference plasmid pAH187_270.

Molecular Analysis

M13 sequence-based polymerase chain reaction (M13-PCR), derived from a RAPD technique, allows differentiating between various strain patterns. M13 typing was performed as described (Glasset et al., 2016). The DNA profiles were analyzed with BioNumerics 7.1 software (Applied Maths). The software compared the DNA profiles and clustered the strains according to their similarity.

The toxin gene profiles were identified by assessing the presence of the *cytK-1, cytK-2, HBLA, HBLC, HBLD, NHEA, NHEB, NHEC, hlyII* and *ces* genes by PCR using specific primers (Glasset et al., 2016). The strains were then clustered into genetic signatures (GS) according to their different combinations of presence/absence patterns (Glasset et al., 2021).

The strains were affiliated to one of the seven known phylogenetic groups according to the partial sequencing of the

panC gene (Guinebretière et al., 2008). The production of the enterotoxins NHE and HBL was tested with the immunological tests BCET-RPLA Toxin Detection (Oxoïd) and Tecra (BDE VIA, 3M-Tecra) kits, respectively (Guinebretière et al., 2002).

Plasmid Curing

Plasmid-curing was tempted to determine the influence of the 270 kb pAH187 plasmid on strain characteristics. Plasmid-curing was investigated through culturing the strains at increased temperature (41°C and 43°C), addition of antibiotics (ampicillin – 50µg/ml or novobiocin - 2ug/ml), or ethidium bromide (15, 100, 125 µg/ml) during repeated or prolonged culture between 5-10 days.

Pathogenicity Island (PAI) Deletion on the pAH187 Plasmid

Knock-out of the region corresponding to the PAI on the pAH187 plasmid carried by the S94 strain was accomplished by double-cross over region substitution. Briefly, using the available sequencing information of the pAH187 plasmid (NC_011655), 1 kb regions upstream (region 130550 to 131543) and downstream (region 174739 to 175734) of the identified PAI were synthesized by the Genecust company (Boynes, France). A spectinomycin-resistance cassette was obtained from pAT28 (Trieu-Cuot et al., 1990). The two fragments upstream and downstream of the PAI were cloned at each side of the cassette into the pAT113 vector (Trieu-Cuot et al., 1991) by the Genecust company. The constructed plasmid was named as pAT113 Δpai-pAH187 and transformed into chemically competent *E. coli* ET12567 and then by conjugation into *B. cereus* S94 strain (Trieu-Cuot et al., 1987; Huys et al., 2004). Briefly, the donor strain and receptor strains were mixed at ratio 14:1 on a sterile membrane filter with a pore size of 0.05 µm (VMWP02500 Milipore) deposited on BHI agar plates for 18 h at 37°C. After mating, bacteria were resuspended from filter with 1.5 mL of colicin solution (Hill and Holland, 1967). The transconjugates were selected on BHI agar plates supplemented with 300 µg/mL of spectinomycin at 37°C. The deletion of the PAI by double recombination event was verified by PCR using primers located upstream and downstream of the cloned region. The corresponding mutant was named S94 Δpai. Due to the size of the entire PAI, it was technically not possible to obtain a complemented strain.

Growth and Morphology

All strains were inoculated into BHI broth and grown at 37°C, 200 rpm. Bacterial growth was followed by measuring the OD at 600 nm at regular intervals.

To determine cellular morphology and size, bacteria were observed on BHI plates. The size of 25 colonies per plate was measured with a graduated scale. Alternatively, bacteria harvested at the end of exponential growth phase were observed under an AxioObserver. ZI Zeiss inverted microscope.

Sporulation/Germination

The sporulation efficiency of the strains was determined in HCT plus 0.3% glucose as previously described (Ramarao and Lereclus, 2005). For germination assays, the spores were incubated in BHI medium for 55 min. Samples were taken at 0, 7 min, 16 min, 25 min, 40 min, 55 min. The number of remaining spores was determined as heat-resistant (85°C for 15 min) CFU on BHI plates and normalized to the initial spore value at T0.

Insect Experiments

Spores were injected at various concentrations between the second and third body segment from the rear of 10 last instar *Galleria mellonella* larvae as previously described (Buisson et al., 2019). The mortality rate was measured after 24 h of infection at 37°C.

Antibiotic Susceptibility

The Minimum Inhibitory Concentrations (MICs) of selected antimicrobial agents were measured by using concentration gradient strips (Etest®, BioMerieux) (Glasset et al., 2018). The following agents were tested: ampicillin[$], cefotaxime, imipenem[$], vancomycin[$], gentamicin[$], rifampicin[$], tetracycline[$], ciprofloxacin[$], chloramphenicol[$], azithromycin, sulfamethoxazole/trimethoprim[$] and clindamycin[$]. Due to scarce availability of interpretative criteria in the literature, clinical breakpoints were used when available ([$]) (Wayne and Clinical and Laboratory Standards Institute (CLSI), 2010).

RESULTS

Comparison of the Three Isolates

Three *B. cereus* isolates were isolated from three different blood cultures of the same patient within a period of 87 days and following intensive antibiotic treatments. No other bacteria were isolated from the blood cultures.

The M13 profiles of the 3 isolates were compared and were highly similar for the 3 isolates, suggesting that the 3 isolates are identical or very similar strains (**Figure 1A**).

In order to further compare the isolates, their genomes were sequenced. Mean size of the draft genomes was 5,533,542bp (range 5318760 [S95] - 5643975 [S94]). Mean GC % was 35.3%. *In silico* MLST analysis determined each strain to belong to the same MLST type 26.

The strains were further characterized for the presence of 10 genes implicated in virulence, the production of Nhe and the phylogenic group. The three isolates possess the *nhe* gene and were high Nhe producers. The *hbl* and *cytK* genes were absent in all isolates. The 3 isolates belong to phylogenetic group III. However, the *ces* gene was present in the two first isolates (S94 and S20) and absent in the last isolate (S95).

The patient received an intensive antibiotic treatment. To assess the potential impact of this treatment on the antibiotic resistance of the strains, the CMI against major antibiotic were measures for the first S94 and the last S95 isolated strains. The two isolates were resistant to ampicillin and cefotaxime. The strains were sensitive to the antibiotics that were administered to the patient. Strikingly, the 94 strain was susceptible to rifampicin whereas S95 strain displayed resistance to rifampicin (**Table 1**).

Identification of a Missing Plasmid in the Last Isolated Strain

Mash analysis of the 3 strains identified the closest strain to S94 and S20 to be AH187 with an average nucleotide identity of

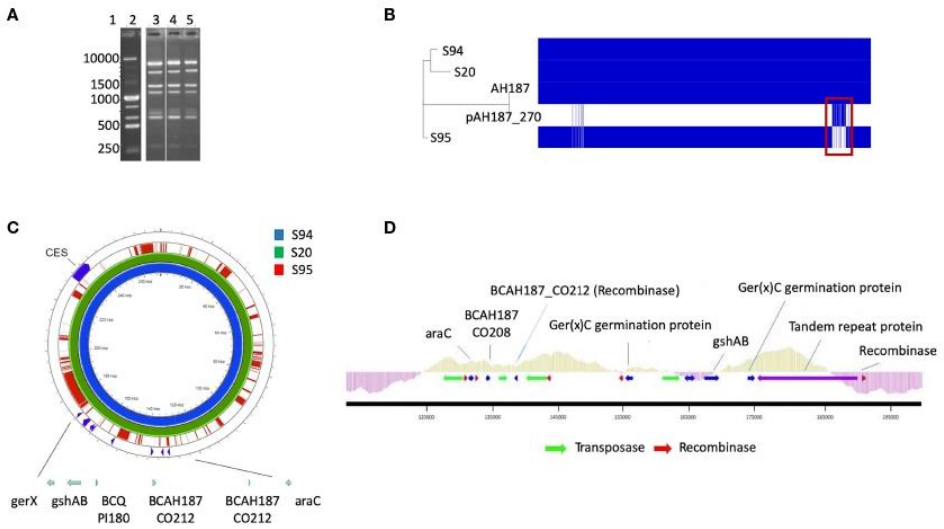

FIGURE 1 | **(A)** M13-PCR fingerprint patterns, Lane 1: 1 kb DNA ladder. Lane 2: reference strain *B cereus* ATCC14579. Lane 3 to 5: S94, S20, S95 *B cereus* strains. **(B)** Visualization of core and accessory genomes of patient isolates S94, S20, S95, along with reference strain *B cereus* AH187 and mega-plasmid pAH187_270, using RAxML-generated phylogenetic tree and presence/absence table generated by Roary. Red box highlights absence of pAH187_270 genes in strain S95. **(C)** Proksee visualization of strains S94, S20, S95 aligned to the plasmid pAH187_270 nucleotide sequences. Key biomarkers are identified within the plasmid (green arrows), as well as the *ces* encoding gene. **(D)** Overview of the PAI. The plasmid region from 125,000 to 192,000bp of pAH187_270 contains all of the plasmid-based biomarkers (blue arrows) and several transposases/recombinases (green and red arrows, respectively). The average GC content is indicated above the genes within the PAI (light green) and in the surrounding regions of the plasmid (purple).

99.9%. The AH187 strain possesses the pAH_187- 270 kb mega-plasmid. Analysis of the core and accessory genomes reveals that nearly all variability among the 3 patient strains results from the accessory genes located on this mega-plasmid (**Figure 1B**).

To further assess the differences among the patient-isolated strains, snps were examined *via* Snippy using the plasmid, pAH187_270, as reference. A significant amount of variation is evident when comparing the S95 patient strain against the mega-plasmid, pAH187_270 (**Table 2**).

Consistently, the pAH187_270 plasmid sequence resulted in nearly 100% coverage for S20 and S94 strains. By contrast, the S95 strain did not demonstrate significant alignment to the pAH187_270 plasmid (**Figure 1C**).

Altogether, the 3 isolates have an almost identical chromosome but differed by the absence of the pAH187_270 plasmid in the S95 isolate compared to the S94 and S20 isolates.

Identification and Reconstruction of a Pathogenicity Island

A closer look at the pAH187_270 plasmid revealed that some of the biomarkers previously identified as characteristic of clinical strains (Kavanaugh et al., 2021) were present on this plasmid (i.e., araC, gshAB, BCQ_PI180) (**Figure 1C**).

We confirmed by WGS that S20 and S94 carried these biomarkers, whereas the S95 strain did not. In addition, S94 and S20 carried the *ces* gene located in the pAH187_270 plasmid whereas S95 did not (not shown).

Based on the NUCmer alignment results, the localisation of the plasmid-based biomarkers of the S94 strain was determined. These biomarkers were located within a 43 kb span of the pAH187_270 plasmid, being distant from the CES operon for cereulide production (**Figure 1C**). We named this region the pathogenicity island (PAI). At first glance, it was observed that the PAI is flanked by resolvases and transposons indicating that they may have been obtained during horizontal gene transfer (**Figure 1D**). Further investigation of the plasmid pAH187 and the PAI revealed typical features used in defining PAIs. First, there is an abundance of direct repeats found in the plasmid. When a higher upper limit is set for maximum size (10,000 bp), 57 repeats of varying size, with 10 repeats of 396 bp clustered in the 175,466 to 189,105 region. However, with a lower limit of 200 bp, 20 hits are detected, with repeats detected on either side of the PAI at approx. 135,000 bp and 185,000 bp. Interestingly, pAH187 possesses a large inverted repeat 2,654 bp long, located 127,621-130,299 and 163,537-160,858, (99% match) found within the PAI. Furthermore, within the PAI, there is an increased presence of resolvases and transposases, which diminish in prevalence immediately outside the PAI. These are believed to play a role in the mobility of the DNA elements and facilitate their transfer and integration. Terminating one end of the PAI, a region, which spans from 175,000bp to 190,000 bp contains numerous tandem repeats, and finally terminates with a Holliday junction resolvase, further confirming the presence of the PAI.

TABLE 1 | MIC results (Etest method) for S94 and S95 *B. cereus* strains for 12 antibiotics.

Key	Ampicillin	Cefotaxime	Imipenem	Vancomycin	Gentamicin	Rifampicin	Tetracyclin	Ciprofloxacin	Chloramphenicol	Azithromycin	Sulf + Trimethoprime	Clindamycin
Recommandation CLSI	S< 0,25 - R >0,5	S < 8 - R > 64	S < 4 - R > 16	S < 4	S < 4 - R > 16	S < 1 - R > 4	S < 4 - R > 16	S < 1 - R > 4	S < 8 - R > 32	?	S < 2/38 - R > 4/ 76	S < 0,5 - R > 4
S94	1,5	64	0,047	1	0,094	**0,19**	0,38	0,047	3	0,19	0,25	0,19
S95	3	64	0,047	3	0,19	**6**	0,19	0,094	1,5	0,125	0,75	0,125

Lastly, PAIs are often accompanied by changes in GC content in the inserted region, and this may be attributed to the DNA arriving from a different species through horizontal gene transfer. The GC content of the PAI was above average, compared to the immediately surrounding regions. It is to note that *B. cereus* is a low-GC-content bacteria and an increase in the GC content may thus indicate an integration of the PAI from a different species. However, as the difference in GC content is not a stark change, it may also represent an insertion or even a fusion event, as *B. cereus* megaplasmids (>100kb) have previously been hypothesized to result from fusion of smaller plasmids given the presence of multiple minireplicons (Zheng et al., 2013).

Several genes are present in the PAI: araC, BCAH187_C0208, BCAH187_C0212 being found at one end, BCN_P218 and BCAH187_C0212_2 towards the middle, and BCQ_PI180, BCQ_PI181, gshAB, 3 germination proteins encoded (including Ger(x)C), and a single protein (DUF11 domain-containing protein) being found on the opposing end of the pathogenicity island (**Table 3**).

Influence of Plasmid Presence on Strain Phenotypes

The first and last isolates, S94 and S95, were evaluated in various phenotypical and functional assays. The two strains have similar growth capacity over time although the S95 strain was slightly impaired (**Figure 2A**). The two strains show no apparent difference in morphology. However, the colony morphology on plate is different with S95 colonies being wider (**Figure 2B**). In average, the size of the colonies was 3 times higher for the S95 strain compared to the S94 strain. In addition, S95 strain showed a drastic diminution in its germination rate compared to the S94 strain (**Figure 2C**). Finally, the S95 strain was severely impaired in its virulence potential compared to the S94 strain in the insect model of infection (**Figure 2D**). The lethal doses 50 (LD50) were $1{,}16.10^{6}$ CFU/mL for the S94 strain and $5{,}29.10^{8}$ CFU/mL for the S95 strain, thus displaying a 456-fold difference.

Taken together, these data strongly suggest that the plasmid pAH187_270 carried by the S94 strain and lost by the S95 strain plays an essential role during *B. cereus* virulence.

Role of the PAI on Strain Phenotypes

To confirm that the pAH187_270 plasmid has an influence on the strain pathogenicity, we first tried to cure the S94 strain from this plasmid. However, all our attempts to cure the plasmid were unsuccessful. Thus, we focussed on the PAI region containing most of the markers previously identified as characteristic of clinical strains. To assess whether the genes located in the PAI may explain the difference in the strain pathogenicity, the S94 strain was deleted for its PAI and the Δpai-mutated strain was compared with the wild type strain in various phenotypical and functional assays.

The strains were observed under the microscope and bacterial morphology showed that the two strains were almost similar in cellular shape and size although the Δpai mutant was slightly impaired in its growth capacity (**Figures 2A, B**).

As at least two germination genes were identified within the PAI (**Figure 1**), the capacity of the wt and mutant strain to sporulate and germinate was assessed. No difference in the

TABLE 2 | Snippy SNP analysis of patient strains against the plasmid pAH187_270 as reference.

Variants	pAH187_270 plasmid		
Strain	**S94**	**S20**	**S95**
Complex	14	14	303
MNP	1	1	10
SNP	60	61	833
Insertion	0	0	2
Deletion	1	1	1
Total	76	77	1149

TABLE 3 | PAI genes with gene position (on the reference genome pAH187_270 - NC_011655.1), putative function and occurrence (%) in the strain collection.

Marker name	BCQ_PI180	gshAB	BCQ_PI181	gerX
Gene name	BCAH187_RS28565	BCAH187_C0244	BCAH187_RS28570	BCAH187_RS28600
Gene position	164163 | 164519 (plasmidic)	167109 | 169376 (plasmidic)	164642 | 165757 (plasmidic)	171639 | 172793 (plasmidic)
Gene length	357 nt	2268 nt	1116 nt	1155 nt
Potential function	helix-turn-helix transcriptional regulator	bifunctional glutamate–cysteine ligase GshA/ glutathione synthetase GshB	S-(hydroxymethyl)glutathione dehydrogenase/ class III alcohol dehydrogenase	Ger(x)C germination protein
% in non clinical strains	9	9	9	9
% in clinical strains	71	71	71	71

sporulation efficiency was observed (not shown). However, the Δpai mutant showed a drastic diminution in its germination rate (**Figure 2C**). The same difference was observed for the S95 and the Δpai mutant compared to the S94 strain, strongly suggesting that the PAI is responsible for the germination efficiency of the initial S94 strain.

Finally, to assess whether the genes located in the PAI may explain the difference in the strain pathogenicity, the S94 and the Δpai mutated strains were evaluated in the *Galleria* infection model (**Figure 2D**). Strikingly, the Δpai mutant was severely impaired in its virulence potential compared to the wild type strain. The lethal doses (LD) was 3.80E+07 CFU/mL for the Δpai mutant strain, thus displaying a 34.5 fold difference, indicating that the PAI plays an important role in *B. cereus* virulence capacity.

The S95 strain showed morphological difference to the Δpai mutant and was even more severely impaired in its virulence capacity. This implies that the genes located within the PAI play an important role during *B. cereus* virulence, but that other genes located elsewhere in the plasmid are also required.

DISCUSSION

Here, we report the identification of a large plasmid, lost over time within the same patient. This plasmid plays an essential role during *B. cereus* germination and virulence in an insect model. Notably, in strain S94, several biomarkers were found on the single large plasmid pAH187_270 within a newly identified pathogenicity island, providing further insights into *B. cereus* pathogenicity and complexity.

Within the *B. cereus sensu lato* group, the carriage of different virulence plasmids was traditionally considered a major contributor to the phenotypic properties that were critical for the speciation of *B. anthracis*, *B. cereus*, and *B. thuringiensis* (Rasko et al., 2007; Adams et al., 2014). However, recent findings suggest a need to reconsider traditional species assignments upon plasmid-mediated pathogenic phenotypes, in particular with the isolation of several *B. cereus* strains from patients with respiratory anthrax-like symptoms and carrying a pXO1-like plasmid (Baldwin, 2020). The identification of the pAH187_270 as an important plasmid for *B. cereus* pathogenicity paves the way for future investigation and may indicate that pAH187_270 could be a marker of clinically relevant *B. cereus* strains.

In particular, a previous study carried out on strains representative of *B. cereus* pathogenicity concluded that most clinical strains possess the combination of 4 genetic biomarkers, named *adhB*, *agrC*, *thiJ* and *BCQ_PI180* (Kavanaugh et al., 2021; Kavanaugh et al., 2022). Strikingly, the biomarker *BCQ_PI180* could be exchanged with other genes (ie: *gshAB, BCQ_PI181, ger (x)C*) giving similar results during the AUC analysis, with an AUC of 0.955 in all cases (Kavanaugh et al., 2021). We consistently showed here that these genes belong to the a PAI located on a large plasmid. The presence of these genes was assessed in a collection of clinical and non clinical strains and revealed that they were present in 25/35 (71%) clinical isolates and 2 of 21 (9%) of non clinical isolates, respectively (**Table 3**) (Kavanaugh et al., 2021), further highlighting their importance during *B. cereus* pathogenesis.

The presence of the *ces* gene is normally associated with emetic *B. cereus* strains, which constitute a cluster of food-borne outbreak (FBO) related strains and represent less than 1% of the strains identified during FBO. This is not surprising as the emetic syndrome is due to the ingestion of the cereulide, pre-formed in food, and does not necessarily require ingestion of the emetic strain

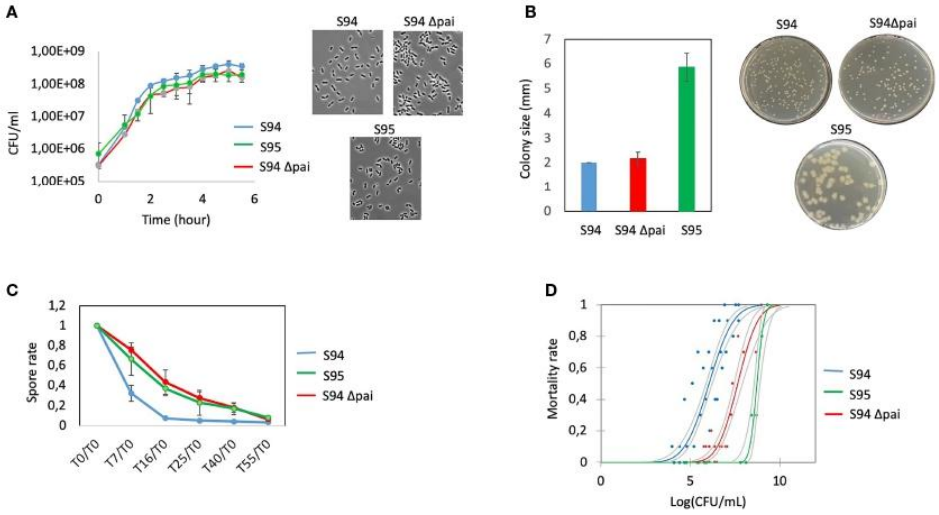

FIGURE 2 | **(A)** left: Determination of growth curves of *B cereus* strains (S94, S95, S94Δpai) by measuring the OD_{600nm} in BHI medium at 37°C during 6.5 hours. Each point is the mean of four independent experiments. Vertical bars indicate standard errors. Right: representative images of microscopic observation of the strains at $DO_{600\ nm}$ = 0.3. **(B)** *B. cereus* strains) were plated on BHI plates to obtained single colonies. Left: the sizes of 25 colonies per plate were measured. The results indicate the mean of three independent experiments with standard errors; Right: representative images of the strains. **(C)** Germination rate efficiency measured over 55 minutes. The spores of the strains were incubated in BHI and at each time point, the remaining heat resistant bacteria (spores) were measured and normalized to the initial spore values at t0. The decrease in spore value indicate the rate of germination. The results indicate the mean of three independent experiments with standard errors. **(D)** Mortality rate of *G mellonella* injected with increasing doses of the strains was assessed 24 hours post-infection. Each dot represents the data for 10 larvae. Several dots are overlapping for the S95 strain.

itself. However, it has been previously shown that several *ces*-positive strains induced non-emetic symptoms (Glasset et al., 2016). This may be due to the fact that other genes, carried by the same plasmid, may have induced these non-emetic symptoms. Similarly, we have previously shown that strains carrying the *ces* gene were found to induce non-gastrointestinal clinical symptoms (Glasset et al., 2018). The markers present on this plasmid may have been at the origin of the symptoms, independently of the *ces* gene. The pAH187 plasmid presents a high degree of sequence similarity to the *B. anthracis* pXO1 plasmid (Rasko et al., 2007), but lacks the pXO1 pathogenicity island. By contrast, we have shown that this plasmid contains a specific pathogenicity island that defines pathogenic *B. cereus* isolates.

Several bacteria carry some of their virulence determinants on specific chromosome or plasmid locations referred to as pathogenicity islands (Parsot, 1994; Cossart and Lecuit, 1998). So far, a pathogenicity island had never been described for *B. cereus*. This island is approximately 50 kb and flanked by resolvases and transposases, likely indicating an acquisition or fusion event. The deletion of this region decreases *B. cereus* virulence in an insect model of infection. Together, it is tempting to speculate that this plasmid carrying the *B. cereus* pathogenic island may define clinical *B. cereus* in the same way that pXO1 and pXO2 define the *B. anthracis* species.

The new discovery of unknown factors located on this plasmid paves the way for future research on their exact roles during *B. cereus* virulence. These data provide new hints into the role of large plasmids and plasmid-hosted genes in the virulence within the *B. cereus* group.

The patient underwent a severe antibiotic treatment and finally recovered from the infection. As the three isolates from this patient were sensitive to the antibiotics used, the treatment might have been successful. On the other hand, it is tempting to speculate that the antibiotic pressure and/or the immune system might have led to a loss of the pAH187_270 plasmid and that the new isolate, cured of the plasmid was rendered less pathogenic and was thus cleared.

In addition, the last isolate showed an acquired resistance to rifampicin, although no rifampicin was given to the patient. Nevertheless, this strongly suggests that, similarly to *S. aureus*, rifampicin should be used with caution to treat *B. cereus* infections.

Taken together, these new findings help in the understanding of *B. cereus* pathogenic potential and complexity and provide further hints into the role of large plasmids in the virulence of *B. cereus* strains. This may provide tools for a better assessment of the risks associated with *B. cereus* hospital contamination to improve hygiene procedure and patient health.

DATA AVAILABILITY STATEMENT

The data presented in this study are deposited in the https://www.ebi.ac.uk/ena/ repository, accession number PRJEB46455.

ETHICS STATEMENT

Ethical review and approval were not required for the study on human participants in accordance with the local legislation and institutional requirements. Written informed consent for participation was not required for this study in accordance with the national legislation and the institutional requirements.

AUTHOR CONTRIBUTIONS

DK, RD, DC, and BG: performed experiments and analyzed data. NR: supervision, analyzed data, writing of manuscript, and funding sources. All authors contributed to the article and approved the submitted version.

FUNDING

This work was supported by the European EJP CARE project from the European Union's Horizon 2020 research and innovation program under Grant Agreement No. 773830.

ACKNOWLEDGMENTS

We warmly thank Laurent Cavalié for the three patient's isolates. We thank Etienne Dervyn for his help in plasmid reconstruction as well as Valentin Loux for bioinformatics support. We are grateful to the INRAE MIGALE bioinformatics platform (http://migale.jouy.inra.fr) for providing computational resources.

REFERENCES

Adams, V., Li, J., Wisniewski, J. A., Uzal, F. A., Moore, R. J., McClane, B. A., et al. (2014). Virulence Plasmids of Spore-Forming Bacteria. *Microbiol. Spectr.* 2 (6). doi: 10.1128/microbiolspec.PLAS-0024-2014

Baldwin, V. M. (2020). You Can't B. Cereus - A Review of Bacillus Cereus Strains That Cause Anthrax-Like Disease. *Front. Microbiol.* 11, 1731. doi: 10.3389/fmicb.2020.01731

Bottone, E. J. (2010). Bacillus Cereus, a Volatile Human Pathogen. *Clin. Microbiol. Rev.* 23 (2), 382–398. doi: 10.1128/CMR.00073-09

Buisson, C., Gohar, M., Huillet, E., and Nielsen-LeRoux, C. (2019). Bacillus Thuringiensis Spores and Vegetative Bacteria: Infection Capacity and Role of the Virulence Regulon PlcR Following Intrahaemocoel Injection of Galleria Mellonella. *Insects* 10 (5), 129. doi: 10.3390/insects10050129

Cadot, C., Tran, S. L., Vignaud, M. L., De Buyser, M. L., Kolsto, A. B., Brisabois, A., et al. (2010). InhA1, NprA and HlyII as Candidates to Differentiate Pathogenic From non-Pathogenic Bacillus Cereus Strains. *J. Clin. Microbiol.* 48, 1358–1365. doi: 10.1128/JCM.02123-09

Carlin, F., Fricker, M., Pielaat, A., Heisterkamp, S., Shaheen, R., Salonen, M. S., et al. (2006). Emetic Toxin-Producing Strains of Bacillus Cereus Show Distinct Characteristics Within the Bacillus Cereus Group. *Int. J. Food Microbiol.* 109 (1-2), 132–138. doi: 10.1016/j.ijfoodmicro.2006.01.022

Cormontagne, D., Rigourd, V., Vidic, J., Rizzotto, F., Bille, E., and Ramarao, N. (2021). Bacillus Cereus Induces Severe Infections in Preterm Neonates: Implication at the Hospital and Human Milk Bank Level. *Toxins (Basel).* 13 (2), 123. doi: 10.3390/toxins13020123

Cossart, P., and Lecuit, M. (1998). Interactions of Listeria Monocytogenes With Mammalian Cells During Entry and Actin-Based Movement: Bacterial Factors, Cellular Ligands and Signaling. *EMBO J.* 17, 3797–3806. doi: 10.1093/emboj/17.14.3797

Fagerlund, A., Lindbäck, T., Storset, A., Granum, P., and Hardy, S. (2008). Bacillus Cereus Nhe is a Pore Forming Toxin With Structural and Functional Properties Similar to ClyA (HlyE, SheA) Family of Haemolysins, Able to Induce Osmotic Lysis in Epithelia. *Microbiol* 154, 693–704. doi: 10.1099/mic.0.2007/014134-0

Fricker, M., Messelhausser, U., Busch, U., Scherer, S., and Ehling-Schulz, M. (2007). Diagnostic Real-Time PCR Assays for the Detection of Emetic Bacillus Cereus Strains in Foods and Recent Food-Borne Outbreaks. *Appl. Environ. Microbiol.* 73 (6), 1892–1898. doi: 10.1128/AEM.02219-06

Glasset, B., Herbin, S., Granier, S., Cavalié, L., Lafeuille, E., Guérin, C., et al. (2018). Bacillus Cereus, a Serious Cause of Nosocomial Infections: Epidemiologic and Genetic Survey. *PloS One* 13 (5), e0194346. doi: 10.1371/journal.pone.0194346

Glasset, B., Herbin, S., Guillier, L., Cadel-Six, S., Vignaud, M. L., Grout, J., et al. (2016). Bacillus Cereus-Induced Food-Borne Outbreaks in France, 2007 to 2014: Epidemiology and Genetic Characterisation. *Euro Surveill* 21 (48), 30413. doi: 10.2807/1560-7917.ES.2016.21.48.30413

Glasset, B., Sperry, M., Dervyn, R., Herbin, S., Brisabois, A., and Ramarao, N. (2021). The Cytotoxic Potential of Bacillus Cereus Strains of Various Origins. *Food Microbiol.* 98, 103759. doi: 10.1016/j.fm.2021.103759

Granum, P. E., and Lund, T. (1997). *Bacillus Cereus* and its Food Poisoning Toxins. *FEMS Microbiol. Lett.* 157 (2), 223–228. doi: 10.1111/j.1574-6968.1997.tb12776.x

Guinebretiere, M. H., Auger, S., Galleron, N., Contzen, M., De Sarrau, B., De Buyser, M. L., et al. (2013). Bacillus Cytotoxicus Sp. Nov. Is a Novel Thermotolerant Species of the Bacillus Cereus Group Occasionally Associated With Food Poisoning. *Int. J. Syst. Evol. Microbiol.* 63 (Pt 1), 31–40. doi: 10.1099/ijs.0.030627-0

Guinebretière, M. H., Broussolle, V., and Nguyen-The, C. (2002). Enterotoxigenic Profiles of Food-Poisoning and Food-Borne *Bacillus Cereus* Strains. *J. Clin. Microbiol.* 40 (8), 3053–3056. doi: 10.1128/JCM.40.8.3053-3056.2002

Guinebretière, M. H., Thompson, F. L., Sorokin, A., Normand, P., Dawyndt, P., Ehling-Schulz, M., et al. (2008). Ecological Diversification in the Bacillus Cereus Group. *Environ. Microbiol.* 10, 851–865. doi: 10.1111/j.1462-2920.2007.01495.x

Haydar, A., Tran, S. L., Guillemet, E., Darrigo, C., Perchat, S., Lereclus, D., et al. (2018). InhA1-Mediated Cleavage of the Metalloprotease NprA Allows Bacillus Cereus to Escape From Macrophages. *Front. Microbiol.* 23, 1063. doi: 10.3389/fmicb.2018.01063

Hill, C., and Holland, I. B. (1967). Genetic Basis of Colicin E Susceptibility in Escherichia Coli. *J. Bacteriol* 94, 677–686. doi: 10.1128/jb.94.3.677-686.1967

Huys, G., D'Haene, K., Collard, J. M., and Swings, J. (2004). Prevalence and Molecular Characterization of Tetracycline Resistance in Enterococcus Isolates From Food. *Appl. Environ. Microbiol.* 70 (3), 1555–1562. doi: 10.1128/aem.70.3.1555-1562.2004

Journal, T. E. (2009). The Community Summary Report on Food-Borne Outbreaks in the European Union in 2007. *EFSA J.* 271.

Kavanaugh, D., Glasset, B., Dervyn, R., Guérin, C., Plancade, S., Cormontagne, D., et al. (2021). New Genetic Biomarkers to Differentiate Non-Pathogenic From Clinically Relevant Bacillus Cereus Strains. *Clin. Microb. Infect.* doi: 10.1016/j.cmi.2021.05.035

Kavanaugh, D., Porrini, C., Dervyn, R., and Ramarao, N. (2022). The Pathogenic Biomarker Alcohol Dehydrogenase Protein Is Involved in Bacillus cereus Virulence and Survival Against Host Innate Defence. *PLoSOne, in press.* doi: 10.1371/journal.pone.0259386

Larsen, M. V., Cosentino, S., Rasmussen, S., Friis, C., Hasman, H., Marvig, R. L., et al. (2012). Multilocus Sequence Typing of Total-Genome-Sequenced Bacteria. *J. Clin. Microbiol.* 50 (4), 1355–1361. doi: 10.1128/JCM.06094-11

Parsot, C. (1994). Shigella Flexneri: Genetics of Entry and Intercellular Dissemination in Epithelial Cells. *Curr. Top. Microbiol. Immunol.* 192, 217–241. doi: 10.1007/978-3-642-78624-2_10

Ramarao, N., and Lereclus, D. (2005). The InhA1 Metalloprotease Allows Spores of the B. Cereus Group to Escape Macrophages. *Cell Microbiol.* 7 (9), 1357–1364. doi: 10.1111/j.1462-5822.2005.00562.x

Ramarao, N., and Sanchis, V. (2013). The Pore-Forming Haemolysins of Bacillus Cereus: A Review. *Toxins* 5, 1119–1139. doi: 10.3390/toxins5061119

Ramarao, N., Tran, S. L., Marin, M., and Vidic, J. (2020). Advanced Methods for Detection of Bacillus Cereus and Its Pathogenic Factors. *Sensors (Basel).* 20 (9), 2667. doi: 10.3390/s20092667

Rasko, D. A., Rosovitz, M. J., Okstad, O. A., Fouts, D. E., Jiang, L., Cer, R. Z., et al. (2007). Complete Sequence Analysis of Novel Plasmids From Emetic and Periodontal Bacillus Cereus Isolates Reveals a Common Evolutionary History Among the B. Cereus-Group Plasmids, Including Bacillus Anthracis Pxo1. *J. Bacteriol* 189 (1), 52–64. doi: 10.1128/JB.01313-06

Seemann, T. (2014). Prokka: Rapid Prokaryotic Genome Annotation. *Bioinformatics* 30 (14), 2068–2069. doi: 10.1093/bioinformatics/btu153

Stenfors Arnesen, L., Fagerlund, A., and Granum, P. (2008). From Soil to Gut: Bacillus Cereus and Its Food Poisoning Toxins. *FEMS Microbiol. Rev.* 32, 579–606. doi: 10.1111/j.1574-6976.2008.00112.x

Tran, S. L., Cormontagne, D., Vidic, J., Andre-Leroux, G., and Ramarao, N. (2020). Structural Modeling of Cell Wall Peptidase CwpFM (EntFM) Reveals Distinct Intrinsically Disordered Extensions Specific to Pathogenic Bacillus Cereus Strains. *Toxins (Basel).* 12 (9), 593. doi: 10.3390/toxins12090593

Trieu-Cuot, P., Carlier, C., Martin, P., and Courvalin, P. (1987). Plasmid Transfer by Conjugation From *Escherichia Coli* to Gram Positive Bacteria. *FEMS Microbiol. Lett.* 48, 289–294. doi: 10.1111/j.1574-6968.1987.tb02558.x

Trieu-Cuot, P., Carlier, C., Poyart-Salmeron, C., and Courvalin, P. (1990). A Pair of Mobilizable Shuttle Vectors Conferring Resistance to Spectinomycin for Molecular Cloning in Escherichia Coli and in Gram-Positive Bacteria. *Nucleic Acids Res.* 18 (14), 4296. doi: 10.1093/nar/18.14.4296

Trieu-Cuot, P., Carlier, C., Poyart-Salmeron, C., and Courvalin, P. (1991). An Integrative Vector Exploiting the Transposition Properties of Tn1545 for Insertional Mutagenesis and Cloning of Genes From Gram-Positive Bacteria. *Gene* 106 (1), 21–27. doi: 10.1016/0378-1119(91)90561-o

Wayne,Clinical and Laboratory Standards Institute (CLSI) (2010). *Methods for Antimicrobial Dilution and Disk Susceptibility Testing of Infrequently Isolated or Fastidious Bacteria; Approved Guideline. 2nd* (CLSI), M45A2E.

Zheng, J., Peng, D., Ruan, L., and Sun, M. (2013). Evolution and Dynamics of Megaplasmids With Genome Sizes Larger Than 100 Kb in the Bacillus Cereus Group. *BMC Evol. Biol.* 13, 262. doi: 10.1186/1471-2148-13-262

Conflict of Interest: The authors declare that the research was conducted in the absence of any commercial or financial relationships that could be construed as a potential conflict of interest.